Doctoral School of the Universitat Jaume I
Doctoral Programme in Industrial Technologies and Materials

Optimal fault estimation and diagnosis strategies: bridging the gap between theory and practice

A dissertation submitted by Ester Sales Setién to obtain the degree of Doctor of Philosophy from the Universitat Jaume I

AUTHOR
Ester Sales Setién

ADVISOR
Dr. Ignacio Peñarrocha Alós

Castellón de la Plana, June 2019

Escuela de Doctorado de la Universitat Jaume I
Programa de Doctorado en Tecnologías Industriales y Materiales

Estrategias óptimas de estimación y diagnóstico de fallos: acercando la teoría a la práctica

Memoria presentada por Ester Sales Setién para optar al grado de doctora por la Universitat Jaume I

AUTORA
Ester Sales Setién

DIRECTOR
Dr. Ignacio Peñarrocha Alós

Castellón de la Plana, Junio 2019

Escola de Doctorat de la Universitat Jaume I
Programa de Doctorat en Tecnologies Industrials i Materials

Estratègies òptimes d'estimació i diagnòstic de fallades: apropant la teoria a la pràctica

Memòria presentada per Ester Sales Setién per a optar al grau de doctora per la Universitat Jaume I

AUTORA
Ester Sales Setién

DIRECTOR
Dr. Ignacio Peñarrocha Alós

Castellón de la Plana, Juny 2019

To my grandmothers

Abstract

Fault diagnosis (FD) has emerged as an effective tool to meet the increasing demands on reliability and safety of modern control systems. Among FD techniques, the strategies based on fault estimation (FE) appear as advanced monitoring methods that give information not only about the moment of appearance and the location of a fault but also about its size and shape, which is of paramount importance for both real-time decision and active fault tolerant control. Fruitful results have been obtained in FE; however, the existing FE methods still posses certain difficulties which limit their application scope.

This thesis addresses some issues arisen from the application of estimation-based FD strategies to different practical systems such as industrial pipe networks, multistage manufacturing processes, wind turbines and wind farms. With this aim, we present different fault estimators relying on model-based augmented observers and, also, various fault evaluators that process the fault estimates provided by the observers in threshold-based decision mechanisms.

The thesis devotes an important effort to the design of these estimation-based FD strategies. The thesis presents the design of fault estimators, the design of fault evaluators and the co-design of fault estimators and evaluators which allow specifying requirements over FD parameters. We use performance parameters which are typical in practice but uncommon in theoretical designs. In the fault estimation step, we present optimal designs which deal with the cumulative squared error due to abrupt faults, the delay in tracking incipient faults, the variance due to noises and the degree of interfault and unknown input (UI) decoupling. Practical UI decoupling is in fact achieved in single-step optimization design problems dealing with other performance requirements. In the fault evaluation step, we introduce optimal designs and co-designs which deal with the minimum isolable fault, the isolation time and the false isolation rate. These proposed optimal designs are mainly formulated using matrix inequalities.

The thesis also deals with the structure of augmented observers for FE. First, we present an enhanced form of augmented observers —proportional multiple-integral and multiple-resonant observers— with an improved performance w.r.t. faults with periodic components. Second, we present a probabilistic design approach that optimally deals with the trade-offs arisen from the structural complexity of augmented observers.

Finally, the methods developed in this thesis are extended to schemes of banks of model-based augmented observers and threshold-based decisions mechanisms. The proposed schemes allow achieving estimation-based FD in systems with non-isolable faults at the expense of some

mild fault simultaneity restrictions. These schemes are also utilized in the thesis for ameliorating the fault estimation and evaluation performance in groups of comparable systems operating under similar conditions.

Resumen

El diagnóstico de fallos (FD, del inglés *Fault Diagnosis*) ha emergido como una herramienta eficaz para responder a las crecientes demandas de fiabilidad y seguridad en los sistemas de control modernos. Entre las técnicas de FD, las estrategias basadas en la estimación de fallos (FE, del inglés *Fault Estimation*) son métodos avanzados de monitoreo que proporcionan información no sólo sobre la aparición y ubicación de un fallo, sino también sobre su tamaño y forma, lo que es de suma importancia para la toma de decisiones en tiempo real y para el control tolerante a fallos activo. Muchos resultados interesantes se han obtenido en el campo de FE; sin embargo, los métodos existentes de FE presentan todavía ciertas limitaciones que dificultan su aplicación.

Esta tesis aborda algunos de los problemas derivados de la aplicación de estrategias de FE a diferentes sistemas prácticos como redes de tuberías industriales, procesos de fabricación multietapa, aerogeneradores y parques eólicos. Con este objetivo, presentamos diferentes estimadores de fallo basados en observadores aumentados y, también, varios evaluadores de fallo que procesan las estimaciones proporcionadas por los observadores en mecanismos de decisión con umbrales.

La tesis se centra en el diseño de estas estrategias de FD basadas en estimación. Así, presentamos diferentes diseños de estimadores, diseños de evaluadores y co-diseños de estimadores y evaluadores que permiten especificar requisitos sobre parámetros que describen el desempeño de la estrategia de FD. En concreto, utilizamos parámetros de desempeño que son típicos en la práctica pero poco comunes en los diseños teóricos. Para la estimación de fallos, presentamos diseños óptimos que tratan con el error cuadrático acumulado ante fallos abruptos, el retraso en el seguimiento de fallos incipientes, la varianza debida a los ruidos y el grado de desacoplamiento de otros fallos y de entrada desconocidas (UIs, del inglés *Unknown Inputs*). En un único problema de optimización, el desacoplamiento práctico de UIs se consigue junto a otros requisitos de desempeño. Para la evaluación de fallos, introducimos diseños y co-diseños óptimos que utilizan el fallo mínimo aislable, el tiempo de aislamiento y la tasa de falsos aislamientos. Los diseños óptimos que se formulan en la tesis se basan, principalmente, en desigualdades matriciales.

La tesis también estudia la estructura de los observadores aumentados para FE. Primero, presentamos una forma mejorada de observadores aumentados — observadores proporcionales múltiple-integrales y múltiple-resonantes — con un comportamiento mejorado frente a fallos con componentes periódicas. En segundo lugar, presentamos un enfoque de diseño probabilístico que aborda de manera óptima los compromisos derivados de la complejidad estructural de los observadores aumentados.

Finalmente, los métodos desarrollados en esta tesis se extienden a esquemas de bancos de observadores aumentados y de mecanismos de decisión. Los esquemas propuestos permiten lograr FE en sistemas con fallos no aislables a costa de algunas restricciones leves sobre la simultaneidad de los fallos. Estos esquemas también se utilizan en la tesis para mejorar las prestaciones de la estimación y la evaluación de fallos en conjuntos de sistemas comparables que operan bajo condiciones similares.

Resum

El diagnòstic de fallades (FD, de l'anglès *Fault Diagnosis*) ha emergit com una eina eficaç per respondre a les creixents demandes de fiabilitat i seguretat en els sistemes de control moderns. Entre les tècniques de FD, les estratègies basades en l'estimació de fallades (FE, de l'anglès *Fault Estimation*) són mètodes avançats de monitorització que proporcionen informació no només sobre l'aparició i la ubicació d'una fallada, sinó també sobre la seua mida i forma, el que és molt important per a la presa de decisions en temps real i per al control tolerant a fallades actiu. Molts resultats interessants s'han obtingut en el camp de FE; tanmateix, els mètodes existents de FE presenten encara limitacions que dificulten la seua aplicació.

Aquesta tesi aborda alguns dels problemes derivats de l'aplicació d'estratègies de FE a diferents sistemes pràctics com xarxes de canonades industrials, processos de fabricació multietapa, aerogeneradors i parcs eòlics. Amb aquest objectiu, presentem diferents estimadors de fallades basats en observadors augmentats i, també, diversos avaluadors de fallades que processen les estimacions proporcionades pels observadors en mecanismes de decisió amb llindars.

La tesi se centra en el disseny d'aquestes estratègies de FD basades en estimació. Així, presentem diferents dissenys d'estimadors, dissenys d'avaluadors i co-dissenys d'estimadors i avaluadors que permeten especificar requisits sobre paràmetres que descriuen el comportament de l'estratègia de FD. En concret, utilitzem paràmetres de comportament que són típics en la pràctica però poc comuns en els dissenys teòrics. Per a l'estimació de fallades, presentem dissenys òptims que tracten amb l'error quadràtic acumulat davant fallades abruptes, el retard en el seguiment de fallades incipients, la variància produïda pels sorolls i el grau de desacoblament d'altres fallades i d'entrades desconegudes (UIs, l'anglès *Unknown inputs*). En un únic problema d'optimització, el desacoblament pràctic d'UIs s'aconsegueix conjuntament amb altres requisits d'execució. Per a l'avaluació de fallades, introduïm dissenys i co-dissenys òptims que utilitzen la fallada mínima aïllable, el temps d'aïllament i la taxa de falsos aïllaments. Els dissenys òptims que es formulen en la tesi es basen, principalment, en desigualtats matricials.

La tesi també estudia l'estructura dels observadors augmentats per a FE. En primer lloc, presentem una forma millorada d'observadors augmentats — observadors proporcionals múltiple-integrals i múltiple-ressonants — amb un comportament millorat davant de fallades amb components periòdiques. En segon lloc, presentem un enfocament probabilístic de disseny que aborda de manera òptima els compromisos derivats de la complexitat estructural dels observadors augmentats.

Finalment, els mètodes desenvolupats en aquesta tesi s'estenen a esquemes de bancs d'observadors augmentats y de mecanismes de decisió. Els esquemes proposats permeten aconseguir FE en sistemes amb fallades no aïllables a canvi de algunes restriccions lleugeres sobre la simultaneïtat de les fallades. Aquests esquemes també s'utilitzen en la tesi per millorar les prestacions de l'estimació i l'avaluació de fallades en conjunts de sistemes comparables que operen en condicions similars.

Funding | *Financiación*

Contrato predoctoral

- Beca Predoctoral de Formación del Profesoraro Universitario (FPU) del Ministerio de Educación, Cultura y Deporte (MECD), Gobierno de España (Ref. FPU14/01592).
- Beca Predoctoral para la Formación de Personal Investigador (FPI) del Programa VALi+d de la Conselleria d'Educació de la Generalitat Valenciana (Ref. ACIF/2015/172).

Participación en actividades

- Proyecto de Investigación "Desarrollo de estrategias de control de grandes parques eólicos off-shore conectados a la red principal mediante enlaces de corriente continua de alta tensión (HVDC) con convertidores por fuente de tensión (VSC)" de la Universitat Jaume I (Ref. P11B2013-51).
- Proyecto de Investigación "Integración de fuentes de energía renovables y control de flujos de potencia en redes HVDC mediante convertidores modulares multinivel" del Ministerio de Economía y Competitividad (Ref. DPI2014-53245-R).
- Proyecto de Investigación "Estrategias de estimación y control para la minimización del coste energético en procesos con perturbaciones variantes y sujetos a periodos tarifarios" del Ministerio de Economía y Competitividad (Ref. TEC2015-69155-R).
- Proyecto de Investigación "Desarrollo de algoritmos de control para sistemas distribuidos implementables mediante estándares industriales" de la Universitat Jaume I (Ref. P11B2015-42).
- Proyecto de Investigación "Interacción entre convertidores y red en sistemas HVDC y HVAC con alta penetración de generación renovable" del Ministerio de Economía, Industria y Competitividad (Ref. DPI2017-84503-R).

Acknowledgements | *Agradecimientos*

En primer lugar, me gustaría expresar mi agradecemiento a mi director y tutor de tesis Ignacio Peñarrocha por la confianza depositada en mi trabajo y por compartir sus inquietudes y su experiencia conmigo durante todo este periodo de formación. También me gustaría dar las gracias al Prof. Ron J Patton por haberme acogido durante mi estancia de investigación en la Universidad de Hull, Reino Unido.

En segundo lugar, quiero acordarme de todos los compañeros con los que he podido interactuar durante estos años. En especial, de mis compañeros de laboratorio Rubén, Carlos, Oscar y David, que me han aportado alegría en mi día a día. También mencionar a Chus, Alexandra, Pepe y Pablo, que me han ayudado a desconectar en los momentos de estrés. También quiero agradecerles su cariño a todas mis *Genias*.

En tercer lugar, quiero agradecer a Luis todo lo que me ha aportado en estos años. Descubrir su mundo interior ha sido mi mayor fuente de felicidad y mi mayor motor para mejorar como persona.

En cuarto lugar, quiero reconocer la labor de mis padres. Gracias a la educación que me han dado y a su apoyo incondicional, la realización de este trabajo ha sido posible. También quiero darle las gracias a mi tía por estar siempre a mi lado.

Finalmente, quiero dedicar estas últimas líneas a mi abuela Rosita y a mi yaya Rosa, dos mujeres luchadoras y trabajadoras cuyo ejemplo ha sido el más inspirador para elaborar esta tesis y lo seguirá siendo para afrontar todos los retos que se me presenten en el futuro.

Contents

List of Figures

List of Tables

Notation

Abbreviations

FD	Fault diagnosis
FI	Fault isolation
FDI	Fault detection and isolation
FDIA	Fault detection, isolation and analysis
FA	Fault analysis
FE	Fault estimation
FTC	Fault tolerant control
AFTC	Active fault tolerant control
PFTC	Passive fault tolerant control
FAR	False alarm rate
FIR	False isolation rate
FDR	Fault detection rate
CSE	Cumulative squared error
MDF	Minimum detectable fault
MIF	Minimum isolable fault
AT	Acknowledgement time
IT	Isolation time
EDD	Expected detection delay
LTI	Linear time-invariant
UI	Unknown input
UIO	Unknown input observer
PI	Proportional integral

PR	Proportional resonant
PMI	Proportional multiple-integral
PMR	Proportional multiple-resonant
PMIR	Proportional multiple-integral multiple-resonant
LMI	Linear matrix inequality
BMI	Bilinear matrix inequality
RMS	Root mean square
FFT	Fast Fourier Transform
RLS	Recursive least squares
LSE	Least-Squares fit estimator
ASE	Estimator in Apley and Shi [11]
DSCE	Estimator in Ding, Shi and Ceglarek [77]
SNE	Estimator presented in Stoica and Nehorai [276]
PLC	Programmable Logic Controller
DCS	Distributed Control System
MMP	Multistage manufacturing process
SPC	Statistical process control
SoV	Stream of Variation
KPC	Key product characteristic
OCMM	Optical coordinate measuring machine
WT	Wind turbine
WF	Wind farm
WS	Wind speed
WSZ	Wind speed zone
PM	Power mode
LIDAR	Laser anemometers
MPPT	Maximum power point tracking

Symbols

$\mathbb{R}$	Real numbers set
$\mathbb{C}$	Complex numbers set
$\bar{\mathbb{C}}_1$	Closed plane outside the unit circle
$\prod$	Product
$\sum$	Summation
$\lvert \cdot \rvert$	Absolute value
$\mathbf{E}\{\cdot\}$, $\mathbb{E}\{\cdot\}$	Expected value
$\mathbf{Pr}\{\cdot\}$, $\mathbb{P}\{\cdot\}$	Probability
$x(t)$	Continuous-time signal at time t
x_k, $x[k]$, $x(k)$	Discrete-time signal at sample k
$\hat{x}_k$	Estimate of x_k
$\widetilde{x}_k$	Estimation error associated to $\hat{x}_k$
$\lVert x_k \rVert_2$	Euclidean norm of vector x_k, $\sqrt{x_k^T\, x_k}$
$\lVert x \rVert_2$	l_2 norm of signal x, $\sqrt{\sum_{k=1}^{\infty} x_k^T\, x_k}$
$\lVert x \rVert_{\text{RMS}}$	RMS norm of signal x, $\lim_{K\to\infty} \sqrt{\frac{1}{K}\, \sum_{k=1}^{K} x_k^T\, x_k}$
$\lVert x_k \rVert_\infty$	Max norm of vector x_k, $\max_i \lvert x_k[i] \rvert$
$\lVert x \rVert_\infty$	l_∞ norm of signal x, $\max_k \max_i \lvert x_k[i] \rvert$
$\mathbf{\Sigma}_x$, $\mathbf{\Sigma}^x$	Covariance matrix of signal x, $\lim_{k\to\infty} \mathbf{E}\{x_k\, x_k^T\}$
$A \in \mathbb{R}^{n\times m}$	Matrix of size $n \times m$
$a \in \mathbb{R}^n$	Vector of size n
$A[i,j]$, $A(i,j)$, A_{ij}	Element in the i-th row and j-th column of matrix A
$A(i)$	i-th row or column of A depending on the context
$a[i]$, $a(i)$, a_i	i-th element in vector a
I_n	Identity matrix of size $n \times n$
$\mathbf{1}_{n\times m}$	Matrix of ones of size $n \times m$
$0_{n\times n}$	Zero matrix of size $n \times n$
a^T	Transpose of vector a
$\text{tr}\{A\}$	Trace of matrix A
$\text{rank}\{A\}$	Rank of matrix A

$\sigma(A)$	Eigenvalues of matrix A
$A \oplus B$	Block diagonal matrix with A and B on its diagonal
$A \otimes B$	Kronecker product of A and B
$A^{\otimes^2}$	Kronecker product of A and A, $A \otimes A$
$A \circ B$	Hadamard product of A and B
A°^2}	Hadamard product of A and A, $A \circ A$
$\text{diag}(A)$	Generates a column vector with the main diagonal of matrix A
$\text{diag}^{-1}(a)$	Generates a diagonal matrix with the elements of a in the diagonal
$\text{vec}(A)$	Generates a vector by stacking the columns of matrix A.
$\text{vec}^{-1}(a)$	Generates a matrix by reordering the elements of vector a into columns
$A \prec B$, $A \succ B$	Matrix $A - B$ is negative definite. Matrix $A - B$ is positive definite
$A \preceq B$, $A \succeq B$	Matrix $A - B$ is negative semidefinite. Matrix $A - B$ is positive semidefinite

Chapter 1

Introduction

1.1 Background

1.1.1 Fault diagnosis objectives

Many engineering systems such as chemical processes, manufacturing systems, engines, power networks, wind energy conversion systems and aerospace systems are subjected to abnormal events or faults. Sensor, actuator or process faults may drastically change the system behavior, resulting in a performance degradation or even danger. As a result, it is of paramount importance to recognize the presence of faults as early as possible and to implement fault tolerant operation for minimizing performance degradation and avoiding dangerous situations [100, 143].

Traditionally, the task of diagnosing and responding to abnormal events in a process has relied on human operators. However, this task has significantly increased in difficulty due to several factors: the increasing complexity and size of modern process plants, the increasing demands on diagnostic activities and the fact that process measurements are often insufficient or incomplete. Hence, a grand challenge for control engineers is the development of fault diagnosis (FD) and fault tolerant control (FTC) strategies. In fact, people in the process industry view this as the next major milestone in control systems research and application [290].

In the last three decades, significant efforts have been made in the field of FD. FD is the procedure to obtain fault information and it includes fault detection and isolation (FDI) and fault identification or analysis (FA). Especially, a lot of attention has been paid to FDI methods; for instance, the review papers by Frank (1990) [95]; Isermann (1997) [138]; Venkatasubramanian, Rengaswamy, Yin & Kavuri (2003) [290]; Isermann (2005) [139]; Zhang & Jiang (2008) [330]; Yin, Ding, Xie & Luo (2014) [315]; Gao, Cecati & Ding (2015) [100, 101]; Yu & Jiang (2015) [318]; Tidriri, Chatti, Verron & Tiplica (2016) [284]; and the books by Himmelblau (1978) [131]; Gertler (1998) [111]; Blanke, Kinnaert, Lunze and Staroswiecki (2006). [29]; Isermann (2006) [140]; Witczak (2007) [301]; Ding (2008 and 2014) [70, 71]; Chen and Patton (2012) [44]; Patton, Frank & Clark (2013) [227].

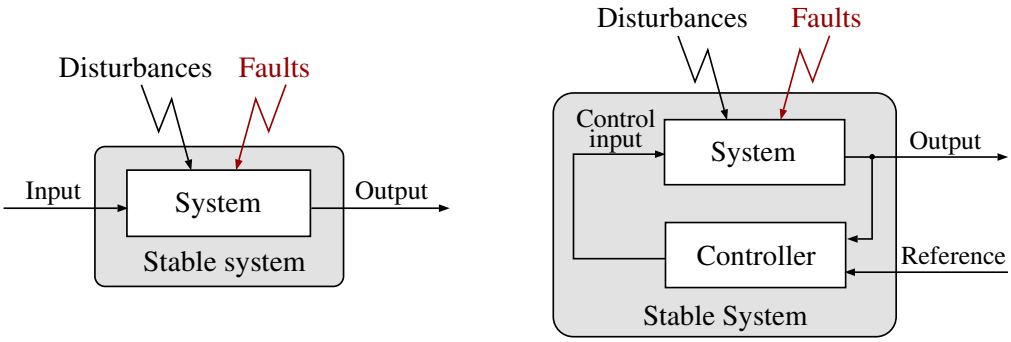

(a) Stable open-loop system (b) Stable closed-loop system

Figure 1.1. Stable systems affected by faults.

On a parallel path, research on FTC has increased progressively. FTC is a control strategy to ensure that a system can continue its operation with satisfactory performance in the presence of faults. Several survey papers and books on FTC are available in the literature. For instance, the survey papers by Rauch (1994) [236] Blanke, Izadi-Zamanabadi, Bøgh & Lunau (1997) [28]; Polycarpou & Vemuri(1998) [232], Zhang & Jiang (2008) [330]; Benosman (2010) [21]; Yu & Jiang (2015) [318]; and the books by Mahmoud, Jiang & Zhang (2003) [193]; Blanke, Kinnaert, Lunze and Staroswiecki (2006). [29]; Zhang, Jiang & Shi (2012) [325]; Hamayun, Edwards & Halim Alwi (2016) [125].

FDI strategies aim to provide information about the appearance (fault detection) and the location (fault isolation) of a fault. However, in FTC designs, not only the information about the appearance and the location of a fault is necessary. The information about its size and shape (fault analysis) is also important. Hence, it seems that most FDI techniques are developed as a diagnostic or monitoring tool, rather than for FTC purposes. Different from FDI methods, fault estimation (FE) aims to provide information about the magnitude and the form of the fault. Hence, as stated in [326], FE appears as a promising bridge between FDI and FTC.

In the FD context, FE is evidently more challenging than FDI and fruitful results were obtained during the past two decades. Commonly, advanced observer-based techniques are utilized for FE [100, 326]. These techniques mainly include augmented observers [102, 103, 163, 306, 339], sliding mode observers [84, 298, 316], adaptive observers [98, 177, 241, 312] and iterative learning observers [50, 136]. However, as detailed by Zhang, Jiang & Shi [325], the existing FE methods posses certain difficulties which limit their application scope. This thesis addresses some issues of the FE problem from a FD practical perspective.

1.1.2 Fault diagnosis architectures

Practical control systems are affected by different kinds of disturbances including unknown inputs (UIs), process disturbances, high-frequency noises and different kinds of uncertainties such as model uncertainties. This thesis considers the case of stable (controlled or uncontrolled) disturbed systems that may be also affected by faults (Fig. 1.1).

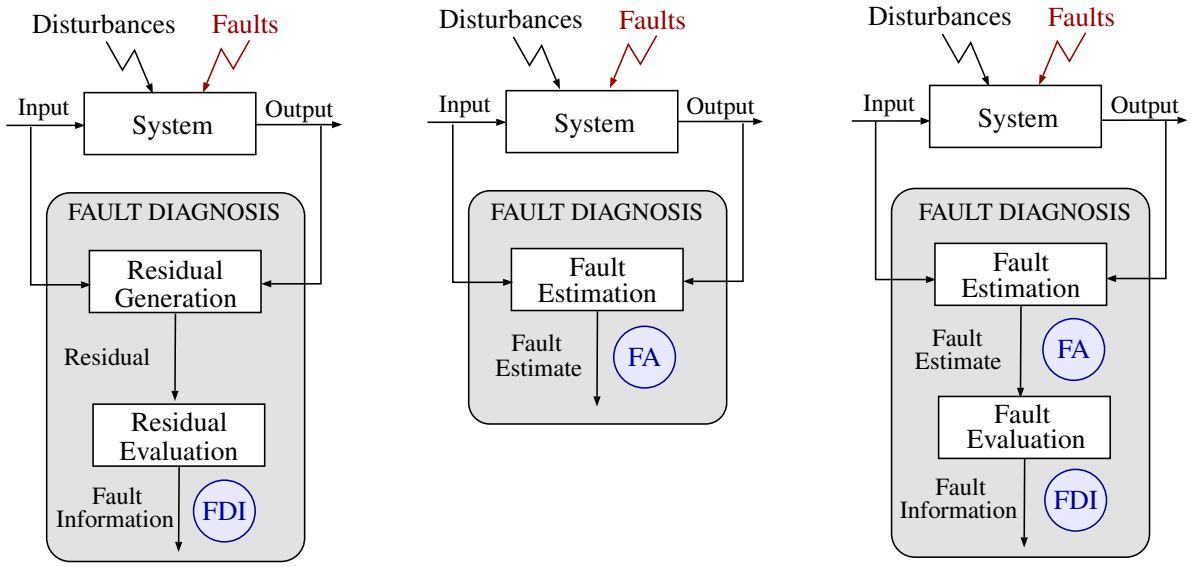

(a) FDI scheme (b) FA scheme (c) Thesis FDI and FA scheme

Figure 1.2. FD architectures.

FDI strategies are based on the generation of residuals, which are signals representing inconsistencies between the measurements and the knowledge from the system. In the absence of all kinds of disturbances, these inconsistencies derive from the presence of faults. However, the presence of disturbances (UIs, process disturbances, noises or model uncertainties) affect the FDI residuals. To face this problem, robust residual generation techniques are utilized. In most cases, however, it is not possible to completely eliminate the effect of all the disturbances on the residuals. Hence, the residuals are generally evaluated in decision mechanisms in order to discern the faults from the disturbances that affect the system [44, 70] (Fig. 1.2.a).

FE strategies, for its part, consist on estimating the value of the faults (Fig. 1.2.b). Some authors consider that robust FE includes detection and isolation because an accurate estimation of the faults implies FDI [170]. However, as in the previous case, it is not always possible to achieve completely error-free fault estimates. Without any further decision mechanism, the decision of whether a specific fault has occurred is delegated to human operators. From a FTC perspective, feedforwarding erroneous fault estimates to a fault tolerant controller in fault-free scenarios also causes a misleading effect that may significantly degrade the system performance.

Motivated by this background, in this thesis, fault analysis is performed by means of FE. The fault estimates are then evaluated in decision mechanisms (which we denote as fault evaluators) in order to reach FDI and decide whether to feed or not a FTC mechanism with these fault estimates (Fig. 1.2.c). Specifically, each fault estimate is independently evaluated from the others; thus, fault detection and fault isolation are addressed simultaneously. Provided that fault isolation (FI) is more involved than fault detection, throughout the thesis, we indistinctly refer to estimation-based FDI or estimation-based FI.

1.2 Challenging problems

This thesis deals with the problems related to the design of fault estimators and evaluators in a FD practical framework. In the following, we briefly describe the major concerns of the thesis which are mainly related to the performance-based optimal design of fault estimators and evaluators with practical FD performance parameters. The results are extended for systems affected by complex uncertain fault forms, systems affected by multiple faults and complex systems with complex disturbances.

Most continuous-time control systems being implemented digitally, discrete-time cases are more meaningful in practice and have a strong engineering background [325]. However, compared with continuous-time systems, fewer and more recent results have been reported for FE in discrete-time systems [323]. Thus, this thesis is devoted to FE and FD in the discrete-time framework.

Performance-based fault estimation

Robust generation techniques in FD (FDI or FE) aim to simultaneously achieve sensitivity to faults and robustness against nuisances [10,277] through the accomplishment of certain trade-off between these properties [241,302]. This issue continues to present significant challenges to both academic and industrial practitioners [228].

Structural methods such as the well-known unknown input observer (UIO) approach [45,106, 120, 163] are used to achieve complete decoupling from disturbances. However, the conditions for complete disturbance decoupling are strong and they are not always verified, at least not for all the nuisances that affect the FD outputs. Alternatively, numerical approaches based on optimization methods can be utilized to attenuate the effect of the disturbances on the FD signals and maximize their fault sensitivity. For instance, the optimization problems based on the well-known $\mathcal{H}_\infty/\mathcal{H}_-$ index [133, 142, 241, 296].

In order to give further physical interpretation to the indices involved in the FD optimization problem, the authors of [49, 327] propose to use the trade-off between the fault detection rate (FDR) and the false alarm rate (FAR). This trade-off has been used in recent works as [331,334] and it is of practical importance in FDI applications. However, although the FAR and the FDR are suitable for FD strategies based on residuals, these indices give little information about other important issues in estimation-based FD methods such as the size of the faults which can be diagnosed, the dynamic behavior or the steady-state accuracy of the results.

In this thesis, we wonder whether practical FE performance parameters from a FD or FTC perspective (e.g., fault estimation delays or variances in steady state due to noises) can be used to design model-based fault estimators. Effectively, as stated in [325], more research on designs considering the performance of FE is needed. Hence, the first challenging problem to be addressed in this thesis can be formulated as follows.

P1. *To design optimal fault estimators taking into account the trade-offs between practical FE performance parameters.*

Generally, in most FE designs, the performance is jointly fixed for all the FE channels (e.g. [106, 302]). However, from a practical perspective not all the faults to which a system is prone impose equal diagnosis demands (e.g. [118, 216]). Designs dealing individually with the performance of each single FE channel would increase the design flexibility. It would also allow handling the coupling effect that appears when faults in other channels appear in the system, which is a rarely studied issue in the literature. This background motivates the following challenging problem of the thesis.

P2. *To independently set the behavior of each FE channel w.r.t. nuisances: UIs, noises and faults in other channels.*

The FD designs including both complete decoupling from certain disturbances and optimal attenuation from the others usually follow a two-steps procedure. For instance, the well-known design of UIOs requires algebraic constraints to achieve UI decoupling [44]. These constraints are generally solved using a particular solution to the problem. Then, the remaining design freedom is used in a numerical second-step design to achieve certain requirements over other performance criteria [180,190,302]. A single-step multiobjective numerical design simultaneously guaranteeing UI decoupling and other performance requirements would reduce the conservatism imposed by the particular solutions to the algebraic constraints and would reduce the complexity of the design procedure. Hence, the challenges **P1** and **P2** are complemented with the following challenging problem **P3**.

P3. *To present single-step designs of optimal fault estimators guaranteeing full UI decoupling and other performance requirements.*

Performance-based fault evaluation

In analogy to the challenging problem **P1**, we wonder whether practical FDI (to which we simply refer as FI) performance parameters can be used to design the decision mechanisms for evaluating the fault estimates (e.g., minimum isolable faults or false isolation rates). We thus introduce the following challenging problem to be tackled in this thesis.

P4. *To design optimal evaluation strategies of fault estimates taking into account the trade-offs between practical FI performance parameters.*

As stated by Ding in [70], the efforts for achieving an optimal diagnosis performance without simultaneously considering the generation and the evaluation function may result in poor diagnosability. Motivated by the integrated designs of residual generators and evaluators in the observer-based approach presented in [327] (extended in works as [1, 49, 294, 295]) and in the set-membership approach presented in [319], we formulate the following promising problem.

P5. *To co-design optimal fault estimators and evaluators taking into account the trade-offs between practical FI performance parameters.*

Many practical applications have explicit FD requirements over time indices (e.g., the FD time requirements in the wind turbine benchmark [216] and in the wind farm benchmark [216]). However, the integrated design becomes specially delicate when it considers isolation time parameters [137, 229]. Hence, we specifically detail this issue in the following problem.

P6. *To introduce isolation time parameters in the co-design of optimal fault estimators and evaluators.*

Fault estimation of complex uncertain fault forms

The essence of augmented observers for FE is to construct an augmented system in which the faults are introduced as an additional state [100, 326]. As an extension of the Luenberger observer, proportional and integral (PI) observers, which have received much attention [163, 305, 339], assume that the faults are constant or step signals. Their applicability is thus limited to the estimation of faults whose variations are slow with respect to the dynamics of the system. By supposing the considered faults to be in the more general form of a polynomial of the time, proportional multiple-integral (PMI) observers were discussed in many works as [102, 103, 156, 306, 322].

As stated in [104], an issue related to the use of PMI observers is that pure high-frequency fault signals cannot be covered by them. On another note, in many practical applications, the faults are periodic signals which can be decomposed into sinusoids of known frequencies (e.g., [157, 240]). The following problem arises from these observations.

P7. *To extend the formulation of PMI observers for FE in order to include resonant terms of known frequency.*

In practice, it is possible to forecast some information about the (polynomial or sinusoidal) order of the faults which are prone to occur. Yet, no exact *a priori* knowledge of this order is available. Hence, the authors in [103, 104] propose to "choose a large order for safety". However, choosing a large order of the faults, increases the order of the corresponding augmented PMI observer and it may degrade its behavior towards faults of lower order. It is then reasonable to study the influence of the complexity of the augmented observer on its tracking ability w.r.t. different types of faults and to take the resulting trade-offs into account in the design:

P8. *To design complex augmented observers taking into account the performance trade-offs derived from their structural complexity.*

Fault estimation and evaluation in systems with numerous faults

One of the main problems in FE arises when the faults affecting a system do not verify fault isolability conditions (i.e., their effect on the measurements cannot be decoupled). Hence, most FE works conservatively consider that the faults verify isolability conditions (e.g., [178, 302]).

However, seldom does this condition hold in practice; specially, if it is protectively considered that, besides possible actuator and process faults, all the sensors may be also affected by faults.

A solution to deal with non-isolable faults is the use of banks of residual generators and evaluators [44, 70]. However, these schemes are usually implemented from a residual-based perspective and each residual in the bank is made sensitive to a subset of faults and insensitive to the other faults. Thus, the following problem states the existing need to extend the concept of bank of residual generators and evaluators to the estimation framework.

P9. *To achieve FE and FI in systems with non-isolable faults using a bank of fault estimators and evaluators.*

Intuitively, a bank-based FE/FI structure imposes some restrictions over the simultaneity of the faults [70]. However, the design flexibility which is gained in each fault estimator and evaluator of the bank make us ask about the possibility of ameliorating the performance of FE/FI schemes (in terms of fault sensitivity and disturbance robustness) at the cost of some simultaneity restrictions over the occurrence of faults. This question is particularly interesting for sets of comparable systems which operate under similar conditions and which very rarely become simultaneously faulty. Then, in this thesis, we address the following problem.

P10. *To ameliorate the performance of FE and FI in replicated systems operating under similar conditions.*

Fault estimation and evaluation in complex practical applications

The application of estimation-based FD techniques becomes particularly difficult in the cases where the system dynamics is complex (e.g., nonlinear time variant systems) or the disturbances affecting the system are complex (e.g., their bounds significantly change along the system operation region or their statistical properties are unknown). In such cases, it is complicated to design tight FD strategies and the designed strategies may result in diagnosis systems with poor diagnosability. Hence, the we formulate the following challenging problem to be addressed in this thesis.

P11. *To design tight FE and FI strategies for complex systems affected by complex disturbances.*

The application of theoretical FD strategies to practical engineering cases also poses a great challenge. It usually demands a considerable modeling effort, the utilization of complex FD techniques and specific challenging performance requirements. Hence, many FD solutions to practical cases in the literature are based on simplified, non-standardized, ad-hoc methods.

This thesis utilizes complex practical applications to motivate and introduce the proposed theoretical contributions. Particularly, we deal with the faults in industrial pipe networks, multistage manufacturing processes, wind turbines and wind farms:

P12. *To apply optimal performance-based FE and FI in complex practical applications: industrial pipe networks, multistage manufacturing processes, wind turbines and wind farms.*

1.3 Thesis outline and contributions

The main goal of this thesis is to bridge the gap between theory and practice in optimal estimation-based fault diagnosis. Inspired by the challenges posed by different practical applications, we develop different kinds of fault estimators and evaluators and we design them using practical FD performance parameters.

The thesis follows a reasonable base line. First, Chapter 2 briefly introduces the basics of FD. Second, Chapter 3, Chapter 4 and Chapter 5 include some initial analysis and comparisons of estimation-based FD strategies. Chapter 6 studies the structure of augmented observers in FE and Chapter 7 presents integral design approaches of fault estimators and evaluators. It also presents structures of banks of fault estimators and evaluators. Chapter 8 and Chapter 9 extend the obtained results to more complex cases.

Throughout the thesis, we motivate the research and we and validate the obtained results using practical applications. We consider the problem of estimation-based FD in industrial pipe networks (Chapter 3), multistage manufacturing processes (Chapter 4), wind turbines (Chapter 7) and wind farms (Chapter 8 and Chapter 9).

Note that each chapter is self-consistent and can be mostly read independently of the others. Most of the content in the thesis derives from published material and, thus, there may be repetitions of preliminary material and some differences in notation between chapters. Let us now introduce an extended summary of the thesis with references to the publications related to each chapter.

Chapter 2: Fault estimation and diagnosis

This chapter aims to give a common framework for the studied problems. First, we introduce the concept of fault and we carefully present the FD terminology used in this thesis. Second, we briefly explain the basics of model-based FD and we detail the advantages of estimation-based schemes over residual-based schemes from a FTC perspective. Finally, we introduce some performance parameters which can be utilized to describe the performance of FE and FI schemes and we motivate the application of these schemes to different engineering applications.

Chapter 3: Comparison of leakage estimation strategies in a real industrial pipe network

This chapter discusses the suitability of two different approaches to face the problems **P1** and **P4** (i.e., the design of fault estimators and evaluators taking into account the trade-off between practical performance parameters in the FD framework). First, we consider a multiplicative approach based on the recursive least square (RLS) identification algorithm. Second, we consider an additive approach based on single-input single-output (SISO) PI observers. In order to examine the advantages and disadvantages of both methods, we consider an accessible practi-

cal application: the problem of leakage estimation in real industrial networks of pipelines and tanks (**P12**).

As discussed in further details in Chapter 3, unlike the multiplicative approach, the additive approach does not impose any signal excitation requirement, the estimation performance is *a priori* parametrizable and does not depend on the inputs. Hence, in this chapter, we show how to algebraically design simple time-invariant SISO PI observers for *a priori* guaranteeing certain trade-off between practical FE performance parameters: the convergence rate under abrupt (step) faults and the variance due to noises (**P1**). Then, we design statistical-based FI decision mechanisms that compare the FE outputs to constant thresholds. In this case, we use the trade-off between the minimum isolable faults (MIFs) and the false isolation rates (FIRs) (**P4**). Provided the application of the proposed strategy to the problem of leakage estimation, we also introduce the concept of "leaked fluid mass until isolation" in the setting of the FI performance trade-off.

Some real data of an industrial pipe network is utilized in the simulations. The real signals are characterized by high noise levels. In order to give a first approximation to the problem **P11**, we give some notes on the influence of the non-Gaussianity of the real measurement noises on the FE and FI response.

The results of this chapter were mainly addressed in:

- **Ester Sales-Setién**, David Tena, and Ignacio Peñarrocha. Comparison of leakage estimation strategies in a real industrial pipe network. *IFAC-PapersOnLine*, 50(1):13550–13555, 2017. *19th World Congress of The International Federation of Automatic Control, IFAC World Congress 2017* (DOI:10.1016/j.ifacol.2017.08.2358).
- **Ester Sales-Setién**, David Tena, and Ignacio Peñarrocha. Estimación de fugas en un sistema industrial mediante modelado por señales aditivas. In *Actas de las XXXVIII Jornadas de Automática (JJAA2017)*, pages 160—166, 2017.

Chapter 4: Estimation of non-stationary process variance in multistage manufacturing processes

Motivated by the conclusions in Chapter 3 for FE and FI schemes based on SISO PI observers, Chapter 4 gives a further insight on the problems **P1** and **P4** and it presents performance-based designs of fault estimators and evaluators utilizing model-based multi-input multi-output (MIMO) PI observers.

In this chapter, we consider a complex practical application: the problem of estimating and isolating variance deviations in multistage manufacturing processes (MMPs). Variance estimation in MMPs is generally handled from a batch-based stationary perspective; hence, this chapter devotes a considerable effort to suitably modeling non-stationary process variances in MMPs from an observer-based perspective (**P11**-**P12**). A time-varying MIMO PI observer is then applied to the model in order to achieve FE.

The problem **P1** is addressed with an approach based on the Kalman filter theory [152]. By considering the fault variations (i.e., the variance deviations) as uncertainties and their covariance as a multivariate tuning parameter, we individually tune the estimation performance of each variance deviation in the MMP. In this case, the design sets the individual trade-off between the convergence rate under abrupt faults (utilizing parameters such as the cumulative squared error or the settling time) and the variance due to noises.

The problem **P4** is simply tackled by developing statistical confidence intervals for the estimations, which fix the trade-off between the MIFs and the FIRs. The main difficulty encountered in the FI step is related to the problem **P11**: the statistical properties of the disturbances are complex. Hence, we first compute a loose confidence interval using the Chevyshev's inequality. Then, we show that the estimation errors approach a Gaussian behavior and we compute a tighter confidence interval taking advantage of this property.

The results of this chapter were mainly addressed in:

- **Ester Sales-Setién**, Ignacio Peñarrocha-Alós, and José V Abellán-Nebot. Estimation of nonstationary process variance in multistage manufacturing processes using a model-based observer. *IEEE Transactions on Automation Science and Engineering*, 16(2):741–754, 2019 (DOI:10.1109/TASE.2018.2856465).

Chapter 5: Performance-based design of proportional integral observers for fault diagnosis

In Chapter 3 and Chapter 4, we gave some approximations to the problems **P1** and **P4** (utilizing the practical background related to the problems **P11** and **P12**). In these chapters we first designed the fault estimators taking into account the trade-off between the convergence rate under abrupt faults and the variance due to noises. Second, we designed the fault evaluators taking into account the trade-off between the MIFs and the FIRs. In this chapter, we give an initial approximation to the problem **P5**: we present two co-design strategies of fault estimators and evaluators taking into account the trade-off between the convergence rate under abrupt faults, the MIFs and the FIRs.

The fault evaluators consist on decision mechanisms that compare the fault estimates provided by a time-invariant MIMO PI observer with constant thresholds. Under the assumption of Gaussian noises, the requirements over the MIFs and the FIRs are translated into requirements over the constant value of the thresholds and the covariance of the steady-state estimates in fault-free scenarios.

In line with the methods introduced in Chapter 4, the first co-design approach is based on the Kalman filter theory. We consider the fault variations as uncertainties whose covariance can be treated as a multivariate tuning parameter. The Lyapunov equations that give the covariance of the estimates in steady state are utilized in an heuristic optimization problem that maximizes the fault sensitivity and assures the required performance specifications.

Alternatively, we formulate an optimization problem based on matrix inequalities. Inspired by the advantages introduced by the previous Kalman-based method, we formulate matrix inequalities that allow bounding the covariance matrix of the estimates due to noises. Then, we bound the cumulative squared error (CSE) under abrupt faults through the $\mathcal{H}_2$ norm of the error dynamics and we formulate it via matrix inequalities. These inequalities are utilized in an optimization problem that minimizes the CSE and assures the required performance specifications.

As discussed in further details in Chapter 5, the comparison of both methods draws some conclusions over their suitability w.r.t. the problem **P2**: the design problem using matrix inequalities allows setting the behavior of each FE channel w.r.t. faults in other channels. In contrast, the Kalman-based approach does not present this feature.

The results of this chapter were mainly addressed in:

- **Ester Sales-Setién**, Ignacio Peñarrocha, Daniel Dolz, and Roberto Sanchis. Performance- based design of PI observers for fault diagnosis in LTI systems under gaussian noises. In *Proceedings of the 3rd Conference on Control and Fault-Tolerant Systems (SysTol2016)*, pages 407—412, 2016 (DOI: 10.1109/SYSTOL.2016.7739784).
- **Ester Sales-Setién**, Ignacio Peñarrocha, Daniel Dolz, and Roberto Sanchis. Diseño basado en prestaciones de observadores PI para el diagnóstico de fallos en sistemas lineales con perturbaciones gaussianas. In *Actas de las XXXVII Jornadas de Automática (JJAA2016)*, 2016.

Chapter 6: Fault estimation via proportional multiple-integral and multiple-resonant observers

Chapter 3, Chapter 4 and Chapter 5 showed the assets of using fault estimators and evaluators based on augmented observers and of designing them with a formulation based on matrix inequalities. Therefore, in the remaining chapters of the thesis, we follow these approaches.

Chapter 6 is focused on the influence of the form of an augmented observer on the FE performance: it deals with the problems **P7** and **P8**. First, we generalize the formulation of the well-known proportional multiple-integral (PMI) augmented observer to enhance the estimation of high-frequency fault signals. We present a novel proportional multiple-integral and multiple-resonant (PMIR) observer for FE and we give its existence conditions (**P7**).

Second, we study the influence of the structural complexity of the augmented observer on the existing trade-off between the steady-state tracking performance w.r.t. complex fault forms and the transient tracking performance w.r.t. simpler fault forms. Motivated by the conclusions of this study, we propose a design strategy that deals with this trade-off from a probabilistic perspective: it takes account on the probability of appearance of each of the fault forms considered by the augmented observer (**P8**).

As the FE observer is applied to systems in environments with stochastic noises, the proposed design is a multiobjective optimization problem based on matrix inequalities which fixes the trade-off between the noise attenuation and the ability to track each fault term included in the observer according to their relative probability of appearance. Bearing in mind the problem **P1**, the noise attenuation is represented by the variance of the estimates in fault-free scenarios (formulated through the $\mathcal{H}_2$ norm of the error dynamics due to noises) and the fault tracking ability is represented by the CSEs w.r.t. each fault term (formulated through the $\mathcal{H}_2$ norm of the error dynamics due to the appearance of these fault terms).

The results of this chapter were mainly addressed in:

- **Ester Sales-Setién** and Ignacio Peñarrocha-Alós. Fault estimation via proportional multiple-integral and multiple-resonant observers for discrete-time systems. *IET Control Theory & Application*, 13(5):659–671, 2019 (DOI:10.1049/iet-cta.2018.5201).

Chapter 7: Multiobjective performance-based designs in fault estimation and isolation and its application to wind turbines

The preceding chapters included some contributions on the performance-based design of fault estimators and evaluators based on augmented observers and threshold-based decision mechanisms for systems affected by noises. Continuing with this issue, Chapter 7 considers both the presence of noises (either Gaussian or non-Gaussian) and of UIs. This chapter develops an all-encompassing approach for all the problems, **P1-P6**, devoted to the issue of performance based designs of estimation-based approaches in the FD framework.

First, we present performance-based optimization design strategies of time-invariant MIMO PI observers that individually set the performance of each FE channel (**P1-P2**). With a view to the problem **P6** (i.e., the inclusion of time isolation indices in the co-design of fault estimators and evaluators), the fault sensitivity of the observer is characterized by its delay to track incipient (ramp) faults. Hence, the proposed design sets the trade-off between the delays to track incipient faults, the FE covariance due to noises, the degree of interfault decoupling and the degree of UI decoupling. The requirements over these criteria are translated into requirements over different $\mathcal{H}_\infty$ norms and covariance bounds of the FE errors. These requirements are formulated via matrix inequalities that we include in an optimization problem. In this chapter, we desire to achieve UI decoupling; the proposed single-step design problem achieves numerical UI decoupling together with other performance requirements (**P3**).

Second, we deal with the problem **P4**. We design the statistical-based constant thresholds of FI decision mechanisms that process the fault estimates provided by the PI observer. In this case, we guarantee certain requirement over one of the following FI indices: the FIRS, the MIFs, the acknowledgement times (ATs) or the isolation times (ITs). For guaranteeing requirements over more than one isolation index, the co-design of the PI observer and the decision mechanisms becomes necessary; hence, we utilize the obtained results to address the problems **P5-P6**.

In this chapter, we apply the proposed FE and FI methods to the systems in a wind turbine (WT): the pitch system, the drive train system and the generator and converter system (**P12**). To do so, we utilize a well-known WT benchmark [216], developed for this purpose, that includes explicit requirements over the ITs and the FIRS. The WT systems are affected by numerous faults and they do not verify fault isolability conditions. Hence, we address this problem (i.e., **P9**) by extending the proposed FE and FI approach to a scheme based on a bank of the previous PI observers and statistical-based decision mechanisms. This bank allows achieving FE and FI at the cost of some fault simultaneity restrictions.

The results of this chapter were mainly addressed in:

- **Ester Sales-Setién** and Ignacio Peñarrocha-Alós. Multiobjective performance-based designs in fault estimation and isolation and its application to wind turbines. *International Journal of Systems Science*, 50(6):1252–1274, 2019 (DOI:10.1080/00207721.2019.1598511).
- **Ester Sales-Setién** and Ignacio Peñarrocha-Alós. Banks of estimators and decision mechanisms for pitch actuator and sensor FE in wind turbines. *IFAC-PapersOnLine*, 51(24):1141—1148, 2018. *10th Symposium on Fault Detection, Supervision and Safety for Technical Processes, SAFEPROCESS2018* (DOI:10.1016/j.ifacol.2018.09.715).
- **Ester Sales-Setién**, Ignacio Peñarrocha, Daniel Dolz, and Roberto Sanchis. Fault detection in the blade and pitch system of a wind turbine with H2 PI observers. *Journal of Physics: Conference Series*, 659(1):012–033, 2015. *12th European Workshop on Advanced Control and diagnosis, ACD2015* (DOI:10.1088/1742-6596/659/1/012033).
- **Ester Sales-Setién**, Ignacio Peñarrocha and Daniel Dolz. Detección de fallos en la orientación de palas en aerogeneradores mediante observadores H2 tipo PI. In *Actas de las XXXVI Jornadas de Automática (JJAA2015)*, 2015.

Chapter 8: Estimation and adaptive diagnosis of decreased power in wind farms: a Markovian jump system approach

Chapter 6 and Chapter 7 thoroughly delved into the problems **P1-P9**. The latter chapters of this thesis aim to extend the obtained results in order to approach the problems **P10-P12**.

In Chapter 8, we consider a challenging practical application: the diagnosis of decreased power generation in wind farms (WFs), and we utilize a well-known WF benchmark developed for this purpose [215] (**P12**). Provided that a WT operates in different power modes and in different wind speed zones, the power generation system of a WT is described by a nonlinear parameter varying model. Taking advantage of the fact that the model parameters can be justifiably considered as Markovian processes, we develop a Markovian jump system approach to estimate power decreases in WTs using a switched PI observer (**P11**).

The properties of the disturbances that affect the system (UIs, uncertainties and noises)

also differ among the operation modes (**P11**). These differences are taken into account in the design of the PI observer, which is performed using a multiobjective optimization problem based on matrix inequalities. The design problem optimally sets the trade-off between the robustness against disturbances and the sensitivity to faults, which are characterized through different $\mathcal{H}_\infty$ norms of the FE error.

As further detailed in Chapter 8, it is difficult to characterize the properties of the fault estimates provided by the observer in fault-free scenarios, taking into consideration also that these properties may differ along the operation modes (**P11**). Hence, a FI mechanism based on basic constant theoretical thresholds would be characterized by a poor isolation capability. In this chapter, we thus propose to evaluate the fault estimates in FI decision mechanisms with adaptive thresholds. The time-varying threshold function is computed with an algorithm designed following a data-driven approach.

The problem **P10** is then addressed by extending the proposed algorithms, obtained for each single WT, to the WF level. We group the WTs in the WF operating under similar conditions and we build a bank of the previous observers and decision mechanisms. The isolation performance is ameliorated at the cost of a restriction on the number of possible simultaneous faulty WTs.

The results of this chapter were mainly addressed in:

- **Ester Sales-Setién** and Ignacio Peñarrocha-Alós. A Markovian jump system approach for the estimation and adaptive diagnosis of decreased power generation in wind farms. *Submitted for journal publication (IET Control Theory & Application)*, October 2018.

Chapter 9: Robust estimation and diagnosis of wind turbine pitch misalignments at a wind farm level

Chapter 9 studies another application problem considered in the WF benchmark [215]: the diagnosis of WT pitch misalignments in WFs (**P12**). As Chapter 9 is the last research chapter of the thesis, it follows a detailed instructional procedure and it notably focuses on the issues derived from the practical application.

Contrary to the power generation system of a WT, the pitch system of a WT can be modeled using a linear model. However, the properties of the uncertainties that affect the pitch system still depend on the operation conditions of the WT. In order to address the problem **P11** and ensure adjusted fault estimates in all operation modes, we use a switched PI observer for FE. In Chapter 8, we considered that the mode switchings were governed by Markovian processes. In this chapter, the conservativeness related to the consideration of arbitrary mode switchings is reduced by alternatively considering that these switchings are infrequent.

In this fashion, we design the switched PI observer through an optimization problem ensuring global stability for all possible switchings and certain local steady-state performance in each operation mode. In this case, the local robustness against UIs is characterized through the corresponding $\mathcal{H}_\infty$ norm of the FE error in each mode. Similarly, the local robustness against

Table 1.1. Thesis outline. Problems addressed per chapter.

	Ch.3	Ch.4	Ch.5	Ch.6	Ch.7	Ch.8	Ch.9
P1	•	•			•		
P2			•		•		
P3					•		
P4	•	•			•		
P5			•		•		
P6					•		
P7				•			
P8				•			
P9					•		
P10						•	•
P11	•	•				•	•
P12	•	•			•	•	•

noises and the local sensitivity to faults are characterized through different $\mathcal{H}_2$ norms of the FE error in each mode. Taking advantage of the results obtained in the previous chapters w.r.t. **P1**, some notes on the physical interpretation of these norms are also given in the chapter.

In this chapter, we build FI decision mechanisms that compare the fault estimates provided by the observer to adaptive thresholds. In this case, we utilize a model-based statistical procedure to compute these thresholds that bound the FE error. Provided the consideration of infrequent mode switchings, we separately bound the FE error due to UIs in each mode by approximating its probability distribution function to a zero-mean uniform distribution. We also bound the Gaussian FE error due to noises making use of its time-varying covariance.

Similarly to Chapter 9, Chapter 8 also addresses the problem **P10** by building banks of the previous observers and decision mechanisms for groups of WTs in the WF operating under similar conditions. Again, the isolation performance is ameliorated at the cost of fault simultaneity restrictions.

The results of this chapter were mainly addressed in:

- **Ester Sales-Setién** and Ignacio Peñarrocha-Alós. Robust estimation and diagnosis of wind turbine pitch misalignments at a wind farm level. *Submitted for journal publication (Renewable Energy)*, June 2018.

Chapter 10: Summary and future research

This last chapter draws some conclusions on the current thesis, whose outline is summarized in Table 1.1. Chapter 10 also discusses exciting research problems for further development on a near future.

1.3.1 List of contributions

The results presented in this thesis mainly correspond to works developed with the author's supervisor where the author has played a key role. The results in Chapter 3 were developed in collaboration with David Tena, while the problematic presented in Chapter 4 was addressed in collaboration with Dr. José V. Abellán-Nebot. The results in Chapter 5 and some preliminary results in Chapter 7 were reviewed by Dr. Roberto Sanchis and Dr. Daniel Dolz[1]. As a summary, listed below are all the publications obtained by the author to date.

Journal papers

1. **Ester Sales-Setién**, Ignacio Peñarrocha-Alós, and José V Abellán-Nebot. Estimation of nonstationary process variance in multistage manufacturing processes using a model-based observer. *IEEE Transactions on Automation Science and Engineering*, 16(2):741–754, 2019 (DOI:10.1109/TASE.2018.2856465, IF:3.667).

2. **Ester Sales-Setién** and Ignacio Peñarrocha-Alós. Fault estimation via proportional multiple-integral and multiple-resonant observers for discrete-time systems. *IET Control Theory & Application*, 13(5):659–671, 2019 (DOI:10.1049/iet-cta.2018.5201, IF:3.296).

3. **Ester Sales-Setién** and Ignacio Peñarrocha-Alós. Multiobjective performance-based designs in fault estimation and isolation and its application to wind turbines. *International Journal of Systems Science*, 50(6):1252–1274, 2019 (DOI:10.1080/00207721.2019.1598511, IF:2.185).

4. **Ester Sales-Setién** and Ignacio Peñarrocha-Alós. A markovian jump system approach for the estimation and adaptive diagnosis of decreased power generation in wind farms. *Submitted for journal publication (IET Control Theory & Application, IF:3.296)*, October 2018.

5. **Ester Sales-Setién** and Ignacio Peñarrocha-Alós. Robust estimation and diagnosis of wind turbine pitch misalignments at a wind farm level. *Submitted for journal publication (Renewable Energy, IF:4.900)*, June 2018.

Book chapters

6. José V Abellán-Nebot, Ignacio Peñarrocha, **Ester Sales-Setién**, and Jian Liu. Optimal inspection/actuator placement for robust dimensional compensation in multistage manufacturing processes. In *Computational Methods and Production Engineering*, pages 31—50. Elsevier, 2017 (DOI:10.1016/B978-0-85709-481-0.00002-1).

[1]This thesis has been accepted by the co-authors of the publications listed above that have waved the right to present them as a part of another PhD thesis.

Conference papers

7. **Ester Sales-Setién** and Ignacio Peñarrocha-Alós. Banks of estimators and decision mechanisms for pitch actuator and sensor FE in wind turbines. *IFAC-PapersOnLine*, 51(24):1141—1148, 2018. *10th Symposium on Fault Detection, Supervision and Safety for Technical Processes, SAFEPROCESS2018* (DOI:10.1016/j.ifacol.2018.09.715).

8. Ignacio Peñarrocha-Alós, **Ester Sales-Setién** and David Tena. Actuator fault tolerant control proposal for PI controlled SISO systems *IFAC-PapersOnLine*, 51(24):680—687, 2018. *10th Symposium on Fault Detection, Supervision and Safety for Technical Processes, SAFEPROCESS2018* (DOI:10.1016/j.ifacol.2018.09.649).

9. **Ester Sales-Setién**, David Tena, and Ignacio Peñarrocha. Comparison of leakage estimation strategies in a real industrial pipe network. *IFAC-PapersOnLine*, 50(1):13550–13555, 2017. *19th World Congress of The International Federation of Automatic Control, IFAC World Congress 2017* (DOI:10.1016/j.ifacol.2017.08.2358).

10. **Ester Sales-Setién**, David Tena, and Ignacio Peñarrocha. Estimación de fugas en un sistema industrial mediante modelado por señales aditivas. In *Actas de las XXXVIII Jornadas de Automática (JJAA2017)*, pages 160—166, 2017.

11. Carlos Díaz-Sanahuja, Ignacio Peñarrocha, Ricardo Vidal Albalate and **Ester Sales-Setién**. Alternativas para el control de la red eléctrica aislada en parques eólicos marinos. In *Actas de las XXXVIII Jornadas de Automática (JJAA2017)*, pages 38—45, 2017.

12. **Ester Sales-Setién**, Ignacio Peñarrocha, Daniel Dolz, and Roberto Sanchis. Performance-based design of PI observers for fault diagnosis in LTI systems under gaussian noises. In *Proceedings of the 3rd Conference on Control and Fault-Tolerant Systems (SysTol2016)*, pages 407—412, 2016 (DOI: 10.1109/SYSTOL.2016.7739784).

13. **Ester Sales-Setién**, Ignacio Peñarrocha, Daniel Dolz, and Roberto Sanchis. Diseño basado en prestaciones de observadores PI para el diagnóstico de fallos en sistemas lineales con perturbaciones gaussianas. In *Actas de las XXXVII Jornadas de Automática (JJAA2016)*, 2016.

14. **Ester Sales-Setién**, Ignacio Peñarrocha, Daniel Dolz, and Roberto Sanchis. Fault detection in the blade and pitch system of a wind turbine with H2 PI observers. *Journal of Physics: Conference Series*, 659(1):012–033, 2015. *12th European Workshop on Advanced Control and diagnosis, ACD2015* (DOI:10.1088/1742-6596/659/1/012033).

15. **Ester Sales-Setién**, Ignacio Peñarrocha and Daniel Dolz. Detección de fallos en la orientación de palas en aerogeneradores mediante observadores H2 tipo PI. In *Actas de las XXXVI Jornadas de Automática (JJAA2015)*, 2015.

Conference papers on Educational Innovation

16. **Ester Sales-Setién** and Ignacio Peñarrocha-Alós. Moodle questionnaires as a self assessment tool for meeting the challenges of diversity in students' background knowledge. In *Proceedings of the 11th Annual International Conference of Education, Research and Innovation (ICERI2018)*, pages 2858—2864, 2018.

17. **Ester Sales-Setién** and Ignacio Peñarrocha-Alós. Desarrollo de cuestionarios para la revisión autónoma y personalizada de conocimientos previos. In *Actas del Congreso Virtual Avances en Tecnologías, Innovación y Desafíos de la Educación Superior (ATIDES2018)*, pages 61–70, 2018.

Chapter 2

Fault estimation and diagnosis

2.1 Concept of fault

2.1.1 Fault versus failure

In compliance with the definitions given in [125, 140, 141], let us first introduce the concepts of fault and failure.

Fault. A fault is an unexpected deviation of at least one feature of a system from the acceptable/standard condition which degrades the system performance.

Failure. A failure is a permanent interruption or a complete breakdown of a component or system which results in its complete inability to perform a specific function.

In order to give a further insight into these concepts, let us consider the system in Fig. 2.1, which is stabilized by a controller. Let us also assume that its performance is described in a two-dimensional space; then, Fig. 2.2 represents the different regions of performance that must be considered [29]:

- the region of required performance,
- the region of degraded performance,
- the region of unacceptable performance and
- the region of danger.

Despite the presence of disturbances, the nominal controller in the execution level makes the fault-free system remain in the region of required performance, where the system satisfies its function. Faults bring the system into the regions of degraded or unacceptable performance whilst failures bring the system into the region of danger.

In the region of degraded performance the system is allowed to remain but the system does not satisfy the required performance. The region of unacceptable performance must be avoided and the region of danger is prohibited due to safety reasons. To deal with these issues, a supervisory layer is introduced into the system. In this layer, we distinguish between the tasks of monitoring and supervision, which are defined as follows [140, 141] (Fig. 2.1).

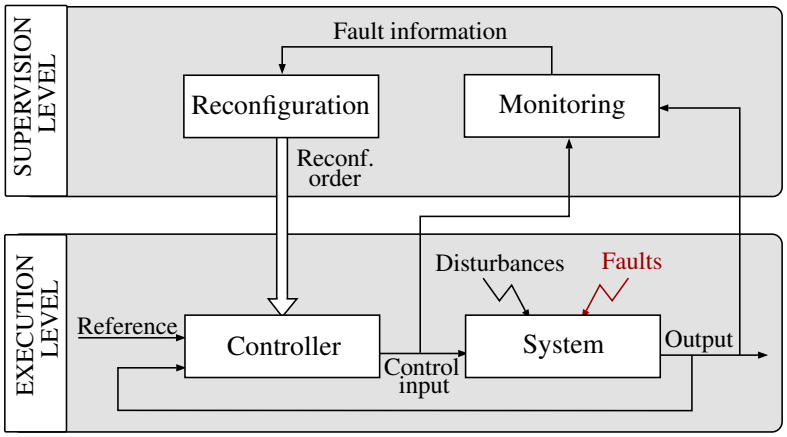

Figure 2.1. Execution and supervision level of a control system subjected to faults.

Monitoring. Determining the conditions of a system by recording information, recognising and indicating anomalies in the behavior.

Supervision. Monitoring a system and taking appropriate actions to maintain the operation in the region of required performance in the case of faults.

At the border of the region of required performance a supervision system is invoked, which diagnoses the faults and demands fault tolerant tasks. The nominal control activity is thus reconfigured to achieve fault-tolerance and upgrade the performance of the system. These fault tolerant tasks (detailed in Section 2.4) are desirable in the region of degraded performance and they become necessary in the region of unacceptable performance. For its part, a safety system interrupting the operation of the system is essential in the region of danger to which the system is brought in the case of failures.

The notions of reliability, maintainability, availability and safety describe the engineering integrity of a system. According to [141, 274], they can be defined as follows.

Reliability. The reliability of a system refers to its resistance to faults and failures. It is defined as the probability that a system performs a required function under normal conditions during a specific period of time.

Maintainability. The maintainability of a system refers to its ease of recovery from a fault or failure. It is defined as the probability of restoring a faulty system to its normal condition within a given timeframe, using the prescribed practices and procedures.

Availability. The availability of a system refers to its ability to be operational when needed. It is defined as the probability that a system performs a required function at any period time. Availability takes into account that faults and failures happen and need some time to repair. Thereby, availability depends on the reliability and maintainability of the system.

Safety. The safety of a system refers to its ability not to cause danger to persons, equipment or the environment.

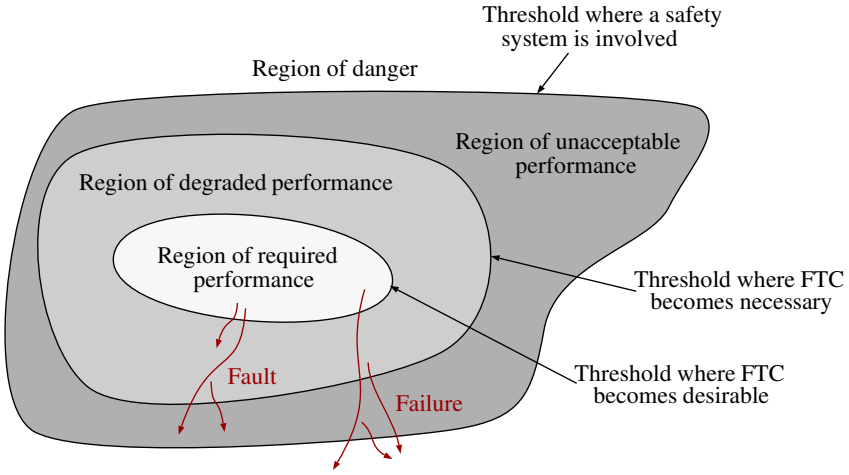

Figure 2.2. Regions of performance (*Source: Prepared by the author on the basis of a figure in [29]*).

To reach high availability, the system must have either reliable components or fast and reliable removal of faults. Fault tolerant tasks cannot change the reliability of the plant components but they improve the reliability and availability of the overall system since it remains operational after the fault appearance [29].

2.1.2 Fault modeling and classification

As motivated in Section 1.2, this thesis focuses on FE and FD in the discrete-time framework. The standard form of the state-space representation of a discrete-time linear time-invariant (LTI) nominal system is given by

$$x_{k+1} = A\,x_k + B\,u_k, \tag{2.1a}$$
$$y_k = C\,x_k + D\,u_k, \tag{2.1b}$$

where $x \in \mathbb{R}^{n_x}$ is the state vector, $u \in \mathbb{R}^{n_u}$ the input vector and $y \in \mathbb{R}^{n_y}$ the output vector. A widely adopted way to model the faults is the *additive* approach, which is followed in this thesis. In this approach, the additive fault vector $f \in \mathbb{R}^{n_f}$ is used to extend (2.1) as

$$x_{k+1} = A\,x_k + B\,u_k + E\,f_k, \tag{2.2a}$$
$$y_k = C\,x_k + D\,u_k + F\,f_k. \tag{2.2b}$$

The input-output transfer matrix representation of (2.2) is

$$y(z) = G_u(z)\,u(z) + G_f(z)\,f(z), \tag{2.3}$$

with

$$G_u(z) = C\,(z\,I - A)^{-1}\,B + D, \qquad G_f(z) = C\,(z\,I - A)^{-1}\,E + F.$$

The i-th fault in the fault vector f_k is denoted as $f_{i,k}$ (i.e., $f_{i,k} = \begin{bmatrix} 0_{1\times i-1} & 1 & 0_{1\times n_f - i} \end{bmatrix} f_k$). Hence, (2.3) can be expressed as

$$y(z) = G_u(z)\,u(z) + \sum_{i=1}^{n_f} G_{f_i}(z)\,f_i(z), \tag{2.4}$$

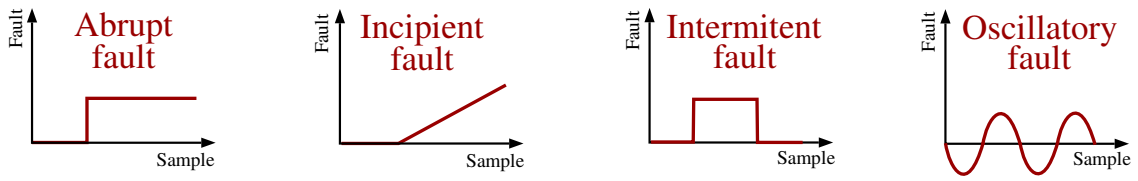

Figure 2.3. Fault classification according to their time characteristics.

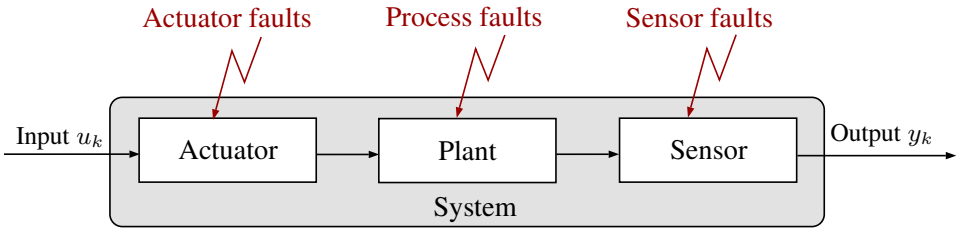

Figure 2.4. Fault classification according to their location.

with

$$G_{f_i}(z) = C\,(z\,I - A)^{-1}\,E_i + F_i,$$

where E_i and F_i denote the i-th column of the matrices E and F, respectively.

The faults can be classified depending upon their time characteristics. Fig. 2.3 shows examples of common fault time functions: abrupt (or step) faults, incipient (drift or ramp) faults, intermittent faults and oscillatory (or sinusoidal) faults. As outlined in Fig. 2.4, the faults can be also classified according to their location as [125, 193]:

Actuator fault. An actuator fault represents the partial or complete loss of a control action.

Sensor fault. A sensor fault represents the incorrect reading from a sensor.

Process fault. A process fault represents malfunctions within the process. It considers all faults that cannot be characterized into the category of actuator or sensor fault.

Actuator faults (f^a), sensor faults (f^s) and process faults (f^p) are additively modeled as

$$x_{k+1} = A\,x_k + B\,(u_k + f_k^a) + E_p\,f_k^p, \tag{2.5a}$$
$$y_k = C\,x_k + D\,(u_k + f_k^a) + f_k^s + F_p\,f_k^p. \tag{2.5b}$$

Defining

$$f_k = \begin{bmatrix} f_k^a \\ f_k^s \\ f_k^p \end{bmatrix}, \quad E = \begin{bmatrix} B & 0 & E_p \end{bmatrix}, \quad F = \begin{bmatrix} D & I & F_p \end{bmatrix},$$

the dynamics (2.5) can be represented using (2.2).

Another extended way to model the faults is the *multiplicative* approach. In practice, malfunctions in the sensors, the actuators and the process may cause changes in the model parameters [70]. These changes can be described by extending (2.1) as

$$x_{k+1} = (A + \Delta A_F)\, x_k + (B + \Delta B_F)\, u_k, \tag{2.6a}$$
$$y_k = (C + \Delta C_F)\, x_k + (D + \Delta D_F)\, u_k, \tag{2.6b}$$

where ΔA_F, ΔB_F, ΔC_F and ΔD_F represent process, actuator and sensor faults. Introducing

$$f_{M,k} = \begin{bmatrix} \Delta A_F\, x_k + \Delta B_F\, u_k \\ \Delta C_F\, x_k + \Delta D_F\, u_k \end{bmatrix}, \quad E_M = \begin{bmatrix} I_{n_x} & 0 \end{bmatrix}, \quad F_M = \begin{bmatrix} 0 & I_{n_y} \end{bmatrix},$$

we can rewrite (2.6) into

$$x_{k+1} = A\, x_k + B\, u_k + E_M\, f_{M,k}, \tag{2.7a}$$
$$y_k = C\, x_k + D\, u_k + F_M\, f_{M,k}. \tag{2.7b}$$

This formulation reveals that, contrary to exogenous additive faults, multiplicative faults depend on the state and the inputs of the system and may affect the system stability [70]. In this way, pure multiplicative faults can be treated following an additive approach as long as their appearance does not unstabilize the system.

2.1.3 Fault versus disturbance

Like faults, disturbances change the plant behavior. The distinction between them is given by the aim of fault tolerant control [29]. The presence of the faults in the system is not known but their effect on the system should be removed by remedial actions. Disturbances are nuisances which are known to be present in the system and whose effects can be handled by appropriately tuned controllers. Faults entail more severe changes and their effect cannot be suppressed by the controllers designed for fault-free scenarios.

Disturbances in the system are often modeled as additive vectors. We distinguish between

- deterministic disturbances or unknown inputs (UIs) and
- stochastic disturbances or noises.

Denoting the UIs as $d \in \mathbb{R}^{n_d}$ and the noises as $w \in \mathbb{R}^{n_w}$, we extend (2.2) as

$$x_{k+1} = A\, x_k + B\, u_k + E\, f_k + B_d\, d_k + B_w\, w_k, \tag{2.8a}$$
$$y_k = C\, x_k + D\, u_k + F\, f_k + D_d\, d_k + D_w\, w_k. \tag{2.8b}$$

The input-output transfer matrix representation of (2.8) is

$$y(z) = G_u(z)\, u(z) + G_f(z)\, f(z) + G_d(z)\, d(z) + G_w(z)\, w(z), \tag{2.9}$$

with

$$G_d(z) = C\,(z\, I - A)^{-1}\, B_d + D_d, \quad G_w(z) = C\,(z\, I - A)^{-1}\, B_w + D_w.$$

Defining $d'_k = \begin{bmatrix} d_k \\ w_k \end{bmatrix} \in \mathbb{R}^{n'_d}$, $B'_d = \begin{bmatrix} B_d & B_w \end{bmatrix}$ and $D'_d = \begin{bmatrix} D_d & D_w \end{bmatrix}$; it yields

$$x_{k+1} = A\,x_k + B\,u_k + E\,f_k + B'_d\,d'_k, \tag{2.10a}$$
$$y_k = C\,x_k + D\,u_k + F\,f_k + D'_d\,d'_k. \tag{2.10b}$$

The input-output transfer matrix representation of (2.10) is

$$y(z) = G_u(z)\,u(z) + G_f(z)\,f(z) + G'_d(z)\,d'(z), \tag{2.11}$$

with

$$G'_d(z) = C\,(z\,I - A)^{-1}\,B'_d + D'_d.$$

Remark 2.1. *Pure process noise (w^p) and pure sensor noise (w^s) can be modeled by means of zeroing the appropriate columns of B_w and H_w (i.e., $w = \begin{bmatrix} w^p \\ w^s \end{bmatrix}$ with $B_w = \begin{bmatrix} B_w^p & 0 \end{bmatrix}$ and $D_w = \begin{bmatrix} 0 & D_w^s \end{bmatrix}$).*

Model uncertainties also disturb the plant behavior. Among a number of expressions for model uncertainties in state-space representation, a standard one is [70]

$$x_{k+1} = (A + \Delta A)\,x_k + (B + \Delta B)\,u_k + E\,f_k, \tag{2.12a}$$
$$y_k = (C + \Delta C)\,x_k + (D + \Delta D)\,u_k + F\,f_k. \tag{2.12b}$$

where ΔA, ΔB, ΔC and ΔD are the model uncertainties. Alternatively, the UI vector (d) can be used to describe a number of different kinds of modeling uncertainties [45]. For instance, for stable systems, (2.12) can be translated into

$$x_{k+1} = A\,x_k + B\,u_k + E\,f_k + B_\Delta\,d_{\Delta,k}, \tag{2.13a}$$
$$y_k = C\,x_k + D\,u_k + F\,f_k + D_\Delta\,d_{\Delta,k}. \tag{2.13b}$$

with

$$d_{\Delta,k} = \begin{bmatrix} \Delta A\,x_k + \Delta B\,u_k \\ \Delta C\,x_k + \Delta D\,u_k \end{bmatrix}, \quad B_\Delta = \begin{bmatrix} I_{n_x} & 0 \end{bmatrix}, \quad D_\Delta = \begin{bmatrix} 0 & I_{n_y} \end{bmatrix}.$$

As detailed in Section (1.1.2), in this thesis, we consider stable (or stabilized) systems. Hence, we use the additive UI vector (d) to represent the modeling uncertainties.

2.2 Fault diagnosis

2.2.1 Fault diagnosis tasks

Fault diagnosis is the procedure to obtain fault information used for fault compensation or scheduled system maintenance. In general, fault diagnosis contains three steps as shown in Fig. 2.5: fault detection, fault isolation and fault identification [29, 112, 325].

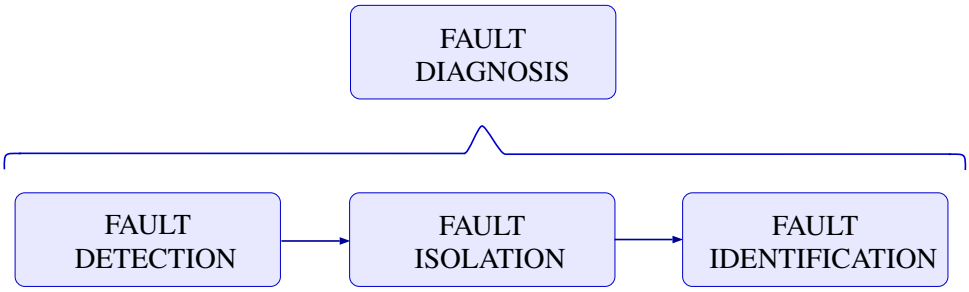

Figure 2.5. Fault diagnosis tasks.

Fault detection. Fault detection is to decide whether a fault has occurred in the system.

Fault isolation. Fault isolation is to find the location of the fault (i.e., the faulty component).

Fault identification or analysis. Fault identification is to identify the magnitude of the fault. This step determines the kind and severity of the fault.

Fault diagnosis (FD) covers fault detection, isolation and analysis (FDIA). In this thesis, as introduced in Section 1.1.2, fault identification or analysis (FA) is obtained by means of fault estimation (FE) strategies and the fault estimates are then used for fault detection and isolation (FDI) purposes, to which we simply refer as estimation-based fault isolation (FI).

2.2.2 System structural properties for fault diagnosis

Corresponding to the tasks in the FD framework, the concepts of fault detectability, isolability and identifiability are introduced to describe the structural properties of the system from the FD perspective. We also introduce the concept of disturbance decoupability. The definitions in this section are the discrete-time version of the ones in [70]. Similar applies to the necessary and sufficient conditions detailed hereafter, whose proof is omitted. The reader is referred to [70] for the detailed proofs in continuous time, provided that it is straightforward to obtain their discrete counterpart.

Recall the system (2.10) described as

$$\begin{aligned} x_{k+1} &= A\,x_k + B\,u_k + E\,f_k + B'_d\,d'_k, \\ y_k &= C\,x_k + D\,u_k + F\,f_k + D'_d\,d'_k. \end{aligned}$$

We define the vector ξ that contains a subset of the faults in vector f, i.e., $\xi_k = \begin{bmatrix} f_{1,k} & \dots & f_{l,k} \end{bmatrix}^T \in \mathbb{R}^l$ with $l \leq n_f$. Its transfer matrix verifies

$$G_\xi(z) = \begin{bmatrix} G_{f_1}(z) & \dots & G_{f_l}(z) \end{bmatrix},$$

and we denote the minimal state-space realization of $G_\xi(z)$ by

$$G_\xi(z) = C\,(z\,I - A)^{-1}\,E_\xi + F_\xi.$$

We also define $\bar{f}_{i,k} = \begin{bmatrix} f_{i,k} \\ d'_k \end{bmatrix} \in \mathbb{R}^{1+n'_d}$.

Fault detectability

Given the system (2.10), a fault f_i is detectable if

$$\left.\frac{\partial y}{\partial f_i}\right|_{f_i=0} df_i \not\equiv 0. \tag{2.14}$$

The definition (2.14) mathematically expresses that a fault f_i is detectable if any occurrence of the fault (from zero to any time function different from zero) leads to a change in the system output.

Theorem 2.1. *([70]) Given the system* (2.10)*, a fault is detectable if and only if* $G_{f_i}(z) \neq 0$.

Fault isolability

Given the system (2.10), the faults f_i $(i = 1, \ldots, l)$ in the fault vector ξ are isolable if

$$\left.\frac{\partial y}{\partial \xi}\right|_{\xi=0} d\xi \not\equiv 0. \tag{2.15}$$

The definition (2.15) mathematically expresses that a group of faults is isolable if any *simultaneous* occurrence of the faults leads to a change in the system output. Note that the definition (2.15) implies that fault detectability is necessary for fault isolability.

Remark 2.2. *The system*

$$x_{k+1} = A\,x_k + E_\xi\,\xi_k, \quad y_k = C\,x_k + F_\xi\,\xi_k, \quad x_0 = 0,$$

is called input observable when $y_k = 0$ *implies* $\xi_k = 0$*, [134]. Except for the assumption on the initial condition* $x_0 = 0$*, the physical meaning of input observability is equivalent to that of isolability of additive faults [70].*

Theorem 2.2. *([70]) Given the system* (2.10)*, the faults in the vector* ξ *are isolable if and only if*

$$\operatorname{rank}\{G_\xi(z)\} = \sum_{i=1}^{l} \operatorname{rank}\{G_{f_i}(z)\}. \tag{2.16}$$

where $\operatorname{rank}\{G(z)\}$ *denotes here the normal rank*[1] *of the transfer matrix* $G(z)$.

Considering that $\sum_{i=1}^{l} \operatorname{rank}\{G_{f_i}(z)\} = l$ and that $\operatorname{rank}\{G_\xi(z)\} \leq \min\{n_y, l\}$, the following corollary to Theorem 2.2 is introduced.

Corollary 2.1. *Given the system* (2.10)*, the faults in the vector* ξ *are isolable only if the number of sensors satisfies* $n_y \geq l$.

[1] The normal rank of a transfer matrix $G(z)$ is the rank of $G(z)$ at all the values of z except for the transmission zeros [151].

The condition in Theorem 2.2 can be alternatively expressed in terms of state-space matrices as detailed in the following corollary.

Corollary 2.2. *([70]) Given the system* (2.10)*, the faults in the vector ξ are isolable if and only if*

$$\operatorname{rank}\begin{bmatrix} A - z\,I & E_\xi \\ C & F_\xi \end{bmatrix} = n_x + l, \tag{2.17}$$

where $\operatorname{rank}\{G(z)\}$ *denotes here the normal rank of the transfer matrix* $G(z)$*.*

Fault identifiability

Given the system (2.10), the faults f_i $(i = 1, \ldots, l)$ in the fault vector ξ are identifiable if the transfer matrix $G_\xi(z)$ is invertible and its inverse is stable and causal. This definition requiring the stability and causality of $G_\xi^{-1}(z)$ expresses the realizability of inverting $G_\xi(z)$ [205].

Theorem 2.3. *([70]) Given the system* (2.10)*, the faults in the vector ξ are perfectly identifiable if and only if*

$$\operatorname{rank}\begin{bmatrix} A - z\,I & E_\xi \\ C & F_\xi \end{bmatrix} = n_x + l, \quad \forall z \in \bar{\mathbb{C}}_1, \tag{2.18}$$

with $\bar{\mathbb{C}}_1$ *being the closed plane outside the unit circle.*

The condition (2.18) implies the condition (2.17) and the condition that the transmission zeros from the faults in ξ to the measurements must be stable [106]. We deduce that fault isolability (and hence fault detectability) is necessary for perfect fault identifiability.

Disturbance decoupability

Given the system (2.10), the disturbance d' can be fully decoupled from the fault f_i if

$$\left.\frac{\partial y}{\partial \bar{f}_i}\right|_{\bar{f}_i = 0} d\bar{f}_i \not\equiv 0. \tag{2.19}$$

The definition (2.19) mathematically expresses that the disturbance d' can be fully decoupled from the fault f_i if any occurrence of the fault f_i leads to a change in the system output despite the presence of any disturbance d'.

Theorem 2.4. *([70, 97]) Given the system* (2.10)*, the disturbance d' can be fully decoupled from a fault f_i if and only if*

$$\operatorname{rank}\left\{\begin{bmatrix} G_{f_i}(z) & G'_d(z) \end{bmatrix}\right\} = \operatorname{rank}\left\{G_{f_i}(z)\right\} + \operatorname{rank}\left\{G'_d(z)\right\}, \tag{2.20}$$

where $\operatorname{rank}\{G(z)\}$ *denotes here the normal rank of the transfer matrix* $G(z)$*.*

The condition in Theorem 2.4 can be alternatively expressed in terms of state-space matrices as follows.

Corollary 2.3. *([70]) Given the system* (2.10)*, the disturbance d' can be fully decoupled from a fault f_i if and only if*

$$\operatorname{rank}\begin{bmatrix} A - z\,I & E_i & B'_d \\ C & F_i & D'_d \end{bmatrix} = 1 + \operatorname{rank}\begin{bmatrix} A - z\,I & B'_d \\ C & D'_d \end{bmatrix}, \tag{2.21}$$

where $\operatorname{rank}\{G(z)\}$ *denotes here the normal rank of the transfer matrix* $G(z)$*.*

Remark 2.3. *Combining Theorem 2.2 and Theorem 2.4, we deduce that the faults in the vector ξ are isolable among them and from the disturbance d' (i.e., the disturbance d' can be fully decoupled from them) if and only if*

$$\operatorname{rank}\left\{\begin{bmatrix} G_\xi(z) & G'_d(z) \end{bmatrix}\right\} = \sum_{i=1}^{l} \operatorname{rank}\left\{G_{f_i}(z)\right\} + \operatorname{rank}\left\{G'_d(z)\right\}. \tag{2.22}$$

The condition (2.22) *can be alternatively expressed in terms of state-space matrices as*

$$\operatorname{rank}\begin{bmatrix} A - z\,I & E_\xi & B'_d \\ C & F_\xi & D'_d \end{bmatrix} = l + \operatorname{rank}\begin{bmatrix} A - z\,I & B'_d \\ C & D'_d \end{bmatrix}. \tag{2.23}$$

2.2.3 Classification of fault diagnosis strategies

Fault diagnosis (FD) strategies are based on exploiting redundancies to generate residuals, which are signals representing inconsistencies between these redundancies. In principle, these inconsistencies derive from the presence of faults. However, the presence of disturbances (e.g., UIs, noises or model uncertainties) also cause inconsistencies that may deviate the residuals. Hence, the residual signals must be evaluated in decision mechanisms in order to discern the faults from the disturbances that affect the system. FD strategies consist thus of two steps:

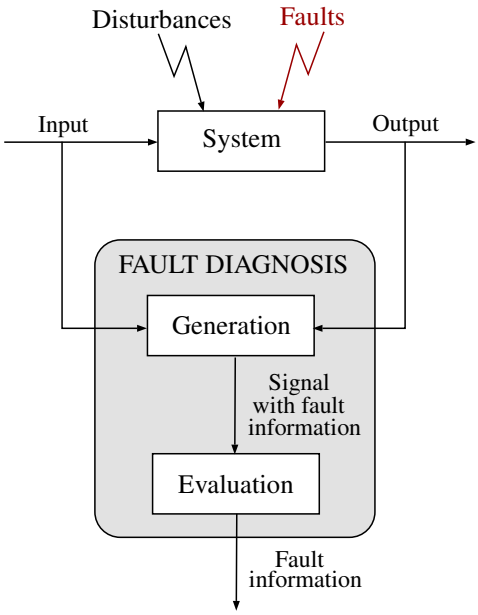

Figure 2.6. Fault diagnosis steps.

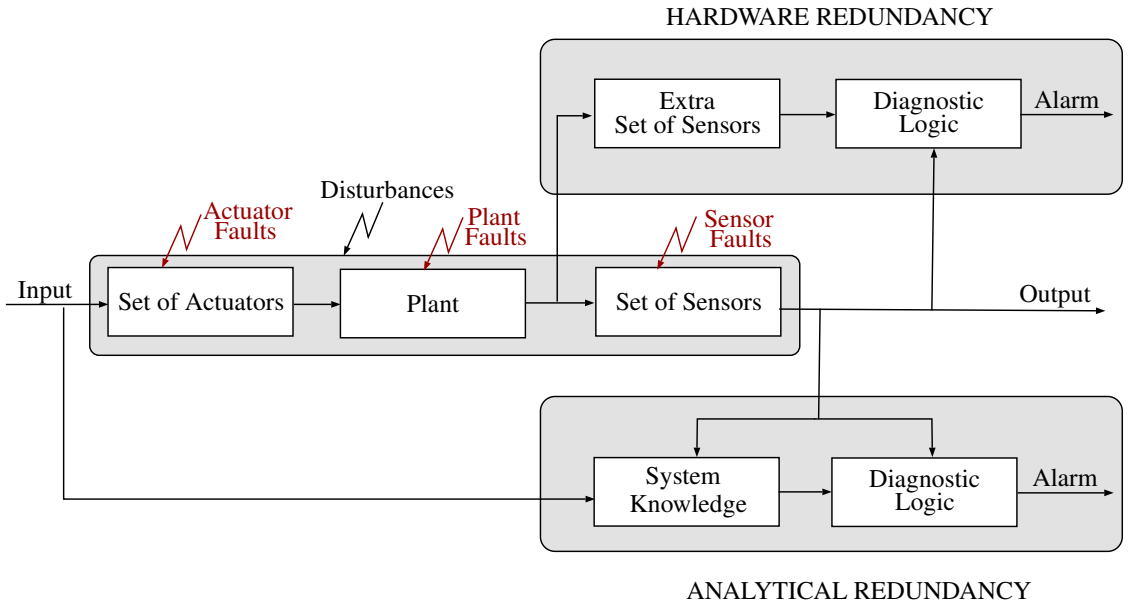

Figure 2.7. Hardware versus analytical redundancy.

1. generating (possibly disturbed) signals containing the faults information and
2. evaluating them in order to detect/isolate/identify the faults;

see Fig. 2.6. A traditional approach to achieve FD is the use of hardware redundancy (e.g., [147, 194]). Although FD techniques based on hardware redundancy are still standard in industrial applications, FD techniques based on analytical redundancy have gain more and more attention since their first appearance in the 1970s [19] and, thus, analytical redundancy has been developed rapidly [330]. According to [140, 325], hardware and analytical redundancy are characterized as follows (Fig. 2.7).

Hardware redundancy. The methods which are based on hardware redundancy utilize multiple lanes of sensors and actuators for duplicating the components of the systems and achieving physical redundancy. These methods are characterized by their high reliability; however, the extra equipment entails additional maintenance costs, weight and space requirements.

Analytical redundancy. The methods which are based on analytical redundancy exploit the redundancy derived from the explicit or implicit knowledge of the system. Analytical redundancy is also called software redundancy because it replaces physical redundancy by mathematical models or patterns which are implemented in computer software. Since no additional hardware is installed in the system, no additional hardware faults are introduced. Therefore, analytical redundancy is potentially more reliable than hardware redundancy [288]. However, it is more challenging due to its need to ensure robustness towards disturbances including model uncertainties, noises and other kinds of disturbances. A comprehensive review of analytical approaches can be found in [100, 101, 137, 289–291].

Traditionally, analytical methods can be categorized into signal-based, data-driven and physical model-based approaches [95, 101]. See the classification in Fig. 2.8 detailed hereafter.

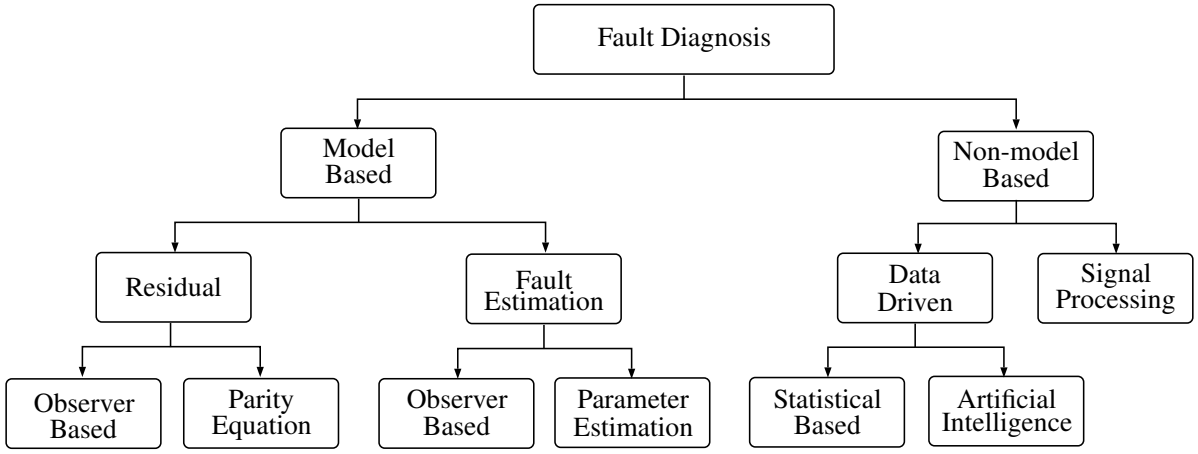

Figure 2.8. Classification of fault diagnosis strategies.

Model-based analytical redundancy. Model-based strategies utilize the mathematical model of the system to achieve analytical redundancy. The reference books in model-based diagnosis [44, 70, 266] detail the basic principles of generating and evaluating model-based signals for FD. Depending on the kind of generated signal, we distinguish between residual-based strategies and FE-based strategies. Depending on the methods which are utilized to generate such signals we distinguish between

- observer-based approaches [97, 326],
- parity equations [31, 75, 223] and
- parameter estimation approaches [94, 110, 145].

Remark 2.4. *Several authors have proved that parity equations lead to certain type of observer structures. Hence, it can be considered that parity-based methods are structurally equivalent to observer-based ones, although the design strategies are different [70].*

Signal processing-based analytical redundancy. Signal processing-based methods achieve analytical redundancy from the *a priori* knowledge of some measurable signal patterns in healthy conditions. They utilize

- time-domain [88, 132],
- frequency-domain [114, 148] or
- time-frequency signal processing techniques such as [39, 55].

Data-driven analytical redundancy. Data-based strategies use the historical data of the system to achieve analytical redundancy because, for complicated industrial processes, a large amount of historical data, rather than a model or a signal pattern, is available [101]. Generally, data-driven approaches are classified into

- statistical-based approaches [71, 203, 315] and
- intelligent FDI approaches including methods such as neural networks [165, 265, 272].

Signal processing-based methods do not require the explicit physical model of the system; however, they are mainly used for steady-state processes and their applicability to multivariable

dynamic systems is limited [70]. Like signal processing-based methods, data-driven methods do not require the explicit physical model of the system; hence, their applicability is extensible to systems with unknown structure. Moreover, the effectiveness of data-driven FD strategies for dynamic systems have been proved umpteen times (e.g., [18,245,314,317]). However, data-driven schemes require complex preprocessing steps involving high computational burden. Taking all these considerations into account, there is an upward trend in developing *hybrid FD* approaches integrating or combining more than one diagnosis strategy [284].

The emphasis on this thesis is on model-based strategies with observers. In the following, we briefly explain the basics of model-based residual methods and fault estimation.

2.3 Model-based fault diagnosis

2.3.1 Residual-based FD schemes

Let us first define residual generation and evaluation [44].

Residual generation. Residual generation consists on processing the input and the output of a monitored system in order to generate signals (residuals, denoted as r) representing the inconsistency between the system variables and the mathematical model of the system.

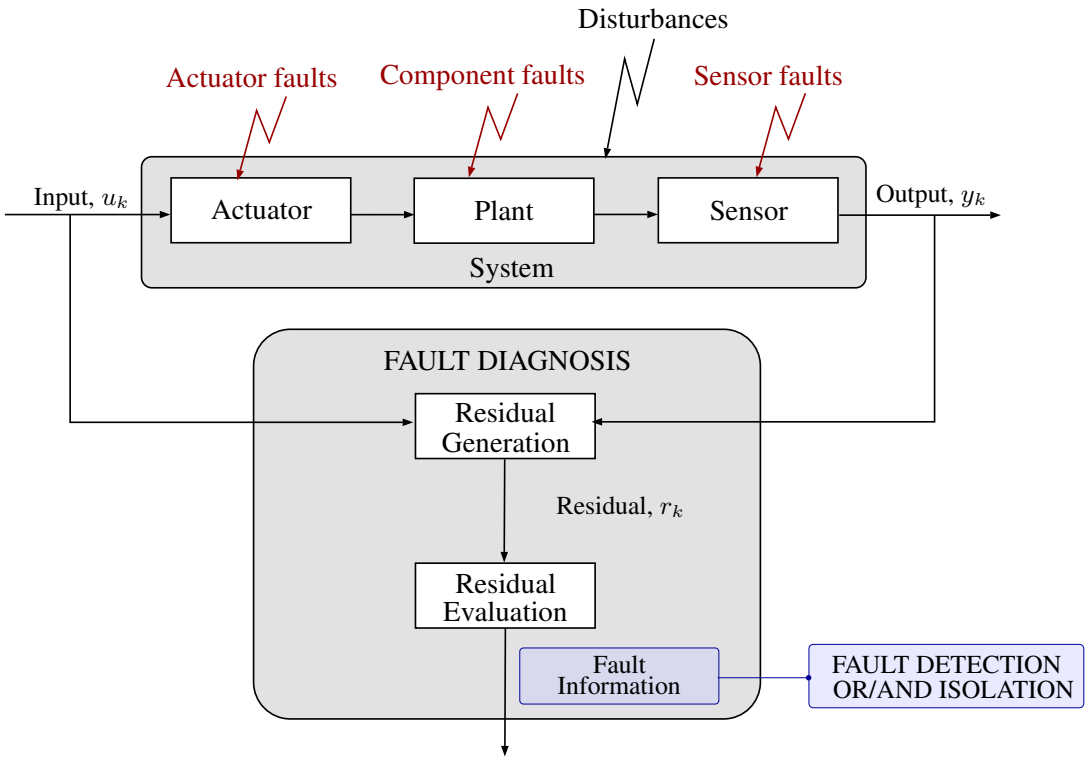

Figure 2.9. General residual-based FD scheme.

Residual evaluation. Residual evaluation consists on processing the residuals by comparing them to certain threshold function in order to get rid of the effect of the disturbances on the residuals and obtain certain fault information.

See the residual generation and evaluation scheme in Fig. 2.9. Depending on whether the generation and evaluation of the residuals is aimed to achieve fault detection or isolation, we distinguish between detection residuals and isolation residuals.

Residuals for fault detection

A residual for fault detection is a signal which must be generated to be sensitive to all the faults affecting the system:

$$r(z) = \sum_{i=1}^{n_f} G_{r,f_i}(z)\, f_i(z), \tag{2.24}$$

where $G_{r,f_i}(z) \neq 0$ $(i = 1, \ldots, n_f)$ is defined as the fault transfer function representing the relation between the detection residual $r(z)$ and the fault $f_i(z)$. Fig. 2.10 depicts this relation for a system with three faults ($n_f = 3$).

Any fault in the system can be then detected by evaluating the residual in a decision mechanism in the form of

$$\begin{cases} \text{if } T(r_k) \geq J_k\ , & f_k \neq 0 \text{ (A fault is present in the system)} \\ \text{otherwise}\ , & f_k = 0 \text{ (No fault is present in the system)} \end{cases}, \tag{2.25}$$

with T and J being the evaluation and threshold function for fault detection.

A general structure for a residual generator is [44]

$$r(z) = H_u(z)\, u(z) + H_y(z)\, y(z), \tag{2.26}$$

with $H_u(z)$ and $H_y(z)$ being realizable, stable transfer matrices. Considering the system (2.2) (i.e., no disturbances affect the system), the residual (2.26) verifies

$$r(z) = \big(H_u(z) + H_y(z)\, G_u(z)\big)\, u(z) + H_y(z)\, G_f(z)\, f(z),$$

which can be alternatively expressed as

$$r(z) = \big(H_u(z) + H_y(z)\, G_u(z)\big)\, u(z) + H_y(z) \sum_{i=1}^{n_f} G_{f_i}(z)\, f_i(z).$$

Hence, in order to generate a residual in the form of (2.24) through (2.26), the transfer matrices $H_u(z)$ and $H_y(z)$ must verify the constraint conditions:

$$H_u(z) + H_y(z)\, G_u(z) = 0, \tag{2.27a}$$

$$H_y(z)\, G_{f_i}(z) \neq 0, \quad i = 1, \ldots, n_f. \tag{2.27b}$$

The existence of a solution to (2.27b) is subjected to the detectability of each fault f_i $(i = 1, \ldots, n_f)$. If this condition is satisfied, the design of the residual (2.26) consists on choosing realizable, stable transfer matrices $H_u(z)$ and $H_y(z)$ satisfying (2.27). The different approaches to generate detection residuals correspond to different parametrizations of these transfer matrices.

Residuals for fault isolation

One of the main approaches to achieve fault isolation is to build a structured residual set [109]. Each residual in the set is aimed to be sensitive to a subset of faults while insensitive to the remaining faults. Performing a threshold test for each residual in the set leads to fault isolation. The main types of structured residual set are dedicated residual sets and generalized residual sets. A simple example of these schemes for a system with three faults is depicted in Fig. 2.11.

Dedicated residual set. A dedicated residual set consists of a set of residuals, each of them being sensitive to one fault and insensitive to the others:

$$r_i(z) = G_{r_i,f_i}(z)\, f_i(z), \quad i = 1, \ldots, n_f, \tag{2.28}$$

where $G_{r_i,f_i}(z) \neq 0$ $(i = 1, \ldots, n_f)$ is defined as the fault transfer function representing the relation between the residual $r_i(z)$ and the fault $f_i(z)$. Then, a simple logic can be used to make the decision about the appearance of a specific fault:

$$\begin{cases} \text{if } T_i\left(r_{i,k}\right) \geq J_{i,k}\ , & f_{i,k} \neq 0 \text{ (The } i\text{-th fault is present in the system)} \\ \text{otherwise}\ , & f_{i,k} = 0 \text{ (The } i\text{-th fault is not present in the system)} \end{cases}, \tag{2.29}$$

with T_i and J_i being the evaluation and threshold function for the i-th residual.

Generalized residual set. A generalized residual set consists of a set of residuals, each of them being sensitive to all but one fault:

$$r_i(z) = \begin{bmatrix} G_{r_i,f_1}(z) & \ldots & G_{r_i,f_{i-1}}(z) & G_{r_i,f_{i+1}}(z) & \ldots & G_{r_i,f_{n_f}}(z) \end{bmatrix} \begin{bmatrix} f_1(z) \\ \vdots \\ f_{i-1}(z) \\ f_{i+1}(z) \\ \vdots \\ f_{n_f}(z) \end{bmatrix}, \quad i = 1, \ldots, n_f. \tag{2.30}$$

where $G_{r_i,f_j}(z) \neq 0$ $(i = 1, \ldots, n_f$ and $j = 1, \ldots, i-1, i+1, \ldots, n_f)$ is defined as the fault transfer function representing the relation between the residual $r_i(z)$ and the fault $f_j(z)$. Then, a simple logic can be used to make the decision about the appearance of a specific fault:

$$\begin{cases} \text{if} \quad \begin{array}{l} T_i\left(r_{i,k}\right) < J_{i,k} \\ T_j\left(r_{j,k}\right) \geq J_{j,k},\ \forall j \neq i \end{array}\ , & f_{i,k} \neq 0 \text{ (The } i\text{-th fault is present in the system)} \\ \text{otherwise}\ , & f_{i,k} = 0 \text{ (The } i\text{-th fault is not present in the system)} \end{cases}. \tag{2.31}$$

From (2.28) and (2.30), we deduce that there is more design freedom in the construction generalized residual sets than in the construction of a dedicated residual set. Hence, generalized residual sets are more common in practice.

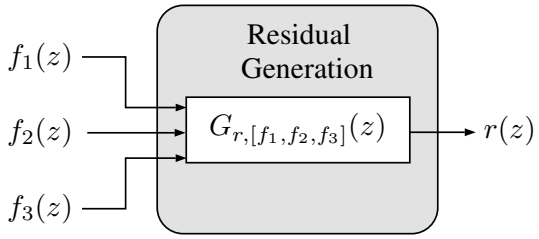

Figure 2.10. Residual for fault detection.

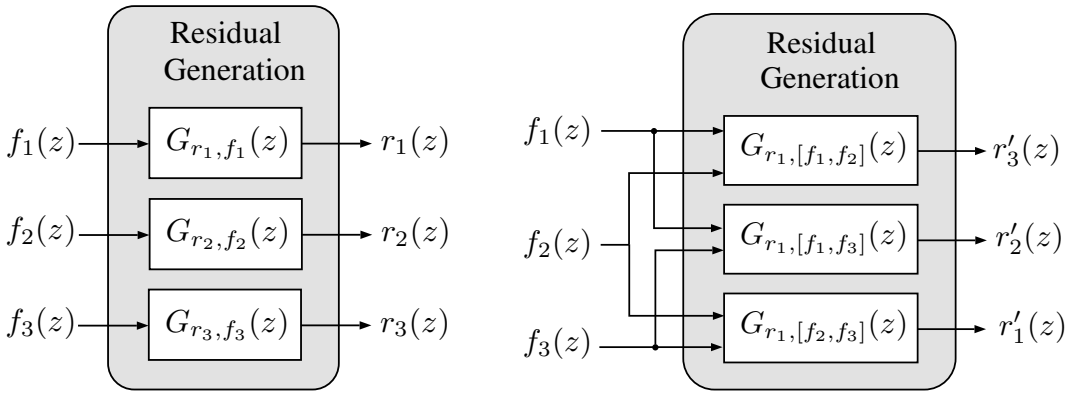

(a) Dedicated scheme **(b)** Generalized scheme

Figure 2.11. Residuals for fault isolation.

Consider the general case in which a residual r^1 must be sensitive to a group of faults $f^1 = \begin{bmatrix} f_1 & \dots & f_l \end{bmatrix}^T \in \mathbb{R}^l$ with $l \leq n_f$ and insensitive to the others ($f^2 = \begin{bmatrix} f_{l+1} & \dots & f_{n_f} \end{bmatrix}^T \in \mathbb{R}^{n_f - l}$) and another residual r^2 must be sensitive to f^2 and insensitive to f^1:

$$r^1(z) = \begin{bmatrix} G_{r^1,f_1}(z) \dots G_{r^1,f_l}(z) \end{bmatrix} \begin{bmatrix} f_1(z) \\ \vdots \\ f_l(z) \end{bmatrix}, \; r^2(z) = \begin{bmatrix} G_{r^2,f_{l+1}}(z) \dots G_{r^2,f_{n_f}}(z) \end{bmatrix} \begin{bmatrix} f_{l+1}(z) \\ \vdots \\ f_{n_f}(z) \end{bmatrix}, \quad (2.32)$$

with $G_{r^1,f_i}(z) \neq 0$ $(i = 1, \dots, l)$ and $G_{r^2,f_i}(z) \neq 0$ $(i = l+1, \dots, n_f)$. The system (2.2) can be expressed as

$$y(z) = G_u(z)\, u(z) + G_f^1(z)\, f^1(z) + G_f^2(z)\, f^2(z),$$

with $G_f^1(z) = \begin{bmatrix} G_{f_1}(z) & \dots & G_{f_l}(z) \end{bmatrix}$ and $G_f^2(z) = \begin{bmatrix} G_{f_{l+1}}(z) & \dots & G_{f_{n_f}}(z) \end{bmatrix}$. The residual generators in the general form of (2.26), i.e.,

$$r^1(z) = H_u^1(z)\, u(z) + H_y^1(z)\, y(z), \quad r^2(z) = H_u^2(z)\, u(z) + H_y^2(z)\, y(z), \quad (2.33)$$

verify

$$r^1(z) = \left(H_u^1(z) + H_y^1(z)\, G_u(z)\right) u(z) + H_y^1(z) \sum_{i=1}^{l} G_{f_i}(z)\, f_i(z) + H_y^1(z)\, G_f^2(z)\, f^2(z),$$

$$r^2(z) = \left(H_u^2(z) + H_y^2(z)\, G_u(z)\right) u(z) + H_y^2(z)\, G_f^1(z)\, f^1(z) + H_y^2(z) \sum_{i=l+1}^{n_f} G_{f_i}(z)\, f_i(z).$$

Hence, in order to generate the residuals (2.32) through the residual generators (2.33), the transfer matrices $H_u^1(z)$ and $H_y^1(z)$ must verify the constraint conditions:

$$H_u^1(z) + H_y^1(z)\, G_u(z) = 0, \tag{2.34a}$$
$$H_y^1(z)\, G_f^2(z) = 0, \tag{2.34b}$$
$$H_y^1(z)\, G_{f_i}(z) \neq 0, \quad i = 1, \ldots, l, \tag{2.34c}$$

and the transfer matrices $H_u^2(z)$ and $H_y^2(z)$ must verify the constraint conditions:

$$H_u^2(z) + H_y^2(z)\, G_u(z) = 0, \tag{2.35a}$$
$$H_y^2(z)\, G_f^1(z) = 0, \tag{2.35b}$$
$$H_y^2(z)\, G_{f_i}(z) \neq 0, \quad i = l+1, \ldots, n_f. \tag{2.35c}$$

The existence of a solution to (2.34c) and (2.35c) is subjected to the detectability of each fault f_i $(i = 1, \ldots, n_f)$. Provided these constraints, the existence of a solution to (2.34b) and (2.35b) is subjected to the isolability of the fault vector f^1 from the fault vector f^2. This condition reveals that fault isolation is more challenging than fault detection.

Observer-based residual generation approaches

Observer-based methods can be utilized for generating both residuals for fault detection and residuals for fault isolation. According to [44], a bank of observers which is devoted to the generation of a dedicated residual set is called a dedicated observer scheme and a bank which is devoted to the generation of a generalized residual set is called a generalized observer scheme.

The main idea of observer-based residual generation methods consists on estimating the output of the system by using an observer. Then, the (weighted) output estimation error is used as a residual. For instance, consider the following observer

$$\hat{x}_{k+1} = A\,\hat{x}_k + B\,u_k + L\,(y_k - C\,\hat{x}_k), \tag{2.36a}$$
$$\hat{y}_k = C\,\hat{x}_k + D\,u_k + K\,(y_k - C\,\hat{x}_k). \tag{2.36b}$$

where $\hat{x}$ is the estimated state, $\hat{y}$ is the estimated output and L and K are constant observer gain matrices of appropriate dimensions. The residuals can be generated as

$$r_k = Q\,(y_k - \hat{y}_k), \tag{2.37}$$

with Q being a weighting matrix.

Provided that only the output estimates are necessary, state estimation is avoidable. Hence, a functional observer as the one presented hereafter can be utilized:

$$z_{k+1} = F\,z_k + K\,y_k + J\,u_k, \tag{2.38a}$$
$$w_k = G\,z_k + R\,y_k + S\,u_k, \tag{2.38b}$$

with F, K, J, G, R and S being the observer gain matrices of appropriate dimensions. z is the state of the functional observer and w is aimed to be an estimate of certain linear combination

of the state $L\,x$ (i.e., $\lim_{k\to\infty}(w_k - L\,x_k) = 0$). In order to generate the residuals, one must design the functional observer to assign $L = C$. The output estimate can be thus obtained as

$$\hat{y}_k = w_k + D\,u_k. \tag{2.39}$$

Then, the residual is obtained with (2.37). See the references [44, 283] for more details on functional observers in the FD framework.

2.3.2 FE-based FD schemes

Let us first define fault estimation and evaluation.

Fault estimation. Fault estimation (FE) consists on processing the input and the output of a monitored system in order to generate a fault estimation vector (denoted as $\hat{f}$) satisfying

$$\lim_{k\to\infty}(\hat{f}_k - f_k) = 0. \tag{2.40}$$

Fault evaluation. Fault evaluation consists on processing each fault estimate $\hat{f}_i$ by comparing it to certain threshold function in order to determine whether this fault is present in the system (fault detection and isolation):

$$\begin{cases} \text{if } T_i\,(\hat{f}_{i,k}) \geq J_{i,k}\,, & f_{i,k} \neq 0 \text{ (The } i\text{-th fault is present in the system)} \\ \text{otherwise}\,, & f_{i,k} = 0 \text{ (The } i\text{-th fault is not present in the system)} \end{cases}. \tag{2.41}$$

with T_i and J_i being the evaluation and threshold function for the detection/isolation of the i-th fault.

Remark 2.5. *In many works, a non-zero fault estimate is supposed to immediately indicate the presence of a fault in the system. Hence, an evaluation stage based on decision mechanisms is omitted. However, as further detailed in Section 2.3.3, the effect of disturbances cannot always be completely removed from the fault estimates. For this reason, in this thesis, we propose to evaluate the fault estimates in FDI decision mechanisms. Provided that isolation is more involved than detection, we refer to these mechanisms as FI decision mechanisms.*

The fault estimation and evaluation scheme is depicted in Fig. 2.12. If we compare this FE-based scheme to the residual-based scheme in Fig. 2.9, the main difference is that FE provides fault identification capabilities while residual-based schemes are limited to fault detection/isolation tasks. As explained in the following section, FE is necessary for many fault tolerant control (FTC) approaches. Hence, this thesis focuses on FE strategies.

The core of the FE problem consists on generating signals with the desired fault information. In analogy to (2.26), we consider the following general structure for FE:

$$\hat{f}(z) = H_u(z)\,u(z) + H_y(z)\,y(z), \tag{2.42}$$

with $H_u(z)$ and $H_y(z)$ being realizable, stable transfer matrices. Considering the system (2.2) (i.e., no disturbances affect the system), the fault estimation vector (2.42) verifies

$$\hat{f}(z) = \left(H_u(z) + H_y(z)\, G_u(z)\right) u(z) + H_y(z)\, G_f(z)\, f(z).$$

Hence, in order to satisfy (2.40), the transfer matrices $H_u(z)$ and $H_y(z)$ must verify the constraint conditions:

$$H_u(z) + H_y(z)\, G_u(z) = 0, \tag{2.43a}$$

$$\lim_{z \to 1} \left(H_y(z)\, G_f(z)\right) = I_{n_f}. \tag{2.43b}$$

The existence of a solution to (2.43) is subjected to the identifiability of each fault f_i ($i = 1, \ldots, n_f$). Provided that fault isolability is necessary for fault identifiability, this fact reveals that FE is more challenging than residual generation.

Observer-based fault estimation approaches

Among FE techniques, there is an upward trend in the use of advanced observers [100]. We distinguish between

- augmented observers [41, 99, 180, 307],
- sliding mode observers [298, 316],
- adaptive observers [177, 241] and

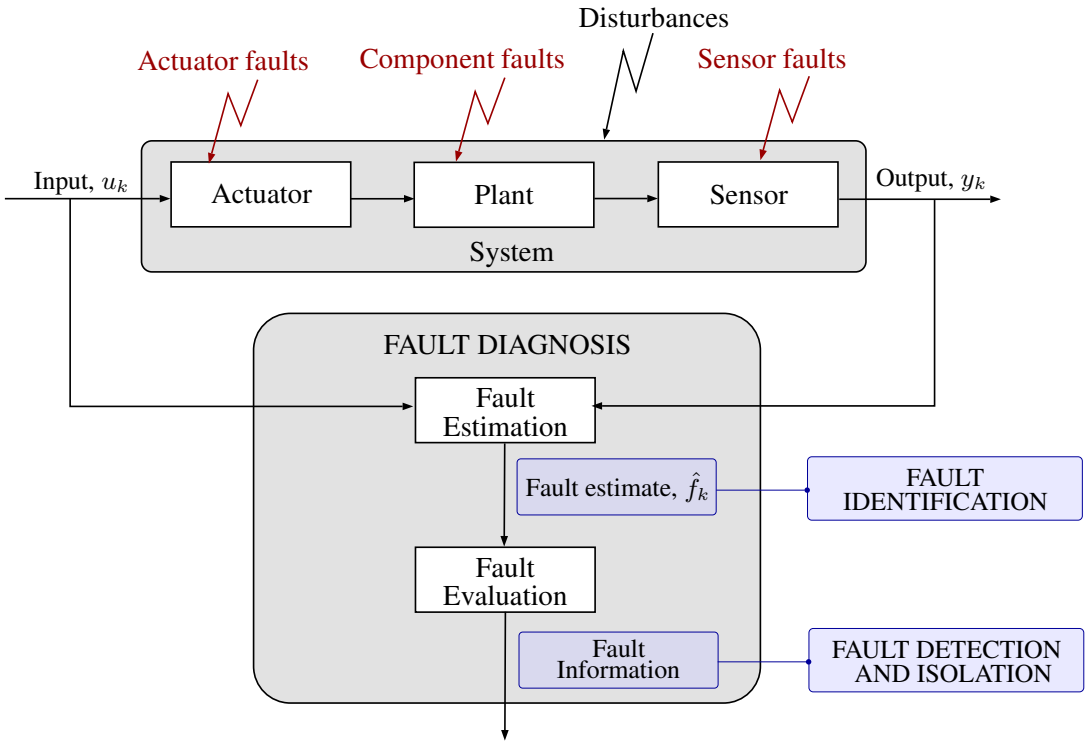

Figure 2.12. General FE-based FD scheme.

- iterative observer schemes [136].

In this thesis, augmented observers are utilized. An augmented observer is based on an augmented model including both the system model and the fault model [99]. Let us consider the following general fault model in the form of

$$\zeta_{k+1} = A_F\,\zeta_k + B_F\,\delta_k, \tag{2.44a}$$
$$f_k = C_F\,\zeta_k, \tag{2.44b}$$

where ζ is the fault state vector, δ is a fault generating vector and A_F, B_F and C_F are the state-space matrices defining the fault model. The model (2.2) is then augmented as

$$z_{k+1} = \mathcal{A}\,z_k + \mathcal{B}\,u_k + \mathcal{E}\,\delta_k, \tag{2.45a}$$
$$y_k = \mathcal{C}\,z_k + D\,u_k, \tag{2.45b}$$
$$f_k = \mathcal{R}\,z_k, \tag{2.45c}$$

where $z = \begin{bmatrix} x \\ \zeta \end{bmatrix}$ denotes the extended state vector. The state-space matrices in (2.45) verify

$$\mathcal{A} = \begin{bmatrix} A & E\,C_F \\ 0 & A_F \end{bmatrix},\ \mathcal{B} = \begin{bmatrix} B \\ 0 \end{bmatrix},\ \mathcal{E} = \begin{bmatrix} 0 \\ B_F \end{bmatrix},\ \mathcal{C} = \begin{bmatrix} C & F\,C_F \end{bmatrix},\ \mathcal{R} = \begin{bmatrix} 0 & C_F \end{bmatrix}.$$

The following model-based augmented observer can be then used to estimate the faults in (2.45)

$$\hat{z}_{k+1} = \mathcal{A}\,\hat{z}_k + \mathcal{B}\,u_k + L\,(y_k - \mathcal{C}\,\hat{z}_k), \tag{2.46a}$$
$$\hat{f}_k = \mathcal{R}\,\hat{z}_k + D\,u_k + K\,(y_k - \mathcal{C}\,\hat{z}_k), \tag{2.46b}$$

where the design observer gain matrices L and K are of appropriate dimensions. Defining the fault estimation error as $\widetilde{f}_k = f_k - \hat{f}_k$ and the extended state estimation error $\widetilde{z}_k = z_k - \hat{z}_k$, it follows that

$$\widetilde{z}_{k+1} = (\mathcal{A} - L\,\mathcal{C})\,\widetilde{z}_k + \mathcal{E}\,\delta_k, \tag{2.47a}$$
$$\widetilde{f}_k = (\mathcal{R} - K\,\mathcal{C})\,\widetilde{z}_k, \tag{2.47b}$$

The input-output transfer matrix representation of (2.47) is $\widetilde{f}(z) = \mathcal{G}_\delta(z)\,\delta(z)$, with $\mathcal{G}_\delta(z) = (\mathcal{R} - K\,\mathcal{C})\big(z\,I - (\mathcal{A} - L\,\mathcal{C})\big)^{-1}\,\mathcal{E}$.

The matrices A_F, B_F and C_F are chosen to guarantee zero steady-state fault estimation errors for the faults which are presumed to affect the system. As the gain matrices L and K must be designed to stabilize the fault estimator (2.46), the output given by $\mathcal{G}_\delta(z)$ under an impulse signal in $\delta(z)$ decays to zero. Therefore, if the realization $(A_F,\,B_F,\,C_F)$ is able to generate the fault signal f from an impulse signal δ, the fault estimation will achieve zero steady-state error. Illustratively, consider the following two examples.

- If it is assumed that the first discrete-time derivative of the faults affecting the system is bounded, A_F, B_F and C_F are fixed to

$$A_F = I_{n_f} \in \mathbb{R}^{n_f \times n_f}, \quad B_F = I_{n_f} \in \mathbb{R}^{n_f \times n_f}, \quad C_F = I_{n_f} \in \mathbb{R}^{n_f \times n_f}. \tag{2.48}$$

  The augmented observer (2.46) with (2.48) is called a discrete-time proportional integral (PI) observer and it is widely utilized in the literature [41,99,323] (see also the works [163, 305,339] on continuous-time PI observers).

- If it is assumed that the n_I-th discrete-time derivative of the faults affecting the system is bounded, A_F, B_F and C_F are fixed to

$$A_F = \begin{bmatrix} I_{n_f} & 0 & 0 & 0 \\ I_{n_f} & I_{n_f} & 0 & 0 \\ 0 & \ddots & \ddots & 0 \\ 0 & 0 & I_{n_f} & I_{n_f} \end{bmatrix} \in \mathbb{R}^{(n_f \cdot n_I) \times (n_f \cdot n_I)}, \tag{2.49a}$$

$$B_F = I_{n_f \cdot n_I} \in \mathbb{R}^{(n_f \cdot n_I) \times (n_f \cdot n_I)}, \quad C_F = \begin{bmatrix} 0 & I_{n_f} \end{bmatrix} \in \mathbb{R}^{n_f \times (n_f \cdot n_I)}. \tag{2.49b}$$

  The augmented observer (2.46) with (2.49) is called a discrete-time proportional multiple-integral (PMI) observer and it is also common in the literature [307] (see also [102, 103, 156, 306, 322] on continuous-time PMI observers).

2.3.3 Robust generation

In Section 2.3.1 and Section 2.3.2, we considered the system (2.2), which is not affected by disturbances. Considering now the system (2.10), the residual (2.26)[2] verifies

$$r(z) = \left(H_u(z) + H_y(z)\, G_u(z)\right) u(z) + H_y(z)\, G_f(z)\, f(z) + H_y(z)\, G'_d(z)\, d'(z). \tag{2.50}$$

The equation (2.50) shows that both the faults and the disturbances affect the residual and, hence, the discrimination between these two effects is difficult. This is the objective of robust FD. Depending on whether the effect of the disturbances is totally or partially decoupled from the residual we distinguish between full and approximate disturbance decoupling.

Full disturbance decoupling

Full (or perfect) disturbance decoupling is defined as the residual design strategy in which the disturbance effect is totally decoupled from the residual:

$$H_y(z)\, G'_d(z) = 0. \tag{2.51}$$

The existence of a solution to (2.51) together with (2.27)[3] requires that the disturbances are decoupable from the faults to which the residual must be sensitive (i.e., their effect on the

[2] The isolation residuals (2.33) and the fault estimator (2.42) are in the same form as (2.26). Hence, in this section, we mainly refer to the results regarding robust residual generation for fault detection.

[3] (2.34c) or (2.35c) in the case of fault isolation and (2.43) in the case of fault estimation.

measurements must be totally decoupled). If this condition is satisfied, perfect disturbance decoupling can be achieved by using different design techniques as eigenstructure assignment approaches [149, 224, 225] or unknown input observers (UIOs) [45, 120, 127, 163, 340]. Provided the importance of the latter approach, we now give some notes on UIOs.

Unknown input observers Consider the system (2.10) with $D'_d = 0$, the full-order observer

$$z_{k+1} = F\, z_k + T\, B\, u_k + K\, y_k, \tag{2.52a}$$
$$\hat{y}_k = C\, z_k + C\, H\, y_k, \tag{2.52b}$$

satisfying the conditions

$$B'_d = H\, C\, B'_d, \tag{2.53a}$$
$$T = I - H\, C, \tag{2.53b}$$
$$F = T\, A - K_1\, C, \tag{2.53c}$$
$$K_2 = F\, H, \tag{2.53d}$$
$$K = K_1 + K_2. \tag{2.53e}$$

is an UIO for residual generation [44]. The residual is then obtained with (2.37).

Theorem 2.5. *([44]) Necessary and sufficient conditions to achieve an UIO from* (2.52) *for the system* (2.10) *with* $D'_d = 0$ *are*

(i) $\operatorname{rank}\{C\, B'_d\} = \operatorname{rank}\{B'_d\}$,

(ii) $\operatorname{rank}\begin{bmatrix} z\, I - A & B'_d \\ C & 0 \end{bmatrix} = n_x + n'_d, \quad \forall z \in \bar{\mathbb{C}}_1.$

The condition (i) is a necessary and sufficient condition for the existence of a solution to (2.53a)[4]. The condition (ii) is equivalent to the condition that the transmission zeros from the disturbances to the measurements must be stable. As detailed in [70], these two conditions are not equivalent to the conditions for perfect disturbance decouplability. While perfect disturbance decoupling just requires the reconstruction of measurable variables for the purpose of generating analytical redundancy, UIOs are used to reconstruct the state variables.

Approximate disturbance decoupling

Approximate (or optimal) disturbance decoupling is defined as the residual design strategy in which the disturbance effect on the residual is attenuated:

$$\|H_y(z)\, G'_d(z)\| = \gamma, \tag{2.54}$$

with γ being certain disturbance attenuation level for some system norm.

[4] A special solution to (2.53a) is $H = B'_d\big((C\, B'_d)^T\, C\, B'_d\big)^{-1}\,(C\, B'_d)^T$.

The decoupability of the disturbances from the faults to which a residual must be sensitive is a strong condition and it makes difficult (if not impossible) to achieve perfect disturbance decoupling in a practical application. In such cases, perfect decoupling is generally sought for a decoupable subset of disturbances (generally unknown inputs) and approximate decoupling is fixed for the others (generally noises).

Approximate disturbance decoupling can be achieved in different manners [70]:

- Approximating $G'_d(z)$ by another transfer matrix $\bar{G}'_d(z)$ satisfying the conditions for perfect disturbance decoupling and designing the residuals so that the effect of $\bar{G}'_d(z)$ is cancelled.
- Designing the residuals so that the effect of $G'_d(z)$ is attenuated.

In this thesis, the latter approach is utilized.

2.3.4 Evaluation strategies

It is clear from Section 2.3.3 that the residuals may be corrupted by disturbances and other uncertainties. To achieve fault diagnosis successfully, a widely accepted procedure is to perform a residual evaluation step as illustrated in Fig. 2.6. A general form of an evaluator is the one presented in (2.25)[5]:

$$\begin{cases} \text{if } T(r_k) \geq J_k \,, & f_k \neq 0 \text{ (A fault is present in the system)} \\ \text{otherwise} \,, & f_k = 0 \text{ (No fault is present in the system)} \end{cases},$$

where T and J denoted the evaluation and threshold function.

Remark 2.6. *The robustness achieved in the signal generation step (i.e., residual generation or fault estimation) is often called active robustness. The robustness achieved in the evaluation step is often called passive robustness [44].*

Different evaluation functions of the residual $r_k \in \mathbb{R}^{n_r}$ are available in the literature. Some standard ones are [70, 74]

- the peak value $T(r_k) = \sqrt{\sum_{i=1}^{n_r} r_{i,k}^2}$,
- the trend peak value $T(r_k) = \sqrt{\sum_{i=1}^{n_r} (r_{i,k} - r_{i,k-1})^2}$ and
- the RMS value $T(r_k) = \sqrt{\frac{1}{T} \sum_{\kappa=k}^{k+N} \sum_{i=1}^{n_r} r_{i,\kappa}^2}$ (N being the size of certain time-window).

In this thesis, peak values are utilized for evaluation purposes [30, 201, 217][6].

The determination of the threshold function is influenced by different factors such as the dynamics of the residual generator and the properties of the disturbances affecting the system. Generally, thresholds functions can be classified into

- constant thresholds computed offline [229, 267] and
- adaptive thresholds computed online [201, 234, 328].

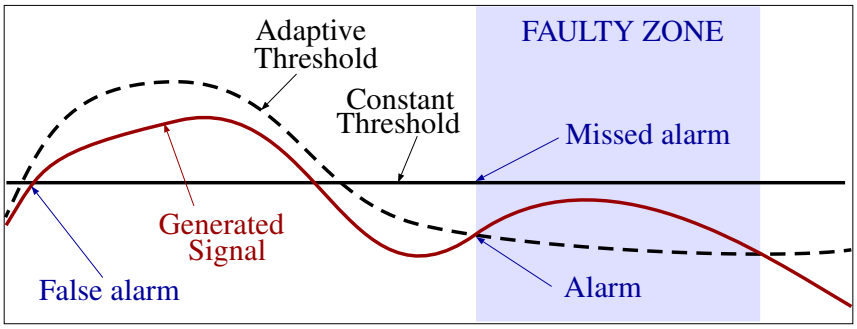

Figure 2.13. Constant versus adaptive thresholds (*Source:Prepared by the author on the basis of a figure in [44]*).

Constant thresholds are less computationally costly than adaptive thresholds. In the case of large manoeuvres, however, fixed thresholds may lead to poor fault diagnosability. The solution to this problem is the use of adaptive thresholds that vary according to the control activity and the UI/noise and the fault signal properties [44]. This concept is illustrated in Fig. 2.13.

There exist two major model-based (online or offline) threshold computation approaches depending on the information which is available for the disturbances affecting the system: statistical methods and deterministic methods.

Statistical methods. Statistical methods are well-established in the statistical framework and they are based on hypothesis testing. The thresholds represent the limits of the confidence intervals for fault diagnosis which are set according to the statistical properties of the residuals in fault-free scenarios. These properties can be derived from the knowledge of the statistical properties of the disturbances affecting the system.

Deterministic methods. Deterministic methods are well-established in robust control theory. The thresholds represent the bounds of the effect of the disturbances on the residuals. They can be derived from the knowledge of the bounds of the disturbances affecting the system.

Note that the main difference between both approaches is that statistical-based thresholding leads to probabilistic diagnosis decisions (the confidence level of the diagnosis decision is lower than 100%) while norm-based thresholding leads to certain diagnosis decisions (the confidence level of the diagnosis decision is equal to 100%).

Remark 2.7. *It is well-known that the theoretical model-based setting of thresholds using deterministic methods may lead to (too) conservative thresholds which result in poor fault diagnosability. Hence, it is the state of the art in real applications to avoid model-based deterministic methods and to set instead data-driven thresholds on the basis of tests in the real application environment [71].*

[5]The decision mechanisms (2.29), (2.31) and (2.41) are in the same form as (2.25). Hence, in this section, we mainly refer to residual evaluation for fault detection.

[6]For scalar residuals or fault estimates ($r_{i,k}$ or $\hat{f}_{i,k}$) the peak value is equivalent to the absolute value (i.e., $T_i(r_{i,k}) = |r_{i,k}|$ and $T_i(\hat{f}_{i,k}) = |\hat{f}_{i,k}|$).

2.4 Fault diagnosis and fault tolerant control

2.4.1 Classification of fault tolerant control strategies

Fault tolerant control (FTC) is a control strategy to ensure that a closed-loop system can continue its operation with the required (satisfactory) performance in the presence of faults (see Section 2.1.1). A comprehensive review on FTC methods can be found in [21, 318, 330]. Generally, FTC methods are classified into passive (PFTC) or active (AFTC) depending on whether they use fixed or reconfigurable control strategies [89].

Passive fault tolerant control. PFTC uses robust controllers against certain classes of presumed faults (Fig. 2.14).

Active fault tolerant control. AFTC uses the fault information provided by a FD scheme to actively reconfigure the control actions so that the acceptable performance of the system can be maintained in the presence of faults(Fig. 2.15).

It is clear that there are two main differences between PFTC and AFTC:

- PFTC does not require FD and AFTC does require it;
- PFTC uses fixed control structures and AFTC reconfigures the controller by changing its parameters or structure.

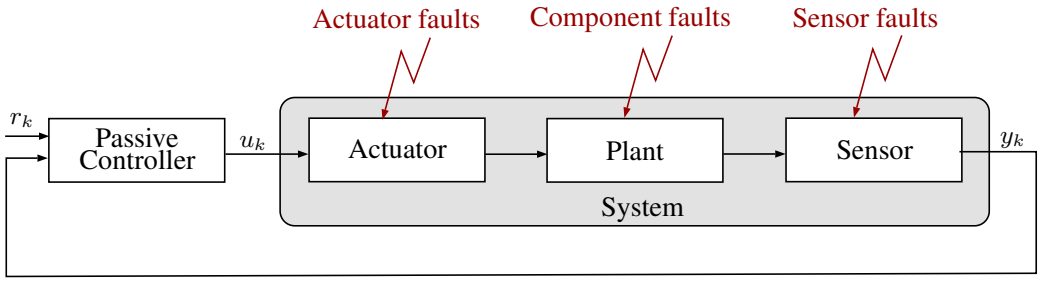

Figure 2.14. General passive FTC scheme.

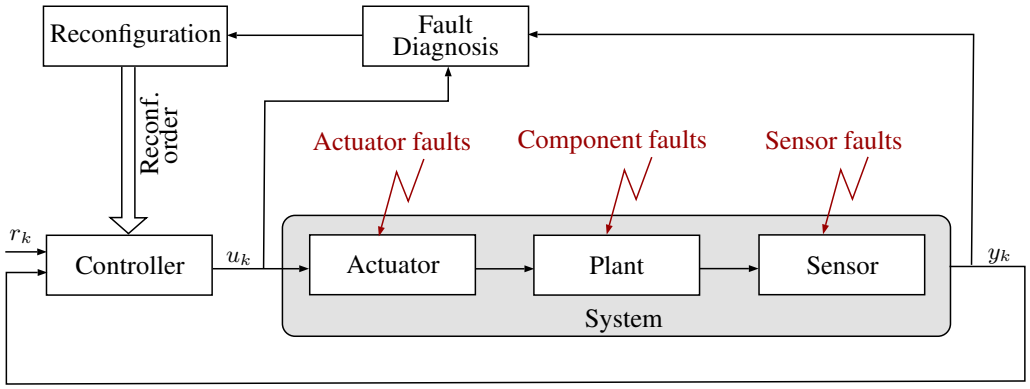

Figure 2.15. General active FTC scheme.

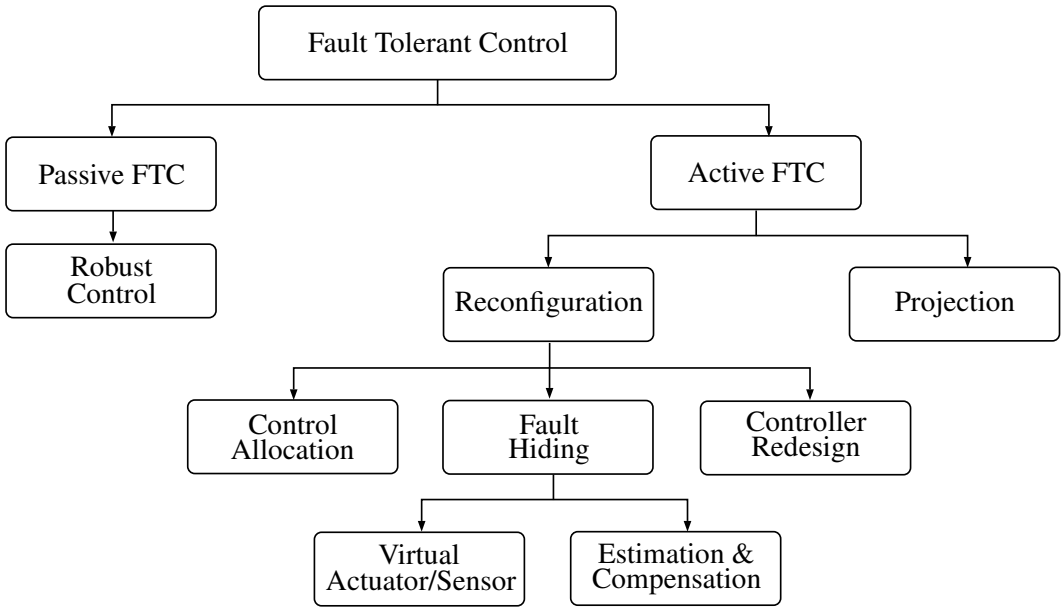

Figure 2.16. Classification of fault tolerant control strategies (*Source: [170]*).

Provided these differences, PFTC is computationally more attractive; however, it requires certain *a priori* knowledge of the faults and it is less versatile than AFTC. Hence, compared with PFTC, AFTC is of broader applicability and it has been the major concern of the FTC community.

As detailed in Fig. 2.16, AFTC can be further classified into projection methods and reconfiguration methods including control allocation, fault hiding and controller redesign strategies.

Projection methods. Projection methods compensate the fault diagnosed at the FD unit by switching the nominal controller to another controller from a set of precomputed (projected) controllers; hence, this method is also called multiple model in the literature [34, 329]. The set of predefined controllers are precomputed for a set of *a priori* presumed faulty situations.

Reconfiguration methods. Reconfiguration methods include three main approaches: control allocation, controller redesign and fault hiding.

- **Control allocation.** Control allocation strategies eliminate the actuator faults diagnosed at the FD unit by reallocating the corresponding control actions to redundant healthy actuators [8, 37, 61].
- **Controller redesign.** Control redesign involves the computation of new parameters of the controller taking into account the fault information from the FD unit. It includes strategies such as model predictive FTC [279, 313].
- **Fault hiding.** Fault hiding approaches use a reconfiguration block between the plant and the nominal controller in order to hide the diagnosed fault to the nominal controller [275]. Fig. 2.17 depicts the basic diagram of the fault hiding method. Currently, two main types of fault hiding methods have been proposed: Virtual actuator/sensor and estimation & compensation.

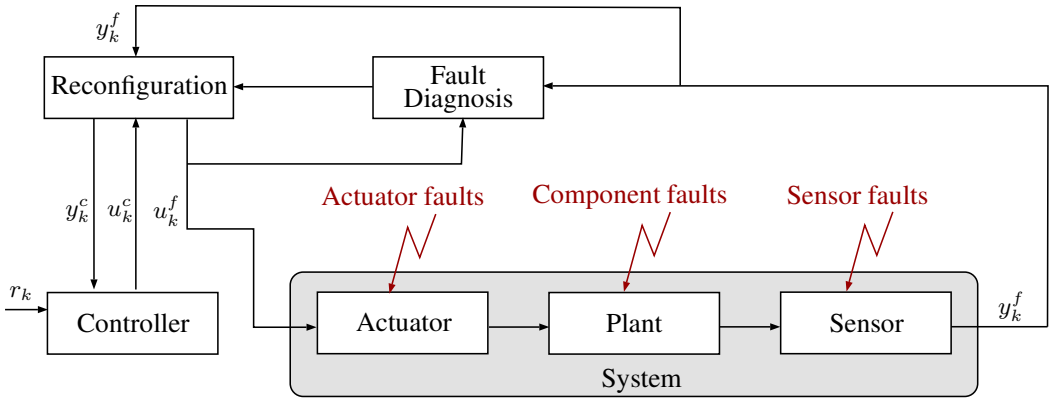

Figure 2.17. General fault hiding scheme.

- In virtual actuator/sensor approaches, the reconfiguration unit uses the faulty system dynamics (deduced from the FD unit) to modify the control action provided by the nominal controller so that the faulty plant behaves as the original healthy one [239,243].
- Estimation & compensation approaches are based on feedforwarding the fault estimates provided by the FD unit to the controller so that it takes this information into account for the computation of the control action [85, 144, 281].

Although projection AFTC methods are more flexible than PFTC approaches, they also present the drawback of requiring some *a priori* knowledge of the presumed faults. Control allocation methods require actuator hardware redundancy and, hence, they are only suitable for overactuated control systems. According to this background, control redesign and fault hiding approaches are considered to be good alternatives to achieve AFTC. Especially, estimation & compensation AFTC methods have become mainstream because they intrinsically integrate diagnosis and FTC tasks [170–172, 179].

2.4.2 Fault diagnosis tasks for fault tolerant control

More often than not, AFTC approaches require FE to achieve their fault tolerant purposes [29]. It is obvious that control redesign and fault hiding methods need the information provided by fault analysis for their functioning. For its part, control allocation and projection methods may not require FE in their implementation. However, FE becomes necessary in projection methods if multiple controllers are predesigned for different degrees of the same isolated fault. FE also becomes necessary in control allocation methods when the faulty actuators are not suppressed and, instead, the control efforts are reorganized among all the actuators.

As explained in Section 2.3.1, residual-based strategies provide FDI information but they are not devoted to FA. Hence, some investigators utilize fault reconstruction methods in order to obtain fault estimates from the generated residuals. However, these reconstructions rely on discrete-event algorithms with complex decisions that entail delays and errors [53, 171]. Hence, FE appears as a powerful alternative to residual-based strategies in an AFTC framework.

This thesis is then focused on the development of observer-based FE strategies which can be utilized in AFTC. As deduced from Section 2.3.3 and Section 2.3.4, the presence of disturbances and noises may lead to non-zero fault estimates in fault-free scenarios. In order to reduce the misleading effect that may be produced by feedforwarding non-zero fault estimates in healthy situations to an active fault tolerant controller, we propose to evaluate the fault estimates in decision mechanisms to achieve FDI (Remark 2.5), to which we simply refer as fault isolation (FI).

2.5 Fault diagnosis performance

2.5.1 Fault estimation performance

Consider certain fault estimator (2.42) satisfying (2.43a). When applied to the system (2.10), the fault estimator verifies

$$\hat{f}(z) = H_y(z)\Big(G_f(z)\,f(z) + G'_d(z)\,d'(z)\Big). \tag{2.55}$$

The performance of the fault estimator can be then described by the behavior of $\hat{f}$ w.r.t. f and w.r.t. d'. In this thesis, we characterize the performance of each fault estimate $\hat{f}_i$ and we distinguish between the effects of the fault f_i and of the other faults f_j $(j = 1, \ldots, i-1, i+1, \ldots, n_f)$. Similarly, we distinguish between the effects of the UIs d and of the noises w:

$$\hat{f}_i(z) = H_y(z)\Big(G_{f_i}(z)\,f_i(z) + \sum_{j=1, j\neq i}^{n_f} G_{f_i}(z)\,f_i(z) + G_d(z)\,d(z) + G_w(z)\,w(z)\Big). \tag{2.56}$$

As illustrated in Fig. 2.18, we refer to these effects using the following nomenclature.

Fault tracking behavior. The fault tracking behavior refers to the behavior of $\hat{f}_i$ when a fault occurs in the i-th fault channel (i.e., $f_i \neq 0$). In order to describe this behavior, we utilize different performance parameters w.r.t. different fault signals. For instance,

- we utilize the *cumulative squared error (CSE)* w.r.t. the fault signals for which the steady-state estimation error is zero.
- we utilize the *fault tracking delay* w.r.t. the fault signals for which the steady-state estimation error is constant.

Fig. 2.19 shows these parameters for the case of a stable PI observer[7].

Interfault coupling. The interfault coupling refers to the effect on $\hat{f}_i$ of the faults in the channels $j \neq i$ (i.e., $f_{j\neq i} \neq 0$). In order to characterize this effect, we utilize the concept of *degree of interfault decoupling*, which refers to some norm bound of this effect.

[7] A stable PI observer guarantees zero steady-state estimation errors when step faults occur and constant steady-state estimation errors when ramp faults occur.

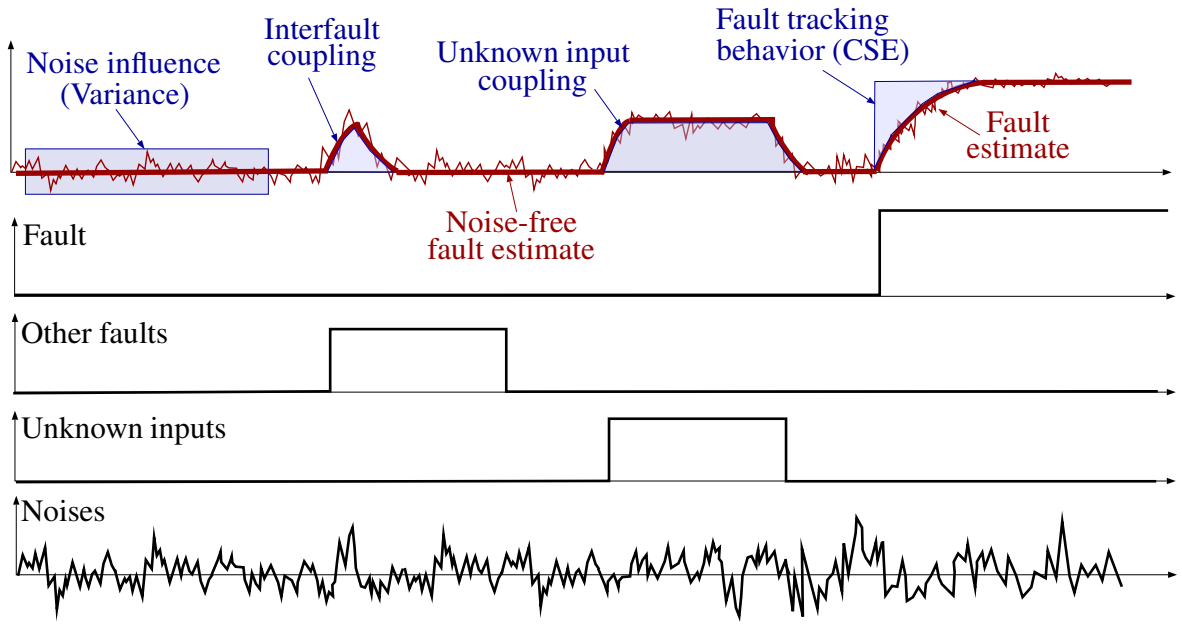

Figure 2.18. Performance characterization in fault estimation.

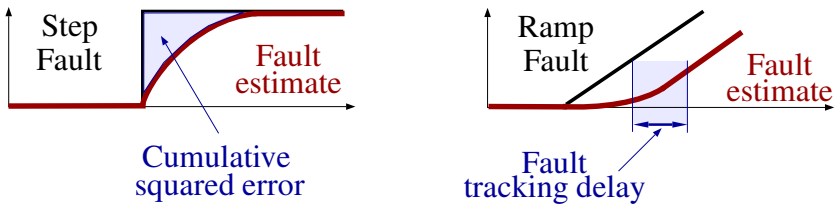

Figure 2.19. Performance parameters for the fault tracking behavior of a PI observer.

UI coupling. The UI coupling refers to the effect on $\hat{f}_i$ of the UIs (i.e., $d \neq 0$). In order to characterize this effect, we utilize the concept of *degree of UI decoupling*, which refers to some norm bound of this effect.

Noise influence. The noise influence refers to the effect on $\hat{f}_i$ of the noises (i.e., $v \neq 0$). In this thesis, it is generally assumed that the noises are zero-mean[8]. Hence, we utilize the *variance due to noises* to characterize this effect.

The design of a fault estimator aims to achieve low CSEs and/or fault tracking delays, high degrees of interfault and UI decoupling and low variances due to noises. The trade-offs that appear for satisfying these four characteristics are called performance trade-offs in fault estimation (Fig. 2.20).

2.5.2 Fault isolation performance

As illustrated in Fig. 2.21, we can characterize the performance of a FI mechanism (i.e., the signal generator and evaluator) using the following standard parameters [44].

[8]This assumption is common for systems affected by stochastic noises (e.g., Kalman filter theory).

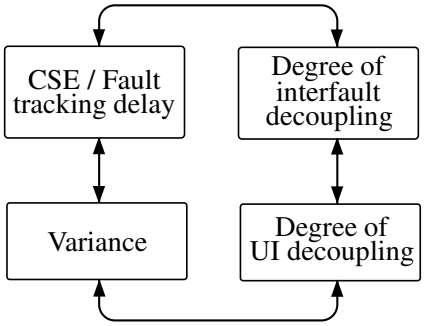

Figure 2.20. Performance trade-offs in fault estimation.

False isolation rate. The false isolation rate is the probability of rising the alarm of fault i when this fault is not present in the system (i.e., $f_i = 0$).

Minimum isolable fault. The minimum isolable fault is the smallest value of a fault f_i that ensures the isolation of this fault.

Isolation time indices. The isolation time indices describe the time delays in isolating the appearance of a fault f_i. We distinguish between

- the *acknowledgement time for isolation*, which refers to the time elapsed between the sample in which f_i reaches the minimum isolable fault and the first sample of isolation of the fault.
- the *isolation time*, which refers to the time elapsed between the appearance of the fault f_i and the first sample of isolation of this fault.

Remark 2.8. *In this thesis, FDI is achieved by means of evaluating the fault estimates provided by model-based observers in threshold-based decision mechanisms. From a diagnosis performance perspective, we assume the non-simultaneity of faults. Hence, we indistinctly refer to detection and isolation performance parameters or to isolation performance parameters.*

The design of a FI mechanism aims to achieve low isolation time indices, low minimum isolable faults and low false isolation rates. The trade-offs that appear for satisfying these

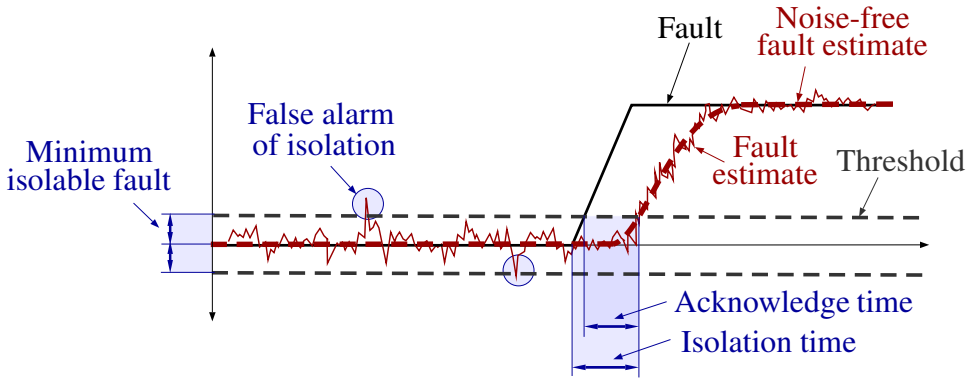

Figure 2.21. Performance characterization in fault isolation.

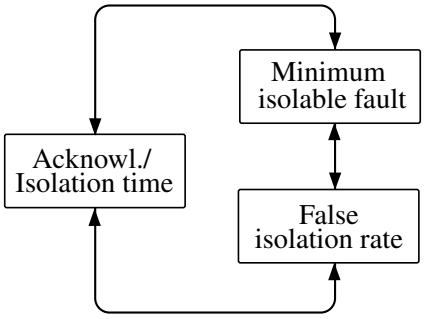

Figure 2.22. Performance trade-offs in fault isolation.

characteristics are called performance trade-offs in FI (Fig. 2.22). As extensively proven in the literature [4,49,72,327], an optimal trade-off between these performance parameters requires an integrated design of the signal generator and evaluator (in this thesis, the model-based observers and the decision mechanisms evaluating the fault estimates).

2.6 Fault diagnosis: applications

The authors in [315] state the need of detailed and comprehensive studies to improve the effectiveness and feasibility of FD systems in industrial environments. In this section, we briefly motivate the development of advanced FD techniques for the practical applications included in the thesis.

Industrial pipe networks. The networks of pipelines and tanks represent major assets of the process industry. However, pipelines may suffer from leakages due to corrosion, erosion or material defects, amongst others. In many cases, the effect of these leakages extends beyond the costs derived from downtimes and product losses because they may be hazardous for the environment or for human beings. Therefore, a lot of attention has been paid to leakage detection [233]. Besides external FD techniques utilizing specialized hardware for leakage detection, there are internal FD techniques that deal with the information provided by the process measurements. Among them, we distinguish between the strategies that rely on the principle of mass conservation and the methods that use analytical models of the dynamics of the fluid inside the pipelines [208]. Unfortunately, except from some contributions (e.g., [237]), most of the works in the literature do not deal with real experimental data. Hence, more research regarding leakage diagnosis in real industrial environments is necessary.

Multistage manufacturing processes. At the manufacturing stage, process engineers are focused on the reduction of process variation. However, process variation reduction throughout the manufacturing process is a challenging task, especially in complex processes such as multistage manufacturing processes (MMPs). Current state of industrial practice in MMPs monitoring is mostly based on statistical approaches, such as statistical process control (SPC) [202]. However, the identification of the root causes has been proved to be arduous when using these methods [187]. More advanced FD techniques require an explicit model of the MMPs. In this field,

one of the most successful approaches is the stream-of-variation (SoV) model [262], a model adapted from the state-space model in control theory for modeling MMPs. Online estimators (e.g., [11, 77]) utilizing batches of manufactured pieces have been successfully applied to SoV models. However, these estimators are mainly applied to MMPs from a stationary perspective. Research in FD for MMPs in non-stationary conditions is thus necessary.

Wind turbines. Undoubtedly, wind energy is a powerful source of sustainable energy (see Appendix A.1). However, wind turbines (WTs) are expensive systems and their maintainability and reliability must be high in order to maximize the amount of generated power and to minimize the costs associated to maintenance operations [199]. A promising strategy to ensure these capabilities is the introduction of advanced FD systems in WTs because, in the state-of-the-art of industrial WTs, FD schemes are simple and most often conservative [216]. Proof of this is the acceptance of the benchmark model presented by Odgaard, Stoustrup & Kinnaert in [216] for the development of advanced FD techniques in WTs, which has received a lot of attention from the researches in the FD field (e.g., [32, 214, 221]). The WT benchmark considers some common WT faults (see Appendix A.3) covering sensor, actuator, and process faults in different WT systems: the pitch system, the drive train system and the generator and converter system. However, most solutions in the bibliography focused either on FDI or on the identification of certain of these faults. It is thus necessary to develop estimation-based FD strategies considering all the faults in the WTs. Moreover, the benchmark includes FDI performance requirements; however, these requirements are generally *a posteriori* studied in the literature. Hence, it is necessary to develop more FD solutions for WTs guaranteeing a predefined FD performance.

Wind farms. Odgaard & Stoustrup presented another benchmark in [215] for FD in WTs at a wind farm (WF) level. Motivated by the conclusions in pioneer works as [168], the authors recognize that some faults which are difficult to diagnose at a WT level can be better handled at the WF level, when the WT is considered in comparison to other WTs of the farm. The WF benchmark considers the following faults: decreased power generation due to debris build-up or erosion, blade misalignments and changes in the drive train damping due to wear and tear. Fewer solutions to this FD problem are available in the literature (e.g., [16, 30, 264]). However, most of these solutions concentrate on FDI purposes and propose the generation and evaluation of open-loop residuals which are very sensitive to disturbances and uncertainties. Moreover, these solutions separately generate and evaluate spatial and temporal residuals. Hence, it is of interest to develop estimation-based closed-loop FD strategies merging the spatial and temporal information provided by the process measurements in WFs.

Chapter 3

Comparison of leakage estimation strategies in a real industrial pipe network

This chapter addresses the leakage estimation problem for a real industrial network of pipelines and tanks. For this aim, we propose two different approaches that rely on the mass conservation principle. The first method models the leakages as multiplicative faults and applies the recursive least square identification algorithm to identify them. The second approach deals with the leakages as additive faults and relies on PI observers for estimating the leakages. We also include a brief performance-based analysis of these methods w.r.t fault diagnosis issues.

3.1 Introduction

The networks of pipelines and tanks represent major assets of the process industry. Regardless of the effort in designing and building the network, pipelines may suffer from leakages due to corrosion, erosion or material defects, amongst others. In many cases, the effect of these leakages extends beyond the costs derived from downtimes and product losses because they may be hazardous for the environment or for human beings. Then, much effort has been devoted to face this problem. Pioneer works in the filed dealt with pipe rehabilitation and replacement issues, [36]. In the last decades, most of the attention has been drawn to leakage detection, [233].

The authors in [107] divide leakage detection methods into two main groups. First, we have the direct or external techniques that require the application of specialized hardware such as optical sensors, acoustic devices or soil monitoring. Second, there are indirect or internal techniques that do not require specialized sensors and deal with the information provided by the process measurements. Among them, Billmann and Isermann [208] distinguish between the strategies that rely on the principle of mass conservation and the methods that use analytical models of the dynamics of the fluid inside the pipeline. The latter enable the detection and

location of smaller leakages w.r.t mass-conservation-based techniques, see [27]. Many contributions such as [292] deal with these analytical methods for leakage identification; however, these strategies require complex models which are very difficult to calibrate and require a trained user [278]. Moreover, some industrial pipe networks are not equipped with pressure transducers and the application of these strategies is not possible. The mass-conservation-based methods, such as the ones present in [9], are easy to use and can be easily implemented since they rely on instrumentation available in every pipeline [80].

Regardless of the model on which they are based, we find leakage indirect identification techniques that use model-based observers for fault diagnosis (FD), like in [286], and other methods that rely on parameter identification techniques, like in [20]. Except from some contributions (i.e., [237]), most of these works do not deal with real data and, in many cases, they assume idealized noise conditions. The authors in [315] state the need of detailed and comprehensive studies to improve the effectiveness and feasibility of FD systems in industrial environments. The main objective of this chapter is to apply and compare the suitability of two different fault estimation (FE) mass-conservation-based techniques for leakage identification in a real industrial pipe network. The first approach is based on parameter identification techniques and the second one is based on model-based observers.

3.1.1 Structure and notation

The outline of this chapter is as follows. First, we state the problem in Section 3.2, where we include the mathematical model of the pipe network and its sensors and we detail the objectives of the chapter. In Section 3.3, we show how to deal with the leakages from a multiplicative point of view. Similarly, Section 3.4 deals with leakage identification from an additive perspective. Section 3.5 compares these two mass-conservation-based approaches and analyses the suitability of these methods from a FD perspective. Section 3.6 applies the techniques to a real network. First, we present the results derived from simulated data and then we show the performance of the algorithms when applied to real industrial data. Finally, Section 3.7 summarizes the main conclusions.

In this chapter, $x(t) \in \mathbb{R}^n$ represents a continuous-time signal at time t and $x[k] \in \mathbb{R}^n$ represents a discrete-time signal at sample k. Expected value is denoted as $\mathbf{E}\{\cdot\}$ and absolute value is denoted as $|\cdot|$.

3.2 Problem statement

Let us consider a group of $i = 1, \ldots, n_v$ fluid storage tanks interconnected through a network of $j = 1, \ldots, n_q$ pipelines. We propose to model this network through the mass balance of each tank i as

$$\dot{M}_i = \sum_{j=1}^{n_q} c_{i,j}\, m_j, \qquad i = 1, \ldots, n_v, \tag{3.1}$$

where m_j is the mass flow rate carried by the pipeline j, $\dot{M}_i$ is the derivative of the mass contained in the tank i and $c_{i,j}$ is a constant describing the relation between the flow of the pipeline j and the variations experienced by the tank i. We have that $c_{i,j} = 0$ if the pipeline is not connected to the tank and $c_{i,j} = \{-1, 1\}$ depending on whether the pipeline extracts fluid from the tank or introduces fluid in it.

Due to the high cost of mass flowmeters such as Coriolis flowmeters, mass flow rates are not generally measured through these devices in industry. It is much more common to find magnetic or pressure-based volumetric flowmeters which are calibrated with a predefined product density, ρ^0. Environmental conditions may affect the product density. In such cases, the actual density, ρ, does not verify $\rho = \rho^0$. Taking this consideration into account, we model the mass flow rate measurement in the pipeline j (denoted as u_j) as

$$u_j = m_j + \eta_j, \tag{3.2}$$

where η_j takes not only account of the sensor noise but also considers the biases produced by the differences between the predefined density, ρ^0, and the actual density, ρ. Similar applies to the mass contained in the tanks. In industry, this mass is computed through the measurements provided by level sensors, the tank dimensions and the predefined product density, ρ^0, i.e.,

$$M_i^0 = \rho_i^0 \, S_i \, h_i,$$

with S_i being the equivalent cross section of the tank i and h_i being the equivalent level measured by the sensors in the i-th tank. Again, we model the mass measurement in the tank i (denoted as s_i) as

$$s_i = M_i + \nu_i, \tag{3.3}$$

where ν_i takes into account sensor noises, density biases and tank dimensions uncertainties.

The previous network might be affected by leakages that corrupt the network. If a leakage occurs, (3.1) does not hold anymore. In the following sections, we present two different approaches to consider possible fluid leakages in the process model. Section 3.3 deals with the leakages as multiplicative faults and Section 3.4 models them as additive faults. The main objective of this chapter is to provide multiplicative and additive leakage estimation algorithms that use the information provided by the input measurements u_j $(j = 1, \ldots, n_q)$ and the output measurements s_i $(i = 1, \ldots, n_v)$. In this chapter, we also aim to characterize the performance of these fault estimators in order to build fault evaluators and achieve fault detection and isolation (FDI).

We desire that the algorithms developed in this thesis can be implemented in industrial hardware such as Programmable Logic Controllers (PLCs) or Distributed Control Systems (DCSs); hence, we work in the discrete domain with the sample time T_s.

3.3 Multiplicative approach for leakage estimation

3.3.1 Leakage identifiability analysis

Let us consider that the previous network may be affected by leakages in its pipelines. We can extend the model (3.1) to take these possible faults into account as

$$\dot{M}_i = \sum_{j=1}^{n_q} (c_{i,j} + c_{i,j}\,\theta_{i,j})\, m_j, \quad i = 1, \ldots, n_v, \tag{3.4}$$

where $\theta_{i,j}$ is a parameter that describes the existence of leakages in the section of the pipeline j between the tank i and the sensor u_j. Then, we have that $\theta_j = 0$ if this leakage does not occur and $\theta_j \neq 0$ when this leakage is present in the network. The mass flow rate of the leakage $\theta_{i,j}$, which we denote as $l_{i,j}$, is given by

$$l_{i,j} = \theta_{i,j}\, m_j. \tag{3.5}$$

Identification algorithms allow identifying as many parameters as sufficiently excited inputs are available per each measured output, see [17,174]. Thus, if we assume that all the mass flow rates m_j are sufficiently excited, each measurement s_i allows identifying all the leakage parameters $\theta_{i,j}$ with $j = 1, \ldots, n_q$. In all, the discrete state-space realization that enables leakage multiplicative identification in the surroundings of the tank i is

$$y_i[k] = D_i\, x_i[k] + E_i\, \eta[k] + \mu_i[k], \tag{3.6}$$

with

$$D_i = \begin{bmatrix} 1+\theta_{i,1} & \ldots & 1+\theta_{i,n_q} \end{bmatrix}, \quad x_i[k] = \begin{bmatrix} c_{i,1}\, u_1[k] & \ldots & c_{i,n_q}\, u_{n_q}[k] \end{bmatrix}^T,$$

$$E_i = \begin{bmatrix} c_{i,1} & \ldots & c_{i,n_q} \end{bmatrix}, \quad \eta[k] = \begin{bmatrix} -\eta_1[k] & \ldots & -\eta_{n_q}[k] \end{bmatrix}^T,$$

and where $y_i[k]$ and $\mu_i[k]$ are the output measurement and its noise defined as

$$y_i[k] = \frac{1}{T_s}\,(s_i[k] - s_i[k-1], \tag{3.7}$$

$$\mu_i[k] = \frac{1}{T_s}\,(\nu_i[k] - \nu_i[k-1]). \tag{3.8}$$

3.3.2 Estimation algorithm

For leakage parameter identification, we transform (3.6) by removing the variables associated to the pipelines which are not connected to the tank i, i.e.,

$$y_i[k] = \bar{D}_i\, \bar{x}_i[k] + \bar{E}_i\, \bar{\eta}[k] + \mu_i[k], \tag{3.9}$$

where $\bar{D}_i$ and $\bar{E}_i$ result from removing the columns j satisfying $c_{i,j} = 0$. Similar applies to the rows of $\bar{x}_i$ and $\bar{\eta}$ w.r.t x_i and η. We denote by $\bar{n}_q$ the resulting number of rows or columns in the previous vectors.

We propose to identify the parameters $\theta_{i,j}$ $(j = 1, \ldots, \bar{n}_q)$ in (3.9) through the following recursive least squares (RLS) algorithm with trace control, see [191]:

$$R_i[k] = \bar{x}_i[k]^T P_i[k-1]\, \bar{x}_i[k] + \lambda, \tag{3.10a}$$
$$L_i[k] = P_i[k-1]\, \bar{x}_i[k]\, R_i[k]^{-1}, \tag{3.10b}$$
$$\bar{D}_i[k-1] = [1 \ \ldots \ 1] + \hat{\theta}_i[k-1]^T, \tag{3.10c}$$
$$\hat{\theta}_i[k] = \hat{\theta}_i[k-1] + L_i[k]\,(y[k] - \bar{D}_i[k-1]\, \bar{x}_i[k]), \tag{3.10d}$$
$$P_i[k] = \frac{1}{\lambda}\,(I - L_i[k]\, \bar{D}_i)\, P_i[k-1], \tag{3.10e}$$
$$\text{if } \ \mathrm{tr}(P_i[k]) > \alpha \ \text{ then } \ P_i[k] = \alpha/\mathrm{tr}(P_i[k])\, P_i[k], \tag{3.10f}$$

with $\hat{\theta}_i[k] = \left[\hat{\theta}_{i,1}[k] \ \cdots \hat{\theta}_{i,\bar{n}_q}[k]\right]^T$ being the vector of identified parameters, $P_i[k]$ the inverse of the weighted information matrix and λ the forgetting factor that must be chosen according to the excitation of the mass flow signal.

3.3.3 Design and performance analysis

The convergence of (3.10) depends on the initial value of the matrix P_i. This matrix must be initialized at a high value to indicate that, initially, there is no information about the process (e.g., $P_i[0] = 10^9 \cdot I$). In the initialization, we do not expect any leakage in the network; thus, we set $\hat{\theta}_i[k]$ to zero.

The estimation error of vector θ_i depends on the forgetting factor λ: a larger value of λ leads to a lower error. The speed of the convergence to the real parameters depends on both the excitation level of the signals and the forgetting factor λ: the convergence under system changes is faster with a lower value of λ. Therefore, λ can be seen as a tuning parameter for setting the trade-off between the FE accuracy and the convergence speed. If the system is sufficiently excited, λ can be chosen close to 0.995, and if not, it must be chosen close to 1.

This method gives no *a priori* information of the estimation error because the signal to noise ratio of the flow signals may change during normal operation. Furthermore, if a signal is mainly constant and does not sufficiently excite the identification algorithm, this approach can give wrong estimations with significant biases [6]. The algorithm should be stopped in the case that all the flow rates become constant and should be only activated if the flows are significantly varying.

3.4 Additive approach for leakage estimation

3.4.1 Leakage identifiability analysis

Let us consider the leakage flows to be additive faults. The process model can be written as

$$\dot{M}_i = \sum_{j=1}^{n_q} c_{i,j}\,(m_j + l_{i,j}), \quad i = 1, \ldots, n_v, \tag{3.11}$$

According to [70], the identifiability of the faults requires their detectability and isolability. A fault is detectable if its variations affect the output measurement of the system. This means that a leakage flow $l_{i,j}$ $(j = 1, \ldots, n_q)$ is detectable through the i-th model in (3.11) if $c_{i,j} \neq 0$. Regarding isolability issues, additive faults are only isolable if the number of faults is not larger than the number of output measurements. Provided that only one output measurement s_i is available per tank, it is just possible to estimate the total leakage flow that occurs in all the pipelines connected to each tank i, i.e.,

$$\dot{M}_i = \sum_{j=1}^{n_q} c_{i,j}\, m_j + f_i, \quad i = 1, \ldots, n_v, \tag{3.12}$$

with

$$f_i = \sum_{l=1}^{n_q} c_{i,j}\, l_{i,j}. \tag{3.13}$$

Finally, let us define the transfer function between the fault f_i and the output measurement s_i as $G_{f_i}(s)$. Identifiability requires the stability and causality of the inverse of $G_{f_i}(s)$. We have that $G_{f_i}^{-1}(s) = s$ and we deduce that f_i is not identifiable through s_i. To face this problem, we propose to consider the measurement of the derivative of M_i to be the output measurement of the system; in this case, we have $G_{f_i}^{-1}(s) = 1$ and we deduce that f_i is identifiable through the measurement of $\dot{M}_i$. The discretization of the state-space model of the system that enables leakage estimation in the surroundings of the tank i is

$$y_i[k] = E_i\, u[k] + E_i\, \eta[k] + \mu_i[k] + f_i[k], \tag{3.14}$$

with

$$u[k] = \begin{bmatrix} u_1[k] & \ldots & u_{n_q}[k] \end{bmatrix}^T.$$

3.4.2 Estimation algorithm

To enhance the steady-state accuracy in additive FE, we propose to use model-based proportional integral (PI) observers. Thus, we model each fault f_i as

$$f_i[k+1] = f_i[k] + \Delta f_i[k], \tag{3.15}$$

where $\Delta f_i[k]$ represents the variation of the fault signal f_i between two consecutive samples. The equation (3.15) allows modeling, for instance, abrupt or step signals ($\Delta f[k]$ only takes a non-zero value at the fault appearance) and incipient or ramp signals ($\Delta f[k]$ takes a constant value). This kind of fault model has been widely used in the literature to analyse the behavior of FD algorithms, see [155, 162]. The proposed single-input single-output (SISO) PI observer for the estimation of the fault f_i is

$$\hat{f}_i[k+1] = \hat{f}_i[k] + l_i(y_i[k] - \hat{f}_i[k] - E_i\, u[k]), \tag{3.16}$$

where $\hat{f}_i$ is the fault estimate and l_i is the gain that updates the prediction obtained from the model with the measurements.

3.4.3 Design and performance analysis

First, let us define the FE error as

$$\widetilde{f}_i[k] = f_i[k] - \hat{f}_i[k]. \tag{3.17}$$

Its dynamics is given by

$$\widetilde{f}_i[k+1] = (1 - l_i)\,\widetilde{f}_i[k] - l_i\,(E_i\,v_i[k] + \mu_i[k]) + \Delta f_i[k] \tag{3.18}$$

and we deduce that l_i places the poles of the dynamics of $\widetilde{f}_i$. For a first-order system, an unambiguous measure of the speed of response is the time constant τ_i defined as

$$\tau_i = -T_s/\ln(1 - l_i). \tag{3.19}$$

This constant fixes, for instance, the 98% settling time towards step faults as $t_{s,98\%} = 4\tau$. Other indices of the temporary behavior of the response include the cumulative squared error (CSE) of the response which is given by

$$\mathrm{CSE}_i = T_s\left(1 - (1 - l_i)^2\right) \tag{3.20}$$

when a step fault occurs.

Second, we denote the covariance of the error $\widetilde{f}_i[k]$ as σ_i^2. To compute σ_i^2, we should take account of the correlation between $\nu_i[k]$ and $\nu_i[k-1]$ inside $\mu_i[k]$, see (3.8). Then, at steady state and when no fault occurs, σ_i^2 satisfies the following Lyapunov equations:

$$\mathcal{F}_i = A_i\,\mathcal{F}_i\,A_i^T + B_i\,\mathcal{V}_i\,B_i^T, \tag{3.21a}$$
$$\sigma_i^2 = R\,\mathcal{F}_i\,R^T, \tag{3.21b}$$

with

$$R = \begin{bmatrix}1 & 0\end{bmatrix},\quad A_i = \begin{bmatrix}l_i/T_s & 1 - l_i\\ 0 & 0\end{bmatrix},\quad B_i = \begin{bmatrix}-l_i\,E_i & -l_i/T_s\\ 0 & 1\end{bmatrix},$$

and $\mathcal{V}_i$ being the covariance of vector $v_i[k] = \begin{bmatrix}\eta[k] & \nu_i[k]\end{bmatrix}$, i.e., $\mathcal{V}_i = \mathbf{E}\left\{v_i[k]\,v_i^T[k]\right\}$.

The equations (3.19)-(3.20) and (3.21) show that there is a trade-off between the tracking ability of the fault estimator and the accuracy of the estimations. To design the fault estimator we can either fix the temporary behavior of the estimation through (3.19) or (3.20) and obtain a certain accuracy of the estimations by (3.21) or vice-versa

3.5 Comparison and FDI architecture

3.5.1 Comparison

Let us briefly compare the multiplicative estimation approach presented in Section 3.3 and the additive estimation approach included in Section 3.4.

- Regarding isolability issues, the additive observer-based approach just estimates the total leakage of all the pipelines connected to a tank i and, unlike the method based on parameter identification, it does not indicate which pipeline j is responsible for the fault.

- Regarding excitability issues, the multiplicative approach requires sufficiently excited inputs. The additive approach does not demand any condition to the inputs.

- Regarding analysis issues, the performance of the estimations obtained through parameter identification cannot be *a priori* characterized as it depends on the excitation of the inputs. In opposite, the performance of the estimations obtained through PI observers is parametrizable and does not depend on the inputs.

3.5.2 FDI architecture

Provided the previous characteristics of the two presented approaches, we propose to use the fault estimates provided by the additive approach (i.e., (3.16)) for FDI purposes. We introduce the following decision mechanism:

$$\begin{cases} \text{if } |\hat{f}_i[k]| \geq f_{m,i} \,, & \text{Fault } f_i \\ \text{otherwise} \,, & \text{No fault } f_i \end{cases} , \tag{3.22}$$

where $f_{m,i}$ denotes the minimum isolable fault f_i and it refers to the constant fault that raises the alarm of fault f_i provided the non-existence of other faults nor noises in the system. Let us define the false isolation rate (FIR), which we denote as ϕ_i, as the probability of rising false alarms regarding the presence of the fault f_i. If we assume that the noises affecting the system are Gaussian, we have that the FE error $\widetilde{f}_i[k]$ is normally distributed with zero mean. Then, $f_{m,i}$ should satisfy the following relation for guaranteeing certain FIR:

$$f_{m,i} = \Phi^{-1}(1 - \phi_i/2)\, \sigma_i, \tag{3.23}$$

where Φ^{-1} is the inverse cumulative distribution function of a normal random variable. The equation (3.23) means that $f_{m,i}$ can be also seen as the quantile used to construct the confidence interval of level $1 - \phi(i)/2$.

Remark 3.1. *If the noises are biased, we must increase the threshold $f_{m,i}$ in an amount equal to $\sum_j |F_{i,j}|\bar{v}_{i,j}$ where $F_{i,j}$ is the static gain from the sensor noise $v_{i,j}$ to the estimated fault $\hat{f}_i$, and $\bar{v}_{i,j}$ is the bias in sensor $v_{i,j}$.*

Remark 3.2. *Once we have diagnosed the presence of a fault in a pipeline connected to the tank i through* (3.22) *and if the inputs m_j are sufficiently excited, we can determine which pipeline j is responsible for the leakage. To do so, we should look for the estimate $\hat{\theta}_{i,j}[k]$ $(j = 1, \ldots, \bar{n}_q)$ that experiences the greatest variation after the fault appearance.*

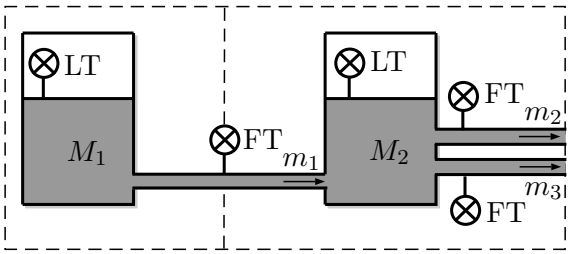

Figure 3.1. Network architecture of tanks, pipelines and transducers.

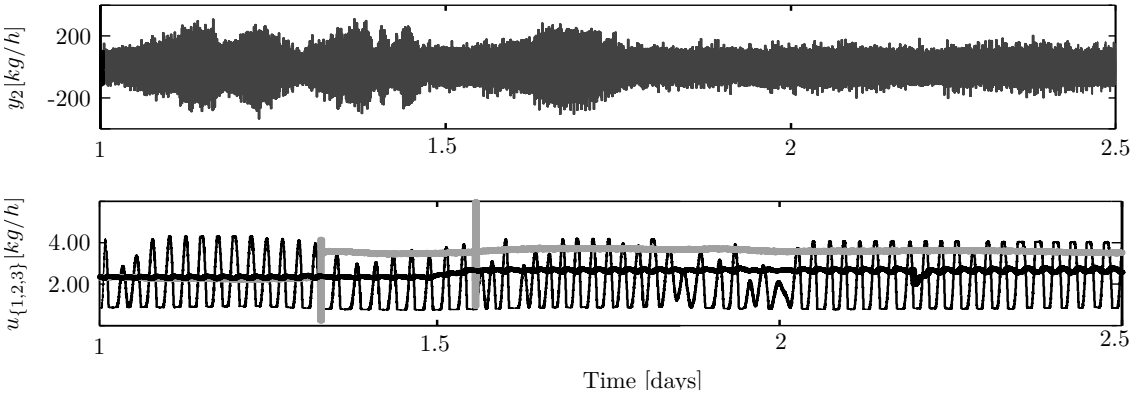

Figure 3.2. Real input and output measurements of the tank 2 ($T_s = 1$).

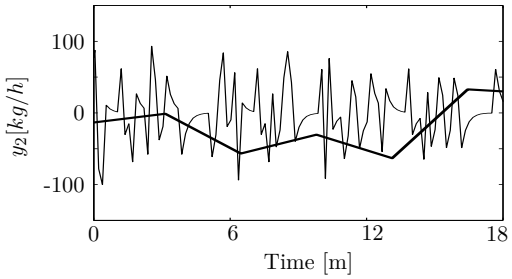

Figure 3.3. Detail in real y_2 data for different sample times (Light: $T_s = 1$, Dark: $T_s = 20$).

3.6 Application

Let us consider the network depicted in Fig. 3.1. There is a raw material storage tank connected with a feeding tank. Let us denote the mass inside these tanks as M_1 and M_2. The maximum capacity of the tanks is, respectively, 10.000 and 800 metric tons. These tanks are connected through a pipeline which delivers a mass flow rate m_1 up to 25 t/h ($c_{1,1} = -1$ and $c_{2,1} = 1$). The feeding tank has two consumers, whose mass flow rates are denoted as m_2 and m_3 ($c_{2,2} = c_{2,3} = -1$). These mass flows are supposed to be, at most, 15 t/h and 10 t/h. All the pipelines are prone to faults ($l_{1,1}$ and $l_{2,1/2/3}$). In this analysis, we focus on the leakage $l_{2,1}$, which refers to the leakage in the section that goes from the flowmeter in the pipeline 1 to the tank 2 [1]. We

[1] In reality, this section of the pipeline 1 is the longest pipe section in the network and it, moreover, is the least accessible pipe section for the operators.

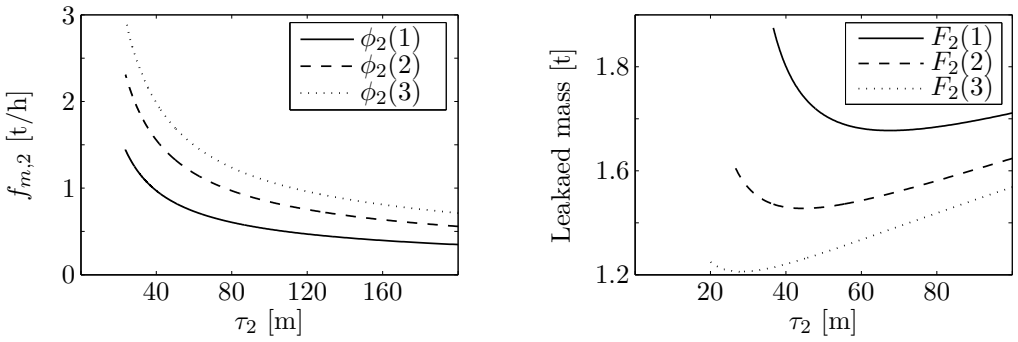

Figure 3.4. Trade-offs of performance for different designs.

apply the previous FE techniques in both simulated data and real industrial data (in which we have added a simulated leakage).

For $T_s = 1$, the measured signals are shown in Fig. 3.2. Fig. 3.3 shows that the quantization in the measurements $s_2[k]$ affects $y_2[k]$ when computed with T_s=1 s: its noise is correlated. If we use T_s=20 s, the correlation disappears at the cost of a maximum delay in the FDI scheme of 20 s. This delay being negligible for the case of study, we choose $T_s = 20$ s for the implementation. In this case, the standard deviation of the measurement noise of $y_2[k]$ is 79.2 t/h. In the worst case, the standard deviation of the measurement noises of $u_1[k]$, $u_2[k]$ and $u_3[k]$ is 0.053 t/h, 0.0026 t/h and 0.022 t/h, respectively. We see that the main handicap of the problem is the difference in the magnitude order between the noise in the tank measurements and the noises in the pipeline measurements. For validation purposes, we also generate simulated data. The simulated data is obtained by generating mass flow rate signals and obtaining the corresponding volume by integration; then, we add Gaussian noises to all the signals with the worst observed real standard deviation.

3.6.1 Additive approach

For the fault estimator (3.16) and the fault evaluator (3.22), we have performed several designs with different constant times τ_2 (from 20 min to 180 min) and FIRs ($\phi(1) = 10^{-3}$, $\phi(2) = 10^{-6}$ and $\phi(3) = 10^{-9}$). Fig. 3.4 (left) shows the minimum isolable fault that corresponds to each design. We see that for a given FIR, the minimum isolable fault $f_{m,2}$ diminish when increasing the time constant of the fault estimator. Achieving certain sensitivity to faults (i.e., given $f_{m,2}$) requires a larger time constant of the estimator if we want to assure lower FIRs.

Under the presence of step faults f_2, the estimator $\hat{f}_2[k]$ behaves as a first-order system with time constant τ_2 and unitary gain. This allows us to obtain the sample in which the fault estimate crosses the threshold and, therefore, the amount of mass that has been leaked until FDI is achieved: $-F\,\tau\,\log(1 - f_m/F)$. In Fig. 3.4 (right), we represent this mass for different estimators (with the time constant indicated in the horizontal axis and with a FIR of 10^{-3}) under three different step faults of size $F_2(1) = 2$ t/h, $F_2(2) = 3$ t/h, and $F_2(3) = 5$ t/h. Given an estimator defined by τ_2 and $f_{m,2}$, it is remarkable that a bigger leakage F_2 makes the FDI

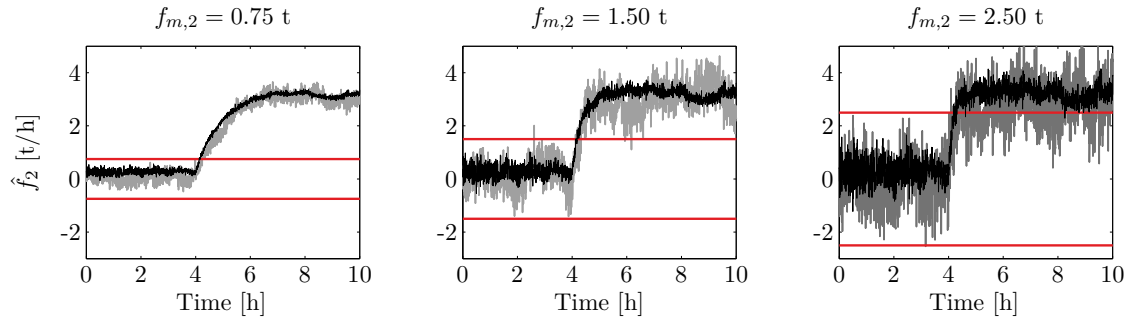

Figure 3.5. Comparison of different designs of additive fault estimation and diagnosis (Dark: Industrial data, Light: Simulated data, Red: Threshold).

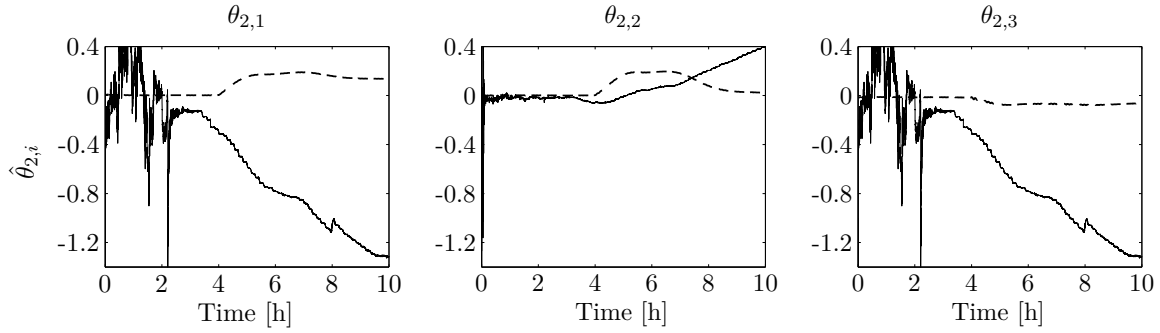

Figure 3.6. Multiplicative fault estimation with $\lambda = 0.999$ (Dark: Industrial data, Dashed: Simulated data with $u_j(1)$).

to occur faster in such a way that less mass leaks. The leaked mass is infinite if the fault F_2 is less than the threshold $f_{m,2}$, and it reaches a minimum at a certain τ_2. As the fault is not known *a priori*, this feature cannot be used to find an optimal fault estimator and evaluator (in the sense of finding the fault estimator and evaluator that assures minimum leaked mass until diagnosis).

In order to test the goodness of the approach, we have fed the algorithm (3.16) with the real data. We have added a step signal of 3 t/h (from the instant 5h) to the measurements of m_1. Recall that his step represents an abrupt leakage in the section of the pipeline 1 that goes from the flowmeter to the tank 2. We have tested the approach for different designs (with three different values of $f_{m,2}$ and a fixed FIR of 10^{-3}); the results are depicted in Fig. 3.5 (black). We can appreciate that in the initial healthy periods the estimation has a bias as explained in (3.2). Note that, for the simulated data, the algorithm (3.16) provides unbiased estimations in the healthy period that satisfy the FIR of the design tightly.

3.6.2 Multiplicative approach

Now, we show the behavior of the RLS algorithm to identify faults in all the pipelines. We have again compared simulated data with the real industrial data. We have simulated a leak by multiplying the measurement of m_1 by 1.2 from the instant 4 h. We can see in Fig. 3.6 the performance of the algorithm with $\lambda = 0.999$, where the simulated data (dotted lines) shows

convergence for the parameter $\hat{\theta}_{2,1}$ (the one with the injected fault), but it shows a bad transient for the other parameters that should be kept to zero (mainly due to the high measurement noises). The application of the algorithm to the real data shows a bad initial transient and no convergence after the fault appearance, mainly due to the scarce excitement of the mass flow rates implied in the identification process (see Fig. 3.2).

3.7 Conclusion

In this chapter, we have analysed the problem of leakage detection in networks of tanks and pipes, whose mass and mass flow rates are measured by noisy sensors. We have described and modeled the problem and we have proposed two different estimation strategies. The first approach models the leakages as multiplicative faults, where identification techniques as the RLS apply. The main drawback of this approach is the requirement of permanently excited signals. The performance of the estimation does also depend on that excitation. The second strategy models the leakages as additive faults and we propose a SISO PI observer for their estimation. This approach does not require any specific excitement of the signals and we are able to characterize the achievable performance despite the presence of high noise levels in the signals. This performance has been characterized by means of the minimum isolable fault, the false isolation rate and the convergence rate under step-like faults. We have shown the relation between these three performance indices for the real industrial data. Finally, we have simulated leaks by means of disturbing the measurements of the flowmeters and we have showed the behavior of both approaches. The validity of the additive approach for leaks in the pipelines that surround certain tank has been proved and we have showed that the multiplicative approach fails with the real data due to its poor excitation.

Chapter 4

Estimation of non-stationary process variance in multistage manufacturing processes

In this chapter we propose a recursive algorithm to estimate the process variance in multistage manufacturing or assembly processes. We use a replicated model that includes the process variance to be estimated as a time-varying state that changes slowly. For this model, we develop an estimation strategy including tuning parameters that play a direct role in the trade-off between the estimation accuracy and the adaptation to changes. We also develop a statistical confidence interval for the estimations which enhances the decision of whether the process variances have changed. Unlike other batch methods in the literature, our proposal is computed recursively, and it allows us to tune the trade-off between the convergence speed and the accuracy without modifying the sample size, which only contains the data of the last manufactured piece.

4.1 Introduction

Nowadays, the highly competitive markets demand customized and high quality products with minimum lead times exerting a great pressure on companies to optimize their resources throughout the product development cycle. At the manufacturing stage, process engineers are focused on the analysis and reduction of process variation to reduce cost, improve product quality and minimize production ramp-up times when new products are launched. However, process variation reduction throughout the manufacturing process is a challenging task, especially in complex processes such as multistage manufacturing processes (MMPs). These processes are those that produce products under multiple setups where the operations conducted at the first stages have an influence on the manufacturing operations down-streams [262]. For instance, the process assembly of automobile bodies is a MMP composed of a series of single stages where, at each stage, the body from previous stages is held in a work-holding structure to assemble

new components and, after the welding operation, the body moves forward to the next stages in order to complete additional assembly operations. In MMPs, statistical process control (SPC) techniques are commonly applied to control the manufacturing process over time by monitoring the quality characteristics of the product. The statistical control charts applied in SPC are effective tools to detect process changes and ensure product quality. However, the identification of root causes that may be inferred from charting results would be significantly limited if the interrelationships between the process variables and the key product characteristics (KPCs) are not explicitly modeled. To overcome this limitation, Li et al. [175] proposed a causation-based T^2 decomposition method where the causal relationships among variables are modeled by a Bayesian network. The interpretation and decomposition of Hotelling's T^2 together with the causal information of the process and the KPCs variables let the proposed SPC method to trace backward from certain quality problems to the variables that are the root causes. An improvement of this method is provided in Verron et al. [293] where the decompositions are computed within the Bayesian network itself.

The state-space model from control theory has also been successfully applied to model the relationships between variation sources and product dimensional quality measurements in MMPs [2, 3, 146, 187, 195, 310, 311, 338]. The use of the state-space model with SPC techniques for root cause identification was proposed in Zou and Tsung [341]. In their work, a multivariate exponential weighted moving average scheme with the generalized likelihood test that fully incorporates directional information based on the state-space model was proved to be an effective solution for process monitoring and fault diagnosis. Besides these SPC techniques, different variation source identification techniques such as those based on MLE estimators, REML estimators and MINQUE estimators have been proposed in MMPs using the state-space model as a linear mixed model. In [336], the application of MLE and MINQUE estimators in MMPs was discussed for estimating both the mean and the variance of the process variation sources. A hypothesis-testing procedure was also developed to provide confidence level of each of the estimation results which let the plant engineers determine if process faults regarding the mean and the variance of the process variation sources exist in terms of statistical significance. However, these methods have been mainly applied in biological and agricultural fields [255] and they are primarily applicable to offline experiments where the sample size is small and the computation time is not a concern. In MMP, large quantity of data may be available and the detection and identification of any process malfunctioning need to be carried out faster and efficiently. For this reason, online estimators with low computation cost and fast response have been investigated in previous researches proving their applicability. A good comparison of online estimators of the variance of the process variation sources (i.e., process variance estimators) and their performance can be found in [78], where the process variance estimators from the research works in [11, 67, 77, 276] were analysed. These estimators entail closed-form expressions and are more cost-effective than the MLE method, particularly for large sample sizes, and are thus more suitable for online quality control. However, the estimators analysed are only adequate when the MMP is stationary since the estimations are based on the sample of data of the last N pieces and only when most of the N pieces are affected by the process faults the estimators can correctly detect and quantify the process variance changes. Therefore, these estimators present a delay in identifying the variation sources which negatively impacts on the efficiency of online

quality control actions. For instance, a certain number of parts may be manufactured before the variation source is identified which compromises the quality in terms of variance of the final product and produces an increase of non-quality costs. To overcome this limitation the application of non-stationary process variance estimators in MMPs has to be investigated.

This chapter discusses the use of a model-based observer that recursively updates the estimated process variance with the measurements from each new processed piece. The observer demands few computational burden and it has an asymptotic behavior We also discuss how to tune the observer for fixing the trade-off between the convergence speed under process variance changes and the steady-state error for stationary process variances.

4.1.1 Structure and notation

This chapter is organized as follows. The problem statement is presented in Section 4.2. Section 4.3 presents the proposed approach for modeling the non-stationary behavior of the process variances in MMPs that enables the application of observer-based strategies for variation source identification. Section 4.4 explains the estimation procedure of the process variance and it details a design strategy of the observer for ensuring a specific performance of the estimator. In Section 4.5 we include the design of confidence intervals for the estimates so as to enhance statistical hypothesis testing for fault diagnosis. Section 4.6 briefly compares the proposed estimates with offline existing estimators and Section 4.7 presents a case of study to validate the approach. Finally, Section 4.8 summarizes the main conclusions of the chapter.

Let $M \in \mathbb{R}^{n\times n}$ be a square matrix and $m \in \mathbb{R}^n$ be some vector. $M[i,j]$ denotes the element in the i-th row and j-th column of M and $m[i]$ denotes the i-th element in m. $I_n \in \mathbb{R}^{n\times n}$ is the identity matrix of size n and $\mathbf{1}_n \in \mathbb{R}^n$ is the unitary column vector of size n. $\mathrm{vec}(M) \in \mathbb{R}^{n^2}$ denotes the vectorization of M and $\mathrm{vec}^{-1}(\mathrm{vec}(M)) = M$. $\mathrm{diag}(M) \in \mathbb{R}^n$ is the operator that returns a column vector with the diagonal entries of M. $\mathrm{diag}^{-1}(\mathrm{diag}(M))$ is a diagonal matrix with the elements $M[i,i]$ in its diagonal. Product is denoted as $\prod$, summation is denoted as $\sum$ and the direct sum is denoted as $\bigoplus$, so that $\bigoplus_i m[i] \in \mathbb{R}^{n\times n}$ is a diagonal matrix containing the elements of m in its diagonal. $M^{\otimes^2}$, and $M^{\circ 2}$ represent the Kronecker and Hadamard product of M and M (i.e., $M^{\otimes^2} = M \otimes M$ and $M^{\circ 2} = M \circ M$). Expected value and probability are denoted as $\mathbf{E}\{\cdot\}$ and $\mathbf{Pr}\{\cdot\}$.

4.2 Problem statement

In a MMP the deviations caused by the variation sources of each stage propagate along the production line. At certain stage the dimensional variability of a piece consists of two components: one derived from the previous stages and another created at the current stage. Since these deviations are much smaller than their corresponding nominal value, they can be represented by a linear state-space model as

$$x_k(i) = A_{k-1}\, x_{k-1}(i) + B_k\, u_k^m(i) + u_k^u(i), \tag{4.1a}$$

$$y_k(i) = C_k\, x_k(i) + v_k(i), \tag{4.1b}$$

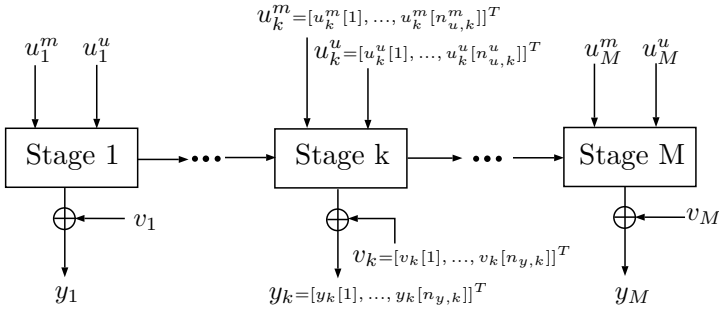

Figure 4.1. Diagram of a MMP.

where $x_k(i) \in \mathbb{R}^{n_{x,k}}$ represents the dimensional variability of piece $i = \{1, ..., \infty\}$ at stage $k = \{1, ..., M\}$. Vector

$$u_k(i) = \begin{bmatrix} u_k^m(i) \\ u_k^u(i) \end{bmatrix} \in \mathbb{R}^{n_{u,k}}$$

(with $n_{u,k} = n_{u,k}^m + n_{u,k}^u$ and $n_{u,k}^u = n_{x,k}$) is the input vector including both the modeled and unmodeled variation sources of the k-th stage affecting the i-th piece. Vector $y_k(i) \in \mathbb{R}^{n_{y,k}}$ is the output vector denoting the measurements of the i-th piece at the k-th stage and $v_k(i) \in \mathbb{R}^{n_{y,k}}$ takes account of the corresponding measurement noises. This kind of stage and piece indexed state-space models, depicted in Fig. 4.1, has been extensively used in MMP applications as shown in [2, 3, 146, 187, 195, 310, 338], which are referred for further modeling details.

As proposed by Apley and Shi [11], model (4.1) can be algebraically transformed into a linear replicated model. Setting the initial conditions to 0, it yields

$$y(i) = \Gamma\, u(i) + v(i), \tag{4.2}$$

where $y(i)$, $u(i)$ and $v(i)$ stand, respectively, for all the measurements, inputs and noises that affect each piece i throughout the MMP, i.e.,

$$y(i) = \begin{bmatrix} y_1(i) \\ \vdots \\ y_M(i) \end{bmatrix},\ u(i) = \begin{bmatrix} u_1(i) \\ \vdots \\ u_M(i) \end{bmatrix},\ v(i) = \begin{bmatrix} v_1(i) \\ \vdots \\ v_M(i) \end{bmatrix},$$

with $y(i) \in \mathbb{R}^{n_y}$, $v(i) \in \mathbb{R}^{n_y}$, $n_y = \sum_k n_{y,k}$ and $u(i) \in \mathbb{R}^{n_u}$, $n_u = \sum_k n_{u,k}$. Matrix Γ can be obtained from A_k, B_k and C_k as explained in the references.

Many works as [78] consider that (4.2) describes a stationary process. For process variance estimation purposes, it is then possible to establish the following relation:

$$\mathbf{\Sigma}_y = \Gamma\, \mathbf{\Sigma}_u\, \Gamma^T + \mathbf{\Sigma}_v, \tag{4.3}$$

where

$$\mathbf{\Sigma}_y = \mathbf{E}\{y\, y^T\}, \tag{4.4a}$$
$$\mathbf{\Sigma}_u = \mathbf{E}\{u\, u^T\}, \tag{4.4b}$$
$$\mathbf{\Sigma}_v = \mathbf{E}\{v\, v^T\}. \tag{4.4c}$$

However, the process variances in (4.3) may change its value at the moment when certain piece i is manufactured. This is due to different effects such as the wear and tear to which the MMP is prone. Then, we can no longer consider the MMP as a stationary process and we rewrite (4.3) as

$$\mathbf{\Sigma}_y(i) = \Gamma\, \mathbf{\Sigma}_u(i)\, \Gamma^T + \mathbf{\Sigma}_v(i), \tag{4.5}$$

where $\mathbf{\Sigma}_y(i)$, $\mathbf{\Sigma}_u(i)$ and $\mathbf{\Sigma}_v(i)$ denote the covariance of the measurements, the variation sources and the measurements noises at the moment when certain piece i is processed, i.e.,

$$\mathbf{\Sigma}_y(i) = \mathbf{E}\{y(i)\, y(i)^T\}, \tag{4.6a}$$
$$\mathbf{\Sigma}_u(i) = \mathbf{E}\{u(i)\, u(i)^T\}, \tag{4.6b}$$
$$\mathbf{\Sigma}_v(i) = \mathbf{E}\{v(i)\, v(i)^T\}. \tag{4.6c}$$

Remark 4.1. *The variables $\mathbf{\Sigma}_y(i)$, $\mathbf{\Sigma}_u(i)$ and $\mathbf{\Sigma}_v(i)$ defined in* (4.6) *are time-varying stochastic variances [158, 186] and they represent the variance of y, u and v for a population of pieces manufactured at the manufacturing conditions of the i-th piece.*

Taking [78] as reference, in this chapter we assume that:

- The underlying distributions of u and v are Gaussian.
- The input vector u is zero-mean since it represents the deviation from the designed nominal position. The variation sources are independent, so that u has a diagonal non-stationary covariance matrix, i.e.,

$$\mathbf{\Sigma}_u(i) = \begin{bmatrix} \sigma_u^2(i)[1] & & 0 \\ & \ddots & \\ 0 & & \sigma_u^2(i)[n_u] \end{bmatrix},$$

  where $\sigma_u^2(i)[p]$ represents the dimensional variance of the p-th variation source of the MMP, i.e., $p = \{1, ..., n_u\}$, at the moment where the i-th piece is manufactured.

- The noise vector v is zero-mean, independent of u and it has a diagonal non-stationary covariance matrix,

$$\mathbf{\Sigma}_v(i) = \begin{bmatrix} \sigma_v^2(i)[1] & & 0 \\ & \ddots & \\ 0 & & \sigma_v^2(i)[n_y] \end{bmatrix},$$

  where $\sigma_v^2(i)[r]$ represents the dimensional variance of the noise of the r-th sensor of the process, i.e., $r = \{1, ..., n_y\}$, at the moment where the i-th piece is manufactured.

- As many works in the field (e.g., [78]), we assume that all the measurement noises have the same variance. Then, we rewrite $\mathbf{\Sigma}_v(i)$ as

$$\mathbf{\Sigma}_v(i) = \sigma_v^2(i)\, I_{n_y},$$

with $\sigma_v^2(i)$ being a scalar that denotes this shared process variance. It is straightforward to extend the results in this chapter to the case where the sensor noises are characterized by different variances[1].

For the sake of readability, we denote the components of $\mathbf{\Sigma}_u(i)$ and $\mathbf{\Sigma}_v(i)$ as $\sigma^2(i)[j]$ with $j = \{1 \dots n_j\}$ and $n_j = n_u + 1$, i.e.,

$$\sigma^2(i)[j] \equiv \begin{cases} \sigma_u^2(i)[j], & j < n_j, \\ \sigma_v^2(i), & j = n_j. \end{cases}$$

The stationary process variance estimator as the ones studied in [78] (i.e., the Least-Squares fit estimator (LSE), the estimator in Apley and Shi (ASE) [11], the estimator in Ding, Shi and Ceglarek (DSCE) [77] and the estimator presented in Stoica and Nehorai (SNE) [276]) use the sampling variance of a batch of N pieces, i.e.,

$$S_y = \frac{\sum_{i=1}^{N} y(i)\, y(i)^T}{N}, \tag{4.7}$$

as an estimate of $\mathbf{\Sigma}_y$ in (4.3). For the study of a non-stationary process, we could propose to infer a time-varying population variance every time that a new piece i is manufactured. If we used the sample provided by the batch of the last N pieces, an estimation of $\mathbf{\Sigma}_y(i)$ in (4.5) would be given by

$$S_y(i) = \frac{\sum_{\iota=i-N}^{i} y(\iota)\, y(\iota)^T}{N}. \tag{4.8}$$

The use of (4.8) is computationally costly since a large sample size (i.e., the data provided by a batch of N pieces) is used for guaranteeing accurate estimates of the process variances $\sigma^2(i)[j]$ and no individual control over the accuracy of each process variance estimate is available. For its part, the use of a sample of large size in (4.7) for ensuring accurate estimates delays the estimation of variance changes and thus the decision of whether the process has experienced faults or not. In this chapter, we propose an alternative strategy for identifying the components of $\mathbf{\Sigma}_u(i)$ and $\mathbf{\Sigma}_v(i)$ and their possible changes taking into account

- the accuracy of the estimations,
- the time needed to track their changes,
- the computational cost,
- the data storage,
- the design flexibility.

To fulfil these requirements we develop a model for MMPs which includes the non-stationary behavior of the process variances $\sigma^2(i)[j]$ and enables the application of observer-based strategies. These strategies allow us to incrementally improve the accuracy of the estimates $\hat{\sigma}^2(i)[j]$ with the data provided by each new piece without the need of storing or using the data of the previous pieces in the computation.

[1] It is well known that the maximum number of different process variances which can be estimated depends on the structural properties of the MMP under consideration. See [70, 337] for studying the diagnosability issues of each case.

4.3 Variation propagation model

In order to develop a model for MMPs with non-stationary process variances of the variation sources and noises we exploit the Gaussian nature of $u(i)$ and $v(i)$ in (4.2). Let us first introduce the following lemma.

Lemma 4.1. *([128]) Let $g(i) \in \mathbb{R}^{n_g}$ be a vector of zero-mean independent Gaussian noises, i.e.,*

$$g(i) \sim \mathcal{N}(0, \mathbf{\Sigma}_g(i)), \tag{4.9}$$

with $\mathbf{\Sigma}_g(i)$ being certain diagonal and varying covariance. If $g_u(i)$ denotes the vector including n_g zero-mean independent Gaussian noises of unitary covariance, i.e.,

$$g_u(i) \sim \mathcal{N}(0, I_{n_g}),$$

vector $g'(i)$ defined as

$$g'(i) = \mathbf{\Sigma}_g(i)^{\frac{1}{2}}\, g_u(i) \tag{4.10}$$

is distributed as (4.9)*.*

Applying Lemma 4.1, the random signals $u(i)$ and $v(i)$ in (4.2) can be rewritten as

$$u(i) = D(i)\,\eta(i), \qquad v(i) = R(i)\,\nu(i). \tag{4.11}$$

where

$$\eta(i) = \begin{bmatrix} \eta(i)[1] \\ \vdots \\ \eta(i)[n_u] \end{bmatrix},\ \nu(i) = \begin{bmatrix} \nu(i)[1] \\ \vdots \\ \nu(i)[n_y] \end{bmatrix}$$

are column vectors containing independent zero-mean Gaussian sequences with unitary time-invariant covariances, i.e.,

$$\mathbf{E}\{\eta(i)\} = 0_{n_u},\ \mathbf{E}\{\eta(i)\,\eta(i)^T\} = I_{n_u}, \tag{4.12a}$$

$$\mathbf{E}\{\nu(i)\} = 0_{n_y},\ \mathbf{E}\{\nu(i)\,\nu(i)^T\} = I_{n_y}, \tag{4.12b}$$

$$\mathbf{E}\{\eta(i)\,\nu(i)^T\} = 0_{n_u \times n_y}. \tag{4.12c}$$

Matrix $D(i)$ contains the standard deviation of the components of $u(i)$, i.e.,

$$D(i) = \begin{bmatrix} \sigma_u(i)[1] & & 0 \\ & \ddots & \\ 0 & & \sigma_u(i)[n_u] \end{bmatrix},$$

and fulfils

$$D(i)\,D(i)^T = \mathbf{\Sigma}_u(i).$$

The same applies to matrix $R(i)$ w.r.t. $v(i)$ (i.e., $R(i) = \sigma_v(i)\ I_{n_y}$). Note that signals $\eta(i)$ and $\nu(i)$ represent the Gaussian variations in $u(i)$ and $v(i)$ while $D(i)$ and $R(i)$ describe the size of

these variations. Applying the decomposition in (4.11), the linear replicated model (4.2) results in

$$y(i) = \begin{bmatrix} \Gamma\, D(i) & R(i) \end{bmatrix} \begin{bmatrix} \eta(i) \\ \nu(i) \end{bmatrix}. \tag{4.13}$$

Defining matrices

$$\Psi(i) = \begin{bmatrix} \Gamma\, D(i) & R(i) \end{bmatrix},\ \zeta(i) = \begin{bmatrix} \eta(i) \\ \nu(i) \end{bmatrix},$$

we rewrite (4.13) as

$$y(i) = \Psi(i)\, \zeta(i). \tag{4.14}$$

For process variance estimation, the information of interest resides in the diagonal terms of the quadratic expression of (4.13). Let us then define the output vector $m(i) \in \mathbb{R}^{n_y}$ as

$$m(i) = y(i) \circ y(i) \equiv \mathrm{diag}\{y(i)\, y(i)^T\}, \tag{4.15}$$

verifying

$$m(i) = \mathrm{diag}\{\Psi(i)\, \zeta(i)\, \zeta(i)^T\, \Psi(i)^T\}. \tag{4.16}$$

Note that $m(i)$ depends on the process variances that we want to estimate. If we define $q(i)$ as the column vector stacking these variances, i.e.,

$$q(i) = \begin{bmatrix} \sigma^2(i)[1] \\ \vdots \\ \sigma^2(i)[n_j] \end{bmatrix} \in \mathbb{R}^{n_j},$$

being $\sigma(i)[j]$ the elements of $D(i)$ and $R(i)$ and, thus, included in $\Psi(i)$, the expected value of $m(i)$ satisfies

$$\mathbf{E}\{m(i)\} = H\, q(i), \tag{4.17}$$

with

$$H = [\Gamma^{\circ 2}\ \ \mathbf{1}_{n_y}] \in \mathbb{R}^{n_y \times n_j},$$

where we have taken into account that $\mathbf{E}\{\zeta(i)\, \zeta(i)^T\} = I_{n_u+n_y}$ (see Appendix D.1.1).

For modeling the non-stationary behavior of the process variances, we propose the following dynamics of the state vector $q(i)$:

$$q(i) = q(i-1) + \Delta q(i-1), \tag{4.18}$$

where

$$\Delta q(i) = \begin{bmatrix} \Delta\sigma^2(i)[1] \\ \vdots \\ \Delta\sigma^2(i)[n_j] \end{bmatrix} \in \mathbb{R}^{n_j}$$

takes account of the process variance differences between two consecutive pieces i and $i+1$. Dynamics of the form of (4.18) have been widely used in the literature to analyse the behavior of estimation algorithms for non-stationary processes. Note that equation (4.18) allows modeling every kind of change experienced by the variables $q(i)[j]$ provided an appropriate form of the

signals $\Delta q(i)[j]$. For instance, abrupt changes in $q(i)[j]$ are produced by impulse signals $\Delta q(i)[j]$ (i.e., $\Delta q(i)[j]$ is only nonzero at the time of the fault appearance), drift changes in $q(i)[j]$ are produced by step signals $\Delta q(i)[j]$ ($\Delta q(i)[j]$ takes a constant value during the fault existence) and parabolic changes in $q(i)[j]$ are produced by ramp signals $\Delta q(i)[j]$.

Thus, the estimations provided by an estimator which takes equation (4.18) into account would vary in value when any kind of fault form appears in the system. However, such estimator only guarantees estimations with zero-mean steady-state errors when abrupt changes affect the system [155, 163, 249]. Thus, the estimations are unbiased when no changes occur and when abrupt changes affect the system. If more general changes occurred, the steady-state estimation errors would not be zero-mean. For instance, if drift changes took place the steady-state estimation errors would be constant [307]). In any case, however, the estimations would vary in value and the changes experienced by the variables $q(i)[j]$ would be detected.

Remark 4.2. *If zero-mean estimation errors were required for changes beyond abrupt deviations, a more general model in the form of*

$$\xi(i) = A_Q\,\xi(i-1) + B_Q\,\Delta q(i-1), \tag{4.19a}$$

$$q(i) = C_Q\,\xi(i) + D_Q\,\Delta q(i), \tag{4.19b}$$

should be considered. In (4.19)*, $\xi(i) \in \mathbb{R}^{n_\zeta}$ is an auxiliary state vector of an appropriate dimension so that the dynamics of the forecast changes can be produced through some matrices (A_Q, B_Q, C_Q, D_Q) and impulse signals $\Delta q(i)$. See [162, 306, 307] for details on the derivation of these models.*

4.4 Estimation of process variance

4.4.1 Model-based observer

For achieving non-stationary process variance estimation, we use a model-based observer. Based on the model defined by equations (4.16)-(4.18), we set up the following estimation algorithm. First, we define $\hat{q}(i)$ as the vector that contains the estimation of $q(i)$, i.e., the process variance estimation. Second, we obtain $m(i)$ with the acquired measurements for piece i using expression (4.15). Then, we estimate $m(i)$ using the last estimated process variance $\hat{q}(i-1)$ and the expression of its expected value given by (4.17), which involves the model information H:

$$\hat{m}(i) = H\,\hat{q}(i-1). \tag{4.20}$$

Finally, we update the process variance estimation with the difference between the measured and estimated output through

$$\hat{q}(i) = \hat{q}(i-1) + L(i)\,\left(m(i) - \hat{m}(i)\right), \tag{4.21}$$

where $L(i)$ is the updating gain matrix which defines the weight between the output prediction error and the last estimated process variance. We define the state estimation error as $\widetilde{q}(i) = q(i) - \hat{q}(i)$ and its dynamics is given by

$$\widetilde{q}(i) = \widetilde{q}(i-1) + \Delta q(i-1) - L(i)\,(m(i) - H\hat{q}(i-1)). \tag{4.22}$$

If we add and subtract $Hq(i)$ to the difference $m(i) - H\hat{q}(i-1)$ in (4.22), the dynamics of $\widetilde{q}(i)$ can be expressed as

$$\widetilde{q}(i) = \Big(I_{n_j} - L(i)\,H\Big)\,(\widetilde{q}(i-1) + \Delta q(i-1)) - L(i)\,t(i), \tag{4.23}$$

with

$$t(i) = m(i) - H\,q(i) \tag{4.24}$$

being a zero-mean random variable as it derives from the difference between $m(i)$ and its expected value.

Remark 4.3. *Notice that an estimate $\hat{q}(i)$ may be negative for some piece i (i.e., $\hat{q}(i) < 0$). Provided that $q(i)$ is a vector stacking variance values and it cannot be negative, we postprocess $\hat{q}(i)$ so as to provide a refined estimate of $q(i)$, which we denote as $\hat{q}_p(i)$:*

$$\hat{q}_p(i) = \begin{cases} \hat{q}(i) & \text{if } \hat{q}(i) \geq 0 \\ 0 & \text{otherwise} \end{cases}.$$

4.4.2 Observer design

In this section, we propose a design of the gain $L(i)$ of the estimation algorithm (4.21). Note that the dynamics in (4.23) can be seen as the estimation error dynamics which is achieved when applying a state observer to a linear system with $\widetilde{q}(i)$ being the state estimation error, $\Delta q(i)$ the process noise, $t(i)$ the measurement noise, I_{n_j} the state matrix and H the output matrix. As the considered process noise $t(i)$ depends on the state, the error dynamics is not linear and simple designs with a constant gain $L(i)$ (as pole placement techniques or stationary Kalman filter approaches) cannot be applied. We then propose a Kalman filter that takes account of the dependence of the noise $t(i)$ on the state which is being estimated (see Appendix D.1.2 and references [52,119] for derivation details). The Kalman gain for observer (4.21) can be computed as

$$\bar{P}(i) = \hat{P}(i-1) + Q(i-1), \tag{4.25a}$$

$$L(i) = \bar{P}(i)\,H^T\,\Big(H\,\bar{P}(i)\,H^T + T(i)\Big)^{-1}, \tag{4.25b}$$

$$\hat{P}(i) = \Big(I_{n_j} - L(i)\,H\Big)\,\bar{P}(i), \tag{4.25c}$$

with

$$Q(i) = \mathbf{E}\{\Delta q(i)\,\Delta q(i)^T\},\;\; T(i) = \mathbf{E}\{t(i)\,t(i)^T\},$$

and where $\hat{P}(i)$ represents the expected covariance of the state estimation error, i.e.,

$$\hat{P}(i) = \mathbf{E}\{\widetilde{q}(i)\,\widetilde{q}(i)^T\}.$$

Remark 4.4. *A necessary condition for the stability of observer* (4.21) *is that the pair (I_{n_j}, H) is observable, which means that the process variances considered in $q(i)$ are diagnosable. This condition is verified whenever the output matrix H verifies*

$$\text{rank}\{H\} \geq n_j. \tag{4.26}$$

For computing the covariances $Q(i)$ and $T(i)$ involved in (4.25), the following considerations should be taken into account.

- Operating algebraically and taking account of the Gaussian nature and the statistical properties (4.12) of the noises $\zeta(i)$, one gets that the covariance matrix $T(i)$ is given by

$$T(i) = (\Psi(i)\,\Psi(i)^T)^{\circ 2}. \tag{4.27}$$

  Relation (4.27) shows the dependence of $T(i)$ on the values $\sigma(i)[j]$ and, thus, on the state vector $q(i)$, which is to be estimated. Provided the slow-varying character of $q(i)$, we have that, in general, $T(i) \simeq T(i-1)$. Then, we propose to approximate covariance $T(i)$ of a piece i by its predicted value from piece $i-1$, i.e.,

$$T(i) \approx \hat{T}(i-1). \tag{4.28}$$

  Matrix $\hat{T}(i-1)$ is computed through (4.27) with the values in the available postprocessed estimated vector $\hat{q}_p(i-1)$.

- The covariance matrix $Q(i)$ is unknown and it can be seen as a multivariate tuning parameter that fixes the performance of the observer. If matrix $Q(i)$ is chosen to be diagonal, as the value of certain element $Q(i)[j,j]$ decreases, the steady-state accuracy of the corresponding estimate improves because the filter is more focused on rejecting the variations $t(i)$. Respectively, if $Q(i)[j,j]$ increases, the tracking ability improves at the cost of a lower measurement noise rejection. For ensuring that $Q(i)$ is in an appropriate order of magnitude, we compute its elements as

$$Q(i) = \Upsilon\,\hat{P}(i)\,\Upsilon, \tag{4.29}$$

  with

$$\Upsilon^2 = \begin{bmatrix} \upsilon_1 & & 0 \\ & \ddots & \\ 0 & & \upsilon_{n_j} \end{bmatrix}$$

  and $\upsilon_j \in [0,1]$ chosen according to the desired performance. This leads to equation (4.25a) as

$$\bar{P}(i) = \hat{P}(i-1) + \Upsilon\,\hat{P}(i-1)\,\Upsilon. \tag{4.30}$$

  Note that equation (4.30) excites more algorithm (4.25) when less knowledge of the states is available and, therefore, $\hat{P}(i)$ has a bigger value. This enhances the initialization of the algorithm.

Remark 4.5. *The proposed algorithm implies computing equations* (4.25) *and* (4.21) *with* $m(i) = y(i)^{\circ 2}$ *every time that a new piece* i *is manufactured in the MMP. At steady state, however, the gain matrix* $L(i)$ *is stationary. For reducing the computational burden, one can use the expressions*

$$L(i) = L(i-1),\ \hat{P}(i) = \hat{P}(i-1), \tag{4.31}$$

instead of (4.25) *whenever* $|\hat{q}(i-1) - \hat{q}(i-2)| \leq \boldsymbol{\Delta}$ *for some given difference* $\boldsymbol{\Delta}$.

Remark 4.6. *Note that algorithm* (4.25) *provides a suboptimal Kalman gain due to the previous approximations and because* $\Delta q(i)$ *is non-zero when process variance changes occur. In any case, the previous design procedure presents the advantage of containing some numerical tuning parameters which can be used to set the trade-off between different estimation performance parameters.*

4.4.3 Estimator properties

The performance of the estimator depends on both the steady-state accuracy and on the delay in tracking the changes defined by $\Delta q(i)$.

Steady-state behavior

Provided the unbiasedness of the estimator in fault-free scenarios (see Section 4.3), the accuracy of the estimator (4.21) when $\Delta q(i) = 0$ is given by the variance of the estimation errors, which we denote as ϕ_j, i.e.,

$$\phi_j = \mathbf{Var}\{\widetilde{q}(i)[j] \mid \Delta q(i) = 0\}. \tag{4.32}$$

The steady-state covariance of the estimation errors due to noises, which we denote as P, is the solution of the following Riccati equation:

$$P = \left(I_{n_j} - \bar{P}\, H^T \left(H\, \bar{P}\, H^T + T\right)^{-1} H\right) \bar{P}, \tag{4.33}$$

with $\bar{P} = P + \Upsilon\, P\, \Upsilon$, and where T is the noise covariance at certain steady state. If we choose matrix Υ to have equal terms (i.e., $\upsilon_j = \upsilon,\ \forall j$), the covariance matrix of the steady-state error is given by

$$P = \frac{\upsilon}{\upsilon + 1}(H(\mathbf{\Sigma}_y \circ \mathbf{\Sigma}_y)^{-1} H^T)^{-1}. \tag{4.34}$$

See Appendix D.1.3 for the derivation of this expression. From (4.34), we deduce that the accuracy of the estimations improves as the design variables υ_j decrease.

Transient behavior

The transient behavior of the estimator can be characterized by the number of pieces whose data must be fed to the estimator in order to track certain change $\Delta q(i)[j]$. We define the settling time of the estimator, which we denote as $\eta_{90,j}$, as the number of pieces which are needed so that $\hat{q}[j]$ changes the 90% of the change experienced by $q[j]$ with $t(i) = 0$. We can also describe the tracking ability of the estimator in terms of the cumulative squared error (CSE) experience by the j-th estimation due to process variance changes and which we define as

$$\varphi_j = \sum_{i=1}^{\infty} \{\widetilde{q}^2(i)[j] \mid t(i) = 0\}. \tag{4.35}$$

According to [191], the response of (4.21) when a unitary step change $\Delta q[j](i)$ occurs is like the response of a first-order system $g(i)$ defined as $g(i) = 1 - (1 + \upsilon_j)^{-i}$ when $t(i) = 0$. In this sense,

the settling time and the CSE of the estimator due to unitary step changes are approximately given by

$$\eta_{90,j} = \frac{-\log(0.1)}{\log(1+\upsilon_j)}, \tag{4.36a}$$

$$\varphi_j = \frac{(1+\upsilon_j)^2}{(1+\upsilon_j)^2 - 1}, \tag{4.36b}$$

see [117]. From (4.36), we deduce that the tracking ability regarding the estimation of $q[j]$ improves when υ_j is increased.

Remark 4.7. *Similarly to $\eta_{90,j}$ we can define $\eta_{\rho,j}$ as the number of pieces which are needed so that $\hat{q}[j]$ achieves the $\rho\%$ of the change experienced by $q[j]$ with $t(i) = 0$ as*

$$\eta_{\rho,j} = \frac{-\log\left(\frac{100-\rho}{100}\right)}{\log(1+\upsilon_j)}. \tag{4.37}$$

4.4.4 Performance-based observer design

As seen in Section 4.4.3, matrix Υ enhances the accomplishment of certain trade-off between the transient and the steady-state tracking performance. Relations (4.36a), (4.36b) and (4.33) can be used to choose the values υ_j $(j = 1, \ldots, n_j)$ so as to set certain trade-off regarding the performance of the estimator. For instance, in order to set certain settling time for the estimation of a unitary step change in $q[j]$, the variable υ_j must be fixed to

$$\upsilon_j = 0.1^{-1/\eta_{90,j}} - 1. \tag{4.38}$$

4.5 Statistical hypothesis testing for fault diagnosis

In steady state (i.e., when no process variance changes occur), we denote the confidence interval offered by an estimate $\hat{q}(i)[j]$ for $q(i)[j]$ as

$$\Omega_j(i) = [\hat{q}(i)[j] - h_j \,,\, \hat{q}(i)[j] + h_j], \tag{4.39}$$

where h_j depends on the confidence level of the interval, $\gamma_j = 1 - \alpha_j$, and on the variance of the estimation $\hat{q}(i)[j]$. Note that, in steady state, the marginal variance of the estimation $\hat{q}[j]$ is $P[j,j]$, which can be obtained through equation (4.33).

Through Chebyshev's inequality [238], we have that

$$\mathbf{Pr}\{q(i)[j] \notin \Omega_j(i)\} \leq P[j,j]/h_j^2. \tag{4.40}$$

Then, if we set h_j as

$$h_j = \sqrt{P[j,j]/\alpha_j^*}, \tag{4.41}$$

we guarantee a bound $\alpha_j \leq \alpha_j^*$ for the confidence level of the interval $\Omega_j(i)$.

Relation (4.40) holds regardless of the probability distribution of $\hat{q}(i)[j]$. We know, however, that when $\Delta q(i) = 0$, the estimation $\hat{q}(i)$ can be expressed as the infinite weighted sum

$$\hat{q}(i) = -\sum_{\iota=1}^{i} \prod_{\kappa=\iota+1}^{i} \Big(I_{n_j} - L(\kappa)\, H\Big)\, L(\iota) t(\iota). \tag{4.42}$$

where the terms $-\prod_{\kappa=\iota+1}^{i} \Big(I_{n_j} - L(\kappa)\, H\Big)\, L(\iota)$ represent the weighting factors and $t(\iota)$ are independent and identically distributed zero-mean random variables with finite variance. One can demonstrate that the sequence of these weighting factors fulfils the conditions on [300] and then one can claim that $\hat{q}(i)$ approaches a normal distribution. Provided these results, we can set h_j to fix the confidence level γ_j to $1 - \alpha_j^*$ as

$$h_j = \Phi_Z^{-1}(1 - \alpha_j^*/2)\, \sqrt{P[j,j]}, \tag{4.43}$$

with $\Phi_Z^{-1}(\cdot)$ being the inverse cumulative distribution function of a standard normal variable. This confidence level is tightener than the one obtained in (4.40) through Chebyshev's inequality.

Remark 4.8. *Provided that $q(i) \geq 0$, we postprocess the value of the limits of $\Omega_j(i)$ so as to provide a refined confidence interval of $q(i)[j]$, which we denote as $\Omega_{j,p}(i)$:*

$$\Omega_{j,p}(i) = \begin{cases} [\hat{q}(i)[j] - h_j\,,\, \hat{q}(i)[j] + h_j] & \text{if } \hat{q}(i)[j] \geq h_j \\ [0\,,\, \hat{q}(i)[j] + h_j] & \text{otherwise} \end{cases}. \tag{4.44}$$

Note that when we use the refined confidence interval $\Omega_{j,p}(i)$ in (4.44) *and h_j is defined through* (4.41)*, we guarantee a bound $\alpha_j \leq \alpha_j^*$ which is looser than the bound which is guaranteed for $\Omega_j(i)$ in* (4.39) *(i.e., the difference between α_j and α_j^* is larger). Similarly, if h_j is defined through* (4.43) *and we use the interval $\Omega_{j,p}(i)$ in* (4.44)*, we just guarantee a bound $\alpha_j \leq \alpha_j^*$ instead of fixing its value to $\alpha_j = \alpha_j^*$ as happens with $\Omega_j(i)$ in* (4.39)*. Thus, if we use $\Omega_{j,p}(i)$ in* (4.44)*, the real confidence level is larger than the one that we have with $\Omega_j(i)$.*

In order to determine whether a process variance of the MMP $q[j]$ has experienced a change $\Delta q[j]$ (i.e., a fault j has appeared), we set the following statistical hypothesis test, where we use $i = 0$ to refer to a piece for which the estimator has achieved the steady state and that has been manufactured with healthy conditions in the MMP:

$$\begin{cases} \mathbf{H_0}: & q(i)[j] \in \Omega_j(0) \\ \mathbf{H_1}: & q(i)[j] \notin \Omega_j(0) \end{cases}. \tag{4.45}$$

Here, the null hypothesis stands for "No change of the j-th process variance" (i.e., "No fault j") and the alternative hypothesis stands for "Change of the j-th process variance" (i.e., "Fault j").

4.6 Comparison with batch-based estimators

As explained in Section 4.2, the batch-based estimators such as the LSE or DSE are offline estimators which are conceived for periodically verify the state of the process. In the following, we compare the properties of these offline estimators with the characteristics of the proposed online approach.

- *Accuracy of the estimations.* In fault-free scenarios, the variance of the estimates provided by batch-based estimators is proportional to $1/N$ (see [78] for details on the corresponding expressions). When using the proposed approach, the variance of the estimates is proportional to $\upsilon/(\upsilon+1)$ if every υ_j is fixed to a common value υ (see (4.34)).
- *Time to track changes.* The delay in tracking changes with the proposed online approach is approximately given by the settling time of the estimator which is defined by the number of pieces $\eta_{98,j}$ in (4.36a) and it is inversely proportional to υ_j. For its part, offline batch-based methods just ensure the diagnosis of a fault if a whole batch of faulty pieces is used in the computation of S_y through (4.7). Then, these methods cannot ensure a tracking delay lower than $2\,N$. Moreover, provided the non-zero variance of the estimates, the manufacturer might not state that a fault has occurred until certain number κ of consecutive faulty estimations are available. In such a case, the number of faulty pieces which must be manufactured in order to state that a fault has occurred is $\eta_{98,j}+\kappa-1$ if the proposed approach is used and $\kappa\,N$ if offline estimators are used.

From these two considerations, we deduce that the existing trade-off between the accuracy of the estimations and their ability to track changes can be set through ν_j for the proposed approach (as explained in Section4.4.3) and through N for batch-based methods . If N is reduced (or if ν_j is increased), the tracking ability increases at the cost of lower estimation accuracies. For accuracies in the same order of magnitude (i.e., $\frac{1}{N}=\frac{\upsilon}{\upsilon+1}$), the time to track changes is $\kappa\,\frac{(\upsilon+1)}{\upsilon}$ for batch-based methods and $\kappa-1-\frac{\log(0.02)}{\log(1+\upsilon_j)}$ for the proposed approach. The tracking ability is thus in the same order of magnitude for both methods if $\kappa=1$ and it gets better for the proposed approach as κ is increased.

Remark 4.9. *Note that if big faults affect the system, it is not necessary that $\hat{q}[j]$ changes the 90% of the change experienced by $q[j]$ in order to detect a fault. If we use $\eta_{\rho,j}$ with $\rho<90$ instead of $\eta_{90,j}$ for the characterization of the tracking ability of the model-based observer, the time that we need in order to detect changes is exponentially reduced. Contrariwise, in no case this time is lower than $(\kappa-1)\,N$ for batch-based methods.*

As stated in Section 4.2, when it comes to estimators, other matters of fact are the computational burden, the volume of stored data and the design flexibility, which are now compared for both methods.

- *Computational Burden.* The algorithms of batch-based estimators (i.e., the LSE and the ASE) require N vector product and summation operations, which are time-consuming.

As the accuracy of such methods improves when N is increased, it happens that there exists a trade-off between the accuracy of the estimations and the computational time of such methods. The computational burden of the proposed observer does not depend on the performance of the estimator because the variance of the estimation can be simply modified by changing the values in Υ. Thus, the computational time is independent of the performance of the estimator.

- *Data Storage.* The sample size of the proposed approach only contains the data of the last manufactured piece. Thus, when certain piece i is manufactured the stored data is $\hat{q}(i-1)$ and $y(i)$. For its part, the sample size of offline approaches contain the data of the last N manufactured piece. Thus, when certain piece i is manufactured the stored data is $y(i-N+1), y(i-N+1), \ldots, y(i-1), y(i-2)$. Again, there exists a trade-off between the accuracy of the estimations and the amount of stored data which is not present in observer-based methods.

- *Design Flexibility.* The trade-off between the ability to track changes and the accuracy of the estimations is collectively set by N for all the estimations $\hat{q}[j]$. Oppositely, this trade-off is individually set by ν_j for each the estimations $\hat{q}[j]$. Thus, the proposed approach enhances the use of different estimations performance requirements for each $q[j]$.

4.7 Case of study

In this section, we set up different assembly processes in order to apply the strategies presented at the previous sections. Even if these processes are simple, the modeling and estimation framework is fairly general and it can be applied to more complex processes.

4.7.1 Single-stage assembly process

First, we study a single-stage automotive body assembly described and modeled by Apley and Shi [11] and studied by Ding et al. [78]. In this single-stage case ($M = 1$), an optical coordinate measuring machine (OCMM) provides 9 measurements ($n_y = 9$). The pieces at this stage are fixed by a 4-way locator, P_1, which produces positioning variability in two directions (i.e., δP_1^x and δP_1^z) and by a 2-way locator, P_2, which only produces positioning variability in one direction (i.e., δP_2^z); thus, $u_k = [\delta P_{1,k}^x \; \delta P_{1,k}^z \; \delta P_{2,k}^z]^T$ and $n_u = 3$. The replicated matrix Γ is

$$\Gamma = \begin{bmatrix} 0.093 & 0.577 & -0.120 \\ 0 & 0 & 0 \\ -0.093 & 0 & 0.843 \\ 0.093 & 0.577 & -0.120 \\ 0 & 0 & 0 \\ 0.647 & 0 & -0.120 \\ -0.370 & 0.577 & 0.482 \\ 0 & 0 & 0 \\ 0.647 & 0 & -0.120 \end{bmatrix}.$$

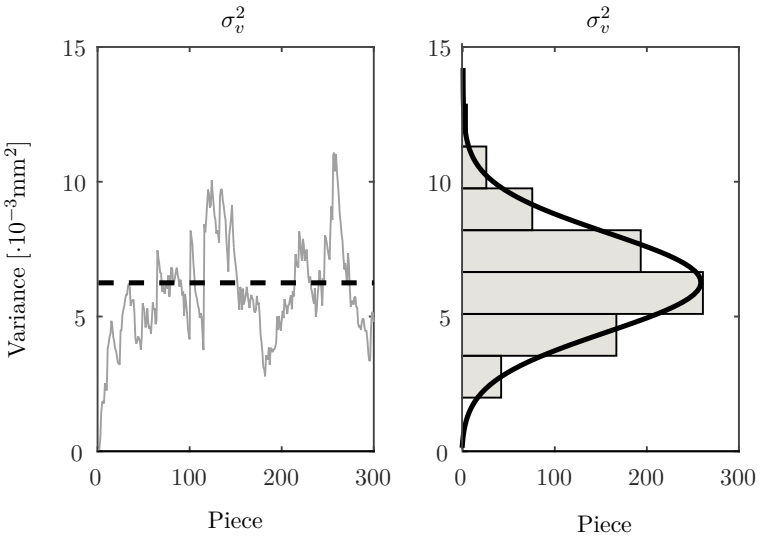

Figure 4.2. Stationary process variance estimation of σ_v^2 ($\upsilon_4 = 0.05$) in the single-stage assembly process. Real (- -), Estimation (Gray —), Fitted Gaussian distribution (Black —).

The sensor accuracy is $(6\sigma)_{sensor} = 0.1$ mm and the tolerance of the pinholes is 0.2 mm. If the tolerance is approximated by the six-sigma value; then, $(6\sigma)_{locator} = 0.2$ mm.

First, we simulate a stationary process of 300 pieces with $q = \begin{bmatrix} 1.1 & 2.5 & 04.4 & 0.6 \end{bmatrix}^T \cdot 10^{-3}$ mm^2 (values taken from [78]). The left-hand side of Fig. 4.2 shows the estimation results for $q[4]$ (i.e., $\hat{q}_p[4]$) when applying an observer with $\Upsilon^2 = 0.05\, I_4$ in (4.29). On the right-hand side of Fig. 4.2, we look at the shape of the probability distribution of $\hat{q}_p[4]$ when running 50 simulation trials and we compare it with a fitted normal density proving a high goodness of fit of the Gaussian distribution. Similar results apply to the other variance estimations $\hat{q}_p[j]$ with $j = \{1, 2, 3\}$, which we do not include due to space constraints. The variance of the estimations provided by different observers are shown in Table 4.1.

In order to compare the proposed online estimators with the process variance estimators based on the sampling variance of a batch of N pieces, we apply these estimators online by inferring a time-varying population variance every time that a new piece i is manufactured from $S_y(i)$ computed through (4.8) (i.e., every time that a new piece i is entirely measured, the estimation is made with the data provided by this piece and by the previous $N-1$ completed pieces). In Fig. 4.3, we compare the relative computational time which is needed to perform the estimation of the previous process for different estimators and different values of the corresponding tuning parameters that lead to different variances of the estimations. As explained in Section 4.6, Fig. 4.3 shows that the computational burden of the proposed observer (KF) does not depend on the performance of the estimator because the variance of the estimation can be simply modified by changing the values in Υ. Oppositely, the algorithms of batch-based estimators (i.e., the LSE and the ASE) require more operations as the estimation accuracy is improved and, thus, the computational time increases with the accuracy. From this figure, we also deduce that the estimator (4.21)-(4.25) is more computationally costly than the LSE and the ASE for estimations of lower accuracies. However, our estimator is more efficient and becomes more

Table 4.1. Variance of the steady-state estimations [$\cdot 10^{-6}$mm^4] for different observers with $\Upsilon^2 = \upsilon\, I_4$.

υ	$\mathbf{Var}\{\hat{q}_p[1]\}$	$\mathbf{Var}\{\hat{q}_p[2]\}$	$\mathbf{Var}\{\hat{q}_p[3]\}$	$\mathbf{Var}\{\hat{q}_p[4]\}$
0.0010	0.0217	0.0103	0.0166	0.0001
0.0152	0.1362	0.1784	0.3443	0.0029
0.0294	0.2322	0.3551	0.6693	0.0051
0.0436	0.3182	0.5384	1.0273	0.0071
0.0579	0.4010	0.7288	1.4120	0.0090
0.0721	0.4880	0.9272	1.8032	0.0109
0.0863	0.5773	1.1415	2.2138	0.0128
0.1005	0.6698	1.3773	2.6695	0.0147
0.1147	0.7640	1.6326	3.1927	0.0167
0.1289	0.8599	1.9116	3.8059	0.0186
0.1431	0.9600	2.2181	4.5634	0.0205
0.1574	1.0698	2.5425	5.5490	0.0224
0.1716	1.1817	2.9035	6.7644	0.0243
0.1858	1.2843	3.3121	8.1135	0.0261
0.2000	1.3797	3.7668	9.6098	0.0280

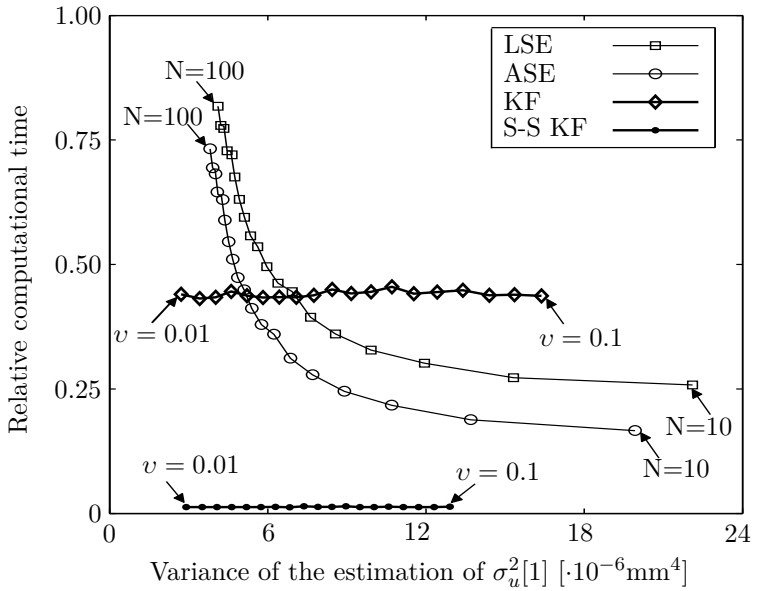

Figure 4.3. Comparison of the computational time which is needed for different estimation accuracies regarding $\sigma_u^2[1]$ at steady state with different estimation strategies.

computationally appealing as the desired accuracy of the estimations is increased. Moreover, if we use relaxation (4.31) (steady-state KF), the computational burden is dramatically reduced for all accuracies.

Fig. 4.4 shows the results provided by three observers with different performance w.r.t. the

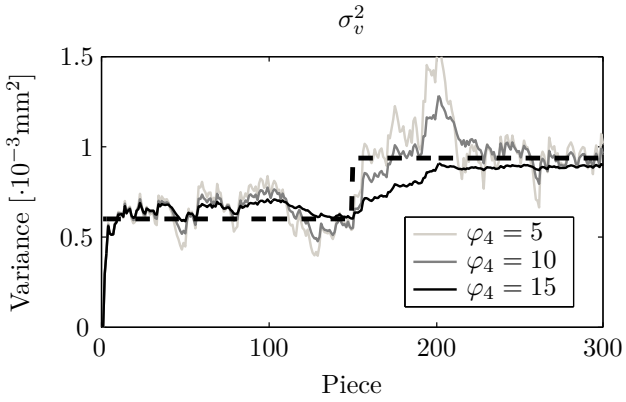

Figure 4.4. Comparison of the performance of different observers used in the single-stage assembly process for the estimation of σ_v^2, which is affected by an abrupt fault. Real (- -), Estimations (—).

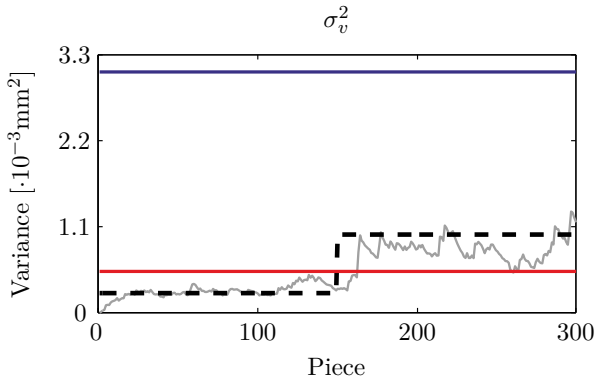

Figure 4.5. Comparison of statistical testing methods with different confidence interval limits ($\gamma_j = 99\%$) for the estimation of σ_v^2 ($\upsilon_4 = 0.05$) in the single-stage assembly process. Real (- -), Estimation (Gray —), Gaussian-based limit (Red —), Chebyshev-based limit (Blue —).

estimation of $q[4]$ when the process of 300 pieces is affected by an abrupt fault which modifies the sensors accuracy from $0.6 \cdot 10^{-3}$ mm^2 to $0.95 \cdot 10^{-3}$ mm^2 at the piece 150. The observers have been designed with requirements over the CSE due to unitary step changes $\Delta q(4)$: $\varphi_4 = 5$ (giving $\upsilon_4 = 0.1$), $\varphi_4 = 10$ (giving $\upsilon_4 = 0.05$) and $\varphi_4 = 15$ (giving $\upsilon_4 = 0.01$). We prove that, as explained in Section 4.4, a smaller CSE (and higher tuning parameter in Υ) results in a better tracking ability at the cost of a lower performance w.r.t. the variance of the process variance estimations. The designer should tune this parameter according to the criticality of the delays in tracking changes.

In Fig. 4.5, we include the estimation results of $q[4]$ provided by the model-based observer designed with $\Upsilon^2 = 0.05\, I_4$ together with the limits of $\Omega_{4,p}(0)$ for both the computation of h_4 through (4.41) and through (4.43) ($\gamma_4 = 99\%$). When no taking account of the Gaussian behavior of the estimations and the limits are computed by means of the Chebyshev's inequality, the confidence interval $\Omega_{4,p}(0)$ is too big and only big variance changes can be detected. On the contrary, the limits of $\Omega_{4,p}(0)$ when computed through (4.43) are tight and smaller faults (as the one being simulated) can be diagnosed.

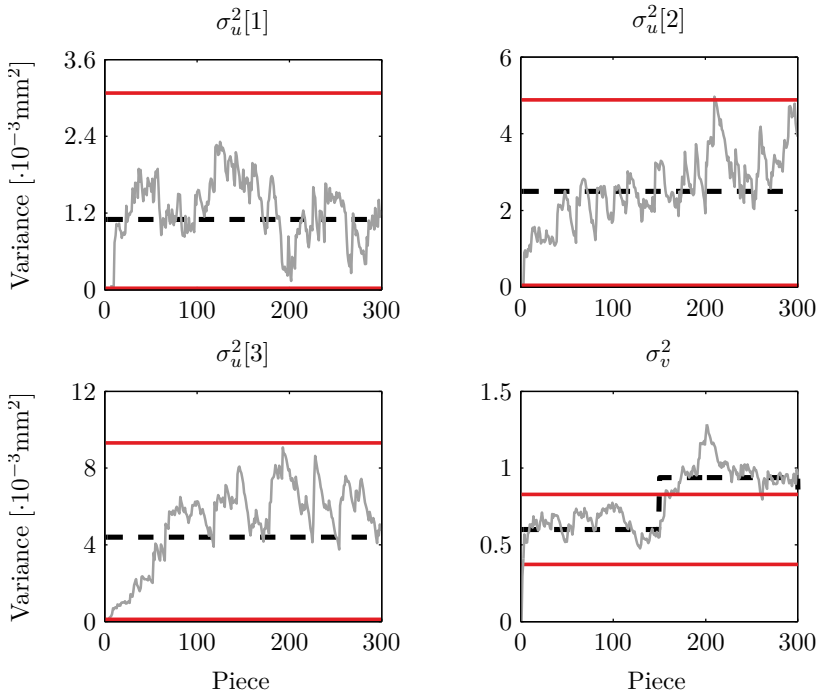

Figure 4.6. Process variance estimation with a model-based observer ($\Upsilon^2 = 0.05\, I_4$) in the single-stage assembly process affected by an abrupt fault in σ_v^2. Real (- -), Estimation (Gray —) Gaussian-based limit with $\gamma_j = 99\%$ (Red —).

Thus, in Fig. 4.6 we include all the estimations provided by the estimator ($\Upsilon^2 = 0.05\, I_4$) for this process with the corresponding the Gaussian-based thresholds of $\Omega_{j,p}(0)$ ($\gamma_j = 99\%$ with $j = \{1, 2, 3, 4\}$). We prove that, although the order of magnitude of the variables involved in $q(i)$ is different, the model-based observer provides appropriate results. Note that the observer depends on $T(i)$, which is a function of $q(i)$ (see (4.25)-(4.27)). Thus, when certain component of $q(i)$ increases its value, so does the variance of the estimations.

Fig. 4.7 shows, for its part, the simulation results (with $\Upsilon^2 = 0.05\, I_4$ and $\gamma_4 = 99\%$) for the process in which we suppose that $\delta P_{1,k}^z$ is affected by an abrupt fault, which doubles its standard deviation from 0.05 mm to 0.1 mm at the piece 150. Then, we have that $q(i)$ in mm^2 is now given by

$$q(i) = \begin{cases} \begin{bmatrix} 1.1 & 2.5 & 4.4 & 0.6 \end{bmatrix}^T \cdot 10^{-3} & \text{if } \; i \in [0, 150) \\ \begin{bmatrix} 1.1 & 10 & 4.4 & 0.6 \end{bmatrix}^T \cdot 10^{-3} & \text{if } \; i \in [150, 300] \end{cases} .$$

As shown in the corresponding figure, the presence of this fault is diagnosed in 52 pieces. If for the simulated fault ($\Delta q[3] = 7.5 \cdot 10^{-3}$ mm^2) this number of corrupted pieces is critical, the designer may decide to build an estimator with higher tuning parameters in Υ^2 at the cost of poorer accuracy.

For the simulations in Fig. 4.6 and Fig. 4.7 we have assumed that no *a priori* knowledge of the variances $\sigma_u^2[j]$ and σ_v^2 is available. Then, the estimator should be initialized at $\hat{q}(0)[j] = 0$ and the estimations increase progressively in value as new measurements are processed. Moreover,

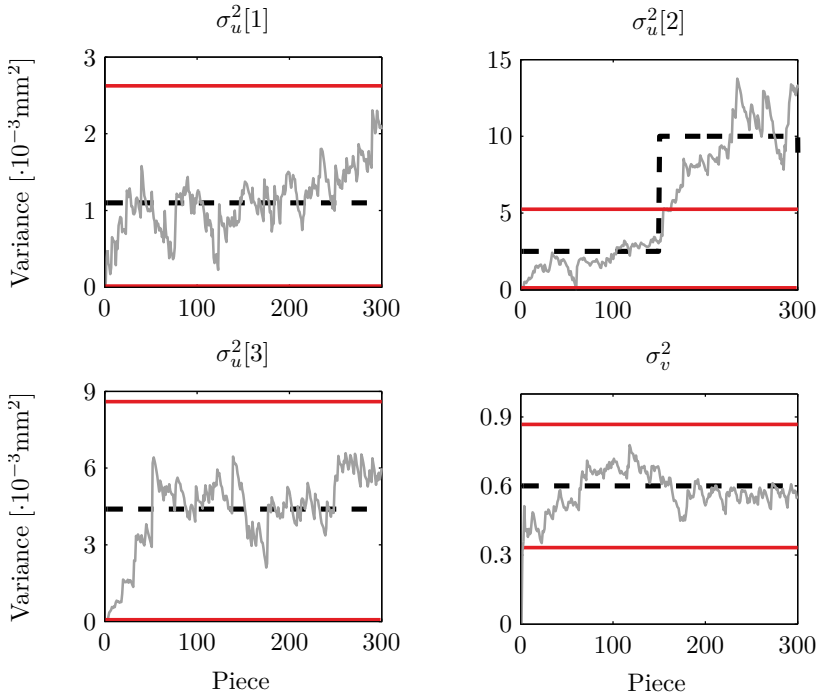

Figure 4.7. Process variance estimation with a model-based observer ($\Upsilon^2 = 0.05\, I_4$) in the single-stage assembly process affected by an abrupt fault in $\sigma_u^2[2]$. Real (- -), Estimation (Gray —) Gaussian-based limit with $\gamma_j = 99\%$ (Red —).

some simulation results in these figures may look as a fault appeared when it does not (e.g., the variation experienced by $\sigma_u^2[2]$ in Fig. 4.6). The reader should notice that these variations are within the confidence intervals designed for a 99% confidence level. If just thinner variations are allowed, the designer should decrease the value of the variables ν_j so that the accuracy of the estimates improves; contrariwise, if these variations should fade faster, the designer should increase the value of the variables ν_j so that the tracking ability of the estimator improves. In Fig. 4.8 we show the estimation of $\sigma_u^2[1]$ for a fault-free scenario. If we use an observer with $\Upsilon^2 = 0.1\, I_4$, the latest simulation results may look as if an abrupt fault appeared but, in any case, the estimation is within the confidence interval for $\gamma_1 = 99\%$ ($\Omega_{j,p}(i) = [0, 3.236]\cdot 10^{-3}$) and no fault is thus diagnosed. If this temporary bias is prohibitive in terms of accuracy, one can use other observers as the ones in the second part of Fig. 4.8, which are designed with $\Upsilon^2 = 0.01\, I_4$ ($\Omega_{j,p}(i) = [0.315, 1.885] \cdot 10^{-3}$ for $\gamma_1 = 99\%$) and $\Upsilon^2 = 0.001\, I_4$ ($\Omega_{j,p}(i) = [0.493, 1.707] \cdot 10^{-3}$ for $\gamma_1 = 99\%$).

4.7.2 Multistage assembly process

Second, we study the two-stage process (M = 2) provided in [78] which was derived from a segment of the simplified automotive body assembly process presented by Ding, Shi and Ceglarek in [77]. This simplified assembly process has been widely used in the literature for analysing diagnosability issues [77, 231], estimation of variance components of variation sources [78] and optimal sensor distribution [76, 200]. In this example, depicted in Fig. 4.9, three workpieces are

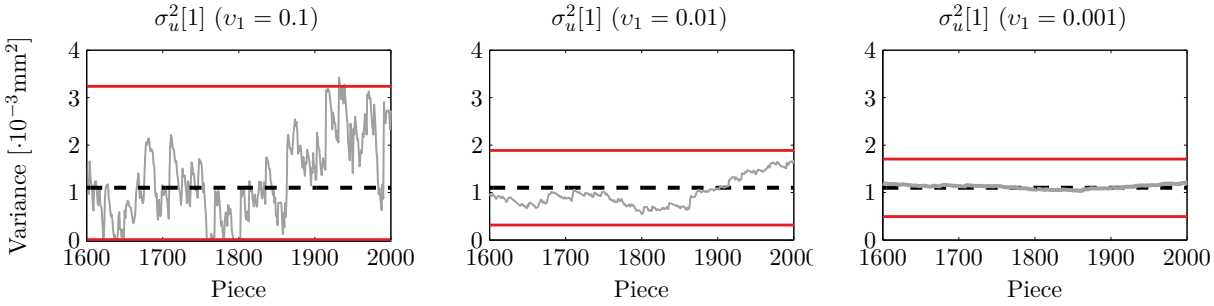

Figure 4.8. Comparison of the performance of different observers used in the single-stage assembly process for the estimation of $\sigma_u^2[1]$ in fault-free scenarios. Real (- -), Estimation (Gray —) Gaussian-based limit with $\gamma_1 = 99\%$ (Red —).

welded together at Stage I. In this stage, there are 9 fixturing variation sources ($n_u = 9$). Once welding operations are completed, the entire assembly is transferred to a dedicated in-process OCMM stage (Stage II) for inspection. High-precision laser-optic coordinate sensors are used to measure two directional coordinates at each of the nine measurement points and, hence, $n_y = 18$. Matrix Γ satisfies

$$\Gamma = \begin{bmatrix} 0 & 0 & 0 & 0.1215 & -0.3846 & 0 & 0 & 0 & 0.2632 \\ 0 & 0 & 0 & 0.0221 & -0.0699 & 0 & 0 & 0 & 0.0478 \\ 0 & 0 & 0 & 0.1215 & -0.3846 & 0 & 0 & 0 & 0.2632 \\ 0 & 0 & 0 & -0.1817 & 0.5944 & 0 & 0 & 0 & -0.4067 \\ 0 & 0 & 0 & -0.0773 & 0.2448 & 0 & 0 & 0 & -0.1675 \\ 0 & 0 & 0 & -0.3379 & 1.0699 & 0 & 0 & 0 & -0.7321 \\ 0 & 0 & 0 & 0.1656 & -0.5245 & 0 & 0 & 0 & 0.3589 \\ 0 & 0 & 0 & -0.3379 & 1.0699 & 0 & 0 & 0 & -0.7321 \\ 0 & 0 & 0 & 0 & 0 & 0 & 0 & 0 & 0 \\ 0 & 0 & 0 & -0.2054 & 0.6503 & 0 & 0 & 0 & -0.445 \\ -1 & 1 & 0 & -0.3110 & 0 & 0.4 & -0.4 & 0 & 0.311 \\ 0 & 0 & 0 & 0.0574 & 0 & -0.24 & 1.24 & 0 & -1.0574 \\ -1 & 1 & 0 & -0.2153 & 0 & 0 & 0 & 0 & 0.2153 \\ 0 & 0 & 0 & -0.2392 & 0 & 1 & 0 & 0 & -0.7608 \\ -1 & 0 & 1 & -0.0957 & 0 & 0 & 0 & 0.4 & -0.3043 \\ 0 & 0 & 0 & 0.0574 & 0 & 0 & 0 & -0.24 & 0.1826 \\ -1 & 0 & 1 & 0 & 0 & 0 & 0 & 0 & 0 \\ 0 & 0 & 0 & -0.2392 & 0 & 0 & 0 & 1 & -0.7608 \end{bmatrix}.$$

The output matrix H which results from Γ does not verify condition (4.26); then, we redefine vector $q(i)$ so that $n_j = \text{rank}\{H\}$ as

$$q(i)[j] = \begin{cases} \sigma_u^2[1] + \sigma_u^2[2] & \text{if } \; j = 1 \\ \sigma_u^2[1] + \sigma_u^2[3] & \text{if } \; j = 2 \\ \sigma_u^2[j+1] & \text{if } \; j \in \{3,4,5,6,7,8\} \\ \sigma_v^2 & \text{if } \; j = 9 \end{cases}.$$

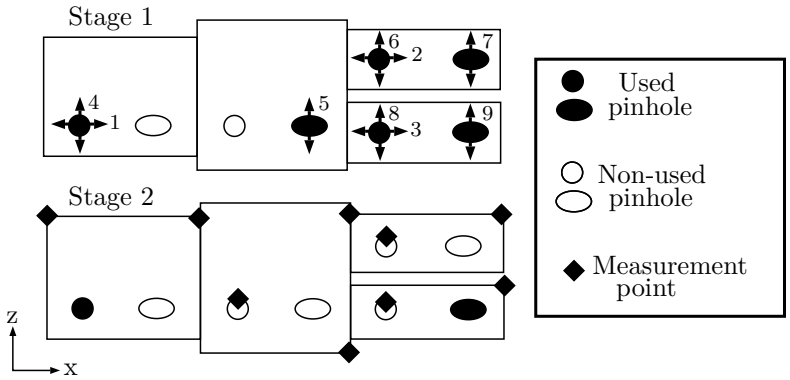

Figure 4.9. Scheme of the two-stage assembly process, adapted from [77, 78].

and we modify matrix H accordingly. This means that in the case of the three first fixturing variation sources we do not identify the process variations individually, but a combination of them.

First, we simulate a process of 2250 pieces with the values

$$\sigma^2(i)[j] = \begin{cases} 4.5 \cdot 10^{-3} & \text{if } \ j = 1 \\ 0.3 \cdot 10^{-3} & \text{if } \ j \in \{2, 3\} \\ 0.5 \cdot 10^{-3} & \text{if } \ j \in \{4, 5, 8, 9\} \\ 1.5 \cdot 10^{-3} & \text{if } \ j = 6 \\ 2.5 \cdot 10^{-3} & \text{if } \ j = 7 \\ 0.0111 \cdot 10^{-3} & \text{if } \ j = 10 \end{cases} .$$

(values in mm^2 taken from [78]). We assume that an abrupt change occurs modifying the variance $\sigma_u^2[6]$ from $1.5 \cdot 10^{-3}$ mm^2 to $3.4 \cdot 10^{-3}$ mm^2 (i.e., doubled standard deviation of the 6-th variation source) at piece 1000. Fig. 4.10 and Fig. 4.11 show the estimation results regarding $\sigma_u^2[j]$ when applying an observer with $\Upsilon^2 = 0.002\, I_9$ in (4.29) and $\gamma_j = 99\%$. Again, we prove that, although the order of magnitude of the variables involved in $q(i)$ is highly different, the model-based observer provides appropriate results.

Now, we simulate a process of 1200 pieces in which standard deviation of the sensors is modified from 0.0033 mm to 0.0100 mm at piece 250. The first simulation depicted in Fig. 4.12 shows the estimation results for this process when using an estimator designed with $\nu_9 = 0.002$ and a Gaussian-based threshold with $\gamma_9 = 99\%$. The second part of this figure shows that the proposed algorithm (with $\nu_9 = 0.002$ and $\gamma_9 = 99\%$) does also track drift faults. In this case, $\sigma_v = 0.0033$ mm before the drift fault and $\sigma_v = 0.0073$ mm 1000 pieces after the fault appears. The drift fault modifies the sensor process variance linearly. The other results compare the performance of estimators with different requirements over the estimation of $q[9]$: $\upsilon_1 = 0.01$, and $\upsilon_1 = 0.001$. Again, we see the trade-offs detailed in Section 4.4. Note that the order of magnitude of the tuning parameter (i.e., υ_j) used in the estimators in Fig. 4.12 is smaller than the order of magnitude of the tuning parameter in the estimators in Fig. 4.4 due to the differences in the values involved in the MMP.

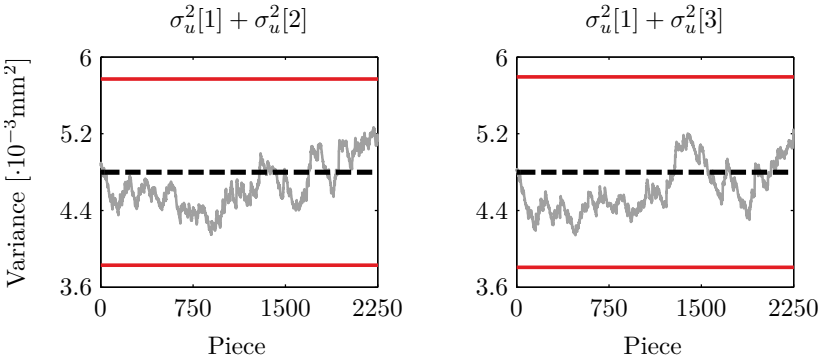

Figure 4.10. Process variance estimation with a model-based observer ($\Upsilon^2 = 0.002\, I_9$) in the multistage assembly process affected by an abrupt fault in $\sigma_u^2[6]$ (Part I, combined process variations). Real (- -), Estimation (Gray —) Gaussian-based limit with $\gamma_j = 99\%$ (Red —).

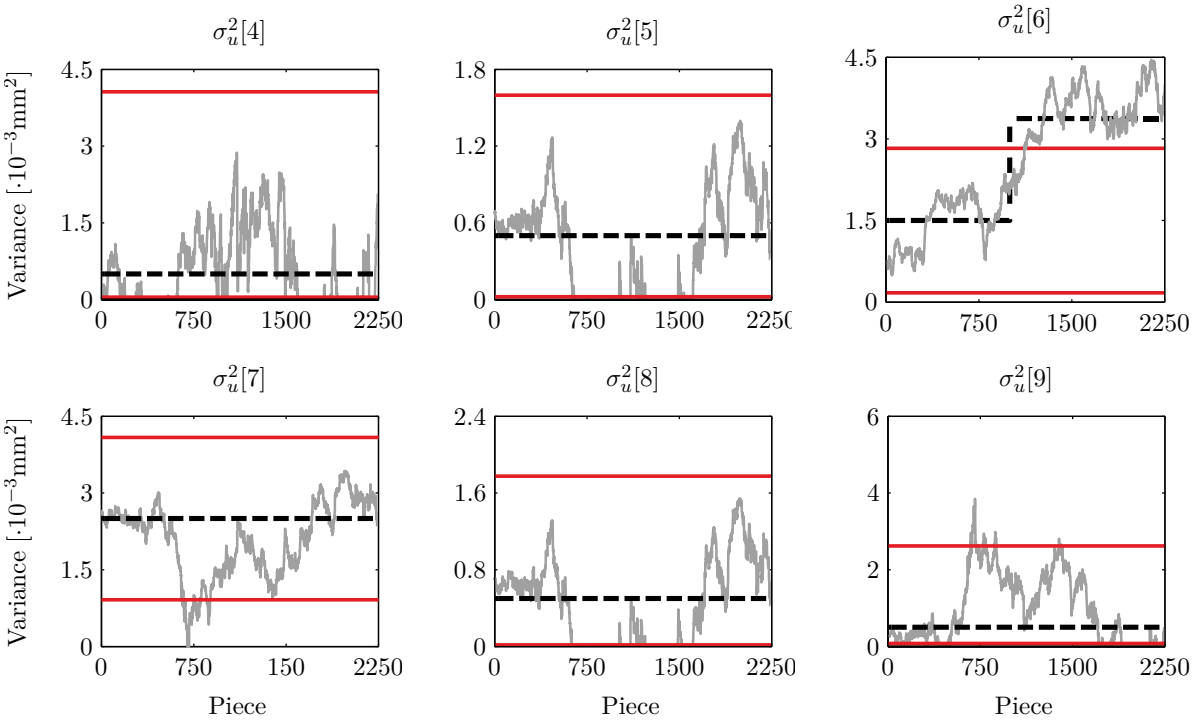

Figure 4.11. Process variance estimation with a model-based observer ($\Upsilon^2 = 0.002\, I_9$) in the multistage assembly process affected by an abrupt fault in $\sigma_u^2[6]$ (Part II, individual process variations). Real (- -), Estimation (Gray —) Gaussian-based limit with $\gamma_j = 99\%$ (Red —).

4.8 Conclusion

In this chapter, we have addressed the non-stationary process variance estimation problem with a recursive algorithm that is updated with the information available from every new manufactured piece. This strategy relaxes the computational burden and the data storage required by other algorithms that use a large sample size for each computation. Furthermore, our approach has a multivariate parameter that tunes the performance in the existing trade-off between the

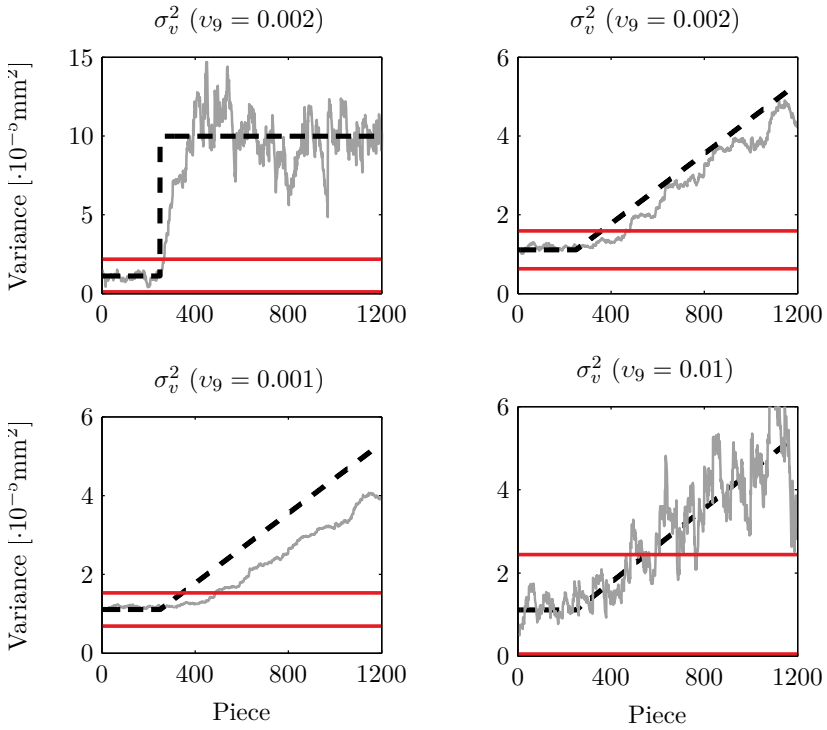

Figure 4.12. Comparison of the performance of different observers used in the multistage assembly process for the estimation of σ_v^2, which is affected by an abrupt fault or a drift fault. Real (- -), Estimation (Gray —) Gaussian-based limit with $\gamma_j = 99\%$ (Red —).

adaptation to process variance changes and the accuracy in stationary periods. We have shown two possible computations of the confidence interval, one based on the Chevyshev's inequality and another which takes account of the Gaussian behavior which is approached by the estimation errors. We have shown in two different examples how to tune the algorithm in order to obtain a desired performance. Future work will include the application of the proposed approach to factory collected and the extension of the approach to obtain not only process variance estimations but also estimations of the mean of the variation sources.

Chapter 5

Performance-based design of proportional integral observers for fault diagnosis

This chapter addresses the fault diagnosis problem for LTI systems under the presence of Gaussian noises through model-based proportional-integral observers with predefined gains. We propose a co-design of fault estimators and evaluators which takes into account the trade-off between physically meaningful parameters such as the false isolation rate, the minimum isolable faults and the cumulative squared error of the fault estimates under abrupt faults. Dynamic fault isolation is also taken into account. In order to solve this design problem, we present two different approaches: one based on the steady-state Kalman filter and another based on convex optimization techniques.

5.1 Introduction

Fault diagnosis (FD) has received much attention in the last decades [44,97,140]. A FD module entails three main tasks: fault detection, isolation and analysis (FDIA). While fault detection consists on determining the appearance of a fault in the system, fault isolation (FI) focuses on its localization and fault analysis (FA) aims to characterize the fault nature [96]. To design these modules, model-based approaches have been widely studied. Broadly speaking, a FDIA system consists of residual generators and evaluators. Among model-based residual generation strategies, there is an upward trend in the use of schemes which rely on observers, see [139,141, 290] and references therein. Given the dual relation between controllability and observability, the enhancement of the steady-state accuracy provided by the integral term in controllers has motivated many researchers to introduce an integral term in the observer design. This type of proportional-integral (PI) observers is proposed in [82, 197, 212] where an augmented state system enables FDIA. On the framework of residual evaluation, statistical methods and norm-based techniques are the most used strategies to achieve optimal processing of the residuals generated by observers [70]. According to [73], an integrated design of both residual generators and evaluators is the key to achieve an optimum FDIA strategy.

When designing a FDIA system the presence of disturbances is the first issue to take into account [201,206,226]. Robust FDIA is an active research area and there are two main different approaches to deal with this problem. First, works as [45,66,225] propose the complete elimination of the effect of these disturbances on the residuals. When complete decoupling is not possible, the effect of these disturbances should be minimized [51,333]. Still, not only must the residuals be robust to disturbances, but they must also be as sensitive as possible to faults [122,332]. In the norm-based context, Zhang and Ding [327] propose to use the trade-off between the false alarm rate (FAR) and the fault detection rate (FDR) to achieve the desired performance of the FD mechanism. However, these parameters give no information about other matters such as the size of the faults which are susceptible to be detected and isolated, the dynamic behavior of the residuals for FDI or their steady-state accuracy for FA. The optimization-based designs in [229,248] include the minimum faults to be detected and a conservative bound of the FAR through Markov's inequality. In those works, under the assumption of Gaussian noises, the FAR is later tightened through involved iterative procedures over the initial optimization problem. In [229], the tracking ability is included in the design through a decay ratio which implies an additional constraint. This conservatism can be avoided thanks to expressing the dynamic behavior of the residuals in terms of their Cumulative Squared Error (CSE) [248].

In this chapter, we propose a FDIA strategy for linear time-invariant (LTI) discrete-time systems affected by Gaussian noises. The proposed FDIA strategy utilizes fault estimation (FE) techniques and it is based on fault estimators (PI observers with constant gains) and fault evaluators (threshold-based decision mechanisms) that focus on isolation tasks. We present two straightforward co-design approaches of the fault estimators and evlautors which take into account all the previous performance aspects. These integrated designs explicitly include tight bounds of the false isolation rate, the minimum isolable faults, the CSE of the fault estimates under abrupt (step) faults and a measure of the dynamic FI. The first technique is based on the steady-state Kalman filter and it is solved through heuristic optimization algorithms. The second one is a norm-based approach with bilinear matrix inequalities (BMI) and we solve it via iterative convex optimization.

5.1.1 Structure and notation

The outline of this chapter is as follows. First, we state the problem in Section 5.2, where we include the mathematical model of the systems under consideration, we present the suggested fault estimation and evaluation strategy and we define the performance parameters to be considered. In Section 5.3, we show how to include these requirements in the two proposed design approaches of the FDIA system. Section 5.4 validates the suggested strategy through simulation results. Finally, Section 5.5 summarizes the main conclusions.

Let M be a square matrix of size $n \times n$. $M(i,i)$ denotes the i-th diagonal element of matrix M, while $M(i)$ denotes its i-th row or column depending on the context. $M \succeq 0$ means that M is positive semidefinite. Similar applies to $\preceq$. The direct sum is denoted as $\bigoplus$. Let $x_k \in \mathbb{R}^n$ represent a signal. $x_k(i)$ denotes the i-th element of vector x_k. Expected value and probability are denoted as $\mathbf{E}\{\cdot\}$ and $\mathbf{Pr}\{\cdot\}$.

5.2 Problem statement

5.2.1 State-space models

Let us consider LTI discrete-time systems defined by the equations

$$x_{k+1} = A\,x_k + B\,u_k + E\,f_k + G\,v_k, \tag{5.1a}$$
$$y_k = C\,x_k + D\,u_k + F\,f_k + H\,v_k, \tag{5.1b}$$

where $x \in \mathbb{R}^{n_x}$ is the state vector, $y \in \mathbb{R}^{n_y}$ is the output vector and $u \in \mathbb{R}^{n_u}$ is the input vector. Vector $v \in \mathbb{R}^{n_v}$ includes zero-mean Gaussian noises of known covariance $\mathbf{E}\{v_k\,v_k^T\} = V$. Finally, vector $f \in \mathbb{R}^{n_f}$ includes the faults affecting the system. We assume that all the faults are detectable, isolable and identifiable.

Remark 5.1. *We introduce the transfer matrix from a fault $f(i)$ to the outputs as $G_{f(i)}[z] = C\,(z\,I - A)^{-1}\,E(i) + F(i)$. According to the results in [70], we state that a fault $f(i)$ of a system of the form (5.1) is detectable if and only if $G_{f(i)}[z] \neq 0$, isolable if and only if*

$$\operatorname{rank}\left[G_{f(1)}[z]\ \ldots\ G_{f(n_f)}[z]\right] = \sum_{i=1}^{n_f} \operatorname{rank}\left(G_{f(i)}[z]\right),$$

and identifiable if and only if the inverse of the transfer matrix $G_{f(i)}[z]$ is realizable and stable.

To reach FDIA objectives, we propose a scheme that relies on model-based PI observers. Thus, we model the faults f_k of (5.1) as

$$f_{k+1} = f_k + \Delta f_k, \tag{5.2}$$

where Δf_k represents the variation of the fault signal between two consecutive instants. The equation (5.2) allows modeling, for instance, abrupt or step signals (Δf_k only takes a non-zero value at the fault appearance) and incipient or ramp signals (Δf_k takes a constant value). This kind of fault model has been widely used in the literature to analyse the behavior of FDIA algorithms, see [155, 162]. To include the faults dynamics, we extend the model (5.1) as

$$z_{k+1} = \bar{A}\,z_k + \bar{B}\,u_k + \bar{G}\,v_k + \bar{E}\,\Delta f_k, \tag{5.3a}$$
$$y_k = \bar{C}\,z_k + \bar{D}\,u_k + \bar{H}\,v_k, \tag{5.3b}$$

where $z_k = \begin{bmatrix} x_k^T & f_k^T \end{bmatrix}^T$ is the extended state vector,

$$\bar{A} = \begin{bmatrix} A & E \\ 0 & I \end{bmatrix},\ \bar{B} = \begin{bmatrix} B \\ 0 \end{bmatrix},\ \bar{G} = \begin{bmatrix} G \\ 0 \end{bmatrix},\ \bar{E} = \begin{bmatrix} 0 \\ I \end{bmatrix},$$

$\bar{C} = \begin{bmatrix} C & F \end{bmatrix}$, $\bar{D} = D$ and $\bar{H} = H$.

5.2.2 Fault estimation and evaluation

For achieving FA, we propose the following fault estimator in the form of a PI observer with predefined gain:

$$\hat{z}_{k+1} = \bar{A}\,\hat{z}_k + \bar{B}\,u_k + L(y_k - \bar{C}\,\hat{z}_k - \bar{D}\,u_k), \tag{5.4a}$$

$$\hat{f}_k = R\,\hat{z}_k, \tag{5.4b}$$

where $\hat{f}$ is the fault estimation vector and L is the gain matrix that updates the prediction obtained from the model with the measurements . R is the matrix that extracts the faults from the extended state z_k, i.e., $f_k = R\,z_k$ with $R = [0_{n_f \times n}\ I_{n_f \times n_f}]$. Recall that we denote as $R(i)$ the i-th row of matrix R; then, a single fault can be extracted as $f_k(i) = R(i)\,z_k$. Let us define the FE error as

$$e_k = f_k - \hat{f}_k, \tag{5.5}$$

whose dynamics is given by

$$\widetilde{z}_{k+1} = (\bar{A} - L\,\bar{C})\,\widetilde{z}_k + (\bar{G} - L\,\bar{H})\,v_k + \bar{E}\,\Delta f_k, \tag{5.6a}$$

$$e_k = R\,\widetilde{z}_k, \tag{5.6b}$$

with $\widetilde{z}_k = z_k - \hat{z}_k$. We denote as Q the covariance of the error e_k, i.e., $Q = \mathbf{E}\{e_k\,e_k^T\}$.

Remark 5.2. *Under null initial conditions and in the absence of faults, the estimation error e_k has a multivariate normal distribution with zero mean and covariance Q because the disturbances and measurement noises are normally distributed with zero mean. The error associated to each fault estimate, $e_k(i)$, is zero-mean normally distributed with variance $Q(i,i)$, corresponding to the marginal distribution of the i-th element in the error vector.*

For FI purposes, we set the following decision mechanism evaluating the fault estimates provided by (5.4):

$$\begin{cases} \text{if } \ |\hat{f}_k(i)| \geq f_{th}(i)\ , & \text{Fault } f(i) \\ \text{otherwise}\ , & \text{No fault } f(i) \end{cases}, \tag{5.7}$$

where $f_{th}(i)$ is the threshold for the isolation of the fault $f(i)$.

Remark 5.3. *We say that there is a fault on the system (fault detection) if any of the alarms for the faults $f(i)$ ($i = 1, \ldots, n_f$) is active. The fact of detecting and isolating a fault through the same decision mechanism* (5.7) *does not introduce any conservatism if we consider the non-simultaneity of faults.*

5.2.3 Performance characterization

According to [44], we define different parameters that allow us to characterize the FI performance of the fault evaluators (5.7) which are based on the fault estimates provided by (5.4). First, the false isolation rate (FIR), which we denote as $\phi(i)$, is the probability of rising false alarms of fault $f(i)$, i.e.,

$$\phi(i) = \mathbf{Pr}\{|\hat{f}_k(i)| \geq f_{th}(i) : f_k(i) = 0\}. \tag{5.8}$$

Second, the minimum isolable fault (MIF), which we denote as $f_m(i)$, is the constant fault that raises the alarm of fault $f(i)$ provided the non-existence of other faults nor noises in the system, i.e.,

$$f_m(i) = \left\{ |f_k(i)| : \begin{array}{l} f_k(i) = f_{k-1}(i), \forall k \\ \lim_{k\to\infty} |\hat{f}_k(i)| \geq f_{th}(i) \end{array} \right\}. \tag{5.9}$$

In this chapter, the previous definition implies $f_{th}(i) = f_m(i)$.

Remark 5.4. *Recall that under null initial conditions and in the absence of faults, each error $e_k(i)$ is normally distributed with zero mean. Hence, the MIF can be also seen as the quantile used to construct the confidence interval of level $1 - \phi(i)/2$. Thus, the following relation holds*

$$f_m(i) = \Phi^{-1}(1 - \phi(i)/2)\, Q(i,i)^{1/2}, \tag{5.10}$$

where Φ^{-1} denotes the inverse cumulative distribution function of a normal random variable.

Third, we define the cumulative squared error (CSE) of a fault estimate $\hat{f}(i)$, which we denote as $\varphi(i)$, as its cumulative estimation error, i.e.,

$$\varphi(i) = \sum_{k=1}^{\infty} e_k^2(i). \tag{5.11}$$

Whilst the FIRs and the MIFs define the accuracy of the FDIA strategy, the CSE of the fault estimates reflects its tracking ability. The aim of this chapter is to co-design the fault estimator (5.4) and the fault evaluator (5.7) to guarantee certain FIRs and MIFs and maximize the fault tracking ability.

5.3 Design of the fault estimator and evaluator

To design the fault estimator (5.4) and the fault evaluator (5.7), we present two different integrated approaches. First, we develop a Kalman-based technique which includes some numerical tuning parameters and we show the difficulty of fixing them according to actual physical meaning. Then, we develop a BMI-based design strategy which explicitly includes physical performance parameters and we solve it through a sequence of convex optimization problems.

5.3.1 Kalman-based fault estimator and evaluator

The following theorem shows how to calculate a predefined gain of the observer (5.4) for the system (5.3) based on the steady-state Kalman filter gain.

Theorem 5.1. *Let us assume that Δf_k has a known constant covariance matrix Γ^{-1}, i.e., $\Gamma^{-1} = \boldsymbol{E}\{\Delta f_k\, \Delta f_k^T\}$. The optimal Kalman gain of the observer* (5.4) *for the system* (5.3) *at steady-state is given by:*

$$L = \bar{A}\, P\, \bar{C}^T\, \mathcal{C}^{-1}, \tag{5.12}$$

with $\mathcal{C} = (\bar{C}\,P\,\bar{C}^T + \bar{H}\,V\,\bar{H}^T)$ *and* P *being the covariance matrix of vector* $\widetilde{z}_k$*, i.e.,* $P = \boldsymbol{E}\{\widetilde{z}_k\,\widetilde{z}_k^T\}$*, which satisfies the following Riccati equation:*

$$P = \bar{A}\,P\,\bar{A}^T + \mathcal{G}\,\mathcal{V}\,\mathcal{G}^T + \bar{A}\,P\,\bar{C}^T\,\mathcal{C}^{-1}\,\bar{C}\,P\,\bar{A}^T, \tag{5.13}$$

with $\mathcal{G} = \bar{G} \oplus \bar{E}$ *and* $\mathcal{V} = V \oplus \Gamma^{-1}$*.*

Proof. See [152]. □

The previous result allows us to obtain a gain L that stabilizes the observer and that takes into account the presence of faults in the system. With the obtained gain L, we obtain the steady-state covariance of the observer error during fault-free scenarios by solving the following Lyapunov equation

$$\begin{aligned} P_0 &= (\bar{A} - L\bar{C})\,P_0\,(\bar{A} - L\bar{C})^T + (\bar{G} - L\bar{H})\,\mathcal{V}\,(\bar{G} - L\bar{H})^T, \\ Q &= RP_0R^T. \end{aligned} \tag{5.14}$$

As the faults are not Gaussian noises, the matrix Γ needed in Theorem 5.1 is neither constant nor known and it can be seen as a tuning parameter whose value can be chosen by the designer to modify the FDIA performance. Thus, increasing Γ improves the accuracy of the fault estimates (as the filter will focus more on rejecting the noises indicated by V), and decreasing Γ improves the tracking ability at the cost of a lower measurement noise rejection. Given (5.10) and for a given FIR, a better estimation accuracy implies achieving a lower MIF.

One design procedure is to look for the value of Γ that leads to a matrix L through (5.12) and (5.13) such that Q in (5.14) satisfies some given performance. The next strategy shows how to design a Kalman-based fault estimator and evaluator guaranteeing certain FIRs and MIFs while the tracking ability of the fault estimates is maximized.

Strategy 5.1. *Let us define a diagonal matrix* $\mathcal{Q}$ *as*

$$\mathcal{Q} = \bigoplus_i \bar{f}_m(i)^2/\Phi^{-1}(1 - \bar{\phi}(i)/2)^2, \tag{5.15}$$

where $\bar{\phi}(i)$ *denotes the desired FIRs and* $\bar{f}_m(i)$ *stands for the desired MIFs. The optimization problem*

$$\begin{aligned} &\text{minimize} \;\; \gamma \\ &\text{subject to} \;\; \mathcal{X}_1 = \left\{ \begin{array}{l} (5.12),\ (5.13),\ (5.14),\ \Gamma \succeq 0, \\ Q \preceq \mathcal{Q},\ tr(\Gamma) \preceq \gamma \end{array} \right\} \end{aligned} \tag{5.16}$$

along the variables P*,* P_0*,* Q*,* L *and* Γ *leads to the fault estimators with the fastest response under faults and guaranteeing the constrained performances when the thresholds of the evaluators are defined as* $f_{th}(i) = \bar{f}_m(i)$*. Matrix* Q *denotes the covariance of the fault estimates at steady-state when no faults occur and is given by* (5.14)*.*

The previous minimization problem can be solved through heuristic optimization approaches such as genetic algorithms.

5.3.2 BMI-based fault estimator and evaluator

The following theorem shows how to design the observer gain L taking into account FDIA performance parameters.

Theorem 5.2. *Consider the PI observer* (5.4) *applied to the system* (5.3)*. If there exist any full matrix L, any symmetric matrices S, $\bar{Q}$ and any n_f symmetric matrices P_i and Γ_i fulfilling*

$$\begin{bmatrix} S & S\,\mathcal{A} & S\,\mathcal{G}\,V \\ \star & S & 0 \\ \star & \star & V \end{bmatrix} \succeq 0, \quad \begin{bmatrix} \bar{Q} & R \\ \star & S \end{bmatrix} \succeq 0, \tag{5.17}$$

and the following constraints for $i = 1, \ldots, n_f$

$$\begin{bmatrix} P_i & P_i\,\mathcal{A} & 0 \\ \star & P_i & R(i)^T \\ \star & \star & I \end{bmatrix} \succeq 0, \quad \begin{bmatrix} P_i & P_i\,\bar{E} \\ \star & \Gamma_i \end{bmatrix} \succeq 0, \tag{5.18}$$

with $\mathcal{A} = \bar{A} - L\,\bar{C}$ and $\mathcal{G} = \bar{G} - L\,\bar{H}$, the following statements hold:

- *In the absence of faults and noises (i.e., $\Delta f_k = v_k = 0$), the error* (5.5) *converges to zero.*
- *In the absence of noises (i.e., $v_k = 0$), the CSE of a fault estimate $\hat{f}(i)$ ($i = \{1, \ldots, n_f\}$) due to a single unitary step fault $f(j)$ with $j = \{1, \ldots, n_f\}$ is bounded as $\varphi(i) \leq \Gamma_i(j, j)$.*
- *In the absence of faults (i.e., $\Delta f_k = 0$), the covariance of the error* (5.5)*, is bounded as $Q \preceq \bar{Q}$.*

Proof. The following items prove each of the statements of Theorem 5.2.

- Let us define the Lyapunov function $V_k^S = \widetilde{z}_k\,S\,\widetilde{z}_k^T$ at each instant k. In the absence of measurement noises and faults after taking Schur's complements on the first linear matrix inequality (LMI) presented at (5.17) and premultiplying the result by $\widetilde{z}_k^T$ and postmultipliying by its transpose, we obtain that $V_{k+1}^S - V_k^S \leq 0$ which assures that the state estimation error (5.5) converges to zero. We get the same result if we define the Lyapunov function $V_k^{P_i} = \widetilde{z}_k\,P_i\,\widetilde{z}_k^T$ at each instant k and we operate on the first LMI presented at (5.18).
- Performing similar steps on each of the second LMIs presented at (5.18) (Schur's complements and operations with Δf_k^T), taking expected value on the results and adding the obtained constraints to the previous one, we get

  $$\mathbf{E}\{V_{k+1}^{P_i}\} - \mathbf{E}\{V_k^{P_i}\} + \mathbf{E}\{e_k^2(i)\} \leq \Delta f_k^T\,\Gamma_i\,\Delta_k,$$

  where we have taken into account the uncorrelation between $\widetilde{z}_k$ and Δf_k. Considering null initial conditions and adding the result from $k = 0$ to $K - 1$ and taking the limit when $K \to \infty$, it yields

  $$\sum_{k=0}^{\infty} e_k^2(i) \leq \sum_{k=0}^{\infty} \Delta f_k^T\,\Gamma_i\,\Delta f_k.$$

If a single unitary step fault $f(j)$ occurs (i.e., $\Delta f_k(j) = 1$ only if $k = 0$) then,

$$\sum_{k=0}^{\infty} e_k^2(i) \leq \Gamma_i(j,j).$$

Hence, by bounding the diagonal elements of Γ_i we constraint the CSEs of each of the fault estimates due to the appearance of different faults, what proves the second statement in Theorem 5.2.

- Applying congruence transformation with $\left[\begin{smallmatrix} S^{-1} & 0 & 0 \\ 0 & I & 0 \\ 0 & 0 & I \end{smallmatrix}\right]$ and Schur's complements on the first LMI in (5.17) we have that

$$\mathcal{A}\, S^{-1}\, \mathcal{A}^T + \mathcal{G}\, V\, \mathcal{G}^T \preceq S^{-1},$$

Comparing this inequality with the steady-state covariance matrix P_0 from (5.14) we have that $P_0 \preceq S^{-1}$ if we assume that $\mathcal{A}$ has stable eigenvalues, which has been demonstrated in the first item. Then, after applying Schur's complements on the second LMI in (5.17) we have

$$R\, S^{-1}\, R^T \preceq \bar{Q},$$

what finally leads to

$$Q = R\, P_0\, R^T \preceq R\, S^{-1}\, R^T \preceq \bar{Q},$$

proving thus the third statement in Theorem 5.2.

□

Taking advantage of the bounds presented in the previous theorem, the next strategy shows how to design a BMI-based fault estimator and evaluator guaranteeing certain FIRs and MIFs while the CSE of the fault estimates is minimized.

Strategy 5.2. *Let us define a diagonal matrix $\mathcal{Q}$ as shown in* (5.15) *with $\bar{\phi}(i)$ the desired FIRs and $\bar{f}_m(i)$ the desired MIFs. The convex optimization problem*

$$\begin{aligned} &\text{minimize } \gamma \\ &\text{subject to } \mathcal{X}_2 = \left\{ \begin{array}{l} (5.17),\ (5.18), \\ \bar{Q} \preceq \mathcal{Q},\ \sum_i^{n_f} \Gamma_i(i,i) \preceq \gamma, \\ \sum_{i,i\neq j}^{n_f} \Gamma_i(j,j) \preceq \epsilon\, \gamma, \forall i,j \end{array} \right\} \end{aligned} \tag{5.19}$$

along the variables S, $\bar{Q}$, P_i, and Γ_i with $\epsilon \geq 0$ and $\epsilon \to 0$ leads to the fault estimators and evaluators with the lowest CSE due to faults and guaranteeing the desired FIRs and MIFs when the thresholds of the evaluators are defined as $f_{th}(i) = \bar{f}_m(i)$. This design also enhances dynamic FI through parameter ϵ.

Remark 5.5. *While the elements $\Gamma_i(i,i)$ $(i = 1, \ldots, n_f)$ quantify the tracking ability of a fault estimate i towards a fault in its own channel, the elements $\Gamma_i(j,j)$ $(i \neq j)$ specify its rejection ability against a fault in a different channel, $f(j)$. This could imply a certain trade-off between tracking and decoupling ability. If the system allows complete dynamic FI, one can set $\epsilon = 0$ in* (5.19)*; but, if this is not possible due to the characteristics of the system, one can include variable ϵ in the optimization design procedure.*

Remark 5.6. *The previous optimization problem entails BMIs and it can be solved through solvers such as the ones presented in [129, 161]. Albeit, it is possible to iteratively solve these inequalities through a sequence of LMI problems following different approaches such as the ones presented in [86], or by a single LMI problem using some slack variables as in [108] at the cost of achieving a lower performance.*

5.4 Example

Let us consider a system (5.1) described by the following matrices

$$A = \begin{bmatrix} 0.2883 & -0.0484 \\ -0.9076 & 0.7753 \end{bmatrix}, \; B = \begin{bmatrix} 0.0059 \\ 1.1532 \end{bmatrix}, \; C = \begin{bmatrix} -2.0756 & -0.1952 \\ -2.0756 & -0.1952 \end{bmatrix}$$

and $D = 0$. We model the presence of three zero-mean uncorrelated Gaussian noises of variance 0.048. These noises affect the system as

$$G = \begin{bmatrix} 0.0059 & 0 & 0 \\ 1.1532 & 0 & 0 \end{bmatrix}, H = \begin{bmatrix} 0 & 1 & 0 \\ 0 & 0 & 1 \end{bmatrix}.$$

We consider that an actuator and a sensor faults may occur, i.e.,

$$E = \begin{bmatrix} -1.1114 & 0 \\ 4.7135 & 0 \end{bmatrix}, F = \begin{bmatrix} 0 & 0 \\ 0 & 1 \end{bmatrix}.$$

For this LTI system, we design fault diagnosers that allow us to recognize actuator and sensor faults above 0.05 and 0.10 respectively ($\bar{f}_m(1) = 0.05$ and $\bar{f}_m(2) = 0.10$). We also impose that there should be 250 samples in average between false alarms ($\bar{\phi}(1) = \bar{\phi}(2) = 0.004$). The constant gain for FE (5.4) obtained by the Kalman-based design approach is

$$L^T = \begin{bmatrix} -0.0362 & 0.2285 & 0.0132 & -0.0127 \\ -0.0025 & -0.0700 & 0.0044 & 0.0325 \end{bmatrix};$$

if we design the observer gain through the BMI-based strategy, the constant gain matrix is

$$L^T = \begin{bmatrix} -0.4607 & 3.6390 & 0.0129 & -0.0227 \\ -0.0236 & 0.1001 & 0.0004 & 0.0227 \end{bmatrix}.$$

In this example, we set up the problem in YALMIP [192] and we successfully solved it with the PENBMI solver [129, 161]. We fixed $\epsilon = 0$.

For verifying the imposed performance restrictions, we first simulate a fault-free process of $3.5 \cdot 10^6$ samples. The Kalman-based results satisfy the FIR bounds ($\phi(1) = 0.0040$ and $\phi(2) = 0.0039$); similar applies to the BMI-based results ($\phi(1) = 0.0039$ and $\phi(2) = 0.0039$). Second, we simulate a process of 3500 samples where the following faults occur

$$f_k^T = \begin{cases} \begin{bmatrix} 15\,\bar{f}_m(1) & 0 \end{bmatrix} & [500, 1500] \\ \begin{bmatrix} 0 & 12\,\bar{f}_m(2) \end{bmatrix} & [2000, 3000] \\ \begin{bmatrix} 0 & 0 \end{bmatrix} & \text{Otherwise} \end{cases}.$$

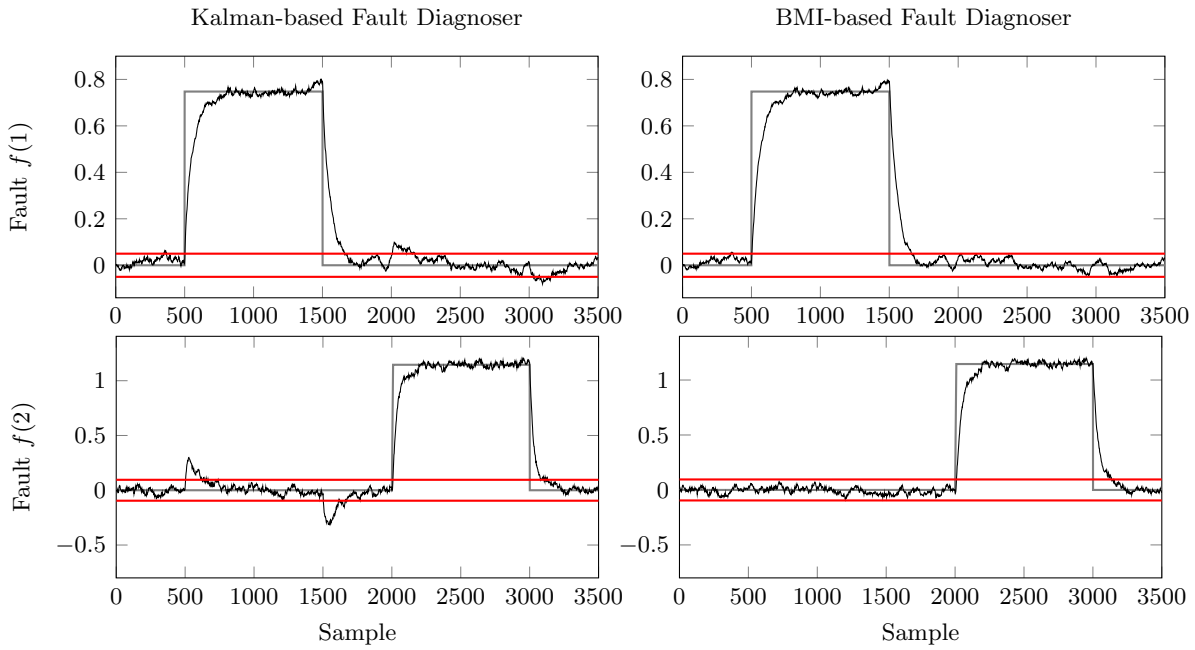

Figure 5.1. Fault diagnosis via different approaches. Fault (Gray), Estimate (Black), Threshold (Red).

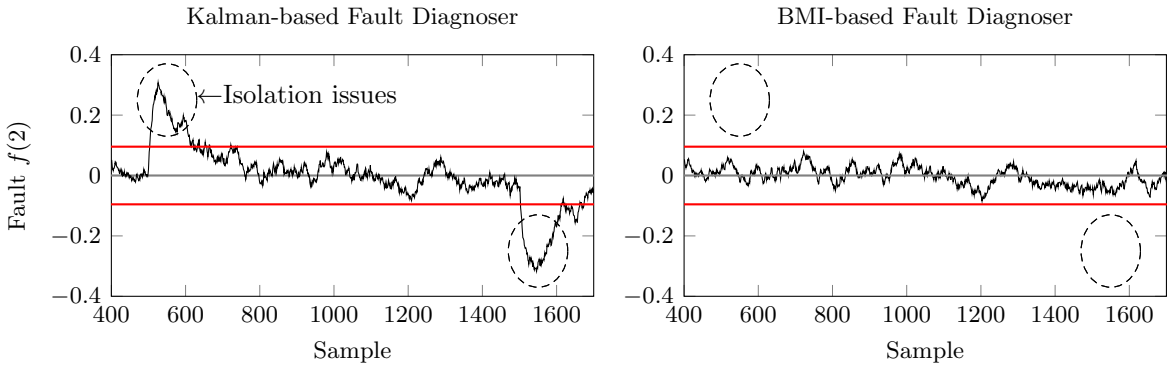

Figure 5.2. Details on fault isolation issues. Fault (Gray), Estimate (Black), Threshold (Red).

Fig. 5.1 shows the simulation results of this process. The CSE during the existence of fault $f(1)$ verifies the bound obtained in the BMI-based optimization problem: $\varphi(1) < \Gamma_1(1,1)\, f(1)^2$ (i.e., $16.96 < 17.25$). The same applies to fault $f(2)$ (i.e., $26.87 < 29.28$). We verify that whilst the BMI-based approach guarantees perfect FI, the Kalman-based design hinders dynamic FI (see the details in Fig. 5.2). One should note that enhancing dynamic FI implies lower minimization capability and, thus, higher CSE versus step-faults. Fig. 5.3 shows this trade-off for the case of study, where we show the optimization result γ for different values of ϵ.

5.5 Conclusions

We have presented two estimation-based FD approaches for solving a fault diagnosis problem with model-based proportional-integral observers under the assumption of Gaussian noises. The

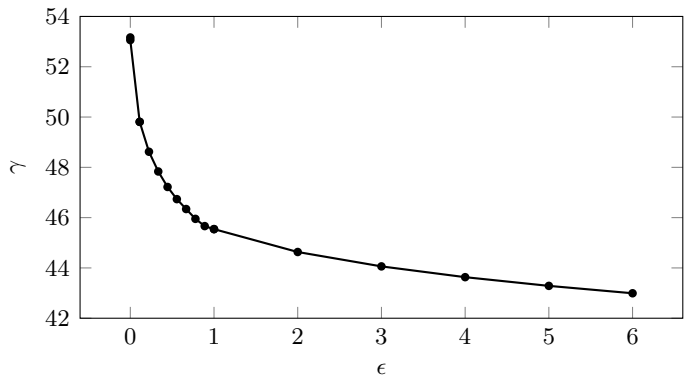

Figure 5.3. Trade-off between dynamic isolation restriction, ϵ, and minimization capability, γ.

design is based on the trade-off between isolation performance indices as the false isolation rate and minimum isolable fault, as well as the fault tracking ability via the cumulative squared error. We have explained how to co-design a fault estimator and evaluator for straightforwardly achieving certain false isolation rates and minimum isolable faults while minimizing the response time under the appearance of faults. We have proposed two designs based on optimization procedures. The first one includes as constraints two discrete Lyapunov equations (steady-state Kalman filter), while the second one includes several BMIs that bound the covariance matrix of the FE error as well as the cumulative squared FE error under step faults. In the BMI approach, one can avoid the dynamic coupling between FE channels, leading to dynamic isolability; while in the Kalman filter approach one cannot state this feature.

Chapter 6

Fault estimation via proportional multiple-integral and multiple-resonant observers

We develop a fault estimation strategy which is based on a novel proportional multiple-integral and multiple-resonant observer. This observer is an extension of the well-known PMI observer and it is able to estimate from low to high-frequency fault signals. The proposed estimation strategy is applied to discrete-time systems which are affected by faults and stochastic noises. We present a multiobjective design strategy of the observer that fixes the trade-offs between practical engineering parameters regarding the noise attenuation and the ability to track each kind of fault dynamics considered by the augmented observer. We study the influence of the order of the observer on the steady-state and transient performance of the estimation of different types of faults. Finally, a numerical example is given to illustrate the effectiveness of the proposed observer, design and characterization.

6.1 Introduction

The increasing complexity and the high costs of practical control systems impose higher demands of reliability and safety. Fault diagnosis, which has been extensively studied over the last decades [29, 44], arises as an effective solution to meet this demand. Among fault diagnosis techniques, fault estimation (FE) appears as an advanced method that gives information not only about the moment (detection) and the location (isolation) of a fault but also about its size and shape (identification), which is of paramount importance for both real-time decision and active fault tolerant control [222, 330].

FE can be realized by utilizing a wide variety of advanced observer techniques such as sliding mode observers [84,298], adaptive observers [98,312], iterative observers [50,136] and augmented observers. The essence of the latter approach is to construct an augmented system in which the faults are introduced as an additional state [100, 326]. As an extension of the Luenberger

observer, proportional and integral (PI) observers, which have received much attention [163, 305, 339], assume that the faults are constant or step signals. Their applicability is thus limited to the estimation of faults whose variations are slow with respect to the dynamics of the system. By supposing the considered faults to be in the more general form of a polynomial of the time, proportional multiple-integral (PMI) observers were discussed in many works as [102, 103, 156, 306, 322]. However and as stated in [104], pure high-frequency fault signals cannot be covered by PMI observers. The development of strategies for estimating the parameters of sinusoidal signals turns out to be an active research area. A comparison study of the most relevant exiting methods can be found in [43]. Usually, the Fast Fourier Transform (FFT) is preferred in stationary conditions. For the estimation of sinusoidal signals with time-varying amplitudes and frequencies different kinds of adaptive techniques, as the ones presented in [42, 209], are commonly utilized. However in many practical applications the faults are periodic signals which can be decomposed into sinusoids of known frequencies. Take as examples the faults related to human consumption of resources such as electricity or water [240], the sensor loss of effectiveness related to the ambient temperature evolution or the faults occurring in power systems of fixed frequency [157]. If the sinusoidal frequencies are known, simpler schemes can be used and it thus seems valuable to extend PMI observers in order to include this resonant dynamics.

It is noticed that fault diagnosis and FE techniques aim to simultaneously make the estimates sensitive to faults and robust against disturbances and noises [10, 277] through the accomplishment of certain trade-off between these properties [241, 302]. In order to characterize the sensitivity of PMI observers to faults, reference works [102, 322] assume that the polynomials of the time describing the faults are of certain order and that their highest-order non-zero time-derivative is bounded. Then, they bound the effect of these time-derivatives of highest order on the FE errors. In practice, it is possible to forecast some information about the polynomial order of the faults which are prone to occur. Yet, no exact *a priori* knowledge of this order is available. Hence, the authors in [103, 104] propose to "choose a large order for safety". However, choosing a large polynomial order of the faults, increases the order of the corresponding augmented PMI observer and it may degrade its behavior towards polynomial faults of lower order. It is then reasonable to ponder to what extent the increasing order of an observer improves its ability to track different type of faults; however, and to the best of the authors' knowledge, no systematic studies have been carried out in order to determine the influence of this allegedly protective election on the overall performance of the fault estimator. It seems then valuable to study the compromises resulting from such election and to provide a design strategy that allows managing the arising trade-offs. In view of this, we propose to characterize the sensitivity of PMI observers to faults by bounding the effect on the estimation error of each polynomial fault term instead of just considering the effect of the highest-order fault terms. This characterization allows designing PMI observers with a different sensitivity to each polynomial fault term according to their individual probability of appearance. Thus, for the same level of disturbance/noise attenuation, a higher ability to track the most probable forms of the fault would be achievable at the cost of a lower performance w.r.t. the less probable fault forms.

Compared with continuous-time systems, fewer and more recent results have been reported for FE in discrete-time systems [323]. In [41, 99, 323], PI estimation techniques are utilized

and in [307] a PMI observer is used for disturbance estimation. It is well known that discrete-time observers are more challenging and practical that continuous-time cases because most continuous-time control systems are implemented digitally [323]. Thus, more effort has to be devoted to FE in discrete-time systems. In any case, it would be straightforward to extend the FE strategies presented in this thesis to continuous-time systems.

6.1.1 Contributions

Inspired by the above background, this chapter uses novel proportional multiple-integral and multiple-resonant observers for FE. We study the performance trade-offs that appear when using complex augmented fault observers for discrete-time systems in environments with stochastic noises and it provides a design strategy that optimally fixes these trade-offs using practical engineering parameters. In all, compared to the relevant existing literature, the main contributions of this chapter are:

- *The existence conditions of proportional multiple-integral and multiple-resonant (PMIR) observers for discrete-time systems are included.* As an extension of the PI and PMI observer existence conditions available in the literature (see [41, 103]), we present the existence conditions of PMIR observers. PMIR observers represent an extension of PMI observers and they include resonant terms. Although these resonant terms are commonly utilized in power systems for building PR controllers [259, 285], PMIR observers are not utilized and their existence conditions are not available in the literature.

- *A multiobjective design of the PMIR observer based on performance trade-offs is presented.* In this chapter, we present a design of the PMIR observer for systems in environments with stochastic noises. The proposed design is a multiobjective optimization problem based on matrix inequalities which fixes certain trade-off between the noise attenuation and the ability to track each fault term included in the observer.Unlike common PMI observer designs which just consider the fault tracking ability w.r.t. the highest-order time-derivative of the fault (e.g., [102, 322]), the proposed design includes the probability of appearance of each kind of fault form considered by the augmented observer and it allows specifying different tracking abilities w.r.t. each fault form.

- *Practical engineering parameters are utilized in the proposed design.* In an aim to bridging the gap between theory and practice [222], the FE performance is characterized by means of practical engineering parameters. The stochastic noise attenuation is represented by the variance of the estimates in fault-free scenarios and the cumulative squared errors due to fault appearances explain the fault tracking ability.

- *The performance of PMIR fault estimators when the system is subject to non-modeled faults is studied.* To reinforce the justification of the probabilistic design approach presented in this chapter and provided that no *a priori* exact knowledge of the dynamics of the faults affecting the system is available, we study the performance of a designed PMIR observer when the system is affected by non-modeled faults. We also study the

influence of the complexity of the considered faults (i.e., the degree of the polynomial and the number of sinusoidal waves included in the augmented observer) on the performance of the estimator w.r.t. fault signals of simpler dynamics.

6.1.2 Structure and notation

The outline of this chapter is as follows. First, we state the problem in Section 6.2. In Section 6.3, we propose a FE strategy based on a novel model-based PMIR observers and, in Section 6.4, we present a multiobjective optimization problem for the design of the estimator. In Section 6.5, we study the fault tracking ability of the designed estimator in both steady state and transients. These characterizations are validated through a numerical example in Section 6.6. Finally, Section 6.7 summarizes the main conclusions and proposes future research topics.

Throughout the chapter, $\mathbb{R}$ denotes the set of real numbers and $\mathbb{C}$ denotes the complex plane. Expected value, probability and absolute value are denoted by $\mathbb{E}\{\cdot\}$, $\mathbb{P}\{\cdot\}$ and $|\cdot|$. Let A be some matrix and a be some vector. $A[i,j]$ denotes the element in the i-th row and j-th column of A and $a[i]$ denotes the i-th element in a. $A \preceq 0$ means that A is negative semidefinite and similar applies to $\succeq$. The trace of matrix A is represented as $\mathrm{tr}(A)$, its rank is given by $\mathrm{rank}(A)$ and $\sigma(A)$ denotes the eigenvalues of A. Let x be a stochastic signal. We write $\|x_k\|_2^2 \triangleq x_k^T\, x_k$ for the Euclidean norm of vector x_k, $\|x\|_2^2 \triangleq \sum_{k=0}^{\infty} \|x_k\|_2^2$ for the l_2 norm of signal x and $\|x\|_{RMS}^2 \triangleq \lim_{k\to\infty} \frac{1}{K} \sum_{k=0}^{K-1} \|x_k\|_2^2$ for its RMS norm. I_n is the identity matrix of size $n \times n$ or of appropriate size when the subindex is omitted; similar applies to $0_{n\times n}$.

6.2 Problem statement

Consider the linear time-invariant (LTI) discrete-time system defined by

$$x_{k+1} = A\,x_k + B\,u_k + E\,f_k + S\,w_k, \tag{6.1a}$$

$$y_k = C\,x_k + D\,u_k + F\,f_k + T\,w_k, \tag{6.1b}$$

with $x \in \mathbb{R}^{n_x}$, $y \in \mathbb{R}^{n_y}$ and $u \in \mathbb{R}^{n_u}$ being the state, output and input vector. Vector $w \in \mathbb{R}^{n_w}$ represents the noise and vector $f \in \mathbb{R}^{n_f}$ includes the faults $f[l]$ with $l = 1, \ldots, n_f$ that affect system (6.1). A, B, C, D, E, F, S and T are known real constant matrices of appropriate dimensions. Note that pure process noise (w^p) and pure sensor noise (w^s) may be considered by means of zeroing the appropriate columns of S and T (i.e., $w = \begin{bmatrix} w^p \\ w^s \end{bmatrix}$ with $S = \begin{bmatrix} S^p & 0 \end{bmatrix}$ and $T = \begin{bmatrix} 0 & T^s \end{bmatrix}$). The following assumptions on the system (6.1) are made.

Assumption 6.1. *The pair (A, C) is observable.*

Assumption 6.2. *The matrices A, C, E and F satisfy*

$$\mathrm{rank} \begin{bmatrix} I_{n_x} - A & -E \\ C & F \end{bmatrix} = n_x + n_f.$$

Assumption 6.3. *The matrices A, C, E and F satisfy*

$$\operatorname{rank}\begin{bmatrix} z\,I_{n_x} - A & -E & 0 \\ 0 & -I_{n_f} & z\,I_{n_f} \\ C & F & 0 \end{bmatrix} = n_x + 2\,n_f$$

for $z \in \{\cos(\omega_r) \pm j\sin(\omega_r)\}$ with $r = 1, \ldots, n_R$.

Assumption 6.4. *The noises in w are zero-mean independent noises of known covariance, i.e., $\mathbb{E}\{w\,w^T\} = W$.*

Assumption 6.5. *We consider that each fault $f[l] = M_l\,f$ (with $M_l = \begin{bmatrix} 0_{1\times l-1} & 1 & 0_{1\times n_f - l} \end{bmatrix}$ and $l = 1, \ldots, n_f$) is in the fairly general form of*

$$f_k[l] = f_k^I[l] + f_k^R[l], \tag{6.2}$$

where $f_k^I[l] = \sum_{i=1}^{n_I} f_k^i[l]$ and $f_k^R[l] = \sum_{r=1}^{n_R} f_k^r[l]$ contain, respectively, the aperiodic and periodic components of the l-th fault which we write as

$$f_k^i[l] = \begin{cases} c_{i,l}\,(k - \kappa_{i,l})^{i-1} & \text{if } \; k \geq \kappa_{i,l} \\ 0 & \text{otherwise} \end{cases}, \tag{6.3a}$$

$$f_k^r[l] = \begin{cases} d_{r,l}\sin[\omega_r\,(k - \bar{\kappa}_{r,l})] & \text{if } \; k \geq \kappa_{r,l} \\ 0 & \text{otherwise} \end{cases}, \tag{6.3b}$$

where $c_{i,l}$ $(i = 1, \ldots, n_I)$ and $d_{r,l}$ $(r = 1, \ldots, n_R)$ are unknown constants, $\kappa_{i,l}$ $(i = 1, \ldots, n_I)$ and $\bar{\kappa}_{r,l}$ $(r = 1, \ldots, n_R)$ are the unknown times of appearance of the corresponding dynamics, and ω_r $(r = 1, \ldots, n_R)$ are the discrete frequencies of the periodic components of the l-th fault.

Remark 6.1. *Assumption 6.1 and Assumption 6.2 are usually made in the FE framework. Assumption 6.3 extends Assumption 6.2 from a high-frequency perspective. Assumption 6.4 is common for systems affected by stochastic noises (e.g., Kalman filter theory).*

Remark 6.2. *Many existing FE techniques assume bounded faults and/or faults with bounded first-time derivative, e.g., [135, 136, 305]. Hence, it is not restrictive to specify Assumption 6.5 including faults with bounded n_I-th time derivative as assumed in PMI observers [307] theory. Moreover, the periodic components of f in Assumption 6.5 allow considering high-frequency faults which, as stated in [104], cannot be covered by the dynamics of the faults assumed in PMI observers. All the fault parameters but the frequencies ω_r $(r = 1, \ldots, n_R)$ are assumed to be unknown. As previously discussed, the knowledge of these frequencies is reasonable in many practical cases (e.g., electrical and power systems).*

Remark 6.3. *Note that $f^I[l]$ can be seen as the n_I-th Taylor series expansion at $k = 0$ for a function g whose derivatives $g^{(n)}$ exist for $n = 1, \ldots, n_I$ on $k = 0$. Likewise, $f^R[l]$ with $\omega_r = r\,\omega_1$ can be seen as the n_R-th order Fourier series expansion for a periodic function g which is integrable on the interval $k \in [0, 2\,\pi/\omega_1]$.*

The faults in the form of (6.2) can be modeled through

$$\xi_{k+1} = A_F\,\xi_k + B_F\,\zeta_k, \tag{6.4a}$$
$$f_k = C_F\,\xi_k, \tag{6.4b}$$

with $\xi = \begin{bmatrix}\xi^I & \xi^R\end{bmatrix}^T \in \mathbb{R}^{n_\xi}$ being the fault state vector verifying $n_\xi = n_f \cdot (n_I + 2 \cdot n_R)$ and $\xi_0 = 0$. Vector $\zeta = \begin{bmatrix}\zeta^I & \zeta^R\end{bmatrix}^T \in \mathbb{R}^{n_\zeta}$ with $n_\zeta = n_f \cdot (n_I + n_R)$ is a vector including the following impulse signals:

$$\zeta_k^I = \begin{bmatrix} c_{n_I,1}\,\delta_{k-\kappa_{n_I,1}} \\ \vdots \\ c_{n_I,n_f}\,\delta_{k-\kappa_{n_I,n_f}} \\ \vdots \\ c_{1,n_f}\,\delta_{k-\kappa_{1,n_f}} \end{bmatrix},\ \zeta_k^R = \begin{bmatrix} d_{n_R,1}\,\delta_{k-\bar{\kappa}_{n_R,1}} \\ \vdots \\ d_{n_R,n_f}\,\delta_{k-\bar{\kappa}_{n_R,n_f}} \\ \vdots \\ d_{1,n_f}\,\delta_{k-\bar{\kappa}_{1,n_f}} \end{bmatrix}.$$

The matrices in (6.4) verify $A_F = \begin{bmatrix} A_F^I & 0 \\ 0 & A_F^R \end{bmatrix}$, $B_F = \begin{bmatrix} B_F^I & 0 \\ 0 & B_F^R \end{bmatrix}$, $C_F = \begin{bmatrix} C_F^I & C_F^R \end{bmatrix}$, with

$$A_F^I = \begin{bmatrix} I_{n_f} & 0 & 0 & 0 \\ I_{n_f} & I_{n_f} & 0 & 0 \\ 0 & \ddots & \ddots & 0 \\ 0 & 0 & I_{n_f} & I_{n_f} \end{bmatrix} \in \mathbb{R}^{(n_f\cdot n_I)\times(n_f\cdot n_I)},$$
$$B_F^I = I_{n_f\cdot n_I} \in \mathbb{R}^{(n_f\cdot n_I)\times(n_f\cdot n_I)},$$
$$C_F^I = \begin{bmatrix} 0 & I_{n_f} \end{bmatrix} \in \mathbb{R}^{n_f\times(n_f\cdot n_I)},$$
$$A_F^R = \left[\begin{array}{ccc|c} 2\cos(\omega_1)\,I_{n_f} & 0 & 0 & \\ 0 & \ddots & 0 & -I_{n_f\cdot n_R} \\ 0 & 0 & 2\cos(\omega_{n_R})\,I_{n_f} & \\ \hline & I_{n_f\cdot n_R} & & 0 \end{array}\right] \in \mathbb{R}^{(n_f\cdot 2\cdot n_R)\times(n_f\cdot 2\cdot n_R)},$$
$$B_F^R = \left[\begin{array}{ccc} \sin(\omega_1)\,I_{n_f} & 0 & 0 \\ 0 & \ddots & 0 \\ 0 & 0 & \sin(\omega_{n_R})\,I_{n_f} \\ \hline & 0 & \end{array}\right] \in \mathbb{R}^{(n_f\cdot 2\cdot n_R)\times(n_f\cdot n_R)},$$
$$C_F^R = \begin{bmatrix} I_{n_f} & \dots & I_{n_f} & 0 \end{bmatrix} \in \mathbb{R}^{n_f\times(n_f\cdot 2\cdot n_R)}.$$

Note that the first n_f elements in ζ refer to the generating signals related to the fault polynomial terms of highest order (i.e., $c_{n_I,l}\,(k-\kappa_{n_I,l})^{n_I-1}$). Therefore, $\zeta[l]$ refers to the polynomial term of highest order of the l-th fault and, more generally, $\zeta[(n_I-i)n_f+l]$ with $i \in [1,\dots,n_I]$ refers to the generating signal related to the term $c_{i,l}\,(k-\kappa_{i,l})^{i-1}$ of this l-th fault. In the following, we will use index m to refer to the m-th generating signal in vector ζ, index $\bar{m}(i,l) \triangleq (n_I-i)n_f+l$ to refer to the generating signal of the polynomial term of power $i-1$ in the fault channel l and index $\breve{m}(r,l) \triangleq (n_I+n_R-r)n_f+l$ to refer to the generating signal of the sinusoidal term

of frequency ω_r in the fault channel l. Thus, applying the $\mathcal{Z}$ transform to (6.4), we get that the transfer functions $G_{f[l],\zeta[m]}(z)$ from the different generating signals $\zeta[m]$ to $f[l]$ are given in

$$f[l](z) = \sum_{i=1}^{n_I} \frac{1}{(1-z^{-1})^i}\, \zeta[\bar{m}(i,l)](z) + \sum_{r=1}^{n_R} \frac{\sin(\omega_r)\, z^{-1}}{1 - 2\,\cos(\omega_r)\, z^{-1} + z^{-2}}\, \zeta[\breve{m}(r,l)](z). \tag{6.5}$$

Remark 6.4. *Although the fault generator model* (6.4) *is built in view of the generation of fault signals in the form of* (6.2)*, any fault signal* $f[l]$ *can be generated through* (6.4) *by any fault input signal* $\zeta[m]$ *with* $m = 1, \ldots, n_\zeta$ *whose* $\mathcal{Z}$ *transform is given by*

$$\zeta[m](z) = \mathcal{Z}^{-1}\left\{G_{f[l],\zeta[m]}(z)\right\}\, \mathcal{Z}\left\{f[l]\right\}.$$

The objective of this chapter is to study the following problem.

Problem 6.1. *Given the LTI discrete-time system* (6.1) *with zero-mean noises and faults in the form of* (6.2)*, it is required to provide a design strategy of an augmented observer that allows us to optimally set the trade-offs between the noise attenuation and the individual abilities to track each polynomial and sinusoidal fault term. It is then also necessary to analyse the effect of these trade-offs on the ability to track non-modeled simpler or more complex faults.*

6.3 Fault estimator

In order to build a model-based fault estimator, we extend the model (6.1) to include the model (6.4) as

$$z_{k+1} = \mathcal{A}\, z_k + \mathcal{B}\, u_k + \mathcal{E}\, \zeta_k + \mathcal{S}\, w_k, \tag{6.6a}$$
$$y_k = \mathcal{C}\, z_k + \mathcal{D}\, u_k + \mathcal{T}\, w_k, \tag{6.6b}$$
$$f_k = \mathcal{R}\, z_k, \tag{6.6c}$$

where $z = \begin{bmatrix} x^T & \xi^T \end{bmatrix}^T$ is the extended state vector and $\mathcal{A} = \begin{bmatrix} A & E\,C_F \\ 0 & A_F \end{bmatrix}$, $\mathcal{B} = \begin{bmatrix} B \\ 0 \end{bmatrix}$, $\mathcal{E} = \begin{bmatrix} 0 \\ B_F \end{bmatrix}$, $\mathcal{S} = \begin{bmatrix} S \\ 0 \end{bmatrix}$, $\mathcal{C} = \begin{bmatrix} C & F\,C_F \end{bmatrix}$, $\mathcal{D} = D$, $\mathcal{T} = T$ and $\mathcal{R} = \begin{bmatrix} 0 & C_F \end{bmatrix}$.

Theorem 6.1. *If Assumption 6.1 and Assumption 6.2 are satisfied, then the extended pair* $(\mathcal{A}, \mathcal{C})$ *is observable.*

Proof. Define $\mathbb{O}(z) = \begin{bmatrix} z\, I_{n_x} - \mathcal{A} \\ \mathcal{C} \end{bmatrix}$. From linear systems theory, the pair $(\mathcal{A}, \mathcal{C})$ is observable if $\operatorname{rank}\{\mathbb{O}(z)\} = n_x + n_\xi$ (with $n_\xi = n_f \cdot (n_I + 2 \cdot n_R)$) for any $z \in \sigma(\mathcal{A})$. In analogy to [41, 103] and since the eigenvalues of $\mathcal{A}$ are equivalent to $\{\sigma(A), 1, \cos(\omega_1) \pm j\sin(\omega_1), \ldots, \cos(\omega_{n_R}) \pm j\sin(\omega_{n_R})\}$, this proof discusses three cases:

(i) If $z \in \sigma(\mathcal{A})$ and $z \notin \{1, \cos(\omega_1) \pm j \sin(\omega_1), \ldots, \cos(\omega_{n_R}) \pm j \sin(\omega_{n_R})\}$, we have

$$\operatorname{rank}\{\mathbb{O}(z)\} = \operatorname{rank}\begin{bmatrix} z\, I_{n_x} - A \\ C \end{bmatrix} + n_\xi$$

and, because of Assumption 6.1, $\operatorname{rank}\{\mathbb{O}(z)\} = n_x + n_\xi$.

(ii) If $z = 1$, we have

$$\operatorname{rank}\{\mathbb{O}(1)\} = \operatorname{rank}\begin{bmatrix} I_{n_x} - A & 0 & 0 & 0 & -E \\ 0 & I_{n_f} & 0 & 0 & 0 \\ 0 & 0 & \ddots & \ddots & 0 \\ 0 & 0 & 0 & I_{n_f} & 0 \\ C & 0 & 0 & 0 & F \end{bmatrix} + n_f 2\, n_R,$$

$$\operatorname{rank}\{\mathbb{O}(1)\} = \operatorname{rank}\begin{bmatrix} I_{n_x} - A & -E \\ C & F \end{bmatrix} + n_f\,(n_I + 2\, n_R - 1)$$

and, because o f Assumption 6.2, $\operatorname{rank}\{\mathbb{O}(1)\} = n_x + n_\xi$.

(iii) For any $r = 1, \ldots, n_R$, if $z = z_r$ with $z_r \triangleq \cos(\omega_r) \pm j \sin(\omega_r)$, we have

$$\operatorname{rank}\{\mathbb{O}(z_r)\} = n_f\,(n_I + 2\, n_R - 2) + \operatorname{rank}\begin{bmatrix} z_r\, I_{n_x} - A & -E & 0 \\ 0 & -\bar{z}_r\, I_{n_f} & I_{n_f} \\ 0 & -I_{n_f} & z_r\, I_{n_f} \\ C & F & 0 \end{bmatrix}. \tag{6.7}$$

with $\bar{z}_r$ being the complex conjugate of z_r. For $\lambda = z_r$, we have

$$-\lambda\, \bar{z}_r\, I_{n_f} + I_{n_f} = 0, \quad \lambda\, I_{n_f} - z_r\, I_{n_f} = 0;$$

because $z_r\, \bar{z}_r = 1$ and we deduce that the second and third row of the matrix in (6.7) are linearly dependent. Thus, it follows that

$$\operatorname{rank}\{\mathbb{O}\,(z_r)\} = n_f\,(n_I + 2\, n_R - 2) + \operatorname{rank}\begin{bmatrix} z_r\, I_{n_x} - A & -E & 0 \\ 0 & -I_{n_f} & z_r\, I_{n_f} \\ C & F & 0 \end{bmatrix}$$

and, because of Assumption 6.3, $\operatorname{rank}\{\mathbb{O}\,(z_r)\} = n_x + n_\xi$.

From (i), (ii) and (iii), we have that $\operatorname{rank}\{\mathbb{O}(z)\} = n_x + n_\xi$ for any $z \in \sigma(\mathcal{A})$. This completes the proof of the theorem. □

Provided the observability of the extended pair $(\mathcal{A}, \mathcal{C})$, the faults are estimated through a model-based observer in the form of:

$$\hat{z}_{k+1} = \mathcal{A}\, \hat{z}_k + \mathcal{B}\, u_k + L\,(y_k - \mathcal{C}\, \hat{z}_k - \mathcal{D}\, u_k)\,, \tag{6.8a}$$

$$\hat{f}_k = \mathcal{R}\, \hat{z}_k + K\,(y_k - \mathcal{C}\, \hat{z}_k - \mathcal{D}\, u_k)\,, \tag{6.8b}$$

where L and K are to be defined and represent the observer gain matrices that update the model-based estimations with the measurements. In analogy to the PMI observers and to the PR controllers which are used in power systems [259, 285] we say that an observer in the from of (6.8) is a proportional multiple-integral and multiple-resonant (PMIR) observer.

Defining the FE error as $\widetilde{f}_k = f_k - \hat{f}_k$ and the extended state estimation error $\widetilde{z}_k = z_k - \hat{z}_k$, it follows that

$$\widetilde{z}_{k+1} = \mathbf{A}\,\widetilde{z}_k + \mathbf{E}\,\zeta_k + \mathbf{S}\,w_k, \tag{6.9a}$$

$$\widetilde{f}_k = \mathbf{R}\,\widetilde{z}_k + \mathbf{T}\,w_k, \tag{6.9b}$$

with $\mathbf{A} = \mathcal{A} - L\,\mathcal{C}$, $\mathbf{E} = \mathcal{E}$, $\mathbf{S} = \mathcal{S} - L\,\mathcal{T}$, $\mathbf{R} = \mathcal{R} - K\,\mathcal{C}$, and $\mathbf{T} = -K\,\mathcal{T}$. If we apply the $\mathcal{Z}$ transform to (6.9), we get

$$\widetilde{f}(z) = G_{\widetilde{f},\zeta}(z)\,\zeta(z) + G_{\widetilde{f},w}(z)w(z), \tag{6.10}$$

being $G_{\widetilde{f},\zeta}(z) = M(z)\mathbf{E}$, $G_{\widetilde{f},w}(z) = M(z)\,\mathbf{S} + \mathbf{T}$ and $M(z) = \mathbf{R}(z\,I - \mathbf{A})^{-1}$. Note that the error sources affecting the FE error are the zero-mean noises in w and the fault variations in ζ. In order to design the fault estimator (6.8), one must choose the observer gain matrices L and K so that certain trade-off between the attenuation from w and from ζ is satisfied.

Remark 6.5. *Note that the PMIR observer* (6.8) *enhances the estimation of simultaneous actuator and sensor faults. Redefining* $\mathcal{R}$ *as* $\mathcal{R} = \mathrm{diag}\{I, C_F\}$*, the observer* (6.8) *can be used as a simultaneous state and fault estimator as proposed in some works, e.g., [102, 106].*

Remark 6.6. *The fault estimator* (6.8) *could be generalized for a continuous system by augmenting the corresponding system model with the continuous form of the fault model* (6.4) *including continuous integrators and resonators. Then, the continuous observer should be constructed in analogy to* (6.8)*.*

6.4 Fault estimator design

In this section, we present an optimization-based design strategy of the observer (6.8). First, the robustness and the fault sensitivity of the observer, represented by norm-bounds regarding the attenuation from the noise w and from each $\zeta[m]$, are formulated using matrix inequalities. Second, these matrix inequalities are numerically transformed so that they can be implemented in a convex optimization design problem. Third, the obtained results are utilized in optimization-based problems for the design of the observer (6.8).

6.4.1 Formulation via matrix inequalities

The robustness and the fault sensitivity of the observer (6.8) are translated into norm-bounds using the formulation based on matrix inequalities in the following theorem.

Theorem 6.2. *Consider the fault estimator* (6.8) *applied to the system* (6.6) *and let* Γ *and* Υ *be certain diagonal matrices. If there exist any matrices* L *and* K *and any symmetric matrices* Q *and* P *fulfilling the matrix inequalities*

$$Q \succ 0, \tag{6.11a}$$
$$\mathbf{A}^T Q \mathbf{A} - Q + \mathbf{R}^T \mathbf{R} \prec 0, \tag{6.11b}$$
$$\mathbf{S}^T Q \mathbf{S} + \mathbf{T}^T \mathbf{T} - \Gamma \prec 0, \tag{6.11c}$$

$$P \succ 0, \tag{6.12a}$$
$$\mathbf{A}^T P \mathbf{A} - P + \mathbf{R}^T \mathbf{R} \prec 0, \tag{6.12b}$$
$$\mathbf{E}^T P \mathbf{E} - \Upsilon \prec 0, \tag{6.12c}$$

the following statements hold :

(i) In the absence of faults and noises (i.e., $\zeta = 0$*,* $w = 0$*), the error* (6.9) *converges to zero.*

(ii) In the absence of faults (i.e., $\zeta = 0$*), error* (6.9b) *is bounded as* $\mathrm{tr}(\mathbb{E}\{\widetilde{f}_k \, \widetilde{f}_k^T\}) < \mathrm{tr}(\Gamma W)$.

(iii) In the absence of noises (i.e., $w = 0$*), if* ζ *is an impulse, error* (6.9b) *is bounded as* $\|\widetilde{f}\|_2^2 < \sum_{m=1}^{n_\zeta} \Upsilon[m,m] \, \zeta_0^2[m]$.

Proof. Define the Lyapunov functions $V_k^Q = \widetilde{z}_k^T Q \, \widetilde{z}_k$ and $V_k^P = \widetilde{z}_k^T P \, \widetilde{z}_k$. The following items prove each statement of Theorem 6.2.

(i) In the absence of faults and noises, premultiplying (6.11b) by $\widetilde{z}_k^T$ and postmultipliying by its transpose, we get

$$V_{k+1}^Q - V_k^Q < 0, \tag{6.13}$$

which assures that the estimation error (6.9) converges to zero . If we perform similar steps on the inequality (6.12b), we get the same result w.r.t. V^P, i.e.,

$$V_{k+1}^P - V_k^P < 0, \tag{6.14}$$

(ii) Premultiplying (6.11c) by w_k^T and postmultipliying by its transpose, summing the obtained constraint to (6.13) and taking expected value on the result, we get

$$\mathbb{E}\{V_{k+1}^Q\} - \mathbb{E}\{V_k^Q\} + \mathrm{tr}(\mathbb{E}\{\widetilde{f}_k \, \widetilde{f}_k^T\}) < \mathrm{tr}(\Gamma W),$$

where we have taken into account the independence between $\widetilde{z}_k$ and w_k and we have applied that $\mathbb{E}\{w_k^T \Gamma \, w_k\} = \mathrm{tr}(\Gamma W)$ and $\mathbb{E}\{\widetilde{f}_k^T \, \widetilde{f}_k\} = \mathrm{tr}(\mathbb{E}\{\widetilde{f}_k \, \widetilde{f}_k^T\})$ because w_k is zero-mean and so does $\widetilde{f}_k$ in the absence of faults [271]. Considering null initial conditions ($\mathbb{E}\{V_0^Q\} = 0$), adding the result from $k = 0$ to $k = K$, dividing the resulting expression by K and taking the limit when $K \to \infty$, it leads to the second statement in Theorem 6.2 because with (6.11a) we have $\mathbb{E}\{V_{K+1}^Q\} \geq 0$.

(iii) Performing similar steps over the inequalities in (6.12) (i.e., operations with ζ_k^T on (6.12c), summation of the obtained constraint to (6.14) and taking expected value on the result), it yields

$$\mathbb{E}\{V_{k+1}^P\} - \mathbb{E}\{V_k^P\} + \mathbb{E}\{\widetilde{f}_k^T\,\widetilde{f}_k\} - \mathbb{E}\{\zeta_k^T\,\Upsilon\,\zeta_k\} < 0.$$

Considering null initial conditions ($\mathbb{E}\{V_0^P\} = 0$), adding the result from $k = 0$ to $k = K$, and provided that ζ_k is an impulse (i.e., $\zeta_k = 0$ for $k \neq 0$), we get $\|\widetilde{f}\|_2^2 < \zeta_0^T\,\Upsilon\,\zeta_0$ because $\mathbb{E}\{V_{K+1}^p\} \geq 0$ and $\mathbb{E}\{\widetilde{f}_k^T\,\widetilde{f}_k\} = \widetilde{f}_k^T\,\widetilde{f}_k$ since ζ_k is deterministic. Provided that matrix Υ is diagonal, we prove the third statement in Theorem 6.2.

□

Remark 6.7. *Note that the third statement in Theorem 6.2 bounds the norm of the FE error w.r.t. each fault input $\zeta[m]$ through the diagonal term $\Upsilon[m,m]$. Hence, different values in the diagonal terms of Υ enhance a design with a different sensitivity w.r.t. each different fault input $\zeta[m]$ ($m = 1,\ldots,n_\zeta$).*

In order to give a discrete-time domain interpretation to these results, the following corollary to Theorem 6.2 can be used. The proof is straightforward and thus is omitted here.

Corollary 6.1. *If the premises in Theorem 6.2 are satisfied, the following statements hold for the estimator* (6.8) *applied to* (6.6)*:*

(i) The sum of the variances of the fault estimates $\hat{f}[l]$ due to noises (i.e., $\gamma = \mathrm{tr}(\mathbb{E}\{\hat{f}_k\,\hat{f}_k^T\})$ with $f = 0$) is bounded as $\gamma < \mathrm{tr}(\Gamma\,W)$.

(ii) The cumulative squared error (CSE)[1] of the FE vector $\hat{f}$ due to a unitary impulse input $\zeta[m]$ (i.e., $\upsilon_m = \|\widetilde{f}\|_2^2$ with $w = 0$ and $\zeta[n] = 0$ for $n = 1,\ldots,m-1,m+1,\ldots,n_\zeta$) is bounded as $\upsilon_m < \Upsilon[m,m]$.

6.4.2 Numerical treatment for convexification

Note that the conditions in Theorem 6.2 are standard in norm-based designs [121,335] and their feasibility depends on the restrictiveness of the chosen values for Γ and Υ. The use of independent closed-loop Lyapunov functions Q and P guarantee a non-conservative design based on these inequalities; however, the design results in a nonlinear problem. To recover convexity without conservatively requiring all specifications to be enforced by a single Lyapunov function [252], i.e., $Q = P$, we can adopt a compromise solution by introducing a slack variable Z [69, 121]. After some Schur complement operation and performing a congruence transformation by $\begin{bmatrix} Z & 0 \\ 0 & I \end{bmatrix}$ to (6.11) and (6.12), we get the linear matrix inequalities (LMIs)

$$\begin{bmatrix} Z^\star - Q & \mathscr{A} & 0 \\ \mathscr{A}^T & Q & \mathbf{R}^T \\ 0 & \mathbf{R} & I \end{bmatrix} \succ 0, \quad \begin{bmatrix} Z^\star - Q & \mathscr{S} & 0 \\ \mathscr{S}^T & \Gamma & \mathbf{T}^T \\ 0 & \mathbf{T} & I \end{bmatrix} \succ 0, \tag{6.15}$$

[1] The CSE experienced by an observer is intrinsically related to its settling time. Hence, higher CSEs imply higher settling times and vice-versa.

$$\begin{bmatrix} Z^\star - P & \mathscr{A} & 0 \\ \mathscr{A}^T & P & \mathbf{R}^T \\ 0 & \mathbf{R} & I \end{bmatrix} \succ 0, \quad \begin{bmatrix} Z^\star - P & Z\,\mathbf{E} \\ \mathbf{E}^T\, Z^T & \Upsilon \end{bmatrix} \succ 0, \tag{6.16}$$

with $Z^\star = Z + Z^T$, $\mathscr{A} = Z\,\mathcal{A} - X\,\mathcal{C}$, $\mathscr{S} = Z\,\mathcal{S} - X\,\mathcal{T}$ and $X = Z\,L$. Here, we have taken into account that the inequality $Z\,Q^{-1}\,Z^T \succeq Z + Z^T - Q$ holds for any strictly positive definite matrix Q and any full-rank matrix Z. Note that it would also be possible to iteratively solve the inequalities (6.11) and (6.12) if we perform Schur complements and we build a sequence of problems of LMIs following different approaches such as the ones presented in [86].

6.4.3 Design optimization problem

The results in Theorem 6.2 could be utilized to design a PMIR observer with a fixed performance w.r.t. noises and faults. In order to solve Problem 1, we use them in an optimization-based design strategy that ensures certain optimal trade-off between the robustness and the individual fault sensitivity of the observer. Let us first introduce the following assumption on the fault input vector ζ.

Assumption 6.6. *There is a non-zero probability that some fault inputs $\zeta[m]$ are zero, i.e., $\mathbb{P}\left\{\bigcup_{m=1}^{n_\zeta} \zeta[m] = 0\right\} \neq 0$.*

Provided Assumption 6.6, we can define the probability of appearance of certain fault input $\zeta[m]$ as $\alpha_m = 1 - \mathbb{P}\{\zeta[m] = 0\}$.

Remark 6.8. *Assumption 6.6 enhances PMIR observer designs in which the fault sensitivity towards the most probable fault forms is preponderant over the fault sensitivity towards less probable fault forms. Hence, the probability of appearance of the faults can be seen as design weights which are given to the different polynomial and sinusoidal fault terms in* (6.2).

Remark 6.9. *It is extended in PMI observer theory to consider that the fault input is $\zeta'_k = \begin{bmatrix} c_{n_I,1} & \dots & c_{n_I,n_f} \end{bmatrix}^T \delta_k \in \mathbb{R}^{n_f}$ and to characterize the fault sensitivity by means of the attenuation from ζ' (e.g., theoretical works [103, 322] and practical works [166, 176]). In this thesis, we extend this approach and we characterize the fault sensitivity by means of the individual attenuation not only from the higher order dynamics generated by ζ' but from all the dynamics generated by ζ. Note that Assumption 6.6 allows considering previous approaches which are achievable if we set $\alpha_m = 1/n_f$ for $m = 1, \dots, n_f$ and $\alpha_m = 0$ for $m = n_f + 1, \dots, n_\zeta$.*

The following two strategies show a proposal of how to use the results in Theorem 6.2 and Corollary 6.1 in a multiobjective optimization problem for designing fault estimators guaranteeing certain trade-off between noise attenuation and fault sensitivity. Let us remark that these design strategies are based on the discrete-time parameters in Corollary 6.1 (variances and CSEs) which are rather intuitive for designers in practical environments. To enhance the individual fault sensitivity approach, we distinguish between the fault unitary impulse inputs for which a specific CSE constraint is necessary ($\zeta[m]$ such that $m \in \Omega$, $\Omega \subset [1, n_\zeta]$) and expected/weighted CSE of the other unitary impulse inputs ($\zeta[m]$ such that $m \notin \Omega$)

Strategy 6.1. *Assume that we want to design an estimator* (6.8) *with:*

- *minimum sum of the variances of the fault estimates* $\hat{f}[l]$ *due to noises (i.e.,* γ*),*
- *certain expected CSE due to the unitary impulse inputs* $\zeta[m]$ *such that* $m \in \Omega$ *(i.e.,* $\sum_{m\in\Omega} \alpha_m \upsilon_m \leq \bar{\upsilon}$*),*
- *certain bounded CSE (i.e.,* $\upsilon_m \leq \bar{\upsilon}_m$*) due to each unitary impulse input* $\zeta[m]$ *such that* $m \in [1, n_\zeta]\backslash\Omega$*,*

To address this design, we set the following convex optimization problem

$$\begin{aligned} \text{minimize} \quad & \operatorname{tr}(\Gamma\, W) \\ \text{subject to} \quad & \sum_{m\in\Omega} \alpha_m \Upsilon[m,m] \leq \bar{\upsilon} \\ & \Upsilon[m,m] \leq \bar{\upsilon}_m, \quad m \in [1, n_\zeta]\backslash\Omega, \\ & (6.15), (6.16) \end{aligned} \tag{6.17}$$

along the variables Z*,* X*,* K*,* Q*,* P*,* Γ *and* Υ *and we define* $L = Z^{-1} X$*.*

Strategy 6.2. *Assume that we want to design a fault estimator* (6.8) *with:*

- *certain bounded sum of the variances of the fault estimates* $\hat{f}[l]$ *due to noises (i.e.,* $\gamma \leq \bar{\gamma}$*),*
- *minimum expected CSE due to the unitary impulse inputs* $\zeta[m]$ *such that* $m \in \Omega \subset [1, n_\zeta]$ *(i.e.,* $\sum_{m\in\Omega} \alpha_m \upsilon_m$*),*
- *certain bounded CSE (i.e.,* $\upsilon_m \leq \bar{\upsilon}_m$*) due to each unitary impulse input* $\zeta[m]$ *such that* $m \in [1, n_\zeta]\backslash\Omega$*,*

To address this design, we set the following convex optimization problem

$$\begin{aligned} \text{minimize} \quad & \sum_{m\in\Omega} \alpha_m \Upsilon[m,m] \\ \text{subject to} \quad & \Upsilon[m,m] \leq \bar{\upsilon}_m, \quad m \in [1, n_\zeta]\backslash\Omega, \\ & \operatorname{tr}(\Gamma\, W) \leq \bar{\gamma} \\ & (6.15), (6.16) \end{aligned} \tag{6.18}$$

along Z*,* X*,* K*,* Q*,* P*,* Γ *and* Υ *and we define* $L = Z^{-1} X$*.*

Remark 6.10. *Although we assume that the system* (6.1) *is not affected by non-zero mean disturbances, it is possible to extend the results presented in this chapter to a system in the form of*

$$\begin{aligned} x_{k+1} &= A\, x_k + B\, u_k + E\, f_k + S\, w_k + S_2\, d_k, \\ y_k &= C\, x_k + D\, u_k + F\, f_k + T\, w_k + T_2\, d_k, \end{aligned}$$

where $d \in \mathbb{R}^{n_d}$ is a bounded vector and S_2 and T_2 are known constant matrices of appropriate dimensions. For such cases, we propose to obtain the matrix inequalities which bound the $\mathcal{H}_\infty$ norm of the dynamics between d and $\widetilde{f}$ and add them in the design strategies of the observer. See [213,326] for details on obtaining this norm using standard matrix inequalities formulation. If unknown input decoupling were necessary, one could guarantee it by constraining the value of this $\mathcal{H}_\infty$ norm to zero or by using the algebraic constraints explained in [70, 106]. To build this Unknown Input Observer (UIO), the rank inequalities in Assumptions 6.2 and 6.3 should be extended as indicated in [106].

6.5 Analysis of the tracking behavior of PMIR observers

In this section, we analyse the tracking behavior of PMIR observers when the system is affected by different types of faults. For this analysis, we omit the effect of the noise w on the fault estimates.

6.5.1 Steady-state analysis

From a steady-state perspective, we have shown that an observer in the form of (6.8) designed through the strategies presented in Section 6.4 experiences a finite cumulative squared error when any fault in the form of (6.2) affects the system. Thus, in such cases, the steady-state error of the estimator is zero. However, seldom is the dynamics of the real faults completely known and it is possible that the real dynamics of a fault affecting the system does not match the assumed model. In the following, we analyse the behavior of the estimator when the system is affected by any polynomial fault and by a sinusoidal fault of any frequency.

Polynomial faults

Let us characterize the steady-state behavior of the PMIR observer (6.8) when the system (6.1) is affected by a polynomial fault of any degree N. To do so, we first introduce a corollary to Theorem 6.2 which gives a bound of the RMS-norm of the FE error as a function of the difference between the degree of the fault (N) and the number of integral terms considered by the PMIR observer (n_I). Then, we obtain a bound of the final value of the estimation error.

Corollary 6.2. *Consider the fault estimator* (6.8) *applied to the system* (6.6)*. If a fault $f[l]$ in the form of $f_k[l] = c_{N,l}\, k^{N-1}$ affects the system, the RMS norm of the l-th FE error is bounded as*

$$\left\|\widetilde{f}[l]\right\|_{RMS} \leq \begin{cases} 0 & \text{if } N \leq n_I \\ \chi_l\, c_{N,l} & \text{if } N = n_I + 1 \\ \infty & \text{if } N > n_I + 1 \end{cases}, \tag{6.19}$$

with $\chi_l = \left\|G_{\widetilde{f}[l],\zeta[l]}(z)\right\|_\infty$ being the $\mathcal{H}_\infty$ norm of the transfer function between $\widetilde{f}[l](z)$ and $\zeta[l](z)$ (i.e., the generating signal for the polynomial term of highest order $c_{n_I,l}\, k^{n_I-1}$).

Proof. Provided equality (6.5) and Remark 6.4, we have that $f_k[l] = c_{N,l}\, k^{N-1}$ (whose $\mathcal{Z}$ transform is $f[l](z) = \frac{c_{N,l}}{(1-z^{-1})^N}$) can be generated as

$$f[l](z) = G_{f[l],\zeta[\bar{m}]}(z)\, \zeta[\bar{m}](z)$$

with

$$\zeta[\bar{m}](z) = \frac{c_{N,l}}{(1-z^{-1})^{N-i}}$$

for any $i = 1, \dots n_I$ (index $\bar{m}$ being equivalent to $\bar{m}(i,l) \triangleq (n_I - i)\, n_f + l$). From Theorem 6.2 we have that $\left\|G_{\widetilde{f},\zeta[m]}(z)\right\|_2^2 \leq \Upsilon[m,m]$ and, thus, $\left\|G_{\widetilde{f}[l],\zeta[m]}(z)\right\|_\infty = \chi_m < \infty$. Then, the RMS norm of $\widetilde{f}[l]$ is bounded as

$$\left\|\widetilde{f}[l]\right\|_{RMS} \leq \chi_{\bar{m}} \left\|\mathcal{Z}^{-1}\left\{\frac{c_{N,l}}{(1-z^{-1})^{N-i}}\right\}\right\|_{RMS}$$

for all $i = 1, \dots, n_I$ and it, thus, verifies

$$\left\|\widetilde{f}[l]\right\|_{RMS} \leq \min_{i=1,\dots,n_I}\left\{\chi_{\bar{m}} \left\|\mathcal{Z}^{-1}\left\{\frac{c_{N,l}}{(1-z^{-1})^{N-i}}\right\}\right\|_{RMS}\right\}.$$

The RMS norm of the signal $\mathcal{Z}^{-1}\left\{\frac{c_{N,l}}{(1-z^{-1})^{N-i}}\right\}$ is zero if $N - i < 1$, finite if $N - i = 1$ (i.e., a step signal), and infinite if $N - i > 1$. Thus, the previous minimum is archived for $i = n_I$ and we have

$$\left\|\widetilde{f}[l]\right\|_{RMS} \leq \chi_l \left\|\mathcal{Z}^{-1}\left\{\frac{c_{N,l}}{(1-z^{-1})^{N-n_I}}\right\}\right\|_{RMS}.$$

because $\bar{m}(n_I, l) = l$, leading to the statement in Corollary 6.2. □

The bound (6.19) in Corollary 6.2 implies that if a fault $f[l]$ in the form of $f_k[l] = c_{N,l}\, k^{N-1}$ affects the system, the steady-state FE error of the l-th fault, i.e., $\lim_{k\to\infty} \widetilde{f}_k[l]$, is bounded as

$$\lim_{k\to\infty} \widetilde{f}_k[l] \leq \begin{cases} 0 & \text{if } N \leq n_I \\ K_l & \text{if } N = n_I + 1 \\ \infty & \text{if } N > n_I + 1 \end{cases}, \tag{6.20}$$

with K_l being a constant which can be obtained through the following procedure.

From Theorem 6.2 we have that $\left\|G_{\widetilde{f},\zeta[m]}(z)\right\|_2^2 \leq \Upsilon[m,m]$ and, thus, $\left\|G_{\widetilde{f}[l],\zeta[m]}(z)\right\|_2 = \phi_m < \infty$. Provided that $G_{\widetilde{f}[l],\zeta[m]}(z) = G_{\widetilde{f}[l],f[l]}(z)\, G_{f[l],\zeta[m]}(z)$ and using the definition of $G_{f[l],\zeta[m]}(z)$ in (6.5), we have that

$$\left\|G_{\widetilde{f}[l],\zeta[\bar{m}]}(z)\right\|_2 = \left\|G_{\widetilde{f}[l],f[l]}(z)\, \frac{1}{(1-z^{-1})^i}\right\|_2 = \phi_m < \infty$$

for all $i = 1, \dots n_I$ (index $\bar{m}$ being equivalent to $\bar{m}(i,l) \triangleq (n_I - i)\, n_f + l$). Thus, we deduce that $\lim_{k\to\infty} \widetilde{f}_k[l] = 0$ when $\zeta_k[\bar{m}] = c_{i,l}\delta_k$. Applying the final value theorem, this result implies that

$$\lim_{z\to 1} G_{\widetilde{f}[l],f[l]}(z)\, \frac{c_{i,l}}{(1-z^{-1})^{i-1}} = 0, \tag{6.21}$$

for all $i = 1, \ldots, n_I$. Let us now decompose $G_{\widetilde{f}[l],f[l]}(z)$ as

$$G_{\widetilde{f}[l],f[l]}(z) = \mathcal{H}_{l,l}(z)\,(1-z^{-1})^p,$$

where $\mathcal{H}_{l,l}(z)$ is a transfer function verifying $\mathcal{H}_{l,l}(1) = \kappa_{l,l}$ ($\kappa_{l,l}$ being a constant) and p represents the number of zeros at $z = 1$ in $G_{\widetilde{f}[l],f[l]}(z)$. Provided that

$$\lim_{z\to 1} \frac{\bar{K}\,(1-z^{-1})^p}{(1-z^{-1})^q} = \begin{cases} 0 & \text{if } q < p \\ \bar{K} & \text{if } q = p \\ \infty & \text{if } q > p \end{cases},$$

we deduce from (6.21) that

$$p \geq n_I \tag{6.22}$$

because $p \geq i$ for all $i = 1, \ldots, n_I$. Applying the final value theorem when a fault $f[l]$ in the form of $f_k[l] = c_{N,l}\,k^{N-1}$ affects the system, we get

$$\begin{aligned} &\lim_{z\to 1} G_{\widetilde{f}[l],f[l]}(z)\,\frac{c_{N,l}}{(1-z^{-1})^{N-1}} = \\ &\lim_{z\to 1} \mathcal{H}_{l,l}(z)\frac{c_{N,l}(1-z^{-1})^p}{(1-z^{-1})^{N-1}} \leq \begin{cases} 0 & \text{if } N \leq n_I \\ \kappa_{l,l}\,c_{N,l} & \text{if } N = n_I + 1 \\ \infty & \text{if } N > n_I + 1 \end{cases} \end{aligned} \tag{6.23}$$

and we deduce that K_l in (6.20) satisfies $K_l = \kappa_{l,l}\,c_{N,l}$.

Remark 6.11. *In essence, the purpose of a fault estimator is to invert the transfer functions from the faults to the measurements [70]. If these transfer functions contain poles which are close to $z = 1$ (i.e., integrators), it may occur that the transfer function from a fault to the corresponding FE error contains p_0 zeros at $z = 1$ (i.e., derivative terms) regardless of the dynamics of the faults included in the estimator. Thus, we rewrite* (6.22) *as $p = n_I + p_0$ with $p_0 \geq 0$ and we have that*

$$\lim_{z\to 1} G_{\widetilde{f}[l],f[l]}(z)\,\frac{c_{N,l}}{(1-z^{-1})^{N-1}} = \lim_{z\to 1} \mathcal{H}_{l,l}(z)\frac{c_{N,l}(1-z^{-1})^{n_I+p_0}}{(1-z^{-1})^{N-1}} = \begin{cases} 0 & \text{if } N \leq n_I + p_0 \\ K_l & \text{if } N = n_I + p_0 + 1 \\ \infty & \text{if } N > n_I + p_0 + 1 \end{cases}$$

with $K_l = \kappa_{l,l}\,c_{N,l}$. Since no a priori knowledge of $p_0 \geq 0$ is available, this equality leads to the bound (6.23).

Sinusoidal faults

Let us now characterize the steady-state behavior of the PMIR observer (6.8) when the system (6.1) is affected by a sinusoidal fault of any frequency ω_N. To do so, we introduce a corollary to Theorem 6.2 which gives a bound of the RMS-norm of the FE error through the difference between the frequency of the fault (ω_N) and the frequencies considered by the PMIR observer ($\omega_r,\ r = 1, \ldots, n_R$). From this bound, we deduce a bound of the steady-state FE error.

Corollary 6.3. *Consider the fault estimator* (6.8) *applied to the system* (6.6)*. If a fault* $f[l]$ *in the form of* $f_k[l] = d_{N,l}\sin(\omega_N\, k)$ *affects the system, the RMS norm of the* l*-th FE error is bounded as*

$$\left\|\widetilde{f}[l]\right\|_{RMS} \leq \begin{cases} 0 & \text{if } \omega_N \in \mho \\ \min\limits_{r=1,\ldots,n_R} \left\{ \chi_{\breve{m}} \frac{d_{N,l}\,|\omega_r^2-\omega_N^2|}{\sqrt{2}\,\omega_N} \right\} & \text{if } \omega_N \notin \mho \end{cases} \tag{6.24}$$

with $\mho = \{\omega_1, \ldots, \omega_{n_R}\}$, $\chi_m = \left\|G_{\widetilde{f}[l],\zeta[m]}(z)\right\|_\infty$ *being the* $\mathcal{H}_\infty$ *norm of the transfer function between* $\widetilde{f}[l](z)$ *and* $\zeta[m](z)$ *and index* $\breve{m}$ *being equivalent to* $\breve{m}(r,l) \triangleq (n_I + n_R - r)\, n_f + l$*.*

Proof. According to the proof of Corollary 6.2, $f_k[l] = d_{N,l}\sin(\omega_N\, k)$ (whose $\mathcal{Z}$ transform is $f[l](z) = \frac{d_{N,l}\sin(\omega_N)\, z^{-1}}{1-2\,\cos(\omega_N)\, z^{-1}+z^{-2}}$) can be generated through $G_{f[l],\zeta[\breve{m}]}(z)$ by

$$\zeta[\breve{m}](z) = \frac{1 - 2\,\cos(\omega_r)\, z^{-1} + z^{-2}}{\sin(\omega_r)\, z^{-1}} \, \frac{d_{N,l}\sin(\omega_N)\, z^{-1}}{1 - 2\,\cos(\omega_N)\, z^{-1} + z^{-2}}.$$

for any $r = 1, \ldots n_R$ (index $\breve{m}$ being equivalent to $\breve{m}(r,l) \triangleq (n_I + n_R - r)\, n_f + l$). The RMS norm of $\widetilde{f}[l]$ is thus bounded as

$$\left\|\widetilde{f}[l]\right\|_{RMS} \leq \min_{r=1,\ldots,n_R} \left\{ \chi_{\breve{m}} \left\| \mathcal{Z}^{-1}\left\{\zeta[\breve{m}](z)\right\} \right\|_{RMS} \right\}$$

which is equivalent to

$$\left\|\widetilde{f}[l]\right\|_{RMS} \leq \min_{r=1,\ldots,n_R} \left\{ \chi_{\breve{m}} \frac{d_{N,l}\,|\omega_r^2-\omega_N^2|}{\sqrt{2}\,\omega_N} \right\}$$

leading to the statement in Corollary 6.3. □

It is straightforward to deduce that the bound (6.24) in Corollary 6.3 implies that if a fault $f[l]$ in the form of $f_k[l] = d_{N,l}\sin(\omega_N\, k)$ affects the system, the peak value of the steady-state estimation error of the l-th fault, i.e., $\widetilde{f}_k[l]$ with k sufficiently large to achieve the sinusoidal steady state, is bounded as ($\mho = \{\omega_1, \ldots, \omega_{n_R}\}$):

$$\max_k |\widetilde{f}_k[l]| \leq \begin{cases} 0 & \text{if } \omega_N \in \mho \\ \min\limits_{r=1,\ldots,n_R} \left\{ \chi_{\bar{\breve{m}}(r,l)} \frac{d_{N,l}\,|\omega_r^2-\omega_N^2|}{\omega_N} \right\} & \text{if } \omega_N \notin \mho \end{cases}$$

6.5.2 Transient analysis

From the analysis in Section 6.5.1, we deduce that, from a steady-state perspective, better results are achieved when the degree n_I of the faults considered by the estimator is increased. However, increasing this degree has its counterpart in the transient behavior of the estimator. First, from (6.21) we have that

$$\lim_{z\to 1} \frac{1}{(1-z^{-1})^q}\, \mathcal{G}_{\widetilde{f}[l],f[l]}(z)\, \frac{1}{(1-z^{-1})^{N-1}} = 0, \;\; \forall q \leq n_I - N.$$

This equality implies that the cumulative error related to the l-th fault is zero whenever $N < n_I$ and that the fault estimate $\hat{f}[l]$ has, thus, an oscillatory behavior. It is worth nothing mentioning that this behavior is undesirable in FE; especially, when the resulting fault estimates are used in fault tolerant control schemes.

Remark 6.12. *Likewise to the analysis performed in Remark 6.11, if we denote the number zeros at $z = 1$ which appear in the estimator regardless of the dynamics of the modeled faults as p_0, the equality in 6.5.2 holds for all $q \leq n_I + p_0 - N$.*

Second and considering $n_R = 0$, the design freedom of an observer in the form of (6.8) is provided by the observer gains $K \in \mathbb{R}^{n_f \times n_y}$ and $L = \begin{bmatrix} L_x \\ L_I \end{bmatrix}$ with $L_x \in \mathbb{R}^{n_x \times n_y}$ and $L_I \in \mathbb{R}^{(n_I \cdot n_f) \times n_y}$. In general and omitting the design effort which is devoted to the satisfaction of noise attenuation constraints, all the design flexibility provided by L_x, L_I and K can be used to ameliorate the ability to track the n_I polynomial terms of the faults. Now, if we design an augmented observer including polynomial faults up to degree $n_I + N$ in its model, the observer gains become K and $L' = \begin{bmatrix} L_x \\ L_N \\ L_I \end{bmatrix}$ with $L_N \in \mathbb{R}^{(N \cdot n_f) \times n_y}$. In such a case and given the structure of the matrices A_F, B_F and C_F in (6.4), the design freedom provided by L_I, L_x and K can be used to ameliorate the ability to track both the first n_I and the last N polynomial terms of the faults. For its part, the design flexibility provided by L_N has no effect on the ability to track the n_I polynomial terms of lower order and and it can only be used to improve the ability to track the N polynomial terms of higher order. In all, we intuitively deduce that the ability to track certain term of a polynomial fault cannot be improved by increasing the order of the augmented observer and that this tracking ability deteriorates as the sensitivity to polynomial terms of higher order is increased. Similar deductions apply to the number of resonators included in a PMIR observer.

6.5.3 Relevance of the proposed design

In this section, we have proved the exiting trade-off between the steady-state accuracy of an augmented observer w.r.t. complex faults and its transient behavior w.r.t. simpler faults. For PMI observers, we have proved that if we choose a large observer order as proposed in the literature [103, 104], the steady-state error is effectively zero for polynomial faults below or equal to this order. It is constant for polynomial faults of one extra order and increasing for polynomial faults of higher-orders (Section 6.5.1). However, we have shown that this election imposes some compromises because it deteriorates the performance of the observer w.r.t. lower-order faults causing a slower and oscillatory response (Section 6.5.2).

This conclusion motivates the design proposed in Section 6.4 which, in contrast to the existing designs in the literature of augmented observers (e.g., [103, 166]), weights the effect of each polynomial degree of the fault. The weighting allows attenuating the negative effect on the transient behavior of the observer w.r.t. low-order faults when extending the observer for taking into account more complex but less probable fault dynamics.

Moreover, the resonant terms that we propose to include in the PMI observer (leading to a PMIR observer) allow considering high-frequency faults without intensively augmenting the negative effect of the noises on the fault estimates. The PMIR architecture maximizes the

observer fault sensitivity around the high-frequencies in which the sinusoidal fault terms are subject to occur. It should also be noted that the existence conditions for PMR observers differ from those of PMI observers (see Theorem 6.1). Thus, it would be possible to design a PMR observer for some systems which do not verify PMI observer existence conditions.

In all, compared with the existing literature of augmented observers, the proposed observer and its design are based on taking these performance trade-offs into account. They allow weighting the effect of the different fault terms according to their the probability of appearance or hazard and they make possible the estimation of resonant fault terms with higher noise attenuation levels.

Example 6.1. *To illustrate the goodness of the approach, consider the example case in which a system is prone to three kinds of faults: a step, a ramp and a sinus of certain high-frequency. We assume that the step and the sinusoidal fault have a high hazard potential due to their abrupt nature whilst the ramp fault is less damaging. A common PMI observer needs to consider two integrators of equal importance in its architecture and to accept low noise attenuation so as to capture the sinusoidal fault. The proposed PMIR observer is able to achieve higher noises attenuations because the resonant term enhances the sinusoidal fault sensitivity. Moreover, for an equal noise attenuation level, faster step fault tracking can be achieved at the cost of a slower response to the less dangerous ramp fault.*

Let us finally remark that the proposed observer does not introduce any complexity in terms of implementation because its architecture is analogous to that of PI and PMI observers. Note that augmented observers are not highly computationally demanding because they avoid complex schemes and computations (e.g., the adaptive laws in [98] involving nonlinear computations or the intermediate computation steps of the iterative observer in [136]). In terms of design, the procedure is based on standard convex optimization problems with LMIS. Moreover, the tuning of the constraining terms in the design is facilitated by the use of intuitive parameters (variances and CSEs).

6.6 Numerical illustrative example

In this section, we are going to numerically show the error effects caused by large-order augmented observers and, consequently, the advantages of weighting in the design the effect of the different fault dynamics included in the observer. Moreover, we are going to study the convenience of including resonant terms in the augmented observer when the system is prone to high-frequency faults. For this purpose, consider a system in the form of (6.1) with matrices

$$A = \begin{bmatrix} 0.700 & 0.300 & 0.200 & -0.003 \\ 0.050 & 0.600 & -0.002 & -0.040 \\ 0.010 & 0.003 & 0.630 & 1 \\ 0 & 0 & 0.010 & 0.600 \end{bmatrix}, \quad B = \begin{bmatrix} 0.0044 & 0.0018 \\ 0.0353 & -0.0755 \\ -0.0559 & 0.0454 \\ -0.0003 & 0.0002 \end{bmatrix}, \quad C = \begin{bmatrix} 1 & 0 & 0 & 0 \\ 0 & -1 & 0 & 0 \end{bmatrix},$$

$$D = 0_{2\times 2}, \quad S = \begin{bmatrix} I_4 & 0_{4\times 2} \end{bmatrix}, \quad T = \begin{bmatrix} 0_{2\times 4} & I_2 \end{bmatrix}.$$

The covariance matrix of the noises is $W = 0.004\, I_6$. In the following, we study the case in which this system is only affected by actuator faults and the case in which it is prone to both actuator and sensor faults. For sake of clarity, unless explicitly stated otherwise, we show the simulation results with $w_k = 0$. The latter does not mean that $w_k = 0$; it only means that we remove the effect of the noises in the figures. For sake of brevity, we just include some of the obtained observer gain matrices. All the observer designs are set up in YALMIP [192] and solved using the solver MOSEK [204].

6.6.1 Actuator fault

Suppose that the system has the following fault distribution matrices

$$E = \begin{bmatrix} -0.0088 & -0.0706 & 0.1118 & 0.0006 \end{bmatrix}^T, \quad F = \begin{bmatrix} 0 & 0 \end{bmatrix}^T,$$

and define the following polynomial fault signals (all of them appearing at $k = 5$ and reaching $f_k = 1$ at $k = 305$):

$$f_{k(N=1)} = \begin{cases} 1 & \text{if } k \geq 5 \\ 0 & \text{otherwise} \end{cases}, \tag{6.25a}$$

$$f_{k(N=2)} = \begin{cases} \frac{1}{300}\,(k-5) & \text{if } k \geq 5 \\ 0 & \text{otherwise} \end{cases}, \tag{6.25b}$$

$$f_{k(N=3)} = \begin{cases} \frac{1}{300^2}\,(k-5)^2 & \text{if } k \geq 5 \\ 0 & \text{otherwise} \end{cases}. \tag{6.25c}$$

Define also the following sinusoidal faults (appearing at $k = 5$):

$$f_{k(\omega_N=\omega_1)} = \begin{cases} \sin[\omega_1\,(k-5)] & \text{if } k \geq 5 \\ 0 & \text{otherwise} \end{cases}, \tag{6.26a}$$

$$f_{k(\omega_N=\omega_2)} = \begin{cases} \sin[\omega_2\,(k-5)] & \text{if } k \geq 5 \\ 0 & \text{otherwise} \end{cases}. \tag{6.26b}$$

with $\omega_1 = 0.24$ rad/sample and $\omega_2 = 2\,\omega_1 = 0.48$ rad/sample.

PMI observers

Let us design PMI observers (i.e., PMIR observers with $n_R = 0$) for different values of n_I ($n_I = 1, 2, 3, 4$). We follow the Strategy 6.2 presented in Section 6.4.3 with a variance noise constraint equal to $\bar{\gamma} = 0.010$. First, we minimize the expected CSE of all the unitary impulse inputs $\zeta[m]$ considering that they have an equal probability of appearance (i.e., $\Omega = [1, n_\zeta]$ and $\alpha_m = 1$ for all m). We obtain the following observer gain matrices:

$$L_{(n_I=1)} = \begin{bmatrix} 0.7587 & 0.0020 & 0.5764 & -0.0384 & 0.0332 \\ -1.6358 & -1.0984 & 0.2149 & 0.8111 & 2.1278 \end{bmatrix}^T,$$

Table 6.1. Estimation errors of the PMI observers ($\bar{\gamma} = 0.010$).

	$n_I = 1$	$n_I = 2$	$n_I = 3$	$n_I = 4$
$N = 1$	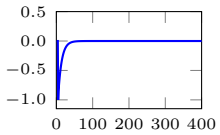	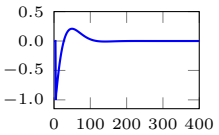	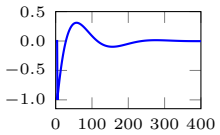	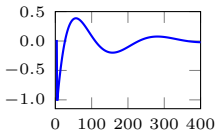
$N = 2$	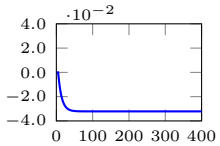	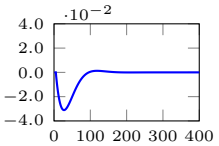	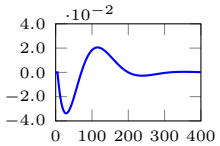	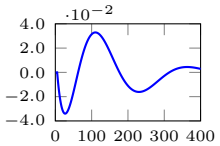
$N = 3$	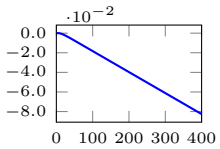	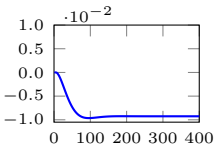	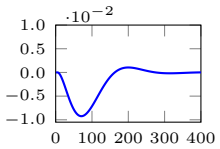	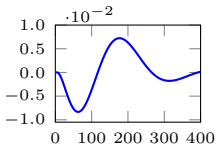
$N = 4$	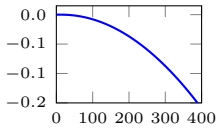	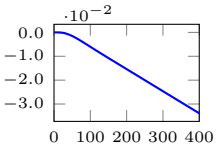	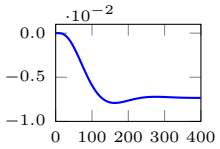	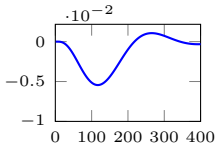

$$L_{(n_I=2)} = \begin{bmatrix} 1.1447 & 0.0381 & 1.6242 & 0.1397 & 0.0098 & -0.0964 \\ -1.9995 & -1.1073 & -1.1448 & 0.7020 & 0.0409 & 1.6390 \end{bmatrix}^T,$$

$$L_{(n_I=3)} = \begin{bmatrix} 1.2351 & 0.0396 & 1.8266 & 0.1439 & 0.0001 & 0.0043 & -0.0571 \\ -2.0857 & -1.1018 & -1.3877 & 0.7132 & 0.0005 & 0.0382 & 1.4430 \end{bmatrix}^T,$$

$$L_{(n_I=4)} = \begin{bmatrix} 0.3157 & -0.0446 & 0.0401 & 0.0530 & 0.0000 & 0.0001 & 0.0028 & 0.0768 \\ -0.6127 & -0.9289 & 0.0684 & 0.5412 & 0.0000 & 0.0008 & 0.0419 & 1.2691 \end{bmatrix}^T,$$

$$K_{(n_I=1)} = \begin{bmatrix} 0.04992.1143 \end{bmatrix}, \quad K_{(n_I=2)} = \begin{bmatrix} -0.1062 & 1.5981 \end{bmatrix},$$

$$K_{(n_I=3)} = \begin{bmatrix} -0.0589 & 1.4035 \end{bmatrix}, \quad K_{(n_I=4)} = 1 \cdot 10^{-9} \begin{bmatrix} 0.0103 & 0.1865 \end{bmatrix}.$$

Table 6.1 includes the FE error $\widetilde{f}$ experienced by each designed observer when the system is subject to each of the polynomial faults (6.25) (i.e., $f_k = f_{k(N)}$ with $N = 1, 2, 3, 4$). We prove that, as detailed in Section 6.5.1, the steady-state error is zero whenever $N \leq n_I$, it is constant if $N = n_I + 1$ and it becomes unbounded if $N > n_I + 1$. For instance, if we study the results in the second column entry of Table 6.1 ($n_I = 2$), the steady-state error is zero towards step faults ($N = 1$) and ramp faults ($N = 2$); it is constant towards parabolic fault signals ($N = 3$); and it is increasing towards cubic fault signals ($N = 4$). The counterpart of augmenting the order of the observer is also shown in the table: the transient behavior becomes more oscillatory as the difference between n_I and N increases (see Section 6.5.2). See, for instance, the case in which $N = 2$: the response of the PMIR observer that includes four integrators ($n_I = 4$) is

Table 6.2. CSE of the PMI observers ($m = n_I - i + 1$).

PMI					
$\bar{\gamma} = 0.010$					
CODE	I1	I2	I2-L	I2-M	I2-H
n_I	1	2	2	2	2
$\bar{\upsilon}_m(i=1)$	-	-	6.20	5.30	4.87
$\upsilon_m\ (i=1)$	4.87	7.28	6.12	5.28	4.87
$\upsilon_m\ (i=2)$	-	3001	3445	6740	566645
$\bar{\gamma} = 0.005$					
CODE	I1	I2	I2-L	I2-M	I2-H
n_I	1	2	2	2	2
$\bar{\upsilon}_m\ (i=1)$	-	-	12.50	10.80	9.70
$\upsilon_m\ (i=1)$	9.67	14.51	12.47	10.78	9.70
$\upsilon_m\ (i=2)$	-	24174	26790	43623	1167520

more oscillatory than the response provided by the PMIR observer that includes two integrators ($n_I = 2$).

Moreover, the results in Table 6.2 show that the CSE experienced under step faults (denoted as $\upsilon_m(i=1)$) is lower with $n_I = 1$ (observer I1) than with $n_I = 2$ (observer I2), being 4.78 vs. 7.28. Then, when step faults occur, I1 behaves better than I2 at the cost of non-zero steady-state estimation errors towards ramp faults.

As proposed in Section 6.5, intermediate solutions can be achieved by designing observers with $n_I = 2$ and adding a constraint on the CSE due to step faults. To do so, we follow the same design strategy (Strategy 6.2 with $\bar{\gamma} = 0.010$) and we constraint the CSE regarding the integrator of lower order[2]. Table 6.2 includes the obtained results. Here, $\bar{\upsilon}_m$ stands for the value of the step CSE constraint (i.e., $\Upsilon[m,m] < \bar{\upsilon}_m$). As this constraint becomes more restrictive (from I2-L to I2-H), the performance of the observer w.r.t. step faults is closer to the performance of a PMI observer with one integrator (I1), but at the cost of worsening the performance w.r.t to ramps (see the values of the CSE experienced under ramp faults denoted as $\upsilon_m(i=2)$). Note that for the most restrictive feasible constraint (i.e, $\bar{\upsilon}_{n_I}$ for $n_I = 2$ equals the value of υ_{n_I} for $n_I = 1$), the performance of the resulting observer (I2-H) w.r.t. step faults equals the performance of I1.

For its part, when imposing more restrictive noise attenuation constraints in the design ($\bar{\gamma} = 0.005$), the CSEs increase and the fault tracking ability of the observers deteriorates for improving the accuracy of the estimates w.r.t. the noises.

Fig. 6.1 shows these trade-offs when simulating the step fault defined in (6.25a). We verify that the response of the observers with $n_I = 2$ approach the response of the observer with $n_I = 1$ as the CSE step fault constraint becomes more restrictive. We also verify that if the

[2]This design is equivalent to the one minimizing the expected CSE of all fault terms and giving a higher probability of appearance to the lower-order fault terms.

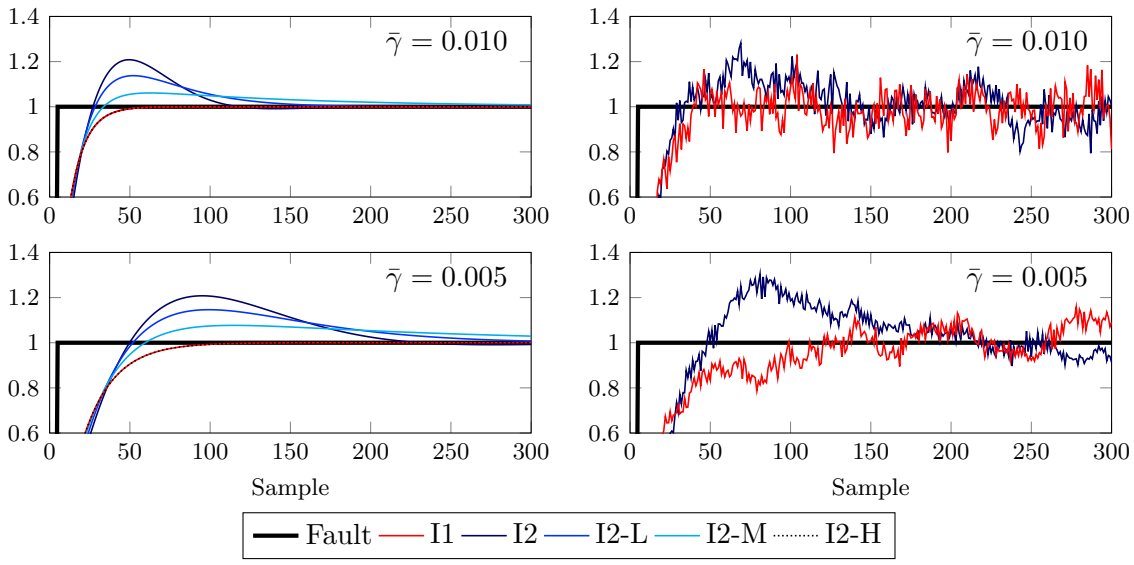

Figure 6.1. Step FE via different PMI observers (Table 6.2) with different noise attenuation constraints. Left: $w_k = 0$. Rigth: ($w_k \neq 0$)

estimates becomes less noisy (with a more restrictive constraint $\bar{\gamma}$), the responses w.r.t. to faults become slower.

PMR observers

Let us now design PMR observers (i.e., PMIR observers with $n_I = 0$) for $n_R = 1, 2$ (with $\omega_1 = 0.24$ rad/sample and $\omega_2 = 2\,\omega_1$) following the same strategy (i.e., Strategy 6.2 in Section 6.4.3). We obtain the following observer gain matrices:

$$L_{(n_R=1)} = \begin{bmatrix} 0.9730 & 0.0560 & 0.7791 & 0.0202 & 0.0030 & -0.0053 \\ -1.0980 & -1.1591 & -0.4720 & 0.7841 & 2.1641 & 2.1956 \end{bmatrix}^T,$$

$$L_{(n_R=2)} = \begin{bmatrix} 0.7027 & 0.0292 & -0.3612 & -0.4559 & 0.0208 & 0.0048 & -0.1637 & -0.0786 \\ -0.5981 & -1.0228 & 1.5289 & 0.5836 & 1.0166 & 1.0747 & 0.9339 & 1.0867 \end{bmatrix}^T,$$

$$K_{(n_R=1)} = \begin{bmatrix} -0.0047 & 2.1946 \end{bmatrix}, \quad K_{(n_R=2)} = \begin{bmatrix} -0.0732 & 2.1615 \end{bmatrix}.$$

Similar deductions as the ones developed for PMI observers hold for PMR observers. The numerical results in Table 6.3 show that increasing the number of resonators in the observer reduces its ability to track the lower-frequency terms which are also included in the observer. Thus, the CSE experienced under a sinusoidal fault of frequency ω_1 (denoted as $\bar{v}_m(r = 1)$) is smaller for the observer just including ω_1 (observer R1) than for the observer including both frequencies ω_1 and ω_2 (observer R2). Again, compromise solutions (R2-L,R2-M and R2-H) can be achieved by designing an observer with both frequencies and imposing a restriction regarding the CSE due to the sinusoidal fault of frequency ω_1 (denoted as $\bar{v}_m(r = 1)$ in the table). The

Table 6.3. CSE of the PMR observers ($m = n_I + n_r - r + 1$).

PMR					
$\bar{\gamma} = 0.010$					
CODE	R1	R2	R2-L	R2-M	R2-H
n_R	1	2	2	2	2
$\bar{\upsilon}_m(r=1)$	-	-	7.00	5.70	4.38
$\upsilon_m(r=1)$	4.37	8.31	7.00	5.70	4.38
$\upsilon_m\ (r=2)$	-	8.10	10.04	15.55	1727
$\bar{\gamma} = 0.005$					
CODE	R1	R2	R2-L	R2-M	R2-H
n_R	1	2	2	2	2
$\bar{\upsilon}_m(r=1)$	-	-	14.00	11.50	8.97
$\upsilon_m\ (r=1)$	8.95	16.65	14.00	11.50	8.97
$\upsilon_m\ (r=2)$	-	15.91	19.88	30.74	2804

results in Table 6.3 also show that higher noise attenuations (e.g., $\bar{\gamma} = 0.005$) impose larger CSEs.

Fig. 6.2 includes the simulation results for these observers ($\bar{\gamma} = 0.010$) when the system is subject to either of the sinusoidal faults defined in (6.26). We verify the numerical results regarding the CSE in Table 6.3 and we prove that the steady-state error is only zero if the frequency ω_N defining the sinusoidal fault signal is within the frequencies ω_r included in the observer. Thus, if the fault is defined as (6.26a), the steady-state error is zero for both observers R1 (designed with $n_R = 1$) and R2 (designed with $n_R = 2$). Contrariwise, if the fault is defined as (6.26b), the steady-state error is only zero for R2.

Comparison of PMI and PMR observers

Let us first obtain the frequency response of the closed-loop transfer function between f and $\hat{f}$ (denoted as $G_{\hat{f},f}$) for the observers in Table 6.2 and Table 6.3 with $\bar{\gamma} = 0.010$. Fig. 6.3 depicts these frequency responses.

First, as deduced in Section 6.6, we verify that the behavior of the PMI observers with two integrators (I2, I2-L and I2-M) is oscillatory: the magnitude of the transfer function is larger than 1 for some low frequencies. We also corroborate that intermediate results between I1 and I2 can be achieved by constraining the CSE due to step faults as proposed in Section 6.4.3. Similar applies to PMR observers.

Fig. 6.3 shows that the 3 dB bandwidth of PMI observers is much lower than ω_1 and ω_2 (0.1 vs. 0.24 and 0.48 rad/sample); thus, poor steady-state estimation results are obtained if we use PMI observers in order to track the pure high-frequency sinusoidal faults defined in (6.26). The unitary gain of $G_{\hat{f},f}$ for R1 at ω_1 ensures zero steady-state errors if the fault (6.26a) affects the system and the same applies to R2 w.r.t. the faults (6.26a) and (6.26b). Contrariwise, if a sinusoidal fault of low frequency (e.g., $0.2\omega_1 = 0.05$ rad/sample) occurs, PMI observers offer

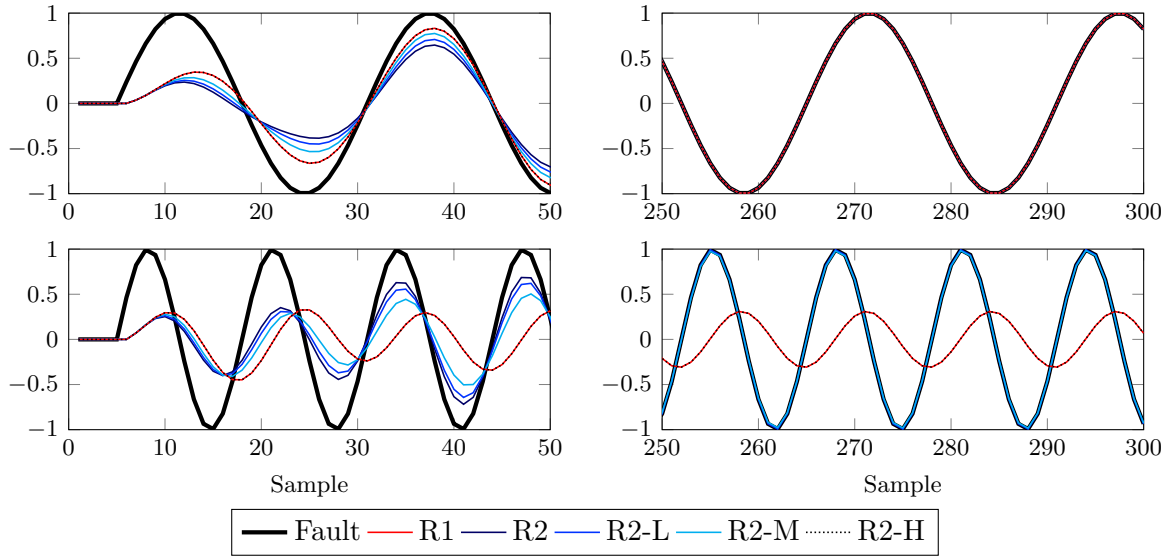

Figure 6.2. Transient and steady-state FE via different PMR observers (Table 6.3 and $\bar{\gamma} = 0.010$) under two sinusoidal faults of frequencies ω_1 and ω_2.

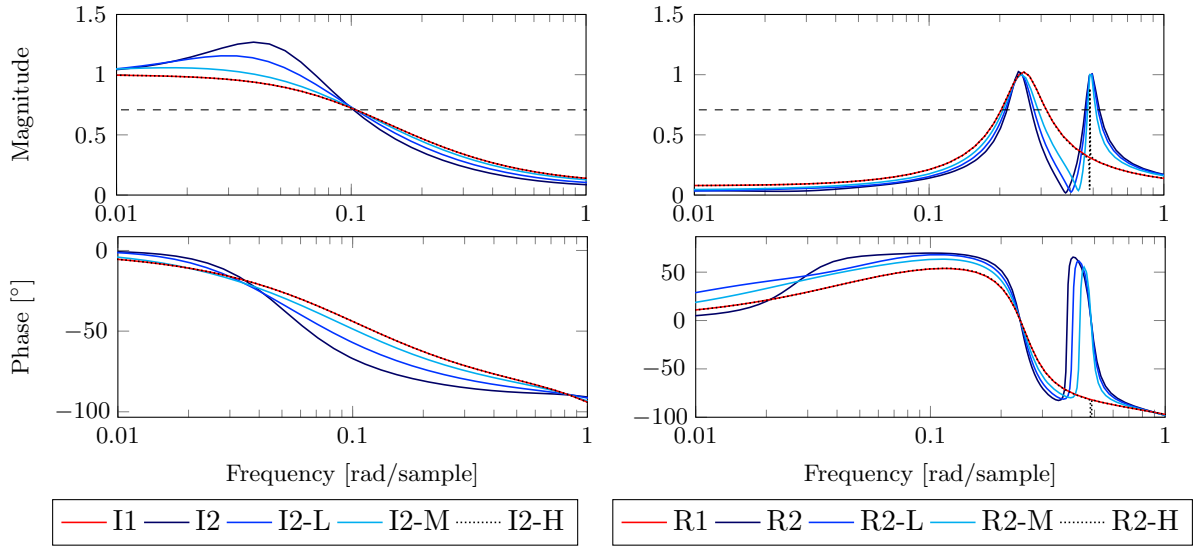

Figure 6.3. Frequency response of the closed-loop transfer function between f and $\hat{f}$ for different PMI and PMR observers (Tables 6.2 and 6.3, $\bar{\gamma} = 0.010$).

much better estimation results than PMR observers. Effectively, the gain of $G_{\hat{f},f}$ for R1 and R2 at low frequencies is barely zero. Fig. 6.6 and Fig. 6.7 illustrate these behaviors. The initial conditions in these simulation are fixed to $x_0 = \begin{bmatrix} 1 & 1 & 1 & 1 \end{bmatrix}$. As stated in Theorem 6.2, the simulation results show that the FE error converges to zero in the absence of faults.

For its part, Fig. 6.4 reveals the effect of the restrictiveness of the noise attenuation constraint included in the design. One verifies that higher noise attenuation constraints impose lower bandwidths. For I1 with $\bar{\gamma} = 0.010$, the 3 dB bandwidth is 0.09 rad/sample; and for I1 with $\bar{\gamma} = 0.005$, it is 0.05 rad/sample. Similarly, the 3 dB bandwidth for R1 reduces from 0.12

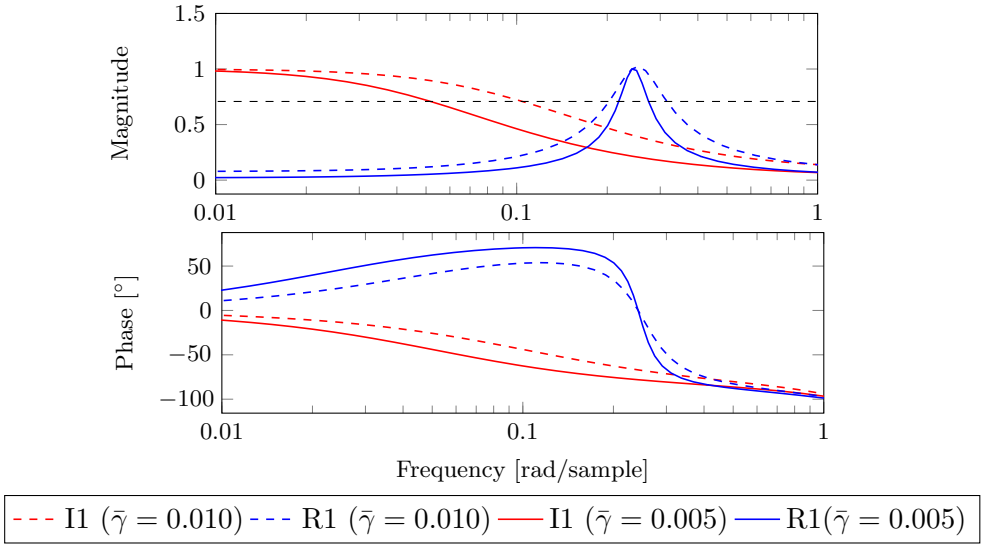

Figure 6.4. Frequency response of the closed-loop transfer function between f and $\hat{f}$ for different PMI and PMR observers (Tables 6.2 and 6.3) designed with different noise attenuation constraints.

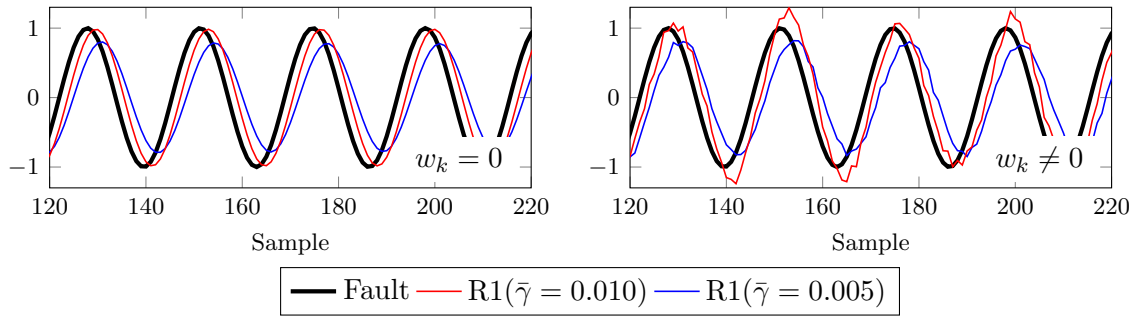

Figure 6.5. Estimation of a sinusoidal fault of frequency $1.05\,\omega_1$ via different PR observers (Table 6.3) designed with different noise attenuation constraints. Results with $w_k = 0$ and $w_k \neq 0$.

to 0.06 rad/sample if $\bar{\gamma}$ varies from 0.010 to 0.005. Hence, we deduce that PMI observers track faults of higher frequencies as the noise is less attenuated and we conclude that the use of the resonant terms proposed in this thesis allow considering high-frequency faults without intensively augmenting the effect of the noise on the fault estimates.

From Fig. 6.4 we also conclude that PMR observers are more robust against uncertainties in the real frequencies of the faults as the attenuation from the noise is reduced. Thus, if a sinusoidal fault of some frequency $(1+\delta)\,\omega_1$ affected the system, R1 with $\bar{\gamma} = 0.010$ would offer better fault tracking results than R1 with $\bar{\gamma} = 0.005$ at the cost of lower noise attenuation. (see Fig. 6.5 including the simulation results for $\delta = 0.05$ with $w_k = 0$ and $w_k \neq 0$).

PMIR observers

Let us now design PMIR observers through the Strategy 2 presented in Section 6.4.3 with different values of n_I and n_R ($\bar{\gamma} = 0.010$). Table 6.4 includes the CSE of these observers (υ_m) w.r.t.

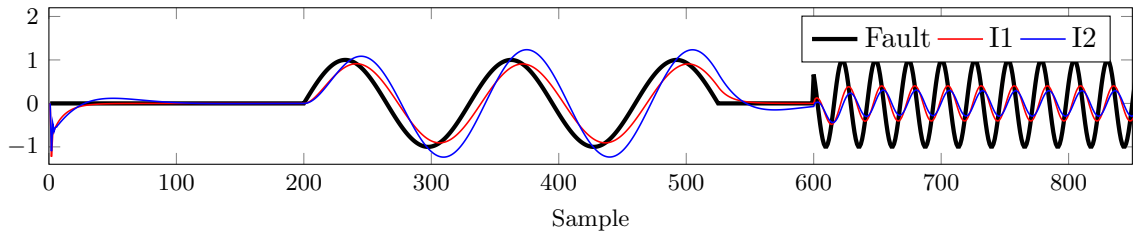

Figure 6.6. Estimation via different PMI observers (Table 6.2, $\bar{\gamma} = 0.010$) of two sinusoidal faults of frequencies $0.20\,\omega_1$ and ω_1.

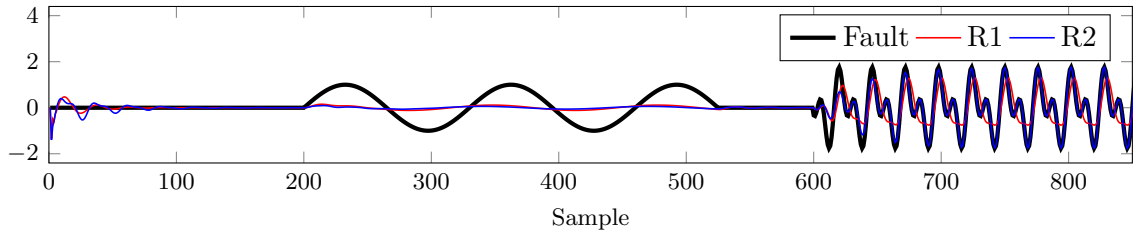

Figure 6.7. Estimation via different PMR observers (Table 6.3 and $\bar{\gamma} = 0.010$) of a sinusoidal fault of frequency $0.20\,\omega_1$ and another of frequencies ω_1 plus ω_2.

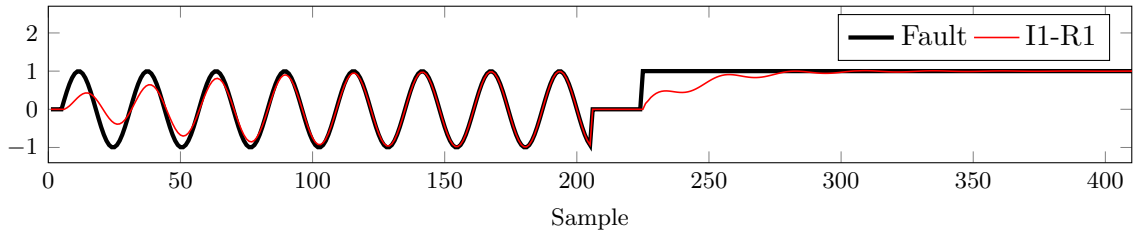

Figure 6.8. Estimation of a step and a sinusoidal fault (frequency ω_1) via a PMIR observer (Table 6.4).

Table 6.4. CSE of the PMIR observers ($\bar{m} = n_I - i + 1$, $\breve{m} = n_I + n_r - r + 1$).

PMIR					
$\bar{\gamma} = 0.010$					
CODE	I1-R1	I1-R2	I1-R2-R	I2-R1	I2-R2
n_I	1	1	1	2	2
$\bar{v}_{\bar{m}}(i=1)$	-	-	-	-	-
$\bar{v}_{\bar{m}}(i=2)$	-	-	-	-	-
$v_{\bar{m}}(i=1)$	8.93	12.64	15.26	7.44	7.42
$v_{\bar{m}}\ (i=2)$	-	-	-	3164	3279
n_R	1	2	2	1	2
$\bar{v}_{\breve{m}}(r=1)$	-	-	9.25	-	-
$\bar{v}_{\breve{m}}(r=2)$	-	-	-	-	-
$v_{\breve{m}}\ (r=1)$	8.53	12.37	9.23	186.79	200.20
$v_{\breve{m}}\ (r=2)$	-	11.98	14.48	-	146.67

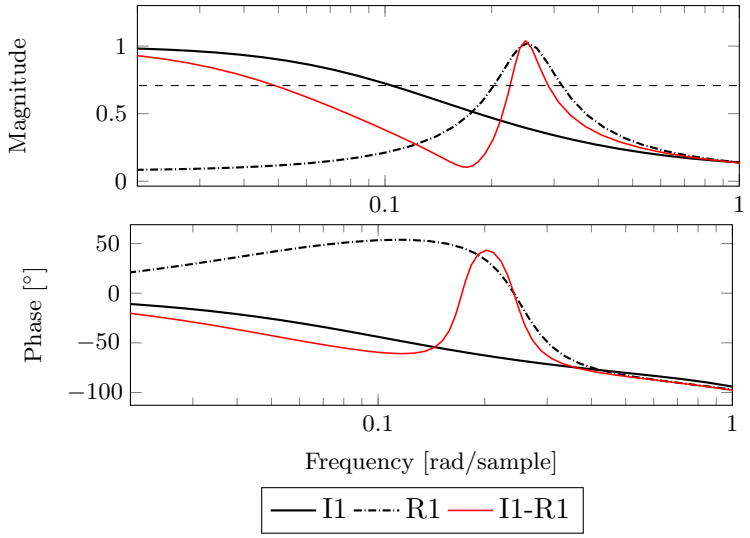

Figure 6.9. Frequency response of the closed-loop transfer function between f and $\hat{f}$ for different PMIR observers (Table 6.4 and $\bar{\gamma} = 0.010$).

different fault terms. Again, we deduce that increasing the order of the observer deteriorates the transient performance of the estimator towards lower-order faults. Compromise solutions can be achieved by imposing a restriction regarding the lower-order CSE constraints. For instance, observer I1-R2 ($n_i = 1$ and $n_r = 2$) offers good results for the high-frequency sinus ($\upsilon_{\check{m}}$ ($r = 2$) equals 11.98) and an intermediate performance for the low-frequency sinus ($\upsilon_{\check{m}}$ ($r = 1$) equals 12.37) and for other low-frequency signals ($\upsilon_{\bar{m}}$ ($i = 1$) equals 12.64). If better results regarding the low-frequency sinus were required, one could design an observer like I1-R2-R with a CSE constraint over the low-frequency sinus (with a value $\bar{\upsilon}_{\check{m}}(r = 1)$ equal to 9.25).

Fig. 6.8 shows the FE results provided by the observer I1-R1 (designed with $n_I = n_R = 1$) when the system is subject to either the step fault defined in (6.25a) or the sinusoidal fault defined in (6.26a). We prove that unlike the so-called PMI observer, this PMIR observer ensures zero steady-state estimation errors for both types of fault signals without increasing the noise effect. Effectively, the frequency response in the first part of Fig. 6.9 shows that the observer I1-R1 ($n_I = n_R = 1$) offers a compromise performance between the performance of I1 ($n_I = 1$) and R1 ($n_R = 1$). The CSE w.r.t. the step fault is 8.93 (vs.4.87 obtained for I1) and 8.53 w.r.t. the sinusoidal fault (vs.4.37 obtained for R1).

6.6.2 Actuator and sensor fault

Consider the situation in which the system suffers from simultaneous actuator (f^a) and sensor (f^s) faults and let $f = \begin{bmatrix} f^a \\ f^s \end{bmatrix}$. Then, one gets accordingly the following distribution matrices ($n_f = 2$):

$$E = \begin{bmatrix} -0.0088 & -0.0706 & 0.1118 & 0.0006 \\ 0 & 0 & 0 & 0 \end{bmatrix}^T, \quad F = \begin{bmatrix} 0 & 0 \\ 1 & 0 \end{bmatrix}^T.$$

Define

$$f^a_{k(N=1)} = \begin{cases} 1 & \text{if } k \in [5, 500] \\ 0 & \text{otherwise} \end{cases}, \tag{6.27a}$$

$$f^s_{k(N=1)} = \begin{cases} 1 & \text{if } k \in [1005, 1500] \\ 0 & \text{otherwise} \end{cases}, \tag{6.27b}$$

$$f^s_{k(\omega_N=\omega_1)} = \begin{cases} \sin[\omega_1 (k-5)] & \text{if } k \in [5, 500] \\ 0 & \text{otherwise} \end{cases}. \tag{6.27c}$$

Let us design PMIR observers using the Strategy 6.2 presented in Section 6.4.3 with $\Omega = [1, n_\zeta]$ and $\alpha_m = 1$ for all m. For $\bar{\gamma} = 0.010$ and for $\bar{\gamma} = 0.005$, we design the observers

- I1 with $n_I = 1$ and $n_R = 0$,
- I2 with $n_I = 2$ and $n_R = 0$,
- R1 with $n_I = 0$ and $n_R = 1$,
- R2 with $n_I = 0$ and $n_R = 2$ and
- I1-R1 with $n_I = 1$ and $n_R = 1$.

Fig. 6.10 shows the simulation results when the fault vector $f_k = \begin{bmatrix} f^a_{k(N=1)} \\ f^s_{k(N=1)} \end{bmatrix}$ affects the system. Note that the deficits in the fault tracking behavior do also affect the isolation capability of the estimator. As explained in Section 6.6.1, if the observer I2 is used, the actuator fault estimate experiences an oscillatory behavior when the step actuator fault occurs. In this case, moreover, the sensor fault estimate does also experience a transient oscillatory deviation. If I1 ($n_i = 1$ and $n_r = 0$) is used instead, the transient deviation is not oscillatory and, thus, the isolation capability of the estimator is improved during transients.

In order to analyse this effect from a steady-state perspective, assume now that $f_k = \begin{bmatrix} f^a_{k(N=1)} \\ f^s_{k(\omega_N=\omega_1)} \end{bmatrix}$. The corresponding simulation results are shown in Fig. 6.11. When the step actuator fault occurs, the observer I1 ($n_i = 1$ and $n_r = 0$) ensures zero steady-state estimation errors that enhance perfect fault isolation in steady state. However, when the sinusoidal sensor fault occurs, the steady-state estimation errors are non-zero and, thus, the fault isolation capability of the estimator is deteriorated. The opposite occurs if the observer R1 ($n_i = 0$ and $n_r = 1$) is used: perfect steady-state fault isolation is guaranteed when sinusoidal faults occur and the problems appear when step faults affect the system. Finally, the observer I1-R1 ($n_i = 1$ and $n_r = 1$) guarantees perfect steady-state fault isolation for both step and sinusoidal faults (see the details in the second part of Fig. 6.11). Thus, we deduce that PMIR observers are useful if different types of faults appear all around the system. For instance, sensor faults may always represent biases (i.e., step faults). However, if sinusoidal actuator faults affect the system, the use of resonators for the sensor FE guarantees perfect steady-state fault isolation and avoids the appearance of steady-state fault interactions.

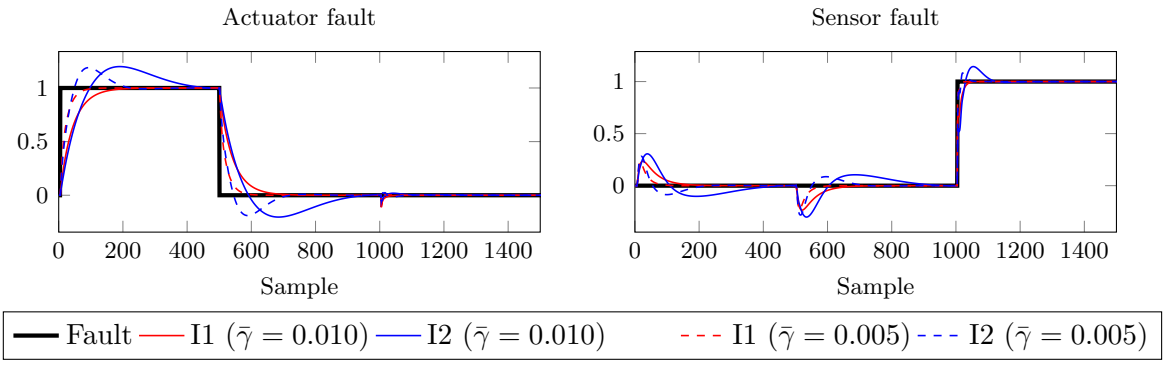

Figure 6.10. Estimation of step actuator and sensor faults via different PMI observers designed with different noise attenuation constraints.

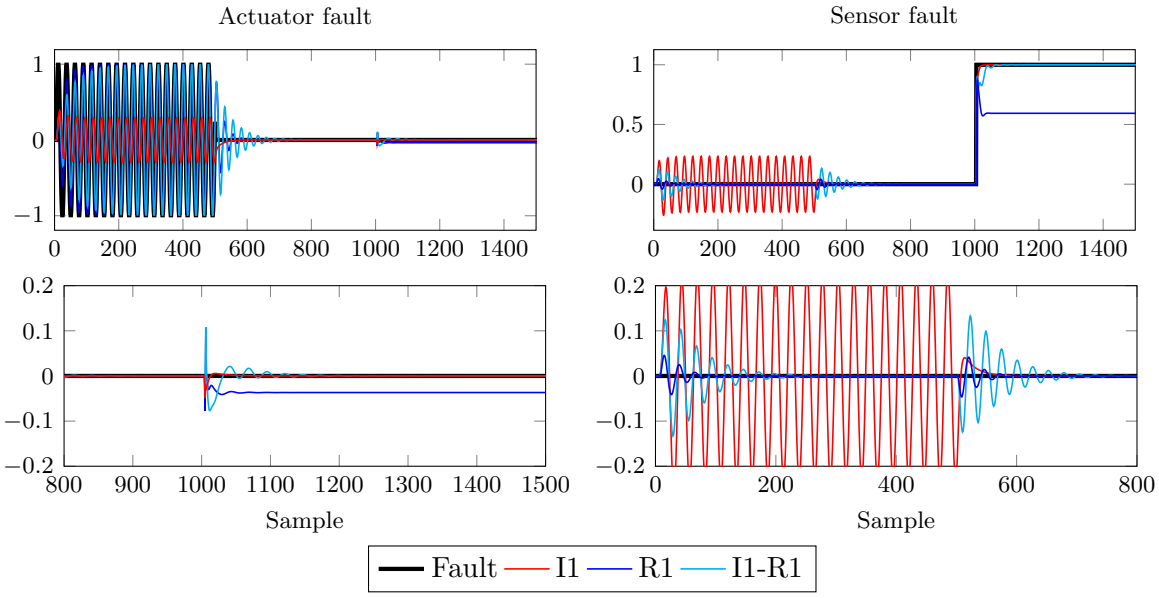

Figure 6.11. FE via different PMIR observers ($\bar{\gamma} = 0.010$) under a sinusoidal actuator fault (ω_1) and a step sensor fault.

6.7 Conclusion

In this chapter, we have generalized the standard formulation of a PMI observer to enhance the estimation of high-frequency fault signals. We have given the conditions for the existence of the novel observer and we have presented a multiobjective design strategy to fix an optimal trade-off between the variance of the estimations in fault-free scenarios and their cumulative squared tracking error in the presence of different faults. We have also included a study which shows the influence of the complexity of the estimator (i.e., the order of the augmented observer) on the existing trade-off between the steady-state and transient tracking performance of the estimator when the system is subject to faults of different complexity. The design and the main conclusions of this study are validated when the proposed FE strategy is applied to a numerical illustrative example. The use of these fault estimates in active FTC strategies highlights as

immediate future work. Future work will also include the application of the approach to practical engineering examples.

Chapter 7

Multiobjective performance-based designs in fault estimation and isolation and its application to wind turbines

In this chapter, we develop a performance-based design of model-based observes and statistical-based decision mechanisms for achieving fault estimation and fault isolation in systems affected by unknown inputs and stochastic noises. First, through semidefinite programming, we design the observers considering different estimation performance indices as the variance of the estimation errors, the time delays in tracking fault signals and the degree of decoupling from unknown inputs and from faults in other channels. Second, we perform a co-design of the observers and decision mechanisms for satisfying certain trade-off between different isolation performance indices: the false isolation rates, the isolation times and the minimum size of the isolable faults. Finally, we extend these results to a scheme based on a bank of observers for the case where multiple faults affect the system and isolability conditions are not verified. To show the effectiveness of the results, we apply these design strategies to a well-known benchmark of wind turbines which considers multiple faults and has explicit requirements over isolation times and false isolation rates.

7.1 Introduction

The importance of the reliability and maintainability of systems has increased over the last decades. Hence, much effort has been devoted to developing fault detection and isolation (FDI) and fault tolerant control (FTC) strategies [100]. On the FTC framework, there are two possible approaches: active and passive FTC. The difference between them is that passive FTC is just an application of robust control that considers faults as uncertainties while active FTC relies on fault diagnosis outputs. The two main approaches regarding FDI are data-based and model-based techniques, see [71] and [44, 70], respectively. Broadly speaking, most FDI systems

consist of residual generators and evaluators; however, research has shown that there are intrinsic difficulties in the use of residuals in active FTC due to the complexity derived from the reconstruction of the faults from the residuals. These reconstructions rely on discrete-event algorithms with complex decisions that entail delays and errors [53, 171]. Active FTC based directly on fault estimation (FE) rather than on FDI seems to provide more immediate and accurate results, see [171, 178]. Among FE techniques, there is an upward trend in the use of advanced observers [100]. Sliding mode observers are used in [298, 316], adaptive observers are applied in [177, 241] and iterative observer schemes are studied in [136]. Augmented observers, which consider the faults as additional states, have received considerable attention [99, 105, 307]. Especially, proportional integral (PI) observers have been intensively studied [41, 180, 305] and applied [190, 242] in the last two decades.

One of the main problems in the use of common FE techniques for active FTC arises when the faults affecting a system are not isolable and it is not possible to build standard observers. Hence, most FE works conservatively consider that the faults verify isolability conditions, e.g., [178,302]. A solution to deal with non-isolable faults is the use of a bank of generalized observers [44, 70]. However, these schemes are usually implemented from a FDI perspective and each observer in the bank is used to provide a residual signal which is sensitive to all but one fault, e.g., [79]. Thus, there is a need to develop more FE approaches based on banks of observers for systems with non-isolable faults.

Another problem in the use of FE for active FTC schemes is the misleading effect produced when feedforwarding non-zero fault estimates in fault-free scenarios. The residual signal in FDI and the fault estimation signal in FE are subjected not only to faults but also to disturbances, which may deviate the estimation outputs. In the FDI framework, in order to make the residual signal sensitive to faults but robust against disturbances, structural methods such as the parametric eigenstructure assignment approach [225] and the unknown input observer (UIO) approach [127, 340] are well-known. Alternatively, numerical approaches based on optimization methods that use the $\mathcal{H}_\infty/\mathcal{H}_-$ and the $\mathcal{H}_\infty/\mathcal{H}_\infty$ indices have gained more attention in FDI research owing to its wide applicability [5, 10, 181]. In the FE framework, multiobjective optimization design approaches are also used in works as [106, 241, 302]. In order to give further physical interpretation to the indices involved in the optimization problem, [49, 327] propose to use the trade-off between the fault detection rate (FDR) and the false alarm rate (FAR). This trade-off is used in recent works as [331, 334] and it is of practical importance in FDI applications. However, although the FAR and the FDR are suitable for FDI methods based on residuals, these indices give little information about other important issues in estimation-based methods such as the size of the faults which are susceptible to occur, the dynamic behavior or the steady-state accuracy of the results. Some initial approaches considering a few of these issues can be found in works as [229, 249, 321]. The iterative design procedures of FDI residuals in [229] involve bounds of the minimum size of the detectable faults (MDF), bounds of the FAR and a decay ratio representing the fault tracking ability of the residuals. In [249] a non-iterative design procedure with the MDF, the FAR and the Cumulative Squared Error (CSE) of the residuals is proposed. For its part, the methods in [321] include new indices as the expected detection delay (EDD) for FDI in statistical processes. In all, as stated in [325], more research on designs considering the performance of model-based FE is needed.

A well-known benchmark for FDI and FTC of wind turbines is developed in [216]. The benchmark takes account of a wide variety of the multiple and diverse faults to which a wind turbine is prone and it sets some FDI performance requirements. A wide variety of solutions based on residuals have been presented for this wind turbine FDI problem, see [214]. Data-based approaches are proposed in works such as [221,268]. Nonetheless, model-based approaches, such as the ones presented in [48,93,251], are more common. Set membership approaches are applied in [93], UIOs are presented in [251] and Kalman filters are developed in [48]. However, there are not solutions that provide *a priori* performance-based designs of the fault diagnosis mechanisms to guarantee the requirements in the benchmark. Hence, the FDI performance is generally tested through an *a posteriori* analysis or simulations. Regarding FTC, both passive and residual-based active FTC strategies have been applied to wind turbines in [32,270]. In [173,254,261,263] active FTC strategies based on FE are applied to wind turbines. However, all these works assume that only certain faults among all the possible ones may affect the turbines. The same assumption is considered in the FE solution presented in [303].

7.1.1 Contributions

In this chapter, FE is achieved by means of PI observers. The fault estimates are then evaluated in statistical-based decision mechanisms to achieve fault isolation (FI). The main contribution of this chapter is the development of novel estimation performance-based design strategies of PI observers. In analogy to the integrated design of residual generators and evaluators in [49,327], we also present novel co-design strategies in the FI framework. We formulate the co-design of PI observers and statistical-based decision mechanisms guaranteeing *a priori* isolation performance requirements. Compared to the relevant existing literature, the novelties of the proposed designs are the following.

- *Designs with a priori performance requirements.* In most cases, the performance of FE and FDI strategies is tested *a posteriori* (e.g., [30, 46]). Hence, the satisfaction of estimation or isolation performance requirements entails iterative procedures. The designs proposed in this chapter guarantee *a priori* performance requirements and, thus, we avoid iterative design procedures.

- *Designs with individual performance requirements.* The designs proposed in this thesis deal with the performance of each single fault estimation/isolation channel. This increases the design flexibility compared with most existing FE and FI designs, where the performance is jointly fixed for all the fault estimation/isolation channels (e.g., [106, 302]).

- *Designs with time-domain performance indices.* In an aim to bridging the gap between theory and practice, we use new performance indices providing further practical and physical interpretation to the norm bounds which are commonly used in FDI and FE designs [178,302]. The proposed observer designs for FE deal with the trade-off between the tracking delays w.r.t. different fault signals and the covariances of the fault estimates due to noises. The proposed co-designs for FI deal with the following isolation performance indices: the false isolation rates, the minimum isolable faults and the isolation times.

- *Single-step numerical designs of observers guaranteeing unknown input and interfault decoupling.* The well-known design of UIOs requires algebraic constraints to achieve unknown input (UI) decoupling [44]. Then, the remaining design freedom is used in a numerical second-step design to achieve certain requirements over other performance criteria [180,190,302]. In this thesis, we propose to use the concept of degree of UI decoupling in order to numerically achieve UI decoupling and other performance requirements in a single-step multiobjective optimization problem. We also introduce the concept of degree of interfault decoupling to deal with the transient FE error which occurs due to the appearance of faults in other channels (e.g., the simulation results in [244,247]). The observer performance indices (covariance due to noises, fault tracking delays and UI and interfault decoupling) are altogether formulated via matrix inequalities in a single-step optimization problem.

We generalize these design strategies to a scheme based on a bank of PI observers and statistical-based decision mechanisms that allow achieving FI and FE in systems where isolability conditions of faults do not hold. Assuming the non-simultaneity of certain number of faults, we extend the concept of residual-based generalized observers [44, 79] from a FE perspective.

To show the goodness of the proposed approaches, we apply the strategies presented in this chapter to the well-known benchmark for FDI and FTC of wind turbines [216]. Unlike works as [173, 303], which just consider the occurrence of a reduced number of possible faults, we achieve the estimation of all the faults affecting the turbines. We also isolate these faults with *a priori* guaranteed isolation performance indices.

7.1.2 Structure and notation

The outline of this chapter is as follows. First, we state the problem in Section 7.2, where we propose a FE and FI strategy based on PI observers and decision mechanisms. In Section 7.3, we present a FE performance-based design of the observer. In Section 7.4, we include a co-design of the observer and decision mechanism for guaranteeing certain trade-off between isolation performance indices. In Section 7.5, we extend the problem to the case in which FI becomes necessary for FE because fault isolability conditions are not verified and standard augmented observers are not applicable. Finally, Section 7.6 presents the results of applying the proposed FE and FI techniques to the wind turbine problem. Section 7.7 summarizes the main conclusions.

Throughout the chapter, $\mathbb{R}$ denotes the set of real numbers. Expected value, probability and absolute value are denoted by $\mathbb{E}\{\cdot\}$, $\mathbb{P}\{\cdot\}$ and $|\cdot|$. Let A be some matrix and a be some vector. A_{ij} denotes the element in the i-th row and j-th column of A and a_i denotes the i-th element in a. $A \preceq 0$ means that A is negative semidefinite and similar applies to $\succeq$. The rank of matrix A is represented as $\text{rank}\{A\}$ and its trace is given by $\text{tr}\{A\}$. Let x be a stochastic process. We write $\|x(k)\|_2^2 \triangleq x(k)^T x(k)$ for the Euclidean norm of vector $x(k)$ and $\|x(k)\|_\infty \triangleq \max_i |x_i(k)|$ for its max norm. $\|x\|_2^2 \triangleq \sum_{k=0}^{\infty} \|x(k)\|_2^2$ denotes the l_2 norm of process x, $\|x\|_{RMS}^2 \triangleq \lim_{k\leftrightarrow\infty} \frac{1}{K} \sum_{k=0}^{K-1} \|x(k)\|_2^2$ denotes its RMS norm and $\|x\|_\infty \triangleq \max_k \max_i |x_i(k)|$ denotes its l_∞ norm. I_n is the identity matrix of size $n \times n$ or of appropriate size when the subindex is omitted; similar applies to $0_{n\times n}$.

7.2 Problem formulation

Let us consider the linear time-invariant (LTI) discrete-time system defined by

$$x(k+1) = A\,x(k) + B\,u(k) + E f(k) + G v(k) + D d(k), \tag{7.1a}$$

$$y(k) = C\,x(k) + F f(k) + H v(k), \tag{7.1b}$$

where $x \in \mathbb{R}^{n_x}$, $y \in \mathbb{R}^{n_y}$ and $u \in \mathbb{R}^{n_u}$ are the state, output and known input vector; $v \in \mathbb{R}^{n_v}$ is the process and sensor noise vector and $d \in \mathbb{R}^{n_d}$ is the UI vector. Vector $f \in \mathbb{R}^{n_f}$ includes all the process, actuator and sensor faults f_i $(i = 1, \ldots, n_f)$ that affect the system [44][1]. We define M_i as the selection matrix verifying $f_i = M_i\, f$ (i.e., $M_i = \begin{bmatrix} 0_{1\times i-1} & 1 & 0_{1\times n_f - i} \end{bmatrix}$). The following assumptions on the system (7.1) are made.

Assumption 7.1. *The pair (A, C) is observable.*

Remark 7.1. *Augmented observers require the observability of the model* (7.1) *as detailed in works as [41, 99]. Hence, Assumption 7.1 is not restrictive from a FE perspective.*

Assumption 7.2. *The faults are detectable, isolable among them and isolable from the UIs.*

Remark 7.2. *The transfer matrix from a fault f_i to the outputs is given by*

$$G_{f_i}(z) = C\,(z\,I - A)^{-1}\,E_i + F_i,$$

where E_i and F_i represent the i-th column of E and F, respectively. The transfer matrix from the UIs to the outputs is given by

$$G_d(z) = C\,(z\,I - A)^{-1}\,D.$$

We define G_{fd} as

$$G_{fd} = \begin{bmatrix} G_{f_1}(z) & \ldots & G_{f_{n_f}}(z) & G_d(z) \end{bmatrix}.$$

According to [70], Assumption 7.2 implies that

$$G_{f_i}(z) \neq 0, \quad \forall i,$$

$$\operatorname{rank}\{G_{fd}(z)\} = \sum_{i=1}^{n_f} \operatorname{rank}\{G_{f_i}(z)\} + \operatorname{rank}\{G_d(z)\}.$$

The detectability of the faults in Assumption 7.2 is a necessary condition for FDI and FE [44, 70]. The isolability condition in Assumption 7.2 is also standard in these frameworks. However, this condition becomes more restrictive as the number of UIs and faults increases [44, 70]. Section 7.5 includes estimation and isolation strategies for the case in which the isolability condition in Assumption 7.2 does not hold.

Assumption 7.3. *The noises are zero-mean and of known covariance, i.e., $\mathbb{E}\{v\,v^T\} = V$. The UIs are norm-bounded, i.e., $\|d\|_\infty \leq \bar{d}$.*

[1]The proposed method entails a more general approach compared with some other existing works that only consider either actuator faults [241] or sensor faults [10, 188].

Remark 7.3. *Vector v takes account of zero-mean stochastic disturbances while vector d takes account of non-zero-mean norm-bounded disturbances. Other disturbances may be also considered in the model* (7.1) *by means of decomposing it into a component included in vector v and a component included in vector d. Pure process noise (v^p) and pure sensor noise (v^s) can be modeled by means of zeroing the appropriate columns of G and H (i.e., $v = \begin{bmatrix} v^p \\ v^s \end{bmatrix}$ with $G = \begin{bmatrix} G^p & 0 \end{bmatrix}$ and $H = \begin{bmatrix} 0 & H^s \end{bmatrix}$). For its part, the UI vector can be also used to describe a number of different kinds of norm-bounded modeling uncertainties [45] (e.g., $d = \Delta A\, x$ with ΔA being the uncertainty regarding the state matrix[2]).*

Assumption 7.4. *The fault discrete derivative $\delta(k) = f(k+1) - f(k)$ is norm-bounded, i.e., $\|\delta\|_\infty \leq \bar{\delta}$.*

Any fault signal verifying Assumption 7.4 (i.e., fault signals with norm-bounded fault discrete derivative δ) can be modeled as

$$\xi(k+1) = A_F\, \xi(k) + B_F\, \delta(k), \tag{7.2a}$$

$$f(k) = C_F\, \xi(k), \tag{7.2b}$$

with

$$A_F = I_{n_f},\ B_F = I_{n_f},\ C_F = I_{n_f}. \tag{7.3}$$

Remark 7.4. *Assumption 7.4 is fairly general because it allows considering a wide range of fault signals which are common in practical applications. For instance, a step (or abrupt) fault signal is generated through* (7.2) *with an impulse signal δ, and a ramp (or drift) fault signal is generated through* (7.2) *with a step signal δ. Note that Assumption 7.4 does not imply any restriction over the upper bound of the fault vector f, which reduces the conservatism compared with some other existing works [188, 241].*

Remark 7.5. *An augmented observer is based on an augmented model including both the system dynamics and the fault dynamics [99, 105]. In the FE literature, fault dynamics verifying Assumption 7.4 are widely utilized leading to the so-called proportional integral (PI) observers [41, 190], which are based on the fault model* (7.2)-(7.3)*. A stable PI observer leads to bounded steady-state FE errors when the system is subjected to fault signals verifying Assumption 7.4. For instance, it leads to zero steady-state errors under step faults and to constant steady-state errors under ramp faults.*

Remark 7.6. *Certain systems may be subjected to complex fault signal forms which do not verify Assumption 7.4. In such cases, the fault estimates provided by a PI observer would increase in value but the estimation errors would not be bounded. To ensure bounded FE errors, the fault state-space matrices* (7.3) *must be replaced by more complex matrices. See, for instance, the state-space matrices in [105, 307] for fault signals in the more general form of a polynomial of the time leading to proportional multiple integral (PMI) observers. Hence, the model* (7.3) *and the strategies developed in this chapter are easily extensible to fault signals which do not verify Assumption 7.4.*

[2] In practice, FE is performed in stable (controlled or uncontrolled) systems. Hence, if ΔA is bounded, the uncertainty $d = \Delta A\, x$ is bounded as x is also bounded.

The model (7.1) is thus augmented as

$$z(k+1) = \mathcal{A}\, z(k) + \mathcal{B}\, u(k) + \mathcal{E}\, \delta(k) + \mathcal{G}\, v(k) + \mathcal{D}\, d(k), \tag{7.4a}$$
$$y(k) = \mathcal{C}\, z(k) + \mathcal{H}\, v(k), \tag{7.4b}$$
$$f(k) = \mathcal{R}\, z(k), \tag{7.4c}$$

where $z = \begin{bmatrix} x \\ \xi \end{bmatrix}$ denotes the extended state vector. The state-space matrices in (7.4) verify $\mathcal{A} = \begin{bmatrix} A & E\,C_F \\ 0 & A_F \end{bmatrix}$, $\mathcal{B} = \begin{bmatrix} B \\ 0 \end{bmatrix}$, $\mathcal{E} = \begin{bmatrix} 0 \\ B_F \end{bmatrix}$, $\mathcal{G} = \begin{bmatrix} G \\ 0 \end{bmatrix}$, $\mathcal{D} = \begin{bmatrix} D^T & 0 \end{bmatrix}^T$, $\mathcal{C} = \begin{bmatrix} C & F\,C_F \end{bmatrix}$, $\mathcal{H} = H$ and $\mathcal{R} = \begin{bmatrix} 0 & C_F \end{bmatrix}$. The following model-based PI observer is proposed to estimate the faults in (7.4)

$$\hat{z}(k+1) = \mathcal{A}\, \hat{z}(k) + \mathcal{B}\, u(k) + L\,(y(k) - \mathcal{C}\, \hat{z}(k))\,, \tag{7.5a}$$
$$\hat{f}(k) = \mathcal{R}\, \hat{z}(k) + K\ (y(k) - \mathcal{C}\, \hat{z}(k))\,, \tag{7.5b}$$

where the design observer gain matrices L and K are of appropriate dimensions. Define the estimation errors $\widetilde{z}(k) = z(k) - \hat{z}(k)$ and $\widetilde{f}(k) = f(k) - \hat{f}(k)$. It follows that

$$\widetilde{z}(k+1) = \bar{\mathcal{A}}\, \widetilde{z}(k) + \bar{\mathcal{G}}\, v(k) + \mathcal{D}\, d(k) + \mathcal{E}\, \delta(k), \tag{7.6a}$$
$$\widetilde{f}(k) = \bar{\mathcal{R}}\, \widetilde{z}(k) + \bar{\mathcal{H}}\, v(k), \tag{7.6b}$$

with $\bar{\mathcal{A}} = \mathcal{A} - L\,\mathcal{C}$, $\bar{\mathcal{G}} = \mathcal{G} - L\,\mathcal{H}$, $\bar{\mathcal{R}} = \mathcal{R} - K\,\mathcal{C}$ and $\bar{\mathcal{H}} = -K\,\mathcal{H}$. Applying the $\mathcal{Z}$ transform to (7.6), we get

$$\widetilde{f}(z) = \mathcal{G}_\delta(z)\, \delta(z) + \mathcal{G}_d(z)\, d(z) + \mathcal{G}_v(z)\, v(z), \tag{7.7}$$

with $\mathcal{G}_\delta(z) = M(z)\mathcal{E}$, $\mathcal{G}_d(z) = M(z)\mathcal{D}$, $\mathcal{G}_v(z) = M(z)\,\bar{\mathcal{G}} + \bar{\mathcal{H}}$ and $M(z) = \bar{\mathcal{R}}(zI - \bar{\mathcal{A}})^{-1}$.

For isolation purposes, we set the following decision mechanisms ($i = 1, \ldots, n_f$) evaluating the fault estimates provided by (7.5):

$$\begin{cases} \text{if } \ |\hat{f}_i(k)| \geq J_i\ , & \text{Fault } i \\ \text{otherwise}\ , & \text{No fault } i \end{cases}, \tag{7.8}$$

where J_i is the isolation threshold of the i-th fault and must be designed.

Remark 7.7. *For FI, it is not necessary to evaluate the fault estimates $\hat{f}$ and appropriate simpler signals (i.e., isolation residuals) can be generated and evaluated instead, e.g., [137, 297]. In this thesis, the fault estimates are evaluated in isolation decision mechanisms in order to decide whether to feed or not an active FTC mechanism with these estimates.*

Remark 7.8. *The decision mechanism* (7.8) *allows simultaneously achieving fault detection and isolation, to which we simply refer as fault isolation. Appendix B shows how to use the fault estimates provided by the observer*(7.5) *in a decision mechanism for pure detection purposes. It also provides some notes on design strategies for guaranteeing a priori detection performance requirements.*

In order to design the observer (7.5) and the decision mechanisms (7.8), one must choose the gain matrices L and K and the thresholds J_i $(i = 1, \ldots, n_f)$. The main objective of this chapter is to solve the following problems

- To provide a design strategy of the observer for guaranteeing certain *a priori* estimation performance requirements.
- To provide a design strategy of the decision mechanisms for guaranteeing one *a priori* isolation performance requirement.
- To provide a co-design strategy of the observer and the decision mechanisms for guaranteeing more than one *a priori* isolation performance requirement.

7.3 Fault estimation

7.3.1 FE Performance Characterization

The performance of the fault estimator (7.5) can be described using the following criteria:

e.1 the fault tracking speed,
e.2 the degree of interfault decoupling,
e.3 the degree of UI decoupling and
e.4 the noise attenuation.

Each element $G_{\delta_{ij}}(z)$ of the transfer matrix $G_\delta(z)$ describes the fault tracking error that the i-th fault estimate (i.e., $\hat{f}_i$) experiences due to the variations of the fault in the channel j (i.e., δ_j). In particular, each diagonal element $G_{\delta_{ii}}(z)$ describes the error $\widetilde{f}_i$ due to δ_i and each off-diagonal term $G_{\delta_{ij}}(z)$ with $j \neq i$ describes the coupling effect that occurs when $\widetilde{f}_i$ increases due to the appearance of a fault in another channel $j \neq i$ (i.e., $\delta_{j\neq i}$). Since the fault tracking speed is strictly related to the fault tracking error, we make use of the $\mathcal{H}_\infty$ norm of the transfer functions $G_{\delta_{ii}}(z)$ $(i = 1, \ldots, n_f)$ to characterize the criterion **e.1.**. Likewise, the criterion **e.2.**, which refers to the degree of decoupling between faults, can be characterized through the $\mathcal{H}_\infty$ norm of the transfer functions $G_{\delta_{ij}}(z)$ $(i = 1, \ldots, n_f,\ j = 1, \ldots, i-1, i+1, \ldots, n_f)$.

Remark 7.9. *There may also be a coupling effect when more than one fault vary simultaneously and it is also desirable to characterize this error. To cope with all these characterizations numerically, we bound each FE error $\widetilde{f}_i$ due to δ as*

$$\lim_{K\to\infty} \sum_{k=0}^{K} \widetilde{f}_i(k)^T\, \widetilde{f}_i(k) \leq \lim_{K\to\infty} \sum_{k=0}^{K} \delta(k)^T\, \Gamma^i\, \delta(k),$$

where the term Γ^i_{ii} stands for the $\mathcal{H}_\infty$ norm of $G_{\delta_{ii}}(z)$, the terms Γ^i_{jj} $(j \neq i)$ stand for the $\mathcal{H}_\infty$ norm of $G_{\delta_{ij}}(z)$ and the off-diagonal terms Γ^i_{jl} $(j \neq l \neq i)$ explain the behavior of the i-th fault estimate towards simultaneous faults.

The dynamics in $\mathcal{G}_d(z)$ determine the effect of the UIs on the fault estimates. Thus, the criterion **e.3** can be characterized through the $\mathcal{H}_\infty$ norm of $\mathcal{G}_d(z)$. Finally, we characterize the criterion **e.4** through the covariance of the FE error due to noises.

Remark 7.10. *In the absence of UIs and faults, the presence of zero-mean noises leads to zero-mean FE errors. In this case, the covariance of $\widetilde{f}$, i.e., $\Sigma = \lim_{k\to\infty} \mathbb{E}\{\widetilde{f}(k)\widetilde{f}(k)^T\}$, is given by the Lyapunov equations*

$$\Sigma^z = \bar{\mathcal{A}}\,\Sigma^z\,\bar{\mathcal{A}}^T + \bar{\mathcal{G}}\,V\,\bar{\mathcal{G}}^T, \tag{7.9a}$$

$$\Sigma = \bar{\mathcal{R}}\,\Sigma^z\,\bar{\mathcal{R}}^T + \bar{\mathcal{H}}\,V\,\bar{\mathcal{H}}^T, \tag{7.9b}$$

which we obtained from (7.7) *with $\delta(z) = 0$, $d(z) = 0$ and using an internal realization of $G_v(z)$.*

The requirements over these criteria can be thus translated into requirements over different $\mathcal{H}_\infty$ norms and covariance bounds of the FE errors. In order to set multiobjective designs with different requirements over these criteria, we use the formulation based on matrix inequalities which is shown in Theorem 7.1.

Theorem 7.1. *Consider the observer* (7.5) *applied to the system* (7.4). *If there exist any matrices L and K, any positive scalar γ_d, any symmetric matrices S, Q, Ξ, P_i and any diagonal matrices Γ^i $(i = 1, \ldots, n_f)$ fulfilling*

$$\begin{bmatrix} Q & Q\,\bar{\mathcal{A}} & Q\,\mathcal{D} & 0 \\ \bar{\mathcal{A}}^T Q & Q & 0 & \bar{\mathcal{R}}^T \\ \bar{\mathcal{D}}^T Q & 0 & \gamma_d\, I & 0 \\ 0 & \bar{\mathcal{R}} & 0 & I \end{bmatrix} \succeq 0, \tag{7.10}$$

$$\begin{bmatrix} S & S\,\bar{\mathcal{A}} & S\,\bar{\mathcal{G}}\,V \\ \bar{\mathcal{A}}^T S & S & 0 \\ V\,\bar{\mathcal{G}}^T S & 0 & V \end{bmatrix} \succeq 0, \quad \begin{bmatrix} \Xi & \bar{\mathcal{R}} & \bar{\mathcal{H}}\,V \\ \bar{\mathcal{R}}^T & S & 0 \\ V\,\bar{\mathcal{H}}^T & 0 & V \end{bmatrix} \succeq 0, \tag{7.11}$$

$$\begin{bmatrix} P_i & P_i\,\bar{\mathcal{A}} & P_i\,\mathcal{E} & 0 \\ \bar{\mathcal{A}}^T P_i & P_i & 0 & \bar{\mathcal{R}}^T M_i^T \\ \bar{\mathcal{E}}^T P_i & 0 & \Gamma^i & 0 \\ 0 & M_i\,\bar{\mathcal{R}} & 0 & I \end{bmatrix} \succeq 0, \quad i = 1, \ldots, n_f; \tag{7.12}$$

the following statements hold:

(i) In the absence of UIs, noises and faults, the extended state estimation error converges to zero.

(ii) The FE error due to UIs is bounded as[3]

$$\|\widetilde{f}\|_{RMS}^2 \leq \gamma_d\,\|d\|_{RMS}^2. \tag{7.13}$$

[3]It is also bounded as $\|\widetilde{f}\|_{RMS}^2 \leq \gamma_d\, n_d^2 \bar{d}^2$ because $\|d\|_{RMS} \leq n_d\,\|d\|_\infty$ and $\|d\|_\infty \leq \bar{d}$.

(iii) The covariance of the FE error due to noises is bounded as

$$\Sigma \preceq \Xi. \tag{7.14}$$

(iv) The FE error due to fault variations is bounded as[4]

$$\|\widetilde{f}_i\|^2_{RMS} \leq \sum_{j=1}^{n_f} \Gamma^i_{jj} \, \|\delta_j\|^2_{RMS}. \tag{7.15}$$

Proof. The following items prove each statement of Theorem 7.1.

(i) Let us define the Lyapunov function $V^Q(k) = \widetilde{z}(k)^T \, Q \, \widetilde{z}(k)$ at each instant k. In the absence of UIs, noises and faults (i.e., $d = 0$, $v = 0$, $\delta = 0$), after taking Schur's complements on (7.10) and premultiplying the result by $\begin{bmatrix} \widetilde{z}(k)^T & d(k)^T \end{bmatrix}$ and postmultipliying by its transpose, we obtain that $V^Q(k+1) - V^Q(k) \leq 0$, which assures that the estimation error (7.6) converges to zero. We get the same result if we define the Lyapunov functions $V^S(k) = \widetilde{z}(k)^T \, S \, \widetilde{z}(k)$ and $V^{P_i}(k) = \widetilde{z}(k)^T \, P_i \, \widetilde{z}(k)$ at each instant k and we perform similar steps on the first inequality in (7.11) and on (7.12) with $\begin{bmatrix} \widetilde{z}(k)^T & v(k)^T \end{bmatrix}$ and $\begin{bmatrix} \widetilde{z}(k)^T & \delta(k)^T \end{bmatrix}$, respectively.

(ii) In the absence of noises and faults (i.e., $v = 0$, $\delta = 0$), after taking Schur's complements on (7.10) and premultiplying the result by $\begin{bmatrix} \widetilde{z}(k)^T & d(k)^T \end{bmatrix}$ and postmultipliying by its transpose, we obtain that

$$V^Q(k+1) - V^Q(k) + \widetilde{f}(k)^T \, \widetilde{f}(k) - \gamma_d \, d(k)^T \, d(k) \leq 0.$$

Considering null initial conditions ($V^Q(0) = 0$) and adding the result from $k = 0$ to $k = K - 1$, it yields

$$\sum_{k=0}^{K-1} \widetilde{f}(k)^T \, \widetilde{f}(k) \leq \sum_{k=0}^{K-1} \gamma_d \, d(k)^T \, d(k),$$

where we have taken into account that $Q \succeq 0$. Dividing this expression by K and taking the limit when $K \to \infty$, it leads to the second statement in Theorem 7.1.

(iii) Applying a congruence transformation with $\begin{bmatrix} S^{-1} & 0 \\ 0 & I \end{bmatrix}$ to the first inequality in (7.11) and taking Schur's complements on the result lead to

$$\bar{\mathcal{A}} \, S^{-1} \, \bar{\mathcal{A}}^T + \bar{\mathcal{G}} \, V \, \bar{\mathcal{G}}^T \preceq S^{-1}.$$

In the absence of UIs and faults (i.e., $d = 0$, $\delta = 0$), the covariance of the estimation error $\widetilde{z}$, $\Sigma^z = \lim_{k \to \infty} \mathbb{E}\{\widetilde{z}(k) \widetilde{f}(z)^T\}$, fulfils the Lyapunov equation (7.9a). Then, we deduce that $\Sigma^z \preceq S^{-1}$ because $\bar{\mathcal{A}}$ has stable eigenvalues as demonstrated in the first item of this proof. Applying Schur's complements on the second inequality in (7.11) we have that

$$\bar{\mathcal{R}} \, S^{-1} \, \bar{\mathcal{R}}^T + K \, \mathcal{H} \, V \, (K \, \mathcal{H})^T \preceq \Xi.$$

[4] It is also bounded as $\|\widetilde{f}_i\|^2_{RMS} \leq \sum_{j=1}^{n_f} \Gamma^i_{jj} \, \bar{\delta}^2$ because $\|\delta_j\|_{RMS} \leq \|\delta\|_\infty$ and $\|\delta\|_\infty \leq \bar{\delta}$.

In the absence of UIs and faults (i.e., $d = 0$, $\delta = 0$), the covariance of the estimation error $\widetilde{f}$, $\Sigma = \lim_{k\to\infty} \mathbb{E}\{\widetilde{f}(k)\widetilde{f}(k)^T\}$, fulfils the Lyapunov equation (7.9b) and we deduce that $\Sigma \preceq \Xi$.

(iv) In the absence of UIs and noises (i.e., $d = 0$, $v = 0$), multiplying (7.12) with $\begin{bmatrix}\widetilde{z}(k)^T & \delta(k)^T\end{bmatrix}$ on the left and by its transpose on the right and performing similar steps as in the second statement, we prove the fourth statement in Theorem 7.1.

□

Remark 7.11. *Optimization-based FE strategies usually characterize the performance of the FE error vector $\widetilde{f}$ w.r.t. the UIs d, the noises v and the fault variations δ, e.g., [106, 172, 302]. In this chapter, we alternatively characterize the performance of each FE error $\widetilde{f}_i$ w.r.t. the noises v (using the bound Ξ_{ii}) and w.r.t. each fault variation δ_j (using the bound Γ^i_{jj}). This approach allows designing estimators satisfying in each fault channel different trade-offs between fault sensitivity and noise attenuation, which is of practical interest in engineering applications. For its part, we just characterize the performance of the entire FE error vector $\widetilde{f}$ w.r.t. the UIs d because we desire to design PI observers ensuring UI decoupling.*

7.3.2 Observer design with FE performance requirements

Let us design the gain matrices L and K of the observer (7.5) for satisfying different requirements over the criteria **e.1**, **e.2**, **e.3** and **e.4**.

From Theorem 7.1, we deduce that if Γ^i_{ii} in (7.12) verifies

$$\Gamma^i_{ii} \leq \bar{\Gamma}^i_{ii}, \tag{7.16}$$

the fault tracking error of the estimate $\hat{f}_i$ w.r.t. the variations described by δ_i is bounded by $\bar{\Gamma}^i_{ii}$. The FE error can be bounded using the constraint (7.16); however, from a reliability perspective, constraints over the criterion **e.1** may be of more practical interest. Since the fault tracking speed depends not only on the fault tracking error but also on the fault signal form, we can choose $\bar{\Gamma}^i_{ii}$ to ensure certain fault tracking speed w.r.t. a specific fault signal form verifying Assumption 7.4. Conservatively, we consider a ramp fault of slope $\Delta_i \neq 0$ occurring in the i-th fault channel[5]. In this case, the fault tracking speed may be described by the steady-state FE delay T_i which is bounded as $T_i \leq \sqrt{\Gamma^i_{ii}}$. To prove it, note that a ramp fault signal is generated through a constant signal δ_i (i.e., $\delta_i(k) = \Delta_i$) and the steady-state FE error is also constant and equal to

$$\lim_{k\to\infty} \widetilde{f}_i(k) = \lim_{z\to 1}(1 - z^{-1})G_{\delta_{ii}}(z)\frac{\Delta_i}{1 - z^{-1}} = G_{\delta_{ii}}(1)\Delta_i = \bar{\widetilde{f}}_i.$$

From the item *(iv)* in Theorem 7.1, we have that if $d = 0$ and $v = 0$,

$$\frac{1}{K}\sum_{k=0}^{K} \widetilde{f}_i(k)^2 \leq \frac{1}{K}\sum_{k=0}^{K} \Gamma^i_{ii}\,\delta_i(k)^2.$$

[5] A constraint regarding the fault tracking speed w.r.t. ramp faults is conservative because it covers the worst-case fault signal form considered in Assumption 7.4 (i.e., a ramp fault of slope $\Delta_i = \bar{\delta}$).

Provided that $\delta_i(k) = \Delta_i$, taking the limit when $K \to \infty$, and computing the square root of the result leads to $|\widetilde{\bar{f}}_i| \leq \sqrt{\Gamma^i_{ii}}\,\Delta_i$. Taking into account that the slope Δ_i describes the proportionality between the increase of f_i and the time elapsed between two different samples, we get the previous bound. Then, if Γ^i_{ii} verifies (7.16), the estimation delay T_i under ramp faults is bounded as $T_i \leq \sqrt{\bar{\Gamma}^i_{ii}}$.

Remark 7.12. *Other fault signal forms verifying Assumption 7.4 could be considered to achieve a constraint over the criterion* ***e.1****. For instance, consider a constant fault of size $\bar{f}_i \neq 0$ occurring in the i-th fault channel. In this case, the fault tracking speed may be described by the cumulative squared error defined as $E_i = \|\widetilde{f}_i(k)\|_2^2$. It is straightforward to prove that $E_i \leq \Gamma^i_{ii}\,\bar{f}_i^2$. Then, if Γ^i_{ii} verifies* (7.16)*, the cumulative squared error E_i under unitary step faults is bounded as $E_i \leq \bar{\Gamma}^i_{ii}$.*

Regarding the criterion **e.2**, if Γ^i_{jj} in (7.12) verifies

$$\Gamma^i_{jj} \leq \bar{\Gamma}^i_{jj}, \tag{7.17}$$

certain degree of interfault decoupling between $\hat{f}_i$ and $\delta_{j\neq i}$ is guaranteed. We define *perfect interfault decoupling* as the characteristic of an estimator verifying $\Gamma^i_{jj} = 0$ for all i and for all $j \neq i$. A numerically sound way of adding these constraints to a semidefinite programming problem involving (7.12) is to set the constraint (7.17) for all i and for all $j \neq i$ and to fix

$$\bar{\Gamma}^i_{jj} := \epsilon_{jj} \tag{7.18}$$

with $\epsilon_{jj} = \varepsilon\,\mathrm{tr}\{\Xi\}/\bar{f}_j$, ε being a small number (e.g., $\varepsilon \leq 10^{-6}$) and $\bar{f}_j$ being the maximum expected value of the j-th fault, which can be derived from the physical constraints of the system. The value (7.18) in the constraint (7.17) makes the estimation error due to fault variations in other channels negligible w.r.t. the estimation error due to noises and we claim that *practical interfault decoupling* is achieved whenever (7.17)-(7.18) is satisfied for all i and for all $j \neq i$. For its part, the use of diagonal matrices Γ^i cancels the errors due to simultaneous variations of faults (i.e., the FE error due to the product $\delta_j\,\delta_l$ with $j \neq l$ is cancelled).

Similarly, certain degree of decoupling from the UIs (criterion **e.3**) is guaranteed if γ_d in (7.10) verifies

$$\gamma_d \leq \bar{\gamma}_d. \tag{7.19}$$

We define *perfect UI decoupling* as the characteristic of an estimator verifying $\gamma_d = 0$. Similarly to (7.18), we numerically address this issue through

$$\bar{\gamma}_d := \epsilon_d \tag{7.20}$$

with $\epsilon = \varepsilon\mathrm{tr}\{\Xi\}/\bar{d}$. Thus, if (7.19)-(7.20) is fulfilled, the FE error due to UIs becomes negligible w.r.t the error due to noises and we claim that *practical UI decoupling* is achieved.

Remark 7.13. *Note that certain degree of interfault and UI decoupling is achievable regardless of the isolability of the faults and UIs. Perfect interfault and UI decoupling are achievable because the system* (7.1) *verifies Assumption 7.2 (i.e., the faults are isolable among them and from the*

UIs). If perfect UI decoupling is achieved, claims (iii) and (iv) in Theorem 7.1 do also hold in the presence of UIs. We consider that they also hold when practical UI decoupling is guaranteed and the UIs are present in the system.

Remark 7.14. *The most extended strategy to build an observer guaranteeing perfect UI decoupling is the use of some algebraic constraints as the ones presented in [70,106,190] for the design of UIOs. Then, the remaining design freedom can be used in a second-step observer design to achieve certain requirements over other performance criteria. Alternatively, we propose to use the numerical constraints* (7.19)-(7.20) *in a design problem involving* (7.10) *to achieve practical UI decoupling. The proposal leads to an homogeneous formulation of all the performance criteria and allows achieving practical UI decoupling together with other estimation performance requirements in a single-step multiobjective optimization problem. Practical UI decoupling refers then to the numerical approach to achieve UI decoupling. In practice, numerical (or practical) UI decoupling is equivalent to structural (or perfect) UI decoupling, which is achieved using algebraic constraints.*

Finally, if matrix Ξ in (7.11) verifies

$$\Xi_{ii} \leq \bar{\Xi}_{ii}, \tag{7.21}$$

certain noise attenuation (criterion **e.4**) is guaranteed in the i-th FE channel. Particularly, (7.21) implies that the marginal variance of $\widetilde{f}_i$ is bounded as $\Sigma_{ii} \leq \bar{\Xi}_{ii}$.

The following two multiobjective design strategies, summarized in Table 7.1, show a proposal of how to use these results for designing the fault estimator (7.5) guaranteeing different estimation performance requirements.

Strategy 7.1. *Let us assume that we want to design a fault estimator* (7.5) *that minimizes certain linear function $f(\cdot)$ of the marginal variances of the FE errors due to noises while it guarantees practical UI and interfault decoupling, and certain FE delays under ramp faults, with T_i^* being the maximum allowed delay in the i-th fault channel. To address this design, we solve the following optimization problem*

$$\begin{aligned} &\text{minimize} \quad f(\Xi_{11}, \ldots, \Xi_{n_f n_f}) \\ &\text{subject to} \quad \{(7.10)-(7.12),\ (7.16)-(7.20),\ \ \forall i, j \neq i\} \end{aligned} \tag{7.22}$$

with

$$\bar{\Gamma}_{ii}^{i} := T_i^* \tag{7.23}$$

in (7.16) *and along the variables S, Q, P^i, Ξ, Γ^i, K, L and γ_d with $i = 1, \ldots, n_f$ and $j = 1, \ldots, n_f$.*

Strategy 7.2. *Let us assume that we want to design a fault estimator* (7.5) *that minimizes certain linear function $f(\cdot)$ of the FE delays under ramp faults while it guarantees practical UI and interfault decoupling, and certain marginal variance of each FE error, with Σ_{ii}^* being the*

Table 7.1. Overview of observer design strategies for guaranteeing estimation performance requirements.

Target	Target Formulation	Observer Design
Practical UI decoupling	$\gamma_d \leq \epsilon_d$	Optimization problem (7.22)-(7.23)
Practical interfault decoupling	$\Gamma^i_{jj} \leq \epsilon_{jj}$, $\forall i, j \neq i$	
Bounded ramp FE delays	$T_i \leq T_i^*$, $\forall i$	
Minimized marginal variances due to noises	min $f(\Sigma_{11}, \ldots, \Sigma_{n_f n_f})$	
Practical UI decoupling	$\gamma_d \leq \epsilon_d$	Optimization problem (7.24)-(7.25)
Practical interfault decoupling	$\Gamma^i_{jj} \leq \epsilon_{jj}$, $\forall i, j \neq i$	
Bounded marginal variances due to noises	$\Sigma_{ii} \leq \Sigma^*_{ii}$, $\forall i$	
Minimized ramp FE delays	min $f(T_1, \ldots, T_{n_f})$	

variance requirement in the i-th fault channel. To address this design, we solve the following optimization problem

$$\begin{aligned} &\text{minimize} \quad f(\Gamma^1_{11}, \ldots, \Gamma^{n_f}_{n_f n_f}) \\ &\text{subject to} \quad \{(7.10)-(7.12),\ (7.17)-(7.21),\ \ \forall i, j \neq i\} \end{aligned} \tag{7.24}$$

with

$$\bar{\Xi}_{ii} := \Sigma^*_{ii} \tag{7.25}$$

in (7.21) *and along the variables* S, Q, P^i, Ξ, Γ^i, K, L *and* γ_d *with* $i = 1, \ldots, n_f$ *and* $j = 1, \ldots, n_f$.

Conservativeness and solvability of the observer design

The multiobjective optimization problems in Strategy 7.1 and Strategy 7.2 are based on the results of Theorem 7.1, whose conditions are standard in norm-based designs [121,335]. The use of independent closed-loop Lyapunov functions Q and P_i ($i = 1, \ldots, n_f$), which are different from the matrix bound S, guarantee non-conservative designs based on the inequalities (7.10)-(7.12) because the estimation error model (7.6) is LTI. However, these designs become nonlinear optimization problems entailing bilinear matrix inequalities (BMIs).

These nonlinear problems can be solved using different solvers such as the ones presented in [129,161]. Unfortunately, these solvers introduce certain degree of conservatism because they only guarantee local solutions. Alternatively, it is possible to iteratively solve the BMIs through a sequence of problems of linear matrix inequalities (LMIs) following different approaches such as the ones presented in [86]. Note that recovering convexity by enforcing $Q = S = P_i$ for all i is not suitable because this approach is too conservative. However, a compromise solution can be also adopted by introducing a slack variable as detailed in works as [69, 121].

Practical interfault and UI decoupling, which are required in Strategy 7.1 and Strategy 7.2, are achievable because the system (7.1) verifies Assumption 7.2. Hence, the solvability of the

optimization problems (7.22) and (7.24) depends on the restrictiveness of the values which are chosen for the performance requirements T_i^* and Σ_{ii}^* $(i = 1, \ldots, n_f)$, respectively. The solvability limits of the performance requirements can be found using the following problems.

- The most restrictive requirements T_i^* $(i = 1, \ldots, n_f)$ guaranteeing the solvability of the design problem in Strategy 7.1 satisfy $T_i^* := \Gamma_{ii}^i$, with Γ_{ii}^i being the solution to the following problem:

$$\begin{aligned} &\text{minimize} && f(\Gamma_{11}^1, \ldots, \Gamma_{n_f n_f}^{n_f}) \\ &\text{subject to} && \{(7.10), (7.12),\ (7.16) - (7.20),\ \ \forall i, j \neq i\} \end{aligned}$$

  along the variables S, Q, P^i, Γ^i, K, L and γ_d with $i = 1, \ldots, n_f$ and $j = 1, \ldots, n_f$.

- The most restrictive requirements Σ_{ii}^* $(i = 1, \ldots, n_f)$ guaranteeing the solvability of the design problem in Strategy 7.2 satisfy $\Sigma_{ii}^* := \Xi_{ii}$, with Ξ_{ii} being the solution to the following problem:

$$\begin{aligned} &\text{minimize} && f(\Xi_{11}, \ldots, \Xi_{n_f n_f}) \\ &\text{subject to} && \{(7.10), (7.11),\ (7.17) - (7.21),\ \ \forall i, j \neq i\} \end{aligned}$$

  along the variables S, Q, P^i, Ξ, K, L and γ_d with $i = 1, \ldots, n_f$ and $j = 1, \ldots, n_f$.

7.4 Fault isolation

7.4.1 FI performance characterization

Motivated by the characterization presented in [44,70], we describe the performance of the fault isolator (7.8) through the following indices:

i.1. the false isolation rates,
i.2. the minimum isolable faults,
i.3. the acknowledgement times and
i.4. the isolation times.

Let us first define a persistent fault f_i satisfying

$$\begin{cases} |f_i(k)| = 0 & \text{if } k < k_0 \\ |f_i(k)| \in (0, \underline{f}_i) & \text{if } k \in [k_0, \underline{k}) \\ |f_i(k)| \geq \underline{f}_i & \text{if } k \geq \underline{k} \end{cases} . \tag{7.26}$$

We define the *false isolation rate* of the fault i, which we denote as ϕ_i, as the probability of rising an isolation alarm of the fault i when $f_i = 0$:

$$\phi_i = \mathbb{P}\{\exists k : |\hat{f}_i(k)| \geq J_i\}. \tag{7.27}$$

Provided $f_{j\neq i} = 0$, $v = 0$ and $d = 0$, we define the *minimum isolable fault* i, which we denote as ψ_i, as the smallest value $\underline{f_i}$ that ensures the isolation of the fault (7.26):

$$\psi_i = \left\{ \begin{array}{l} \min \underline{f_i} \\ \text{s.t.} \quad \exists k \geq \underline{k} : |\hat{f}_i(k)| \geq J_i \end{array} \right\}. \tag{7.28}$$

Under these conditions (i.e., $f_{j\neq i} = 0$, $v = 0$ and $d = 0$), we define the *acknowledgement time* of the fault i, which we denote as ϑ_i, as the time elapsed between $\underline{k}$ and the first sample of isolation of the fault (7.26):

$$\vartheta_i = \left\{ \begin{array}{l} \min\limits_{k\geq \underline{k}} k - \underline{k} \\ \text{s.t.} \quad |\hat{f}_i(k)| > J_i \end{array} \right\}. \tag{7.29}$$

We define the *isolation time* of the fault i, which we denote as τ_i, as the time elapsed between the appearance of the fault (7.26) at k_0 and the first sample of isolation of this fault:

$$\tau_i = \underline{k} - k_0 + \vartheta_i. \tag{7.30}$$

7.4.2 Mechanisms design with FI requirements

Assume that the model-based observer (7.5) has been designed through the strategies presented in Section 7.3.2 and the fault estimate $\hat{f}_i$ provided by such observer (with prefixed stabilising gains L and K) is used in the decision mechanism (7.8). In the following, we show how to design the threshold J_i of the decision mechanism (7.8) for guaranteeing certain requirement over one isolation performance index.

Regarding the index **i.1**, if $f_i = 0$ and perfect UI and interfault decoupling are achieved, the fault estimate $\hat{f}_i$ is zero-mean and its variance is given by the marginal variance Σ_{ii}, which can be computed through (7.9). Then, through Chebyshev's inequality[6] and the definition (7.27), we have that

$$\phi_i \leq \Sigma_{ii}/J_i^2, \tag{7.31}$$

and we can set J_i as

$$J_i := \sqrt{\Sigma_{ii}/\phi_i^*}. \tag{7.32}$$

to guarantee the bound $\phi_i \leq \phi_i^*$.

Remark 7.15. *Provided UI and interfault decoupling, if the noises v are Gaussian, we have that $\hat{f}_i \sim \mathcal{N}(0, \Sigma_{ii})$ and we can set J_i to fix the index **i.1** to ϕ_i^* as*

$$J_i := \Phi_Z^{-1}(1 - \phi_i^*/2)\,\sqrt{\Sigma_{ii}}, \tag{7.33}$$

with $\Phi_Z^{-1}(\cdot)$ being the inverse cumulative distribution function of a standard normal variable[7].

[6] If $a > 0$ and x is a random variable of mean μ and variance σ, then $\mathbb{P}\{|x - \mu| > a\,\sigma\} \leq 1/a^2$.

[7] Note that the threshold J_i defined as (7.33) ensures $\phi_i \equiv \phi_i^*$ in the case of Gaussian noises while the threshold J_i defined as (7.32) ensures the bound $\phi_i \leq \phi_i^*$ regardless of the statical distribution of the noises.

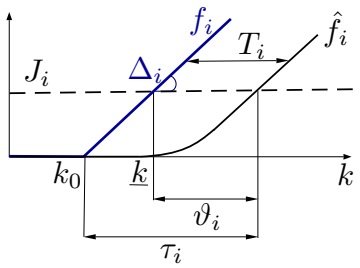

Figure 7.1. Time isolation indices in the presence of a ramp fault.

The minimum isolable fault i depends on the form of the fault signal f_i, see the definition (7.28). Then, we can just ensure certain index **i.2** w.r.t. a specific fault signal form verifying Assumption 7.4 and the conditions (7.26). The straightforward case is the occurrence of a non-zero step fault in the i-th fault channel because the minimum isolable fault coincides with the threshold of the isolation mechanism, i.e.,

$$\psi_i \equiv J_i. \tag{7.34}$$

Hence, we can fix the minimum isolable constant fault i to ψ_i^* by setting

$$J_i := \psi_i^*. \tag{7.35}$$

The time indices **i.3** and **i.4** do also depend on the form of the exogenous fault signal f_i, see (7.29) and (7.30). Then, we can just ensure certain time indices w.r.t. a specific fault signal form verifying Assumption 7.4 and the conditions (7.26). In analogy to the estimation performance criterion **e.1**, we consider the occurrence of a ramp fault of slope $\Delta_i \neq 0$ in the i-th fault channel, see Fig. 7.1. If the estimation error has achieved the steady state when the fault exceeds J_i, the acknowledgement time of the fault i is the steady-state estimation delay T_i (i.e., $\vartheta_i \equiv T_i$) and the isolation time of the fault i satisfies

$$\tau_i \equiv J_i/\Delta_i + T_i, \tag{7.36}$$

where J_i/Δ_i characterizes the time that the ramp fault requires to achieve J_i. In all, $\vartheta_i \equiv T_i$ is determined by the observer and it cannot be modified by varying J_i. Provided certain T_i, we can set

$$J_i := \Delta_i(\tau_i^* - T_i) \tag{7.37}$$

to fix the isolation time to τ_i^* (i.e., $\tau_i \equiv \tau_i^*$) if $\tau_i^* > T_i$ and Δ_i is known. Note that the slope Δ_i is not generally known and requirements over the acknowledgement time ϑ_i are more general.

The mechanism design strategies presented in this section are summarized in Table 7.2. Note that once J_i is designed to guarantee one isolation performance index, the other indices can be computed through (7.31), (7.34) and (7.36).

7.4.3 Co-design with FI requirements

The strategies presented in Section 7.4.2 show how to design the decision mechanism (7.8) to ensure one requirement over the index **i.1**, **i.2.** or **i.4** when the gain matrices L and K of the

Table 7.2. Overview of mechanism design strategies for guaranteeing one isolation performance requirement.

Target	Target Formulation	Mechanism Design
Bounded false isolation rate	$\phi_i \leq \phi_i^*$	Obtain Σ_{ii} with (7.9) Equality (7.32)†
Certain minimum isolable constant fault	$\psi_i \equiv \psi_i^*$	Equality (7.35)
Certain ramp fault isolation time (slope Δ_i)	$\tau_i \equiv \tau_i^*$	Equality (7.37)

†Equality (7.33) with Gaussian noises ensures $\phi_i \equiv \phi_i^*$.

observer (7.5) are prefixed (i.e., the gains are already designed). In order to achieve an isolator guaranteeing two or more requirements over these indices, it is necessary to perform a co-design of the observer (7.5) and the decision mechanisms (7.8). The following strategies, summarized in Table 7.3, show a proposal of how to perform this co-design for guaranteeing more than one isolation performance requirement.

Strategy 7.3. *Assume that we desire to ensure altogether certain false isolation rates ϕ_i^* $(i = 1, \ldots, n_f)$, certain minimum isolable constant faults ψ_i^* $(i = 1, \ldots, n_f)$ and minimum acknowledgement times under ramp faults (and thus minimum isolation times under ramp faults). To ensure these requirements, we first design the observer* (7.5) *through Strategy 7.2 with the value*

$$\Sigma_{ii}^* := \phi_i^* \, {\psi_i^*}^2 \tag{7.38}$$

in (7.25) *for all i. Second, with the obtained gains L and K, we compute Σ through* (7.9)[8] *and we set the isolation thresholds through* (7.32) *with ϕ_i^* for all i.*

Remark 7.16. *If the noises v that affect the system* (7.1) *are Gaussian, the constraint* (7.38) *can be replaced by*

$$\Sigma_{ii}^* := {\psi_i^*}^2 / \Phi_Z^{-1}(1 - \phi_i^*/2)^2 \tag{7.39}$$

and each isolation threshold can be set through (7.33) *with ϕ_i^*.*

Strategy 7.4. *Now, assume that we desire to ensure altogether certain false isolation rates ϕ_i^* $(i = 1, \ldots, n_f)$, certain acknowledgement times under ramp faults ϑ_i^* $(i = 1, \ldots, n_f)$ and we desire to minimize the minimum isolable faults. To ensure these requirements, we first design the observer* (7.5) *through Strategy 7.1 with the value*

$$T_i^* := \vartheta_i^* \tag{7.40}$$

in (7.23) *for all i. Second, with the obtained gains L and K, we compute Σ through* (7.9) *and we set the isolation thresholds through* (7.32) *(or* (7.33) *if the noises are Gaussian) with ϕ_i^* for all i.*

[8]Strategy 7.2 guarantees practical UI and interfault decoupling and thus, in the fault-free scenarios, signal $\hat{f}_i$ is zero-mean and its variance is given by the marginal variance Σ_{ii}.

Table 7.3. Overview of co-design strategies for guaranteeing isolation performance requirements.

Target	Target Formulation	Observer Design	Mechanisms Design
Bounded false isolation rates	$\phi_i \leq \phi_i^*, \forall i$	Optimization problem (7.24)-(7.25)† $\Sigma_{ii}^* := \phi_i^* \psi_i^{*2}, \forall i$	Obtain Σ (7.9) Equality (7.32)‡
Bounded minimum isolable constant faults	$\psi_i \leq \psi_i^*, \forall i$		
Minimized ramp fault isolation times	$\min f(\tau_1, \ldots, \tau_{n_f})$		
Minimized ramp fault acknowledgement times	$\min f(\vartheta_1, \ldots, \vartheta_{n_f})$		
Bounded false isolation rates	$\phi_i \leq \phi_i^*, \forall i$	Optimization problem (7.24)-(7.25) $T_i^* := \vartheta_i^*, \forall i$	Obtain Σ (7.9) Equality (7.32)‡
Bounded ramp fault acknowledgement times	$\vartheta_i \leq \vartheta_i^*, \forall i$		
Minimized minimum isolable constant faults	$\min f(\psi_1, \ldots, \psi_{n_f})$		
Bounded minimum isolable constant faults	$\psi_i \leq \psi_i^*, \forall i$	Optimization problem (7.24)-(7.25) $T_i^* := \vartheta_i^*, \forall i$	Equality (7.35)
Bounded ramp fault acknowledgement times	$\vartheta_i \leq \vartheta_i^*, \forall i$		
Minimized false isolation rates	$\min f(\phi_1, \ldots, \phi_{n_f})$		

†$\Sigma_{ii}^* := \psi_i^{*2}/\Phi_Z^{-1}(1-\phi_i^*/2)^2$ with Gaussian noises.

‡Equality (7.33) with Gaussian noises.

Remark 7.17. *Note that if we desire to ensure altogether certain acknowledgement times under ramp faults ϑ_i^* $(i = 1, \ldots, n_f)$, certain minimum isolable constant faults ψ_i^* $(i = 1, \ldots, n_f)$ and we desire to minimize the false isolation rates, we just have to design the observer* (7.5) *through Strategy 7.1 with the value $T_i^* := \vartheta_i^*$ and set $J_i := \psi_i^*$ for all i.*

Remark 7.18. *In order to achieve an isolator which guarantees certain isolation times τ_i^* under ramp faults of slope Δ_i $(i = 1, \ldots, n_f)$, certain false isolation rates ϕ_i^* $(i = 1, \ldots, n_f)$ while it minimizes the minimum isolable constant faults, we must design the observer* (7.5) *through Strategy 7.1 with $T_i^* := \tau_i^* - 1/\Delta_i \sqrt{\Xi_{ii}/\phi_i^*}$ in* (7.23) *for all i. The constraint* (7.23) *becomes, then, nonlinear. Provided this nonlinearity and given that slope Δ_i is generally unknown, we use Strategy 7.4 whenever requirements over time isolation indices appear in the co-design.*

7.5 FE and FI with a bank of observers

In this section, we address the case in which the faults and the UIs in the system (7.1) are not isolable (i.e., $\text{rank}\{G_{fd}(z)\} < \sum_{i=1}^{n_f} \text{rank}\{G_{f_i}(z)\} + \text{rank}\{G_d(z)\}$) and, thus, it is not possible to build model-based observers that guarantee both decoupling from the UIs and appropriate

fault estimates. Then, we design several observers (i.e., a bank of observers), each of them taking only into account a subset of all the faults to which the system is prone. Assuming that all the faults in the system are not simultaneous, we build a bank of decision mechanisms for the bank of observers which enhances, first, FI and, then, FE.

Remark 7.19. *As detailed in Remark 7.13, certain degree of UI decoupling is achievable regardless of the isolability of the faults from the UIs. In this section, we assume that practical UI decoupling is required and intermediate solutions guaranteeing certain degree of UI decoupling do not fulfil the required performance.*

Remark 7.20. *Consider the case in which certain requirements over estimation or isolation performance indices compromise FE or FI w.r.t. other performance indices. Although not being necessary in terms of isolability conditions, the use of a bank of observers leads to a better performance w.r.t the compromised indices at the cost of new restrictions over the simultaneity of faults. This situation gives a further motivation to the strategies developed in this section.*

7.5.1 Bank of observers and decision mechanisms for FE and FI

Let us denote the set of all possible faults as $S = \{f_1, \dots, f_{n_f}\}$ and the set of the corresponding ordered indices as $\pi = \{1, \dots, n_f\}$ (i.e., $\pi_i = i$). We split the model (7.1) into a bank of m submodels. Each submodel b (with $b = 1, \dots, m$) takes account of a subset $S^b \subset S$ of $n_s < n_f$ faults (with ordered indices $\pi^b \subset \pi$) while it ignores the other faults. Every fault of the system is at least considered by one submodel in the bank (i.e., $S = \bigcup_b S^b$) and $S^b \neq S^c$ for $b \neq c$. The number of submodels in the bank is thus

$$m = \mathbf{C}_{n_s}^{n_f} = \frac{n_f!}{n_s!\,(n_f - n_s)!}. \tag{7.41}$$

We denote the vector that stacks the faults which are taken into account by the b-th submodel as f^b and the vector that stacks the faults which are ignored by this submodel as $f^{\setminus b}$. The b-th submodel is

$$x(k+1) = A\,x(k) + B\,u(k) + E^b\,f^b(k) + G\,v(k) + D\,d(k), \tag{7.42a}$$

$$y(k) = C\,x(k) + F^b\,f^b(k) + H\,v(k), \tag{7.42b}$$

with E^b and F^b being the result of stacking the columns of E and F indexed by π^b. The size n_s of the subsets S^b must be chosen in order to guarantee the isolability of all the fault vectors f^b in the presence of UIs. For all b, we must have that

$$\operatorname{rank}\{G_{f^b d}(z)\} = \sum_{l=1}^{n_s} \operatorname{rank}\left\{G_{f_l^b}(z)\right\} + \operatorname{rank}\left\{G_d(z)\right\}, \tag{7.43}$$

with $G_{f_l^b}(z) = C\,(z\,I - A)^{-1}\,E_l^b + F_l^b$ and $G_{f^b d}(z) = \left[G_{f_1^b}(z) \dots G_{f_{n_s}^b}(z) \quad G_d(z)\right]$. Due to the additive nature of the faults and the UIs in (7.1), it is not possible to guarantee the condition (7.43) if $n_s > n_y - n_d$. Then, we set n_s as the maximum number less than or equal to $n_y - n_d$ such that the condition (7.43) holds for all the submodels in the bank.

In analogy to (7.4), we augment each submodel (7.42) with the dynamics of the fault vector f^b (i.e., $A_F^b = I_{n_s},\ B_F^b = I_{n_s},\ C_F^b = I_{n_s}$). Then, likewise to (7.5), we build a bank of observers in the form of

$$\hat{z}^b(k+1) = \mathcal{A}^b\,\hat{z}^b(k) + \mathcal{B}^b\,u(k) + L^b(y(k) - \mathcal{C}^b\,\hat{z}^b(k)), \tag{7.44a}$$

$$\hat{f}^b(k) = \mathcal{R}^b\,\hat{z}^b(k) + K^b\,(y(k) - \mathcal{C}^b\,\hat{z}^b(k)), \tag{7.44b}$$

with L^b and K^b being the observer gain matrices of the b-th observer of appropriate dimensions. Vector $\hat{f}^b$ is the estimated fault and $\hat{z}^b$ is the estimated extended state.

Note that (7.42) models the behavior of the system (7.1) when the faults $f^{\setminus b}$ are not present in the system (i.e., $f^{\setminus b} = 0$). Then, $\hat{f}^b$ is only reliable when $f^{\setminus b} = 0$. We know that a fault f_i is zero if $\hat{f}_l^b = 0$ with $\pi_l^b = i$ for some estimator b. If n_s or more simultaneous faults occur, there are no zero-value fault estimates and all the estimates provided by the bank are thus corrupted. This means that it is only possible to discern reliable estimates when no more than $n_s - 1$ simultaneous faults are present in the system and that FE and FI are only possible if $n_s > 1$. In all, Algorithm 1 summarizes the strategy to build the bank of observers guaranteeing the isolation and estimation of the maximum possible number of simultaneous faults.

Remark 7.21. *Assume that the condition* (7.43) *does not hold for all submodels b if $n_s > 1$.*

- *If* (7.43) *holds at least for some submodels b when $n_s > 1$ and all the faults f_i ($i = 1, \ldots, n_f$) are considered within these submodels, we extend them with $A_F^b = I_{n_s},\ B_F^b = I_{n_s},\ C_F^b = I_{n_s}$ and we build the corresponding observers* (7.44)*. We extend the other submodels which do not verify* (7.43) *with $A_F^b = 0_{n_s \times n_s},\ B_F^b = I_{n_s},\ C_F^b = I_{n_s}$ and we build the corresponding observers* (7.44)*. In this case, the latter observers are only used for FI purposes and allow discerning the reliability of the outputs provided by the first group of observers, which are used for FE purposes. See the details in [250]*[9].
- *Otherwise, a transformation of the system, as proposed in [182], must be done (leading to new a fault vector f).*

In noisy environments, there are not zero-value fault estimates. This means that decision mechanisms based on thresholds are necessary for both FI and FE. Likewise to (7.8), we set the following decision mechanism which enables FI when no more than $n_s - 1$ simultaneous faults occur

$$\begin{cases} \text{if } \ |\hat{f}_l^b(k)| \geq J_l^b \ \ \forall (b,l) : \pi_l^b = i\ , & \text{Fault } i \\ \text{otherwise}\ , & \text{No fault } i \end{cases} . \tag{7.45}$$

with J_l^b being the isolation threshold of the l-th fault in the b-th bank.

For FE, we rely on $\hat{f}_l^b$ as an estimate of $f_{\pi_l^b}$ whilst no fault in $f^{\setminus b}$ has been isolated through (7.45). If a set B of more than one estimator in the bank provides a reliable estimation of a fault f_i, we define $\hat{f}_i$ through the reliable estimator with better performance w.r.t. certain isolation performance index

$$\hat{f}_i(k) := \{\hat{f}_l^{b^*}(k) : i = \pi_l^{b^*}\}, \tag{7.46}$$

[9] Once a fault is accommodated, the observers in the bank must be reset to avoid the existence of wrong initial conditions derived from the previous presence of ignored faults.

Algorithm 1 Strategy to construct the bank of observers.

$n_s \leftarrow n_y - n_d$
while $n_s > 1$ **do**
  compute m with (7.41)
  construct m subsets S^b verifying $S = \bigcup_b S^b$ and $S^b \neq S^c$ for $b \neq c$
  construct the bank of m submodels (7.42)
  if the condition (7.43) is verified for all b **then**
    construct the bank of m observers (7.44)
    end algorithm
  else
    $n_s \leftarrow n_s - 1$
  end if
end while
if $n_s = 1$ **then**
  apply the strategies in Remark 7.21
end if

with

$$b^* = \{\underset{b \in B}{\operatorname{argmin}} \ \alpha_l^b : \pi_l^b = i\},$$

and α_l^b certain isolation performance index reflecting and improved isolation performance as it decreases.

7.5.2 FI performance characterization and co-design with FI requirements

The isolation index **i.1** of a fault i, ϕ_i, depends on the false alarms of every pair $\hat{f}_l^b$ and J_l^b with $\pi_l^b = i$, i.e.,

$$\phi_i = \mathbb{P}\left\{ \bigcap_{(b,l):\pi_l^b = i} \exists k : |\hat{f}_l^b(k)| \geq J_l^b \right\}, \tag{7.47}$$

when $f_i = 0$. Note that the events $X_j =$ " $\exists k : |\hat{f}_l^b(k)| \geq J_l^b$ " in (7.47) (with $j = 1, \ldots, n_j$ and n_j the number of pairs (b, l) satisfying $\pi_l^b = i$) are not independent and ϕ_i depends on the conditional probability of each event X_j subject to the occurrence of the others. Starting from event X_1, we have that

$$\phi_i = \mathbb{P}\{X_1\} \cdot \mathbb{P}\{X_2/X_1\} \cdot \ldots \cdot \mathbb{P}\left\{X_{n_j}/X_1 \cap \ldots \cap X_{n_j-1}\right\}. \tag{7.48}$$

This equality holds when starting from any event X_j and, thus, we have that

$$\phi_i \leq \mathbb{P}\{X_j\}$$

for $j = 1, \ldots, n_j$. The conditional probabilities in (7.48) are close to 1 because, in practice, the same noises affect all the observers simultaneously. Hence, we deduce that ϕ_i is tightly bounded by

$$\phi_i \leq \min_{(b,l):\pi_l^b = i} \phi_l^b, \tag{7.49}$$

where ϕ_l^b satisfies (7.27) for the b-th estimator. Regarding the index **i.1**, the minimum isolable constant fault i, ψ_i, is given by

$$\psi_i = \max_{(b,l):\pi_l^b=i} \psi_l^b, \tag{7.50}$$

where ψ_l^b satisfies (7.28) for the b-th estimator. Analogous definitions apply to the time indices **i.3** and **i.4**.

In order to design the observers and decision mechanisms of the bank for satisfying global isolation performance requirements, we make use of these characterizations. The following two strategies show a proposal of how to perform the co-design of each observer and the corresponding thresholds for guaranteeing different isolation requirements.

Strategy 7.5. *Assume that we desire to ensure altogether certain false isolation rates ϕ_i^* $(i = 1, \ldots, n_f)$, certain minimum isolable constant faults ψ_i^* $(i = 1, \ldots, n_f)$ and minimum acknowledgement times under ramp faults. To ensure these requirements, we perform m independent designs. In each of them, we design a different observer b of the bank and the corresponding thresholds J_l^b $(l = 1, \ldots, n_s)$ through Strategy 7.3 with requirements ϕ_i^* and ψ_i^* whenever $\pi_l^b = i$.*

Strategy 7.6. *Assume that we desire to ensure altogether certain false isolation rates ϕ_i^* $(i = 1, \ldots, n_f)$, certain acknowledgement times under ramp faults ϑ_i^* $(i = 1, \ldots, n_f)$ and we want to minimize the minimum isolable constant faults. To ensure these requirements, we perform m independent designs. In each of them, we design a different observer b of the bank and the corresponding thresholds J_l^b $(l = 1, \ldots, n_s)$ through Strategy 7.4 with requirements ϕ_i^* and ϑ_i^* whenever $\pi_l^b = i$.*

7.6 Case of study: FE and FI in a wind turbine

The benchmark in [216] describes a three-bladed horizontal wind turbine which consists of four main systems: the generator and converter, the drive train, the blade and pitch and the controller[10]. The strategies developed in this thesis are independent of the control scheme and can be implemented regardless of the control law. In this section, we apply the proposed fault estimators and isolators to the first three systems.

7.6.1 State-space models

In the following, we model the wind turbine systems through the continuous model

$$\dot{x} = A^c x + B^c u + E^c f + G^c v + D^c d, \tag{7.51a}$$

$$y = C^c x + F^c f + H^c v. \tag{7.51b}$$

The sate-space matrices of the realizations are detailed in Appendix D.2.1. Reference [216], which is referred for further modeling details, specifies that the noises that affect the wind turbine benchmark are Gaussian.

[10] Some notes on the operation principle of wind turbines are included in Appendix A.2.

Generator and Converter System. This system can be modeled as a first order closed-loop system between the torque reference, $\tau_{g,r}$, and the non-deviated torque $\tau_{g,n}$. The actual generator torque, τ_g, is given by $\tau_g = \tau_{g,n} + \Delta\tau_{g,n}$, where $\Delta\tau_{g,n}$ is the offset representing the converter fault. Let $\tau_{g,m}$ and v_{τ_g} be the measurement of τ_g and the corresponding additive noise; then, we have

$$x \triangleq \tau_{g,n},\ \ u \triangleq \tau_{g,r},\ \ y \triangleq \tau_{g,m},\ \ f \triangleq \Delta\tau_{g,n},\ \ v \triangleq v_{\tau_g},\ \ d \triangleq \emptyset.$$

Drive Train System. The drive train dynamics is represented by a two-mass model involving the rotor speed, ω_r, the generator speed, ω_g and the torsion angle of the drive train, θ_{rg}. This system is fed with the actual generator torque, τ_g, and the aerodynamic torque from the wind, τ_a. Provided that the real generator torque is not available, we model this input as the difference between its measurement, $\tau_{g,m}$, and the corresponding additive sensor noise, $v_{\tau_{g,m}}$. The aerodynamic torque may be obtained through the wind speed and the power coefficient, C_p, which is a nonlinear function of ω_r, the wind speed and the pitch angles of the turbine. In practice, it is very difficult to know the real distribution of C_p and the measurements of the wind speed provided by anemometers are rather inaccurate. Thus, we consider τ_a to be an UI, which is a widely extended assumption in the bibliography, see [217]. Both drive train speeds are measured by the redundant sensors ω_{r,m_1}, ω_{r,m_2}, ω_{g,m_1} and ω_{g,m_2} and we model their possible faults as the additive signals $\Delta\omega_{r,m_1}$, $\Delta\omega_{r,m_2}$, $\Delta\omega_{g,m_1}$ and $\Delta\omega_{g,m_2}$. Similar applies to their corresponding sensor noise. In all, the state-space vectors are

$$\begin{aligned}
x &\triangleq \begin{bmatrix}\omega_r & \omega_g & \theta_{rg}\end{bmatrix}^T,\\
u &\triangleq \tau_{g,m},\\
y &\triangleq \begin{bmatrix}\omega_{r,m_1} & \omega_{r,m_2} & \omega_{g,m_1} & \omega_{g,m_2}\end{bmatrix}^T,\\
v &\triangleq \begin{bmatrix}v_{\omega_{r,m_1}} & v_{\omega_{r,m_2}} & v_{\omega_{g,m_1}} & v_{\omega_{g,m_2}} & v_{\tau_{g,m}}\end{bmatrix}^T,\\
f &\triangleq \begin{bmatrix}\Delta\omega_{r,m_1} & \Delta\omega_{r,m_2} & \Delta\omega_{g,m_1} & \Delta\omega_{g,m_2}\end{bmatrix}^T,\\
d &\triangleq \tau_a.
\end{aligned}$$

Blade and Pitch System. The hydraulic pitch system of each of the blades $p = 1, 2, 3$ is modeled as a second order closed-loop system between the reference angle provided by the wind turbine controller, β_r, and the averaged measurement, $\beta_{m(p)}$, provided by two redundant sensors, $\beta_{m_1(p)}$ and $\beta_{m_2(p)}$. Both sensors entail measurement noises that disturb the closed loops. Provided that only the closed-loop indices (ω_{n_0} and ξ_0) are known, we model these disturbances as additive signals $v_{\beta_{1(p)}}$ and $v_{\beta_{2(p)}}$ which affect both the measurements and the reference. Similar applies to sensor faults, which we denote as $\Delta\beta_{m_1(p)}$ and $\Delta\beta_{m_2(p)}$ (See Fig. 7.2). The pitch actuator may also suffer from dynamic changes. If we denote the deviations of ω_{n_0} and ξ_0 as $\Delta\omega_{n(p)}$ and $\Delta\xi_{(p)}$ (i.e., $\omega_{n(p)} = \omega_{n_0} + \Delta\omega_{n(p)}$ and $\xi_{(p)} = \xi_0 + \Delta\xi_{(p)}$), the actuator fault can be modeled as an additive signal in the form of

$$f_{\beta_a(p)} = (\Delta w^2_{n(p)} + 2w_{n_0}\Delta w_{n(p)})(\beta_r - \beta_{(p)}) - 2\,(\xi_0\Delta w_{n(p)} + w_{n_0}\Delta\xi_{(p)} + \Delta\xi_{(p)}\Delta w_{n(p)})\dot{\beta}_{(p)}.$$

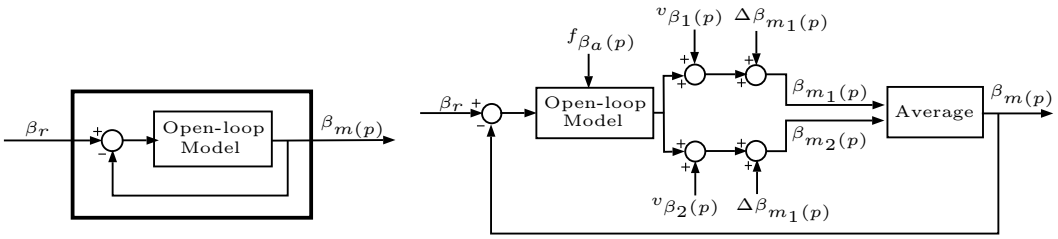

Available Closed-loop Model — Actual Feedback Implementation Model

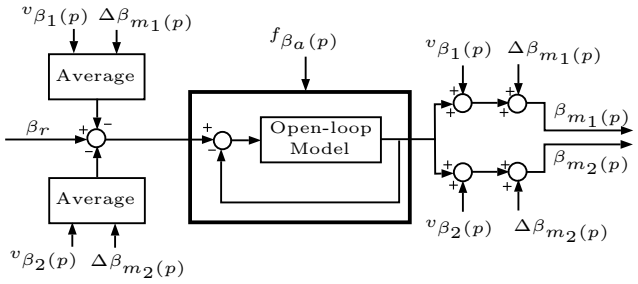

Equivalent Feedback Implementation Model

Figure 7.2. Architecture of the pitch system.

In all, the state-space vectors of each pitch system are

$$
\begin{aligned}
x &\triangleq \begin{bmatrix} \beta_{(p)} & \dot{\beta}_{(p)} \end{bmatrix}^T, \\
u &\triangleq \beta_r, \\
y &\triangleq \begin{bmatrix} \beta_{m_1(p)} & \beta_{m_2(p)} \end{bmatrix}^T, \\
v &\triangleq \begin{bmatrix} v_{\beta_{1(p)}} & v_{\beta_{2(p)}} \end{bmatrix}^T, \\
f &\triangleq \begin{bmatrix} f_{\beta_a(p)} & \Delta\beta_{m_1(p)} & \Delta\beta_{m_2(p)} \end{bmatrix}^T, \\
d &\triangleq \emptyset.
\end{aligned}
$$

7.6.2 Fault estimation and isolation

FE and FI architecture

We discretize the models (7.51) with the sample time $T_s = 0.01$ s and we obtain the matrices A, B, C, D, E, F, G and H in (7.1). The converter faults fulfil the necessary condition for fault isolability in Assumption 7.4; however, the drive train and the pitch faults do not verify it. Then, we split these two models as detailed in Section 7.5. For the drive train system, the strategy summarized in Algorithm 1 leads to $n_s = 3$ and $m = 4$:

$$
\begin{aligned}
S^1 &= \{f_1, f_2, f_3\}, \quad S^2 = \{f_1, f_2, f_4\}, \quad S^3 = \{f_1, f_3, f_4\}, \quad S^4 = \{f_2, f_3, f_4\}, \\
\pi^1 &= \{1, 2, 3\}, \qquad \pi^2 = \{1, 2, 4\}, \qquad \pi^3 = \{1, 3, 4\}, \qquad \pi^4 = \{2, 3, 4\};
\end{aligned}
$$

Table 7.4. Fault signature matrix in the drive train system (☒:Sensitive, ☐:Ignored).

	$\hat{f}_1^1$	$\hat{f}_2^1$	$\hat{f}_3^1$	$\hat{f}_1^2$	$\hat{f}_2^2$	$\hat{f}_3^2$	$\hat{f}_1^3$	$\hat{f}_2^3$	$\hat{f}_3^3$	$\hat{f}_1^4$	$\hat{f}_2^4$	$\hat{f}_3^4$
$f_1 = \Delta\omega_{r,m_1}$	☒			☒			☒			☐	☐	☐
$f_2 = \Delta\omega_{r,m_2}$		☒			☒		☐	☐	☐	☒		
$f_3 = \Delta\omega_{g,m_1}$			☒	☐	☐	☐		☒			☒	
$f_4 = \Delta\omega_{g,m_2}$	☐	☐	☐			☒			☒			☒

Table 7.5. Fault signature matrix in the pitch systems (☒:Sensitive, ☐:Ignored).

	$\hat{f}_1^1$	$\hat{f}_2^1$	$\hat{f}_1^2$	$\hat{f}_2^2$	$\hat{f}_1^3$	$\hat{f}_2^3$
$f_1 = f_{\beta_a(p)}$	☒		☒		☐	☐
$f_2 = \Delta\beta_{m_1(p)}$		☒	☐	☐	☒	
$f_3 = \Delta\beta_{m_2(p)}$	☐	☐		☒		☒

then, FI is only guaranteed if no more than two simultaneous faults occur. For each pitch system, the strategy summarized in Algorithm 1 indicates that the procedure in Remark 7.21 must be applied. We get $n_s = 2$ and $m = 3$:

$$S^1 = \{f_1, f_2\}, \quad S^2 = \{f_1, f_3\}, \quad S^3 = \{f_2, f_3\},$$
$$\pi^1 = \{1, 2\}, \quad \pi^2 = \{1, 3\}, \quad \pi^3 = \{2, 3\}.$$

The isolability condition (7.43) holds for the subsets S^1 and S^2, and all the faults of the pitch system are considered within these subsets. For the subset S^3 the condition (7.43) does not hold and we must use $A_F^b = 0$, $B_F^b = I$, $C_F^b = I$ to extend this submodel. Further explanations regarding this issue are included in Appendix D.2.3.

For each of the resulting submodels, we define the observers (7.44) and the corresponding decision mechanisms (7.45). The signature matrices are presented in Table 7.4 and Table 7.5, where ☒ indicates that the estimate f_l^b is devoted to the estimation of the fault f_i and ☐ indicates that the fault f_i is ignored by the observer b and it may corrupt the estimates f_l^b with $l = 1, \ldots, n_s$. For each of the resulting submodels, we define the observers (7.44) and the corresponding decision mechanisms (7.45).

FE and FI design

Let us first perform different observer designs to study the existing trade-offs between the estimation performance criteria detailed in Section 7.3.1[11]. Fig. 7.3 (left) shows the estimation performance results for different observers designed through Strategy 7.1 for the converter system. One verifies that imposing more restrictive constraints over the ramp fault tracking delay T_{11} leads to higher marginal variances due to noises Σ_{11}. Fig. 7.4 includes the details on the frequency response of the closed-loop transfer function between f and $\hat{f}$ for some of these observers (Observer A with $T_{11} = 1$ samples, Observer B with $T_{11} = 3$ samples and Observer C

[11]The problems are set up in YALMIP [192] and we successfully solve them with the PENBMI solver [129]. For sake of brevity, we do not include the value of the obtained gain matrices.

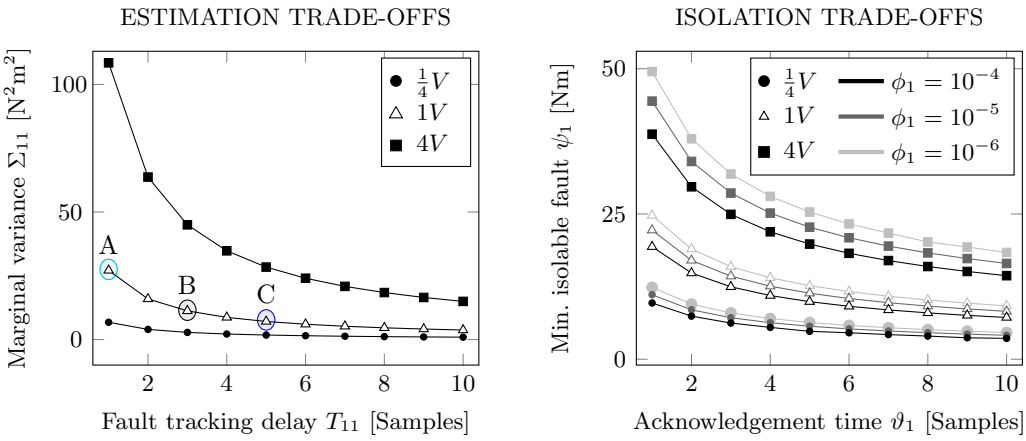

Figure 7.3. Estimation and isolation performance trade-offs in the converter system.

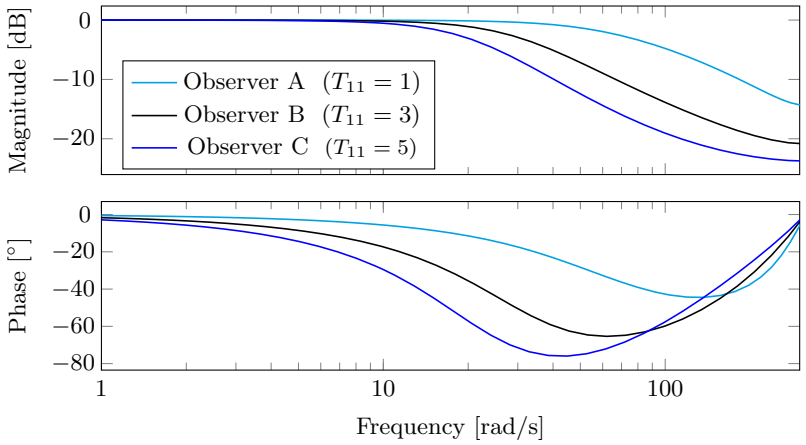

Figure 7.4. Frequency response of the closed-loop transfer function between f and $\hat{f}$ (Converter system).

with $T_{11} = 5$ samples). Provided the physical proprieties of the converter system, the transfer function between f and $\hat{f}$ coincides with the transfer function between v and $\hat{f}$. One verifies then that the observers with a higher bandwidth and a lower phase lag (i.e., fastest response under the appearance of faults) are characterized by higher magnitudes at high frequencies (i.e., higher noise influence). Fig. 7.3 (left) also represents the effect of performing these designs in situations of amplified (i.e., $4V$) and attenuated (i.e., $1/4V$) noises, where V denotes the noise covariance in the benchmark. When the noises affecting the systems increase in variance, the same fault tracking delays imply higher variances.

Now, we perform the observer and decision mechanism co-design in Strategy 7.4 with different acknowledgement time requirements. Fig. 7.3 (right) depicts the trade-offs between the isolation performance indices defined in Section 7.4.1. Again, imposing more restrictive time constraints leads to higher minimum isolable constant faults for certain level of false alarms. For its part, increasing the false isolation rate reduces the value of the minimum isolable constant faults for certain acknowledgement time of ramp faults.

To fulfil the requirements in the benchmark [216], we now design the observers and decision

Table 7.6. Minimum isolable constant faults.

Fault	Minimum Isolable Fault	Fault	Minimum Isolable Fault
$\Delta\omega_{r,m_1}$	0.151 rad/s	$\Delta\tau_{g,n}$	14.300 Nm
$\Delta\omega_{r,m_2}$	0.151 rad/s	$f_{\beta_a(p)}$	$0.933°/s^2$
$\Delta\omega_{g,m_1}$	0.295 rad/s	$\Delta\beta_{m_1(p)}$	0.063°
$\Delta\omega_{g,m_2}$	0.295 rad/s	$\Delta\beta_{m_2(p)}$	0.063°

Table 7.7. Wind turbine benchmark fault scenario description.

Fault code	System	Fault signal	Fault type	Time occurrence TS1
GC-1	Generator	$\Delta\tau_{g,n}$	offset	$t \in [3800, 3900]$ s
DT-1	Drive Train	$\Delta\omega_{r,m_1}$	fixed value	$t \in [1500, 1600]$ s
DT-2	Drive Train	$\Delta\omega_{r,m_2}$, $\Delta\omega_{g,m_1}$	gain factor	$t \in [1000, 1100]$ s
P1-1	Pitch 1	$\Delta\beta_{m_1(1)}$	fixed value	$t \in [2000, 2100]$ s
P2-1	Pitch 2	$\Delta\beta_{m_2(2)}$	gain factor	$t \in [2300, 2400]$ s
P2-2	Pitch 2	$f_{\beta_a(2)}$	change dynamics	$t \in [2900, 3000]$ s
P3-1	Pitch 3	$\Delta\beta_{m_1(3)}$	fixed value	$t \in [2600, 2700]$ s
P3-2	Pitch 3	$f_{\beta_a(3)}$	change dynamics	$t \in [3400, 3500]$ s

mechanisms of the three wind turbine systems through Strategy 7.4.

Although the benchmark [216] highlights the necessity of isolating the faults occurring in the wind turbine systems, it only explicitly specifies requirements over detection performance indices. Thus, we equal the requirements over the false detection rates and the detection times in the benchmark to the requirements over the false isolation rates and the isolation times, respectively. In order to directly apply our approach, we approximate the requirements over the isolation times to requirements over the acknowledgement times of ramp faults and we perform the co-design of each pair of observer and mechanism in the banks. In number of samples, we have $\vartheta_1^* = 3$ for the converter, $\vartheta_{\{1,2,3,4\}}^* = 10$ for the drive train system, and $\vartheta_1^* = 8$, $\vartheta_{\{2,3\}}^* = 10$ for the pitch system. The required false isolation rate is $\phi_i^* = 10^{-5}$ for all the systems. We use the summation (i.e., $\sum_{l=1}^{n_s} \Xi_{ll}$) as the function $f(\Xi_{11}, \ldots, \Xi_{n_s n_s})$ being minimized in the optimization problem. The obtained minimum isolable constant faults are indicated in Table 7.6.

7.6.3 Simulation results

The wind turbine benchmark presents a scenario of 4400 s in which different faults occur. Within the listing of the possible faults, the benchmark test sequences choose the subset of faults in Table 7.7. The benchmark considers seven different test signal sets; they are formed by time-shifting the occurrence of the faults defined in the original test sequence (TS1), which is described in Table 7.7.

Illustratively, let us first simulate the time response of the Observers A, B and C defined in Fig. 7.4 to estimate the converter fault in the test set TS1. Fig. 7.5 (left) shows the estimation

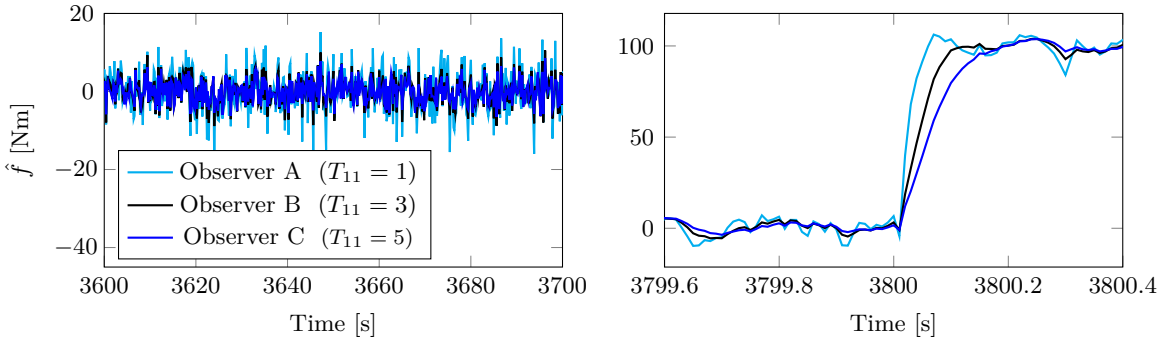

Figure 7.5. FE in the converter with different observers (test set TS1).

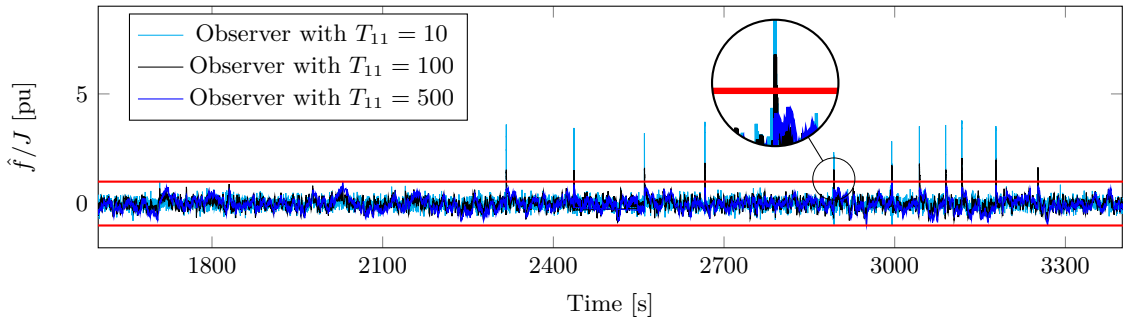

Figure 7.6. FE in the converter with model parameter changes (test set TS1).

results in fault-free samples and Fig. 7.5 (right) shows the estimation results during the fault appearance. The simulation results validate the estimation trade-offs indicated in Fig. 7.3 (left).

Let us also analyse the effect of the restrictiveness of the time constraints on the sensitivity to parameter changes in the model. Fig. 7.6 shows the effect produced by a 5% relative change in the parameter defining the converter dynamics. We verify that the sensitivity to parameter changes increases as the time constraints become more restrictive. The reader is referred to Remark 7.3 and equation (7.7) to obtain the algebraic expression of the effect of the parameter changes on the FE error[12].

Now, we test the behavior of the observers and decision mechanics that we have designed with the isolation performance constraints in the benchmark. If we simulate the different test sets proposed in the benchmark through several Monte Carlo simulations for different noises, we verify that all the results verify the false isolation rate restriction tightly. The isolation times of the faults are summarized in Table 7.8. As an example, Fig. 7.7 details the isolation times obtained for the fault **DT1-1**. Note that the minimum isolation times fulfil the requirements in the benchmark. The cases in which the time requirement is exceeded refer to scenarios with variable fault signals which do not always exceed the achieved minimum isolable fault. For instance, there are cases in which the fault **P3-2** is present in the system but the pitch reference

[12]If the uncertainties regarding parameter changes lead to poor estimation results, these uncertainties must be modeled as UIs (see Remark 7.3) and certain degree of UI decoupling (i.e., constraint (7.19)) must be introduced as an additional requirement in the observer design.

Table 7.8. Isolation times (IT) in number of samples of the Monte Carlo simulation.

Fault scenario	IT Requirement	Minimum IT	Mean IT	Maximum IT
GC-1	3	2	2.19	3
DT-1	10	2	4.36	11
DT-2	10	2	2	2
P1-1	10	2	2	2
P2-1	10	6	223.8	737
P2-2	8	2	2.56	7
P3-1	10	2	2.46	13
P3-2	8	1145	1793.4	2322

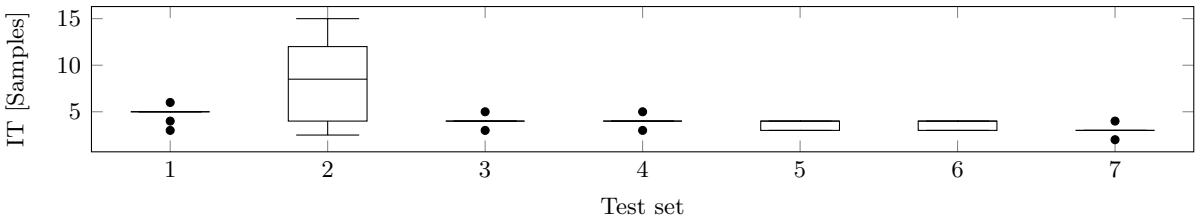

Figure 7.7. Isolation time (IT) of the fault **DT-1** for the test sets in the benchmark.

is barely zero. In such cases, there is no chance to detect or isolate the changes experienced by the pitch dynamics. Other proposals available in the bibliography provide similar results regarding this issue. In any case, if the designer decides that missisolating these small faults may be prohibitive, it would be possible to redesign the fault isolators through Strategy 7.5 as explained in Section 7.5. Note that numerical comparisons with other strategies in the literature are difficult because most existing works are devoted to fault detection and fault isolation and estimation are not included. Moreover, they study indices as the FDR instead of the physically meaningful parameters required on the benchmark (i.e., isolation times, minimum isolable faults, etc.).

In the following, we include the figures showing the FE and FI results in the test set TS1 (described in Table 7.7). First, Fig. 7.8 shows the estimation signal and the corresponding isolation threshold for the converter system, which is affected by **GC-1**. Fig. 7.9 shows the outputs provided by the bank built for FE and FI in the drive train system, which is affected by **DT-1** and **DT-2**. It is straightforward to verify that applying (7.45)-(7.46), the isolation and the estimation of the faults **DT-1** and **DT-2** is achieved.

Regarding the pitch system, Fig. 7.10 (details in Fig. 7.11) shows the results for the third pitch system, which is affected by both **P3-1** and **P3-2**. The figure includes the fault estimates and the thresholds corresponding to the relied observers in the bank. Note that the observer which provides the estimate of the fault $f_3 = \Delta\beta_{m_2(p)}$ (i.e., the pair with better isolation optimized performance index) becomes non-reliable when $f_2 = \Delta\beta_{m_1(p)}$ is present in the system. In this case, the estimation is provided by another pair in the bank with a poorer minimum

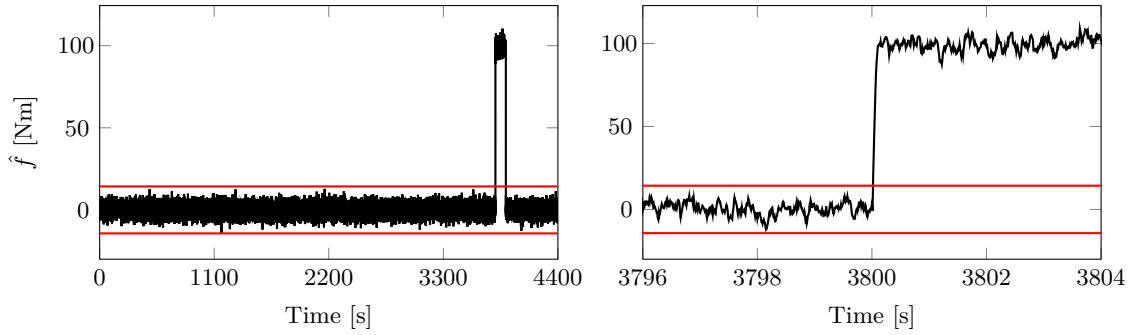

Figure 7.8. FE and FI in the converter (test set TS1).

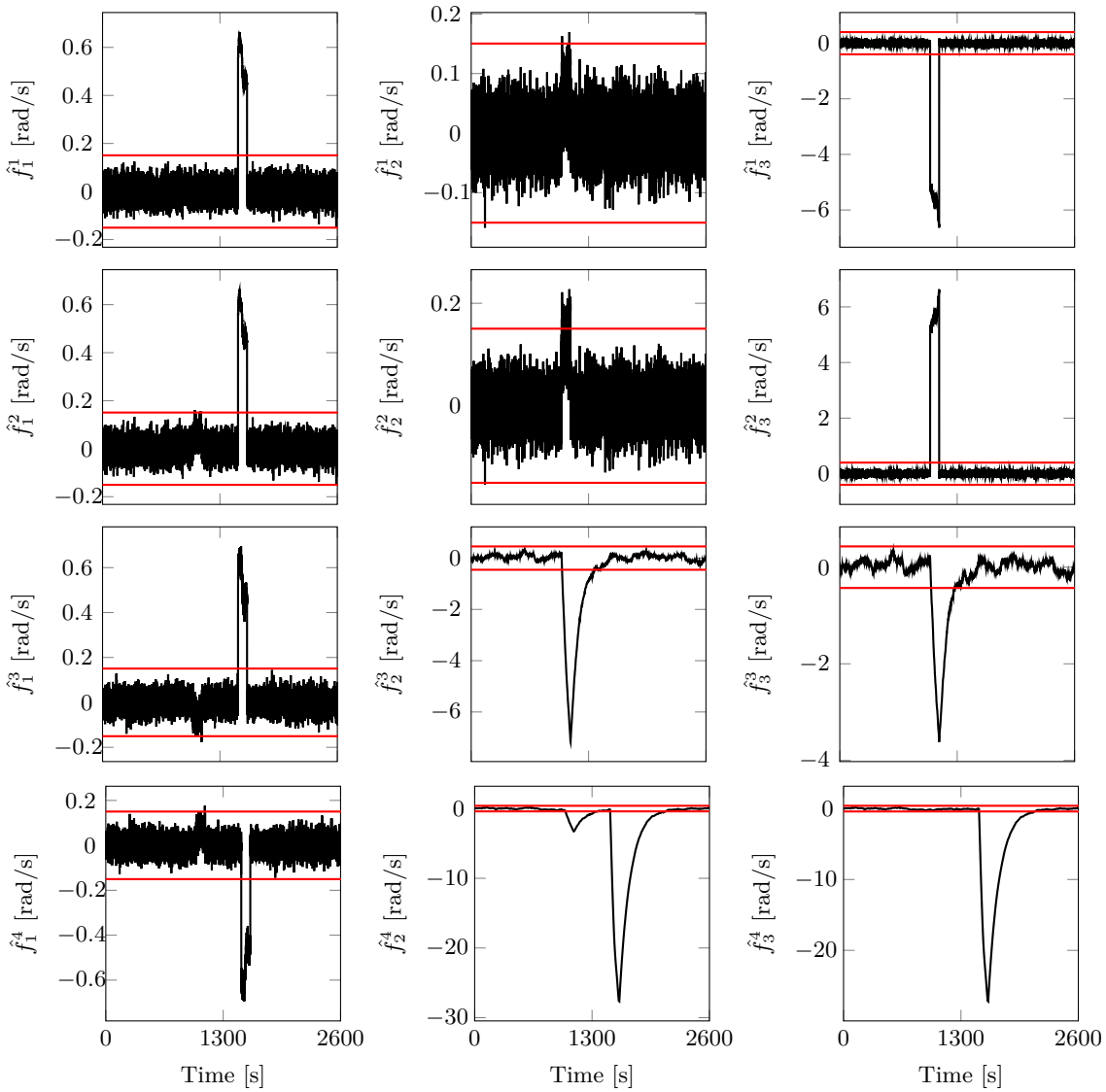

Figure 7.9. Bank of observers and decision mechanisms in the drive train (test set TS1).

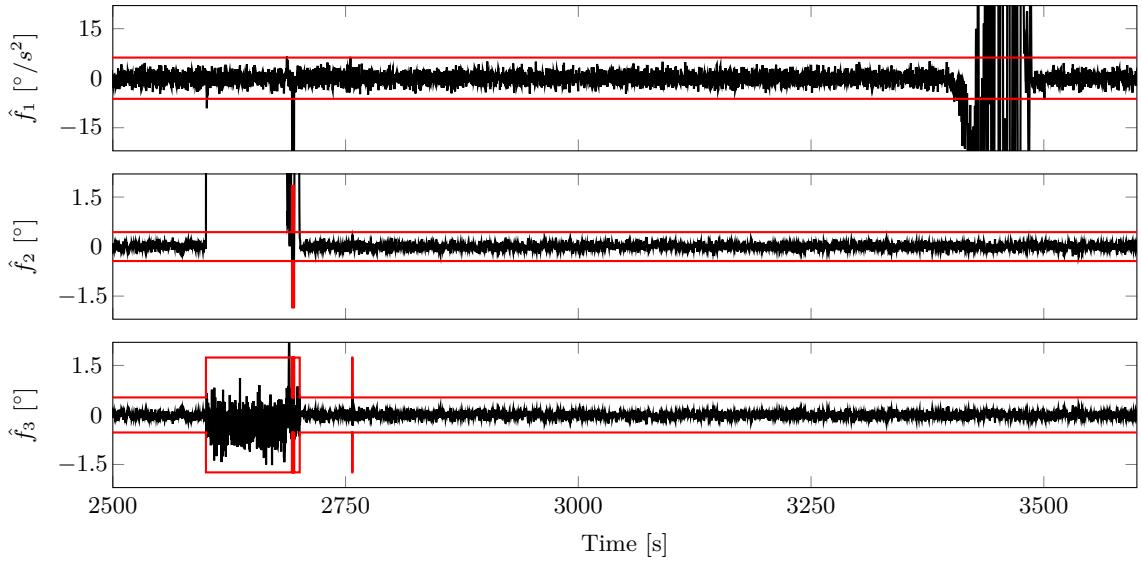

Figure 7.10. FE and FI in the third pitch system in the (test set TS1).

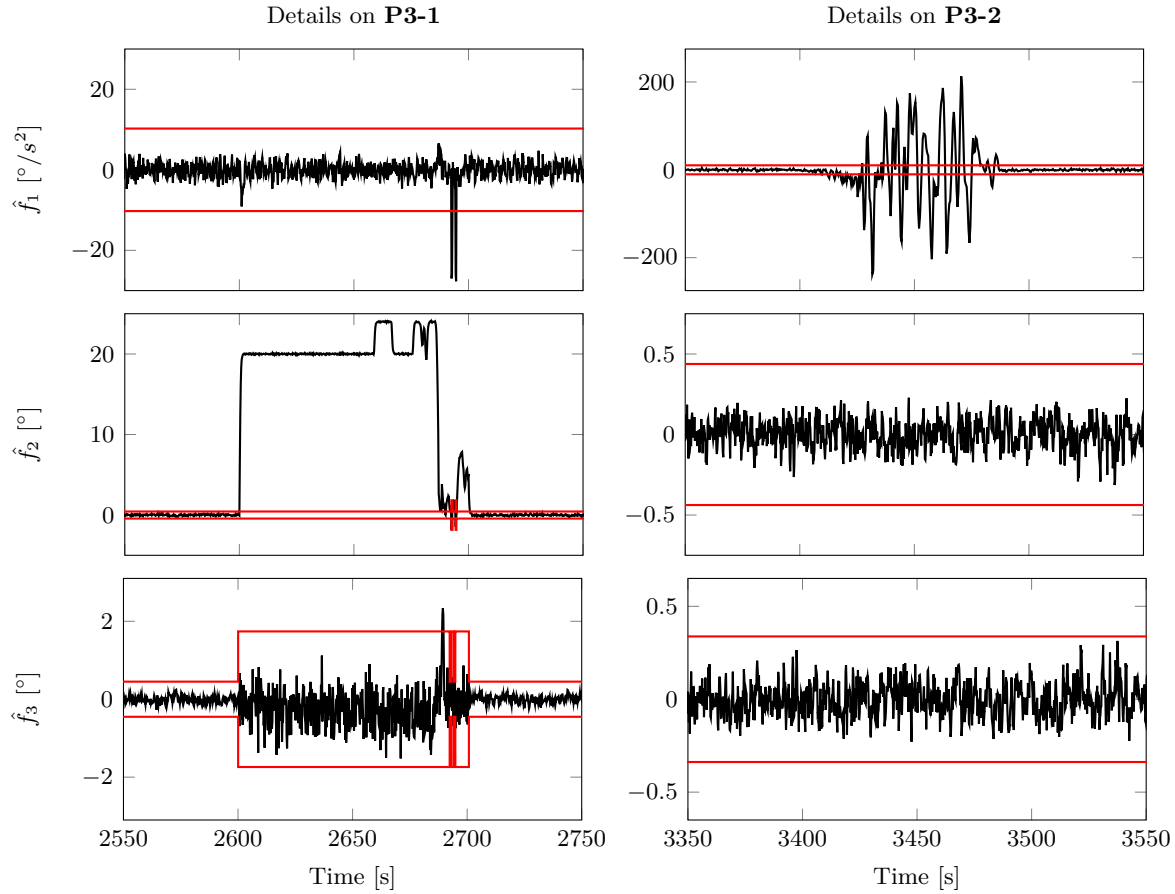

Figure 7.11. Details of FE and FI in the third pitch system (test set TS1).

isolable fault. For ease of space, we do not include the results for the first and second pitch systems.

7.7 Conclusion

In this chapter, we have developed performance-based designs of model-based observes and statistical-based decision mechanisms for achieving FE and FI in systems affected by unknown inputs and stochastic noises. First, we have presented FE performance-based designs of PI observers taking into account the trade-off between the degree of UI and interfault decoupling, the delay to track fault variations and the covariance due to noises. Second, we have presented FI performance-based co-designs of the observers and decision mechanisms taking into account the trade-off between the false isolation rates, the minimum isolable faults and the isolation times. Finally, we have extended the results to a scheme based on a bank of observers and decision mechanisms which provides a solution for FI and FE in systems where fault isolability conditions do not hold and it is not possible to achieve FE through standard observers. We have applied this procedure to a well-known benchmark that has explicit isolation requirements and we have shown that we fulfil all these requirements by just including them as constraints in the designs.

Chapter 8

Estimation and adaptive diagnosis of decreased power in wind farms: a Markovian jump system approach

Blade erosion and debris build-up decrease the power production of wind turbines, reducing their reliability and availability. The diagnosis of this fault is necessary to actively address the problem. In this chapter, we propose a Markovian jump model of the power generation system of a wind turbine and we present a closed-loop model-based observer to estimate the faults related to energy losses. The observer is designed through an $\mathcal{H}_\infty$-based optimization problem that fixes the trade-off between the observer fault sensitivity and robustness. The fault estimates provided by the observer are then used in data-based decision mechanisms for achieving fault detection and isolation. The performance of the diagnosis strategy is then ameliorated in a wind farm level scheme that uses a bank of the aforementioned observers and decision mechanisms. Finally, the proposed approach is tested using a well-known benchmark in the context of wind farm fault diagnosis.

8.1 Introduction

Wind energy is considered as a powerful source of sustainable energy. However, wind turbines (WTs) are expensive systems and their maintainability and reliability must be high. Fouling of the rotor blades with ice or insects, as well as erosion, is an important root cause of faults and it is expected to increase in significance as more WTs are situated in locations with higher wind speeds (WSs) [199, 282]. As stated in [64], the major problem related to debris build-up and erosion is the reduction of the overall WT aerodynamic efficiency leading to unpredicted reductions in power production. Besides possible human safety risks, debris build-up may also cause mass and aerodynamic imbalances, damaging all WT components.

As discussed in [220], the diagnosis of debris build-up can be done using direct or indirect measurements. Direct methods are based on the detection of some change of physical properties

such as mass, electrical or thermal properties. Hence, they often require extra equipment, which augment the installation and maintenance costs and the weight and space requirements. For its part, indirect methods are mainly based on detecting the reduction in power production. These methods do not require extra hardware because they use WT control measurements. They require, however, the WTs to be in operation. Their main disadvantage is that energy losses may be also the consequence of other phenomena which are, nonetheless, generally easily distinguishable from debris build-up. For instance, consider the occurrence of an electric fault in the WT generator. In this case, the deviation of the generator torque from its reference, which can be deduced from the generator torque measurement, provides an immediate and accurate diagnosis of the electric fault leading to its straightforward isolation from debris build-up or erosion [216].

The indirect fault diagnosis (FD) of decreased power generation due to debris build-up or erosion is one of the objectives of the realistic and widely accepted wind farm (WF) benchmark presented in [215]. The benchmark includes the WF power generation model which is based on the well-known power curve of a WT. Basically, two kinds of residuals are used in the bibliography [16, 30, 33, 83, 264] to diagnose power reductions in the benchmark. At a WT level, temporal residuals represent the inconsistencies between the power generation model output and the generated power measurement of a single WT. At a WF level, spatial residuals represent the inconsistencies between the generated power measurements of different WTs. Borcehrsen et al. [33] utilize open-loop temporal residuals in dynamical cumulative sums. Alternatively, Duviella et al. [83] present a FD approach based on spatial residuals and Blesa et al. [30] compute both spatial and open-loop temporal residuals via nonlinear parameter varying parity equations. For its part, Badihi et al. [16] merge both approaches. The authors use the generation model of the WTs to compute the power differences among the WF; then, they compare them to the measured power differences. They also present an approach which replaces the generation model by fuzzy inference mechanisms. Similarly, Simani et al. [264] present fuzzy and neural networks techniques.

The power generation model of a WT is affected by various non-negligible disturbances: mean WS estimation errors, turbulences, vibrations and measurement noises [215]. Hence, the WT level open-loop temporal residuals in [30, 33] may be significantly disturbed. The spatial residuals in [16, 30, 83] are not affected by mean WS estimation errors because they compare WTs working under the same wind conditions. For instance, the methods in [16] require that all the WTs in the WF operate under the same wind conditions. However, in most cases, the WTs operate in different conditions and WS estimation errors still affect the spatial residuals. In all, it is of interest to develop closed-loop strategies with a better performance w.r.t. disturbances at a WT level and at a WF level for groups of WTs affected not only by identical but also by similar wind conditions. Specially, if the FD objectives require not only the information about the appearance and the location of a fault (fault detection and isolation or FDI) but also about its size and shape (fault estimation or FE). FE is of paramount importance for both real-time decisions and active fault tolerant control (AFTC) [330] such as power demand redistribution among the WF.

The closed-loop power generation system of a WT is a parametric loop because the WT operates in different WS zones and under different WT operating modes [54]. Moreover, the

stochastic characteristic of the wind brings further difficulty to the design of closed-loop FE strategies. In the literature, many authors conclude that the WS behavior can be explained as a Markovian process [40, 198]. This behavior has been exploited in recent WT control schemes as the ones in [63, 184, 185]; however, up to date, there has been no work taking advantage of the Markovian behavior of the wind to design FE strategies.

Motivated by the above background, in this work, we develop a Markovian jump system approach for closed-loop FE of decreased power generation in a WF. First, we develop a WT level approach; then, we extend it to the WF level for groups of nearby WTs working under similar wind conditions. FE techniques must be simultaneously robust against uncertainties and noises [106] and sensitive to faults through the accomplishment of certain trade-off between these properties [327]. In this paper, we use the $\mathcal{H}_\infty$ performance of the proposed model-based observer to characterize these properties and to set up an optimal observer design strategy based on linear matrix inequalities (LMIs). Providing a systematic performance-based optimal approach for tuning the FE observer is an advantage when compared to other algorithm designs, where some user expertise is necessary. For instance, numerical extensive simulations and trial and error procedures are necessary to tune the algorithms in [264].

To achieve FDI, we evaluate the fault estimates provided by the proposed observer into decision mechanisms based on thresholds. Model-based thresholding usually leads to too conservative results which are characterized by poor fault detectability and isolability [71], notably in the cases of Markovian jump systems [246]. Therefore, we utilize a data-driven FDI approach based on adaptive thresholds for evaluating the FE output provided by the model-based observer. The proposed adaptive mechanism enhances a tight FDI adjustment in the different WS zones and WT operating modes when compared to the constant thresholds in [16, 33, 264].

8.1.1 Challenges

The proposed Markovian jump system approach for FE and adaptive FDI entails the following challenges.

1. Obtaining a linear parameter varying state-space model of the power generation system of a WT, which is based on nonlinear power curves and consists of two operation modes. To do so, we define a parameter vector containing the WS acting on a WT and the difference between the demanded and the generated power. In this work, the power curves in the WF benchmark [215] are utilized. In reality, these curves can be obtained through different methods such as random forest, method of bins, k-nearest neighbours or support vector regression [115].

2. Modeling the stochastic behavior of the parameters as Markovian processes. Obtaining a suitable partition of the parameter set taking its discontinuities into account. Computing the transition probabilities between subsets.

3. Building an augmented model-based observer for FE of decreased power generation in a WT. Designing the observer through a multiobjective optimization problem that guarantees certain optimal trade-off between the robustness against disturbances/uncertainties

and the sensitivity to faults. To do so, we use the $\mathcal{H}_\infty$ performance of the observer, which we formulate using linear matrix inequalities (LMIs) for Markovian processes and convex polytopic sets.

4. Building an adaptive threshold-based decision mechanism for FDI of decreased power generation in a WT. Proposing an algorithm for computing a tight adaptive threshold piecewise on the WT operation mode. Tuning the algorithm with fault-free datasets using data-driven techniques.

5. Extending the WT level model-based FE and data-driven FDI approach to the WF level. To do so, we group the WTs operating under similar wind conditions and we use a bank of the previous observers and decision mechanisms that automatically merges the information provided by the temporal and spatial relations in the WF according to the degree of shared uncertainty among the WTs.

8.1.2 Structure and notation

The reminder of this chapter is organized as follows. Section 8.2 gives the problem formulation and Section 8.3 presents a Markovian jump modeling of the power generation system of a WT. In Section 8.4, we develop a wind turbine level model-based FE strategy and, in Section 8.5, the FE output is utilized in a data-based FDI algorithm. Then, in Section 8.6, these strategies are extended to the wind farm level. Simulation results are reported in Section 8.8 followed by some concluding remarks in Section 8.9.

Let a be some vector and A and B be some matrix. The size of a is denoted as n_a and $a[i]$ denotes the i-th element in a. $A \preceq 0$ means that A is negative semidefinite and similar applies to $\succeq$. The direct sum is represented as $\oplus$ and the Kronecker product is represented as $\otimes$. I_n is the identity matrix of size $n \times n$, $\mathbf{1}_{n\times m}$ is a matrix of ones of size $n \times m$ and $0_{n\times m}$ is the zero matrix of size $n \times m$ (all of these matrices being of appropriate dimensions when the subindex is omitted). Expected value and absolute value are denoted by $\mathbb{E}\{\cdot\}$ and $|\cdot|$. Let x_k be a vector of stochastic signals at a sample k. We write $\|x_k\|_\infty \triangleq \max_i |x_k[i]|$ for the max norm of vector x_k. We write $\|x\|_\infty \triangleq \max_k \max_i |x_k[i]|$ for the l_∞ norm of signal x, $\|x\|_2^2 \triangleq \lim_{K\to\infty} \sum_{k=1}^{K} x_k^T x_k$ for its l_2 norm and $\|x\|_{\text{RMS}}^2 = \lim_{K\to\infty} \frac{1}{K} \sum_{k=1}^{K} x_k^T x_k$ for its RMS norm.

8.2 Problem statement

8.2.1 Wind farm benchmark description

Consider the WF benchmark [215] with 9 WTs of 4.8 MW and the layout shown in Fig. 8.1. We name the WTs according to the existing wind direction (see the example in Fig. 8.1) and we consider that the wind is perpendicular to the rows of WTs (which are numbered as $i = 1, \ldots, Y$ and Y is the number of rows for the considered wind direction) and parallel to the columns of WTs (which are numbered as $j = 1, \ldots, Z$ and Z is the number of columns for the considered

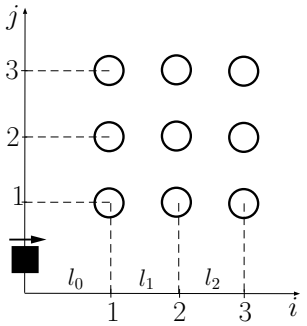

Figure 8.1. Layout of the WF benchmark ($l_0 = 1150$ m and $l_1 = l_2 = 1138.44$ m). →: Wind direction, ◯: Wind turbine, ■: Wind mast.

wind direction). We denote the distance between two rows i and $i+1$ as l_i. There is a wind mast that measures the wind speed at row $i = 0$:

$$v^0 = \hat{v}^0 + \widetilde{v}^0, \tag{8.1}$$

with v^0 being the wind speed at the wind mast, $\hat{v}^0$ being its measurement and $\widetilde{v}^0$ being the corresponding sensor noise. The wind speed acting on the WT (i, j), denoted as $v^{i,j}$, can be modeled as

$$v^{i,j} = v^i + \widetilde{v}_t^{i,j}, \tag{8.2}$$

where v^i is the mean wind speed acting on the WTs in the i-th row and $\widetilde{v}_t^{i,j}$ is a zero-mean turbulence component of known variance ($\sigma_t^2 = 0.2$ m^2/s^2).

The static available power in the WT (i, j), denoted as $P_s^{i,j}$, represents the theoretical maximal generated power in the WT and it depends on $v^{i,j}$ as shown in Fig. 8.2. This power curve is extensively used in monitoring of wind farms (e.g., [115,196]) and it consists of four zones delimited by three different wind speeds: the cut-in (v_{cut-in} =4 m/s), the rated (v_{rated} =12.5 m/s) and the cut-out ($v_{cut-out}$ =25 m/s) wind speed [54]:

- *Zone I* with $v^{i,j} < v_{cut-in}$. In this zone, the aerodynamic torque is not sufficient to overcome the WT inertia and $P_s^{i,j} = 0$.
- *Zone II* or partial load region with $v_{cut-in} \leq v^{i,j} < v_{rated}$. Maximum power point tracking (MPPT) techniques are performed in this region. For MPPT, the pitch angle is held at zero degrees and the generator moment is adjusted to keep the power coefficient of the WT at a maximum value. Hence, $P_s^{i,j}$ becomes a nonlinear function of $v^{i,j}$.
- *Zone III* or full load region with $v_{rated} \leq v^{i,j} < v_{cut-out}$. In this zone, the pitch angle is controlled to keep the static available power not higher than the WT nominal power (i.e., $P_s^{i,j} = P_{nom}$).
- *Zone IV* with $v^{i,j} \geq v_{cut-out}$. The turbine is pitched out to stop the rotation due to security reasons and $P_s^{i,j} = 0$.

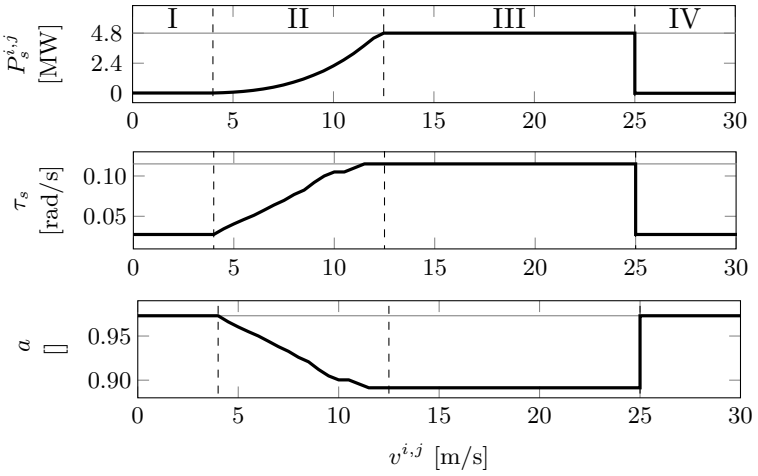

Figure 8.2. Power curve $P_s^{i,j}(v^{i,j})$ and continuous and discrete transfer coefficient curves $\tau_s(v^{i,j})$ and $a(v^{i,j})$. Values borrowed from [215].

According to [215], changes in the generated power will be instantaneous; thus, the static available power in the WT (i, j), denoted as $P_s^{i,j}$, is filtered by a first-order transfer function. This transfer function is characterized by the wind-dependent transfer coefficient τ_s in Fig. 8.2. In all, the dynamic available power in a WT, named after $P_a^{i,j}$, is modeled as

$$\dot{P}_a^{i,j} = \tau_s(v^{i,j}) \left(P_s^{i,j}(v^{i,j}) - P_a^{i,j} \right). \tag{8.3}$$

The WF controller feeds each turbine with the WT static power reference, denoted as P_t. The WT also behaves as a low-pass filter to changes in the power reference; thus, the dynamic power reference of a turbine, P^r, fulfils

$$\dot{P}_r = \tau_r \left(P_t - P_r \right), \tag{8.4}$$

where τ_r is a known transfer function coefficient ($\tau_r = 1.2$ rad/s).

Remark 8.1. *The network operator demands certain power to the WF that ensures a reliable connection of the farm to the electrical grid. This power demand is determined in different modes such as delta, absolute and frequency regulation modes [15]. The WF controller computes the WF static power reference, denoted as P_f, as a function of this demanded power and the power generated by the WF. See [126, 160] for examples of WF power reference computation algorithms. Then, the WF controller feeds each turbine with the WT static power reference, P_t. In this case, the simple distribution algorithm $P_t = \frac{P_f}{YZ}$ is utilized.*

Depending on the values of the dynamic available power $P_a^{i,j}$ and the dynamic power reference P_r, each WT operates in one of the following two main working modes:

- If $P_a^{i,j} < P_r$, the control objective is to maximize the amount of power harvested from the wind and, thus, the generated power equals the dynamic available power in the WT.

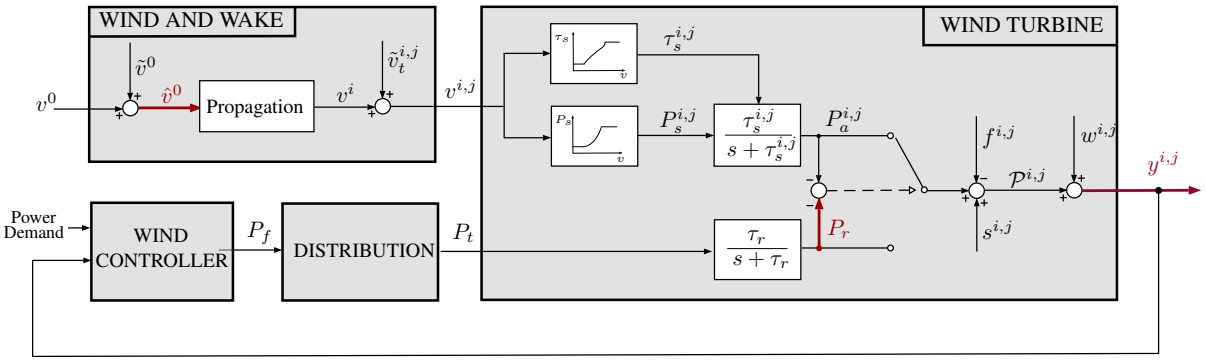

Figure 8.3. Structure of the WF benchmark. The signals which are available for FE and FDI are depicted in red.

- If $P_a^{i,j} \geq P_r$, the control objective is to maintain the generated electrical power equal to the reference.

This behavior can be modeled as

$$\mathcal{P}^{i,j} = \begin{cases} P_a^{i,j} - f^{i,j} + s^{i,j} & \text{if } P_a^{i,j} < P_r \\ P_r \quad - f^{i,j} + s^{i,j} & \text{otherwise} \end{cases}, \tag{8.5}$$

where $\mathcal{P}^{i,j}$ is the power generated by the turbine (i,j) and $s^{i,j}$ is a disturbance modeling the drive train oscillations that influence the electrical power generation (i.e., $s^{i,j} = \gamma_p \sin(\sigma_p\, 2\,\pi\, t)$ with $\gamma_p = 1000$ W and $\sigma_p = 10$ Hz). The additive element $f^{i,j}$ is the fault representing a decreased power generation and it is caused by changes in the aerodynamics of the WT due to phenomena such as debris build-up or blade erosion.

The power $\mathcal{P}^{i,j}$ is measured by a sensor whose noise, $w^{i,j}$, can be realistically described by a zero-mean Gaussian noise with variance $\sigma_w^2 = 2.5 \cdot 10^5$ W^2. Denoting the generated power measurement as $y^{i,j}$, we have

$$y^{i,j} = \mathcal{P}^{i,j} + w^{i,j}. \tag{8.6}$$

8.2.2 FE and FDI signals

The objective of this chapter is to develop an estimation and diagnosis strategy of the faults representing a decreased power generation in the WTs of the WF.

The generated power measurements $y^{i,j}$ $(i = 1,\ldots,Y,\ j = 1,\ldots,Z)$, the dynamic power reference P^r and the wind speed measurement at the wind mast $\hat{v}^0$, are available for FE and FDI (see Fig. 8.5). We assume that the wind speed at the WTs is not measured and, thus, $v^{i,j}$ must be estimated. As detailed in Appendix C.2, the measurements $\hat{v}^0$ can be used to estimate the mean wind speed v^i through some propagation strategy. Denoting the propagated mean wind speed as $\hat{v}^i$, it yields

$$v^{i,j} = \hat{v}^i + \widetilde{v}_p^i + \widetilde{v}_t^{i,j}, \tag{8.7}$$

where $\widetilde{v}_p^i$ is the propagation error (i.e., $\widetilde{v}_p^i = v^i - \hat{v}^i$), which derives from both the propagation model mismatch and the use of the noisy measurement $\hat{v}^0$ in the propagation scheme. Note that the total wind speed estimation error verifies

$$\widetilde{v}^{i,j} = \widetilde{v}_p^i + \widetilde{v}_t^{i,j},$$

where the propagation error $\widetilde{v}_p^i$ is common for all the turbines in the i-th row while the turbulence $\widetilde{v}_t^{i,j}$ is different for each turbine (i,j).

It is well known that most continuous-time control systems are implemented digitally [323]. Thus, we present a discrete-time FE and FDI algorithm[1]. The following assumption on the fault $f^{i,j}$ is made.

Assumption 8.1. *The variation $\delta^{i,j}$ of the fault $f^{i,j}$ (i.e., $\delta_k^{i,j} = f_{k+1}^{i,j} - f_k^{i,j}$) belongs to $l_2[0,\infty)$.*

Remark 8.2. *Assumption 8.1 is common in FE and it considers faults whose variations are slow with respect to the dynamics of the system and it can cover the typical faults in engineering systems such as abrupt faults and incipient faults [99, 323]. In any case, the strategies developed in this chapter can be easily extended to faults with more complex dynamics (cf. [307]).*

8.3 Markovian jump discrete state-space modeling

8.3.1 Parameter varying discrete state-space modeling

First, we develop the discrete state-space model of the power generation system described in Section 8.2. Define

$$a(v^{i,j}) = e^{-\tau_s(v^{i,j})\,T_s}, \quad b(v^{i,j}) = 1 - a(v^{i,j}), \tag{8.8}$$

with T_s being the sampling time that we fix to 1 s, see Fig. 8.2. Defining the state $x^{i,j} = P_a^{i,j}$ and the inputs $u(v^{i,j}) = P_s^{i,j}(v^{i,j})$ and $r = P_r$; it yields,

$$x_{k+1}^{i,j} = a(v_k^{i,j})\, x_k^{i,j} + b(v^{i,j})\, u(v_k^{i,j}), \tag{8.9a}$$

$$y_k^{i,j} = c(\Delta_k^{i,j})\, x_k^{i,j} + d(\Delta_k^{i,j})\, r_k - f_k^{i,j} + s_k^{i,j} + w_k^{i,j}, \tag{8.9b}$$

where $\Delta^{i,j}$ is the power difference defined as

$$\Delta^{i,j} = P_a^{i,j} - P_r = x^{i,j} - r \tag{8.10}$$

and with

$$c(\Delta^{i,j}) = \begin{cases} 1 & \text{if } \Delta^{i,j} < 0 \\ 0 & \text{otherwise} \end{cases}, \tag{8.11a}$$

$$d(\Delta^{i,j}) = \begin{cases} 0 & \text{if } \Delta^{i,j} < 0 \\ 1 & \text{otherwise} \end{cases}. \tag{8.11b}$$

[1] It would be also possible to straightforwardly formulate the continuous-time version of the FE and FDI strategy presented in this chapter and to discretize the obtained result for implementation.

The faults verifying Assumption 8.1 can be modeled through

$$f_{k+1}^{i,j} = f_k^{i,j} + \delta_k^{i,j}, \tag{8.12}$$

where $\delta^{i,j}$ is the fault variation. Defining the extended state vector $z^{i,j} = \begin{bmatrix} x^{i,j} & f^{i,j} \end{bmatrix}^T$ and the parameter vector $\theta^{i,j} = \begin{bmatrix} v^{i,j} & \Delta^{i,j} \end{bmatrix}^T$, we augment the system (8.9) into

$$z_{k+1}^{i,j} = \underbrace{\begin{bmatrix} a(v_k^{i,j}) & 0 \\ 0 & 1 \end{bmatrix}}_{A(\theta_k^{i,j})} z_k^{i,j} + \underbrace{\begin{bmatrix} b(v_k^{i,j}) \\ 0 \end{bmatrix}}_{B(\theta_k^{i,j})} \underbrace{u(v_k^{i,j})}_{u(\theta_k^{i,j})} + \underbrace{\begin{bmatrix} 0 \\ 1 \end{bmatrix}}_{E} \delta_k^{i,j}, \tag{8.13a}$$

$$y_k^{i,j} = \underbrace{\begin{bmatrix} c(\Delta_k^{i,j}) & -1 \end{bmatrix}}_{C(\theta_k^{i,j})} z_k^{i,j} + \underbrace{d(\Delta_k^{i,j})}_{D(\theta_k^{i,j})} r_k + s_k^{i,j} + w_k^{i,j}, \tag{8.13b}$$

$$f_k^{i,j} = \underbrace{\begin{bmatrix} 0 & 1 \end{bmatrix}}_{F} z_k^{i,j}. \tag{8.13c}$$

For ease of readability, let us omit hereafter the dependence of the variables on the number of turbine (i, j) (e.g., z_k stands for $z_k^{i,j}$). The extended system model (8.13) results in

$$z_{k+1} = A(\theta_k)\, z_k + B(\theta_k)\, u(\theta_k) + E\, \delta_k, \tag{8.14a}$$

$$y_k = C(\theta_k)\, z_k + D(\theta_k)\, r_k + s_k + w_k, \tag{8.14b}$$

$$f_k = F\, z_k. \tag{8.14c}$$

The system dynamics (8.14) depends on the system matrices $A(\theta_k)$, $B(\theta_k)$, $C(\theta_k)$ and $D(\theta_k)$. According to (8.8) and (8.13), the behavior of $A(\theta_k)$ and $B(\theta_k)$ switches between the estimated wind speed zones as shown in Fig. 8.2. According to (8.11) and (8.13), $C(\theta_k)$ and $D(\theta_k)$ are switching matrices whose value depends on the WT working mode determined by the sign of the parameter Δ_k.

8.3.2 Markovian jump discrete state-space modeling

The parameters v and Δ can be considered to be bounded by the sets

$$v \in \Omega_v, \quad \Omega_v := \{\underline{v} < v < \bar{v}\}, \tag{8.15a}$$

$$\Delta \in \Omega_\Delta, \quad \Omega_\Delta := \{\underline{\Delta} < \Delta < \bar{\Delta}\}, \tag{8.15b}$$

where $\underline{v}$, $\bar{v}$, $\underline{\Delta}$ and $\bar{\Delta}$ are the minimum and maximum possible values of these parameters (which we fix to $\underline{v} = 0$ m/s, $\bar{v} = 30$ m/s, $\underline{\Delta} = -4.8$ MW and $\bar{\Delta} = 4.8$ MW). The parameter vector $\theta = \begin{bmatrix} v \\ \Delta \end{bmatrix}$ lies then in $\Theta = \Omega_v \times \Omega_\Delta$. Let us partition the parameter set Θ into N subsets $\Theta^{(p)}$ (i.e., $\Theta = \{\Theta^{(p)}\}_{p \in \{1,\dots,N\}}$) by dividing Ω_v into N_v intervals $\Omega_v^{(p_v)}$ (i.e., $\Omega_v = \{\Omega_v^{(p_v)}\}_{p_v \in \{1,\dots,N_v\}}$) and Ω_Δ into N_Δ intervals $\Omega_\Delta^{(p_\Delta)}$ (i.e., $\Omega_\Delta = \{\Omega_\Delta^{(p_\Delta)}\}_{p_\Delta \in \{1,\dots,N_\Delta\}}$), i.e.,

$$\Theta = \Big\{ \underbrace{(\Omega_v^{(1)}, \Omega_\Delta^{(1)})}_{\Theta^{(1)}}, \dots, (\Omega_v^{(1)}, \Omega_\Delta^{(p_\Delta)}), \dots, (\Omega_v^{(p_v)}, \Omega_\Delta^{(1)}), \dots, \underbrace{(\Omega_v^{(p_v)}, \Omega_\Delta^{(p_\Delta)})}_{\Theta^{(N)}} \Big\} \tag{8.16}$$

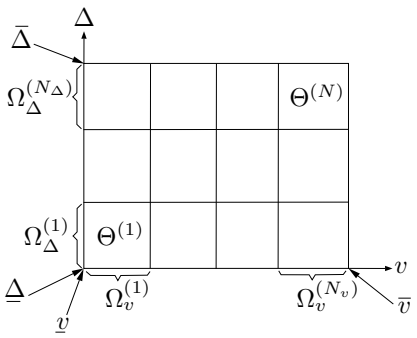

Figure 8.4. Partition of the two-dimensional parameter set.

with $N = N_v \cdot N_\Delta$ (see Fig. 8.4). The partition is one such that each interval $\Omega_v^{(p_v)}$ lies in a single wind speed zone and each interval $\Omega_\Delta^{(p_\Delta)}$ lies in a single WT working mode (see Table 8.1).

For such partition, the system state-space matrices $C(\theta_k)$ and $D(\theta_k)$ associated with $\theta_k \in \Theta^{(p)}$ are constant and they can be expressed as

$$C(\theta_k) = C_p, \quad D(\theta_k) = D_p. \tag{8.17}$$

The system state-space matrices $A(\theta_k)$ and $B(\theta_k)$ associated with $\theta_k \in \Theta^{(p)}$ are constant if the interval $\Omega_v^{(p_v)}$ defining $\Theta^{(p)}$ (i.e., $\Theta^{(p)} = (\Omega_v^{(p_v)}, \Omega_\Delta^{(p_\Delta)})$) lies in the wind speed zones I, III or IV (i.e., $\Omega_v^{(p_v)} \in [\underline{v}, v_{cut-in}) \cup [v_{rated}, \overline{v})$) because the discrete transfer coefficient $a(v)$ is constant in these zones. If the interval $\Omega_v^{(p_v)}$ lies in the zone II (i.e., $\Omega_v^{(p_v)} \in [v_{cut-in}, v_{rated})$), these matrices are not constant because the discrete transfer coefficient $a(v)$ is described by the function in Fig. 8.2. In all, we express the matrices $A(\theta_k)$ and $B(\theta_k)$ associated with $\theta_k \in \Theta^{(p)}$ as

$$A(\theta_k) = \sum_{m=1}^{M} \alpha_p^m(\theta_k) A_p^m, \quad B(\theta_k) = \sum_{m=1}^{M} \alpha_p^m(\theta_k) B_p^m, \tag{8.18}$$

with $\sum_{m=1}^{M} \alpha_p^m(\theta_k) = 1$ and $0 \leq \alpha_p^m(\theta_k) \leq 1$ for $m = 1, \ldots, M$. The matrix A_p^m denotes the m-th vertex of the convex polytope in which $A(\theta_k)$ lies whenever $\theta_k \in \Theta^{(p)}$. Note that in the wind speed zones I, III and IV, we have $A_p^m = A_p$ and $\alpha_p^m = 1/M$ for $l = 1, \ldots, M$. Similar applies to $B(\theta_k)$.

Define the membership signal ξ^v whose value at a sample k equals the number p_v of the interval $\Omega_v^{(p_v)}$ in which the wind speed v lies at the sample k; similar applies to ξ^Δ w.r.t. Δ and to ξ w.r.t. θ:

$$\xi_k^v = p_v \quad \text{if} \quad v_k \in \Omega_v^{(p_v)}, \tag{8.19a}$$

$$\xi_k^\Delta = p_\Delta \quad \text{if} \quad \Delta_k \in \Omega_\Delta^{(p_\Delta)}, \tag{8.19b}$$

$$\xi_k = p \quad \text{if} \quad \theta_k \in \Theta^{(p)}. \tag{8.19c}$$

Research has shown that the stochastic behavior of the mean wind speed can be represented as a Markovian process [40,198]. This behavior has been exploited in recent WT control strategies

p_v	Wind speed boundaries	Wind zone
1	$\underline{v} \leq v < v_1$	Zone I
2	$v_1 \leq v < v_2$	Zone I
$\vdots$	$\vdots$	$\vdots$
n_1	$v_{n_1-1} \leq v < v_{cut-in}$	Zone I
n_1+1	$v_{cut-in} \leq v < v_{n_1+1}$	Zone II
$\vdots$	$\vdots$	$\vdots$
n_2	$v_{n_2-1} \leq v < v_{rated}$	Zone II
n_2+1	$v_{rated} \leq v < v_{n_2+1}$	Zone III
$\vdots$	$\vdots$	$\vdots$
n_3	$v_{n_3-1} \leq v < v_{cut-out}$	Zone III
n_3+1	$v_{cut-out} \leq v < v_{n_3+1}$	Zone IV
$\vdots$	$\vdots$	$\vdots$
N_v	$v_{N_v-1} \leq v < \bar{v}$	Zone IV

p_Δ	Power difference boundaries	Working mode
1	$\underline{\Delta} \leq \Delta < \Delta_1$	$P_a < P_r$
2	$\Delta_1 \leq \Delta < \Delta_2$	$P_a < P_r$
$\vdots$	$\vdots$	$\vdots$
n_1'	$\Delta_{n_1'-1} \leq \Delta < 0$	$P_a < P_r$
$n_1'+1$	$0 \leq \Delta < \Delta_{n_1'+1}$	$P_a \geq P_r$
$\vdots$	$\vdots$	$\vdots$
N_Δ	$\Delta_{N_\Delta-1} \leq \Delta < \bar{\Delta}$	$P_a \geq P_r$

Table 8.1. Partition of the parameter sets Ω_v and Ω_Δ.

as the ones in [63, 184, 185]. Motivated by this research, we assume that that $\{\xi_k^v\}$ is a discrete homogeneous Markov chain taking values in the finite set $\{1, \ldots, N_v\}$. Since the mean wind speed affects the WT working mode, we also assume that $\{\xi_k^\Delta\}$ is a discrete homogeneous Markov chain taking values in the finite set $\{1, \ldots, N_\Delta\}$. Both assumptions are considered in the following assumption over $\{\xi_k\}$.

Assumption 8.2. *The membership $\{\xi_k\}$ is governed by a discrete homogeneous Markov chain whose states are in the finite set $S = \{1, \ldots, N\}$ with the transition probability matrix*

$$\Pi = \begin{bmatrix} \pi_{11} & \cdots & \pi_{1N} \\ \vdots & \vdots & \vdots \\ \pi_{N1} & \cdots & \pi_{NN} \end{bmatrix} \in \mathbb{R}^{N \times N} \tag{8.20}$$

and π_{pq} being the transition probability defined as

$$\pi_{pq} = \mathbf{Pr}\{\xi_{k+1} = q | \xi_k = p\}, \tag{8.21}$$

where $\sum_{q=1}^{N} \pi_{pq} = 1$ *for any* $p \in S$.

Remark 8.3. *([257]) Provided* (8.16)*, the transition probability matrix* Π *satisfies* $\Pi = \Pi^v \otimes \Pi^\Delta$*, with*

$$\begin{aligned}
\Pi^v &= [\pi^v_{p_v q_v}]_{p_v, q_v \in \{1,\dots,N_v\}},\\
\Pi^\Delta &= [\pi^\Delta_{p_\Delta q_\Delta}]_{p_\Delta, q_\Delta \in \{1,\dots,N_\Delta\}},\\
\pi_{p^v q^v} &= \mathbf{Pr}\{\xi^v_{k+1} = q_v | \xi^v_k = p_v\},\\
\pi_{p^\Delta q^\Delta} &= \mathbf{Pr}\{\xi^\Delta_{k+1} = q_\Delta | \xi^\Delta_k = p_\Delta\}.
\end{aligned}$$

Remark 8.4. *([210]) The probabilities* π_{pq} *can be obtained through numerical simulations by sampling the data in the separate subsets* $\Theta^{(p)}$ *and computing*

$$\pi_{pq} = \frac{\textit{observed transitions from state } p \textit{ to } q}{\textit{observed occurrences of state } p}.$$

Similar applies to $\pi_{p_v q_v}$ *and* $\pi_{p_\Delta q \Delta}$.

8.4 FE at a wind turbine level

8.4.1 FE architecture

To achieve FE, we build the following model-based observer for the extended system (8.14):

$$\hat{z}_{k+1} = A(\hat{\theta}_k)\,\hat{z}_k + B(\hat{\theta}_k)\,u(\hat{\theta}_k) + L(\hat{\theta}_k)\,\left(y_k - C(\hat{\theta}_k)\,\hat{z}_k - D(\hat{\theta}_k)\,r_k\right), \tag{8.22a}$$

$$\hat{f}_k = F\,\hat{z}_k + K(\hat{\theta}_k)\,\left(y_k - C(\hat{\theta}_k)\,\hat{z}_k - D(\hat{\theta}_k)\,r_k\right), \tag{8.22b}$$

where $\hat{\theta} = \begin{bmatrix}\hat{v} & \hat{\Delta}\end{bmatrix}^T$ is the estimated parameter vector in which $\hat{v}$ is the open-loop propagated wind speed (see (8.7)) and $\hat{\Delta}$ is the closed-loop estimated power difference computed as $\hat{\Delta} = P^r - \hat{x}$ (with $\hat{x}$ being the first state of $\hat{z}$)[2]. The estimated parameter vector $\hat{\theta}$ does also lie in the set Θ, partitioned into the subsets $\{\Theta^{(p)}\}_{p\in\{1,\dots,N\}}$ as explained in Section 8.3.2.

The matrices $L(\hat{\theta}_k) \in \mathbb{R}^{2\times 1}$ and $K(\hat{\theta}_k) \in \mathbb{R}^1$ are the parameter-dependent design gain matrices of appropriate dimensions. Provided the switching behavior of the system state-space matrices in (8.17)-(8.18), we fix $L(\hat{\theta}_k) \in \mathbb{R}^{2\times 1}$ and $K(\hat{\theta}_k) \in \mathbb{R}^1$ as

$$L(\hat{\theta}_k) = L_p \quad \text{if} \quad \hat{\theta}_k \in \Theta^{(p)}, \tag{8.23a}$$

$$K(\hat{\theta}_k) = K_p \quad \text{if} \quad \hat{\theta}_k \in \Theta^{(p)}, \tag{8.23b}$$

where L_p and K_p are constant matrices associated to $\hat{\theta}_k \in \Theta^{(p)}$ and must be designed. Given (8.19), these matrices can be also expressed as $L(\hat{\theta}_k) = L_p$ if $\hat{\xi}_k = p$ and $K(\hat{\theta}_k) = K_p$ if $\hat{\xi}_k = p$.

[2]It would be possible to define $\hat{\Delta}$ as the open-loop estimated power difference computed as $\hat{\Delta} = P^r - \frac{\tau_s(\hat{v}^{i,j})}{s+\tau_s(\hat{v}^{i,j})} P_s^{i,j}(\hat{v}^{i,j})$. We choose to use the closed-loop estimated power difference in order to reduce the parameter estimation error.

Remark 8.5. *Note that certain degree of conservatism is introduced when using switched observer gain matrices in the form of* (8.23) *for the regions lying in the wind speed zone II, where the state-space matrices* $A(\hat{\theta}_k)$ *and* $B(\hat{\theta}_k)$ *are not constant (see* (8.18)*). Even though switched polytopic gain matrices could be used instead, the small variations experienced by these matrices (see Fig. 8.2) justify the choice in* (8.23) *that reduces the observer complexity.*

Define the extended state estimation error as $\widetilde{z}_k = z_k - \hat{z}_k$ and the FE error as $\widetilde{f}_k = f_k - \hat{f}_k$. It follows that

$$\widetilde{z}_{k+1} = \Big(A(\hat{\theta}_k) - L(\hat{\theta}_k)\, C(\hat{\theta}_k)\Big)\, \widetilde{z}_k + E\, \delta_k + \bar{R}\, g_k - L(\hat{\theta}_k)\, \Big(R\, h_k + s_k + w_k\Big), \tag{8.24a}$$

$$\widetilde{f}_k = \Big(F - K(\hat{\theta}_k)\, C(\hat{\theta}_k)\Big)\, \widetilde{z}_k - K(\hat{\theta}_k)\, \Big(R\, h_k + s_k + w_k\Big), \tag{8.24b}$$

with $\bar{R} = \begin{bmatrix} 1 & 0 \end{bmatrix}^T$. The error depends then on the fault variation δ_k, the oscillation s_k, the noise w_k and the disturbances $g_k = g_k(\hat{\theta}_k, \theta_k)$ and $h_k = h_k(\hat{\theta}_k, \theta_k)$, which stem from using $\hat{\theta}$ instead of θ in the estimation algorithm. As (8.24) refers to the turbine (i, j), g_k and h_k refer in fact to $g_k^{i,j}$ and $h_k^{i,j}$ defined as

$$g_k^{i,j} = \Big(a(v_k^{i,j}) - a(\hat{v}_k^i)\Big) x_k^{i,j} + \Big(\bar{u}(v_k^{i,j}) - \bar{u}(\hat{v}_k^i)\Big), \tag{8.25a}$$

$$h_k^{i,j} = \Big(c(\Delta_k^{i,j}) - c(\hat{\Delta}_k^{i,j})\Big)\, x_k^{i,j} + \Big(d(\Delta_k^{i,j}) - (\hat{\Delta}_k^{i,j})\Big)\, r_k, \tag{8.25b}$$

with $\bar{u}(v_k^{i,j}) = b(v_k^{i,j})\, u(v_k^{i,j})$. Specifically, $g_k^{i,j}$ stands for the disturbance derived from the open-loop wind propagation strategy and $h_k^{i,j}$ is the disturbance derived from the closed-loop dynamic available power estimation strategy. Note that $h_k^{i,j}$ is in fact equal to 0 (if the WT operating mode is correctly estimated) or to the difference $\Delta^{i,j}$ (otherwise).

Provided (8.7), $g_k^{i,j}$, which is caused by the total wind speed estimation error, can be expressed as

$$g_k^{i,j} = e_k^i + \varepsilon_k^{i,j}, \tag{8.26}$$

where e_k^i is caused by the wind propagation error and $\varepsilon_k^{i,j}$ is caused by the wind turbulence, i.e.,

$$e_k^i = \Big(a(v_k^i) - a(\hat{v}_k^i)\Big) x_k^{i,j} + \Big(\bar{u}(v_k^i) - \bar{u}(\hat{v}_k^i)\Big), \tag{8.27a}$$

$$\varepsilon_k^{i,j} = \Big(a(v_k^{i,j}) - a(v_k^i)\Big) x_k^{i,j} + \Big(\bar{u}(v_k^{i,j}) - \bar{u}(v_k^i)\Big). \tag{8.27b}$$

In (8.27), the first summands are negligible w.r.t. to the second summands. Hence, we omit the dependence of the disturbance e^i on the column j. The following assumption on e^i, $\varepsilon^{i,j}$ and $h^{i,j}$ is made.

Assumption 8.3. *The disturbances* e^i, $\varepsilon^{i,j}$ *and* $h^{i,j}$ *can be considered to be bounded as*

$$\|e^i\|_\infty \leq \bar{e}_p, \quad \|\varepsilon^{i,j}\|_\infty \leq \bar{\varepsilon}_p, \quad \|h^{i,j}\|_\infty \leq \bar{h}_p, \quad \text{if } \theta \in \Theta^{(p)}. \tag{8.28}$$

Details on the computation of these bounds are included in Appendix D.3.1. Note that it would have been possible to consider a row-dependent bound of the disturbance caused by the propagation error (i.e., $|e^i| \leq \bar{e}_p^i$) because this error generally increases with the distance to the wind mast. For sake of simplicity, we introduce some conservatism by neglecting this dependence. Hence, $\bar{e}_p$ verifies $\bar{e}_p = \max_i \bar{e}_p^i$.

For brevity, we omit again the dependence on the number of row i and on the number column j. Taking (8.26) and (8.28) into account, the summands $\bar{R}\, g_k$ and h_k in (8.24) can be expressed as

$$\bar{R}\, g_k = \mathcal{G}(\hat{\theta}_k)\, \lambda_k + G(\hat{\theta}_k)\, \mu_k, \quad h_k = H(\hat{\theta}_k)\, \varphi_k, \tag{8.29}$$

with $\lambda_k \in [-1, 1]$, $\mu_k \in [-1, 1]$ and $\varphi_k \in [-1, 1]$ satisfying

$$\lambda_k = e_k/\bar{e}_p, \quad \mu_k = \varepsilon_k/\bar{\varepsilon}_p, \quad \varphi_k = h_k/\bar{h}_p, \tag{8.30}$$

if $\theta_k \in \Theta^{(p)}$ and where $\mathcal{G}(\hat{\theta}_k)$, $G(\hat{\theta}_k)$ and $H(\hat{\theta}_k)$ are defined as

$$\mathcal{G}(\hat{\theta}_k) = \mathcal{G}_p \quad \text{if} \quad \hat{\theta}_k \in \Theta^{(p)}, \qquad \mathcal{G}_p = \bar{R}\, \bar{e}_p, \tag{8.31a}$$

$$G(\hat{\theta}_k) = G_p \quad \text{if} \quad \hat{\theta}_k \in \Theta^{(p)}, \qquad G_p = \bar{R}\, \bar{\varepsilon}_p, \tag{8.31b}$$

$$H(\hat{\theta}_k) = H_p \quad \text{if} \quad \hat{\theta}_k \in \Theta^{(p)}, \qquad H_p = \bar{h}_p. \tag{8.31c}$$

In all, we rewrite (8.24) as

$$\widetilde{z}_{k+1} = \mathcal{A}(\hat{\theta}_k)\, \widetilde{z}_k + \mathcal{B}(\hat{\theta}_k)\, \mathcal{W}_k + E\, \delta_k, \tag{8.32a}$$

$$\widetilde{f}_k = \mathcal{C}(\hat{\theta}_k)\, \widetilde{z}_k + \mathcal{D}(\hat{\theta}_k)\, \mathcal{W}_k, \tag{8.32b}$$

with

$$\begin{aligned}
\mathcal{A}(\hat{\theta}_k) &= A(\hat{\theta}_k) - L(\hat{\theta}_k)\, C(\hat{\theta}_k), \\
\mathcal{C}(\hat{\theta}_k) &= F - K(\hat{\theta}_k)\, C(\hat{\theta}_k), \\
\mathcal{B}(\hat{\theta}_k) &= \begin{bmatrix} \mathcal{G}(\hat{\theta}_k) & G(\hat{\theta}_k) & -L(\hat{\theta}_k)\, H(\hat{\theta}_k) & -L(\hat{\theta}_k) & -L(\hat{\theta}_k) \end{bmatrix}, \\
\mathcal{D}(\hat{\theta}_k) &= \begin{bmatrix} 0 & 0 & -K(\hat{\theta}_k)\, H(\hat{\theta}_k) & -K(\hat{\theta}_k) & -K(\hat{\theta}_k) \end{bmatrix}, \\
\mathcal{W}_k &= \begin{bmatrix} \lambda_k & \mu_k & \varphi_k & s_k & w_k \end{bmatrix}^T.
\end{aligned}$$

Note that $\mathcal{A}_p(\hat{\theta}_k)$, $\mathcal{B}_p$, $\mathcal{C}_p$ and $\mathcal{D}_p$ are defined using the corresponding matrices associated with $\theta_k \in \Theta^{(p)}$ (e.g., $\mathcal{A}_p(\hat{\theta}_k) = \sum_{m=1}^{M} \alpha_p^m(\hat{\theta}_k)(A_p^m - L_p\, C_p)$ and $\mathcal{C}_p = F - K_p\, C_p$).

8.4.2 FE design

The FE error caused by δ describes the fault sensitivity of the observer and the error caused by $\mathcal{W}$ describes the robustness of the observer against disturbances and noises. We characterize them through the $\mathcal{H}_\infty$ performance of the observer w.r.t. δ and $\mathcal{W}$, respectively. To that end, we use the formulation based on LMIs in the following theorem. For the sake of generality, we denote the size of the inputs in (8.32) as n_δ, n_λ, n_μ, n_φ, n_s and n_w verifying $n_\delta = n_\lambda = n_\mu = n_\varphi = n_s = n_w = 1$ in this case of FE at a WT level.

Theorem 8.1. *Consider the observer* (8.22) *applied to the system* (8.14)*. If there exist positive scalars* γ_λ*,* γ_μ*,* γ_φ*,* γ_s*,* γ_w *and* γ_δ*; full matrices of appropriate dimensions* X_p*,* K_p *and* V_p*; and symmetric matrices of appropriate dimensions* Q_p*, for* $p, q = 1, \ldots, N$ *and* $m = 1, \ldots M$ *fulfilling the LMIs*

$$\Xi_p^m = \begin{bmatrix} \Omega_p & \bar{\Lambda}_p^{m\,T} & \bar{\Phi}_p^T & 0 \\ \bar{\Lambda}_p^m & Q_p & 0 & \mathcal{C}_p^T \\ \bar{\Phi}_p & 0 & \Gamma & \Upsilon_p^T \\ 0 & \mathcal{C}_p & \Upsilon_p & I \end{bmatrix} \succ 0, \tag{8.33}$$

with

$$\begin{aligned}
\Omega_p =& \bigoplus_{q=1}^{N} V_p + V_p^T - Q_q, \\
\bar{\Lambda}_p^m =& \begin{bmatrix} \sqrt{\pi_{p1}}\,\Lambda_p^m & \ldots & \sqrt{\pi_{pN}}\,\Lambda_p^m \end{bmatrix}, \\
\Lambda_p^m =& V_p\,A_p^m - X_p\,C_p, \\
\bar{\Phi}_p =& \begin{bmatrix} \sqrt{\pi_{p1}}\,\Phi_p & \ldots & \sqrt{\pi_{pN}}\,\Phi_p \end{bmatrix}, \\
\Phi_p =& \begin{bmatrix} V_p\,\mathcal{G}_p & V_p\,G_p & -X_p\,H_p & -X_p & -X_p & V_p\,E \end{bmatrix}, \\
\Upsilon_p =& \begin{bmatrix} 0 & 0 & -K_p\,H_p & -K_p & -K_p & 0 \end{bmatrix}, \\
\mathcal{C}_p =& F - K_p\,C_p, \\
\Gamma =& \gamma_\lambda\,I_{n_\lambda} \oplus \gamma_\mu\,I_{n_\mu} \oplus \gamma_\varphi\,I_{n_\varphi} \oplus \gamma_s\,I_{n_s} \oplus \gamma_w\,I_{n_w} \oplus \gamma_\delta\,I_{n_\delta},
\end{aligned}$$

then defining $L_p = V_p^{-1}\,X_p$*, the following statements hold for all* $\hat{\theta}_k \in \Theta$*.*

1. *In the absence of disturbances, noises and faults (i.e.,* $\mathcal{W}_k = 0$ *and* $\delta_k = 0$*), the extended state estimation error* (8.32) *converges asymptotically to zero in average.*

2. *Under null initial conditions, the expected value of the FE error is bounded as*

$$\begin{aligned}
\mathbb{E}\{\|\widetilde{f}\|_{\text{RMS}}^2\} <& \gamma_\lambda\,n_\lambda\,\|\lambda\|_\infty^2 + \gamma_\mu\,n_\mu\,\|\mu\|_\infty^2 + \gamma_\varphi\,n_\varphi\,\|\varphi\|_\infty^2 + \gamma_s\,\|s\|_{\text{RMS}}^2 + \\
& \gamma_w\,\|w\|_{\text{RMS}}^2 + \gamma_\delta\,n_\delta\,\|\delta\|_\infty^2,
\end{aligned} \tag{8.34}$$

with $\mathbb{E}\{\|\widetilde{f}\|_{\text{RMS}}^2\} = \lim_{K\to\infty} \frac{1}{K} \sum_{k=1}^{K} \mathbb{E}\{\widetilde{f}_k^T\,\widetilde{f}_k | \hat{\theta}_{k-1} \in \Theta^{(p)}\}$.

Proof. If (8.33) holds for $p, q = 1, \ldots, N$, we have that $Q_q \succ 0$ and that V_p is a nonsingular matrix because $V_p + V_p^T - Q_q \succ 0$. Hence, we can state that $(Q_q - V_p)\,Q_q^{-1}\,(Q_q - V_p)^T \succeq 0$ which implies that

$$V_p + V_p^T - Q_q \preceq V_p\,Q_q^{-1}\,V_p^T.$$

Thus, the matrix inequalities which result from replacing $V_p + V_p^T - Q_q$ by $V_p\,Q_q^{-1}\,V_p^T$ in (8.33) are also positive definite. Let us substitute X_p by $V_p\,L_p$ and apply a congruence transformation by $\left(\bigoplus_{q=1}^{N} V_p^{-1}\right) \oplus I$ to the result. Multiplying the matrix inequality by $\alpha_p^m(\hat{\theta}_k)$, summing for

$m = 1, \ldots, M$, taking Schur's complements, pre-multiplying the result by $\begin{bmatrix} \widetilde{z}_k^T & \mathcal{W}_k^T & \delta_k^T \end{bmatrix}$ and post-multiplying by its transpose lead to

$$\begin{aligned} &\sum_{q=1}^{N} \pi_{pq} \left(\mathcal{A}_p(\hat{\theta}_k) \widetilde{z}_k + \mathcal{B}_p \mathcal{W}_k + E\delta_k \right)^T Q_q \left(\mathcal{A}_p(\hat{\theta}_k) \widetilde{z}_k + \mathcal{B}_p \mathcal{W}_k + E\,\delta_k \right) - \widetilde{z}_k^T Q_p\, \widetilde{z}_k + \\ &\widetilde{f}_k^T \widetilde{f}_k - \gamma_\lambda\, \lambda_k^T \lambda_k - \gamma_\mu\, \mu_k^T \mu_k - \gamma_\varphi\, \varphi_k^T \varphi_k - \gamma_s\, s_k^T\, s_k - \gamma_w\, w_k^T\, w_k - \gamma_\delta\, \delta_k^T\, \delta_k < 0, \end{aligned} \tag{8.35}$$

for all $p = 1, \ldots, N$ and where we have taken into account that $\sum_{m=1}^{M} \alpha_p^m(\hat{\theta}_k) = 1$.

Now, let us define the Lyapunov function $V_k = \widetilde{z}_k^T\, Q(\hat{\theta}_k)\, \widetilde{z}_k$ equal to $V_k = \widetilde{z}_k^T\, Q_p\, \widetilde{z}_k$ for $\hat{\theta}_k \in \Theta^{(p)}$ and $p = 1, \ldots, N$.

1. In the absence of disturbances noises and faults (i.e., $\mathcal{W}_k = 0$ and $\delta_k = 0$), expression (8.35) leads to

$$\widetilde{z}_k^T \Big(\sum_{q=1}^{N} \pi_{pq}\, \mathcal{A}_p(\hat{\theta}_k)\, Q_q\, \mathcal{A}_p(\hat{\theta}_k) \Big) \widetilde{z}_k - \widetilde{z}_k^T\, Q_p\, \widetilde{z}_k < 0,$$

   for all $p = 1, \ldots, N$, which assures $\mathbb{E}\{V_{k+1} | \hat{\theta}_k \in \Theta^{(p)}\} - V_k < 0$ guaranteeing that the extended state estimation error (8.32) converges asymptotically to zero in average for all $\hat{\theta}_k \in \Theta$.

2. For brevity, let us denote $\mathbb{E}\{V_{k+1} | \hat{\theta}_k \in \Theta^{(p)}\}$ as $\mathbb{E}\{V_{k+1} | \hat{\theta}_k\}$ and let us not include in the next that the inequalities are fulfilled for all $\hat{\theta}_k \in \Theta$. Taking conditional expectation given $\hat{\theta}_{k-1}$ over expression (8.35) leads to

$$\begin{aligned} &\mathbb{E}\{V_{k+1} | \hat{\theta}_k\} - \mathbb{E}\{V_k | \hat{\theta}_{k-1}\} + \mathbb{E}\{\widetilde{f}_k^T \widetilde{f}_k | \hat{\theta}_{k-1}\} - \gamma_\lambda\, n_\lambda \|\lambda\|_\infty^2 - \gamma_\mu\, n_\mu \|\mu\|_\infty^2 - \\ &\gamma_\varphi\, , n_\varphi \|\varphi\|_\infty^2 - \gamma_s\, \|s\|_{\mathrm{RMS}}^2 - \gamma_w\, \|w\|_{\mathrm{RMS}}^2 - \gamma_\delta\, n_\delta \|\delta\|_\infty^2 < 0, \end{aligned} \tag{8.36}$$

   because $\mathbb{E}\{V_{k+1} | \hat{\theta}_k | \hat{\theta}_{k-1}\} = \mathbb{E}\{V_{k+1} | \hat{\theta}_k\}$ and the exogenous signals are independent of $\hat{\theta}_{k-1}$. In (8.36), we have also taken into account that λ is a deterministic signal and

$$\mathbb{E}\{\lambda_k^T \lambda_k\} = \lambda_k^T \lambda_k \leq n_\lambda \|\lambda\|_\infty^2$$

   (similar applies to μ, φ and δ), and that $\mathbb{E}\{s_k^T s_k\} = \|s\|_{\mathrm{RMS}}^2$ because s_k is zero-mean (similar applies to w_k).

   Under null initial conditions ($V_0 = 0$), adding the aforementioned expression from $k = 0$ to $k = K - 1$ leads to

$$\begin{aligned} \sum_{k=0}^{K-1} \mathbb{E}\{\widetilde{f}_k^T \widetilde{f}_k | \hat{\theta}_{k-1}\} < \sum_{k=0}^{K-1} \Big(&\gamma_\lambda\, n_\lambda \|\lambda\|_\infty^2 + \gamma_\mu\, n_\mu \|\mu\|_\infty^2 + \gamma_\varphi\, n_\varphi \|\varphi\|_\infty^2 + \\ &\gamma_s\, \|s\|_{\mathrm{RMS}}^2 + \gamma_w\, \|w\|_{\mathrm{RMS}}^2 + \gamma_\delta\, n_\delta \|\delta\|_\infty^2 \Big), \end{aligned}$$

   because $\sum_{k=0}^{K-1} \Big(\mathbb{E}\{V_{k+1} | \hat{\theta}_k\} - \mathbb{E}\{V_k | \hat{\theta}_{k-1}\} \Big) = \mathbb{E}\{V_{K+1} | \hat{\theta}_K\}$ and $\mathbb{E}\{V_{K+1} | \hat{\theta}_K\} > 0$. Dividing this expression by K and taking the limit when K tends to infinity leads to (8.34).

□

There exists thus a trade-off between ameliorating the fault tracking ability of the observer and its robustness [106]. From the practical viewpoint, it is of considerable interest to achieve certain tracking ability and to minimize the effect of the disturbances and noises on the estimations [327]. Thus, we propose to design the observer gain matrices through the following optimization problem:

$$\begin{aligned} \text{minimize} \quad & \gamma_\lambda n_\lambda \|\lambda\|_\infty^2 + \gamma_\mu n_\mu \|\mu\|_\infty^2 + \gamma_\varphi n_\varphi \|\varphi\|_\infty^2 + \\ & \gamma_s \|s\|_{\text{RMS}}^2 + \gamma_w \|w\|_{\text{RMS}}^2 \\ \text{subject to} \quad & \gamma_\delta \leq \bar{\gamma}_\delta, \\ & \Xi_p^m \succ 0, \ \ \forall p, m \end{aligned} \tag{8.37}$$

along the variables γ_λ, γ_μ, γ_φ, γ_s, γ_w, γ_δ, X_p, K_p, V_p, Q_p and P_p ($p = 1, \ldots, N$) and with $\bar{\gamma}_\delta$ being the required $\mathcal{H}_\infty$ performance describing the fault tracking ability of the observer.

Remark 8.6. *The use of the signals* (8.30) *in the design process allows considering the differences in the bounds* (8.28) *among the different subsets* $\Theta^{(p)}$*. Effectively, we now have that the value of these bounds is introduced through the matrices* $\mathcal{G}_p$*,* G_p *and* H_p *and* $\|\lambda\|_\infty^2 = \|\mu\|_\infty^2 = \|\varphi\|_\infty^2 = 1$*. If the signals* e*,* ϵ *and* h *were used instead, the maximum value of the bounds* (8.28) *(e.g.,* $\max_p \bar{e}_p$*) would be the only information introduced in the design. Note also that if the bounds* (8.28) *are not completely accurate,* $\|\lambda\|_\infty^2$*,* $\|\mu\|_\infty^2$ *and* $\|\varphi\|_\infty^2$ *can be considered as tuning parameters regarding the bounding accuracy. Similar applies to* $\|s\|_{\text{RMS}}^2$ *and* $\|w\|_{\text{RMS}}^2$ *that can be easily derived from the known parameters* γ_p *and* σ_w *but whose values can be increased with the uncertainty over these parameters.*

Taking Remark 8.5 and Remark 8.6 into account, we deduce that the conservatism is reduced when a lot of gridding intervals are utilized for the partition of the set Θ. Hence, the density N of the grid $\{\Theta^{(p)}\}_{p\in\{1,\ldots,N\}}$ is to be determined from a trade-off between having a few gridding intervals that ensure reduced computational burden but introduce conservatism or having a lot of gridding intervals causing heavy computational times but reduced performance conservatism [56, 218]. As specified in Appendix D.3.1, we choose $N_v = 6$ and $N_\Delta = 4$. This gridding is *a posteriori* validated through the numerical simulations in Section 8.8.

8.5 FDI at a Wind Turbine Level

We set the following decision mechanism for FDI:

$$\begin{cases} \text{if } |\hat{f}_k| \geq J_k \,, & \text{Fault} \\ \text{otherwise} \,, & \text{No fault} \end{cases}, \tag{8.38}$$

where J is an adaptive threshold covering the uncertainties affecting the fault estimate in fault-free conditions. As recalled in [71], the model-based setting of thresholds usually leads to too conservative thresholds which result in poor fault diagnosability. It is the state of the art in real applications to optimally set thresholds on the basis of tests in the real application environment. In this context, we propose to compute the threshold through a multivariate linear model over the estimated parameters $\hat{\theta}$ and to obtain the coefficients of this model using a set of fault-free training data as detailed hereafter.

Remark 8.7. *Norm-based constant thresholding can be performed using the RMS-norm bound of the FE error in* (8.34) *(with* $\gamma_\delta = 0$*). Assuming zero-mean disturbances, one can apply the Chebyshev's inequality and obtain a stochastic threshold for certain confidence level. However, this approach ignores the real statistical distribution of the error and leads to too loose bounds [229]. Alternatively, assuming bounded noises, a deterministic threshold can be directly obtained by bounding the peak-norm of the FE error due to disturbances through the* l_1*-norm of* (8.22)*. However, this approach is even more conservative because it bounds the worst-case scenario, which rarely occurs in practice.*

Provided the switching behavior of the system, we use different coefficients for each WT working mode. For this purpose, we define $\hat{\eta}^M$ $(M = 1, 2, 3)$ as a signal indicating whether the WT is estimated to be operating in mode M:

$$\hat{\eta}_k^1 = \begin{cases} 1 & \text{if } \hat{\xi}_k^\Delta \in [1,\, n_1' - n'] \\ 0 & \text{otherwise} \end{cases}, \tag{8.39a}$$

$$\hat{\eta}_k^2 = \begin{cases} 1 & \text{if } \hat{\xi}_k^\Delta \in (n_1' - n',\, n_1' - n'] \\ 0 & \text{otherwise} \end{cases}, \tag{8.39b}$$

$$\hat{\eta}_k^3 = \begin{cases} 1 & \text{if } \hat{\xi}_k^\Delta \in (n_1' - n',\, N_\Delta] \\ 0 & \text{otherwise} \end{cases}, \tag{8.39c}$$

with $\hat{\xi}_k^\Delta$ being the estimated membership function of power difference (i.e., $\hat{\xi}_k^\Delta = p_\Delta \,|\, \hat{\Delta}_k \in \Omega_\Delta^{(p_\Delta)}$) and n' being a design parameter that defines an uncertain intermediate mode. Effectively, mode $M = 1$ refers to the cases where $\hat{\Delta}_k < \Delta_{n_1'-n'} \leq 0$ and the generated power equals the dynamic available power in the WT. Mode $M = 3$ refers to the cases where $0 \leq \Delta_{n_1'-n'} \leq \hat{\Delta}_k$ and the generated power equals the dynamic power reference (see Table 8.1). For its part, mode $M = 2$ is the transition mode defined by $n' > 0$ that takes the working mode estimation error into account. In all, the proposed multivariate linear model for computing the adaptive threshold is

$$J_k = X_k\, \beta, \tag{8.40}$$

with X_k being the variable vector defined as

$$X_k = \left[\begin{array}{ccc|ccc|ccc} \hat{\eta}_k^1 & \hat{\eta}_k^2 & \hat{\eta}_k^3 & \hat{\eta}_k^1\hat{v}_k & \hat{\eta}_k^2\hat{v}_k & \hat{\eta}_k^3\hat{v}_k & \hat{\eta}_k^1\hat{\Delta}_k & \hat{\eta}_k^2\hat{\Delta}_k & \hat{\eta}_k^3\hat{\Delta}_k \end{array}\right]$$

and $\beta \in \mathbb{R}^{9\times 1}$ being the coefficient vector. Thus, in Mode M, the threshold verifies $J_k = \beta[M] + \hat{v}_k\, \beta[M+3] + \hat{\Delta}_k\, \beta[M+6]$.

Remark 8.8. *Less conservative thresholds would be achievable by taking account of all the switchings of* $\hat{\theta}_k$ *among the subsets of the parameter vector. To do so, the alternative variable vector* $\bar{X}_k = \left[\hat{\bar{\eta}}_k^1 \;\; \ldots \;\; \hat{\bar{\eta}}_k^N\right] \otimes \left[1 \;\; \hat{\theta}_k^T\right]$ *(with* $\bar{\beta} \in \mathbb{R}^{3N\times 1}$*) would be used instead. Here,* $\hat{\bar{\eta}}_k^p$ *is equal to 1 if* $\hat{\xi}_k = p$ *and it is equal to 0 otherwise. Similarly, it would be possible to take account of the process dynamic behavior by using the alternative variable vector* $\bar{X}_k' = \left[X_k \;\; \ldots \;\; X_{k-O}\right]$ *(with* $\bar{\beta}' \in \mathbb{R}^{3O\times 1}$ *and* O *being the number of past considered samples). However, the simplified form in* (8.40) *reduces the complexity of the threshold computation while it has provided satisfactory results in the simulations in Section 8.8.*

To obtain β, we collect the data of N_T samples in fault-free conditions, we run the estimator (8.22) and we construct the matrices

$$\mathcal{X} = \begin{bmatrix} X_1 \\ \vdots \\ X_{N_T} \end{bmatrix}, \quad \hat{\mathcal{F}} = \begin{bmatrix} |\hat{f}_1| \\ \vdots \\ |\hat{f}_{N_T}| \end{bmatrix}. \tag{8.41}$$

Remark 8.9. *To obtain a fault-free training dataset two approaches are possible. If a realistic simulator of the WF is available, the designer can excite it with all possible power demands and WS profiles and collect the output data. Alternatively, the designer can collect historical data covering all possible power demands and WS profiles. For newly-built systems, one can use either the corresponding simulator or the historical data of its initial operation by assuming that no faults affect the system during this initial period.*

Then, we solve the following optimization problem

$$\begin{aligned} \underset{\beta,\,\epsilon>0}{\text{minimize}} \quad & \sigma\,(\hat{\mathcal{F}} - \mathcal{X}\,\beta)^T(\hat{\mathcal{F}} - \mathcal{X}\,\beta) + (1-\sigma)\,\epsilon\,N_T^2 \\ \text{subject to} \quad & |\hat{f}_k| < \mathcal{X}_k\,\beta < |\hat{f}_k| + \epsilon, \quad k = 1, \ldots, N_T \end{aligned} \tag{8.42}$$

with $\sigma \in [0, 1]$ being a weighting factor. The optimization problem (8.42) guarantees that the collected fault estimates do not exceed the threshold and it minimizes a weighted combination of the quadratic accumulated difference and the maximum difference (denoted as ϵ) between the threshold and the simulated data. Note that the multiplicand N_T^2 in (8.42) is used to regularize the minimized terms. The proposed FE and FDI strategies are summarized in Fig. 8.5.

Remark 8.10. *The sampling False Alarm Rate (FAR) obtained from* (8.42) *is equal to 0. If the resulting threshold is too conservative, one can fix FAR=$\frac{\phi}{T}$ by performing ϕ iterations in which the optimization problem* (8.42) *is solved and the most conservative data (i.e.,$|\hat{f}_{\bar{k}}|$ and $X_{\bar{k}}$ such that $\bar{k} = \text{argmin}_{k\in[1,N]}\,|\hat{f}_k| - X_k\,\beta)$ is eliminated from $\mathcal{F}$ and $\mathcal{X}$ for the next iteration.*

Remark 8.11. *Recall that, for brevity, we have omitted the dependence of the variables on the number of row i and on the number of column j. Hence, let us remark that the inequality in* (8.38) *stands in fact for $|\hat{f}_k^{i,j}| \geq J_k$. The threshold J does not depend on the number of WT (i, j) because the disturbances and noises affecting the estimation error $\tilde{f}^{i,j}$ are equally bounded for all the WTs in the farm.*

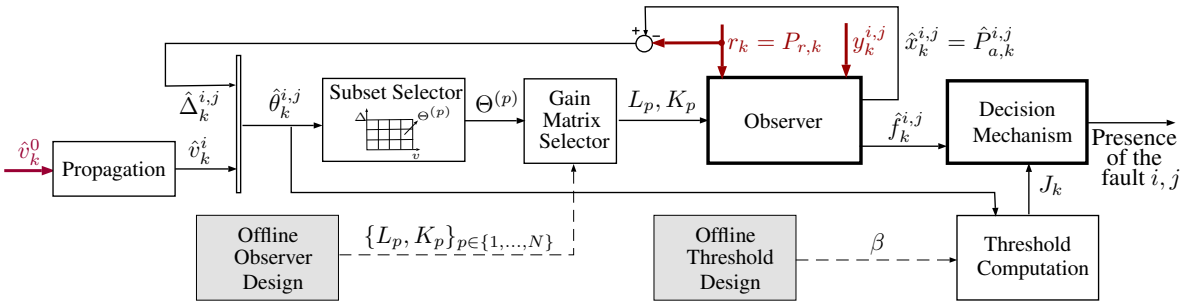

Figure 8.5. FE and FDI strategy at a wind turbine level.

8.6 FE and FDI at a wind farm level

The performance of the observer (8.22) and the decision mechanism (8.38) may be compromised if the bounds of the disturbances in Assumption 8.3 are too large. A solution to mitigate this effect is to totally decouple the FE error from these signals instead of attenuating their effect through the robust design in (8.37). However, a necessary condition for achieving disturbance decoupling is that the faults and the disturbances have a totally decoupled effect on the measurements and this is not possible from a WT level perspective because there is just one measurement which is simultaneously affected by the faults and the disturbances. At the WF level, we can consider altogether the WTs in the same row because the disturbance caused by the wind propagation error (i.e., the disturbance e^i) is common to all these WTs. As detailed hereafter, when all the WTs in a row are prone to the power fault, e^i does not verify disturbance decoupling conditions either. However, in this case, it is possible to build a bank of observers and decision mechanisms that allow achieving the decoupling from e^i at the cost of some fault simultaneity restrictions (cf. [70]).

Remark 8.12. *We have here considered that e^i is caused by the wind propagation error and that $\epsilon^{i,j}$ takes account of the uncertainties caused by the individual turbulence. If for any wind direction or for any other WF layouts there were no sufficient WTs per row in order to build the bank of observers, we would consider groups i of close WTs and divide the uncertainty caused by the wind propagation error into a common disturbance e^i and a non-common disturbance which would be considered together with the turbulence by $\epsilon^{i,j}$.*

To do so, let us first define the auxiliary vectors

$$\boldsymbol{f}^{\boldsymbol{l}}(i) = \begin{bmatrix} f^{i,1} & \dots & f^{i,l-1} & f^{i,l+1} & \dots & f^{i,Z} \end{bmatrix}^T \in \mathbb{R}^{Z-1}, \tag{8.43a}$$

$$\boldsymbol{\delta}^{\boldsymbol{l}}(i) = \begin{bmatrix} \delta^{i,1} & \dots & \delta^{i,l-1} & \delta^{i,l+1} & \dots & \delta^{i,Z} \end{bmatrix}^T \in \mathbb{R}^{Z-1}, \tag{8.43b}$$

where Z denoted the number columns for the considered wind direction. The vector $\boldsymbol{f}^{\boldsymbol{l}}(i)$ considers all the faults of the WTs in the i-th row but the fault of the WT in the l-th column $f^{i,l}$. Similar applies to $\boldsymbol{\delta}^{\boldsymbol{l}}(i)$ w.r.t. the fault variations in (8.12). The model of the power generation systems of the i-th row of WTs including the dynamics of $\boldsymbol{f}^{\boldsymbol{l}}(i)$ can be written as

$$\boldsymbol{z}^{\boldsymbol{l}}_{k+1}(i) = \boldsymbol{A}(\boldsymbol{\theta}_k(i)) \underbrace{\begin{bmatrix} x^{i,1}_k \\ \vdots \\ x^{i,Z}_k \\ \hline \boldsymbol{f}^{\boldsymbol{l}}(i) \end{bmatrix}}_{\boldsymbol{z}^{\boldsymbol{l}}_k(i)} + \boldsymbol{B}(\boldsymbol{\theta}_k(i)) \underbrace{\begin{bmatrix} u(v^{i,1}_k) \\ \vdots \\ u(v^{i,Z}_k) \end{bmatrix}}_{\boldsymbol{u}(\boldsymbol{\theta}_k(i))} + \underbrace{\begin{bmatrix} 0 \\ \hline I_{Z-1} \end{bmatrix}}_{\boldsymbol{E}} \boldsymbol{\delta}^{\boldsymbol{l}}_k(i), \tag{8.44a}$$

$$\underbrace{\begin{bmatrix} y^{i,1}_k \\ \vdots \\ y^{i,Z}_k \end{bmatrix}}_{\boldsymbol{y}_k(i)} = \boldsymbol{C}^{\boldsymbol{l}}(\boldsymbol{\theta}_k(i))\, \boldsymbol{z}^{\boldsymbol{l}}_k(i) + \boldsymbol{D}(\boldsymbol{\theta}_k(i))\, r_k + \underbrace{\begin{bmatrix} 0_{(l-1)\times 1} \\ 1 \\ 0_{(Z-l)\times 1} \end{bmatrix}}_{\boldsymbol{U}^{\boldsymbol{l}}} f^{i,l}_k + \underbrace{\begin{bmatrix} s^{i,1}_k \\ \vdots \\ s^{i,Z}_k \end{bmatrix}}_{\boldsymbol{s}_k(i)} + \underbrace{\begin{bmatrix} w^{i,1}_k \\ \vdots \\ w^{i,Z}_k \end{bmatrix}}_{\boldsymbol{w}_k(i)}, \tag{8.44b}$$

with

$$\boldsymbol{A}(\boldsymbol{\theta}_k(i)) = \left[\begin{array}{ccc|c} a(v_k^{i,1}) & 0 & 0 & 0 \\ 0 & \ddots & 0 & 0 \\ 0 & 0 & a(v_k^{i,Z}) & 0 \\ \hline 0 & 0 & 0 & I_{Z-1} \end{array}\right], \quad \boldsymbol{B}(\boldsymbol{\theta}_k(i)) = \left[\begin{array}{ccc} b(v_k^{i,1}) & 0 & 0 \\ 0 & \ddots & 0 \\ 0 & 0 & b(v_k^{i,Z}) \\ \hline 0 & 0 & 0 \end{array}\right],$$

$$\boldsymbol{C}^{\boldsymbol{l}}(\boldsymbol{\theta}_k(i)) = \left[\begin{array}{ccc|cc} c(\Delta_k^{i,1}) & 0 & 0 & -I_{l-1} & 0 \\ 0 & \ddots & 0 & 0 & 0 \\ 0 & 0 & c(\Delta_k^{i,Z}) & 0 & -I_{Z-l} \end{array}\right], \quad \boldsymbol{D}(\boldsymbol{\theta}_k(i)) = \begin{bmatrix} d(\Delta_k^{i,1}) \\ \vdots \\ d(\Delta_k^{i,Z}) \end{bmatrix},$$

and where $\boldsymbol{z}^{\boldsymbol{l}}(i) \in \mathbb{R}^{2\,Z-1}$ is the extended state vector, $\boldsymbol{y}(i) \in \mathbb{R}^Z$ is the measurement vector and $\boldsymbol{w}(i) \in \mathbb{R}^Z$ and $\boldsymbol{s}(i) \in \mathbb{R}^Z$ are the disturbance vectors. For its part, $\boldsymbol{\theta}(i)$ stands for the parameter vector defined as

$$\boldsymbol{\theta}(i) = \begin{bmatrix} \theta^{i,1} & \dots & \theta^{i,Z} \end{bmatrix}^T \in \mathbb{R}^{2\,Z}. \tag{8.45}$$

Assumption 8.4. *The parameter vectors $\theta^{i,j}$ of all the turbines in the i-th row belong to the same subset $\Theta^{(p)}$ at each sample k (i.e., $\theta_k^{i,j} \in \Theta^{(p)}$ for $j = 1, \dots, Z$). Hence, $\boldsymbol{\theta}(i)$ lies in the ordered parameter set $\boldsymbol{\Theta}$ of N subsets $\boldsymbol{\Theta}^{(p)}$ (i.e., $\boldsymbol{\Theta} = \{\boldsymbol{\Theta}^{(1)}, \dots, \boldsymbol{\Theta}^{(N)}\}$) defined as $\boldsymbol{\Theta}^{(p)} = (\Theta^{(p)}, \dots, \Theta^{(p)})$.*

Remark 8.13. *Assumption 8.4 seeks reducing the computational burden of the design and implementation of a switched observer based on the model* (8.44)*. However, in reality, it may in fact happen that not all the parameter vectors $\theta^{i,j}$ of the i-th row belong to the same subset $\Theta^{(p)}$ at certain sample k. In such cases, we neglect these differences and we consider that $\boldsymbol{\theta}_k(i)$ belongs to the closest subset $\boldsymbol{\Theta}^{(p)}$. In any case, if more precise results were required, Assumption 8.4 would be omitted and the parameter set would be alternatively defined as $\boldsymbol{\Theta}' = \{\Omega_v \times \Omega_\Delta \times \dots \times \Omega_v \times \Omega_\Delta\}$. The partition of Ω_Δ and Ω_v as detailed in Section 8.3.2 would then lead to N^Z subsets $\boldsymbol{\Theta}'^{(p)}$.*

Omitting hereafter the dependence on the number of row i (e.g., $\boldsymbol{z}_k^{\boldsymbol{l}}$ stands for $\boldsymbol{z}_k^{\boldsymbol{l}}(i)$), it yields

$$\boldsymbol{z}_{k+1}^{\boldsymbol{l}} = \boldsymbol{A}(\boldsymbol{\theta}_k)\, \boldsymbol{z}_k^{\boldsymbol{l}} + \boldsymbol{B}(\boldsymbol{\theta}_k)\, \boldsymbol{u}(\boldsymbol{\theta}_k) + \boldsymbol{E}\, \boldsymbol{\delta}_k^{\boldsymbol{l}}, \tag{8.46a}$$

$$\boldsymbol{y}_k = \boldsymbol{C}^{\boldsymbol{l}}(\boldsymbol{\theta}_k)\, \boldsymbol{z}_k^{\boldsymbol{l}} + \boldsymbol{D}(\boldsymbol{\theta}_k)\, r_k + \boldsymbol{U}^{\boldsymbol{l}}\, f_k^{i,l} + \boldsymbol{s}_k + \boldsymbol{w}_k, \tag{8.46b}$$

$$\boldsymbol{f}_k^{\boldsymbol{l}} = \boldsymbol{F}\, \boldsymbol{z}_k^{\boldsymbol{l}}, \tag{8.46c}$$

with $\boldsymbol{F} = \begin{bmatrix} 0 & I_{Z-1} \end{bmatrix}$.

8.6.1 FE and FDI architecture

In analogy to (8.22), the following model-based observer is built for the extended system (8.46):

$$\hat{\boldsymbol{z}}_{k+1}^{\boldsymbol{l}} = \boldsymbol{A}(\hat{\boldsymbol{\theta}}_k)\, \hat{\boldsymbol{z}}_k^{\boldsymbol{l}} + \boldsymbol{B}(\hat{\boldsymbol{\theta}}_k)\, \boldsymbol{u}(\hat{\boldsymbol{\theta}}_k) + \boldsymbol{L}^{\boldsymbol{l}}(\hat{\boldsymbol{\theta}}_k)\Big(\boldsymbol{y}_k - \boldsymbol{C}^{\boldsymbol{l}}(\hat{\boldsymbol{\theta}}_k)\, \hat{\boldsymbol{z}}_k^{\boldsymbol{l}} - \boldsymbol{D}(\hat{\boldsymbol{\theta}}_k)\, r_k\Big), \tag{8.47a}$$

$$\hat{\boldsymbol{f}}_k^{\boldsymbol{l}} = \boldsymbol{F}\, \boldsymbol{z}_k^{\boldsymbol{l}} + \boldsymbol{K}^{\boldsymbol{l}}(\hat{\boldsymbol{\theta}}_k)\Big(\boldsymbol{y}_k - \boldsymbol{C}^{\boldsymbol{l}}(\hat{\boldsymbol{\theta}}_k)\, \hat{\boldsymbol{z}}_k^{\boldsymbol{l}} - \boldsymbol{D}(\hat{\boldsymbol{\theta}}_k)\, r_k\Big). \tag{8.47b}$$

where $\boldsymbol{L^l}(\hat{\boldsymbol{\theta}}) \in \mathbb{R}^{(2\,Z-1)\times Z}$ and $\boldsymbol{K^l}(\hat{\boldsymbol{\theta}}) \in \mathbb{R}^{(Z-1)\times Z}$ are the gain matrices of the observer that we fix to

$$\boldsymbol{L^l}(\hat{\boldsymbol{\theta}}) = \boldsymbol{L_p^l} \quad \text{if} \quad \hat{\boldsymbol{\theta}} \in \boldsymbol{\Theta}^{(p)}, \tag{8.48a}$$

$$\boldsymbol{K^l}(\hat{\boldsymbol{\theta}}) = \boldsymbol{K_p^l} \quad \text{if} \quad \hat{\boldsymbol{\theta}} \in \boldsymbol{\Theta}^{(p)}. \tag{8.48b}$$

Define $\tilde{\boldsymbol{z}}_k^{\boldsymbol{l}} = \boldsymbol{z}_k^{\boldsymbol{l}} - \hat{\boldsymbol{z}}_k^{\boldsymbol{l}}$ and $\tilde{\boldsymbol{f}}_k^{\boldsymbol{l}} = \boldsymbol{f}_k^{\boldsymbol{l}} - \hat{\boldsymbol{f}}_k^{\boldsymbol{l}}$. It follows that

$$\tilde{\boldsymbol{z}}_{k+1}^{\boldsymbol{l}} = \boldsymbol{\mathcal{A}^l}(\hat{\boldsymbol{\theta}}_k)\tilde{\boldsymbol{z}}_k^{\boldsymbol{l}} + \boldsymbol{\mathcal{B}^l}(\hat{\boldsymbol{\theta}}_k)\boldsymbol{\mathcal{W}}_k + \boldsymbol{E}\,\boldsymbol{\delta}_k^{\boldsymbol{l}} - \boldsymbol{L^l}(\hat{\boldsymbol{\theta}}_k)\boldsymbol{U^l} f_k^{i,l}, \tag{8.49a}$$

$$\tilde{\boldsymbol{f}}_k^{\boldsymbol{l}} = \boldsymbol{\mathcal{C}^l}(\hat{\boldsymbol{\theta}}_k)\,\tilde{\boldsymbol{z}}_k^{\boldsymbol{l}} + \boldsymbol{\mathcal{D}^l}(\hat{\boldsymbol{\theta}}_k)\,\boldsymbol{\mathcal{W}}_k - \boldsymbol{K^l}(\hat{\boldsymbol{\theta}}_k)\,\boldsymbol{U^l} f_k^{i,l}, \tag{8.49b}$$

with

$$\begin{aligned}
\boldsymbol{\mathcal{A}^l}(\hat{\boldsymbol{\theta}}_k) &= \boldsymbol{A}(\hat{\boldsymbol{\theta}}_k) - \boldsymbol{L^l}(\hat{\boldsymbol{\theta}}_k)\,\boldsymbol{C^l}(\hat{\boldsymbol{\theta}}_k),\\
\boldsymbol{\mathcal{C}^l}(\hat{\boldsymbol{\theta}}_k) &= \boldsymbol{F} - \boldsymbol{K^l}(\hat{\boldsymbol{\theta}}_k)\,\boldsymbol{C^l}(\hat{\boldsymbol{\theta}}_k),\\
\boldsymbol{\mathcal{B}^l}(\hat{\boldsymbol{\theta}}_k) &= \begin{bmatrix} \boldsymbol{\mathcal{G}}(\hat{\boldsymbol{\theta}}_k) & \boldsymbol{G}(\hat{\boldsymbol{\theta}}_k) & -\boldsymbol{L^l}(\hat{\boldsymbol{\theta}}_k)\boldsymbol{H}(\hat{\boldsymbol{\theta}}_k) & -\boldsymbol{L^l}(\hat{\boldsymbol{\theta}}_k) & -\boldsymbol{L^l}(\hat{\boldsymbol{\theta}}_k) \end{bmatrix},\\
\boldsymbol{\mathcal{D}^l}(\hat{\boldsymbol{\theta}}_k) &= \begin{bmatrix} 0 & 0 & -\boldsymbol{K^l}(\hat{\boldsymbol{\theta}}_k)\boldsymbol{H}(\hat{\boldsymbol{\theta}}_k) & -\boldsymbol{K^l}(\hat{\boldsymbol{\theta}}_k) & -\boldsymbol{K^l}(\hat{\boldsymbol{\theta}}_k) \end{bmatrix},\\
\boldsymbol{\mathcal{W}}_k &= \begin{bmatrix} \lambda_k & \boldsymbol{\mu}_k & \boldsymbol{\varphi}_k & \boldsymbol{s}_k & \boldsymbol{w}_k \end{bmatrix}^T.
\end{aligned}$$

We have that λ_k, $\boldsymbol{\mu}_k$ and $\boldsymbol{\varphi}_k$ stand in fact for $\lambda_k(i)$, $\boldsymbol{\mu}_k(i)$ and $\boldsymbol{\varphi}_k(i)$ which are defined in analogy to (8.30) as

$$\lambda_k(i) = e_k^i/\bar{e}_p, \quad \boldsymbol{\mu}_k(i) = \begin{bmatrix} {\varepsilon_k}^{i,1}/\bar{\varepsilon}_p \\ \vdots \\ {\varepsilon_k}^{i,Z}/\bar{\varepsilon}_p \end{bmatrix}, \quad \boldsymbol{\varphi}_k(i) = \begin{bmatrix} {h_k}^{i,1}/\bar{h}_p \\ \vdots \\ {h_k}^{i,Z}/\bar{h}_p \end{bmatrix},$$

if $\theta_k \in \Theta^{(p)}$. For its part, $\boldsymbol{\mathcal{G}}(\hat{\boldsymbol{\theta}}_k)$, $\boldsymbol{G}(\hat{\boldsymbol{\theta}}_k)$ and $\boldsymbol{H}(\hat{\boldsymbol{\theta}}_k)$ satisfy

$$\boldsymbol{\mathcal{G}}(\hat{\boldsymbol{\theta}}_k) = \boldsymbol{\mathcal{G}}_p \quad \text{if} \quad \hat{\boldsymbol{\theta}}_k \in \Theta^{(p)}, \qquad \boldsymbol{\mathcal{G}}_p = \bar{\boldsymbol{R}}_0\,\bar{e}_p, \tag{8.50a}$$

$$\boldsymbol{G}(\hat{\boldsymbol{\theta}}) = \boldsymbol{G}_p \quad \text{if} \quad \hat{\boldsymbol{\theta}}_k \in \Theta^{(p)}, \qquad \boldsymbol{G}_p = \bar{\boldsymbol{R}}\,\bar{\varepsilon}_p, \tag{8.50b}$$

$$\boldsymbol{H}(\hat{\boldsymbol{\theta}}_k) = \boldsymbol{H}_p \quad \text{if} \quad \hat{\boldsymbol{\theta}}_k \in \Theta^{(p)}, \qquad \boldsymbol{H}_p = \boldsymbol{R}\,\bar{h}_p, \tag{8.50c}$$

with $\bar{\boldsymbol{R}}_0 = \begin{bmatrix} \mathbf{1}_{Z\times 1} \\ 0_{(Z-1)\times 1} \end{bmatrix}$, $\bar{\boldsymbol{R}} = \begin{bmatrix} I_Z \\ 0_{(Z-1)\times 1} \end{bmatrix}$ and $\boldsymbol{R} = I_Z$. As previously specified, $\lambda_k(i)$ is a single disturbance modeling the wind propagation error and it affects all the turbines simultaneously.

In all, the signals affecting the $\boldsymbol{l}$-th observer are the fault generators $\boldsymbol{\delta^l}$ (with $n_{\boldsymbol{\delta}} = Z-1$), the disturbances in $\boldsymbol{\mathcal{W}}$ (with $n_\lambda = 1$ and $n_{\boldsymbol{\mu}} = n_{\boldsymbol{\varphi}} = n_{\boldsymbol{s}} = n_{\boldsymbol{w}} = Z$) and the fault $f^{i,l}$ which can be now considered as a new "disturbance". Following the approaches in [70], one can verify that it is now possible to decouple $\boldsymbol{f^l}$ from λ if the new "disturbance" $f^{i,l}$ is ignored. Note that if $f^{i,l}$ was not ignored and its dynamics was considered together with the dynamics of $\boldsymbol{f^l}$, λ would not verify disturbance decoupling conditions because it would not be possible to distinguish this disturbance from the occurrence of simultaneous faults in all the turbines in the row.

Hence, we propose to ignore the presence of the fault $f^{i,l}$ and to design the observer (8.47) through the optimization problem

$$\begin{array}{ll} \text{minimize} & \gamma_\mu n_{\boldsymbol{\mu}} \|\mu\|_\infty^2 + \gamma_\varphi n_{\boldsymbol{\varphi}} \|\varphi\|_\infty^2 + \gamma_s \|\boldsymbol{s}\|_{\text{RMS}}^2 + \\ & \gamma_w \|\boldsymbol{w}\|_{\text{RMS}}^2 \\ \text{subject to} & \gamma_\lambda = 0, \quad \gamma_\delta \leq \bar{\gamma}_\delta, \\ & \boldsymbol{\Xi}_p^m \succ 0, \ \ \forall p, m \end{array} \tag{8.51}$$

with $\boldsymbol{\Xi}_p^m$ built in analogy to Ξ_p^m with the matrices in (8.49) replacing the matrices in (8.32). The new constraint $\gamma_\lambda = 0$ ensures now the decoupling from λ.

In the absence of the ignored fault $f^{i,l}$, we can thus set the following decision mechanisms ($j = 1, \ldots, l-1, l+1, \ldots, Z$):

$$\begin{cases} \text{if } |\hat{\boldsymbol{f}}_k^{\boldsymbol{l}}[j]| \geq \boldsymbol{J}_k \ , & \text{Fault } \boldsymbol{f^l}[j] \\ \text{otherwise} \ , & \text{No fault } \boldsymbol{f^l}[j] \end{cases} . \tag{8.52}$$

The adaptive threshold $\boldsymbol{J}$ does not depend on the number of turbine (i, j) nor on the number of ignored fault l (see Remark 8.11) and it is designed following the strategy presented in Section 8.5. The decoupling from λ enhances FDI because the thresholds $\boldsymbol{J}$ in (8.52) are now smaller than the thresholds J in (8.38).

However, if the fault $f^{i,l}$ is present in the system, the decision mechanisms (8.52) are no longer reliable. Hence, we build a bank of $\boldsymbol{l} = 1, \ldots Z$ observers, each of them taking account of the fault $\boldsymbol{f^l}$ and ignoring the fault $f^{i,l}$. An observer $\boldsymbol{l}$ and the corresponding decision mechanisms are reliable if the absence of the fault $f^{i,l}$ is diagnosed by the decision mechanisms of at least another reliable observer $\boldsymbol{l'}$ ($\boldsymbol{l'} \neq \boldsymbol{l}$). In turn, the reliability of $\boldsymbol{l'}$ implies that the decision mechanisms of the $\boldsymbol{l}$-th observer diagnose the absence of the fault $f^{i,l'}$. In all, the proposed bank of observer and decision mechanisms enables FE and FDI whenever 2 of the faults in a row i are not present in the system (i.e., there are no more than $Z-2$ simultaneous faults in a row). FE and FDI are then achieved with any of the reliable observers and decision mechanisms of the bank.

8.7 Benefits of the proposed approach

Compared to the relevant existing literature, the benefits of the proposed approach are the following.

- The proposed approach utilizes a reduced number of measurements: the power reference, the generated power and the WS at the wind mast. This reduces the information needs w.r.t. other techniques such as the one in [33] (requiring the rotor speed measurement) or in [264] (requiring the collective pitch angle measurement). It does not either require the information about the presumed fault size as it is in [33].

- The residual-based techniques in [30, 33, 83] are focused on FDI tasks. Contrariwise, the proposed approach is focused on both FE (Section 8.4) and FDI (Section 8.5), being more suitable for the development of AFTC strategies.
- The proposed closed-loop approach is more actively robust against disturbances and uncertainties than the open-loop methods in [16, 30, 33, 83].
- The Markovian jump system approach is a non-conservative procedure to handle the nonlinearities in the power generation model. It facilitates the adaptation to the different levels of uncertainties and disturbances along the parameter set, leading to a less restrictive compromise between fault sensitivity and robustness.
- The proposed observer design in Section 8.4.2 guarantees certain fault sensitivity with optimal disturbance rejection. This performance is not guaranteed in [16,30,33,83]. where more ad-hoc and user knowledge-based tuning procedures are utilized to set this trade-off.
- In contrast to the constant thresholds in [16, 33, 264], the adaptive FDI mechanisms presented in Section 8.5 allow the adjustment of the thresholds to the different WS zones and WT operating modes. The proposed data-driven design of the FDI thresholds provides tight bounds for the fault estimates obtained via Markovian observers. This allows a more rapid detection and isolation of small faults w.r.t. model-based adaptive thresholds as the ones used in [30], which moreover require precise bounds of the uncertainties.
- The WF level scheme proposed in Section 8.6 is based on a systematic multi-input multi-ouput (MIMO) observer that automatically merges the information acquired from temporal and spatial inconsistencies depending on the level of shared uncertainties among the group of considered WTs. Hence, it is more easily extensible to different WF layouts and wind direction than the residuals in [16, 30, 83, 264], which assume identical wind conditions among groups of WTs.

8.8 Simulation results

The WF benchmark [215] includes the wind data of 4400 s for numerical simulations. The wind directions in Fig. 8.6 are considered in the benchmark. The application of the proposed WT level strategy is independent of the WF layout and of the wind direction. The WF level approach requires to group the nearby turbines and to bound the shared uncertainties caused by the wind (see Remark 8.12). In the first wind direction, we distinguish three rows and three columns of WTs and, in this case, we simply group the turbines by rows. In the second wind direction, there exist 5 rows of WTs; however, for the application of the WF level FE and FDI strategy, we group the WTs as shown in Fig. 8.6. Due to space constraints, in the following, we just include the simulation results for the first wind direction. Similar WF level results are obtained for the other wind direction.

First, we create a fault-free training dataset and a validation dataset by considering 10 different dynamic power reference cases (see some example cases in the first row of Table 8.2).

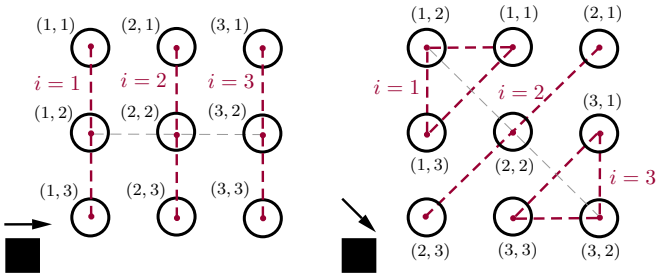

Figure 8.6. Rows/groups of WTs in the WF benchmark depending on the wind direction (→). ◯: Wind turbine, ■: Wind mast.

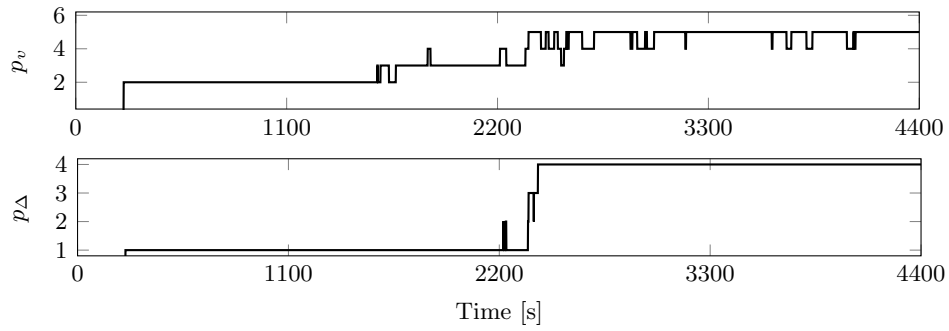

Figure 8.7. Case A subsets. Turbine ($i = 1$, $j = 1$).

Note that it is not possible to consider different wind speed scenarios because only the data related to one wind speed profile is available in the benchmark (detailed in Appendix C). The transitions experienced by the training dataset (see the example in Fig. 8.7) are utilized for computing the transition probability matrix of the Markovian process[3] . Then, we perform the design of the WT level observer (8.22) through the optimization problem (8.37) and of the WF level observer (8.47) through the optimization problem (8.51). For both designs, we fix the required $\mathcal{H}_\infty$ performance describing the observer fault sensitivity to $\bar{\gamma}_\delta = 1$. The values included in the designs are specified in Table D.5 and Table D.6 of Appendix D.3.1. The fault-free training dataset is subsequently utilized to obtain the thresholds of the data-based decision mechanisms. For each training case, we run the designed estimator ((8.22) for the WT level approach and (8.47) for the WF level approach). Then, we construct the matrices (8.41) with all the estimated data and we solve the optimization problem (8.42)[4].

The figures in Table 8.2 show the simulation results for some fault-free training and validation cases. The estimates are in black and the thresholds are in red. For ease of comprehension, we include both the figures comparing the real estimates in MW (i.e., $\hat{f}_k$ at a WT level or $\hat{\boldsymbol{f}}_k^{\boldsymbol{l}}[j]$ at a WF level) with the real thresholds (i.e., J_k or $\boldsymbol{J}_k$) and the figures comparing normalized FE variables (i.e., $\hat{f}_k/J_k$ at a WT level or $\hat{\boldsymbol{f}}_k^{\boldsymbol{l}}[j]/\boldsymbol{J}_k$ at a WF level) with unitary thresholds. First, we

[3]The transition probabilities are computed with the open-loop estimated power difference because the closed-loop estimates are not yet available.

[4]All the designs are set up in YALMIP [192] and solved using the solver MOSEK [204]. For simplification, we omit the obtained results.

Table 8.2. FE and FDI in the fault-free WT ($i = 1, j = 1$). ■: Training cases (A,B,C), □: Test cases (1,2).

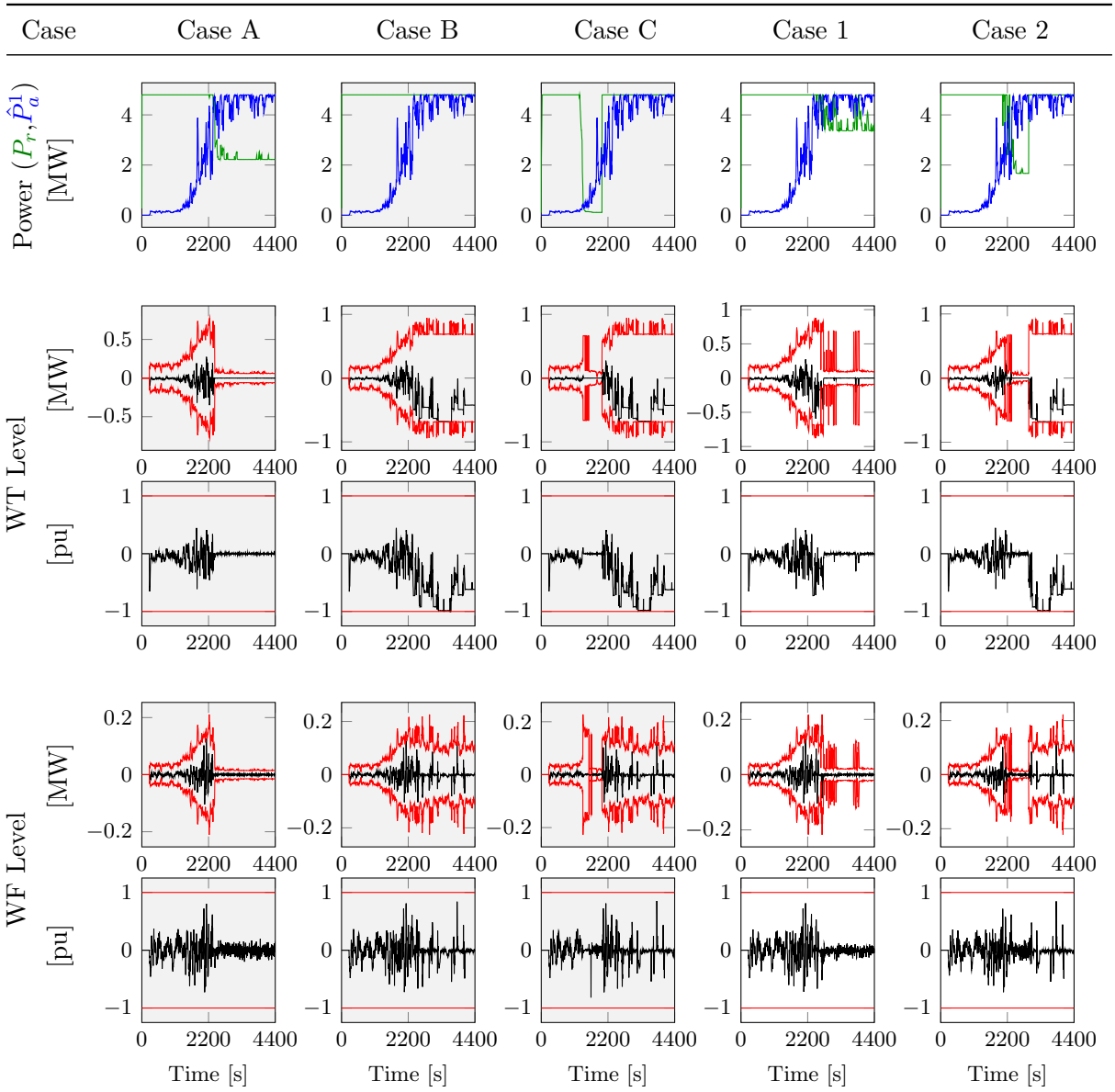

verify that the WF level approach enhances fault diagnosability w.r.t. the WT level approach: the minimum diagnosable faults are in the order of 0.2 MW at the WF level and in the order of 0.5-1 MW at the WT level. Second, we deduce that more accurate fault estimates are obtained when the power generated by the WT equals the dynamic power reference, P_r, and not the dynamic available power, $\hat{P}_a^i$. Effectively, in this WT working mode, the uncertainties derived from the wind speed estimation error disappear because the WT is available to generate the amount of requested power.

Now, let us consider Case 1 and suppose that the turbine ($i = 1$, $j = 1$) is affected by a 40% power degradation during the period **T1** (defined as [1000, 1100] s) and by a 3% power

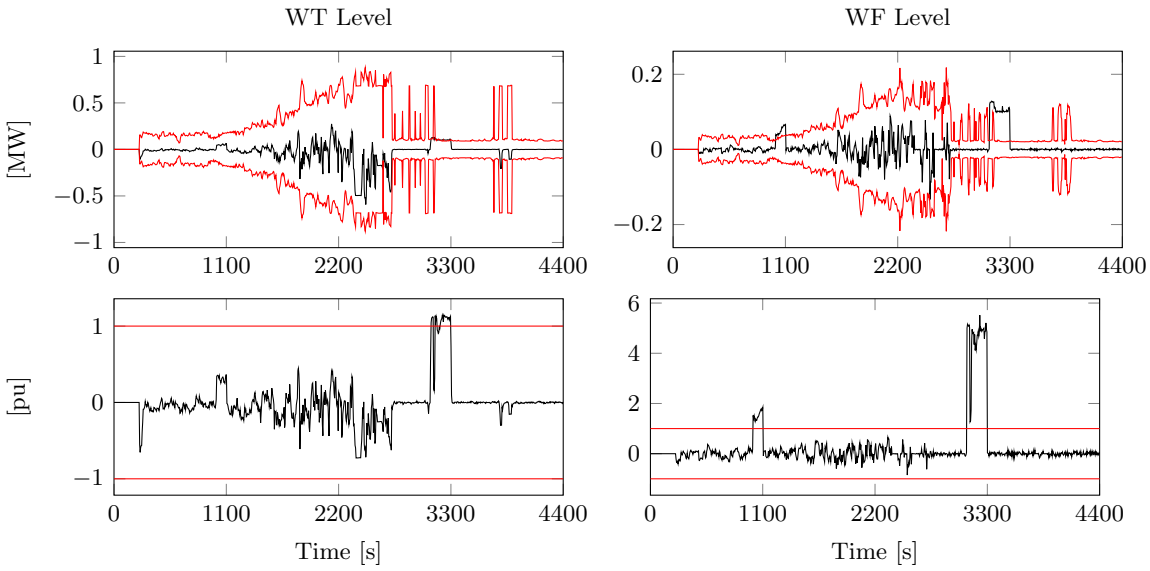

Figure 8.8. FE and FDI in the WT ($i = 1$, $j = 1$). Case 1 with 40% power degradation during **T1** and 3% power degradation during **T2**.

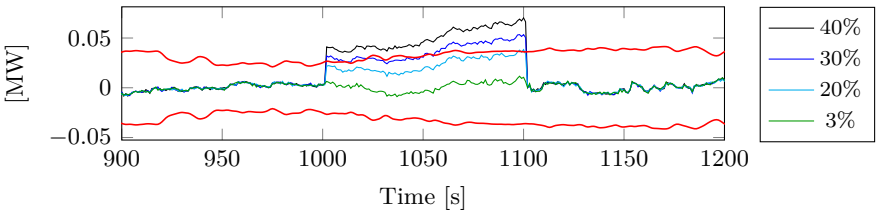

Figure 8.9. WF level FE and FDI in the WT ($i = 1$, $j = 1$). Case 1 with different power degradation levels during **T1**.

degradation during the period **T2** (defined as [3200, 3300] s). The WT level and WF level FE and FDI results are depicted in Fig. 8.8. One verifies that the first fault is only diagnosed at the WF level and the second fault, although being also diagnosed at the WT level, it is more clearly distinguishable at the WF level. If we study Case 1 (see Table 8.2), we verify that relative power degradations are more difficult to diagnose during **T1** than during **T2** because, in this case, the amount of generated power is smaller and, moreover, the generated power equals the dynamic available power and the level of uncertainties is thus bigger. Hence, small relative power degradations are hard to diagnose during this period (see some examples in Fig. 8.9).

Finally, we consider the whole WF and the Case 2 in Table 8.2. We assume that the turbine ($i = 1$,$j = 3$) is affected by a relative power degradation of 50% during **T1** and that the turbine ($i = 2$,$j = 1$) is affected by a relative power degradation of 20% during **T2**. Fig. 8.10 shows the WF level simulation results for all the WTs in the farm. We verify that the proposed approach allows FE and FDI in the WF. Moreover, the proposed approach allows simultaneous faults in the farm: if the WT level approach is utilized, no simultaneity restrictions apply; if the WF level approach is utilized, the only restriction for achieving FE is that there should be two simultaneous fault-free turbines per row (i.e., only a faulty turbine per row in this case).

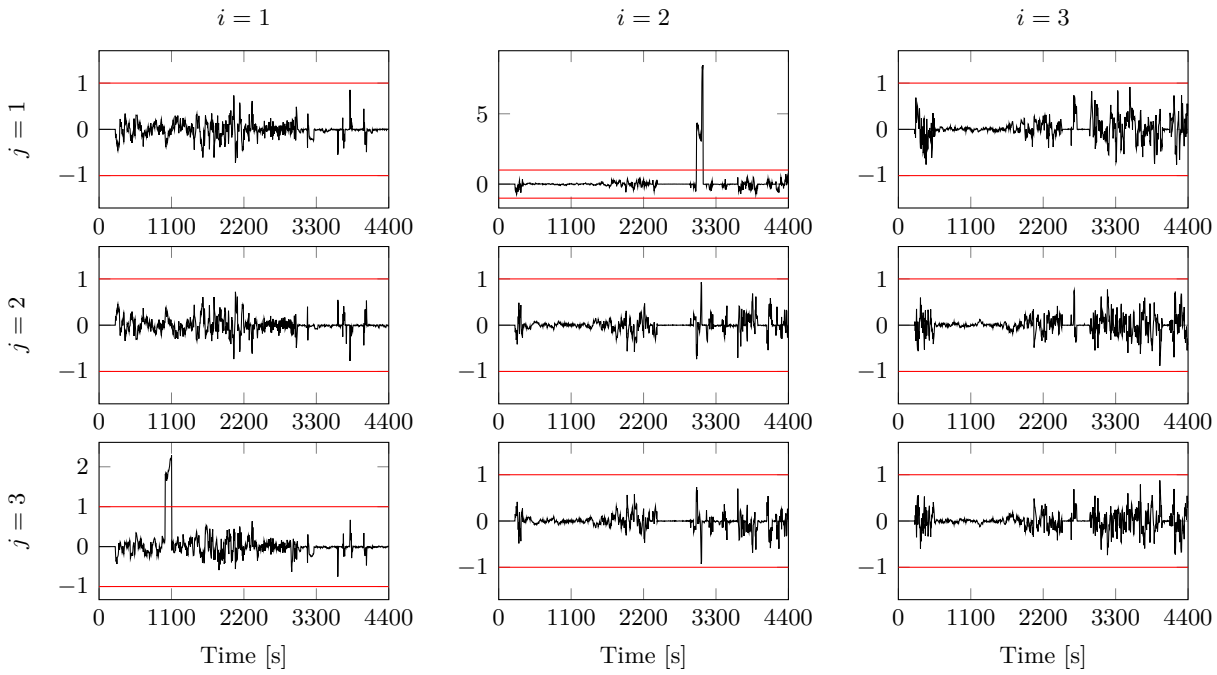

Figure 8.10. WF level FE and FDI in the WF [pu]. Case 2 with 50% power degradation in the turbine ($i = 1$,$j = 3$) during **T1** and 20% power degradation in the turbine ($i = 2$,$j = 1$) during **T2**.

8.9 Conclusion

This chapter proposed a novel closed-loop FE scheme for the estimation of decreased power generation in WTs due to blade erosion and debris build-up, which also cause other WT damages. The model-based strategy is based on the Markovian jump system model of the power generation system of a WT and it thus covers all the wind speed zones and WT operating modes. The FE output is also utilized for FDI in tighten data-based decision mechanisms. The approach is first applied to a single WT and then generalized from a WF perspective. The WF approach has the advantage of being easily applicable to different wind directions and layouts by simply adjusting the level of shared uncertainty by the considered groups of nearby turbines. The extension of the proposed approach to other WT systems and the use of the obtained fault estimates in active FTC strategies highlight as immediate future work.

Chapter 9

Robust estimation and diagnosis of wind turbine pitch misalignments at a wind farm level

Wind turbine pitch misalignments provoke aerodynamic asymmetries which can cause severe damage of the turbine and its components. The diagnosis of these wind turbine faults at a wind farm level has emerged as an effective solution to the problem. In this chapter, we propose a model-based strategy to estimate and diagnose pitch misalignments at a wind farm level. Fault estimation is addressed by using a switched observer that assumes bounded wind propagation errors. These estimates are used in statistical-based decision mechanisms for achieving fault detection and isolation. The observer design takes account on the trade-off between the cumulative squared errors due to faults and the root mean square errors due to noises and uncertainties. The thresholds of the decision mechanisms are fixed using the False Alarm Rate criterion. The diagnosis performance is then ameliorated with a scheme that uses a bank of the aforementioned observers and decision mechanisms. Finally, the proposed approach is tested using a well-known benchmark in the context of wind farm fault diagnosis.

9.1 Introduction

Wind energy has grown in importance over the last two decades as it has proven to be a promising and powerful source of renewable energy [87]. However, the maintainability and reliability of wind turbines (WTs) is still a challenging and critical issue due to the high costs associated to maintenance operations [235]. The issues related to the pitch system are of particular interest to the wind industry due to their long downtimes and high failure rates [130, 235]. These issues include actuator, sensor and imbalance faults [23, 113, 168, 261]. A common pitch imbalance fault is aerodynamic asymmetry, which may be caused by the misalignment of one or more blades. This misalignment can be originated by several factors, including high wind shear and

manufacturing, installation or control errors [113, 260]. In general, aerodynamic asymmetries represent a significant problem for WTs, as also witnessed by the fact that certification guidelines require relatively small pitch misalignments [22]. When a blade misalignment is present, the loadings experienced by the blades are not balanced which results in vibrations that negatively affect other components of the turbine. Moreover, the power quality is degraded and the power generation efficiency is reduced [260].

It is widely recognized that pitch actuator and sensor faults can be dealt with at the WT level. A well-established benchmark for actuator and sensor fault diagnosis (FD) in WTs was presented in [216]. Several solutions have been proposed showing the effectiveness of FD for predictive maintenance. Although some data-based methods being available, e.g., [68, 221], most solutions deal with model-based FD techniques, see [153, 173, 189, 258, 304]. However, imbalance faults are more challenging. As stated by [113], most exiting methods for imbalance fault diagnosis require additional sensors such as vibrational sensors [150, 169, 211]. This extra equipment is inevitably subject to failures and it is generally difficult to access. Thus, current-based imbalance diagnosis methods have gained more attention [113, 260]. However, as recognized by [113], there are intrinsic challenges in using current signals for imbalance diagnosis: the characteristic frequencies of imbalance faults depend on the shaft rotating frequency and the useful information in current signals for FD is characterized by a low signal-to-noise ratio.

Another approach is to diagnose imbalance faults at a wind farm (WF) level. In [168], a WF data-mining approach was developed for monitoring blade imbalance faults. Motivated by this work, a new benchmark has been presented in [215] for FD in WTs at a WF level. The authors recognize that some faults which are difficult to diagnose at a WT level can be better handled at the WF level, when the WT is considered in comparison to other WTs of the farm. Fewer solutions to this problem can be found in the bibliography: data-driven approaches are presented in [83, 267] and model-based strategies are developed in [30, 33]. Duviella et al. [83] present an evolving classification method and Simani et al. [267] develop a FD strategy based on fuzzy logic. Borcehrsen et al. [33] use dynamical cumulative sums for FD and Blesa et al. [30] address the problem using interval nonlinear parameter varying parity equations.

One of the main interests in diagnosing pitch imbalances is the development of individual pitch fault-tolerant controllers that accommodate the aforementioned faults for achieving load mitigation [54]. The WF solutions in [30, 33, 83, 267] are focused on fault detection and isolation (FDI) tasks and they propose consistency checking methods which are based on computing the difference, called residual, between the modeled and the real behavior of the system [44, 297]. Research has shown that there are intrinsic difficulties in the use of residuals in active fault tolerant control (FTC) due to the complexity derived from the reconstruction of the faults from the residuals [171]. Active FTC based directly on fault estimation (FE) rather than on residual-based techniques seems to provide more immediate and accurate results, see [171]. Thus, Siminai et al. [264] extended the work in [267] to cover FE. They develop data-driven solutions which rely on fuzzy models and neural networks.

In this chapter, we propose a model-based strategy for FE and FDI of pitch misalignments. This model is affected by uncertainties that depend on the operation conditions of the WT;

hence, we develop a switched observer for FE [280]. These uncertainties derive from the open-loop scheme which is used for wind propagation; however, just the information of their bounds is necessary to design the observer. Thus, the proposed method has the feature of being easily extensible to other wind propagation strategies. It is noticed that FE techniques aim to simultaneously make the estimates sensitive to faults and robust against uncertainties and noises [277] through the accomplishment of certain trade-off between these properties [299, 327]. In an aim to bridging the gap between theory and practice, we propose to use common engineering performance parameters in the fault estimator design. Thus, we use the trade-off between the cumulative squared error experienced by the estimates due to faults and the root mean square of the estimation signals due to noises and uncertainties. Then, the fault estimates are evaluated in statistical-based decision mechanisms for FDI, which we design for guaranteeing certain False Isolation Rate (FIR). The proposed FE and FDI strategy is validated using the benchmark [215]. Through numerical simulations, we show the effect of the intuitive design settings on the performance of the results.

9.1.1 Structure and notation

The rest of this chapter is organized as follows. Section 9.2 gives the problem formulation. Section 9.3 presents the wind propagation scheme used in this chapter and its characterization. In Section 9.4 we present the proposed performance-based FE and FDI strategy, whose design we detail in Section 9.5. In Section 9.6 we present an improvement of performance which can be made at the cost of some restrictions regarding the simultaneity of faults. Simulation results are reported in Section 9.7 to show the effectiveness of the proposed approach, followed by some concluding remarks in Section 9.8.

Let A and B be some matrix and a be some vector. $A[i,j]$ denotes the element in the i-th row and j-th column of A and $a[i]$ denotes the i-th element in a. $A \preceq 0$ means that A is negative semidefinite and similar applies to $\succeq$. The trace of matrix A is represented as $\mathrm{tr}(A)$. Let x_k be a vector of stochastic signals at a sample k. We write $\|x_k\|_\infty \triangleq \max_i |x_k[i]|$ for the max norm of vector x_k. We write $\|x\|_\infty \triangleq \max_k \max_i |x_k[i]|$ for the l_∞ norm of signal x, $\|x\|_2^2 \triangleq \lim_{K\to\infty} \sum_{k=1}^{K} x_k^T\, x_k$ for its l_2 norm and $\|x\|_{RMS}^2 = \frac{1}{K}\,\|x\|_2^2$ for its RMS norm. Expected value, probability and absolute value are denoted by $\mathbb{E}\{\cdot\}$, $\mathbb{P}\{\cdot\}$ and $|\cdot|$. I_n is the identity matrix of size $n \times n$, $\mathbf{1}_{n\times m}$ is a matrix of ones of size $n \times m$ and 0 is the zero matrix of appropriate dimensions.

9.2 Problem statement

Consider the WF benchmark consisting of $N = 9$ WTs of 4.8 MW. The benchmark considers two possible wind directions: 0° and 45°. The WTs can be named according to the wind direction as shown in Fig. 9.1. We consider that the wind is perpendicular to the rows of WTs, which are numbered as $i = 1, \ldots, n_i$ and parallel to the columns of WTs, which are numbered as $j = 1, \ldots, n_j$. There is a wind mast at row $i = 0$ which measures the wind speed. We denote the

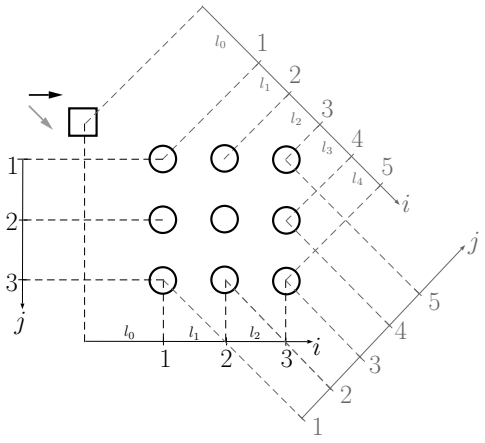

Figure 9.1. Layout of the WF benchmark (◯: Wind turbine, □: Wind mast, →: Wind direction). Black: 0° layout, Gray: 45° layout.

distance between two consecutive rows i and $i+1$ as l_i. For the 0° layout, we have $l_0 = 1150$ m and $l_i = 1138.44$ m for all $i \neq 0$.

According to [116, 215], the collective pitch system of a WT (i, j) can be modeled as a first order close-loop system between the collective pitch, named after $\beta^{i,j}$, and the collective pitch reference, named after $\beta_r^{i,j}$:

$$\beta^{i,j}(s) = \frac{\tau_\beta}{s + \tau_\beta} \beta_r^{i,j}(s), \tag{9.1}$$

where τ_β is a known constant transfer function coefficient ($\tau_\beta = 1.6$ rad/s). The collective pitch reference is a nonlinear function $g(\cdot)$ of the dynamic power reference, P^r, and the effective wind speed acting on the blades of the turbine (i, j), $\nu^{i,j}$:

$$\beta_r^{i,j} = g\left(\nu^{i,j}, P^r\right), \tag{9.2}$$

see Fig. 9.2 (values borrowed from the look up tables in [215]). The dynamic power reference on which the collective pitch reference depends is known. The WF controller computes the WF static power reference, denoted as P^f, as a function of the power requested by the operator and the power generated by the WF and it feeds each turbine with P^t verifying $P^t = P^f/N$. Then, the dynamic power reference of a turbine, P^r, fulfils

$$P^r(s) = \frac{\tau_p}{s + \tau_p} P^t(s), \tag{9.3}$$

where τ_p is a known transfer function coefficient ($\tau_p = 1.2$ rad/s). For its part, the effective wind speed is not known and only the measurement of the wind speed at the wind mast is available.

The misalignment of one or more blades of turbine (i, j) can be modeled as an additive fault, denoted $f^{i,j}$, affecting the measurement of the collective pitch angle $\beta^{i,j}$, denoted as $y^{i,j}$. The corresponding zero-mean Gaussian sensor noise of known variance ($\sigma_w^2 = 0.3^{\circ^2}$) is named after $w^{i,j}$. The objective of this chapter is to develop a FE and FDI strategy for the blade misalignment of the WTs in the WF.

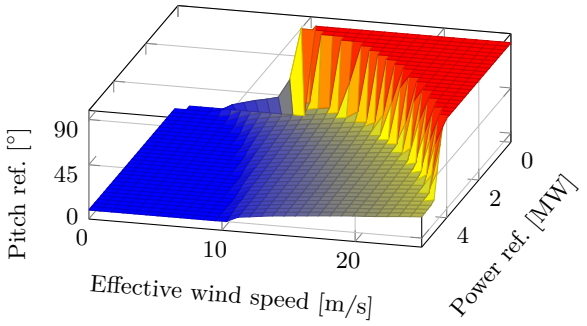

Figure 9.2. Nonlinear function $g\left(\nu^{i,j}, P^r\right)$.

9.3 Wind and pitch reference estimation

The first step to estimate the pitch misalignment faults is to provide an open-loop estimation strategy of the pitch reference which depends on the unknown effective wind speed. In this section, we first propose a propagation strategy to estimate this wind speed and we bound the errors associated to the wind speed estimation. Then, we use the estimated wind speed to estimate the pitch reference and we bound the pitch reference open-loop estimation error. See the open-loop estimation box in Fig. 9.4

9.3.1 Wind estimation

The wind speed acting on the WT (i, j), $\nu^{i,j}$, depends on the mean wind speed acting on the WTs in the i-th row, denoted as ν^i, and a zero-mean turbulence component of known variance ($\sigma_t = 0.2$ m^2/s^2), which we denote as $\widetilde{\nu}_t^{i,j}$:

$$\nu^{i,j} = \nu^i + \widetilde{\nu}_t^{i,j}. \tag{9.4}$$

The mean wind speed ν^i is not known and only the measurement of the wind speed at the wind mast is available:

$$\nu^0 = \hat{\nu}^0 + \widetilde{\nu}^0, \tag{9.5}$$

with ν^0 being the wind speed at the wind mast, $\hat{\nu}^0$ being its measurement and $\widetilde{\nu}^0$ being the corresponding sensor noise. From $\hat{\nu}^0$, we can estimate the mean wind speed acting on the WTs in the i-th row, ν^i, as detailed in Appendix C.2. Denoting the propagated mean wind speed as $\hat{v}^i$, the mean wind speed fulfils

$$\nu^i = \hat{\nu}^i + \widetilde{\nu}_p^i, \tag{9.6}$$

where $\widetilde{\nu}_p^i$ is the propagation error. This error derives from both the use of the noisy measurement $\hat{\nu}^0$ and the propagation model mismatch. Fig. C.1 in Appendix D.4.1 shows the wind speed estimation results for the turbines in the 0° layout.

From (9.4) and (9.6), we deduce that $\nu^{i,j}$ satisfies

$$\nu^{i,j} = \hat{\nu}^i + \widetilde{\nu}^{i,j}, \tag{9.7}$$

where $\widetilde{\nu}^{i,j}$ is the total wind speed estimation error and it verifies

$$\widetilde{\nu}^{i,j} = \widetilde{\nu}_p^i + \widetilde{\nu}_t^{i,j}. \tag{9.8}$$

Note that the propagation error $\widetilde{\nu}_p^i$ is common for all the turbines in the i-th row while the turbulence $\widetilde{\nu}_t^{i,j}$ is different for each turbine (i,j). The following assumption on these errors is made.

Assumption 9.1. *The errors in* (9.8) *can be considered to be bounded as follows.*

- *The propagation error $\widetilde{\nu}_p^i$ of the turbines in the i-th can be considered to be bounded as $|\widetilde{\nu}_p^i| \leq \lambda_p^i$, where λ_p^i is different for each row of turbines i (the propagation error increases with the distance between the wind mast and the turbines).*
- *The turbulence $\widetilde{\nu}_t^{i,j}$ of the turbine (i,j) can be considered to be bounded as $|\widetilde{\nu}_t^{i,j}| \leq \lambda_t$. We compute λ_t as $\lambda_t = 3\,\sigma_t$.*

In Appendix D.4.1 we validate the computation of these bounds through numerical simulations. Let us remark that this procedure is usually employed in observer-based applications [164, 309].

Remark 9.1. *The FE and FDI strategies developed in this chapter are independent of the wind propagation scheme. If other wind propagation strategies were used, the bounds λ_p^i would vary accordingly. Similar applies to the turbulence component that, if considered to be differently distributed, it would be bounded with a different value λ_t.*

9.3.2 Pitch reference estimation

The estimate $\hat{\nu}^i$ of the effective wind speed $\nu^{i,j}$ given by (C.2) is used to estimate the pitch reference (9.2) of the turbines in the i-th row as

$$\hat{\beta}_r^{i,j} = g\,(\hat{\nu}^i, P^r). \tag{9.9}$$

From (9.8), we deduce that the pitch reference estimation error can be disaggregated as

$$g\,(\nu^{i,j}, P^r) - g\,(\hat{\nu}^i, P^r) = \underbrace{g\,(\nu^{i,j}, P^r) - g\,(\nu^i, P^r)}_{\widetilde{u}^{i,j}} + \underbrace{g\,(\nu^i, P^r) - g\,(\hat{\nu}^i, P^r)}_{\widetilde{u}^i}, \tag{9.10}$$

where $\widetilde{u}^i$ derives from the propagation error $\widetilde{\nu}_p^i$ (i.e., $\widetilde{\nu}_p^i = \nu^i - \hat{\nu}^i$) and $\widetilde{u}^{i,j}$ derives from the turbulence $\widetilde{\nu}_t^{i,j}$ (i.e., $\widetilde{\nu}_t^{i,j} = \nu^{i,j} - \nu^i$). Thus, the error $\widetilde{u}^i$ is common for all the turbines in the i-th row while $\widetilde{u}^{i,j}$ is different for each turbine. For certain row i and for certain value of the estimated wind speed and of the dynamic power reference, one could compute the bounds of

these errors with the values λ_p^i and λ_t (which are the bounds of the wind speed estimation errors in Assumption 9.1) as

$$|\widetilde{u}^i| \leq \max \left\{ \begin{array}{l} |g\left(\hat{\nu}^i + \lambda_p^i, P^r\right) - g\left(\hat{\nu}^i, P^r\right)|, \\ |g\left(\hat{\nu}^i - \lambda_p^i, P^r\right) - g\left(\hat{\nu}^i, P^r\right)| \end{array} \right\}, \tag{9.11a}$$

$$|\widetilde{u}^{i,j}| \leq \max \left\{ \begin{array}{l} |g\left(\hat{\nu}^i + \lambda_p^i + \lambda_t, P^r\right) - g\left(\hat{\nu}^i + \lambda_p^i, P^r\right)|, \\ |g\left(\hat{\nu}^i + \lambda_p^i - \lambda_t, P^r\right) - g\left(\hat{\nu}^i + \lambda_p^i, P^r\right)|, \\ |g\left(\hat{\nu}^i - \lambda_p^i + \lambda_t, P^r\right) - g\left(\hat{\nu}^i - \lambda_p^i, P^r\right)|, \\ |g\left(\hat{\nu}^i - \lambda_p^i - \lambda_t, P^r\right) - g\left(\hat{\nu}^i - \lambda_p^i, P^r\right)| \end{array} \right\}. \tag{9.11b}$$

Note that we express these bounds in terms of $\hat{\nu}^i$ because the variables $\nu^{i,j}$ and ν^i are not available. Since the function $g\left(\cdot\right)$ is nonlinear, these errors are different for the different values of $\hat{\nu}^i$ and P^r. Then, the following assumption is made.

Assumption 9.2. *The errors in* (9.10) *can be considered to be bounded as*

$$|\widetilde{u}^i| \leq \lambda_1^i(\hat{\nu}^i, P^r), \tag{9.12a}$$

$$|\widetilde{u}^{i,j}| \leq \lambda_2^i(\hat{\nu}^i, P^r), \tag{9.12b}$$

where $\lambda_1^i(\hat{\nu}^i, P^r)$ *and* $\lambda_2^i(\hat{\nu}^i, P^r)$ *are different for each row* i *and depend on the inputs of the function* $g\left(\cdot\right)$.

The variables $\hat{\nu}^i$ and P^r can be considered to be bounded by the sets

$$\hat{\nu}^i \in \Omega_\nu, \;\; \Omega_\nu := \{\underline{\nu} < \hat{\nu}^i < \bar{\nu}\}, \tag{9.13a}$$

$$P^r \in \Omega_p, \;\; \Omega_p := \{\underline{P} < P^r < \bar{P}\}, \tag{9.13b}$$

where $\underline{\nu}$, $\bar{\nu}$, $\underline{P}$ and $\bar{P}$ are the minimum and maximum possible values of these parameters (which we fix to $\underline{\nu} = 0$ m/s, $\bar{\nu} = 25$ m/s, $\underline{P} = 0$ MW and $\bar{P} = 4.8$ MW). The parameter vector $\theta = \begin{bmatrix} \hat{\nu}^i \\ P^r \end{bmatrix}$ lies then in $\Theta = \Omega_\nu \times \Omega_p$. Let us partition the parameter set Θ into N_θ subsets $\{\Theta^{(q)}\}_{q\in\{1,\ldots,N_\theta\}}$ by dividing Ω_ν into N_ν intervals (i.e., $\{\Omega_\nu^{(q_\nu)}\}_{q_\nu\in\{1,\ldots,N_\nu\}}$) and Ω_p into N_p intervals (i.e., $\{\Omega_p^{(q_p)}\}_{q_p\in\{1,\ldots,N_p\}}$). Thus, we have $N_\theta = N_\nu \cdot N_p$ (see Fig. 9.3). For each row i, $\widetilde{u}^i$ and $\widetilde{u}^{i,j}$ are bounded as

$$|\widetilde{u}^i| \leq \lambda_{1,q}^i \quad \text{if } \theta \in \Theta^{(q)}, \tag{9.14a}$$

$$|\widetilde{u}^{i,j}| \leq \lambda_{2,q}^i \quad \text{if } \theta \in \Theta^{(q)}, \tag{9.14b}$$

where

$$\lambda_{1,q}^i = \max_{\theta\in\Theta^{(q)}} \left\{ \begin{array}{l} |g\left(\hat{\nu}^i, P^r\right) - g\left(\hat{\nu}^i + \lambda_p^i, P^r\right)| \\ |g\left(\hat{\nu}^i, P^r\right) - g\left(\hat{\nu}^i - \lambda_p^i, P^r\right)| \end{array} \right\}. \tag{9.15}$$

Similar applies to $\lambda_{2,q}^i$, whose value is deduced from (9.11b) along the values θ such that $\theta \in \Theta^{(q)}$. In Appendix D.4.1, we detail the computation of these bounds (we choose $N_\nu = N_p = 7$).

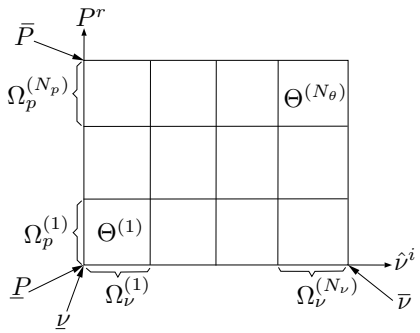

Figure 9.3. Partition of the two-dimensional parameter set ($N_\nu = 4$ and $N_p = 3$)

9.4 FE and FDI of pitch misalignments

In this section we develop a model-based FE and FDI strategy of the misalignment of the blades of the WTs in the WF. It is well known that most continuous-time control systems are implemented digitally [323]. Thus, we develop the discrete state-space model of the pitch system described in Section 9.2:

$$\beta_{k+1}^{i,j} = \alpha\, \beta_k^{i,j} + (1-\alpha)\, g\,(\nu_k^{i,j}, P_k^r), \tag{9.16a}$$

$$y_k^{i,j} = \beta_k^{i,j} + f_k^{i,j} + w_k^{i,j}. \tag{9.16b}$$

The discrete transfer function coefficient α is derived from τ_β in (9.1) with an appropriate sampling time, which we fix to $T_s = 0.1$ s. The following assumption on the faults $f^{i,j}$ is made.

Assumption 9.3. *Define the variation $\delta^{i,j}$ of the fault $f^{i,j}$ as*

$$\delta^{i,j}(k) = f^{i,j}(k+1) - f^{i,j}(k). \tag{9.17}$$

We assume that $\delta^{i,j}$ is energy bounded.

The faults verifying Assumption 9.3 can be modeled through

$$\xi_{k+1}^{i,j} = a_F\, \xi_k^{i,j} + b_F\, \delta_k^{i,j}, \tag{9.18a}$$

$$f_k^{i,j} = c_F\, \xi_k^{i,j}, \tag{9.18b}$$

with $\xi^{i,j}$ being the fault state and $a_F = b_F = c_F = 1$. Any individual fault $f[j] = f^{i,j}$ is extracted from f as $f[j] = F^j\, f$ where F^j is the selection matrix defined as $F^j = \begin{bmatrix} \mathbf{0}_{j-1} & 1 & \mathbf{0}_{n_j - j} \end{bmatrix}$.

Remark 9.2. *Assumption 9.3 is common in FE and it considers faults whose variations are slow with respect to the dynamics of the system and it can cover the typical faults in engineering systems such as abrupt faults and incipient faults [99, 323]. In any case, the strategies developed in this work can be easily extended to systems whose faults do not verify Assumption 9.3. If more complex fault signals affected the system, model* (9.18) *should be modify accordingly. See, for instance, the models developed in [307] for faults in the form of a polynomial of the time.*

Provided Assumption 9.3, we extend the model (9.16) to include the dynamics (9.18). As explained in Section 9.3.2, the estimated pitch reference is the same for all the turbines in the i-th row. Thus, we model all these turbines simultaneously. In all, the discrete extended state-space model of the pitch systems of the i-th row of WTs is given by the following model with $z \in \mathbb{R}^{2\,n_j}$ being the extended state vector that stacks the collective pitch angles $\beta^{i,j}$ and the fault states $\xi^{i,j}$ of the turbines in the i-th row from $j = 1$ to $j = n_j$. Similar applies to $u \in \mathbb{R}^{n_j}$, $y \in \mathbb{R}^{n_j}$, $w \in \mathbb{R}^{n_j}$, $f \in \mathbb{R}^{n_j}$ and $\delta \in \mathbb{R}^{n_j}$, which are the input, output, noise, fault and fault generator vectors.

$$z_{k+1} = \underbrace{\left[\begin{array}{c|c} \alpha\, I_{n_j} & 0 \\ \hline 0 & I_{n_j} \end{array}\right]}_{A} \underbrace{\left[\begin{array}{c} \beta_k^{i,1} \\ \vdots \\ \beta_k^{i,n_j} \\ \hline \xi_k^{i,1} \\ \vdots \\ \xi_k^{i,n_j} \end{array}\right]}_{z_k} + \underbrace{\left[\begin{array}{c|c} (1-\alpha)\, I_{2\,n_j} \end{array}\right]}_{B} \underbrace{\left[\begin{array}{c} g\left(\nu_k^{i,1}, P_k^r\right) \\ \vdots \\ g\left(\nu_k^{i,n_j}, P_k^r\right) \\ \hline 0 \end{array}\right]}_{u_k} + \underbrace{\left[\begin{array}{c} 0 \\ \hline I_{n_j} \end{array}\right]}_{D} \underbrace{\left[\begin{array}{c} \delta_k^{i,1} \\ \vdots \\ \delta_k^{i,n_j} \end{array}\right]}_{\delta_k},$$

$$\underbrace{\left[\begin{array}{c} y_k^{i,1} \\ \vdots \\ y_k^{i,n_j} \end{array}\right]}_{y_k} = \underbrace{\left[\begin{array}{cc} I_{n_j} & I_{n_j} \end{array}\right]}_{C} z_k + \underbrace{\left[\begin{array}{c} w_k^{i,1} \\ \vdots \\ w_k^{i,n_j} \end{array}\right]}_{w_k},$$

$$\underbrace{\left[\begin{array}{c} f_k^{i,1} \\ \vdots \\ f_k^{i,n_j} \end{array}\right]}_{f_k} = \underbrace{\left[\begin{array}{cc} 0 & I_{n_j} \end{array}\right]}_{R} z_k,$$

In summary, we have

$$z_{k+1} = A\, z_k + B\, u_k + D\, \delta_k, \tag{9.19a}$$

$$y_k = C\, z_k + w_k, \tag{9.19b}$$

$$f_k = R\, z_k, \tag{9.19c}$$

$$f_k[j] = F^j\, f_k. \tag{9.19d}$$

The pitch references $g\left(\nu^{i,j}, P^r\right)$ are not available. Then, we build a model-based observer for the system (9.19) based on the open-loop estimates (9.9). Provided that the bounds of the errors associated to these estimated variables depend on θ, we propose to use parameter-dependent gain matrices in the observer. Then, we have the following fault estimator

$$\hat{z}_{k+1} = A\, \hat{z}_k + B \underbrace{\left[\begin{array}{c} \mathbf{1}_{n_j \times 1} \\ 0 \end{array}\right] g\left(\hat{\nu}_k^i, P_k^r\right)}_{\hat{u}_k} + L(\theta_k)\left(y_k - C\, \hat{z}_k\right), \tag{9.20a}$$

$$\hat{f}_k = R\, \hat{z}_k + K(\theta_k)\left(y_k - C\, \hat{z}_k\right), \tag{9.20b}$$

where $L(\theta_k)$ and $K(\theta_k)$ are the parameter-dependent design gain matrices of appropriate dimensions. Given the bounds in (9.14), we define $L(\theta_k)$ and $K(\theta_k)$ as

$$L(\theta_k) = L_q \quad \text{if } \theta_k \in \Theta^{(q)}, \tag{9.21a}$$

$$K(\theta_k) = K_q \quad \text{if } \theta_k \in \Theta^{(q)}, \tag{9.21b}$$

and the design gain matrices become the finite set of gain matrices L_q and K_q with $q = 1, \ldots, N_\theta$ (i.e., $L(\theta_k) \in \{L_1, \ldots, L_q, \ldots, L_{N_\theta}\}$ and $K(\theta_k) \in \{K_1, \ldots, K_q, \ldots, K_{N_\theta}\}$). Define the extended state estimation error as $\widetilde{z}_k = z_k - \hat{z}_k$ and the fault estimation error as $\widetilde{f}_k = f_k - \hat{f}_k$. It follows that

$$\widetilde{z}_{k+1} = (A - L(\theta_k)\, C)\, \widetilde{z}_k + B\,(u_k - \hat{u}_k) + D\,\delta_k - L(\theta_k)\, w_k, \tag{9.22a}$$

$$\widetilde{f}_k = (R - K(\theta_k)\, C)\, \widetilde{z}_k - K(\theta_k)\, w_k. \tag{9.22b}$$

The difference $u_k - \hat{u}_k$ refers to the pitch reference estimation errors. As detailed in Section 9.3.2, this error can be disaggregated as

$$u_k - \hat{u}_k = \begin{bmatrix} g\,(\nu_k^{i,1}, P_k^r) - g\,(\hat{\nu}_k^i, P_k^r) \\ \vdots \\ g\,(\nu_k^{i,n_j}, P_k^r) - g\,(\hat{\nu}_k^i, P_k^r) \\ 0 \end{bmatrix} = \underbrace{\begin{bmatrix} \mathbf{1}_{n_j \times 1} \\ 0 \end{bmatrix}}_{E_0} \underbrace{\widetilde{u}_k^i}_{p_k} + \underbrace{\begin{bmatrix} I_{n_j} \\ 0 \end{bmatrix}}_{F_0} \underbrace{\begin{bmatrix} \widetilde{u}_k^{i,1} \\ \vdots \\ \widetilde{u}_k^{i,n_j} \end{bmatrix}}_{t_k}. \tag{9.23}$$

where p_k is the pitch reference estimation error due to the error on the wind speed propagation scheme and it is common to all the turbines in the i-th row. Vector t_k contains the pitch reference estimation error due to the wind speed estimation error caused by the turbulence of each turbine. Provided the bounds (9.14), we deduce that the vectors p_k and t_k are bounded as

$$\|p_k\|_\infty \leq \lambda_{1,q}^i \quad \text{if } \theta_k \in \Theta^{(q)}, \tag{9.24a}$$

$$\|t_k\|_\infty \leq \lambda_{2,q}^i \quad \text{if } \theta_k \in \Theta^{(q)}. \tag{9.24b}$$

Remark 9.3. *Since p_k is common to all the turbines in the i-th row, the effect of the wind propagation error on FE is diminished when all these turbines are considered simultaneously by the same observer. This is the main reason to build one fault estimator* (9.20) *for each row of turbines i.*

Regarding FDI, we set the following set of fault evaluators ($j = 1, \ldots, n_j$):

$$\begin{cases} \text{if } |\hat{f}_k[j]| \geq J_k[j]\,, & \text{Fault } f[j] \\ \text{otherwise}\,, & \text{No fault } f[j] \end{cases}, \tag{9.25}$$

where $J[j]$ is an adaptive threshold to be computed online. Note that the fault evaluator (9.25) achieves fault detection and fault isolation simultaneously. For simplicity sake and considering that fault isolation (FI) implies fault detection, the remainder of this chapter utilizes the term FI to refer to FDI.

In the following, we present a multiobjective approach to design offline the gain matrices L_q and K_q ($q = 1, \ldots, N_\theta$) of the model-based observer and to compute online the adaptive thresholds $J[j]$ of the decision mechanism.

9.5 Fault estimator and evaluator design

9.5.1 Fault estimator design

From (9.22)-(9.23), it yields

$$\widetilde{z}_{k+1} = (A - L(\theta_k)\, C)\, \widetilde{z}_k + E\, p_k + F\, t_k + D\, \delta_k - L(\theta_k)\, w_k, \tag{9.26a}$$

$$\widetilde{f}_k = (R - K(\theta_k)\, C)\, \widetilde{z}_k - K(\theta_k)\, w_k, \tag{9.26b}$$

with $E = B\, E_0$ and $F = B\, F_0$. The fault estimation error depends on the following exogenous signals:

(a) the fault generator δ satisfying Assumption 9.3,

(b) the noises w satisfying $w \sim \mathcal{N}(0, W)$ with $W = \sigma_w^2\, I_{n_j}$,

(c) the unknown inputs p and t satisfying the bounds (9.24).

The error caused by δ describes the fault tracking ability of the observer and the errors caused by w, p and t describe the robustness of the observer against noises and uncertainties. Hence, we propose to characterize the fault tracking ability of the observer by the cumulative squared error (CSE) experienced by each estimate $\hat{f}[j]$ (i.e., $\|\widetilde{f}[j]\|_2^2 = \sum_{k=1}^{\infty} \widetilde{f}[j]^2$) when it faces a unitary impulse $\delta[m]$ (which generates a unitary step fault $f[m]$):

$$\gamma_m^j = \max_{\theta \in \Theta} \frac{\|\widetilde{f}[j]\|_2^2}{\|\delta[m]\|_2^2}, \qquad \begin{array}{c} \delta_k[m] = \{1, 0, 0, \ldots\}, \\ \delta[n] = 0,\ \forall n \neq m, \\ w = 0,\ p = 0,\ t = 0. \end{array} \tag{9.27a}$$

Similarly, we characterize the robustness of the observer by the root-mean-square (RMS) error experienced by estimate $\hat{f}[j]$ (i.e., $\|\widetilde{f}[j]\|_{RMS} = \lim_{K \to \infty} \sqrt{\frac{1}{K} \sum_{k=1}^{K} \widetilde{f}[j]^2}$) due to the noises (b) and the UIs (c):

$$\gamma_w^j = \max_{\theta \in \Theta} \frac{\|\widetilde{f}[j]\|_{RMS}^2}{\sigma_w^2}, \qquad \delta = 0,\ p = 0,\ t = 0; \tag{9.27b}$$

$$\gamma_p^j = \max_{\theta \in \Theta} \frac{\|\widetilde{f}[j]\|_{RMS}^2}{\|p\|_\infty^2}, \qquad \delta = 0,\ w = 0,\ t = 0; \tag{9.27c}$$

$$\gamma_t^j = \max_{\theta \in \Theta} \frac{\|\widetilde{f}[j]\|_{RMS}^2}{\|t\|_\infty^2}, \qquad \delta = 0,\ w = 0,\ p = 0. \tag{9.27d}$$

There exists thus a trade-off between ameliorating the fault tracking ability of the observer and its robustness [106, 249]. From the practical viewpoint, it is of considerable interest to achieve certain tracking ability and to minimize the effect of the noises and uncertainties on the estimations [327]. Thus, we propose to design the observer gain matrices through the following optimization problem

$$\begin{array}{ll} \underset{\{L_q, K_q\}_{q \in \{1, \ldots, n_\theta\}}}{\text{minimize}} & \displaystyle\sum_{j=1}^{n_j} \left(\gamma_w^j\, \sigma_w^2 + \gamma_p^j\, \|p\|_\infty^2 + \gamma_t^j\, \|t\|_\infty^2 \right) \\ \text{subject to} & \gamma_m^j \leq \bar{\gamma}_m^j\,, \quad \forall j, m \\ & \text{stability of (9.26)}\,, \quad \theta \in \Theta \end{array} \tag{9.28}$$

Remark 9.4. *Note that γ_m^j with $m \neq j$ denotes the CSE experienced by the fault estimate in the j-th fault channel due to a unitary step fault in another channel m while γ_j^j denotes the CSE experienced due to a unitary step fault in the own channel j. Hence, the CSE requirements $\bar{\gamma}_m^j$ $(m = 1, \ldots, j-1, j+1, \ldots, n_j)$ are generally chosen to be smaller than the corresponding CSE requirement*[1] *$\bar{\gamma}_j^j$.*

The system (9.26) operates in a finite set of multiple modes because

$$L(\theta_k) \in \{L_q\}_{q\in\{1,\ldots,n_\theta\}}\,, \tag{9.29a}$$

$$K(\theta_k) \in \{K_q\}_{q\in\{1,\ldots,n_\theta\}}\,. \tag{9.29b}$$

A general theory of such systems is developed in the switched systems community [62, 183, 273]. The results for switched systems under arbitrary switchings are rather conservative and much tighter results can be developed if further assumptions hold [123]. Take as an example a Markovian jump linear system where the switching process can be described by a Markov chain [57]. In this work, we consider that the parameter θ is slow-varying compared to the dynamics of (9.26). Thus, the membership of θ to a subset $\Theta^{(q)}$ infrequently switches to another subset $\Theta^{(p\neq q)}$. In this fashion, we translate the optimization problem (9.28) into another design problem ensuring global stability in the set Θ and certain local steady-state performance in each subset $\Theta^{(q)}$:

$$\begin{aligned} \underset{\{L_q,K_q\}_{q\in\{1,\ldots,n_\theta\}}}{\text{minimize}} \quad & \sum_{q=1}^{N_\theta}\sum_{j=1}^{n_j}\left(\gamma_{w,q}^j\,\sigma_w^2 + \gamma_{p,q}^j\,(\lambda_{1,q}^i)^2 + \gamma_{t,q}^j\,(\lambda_{2,q}^i)^2\right) \\ \text{subject to} \quad & \gamma_{m,q}^j \leq \bar{\gamma}_m^j\,, \quad \forall j, m, q \\ & \text{stability of (9.26)}\,, \quad \theta \in \Theta \end{aligned} \tag{9.30}$$

where $\gamma_{m,q}^j$, $\gamma_{w,q}^j$, $\gamma_{p,q}^j$, $\gamma_{t,q}^j$ denote the maximums in (9.27) when $\theta \in \Theta^{(q)}$, e.g.,

$$\gamma_{m,q}^j = \max_{\theta\in\Theta^{(q)}} \frac{\|\widetilde{f}[j]\|_2^2}{\|\delta[m]\|_2^2}, \qquad \begin{array}{c} \delta_k[m] = \{1, 0, 0, \ldots\}, \\ \delta[n] = 0,\ \forall n \neq m, \\ w = 0,\ p = 0,\ t = 0. \end{array} \tag{9.31}$$

Unlike γ_m^j, γ_w^j, γ_p^j, γ_t^j, which depend on $\{L_q, K_q\}_{q\in\{1,\ldots,n_\theta\}}$, $\gamma_{m,q}^j$, $\gamma_{w,q}^j$, $\gamma_{p,q}^j$, $\gamma_{t,q}^j$ only depend on L_q and K_q. Note that in (9.30), we have taken into account that $\|p\|_\infty \leq \lambda_{1,q}^i$ if $\theta \in \Theta^{(q)}$ because $\|p_k\|_\infty$ satisfies (9.24). Similar applies to $\|t\|_\infty$. In all, an observer designed through the optimization problem (9.30) is globally stable inside the set Θ regardless of the parameter dynamics and it guarantees certain local performance trade-off in each subset $\Theta^{(q)}$ provided infrequent changes of subset membership. Similar approaches are utilized in practical works as [25, 47, 308].

Remark 9.5. *The density N_θ of the grid $\{\Theta^{(q)}\}$ is to be determined from a trade-off between having*

[1] In order to approximately fix the χ% settling times of the observer, we can approximate the fault observer responses to the response of a first-order system. Hence, if we fix $\bar{\gamma}_j^j = \frac{1}{1-(1+\log(1-\chi/100)/\bar{T}^j)^2}$, the χ% settling time of the j-th fault estimate due to a step fault $f[j]$ is approximated to $\bar{T}^j$.

- *a few gridding intervals that ensure reduced computational burden and infrequent changes of subset membership but introduce conservatism,*
- *a lot of gridding intervals causing heavy computational time and more frequent changes of subset membership but reducing performance conservatism.*

As previously specified, we choose $N_\nu = N_p = 7$ (see Appendix D.4.1). This gridding is a posteriori validated through the numerical simulations in Section 9.7.

Regarding the stability requirement in (9.30), it should be noted that even when all the subsystems of a switched system are stable, such a system may fail to preserve stability. It is well-known in switched systems theory that a necessary and sufficient condition to ensure the stability of (9.26) is the existence of N_θ positive-definite matrices $P_1, \ldots, P_{N_\theta}$ satisfying ([62])

$$(A - L_q\, C)^T\, P_p\, (A - L_q\, C) - P_q \preceq 0, \quad \forall (q,p) \in \{1, \ldots N_\theta\} \times \{1, \ldots N_\theta\}. \tag{9.32}$$

Regarding the performance requirements in (9.30), let us apply the $\mathcal{Z}$ transform to (9.26) when $\theta \in \Theta^{(q)}$; it yields

$$\widetilde{f}[j](z) = \sum_{m=1}^{n_j} \Big(G^j_{m,q}(z)\, \delta[m](z) \Big) + G^j_{w,q}(z)\, w(z) + G^j_{p,q}(z)\, p(z) + G^j_{t,q}(z)\, t(z), \tag{9.33}$$

with

$$G^j_{m,q}(z) = -M^j_q(z)\, D\, (F^m)^T, \tag{9.34a}$$
$$G^j_{w,q}(z) = M^j_q(z)\, L_q + K_q, \tag{9.34b}$$
$$G^j_{p,q}(z) = M^j_q(z)\, E, \tag{9.34c}$$
$$G^j_{t,q}(z) = M^j_q(z)\, F, \tag{9.34d}$$

and $M^j_q(z) = F^j\, (R - K_q\, C)(z\, I - A + L_q\, C)^{-1}$. It is well-known that $\gamma^j_{m,q}$, $\gamma^j_{w,q}$, $\gamma^j_{p,q}$, $\gamma^j_{t,q}$ fulfil ([269])

$$\gamma^j_{m,q} = \|G^j_{m,q}(z)\|_2^2, \tag{9.35a}$$
$$\gamma^j_{w,q} = \|G^j_{w,q}(z)\|_2^2, \tag{9.35b}$$
$$\gamma^j_{p,q} \leq \|G^j_{p,q}(z)\|_\infty^2, \tag{9.35c}$$
$$\gamma^j_{t,q} \leq \|G^j_{t,q}(z)\|_\infty^2, \tag{9.35d}$$

where $\|G(z)\|_2$ and $\|G(z)\|_\infty$ denote, respectively, the $\mathscr{H}_2$ norm and the $\mathscr{H}_\infty$ norm of a system $G(z)$. In all, (9.30) can be rewritten as

$$\begin{array}{ll} \underset{\{L_q, K_q, P_q, Q_q\}_{q \in \{1,\ldots,n_\theta\}}}{\text{minimize}} & \displaystyle\sum_{q=1}^{N_\theta} \sum_{j=1}^{n_j} \Big(\|G^j_{w,q}(z)\|_2^2\, \sigma_w^2 + \|G^j_{p,q}(z)\|_\infty^2\, (\lambda^i_{1,q})^2 + \|G^j_{t,q}(z)\|_\infty^2\, (\lambda^i_{2,q})^2 \Big) \\ \text{subject to} & \|G^j_{m,q}(z)\|_2^2 \leq \bar{\gamma}^j_m\,, \quad \forall j, m, q \\ & \text{matrix inequalities in (9.32)} \end{array} \tag{9.36}$$

This optimization problem ensures global stability in the set Θ and certain local steady-state performance in each subset $\Theta^{(q)}$. It can be solved using different numerical approaches as genetic algorithms. In the following we briefly show how to translate this problem into a convex optimization problem based on linear matrix inequalities (LMIs).

Convex formulation of the observer design optimization problem

The observer design optimization problem (9.36) can be reformulated as a multiobjective convex optimization problem as follows.

$$\begin{aligned} \text{minimize} \quad & \sum_{q=1}^{N_\theta} \sum_{j=1}^{n_j} \left(\gamma_{w,q}^{j}\, \sigma_w^2 + \gamma_{p,q}^{j}\, (\lambda_{1,q}^{i})^2 + \gamma_{t,q}^{j}\, (\lambda_{2,q}^{i})^2 \right) \\ \text{subject to} \quad & \Xi_{q,p}^{1} \succeq 0, \qquad\qquad \forall (q,p) \in \{1,\dots N_\theta\} \times \{1,\dots N_\theta\} \\ & \Xi_{q,j}^{\{2,3,4,5,6,7\}} \succeq 0, \quad \forall (q,j) \in \{1,\dots N_\theta\} \times \{1,\dots n_j\} \end{aligned} \tag{9.37}$$

along the full-rank matrices Q_q, K_q, X_q; symmetric matrices $P_{q,j}$, $R_{q,j}$, $S_{q,j}$, $T_{q,j}$, $V_{q,j}$; and scalars $\gamma_{q,j}^{w}$, $\gamma_{q,j}^{p}$ and $\gamma_{q,j}^{t}$ for $q = 1,\dots,N_\theta$ and $j = 1,\dots,n_j$. The LMIs in (9.37) are defined as[2]

$$\Xi_{q,p}^{1} = \begin{bmatrix} Q_q + Q_q^T - P_p & \Xi_q \\ \star & P_q \end{bmatrix}, \tag{9.38a}$$

$$\Xi_{q,j}^{2} = \begin{bmatrix} Q_q + Q_q^T - R_{q,j} & \Xi_q & 0 \\ \star & R_{q,j} & \Psi_q^j \\ \star & \star & I \end{bmatrix}, \quad \Xi_{q,j}^{3} = \begin{bmatrix} Q_q + Q_q^T - R_{q,j} & Q_q\, D \\ \star & \Gamma_q^j \end{bmatrix}, \tag{9.38b}$$

$$\Xi_{q,j}^{4} = \begin{bmatrix} Q_q + Q_q^T - S_{q,j} & \Xi_q & 0 \\ \star & S_{q,j} & \Psi_q^j \\ \star & \star & I \end{bmatrix}, \quad \Xi_{q,j}^{5} = \begin{bmatrix} Q_q + Q_q^T - S_{q,j} & X_q & 0 \\ \star & \gamma_{w,q}^{j} I & (F^j\, K_q)^T \\ \star & \star & I \end{bmatrix} \tag{9.38c}$$

$$\Xi_{q,j}^{6} = \begin{bmatrix} Q_q + Q_q^T - T_{q,j} & \Xi_q & Q_q\, E & 0 \\ \star & T_{q,j} & 0 & \Psi_q^j \\ \star & \star & \gamma_{p,q}^{j} I & 0 \\ \star & \star & \star & I \end{bmatrix}, \tag{9.38d}$$

$$\Xi_{q,j}^{7} = \begin{bmatrix} Q_q + Q_q^T - V_{q,j} & \Xi_q & Q_q\, F & 0 \\ \star & V_{q,j} & 0 & \Psi_q^j \\ \star & \star & \gamma_{t,q}^{j} I & 0 \\ \star & \star & \star & I \end{bmatrix}, \tag{9.38e}$$

with $\Xi_q = Q_q\, A - X_q\, C$, $\Psi_q^j = (F^j\, R - F^j\, K_q\, C_q)^T$ and

$$\Gamma_q^j = \begin{bmatrix} \bar{\gamma}_1^j & 0 & 0 \\ 0 & \ddots & 0 \\ 0 & 0 & \bar{\gamma}_{n_j}^j \end{bmatrix}. \tag{9.39}$$

[2]The symbol $\star$ in a block matrix denotes the blocks induced by symmetry.

The gains L_q are then defined as $L_q = Q_q^{-1} X_q$. The proofs associated to this procedure are similar to the ones presented in the previous chapters of the thesis and can be derived from the reference works [62,69,252,324], where it is shown how to translate a multiobjective optimization problem into a convex optimization problem based on LMIs by means of introducing of slack variables, here named after $\{Q_q\}_{q\in\{1,\dots,N_\theta\}}$.

9.5.2 Fault evaluator design

To characterize the behavior of the FI decision mechanism (9.25) that evaluates the fault estimates provided by the observer (9.20), we propose to use the parameters defined as follows.

- The *false isolation rate* (FIR) of the fault j, which we denote as ϕ^j, is the probability of rising alarms of the j-th fault when no fault exists (i.e., $f = 0$).
- The *minimum isolable fault* j (MIF), which we denote as υ^j, is the smallest value of a constant fault $f[j]$ which ensures that the alarm of fault j raises at some sample k_j provided the non-existence of other faults and disturbances (i.e., $f[m \neq j] = 0$, $w = 0$, $p = 0$, $t = 0$).
- The *isolation time* (IT) of fault j, which we denote as τ^j, is the time elapsed between the sample k_a of appearance of a fault $f[j]$ and the sample k_j in which the alarm is raised provided the non-existence of other faults and disturbances (i.e., $f[m \neq j] = 0$, $w = 0$, $p = 0$, $t = 0$).

The decision mechanisms (9.25) consist of both the thresholds $J[j]$ and the estimates $\hat{f}[j]$ provided by (9.20). The values of the thresholds $J[j]$ fix the trade-off between the certainness and uncertainness of the FI decision. Then, for certain estimator (9.20), as the thresholds $J[j]$ increase, so does the certainness of the decisions and the FIRs decrease while the MIFs and ITs increase. Since the observer gain matrices are already designed through the optimization problem (9.36), we can only arbitrarily fix the thresholds $J[j]$. Hence, it is only possible to guarantee a performance requirement over one of the aforementioned isolation performance parameters. We propose to online compute the adaptive thresholds for guaranteeing certain FIRs of the fault evaluator.

The requirement over the FIRs concerns the case in which $\delta = 0$ and $f = 0$ (i.e., $\hat{f} = -\widetilde{f}$). In this case, the estimation error sources are the noises (b) and the UIs (c). In the following, we characterize the probability that, in the absence of faults, $\hat{f}[j]$ exceeds certain value due to each of these error sources.

- The signal $\hat{f}[j]$ due to the noises w is zero-mean and Gaussian because the noises w are zero-mean and Gaussian. Its time-varying variance is equal to the marginal variance of the fault estimation error $\widetilde{f}[j]$, which is given by the j-th diagonal element of $\mathbf{\Sigma}_k^f = \mathbb{E}\{\hat{f}_k \hat{f}_k^T\}$ (i.e., $\mathbf{\Sigma}_k^f[j,j]$) and it can be computed as

$$\mathbf{\Sigma}_{k+1} = (A - L(\theta_k)\, C)\, \mathbf{\Sigma}_k\, (A - L(\theta_k)\, C)^T + L(\theta_k)\, W\, L(\theta_k)^T, \tag{9.40a}$$

$$\mathbf{\Sigma}_k^f = (R - K(\theta_k)\, C)\, \mathbf{\Sigma}_k\, (R - K(\theta_k)\, C)^T + K(\theta_k)\, W\, K(\theta_k)^T, \tag{9.40b}$$

with $L(\theta_k)$ and $K(\theta_k)$ being selected through (9.21)[3]. Taking account of the properties of the probability distribution function of a zero-mean Gaussian variable, if $\delta = 0$, $p = 0$ and $t = 0$, we have that

$$\mathbb{P}\left\{|\hat{f}_k[j]| > \Phi_Z^{-1}(1-\phi^j/2)\sqrt{\mathbf{\Sigma}_k^f[j,j]}\right\} \leq \phi^j, \tag{9.41}$$

with $\Phi_Z^{-1}(\cdot)$ being the inverse cumulative distribution function of a standard normal variable.

- The statistical properties of the signal $\hat{f}[j]$ due to the UIs p and t are unknown. Thus, we propose to approximate its probability distribution function to a zero-mean uniform distribution. If $\theta \in \Theta^{(q)}$, $\delta = 0$, $w = 0$ and $t = 0$, the inequality

$$\|\widetilde{f}[j]\|_{RMS} \leq \|G_{p,q}^j(z)\|_\infty \lambda_{1,q}^i \tag{9.42}$$

holds for infrequent changes of subset membership[4]. Thus, taking account of the properties of the probability distribution function of a zero-mean uniform variable[5] , we have that

$$\mathbb{P}\left\{|\hat{f}_k[j]| > \sqrt{3}\,\|G_{p,q}^j(z)\|_\infty \lambda_{1,q}^i\right\} \approx 0. \tag{9.43}$$

Similar applies to the error caused by t.

Given these probabilities, we online compute the adaptive thresholds $J[j]$ for approximately bounding the FIRs (i.e., $\phi^j \lessapprox \bar{\phi}^j$ for $j = 1, \ldots, n_j$) as

$$J_k[j] = \Phi_Z^{-1}(1-\bar{\phi}^j/2)\sqrt{\mathbf{\Sigma}_k^f[j,j]} + \bar{p}(\theta_k) + \bar{t}(\theta_k), \quad \forall j \tag{9.44}$$

with

$$\bar{p}(\theta_k) = \bar{p}_q \quad \text{if } \theta_k \in \Theta^{(q)}, \tag{9.45a}$$
$$\bar{t}(\theta_k) = \bar{t}_q \quad \text{if } \theta_k \in \Theta^{(q)}, \tag{9.45b}$$

and where $\bar{p}$ and $\bar{t}$ are computed offline as

$$\bar{p}_q = \sqrt{3}\,\|G_{p,q}^j(z)\|_\infty \lambda_{1,q}^i, \tag{9.46a}$$
$$\bar{t}_q = \sqrt{3}\,\|G_{t,q}^j(z)\|_\infty \lambda_{2,q}^i, \tag{9.46b}$$

with the designed gains L_q and K_q for $q = 1, \ldots, N_\theta$. In all, the proposed FE and FI strategy is summarized in Fig. 9.4.

[3]These Riccati equations have been obtained with $\delta(z) = 0$, $p(z) = 0$, $t(z) = 0$ and using an internal realization of the transfer function between w and $\widetilde{f}$.

[4]From the definition of $\gamma_{p,q}^j$, we have $\|\widetilde{f}[j]\|_{RMS} \leq \gamma_{p,q}^j \|p\|_\infty$; from (9.35), we have $\gamma_{p,q}^j \leq \|G_{p,q}^j(z)\|_\infty$; and from (9.24), we have $\|p\|_\infty \leq \lambda_{1,q}^i$.

[5]If x is a zero-mean uniform variable, then $|x| < \sqrt{3}\,\|x\|_{RMS}$.

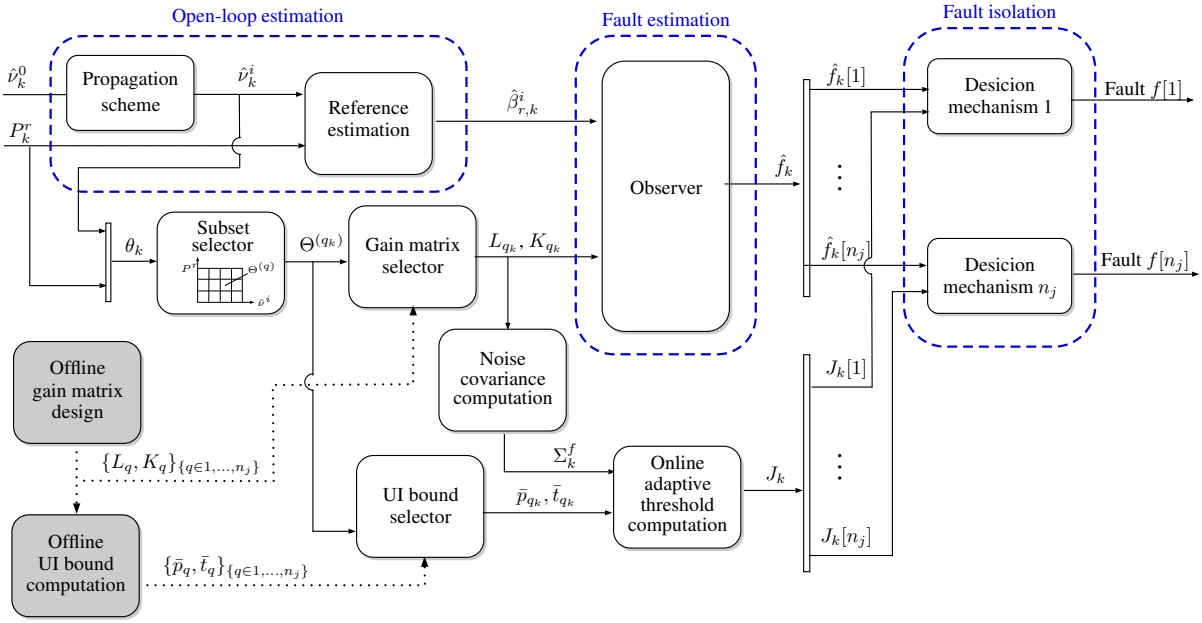

Figure 9.4. FE and FI strategy for each row of turbines i.

Remark 9.6. *In order to avoid false alarms when the membership of θ to a subset $\Theta^{(q)}$ changes to a subset $\Theta^{(p\neq q)}$ such that $(\bar{p}_q + \bar{t}_q) > (\bar{p}_p + \bar{t}_p)$ we use the refined adaptive threshold $J_k^*[j]$ defined as*

$$J_k^*[j] = \begin{cases} \alpha_j\, J_{k-1}^*[j] + (1-\alpha_j)\, J_k[j] & \text{if } J_k[j] < J_{k-1}^*[j] \\ J_k[j] & \text{otherwise} \end{cases}, \tag{9.47}$$

with α_j defining a sufficiently slow filter which can be validated through numerical simulations (we choose $\alpha_j = 0.90$).

Remark 9.7. *The propagation error p is a high-frequency signal and we can model its dynamics as $p(z) = \frac{z-1}{z-\alpha_f}\,\eta(z)$ where η is a random variable verifying $\|\eta\|_\infty = \|p\|_\infty$ and $\alpha_f \lessapprox 1$ (we choose $\alpha_f = 0.99$). Thus, we replace $\|G_{p,q}^j(z)\|_\infty$ by $\|G_{p,q}^j(z)\,\frac{z-1}{z-\alpha_f}\|_\infty$ in (9.46a) . Similar applies to t; hence, we replace $\|G_{t,q}^j(z)\|_\infty$ by $\|G_{t,q}^j(z)\,\frac{z-1}{z-\alpha_f}\|_\infty$ in (9.46b). With this, we give more weight to high-frequency components w.r.t. low-frequency components that would lead to a conservative computation of the thresholds of the decision mechanisms.*

9.6 Improvement of performance with fault simultaneity restrictions

The dependence of the thresholds on the variances of the noises and on the peak bounds of the UIs (see (9.44)) may compromise the performance of the fault evaluator. Even if the effect of the noises and UIs is attenuated (see the optimization problem (9.36)), large values of the variances of the noises and, especially, of the bounds of the UIs may lead to large values of the MIFs and ITs. In such a case, it would not be possible to detect and isolate through (9.25) the

occurrence of small faults to which the system may be prone. Thus, we propose to improve the FI performance at the cost of a constraint regarding the simultaneity of faults.

To do so, we build a bank of n_j observers b ($b = 1, \ldots, n_j$). Each observer b aims to estimate the auxiliary fault vector

$$\bar{f}_k^b = \left[\begin{array}{cccccc} f_k^{i,1} & \ldots & f_k^{i,b-1} & f_k^{i,b+1} & \ldots & f_k^{i,n_j} \end{array} \right].$$

The discrete state-space model of the pitch systems of the i-th row of WTs including the dynamics of $\bar{f}^b$ can be written as

$$\bar{z}_{k+1}^b = \bar{A}\,\bar{z}_k^b + \bar{B}\,u_k + \bar{D}\,\bar{\delta}_k^b, \tag{9.48a}$$

$$y_k = \bar{C}\,\bar{z}_k^b + w_k + \bar{G}^b\,f_k^{i,b}, \tag{9.48b}$$

$$\bar{f}_k^b = \bar{R}\,\bar{z}_k^b, \tag{9.48c}$$

with

$$\bar{z}_k^b = \left[\begin{array}{cccc|cccccc} \beta_k^{i,1} & \ldots & \beta_k^{i,n_j} & \xi_k^{i,1} & \ldots & \xi_k^{i,b-1} & \xi_k^{i,b+1} & \ldots & \xi_k^{i,n_j} \end{array} \right],$$
$$\bar{\delta}_k^b = \left[\begin{array}{cccccc} \delta_k^{i,1} & \ldots & \delta_k^{i,b-1} & \delta_k^{i,b+1} & \ldots & \delta_k^{i,n_j} \end{array} \right],$$

$\bar{A} = \begin{bmatrix} \alpha\, I_{n_j} & 0 \\ 0 & I_{n_j-1} \end{bmatrix}$, $\bar{B} = (1-\alpha)\, I_{2\,n_j-1}$, $\bar{D} = \begin{bmatrix} 0 \\ I_{n_j-1} \end{bmatrix}$, $\bar{C} = \begin{bmatrix} I_{n_j} & I_{n_j-1} \end{bmatrix}$, $\bar{G}^b = \begin{bmatrix} 0_{(b-1)\times 1} \\ 1 \\ 0_{(n_j-b)\times 1} \end{bmatrix}$

and $\bar{R} = \begin{bmatrix} 0 & I_{n_j-1} \end{bmatrix}$. Then, each model-based observer b can be built as

$$\hat{\bar{z}}_{k+1}^b = \bar{A}\,\hat{\bar{z}}_k^b + B\,\hat{u}_k + \bar{L}_k^b\,(y_k - \bar{C}\,\hat{\bar{z}}_k^b), \tag{9.49a}$$

$$\hat{\bar{f}}_k^b = \bar{R}\,\hat{\bar{z}}_k^b + \bar{K}_k^b\,(y_k - \bar{C}\,\hat{\bar{z}}_k^b). \tag{9.49b}$$

Define $\tilde{\bar{z}}^b = \bar{z}^b - \hat{\bar{z}}^b$ and $\tilde{\bar{f}}^b = \bar{f}^b - \hat{\bar{f}}^b$. It follows that

$$\tilde{\bar{z}}_{k+1}^b = (\bar{A} - \bar{L}_k^b\,\bar{C})\,\tilde{\bar{z}}_k^b + \bar{E}\,p_k + \bar{F}\,t_k + \bar{D}\,\bar{\delta}_k^b - \bar{L}_k^b\,w_k, \tag{9.50a}$$

$$\tilde{\bar{f}}_k^b = (\bar{R} - \bar{L}_k^b\,\bar{C})\,\tilde{\bar{z}}_k^b - \bar{K}_k^b\,w_k - \bar{G}^b\,f_k^{i,b}, \tag{9.50b}$$

with $\bar{E}$ and $\bar{F}$ being built in analogy to E and F. The exogenous signals affecting the observer b are not only the fault generator $\bar{\delta}^b$, the noises w and the unknown inputs p and t but also the fault $f^{i,b}$. We propose to omit the dependence of the error on the fault $f^{i,b}$ and to design the gain matrices of each observer (9.49) following the approach presented in Section 9.5 (the matrices $\bar{A}$, $\bar{C}$, $\bar{D}$, $\bar{E}$, $\bar{F}$, $\bar{L}^b$ and $\bar{K}^b$ in the place of the matrices A, C, D, E, F, L and K). Note that, in this case, the restriction regarding the CSE requirement of the b-th fault will not appear in the optimization problem (9.30). This extra design freedom is then used to achieve a greater minimization of the effect of the noises and the UIs on the fault estimates.

In the absence of the fault $f^{i,b}$, we can thus set the following decisions ($j = 1, \ldots, n_j - 1$) for the b-th observer:

$$\left\{ \begin{array}{ll} \text{if } |\hat{\bar{f}}_k^b[j]| \geq \bar{J}_k^b[j]\,, & \text{Fault } \bar{f}^b[j] \\ \text{otherwise}\,, & \text{No fault } \bar{f}^b[j] \end{array} \right., \tag{9.51}$$

where $J^b[j]$ is designed following the strategies in Section 9.5. Note that the thresholds $\bar{J}^b[j]$ in (9.51) are smaller than the thresholds $J[j]$ in (9.25): when omitting the presence of the fault $f^{i,b}$, we achieve a greater attenuation from noises and UIs.

If the fault $f^{i,b}$ is present in the system, the decision mechanisms (9.51) which are based on the b-th observer are no longer reliable. Thus, an observer b and the corresponding decision mechanisms are reliable if the absence of the fault $f^{i,b}$ is diagnosed by the decision mechanisms of at least one reliable observer c ($c \neq b$). In turn, the reliability of c implies that the decision mechanisms of the b-th observer diagnose the absence of the fault $f^{i,c}$, see Fig. 9.5. In all, the proposed bank of observer and decision mechanisms enables FE and FI whenever 2 of the faults in a row i are not present in the system (i.e., there are no more than $n_j - 2$ simultaneous faults in a row). FE and FI are obtained with any of the reliable observers and decision mechanisms of the bank. The strategy is summarized in Fig. 9.6.

9.7 Simulation results

The benchmark [215] includes a scenario of 4400 s in which different faults occur. In the first period between 0 s and 2300 s, the WF cannot deliver the required power, while it can do so in the second period between 2300 s and 4400 s. The collective pitch system of the turbines $(1,1)$ and $(2,2)$ of the 0° layout are affected by misalignment of the blades causing an offset of 0.3° in the pitch angle measurements, see Table 9.1. In the following, we include the FE and FI results that we obtain with the proposed approach. All the observer designs are translated into multiobjective convex optimizations as detailed in (9.37), set up in YALMIP [192] and solved using the solver MOSEK [204]. For simplification, we omit the obtained observer matrix gains

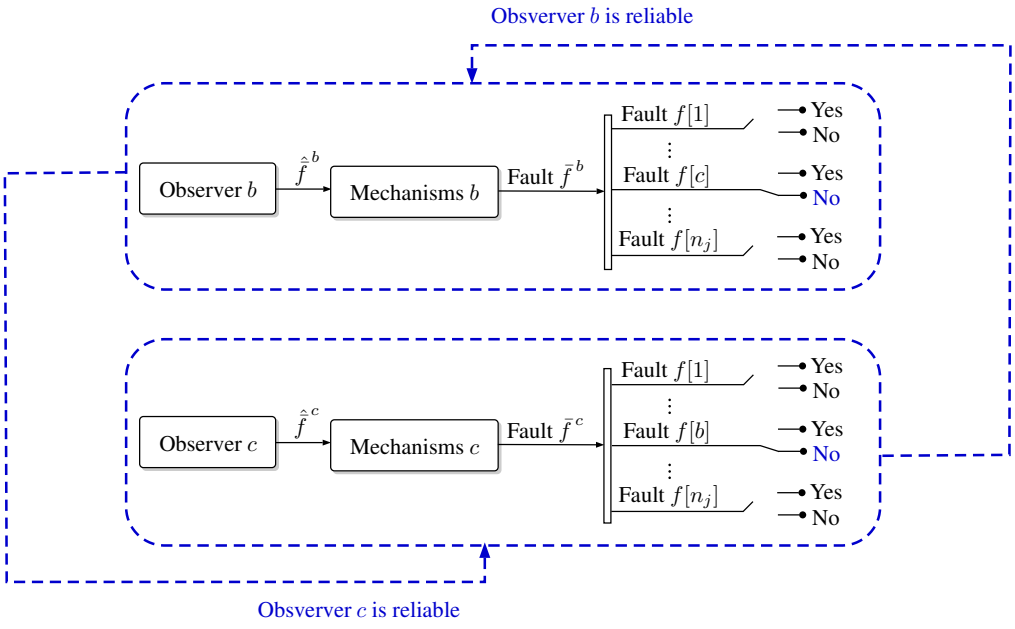

Figure 9.5. Reliability chain in the bank of observers and decision mechanisms.

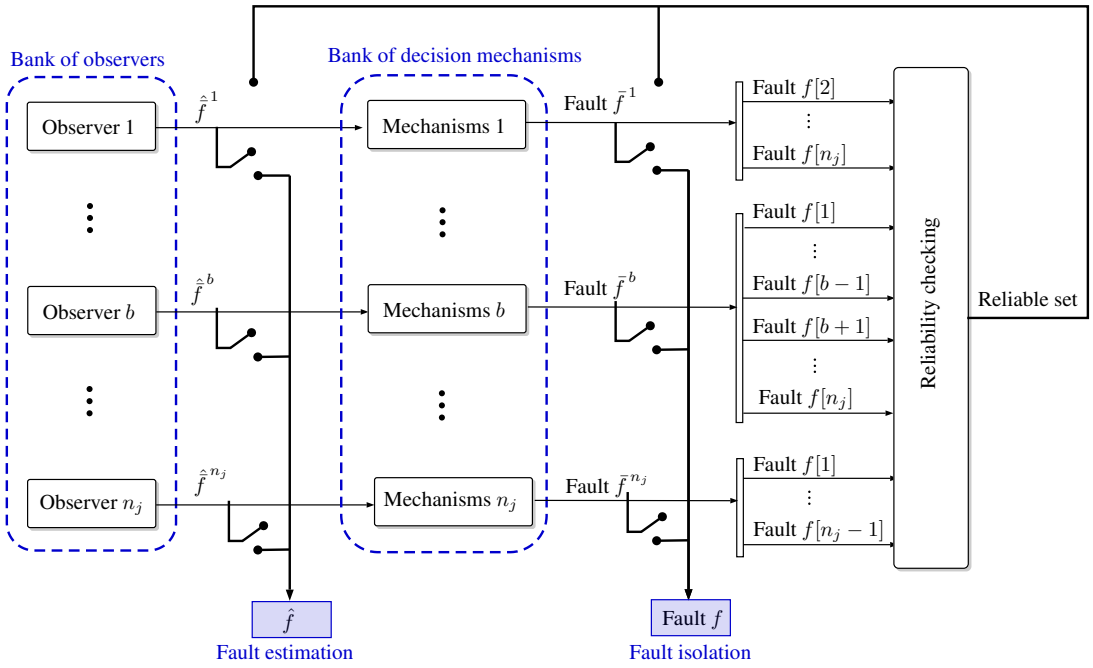

Figure 9.6. Bank of observers and decision mechanisms for FE and FI in each row of turbines i.

$\{L_q, K_q\}_{\{1,\dots,N_\theta\}}$ and the obtained bounds $\{\bar{p}_q, \bar{t}_q\}_{\{1,\dots,N_\theta\}}$. Let us remark that in the figures of the section, unless explicitly stated otherwise, the fault estimates are in black and the FI thresholds are in red.

For the 0° layout, we build a bank of observers and decision mechanisms for each row of turbines ($i = 1, 2, 3$) as explained in Section 9.6. Let us perform different observer designs with different values of the CSE requirements $\bar{\gamma}_j^j$ and let us use $\bar{\gamma}_m^j = \bar{\gamma}_j^j/100$ for all $m \neq j$ in these designs (See Remark 9.4). If we denote as $\bar{\psi}^j$ the CSE requirement $\bar{\gamma}_j^j$ when taking into account the sampling time T_s (i.e., $\bar{\psi}^j = \bar{\gamma}_j^j T_s$), we use $\bar{\psi}^j = [1, 5, 10, 20, 30, 50]^{\circ 2} s$ for $j = 1, \dots, n_j$. The FIR criteria with $\bar{\phi}^j = 1 \cdot 10^{-5}$ (i.e., one false alarm each 1000s) for $j = 1, \dots, n_j$ is used to compute the thresholds of the decision mechanisms. Fig. 9.7 shows the effect of varying the CSE in the turbine ($i = 1, j = 1$), which is affected by the fault **F1**. As an example, the details on the results with $\bar{\psi}^j = 30^{\circ 2} s$ are depicted in Fig. 9.8. Fig. 9.9 shows the results for the turbine ($i = 2, j = 2$), which is affected by the fault **F2**, and Fig. 9.10 shows the results for the turbine ($i = 1, j = 2$), which operates in fault-free conditions. The results on the left hand side of the figures include the variables $\hat{f}[j]$ (black) and $J[j]$ (red) while the results on the right hand side compare the normalized variable $\hat{f}[j]/J[j]$ (black) with a unitary threshold (red).

Fault ID	0° layout	45° layout	Time occurrence
F1	$(i = 1, j = 1)$	$(i = 1, j = 3)$	[1300,1400] s
F2	$(i = 2, j = 2)$	$(i = 3, j = 3)$	[3300,3400] s

Table 9.1. Fault scenario description.

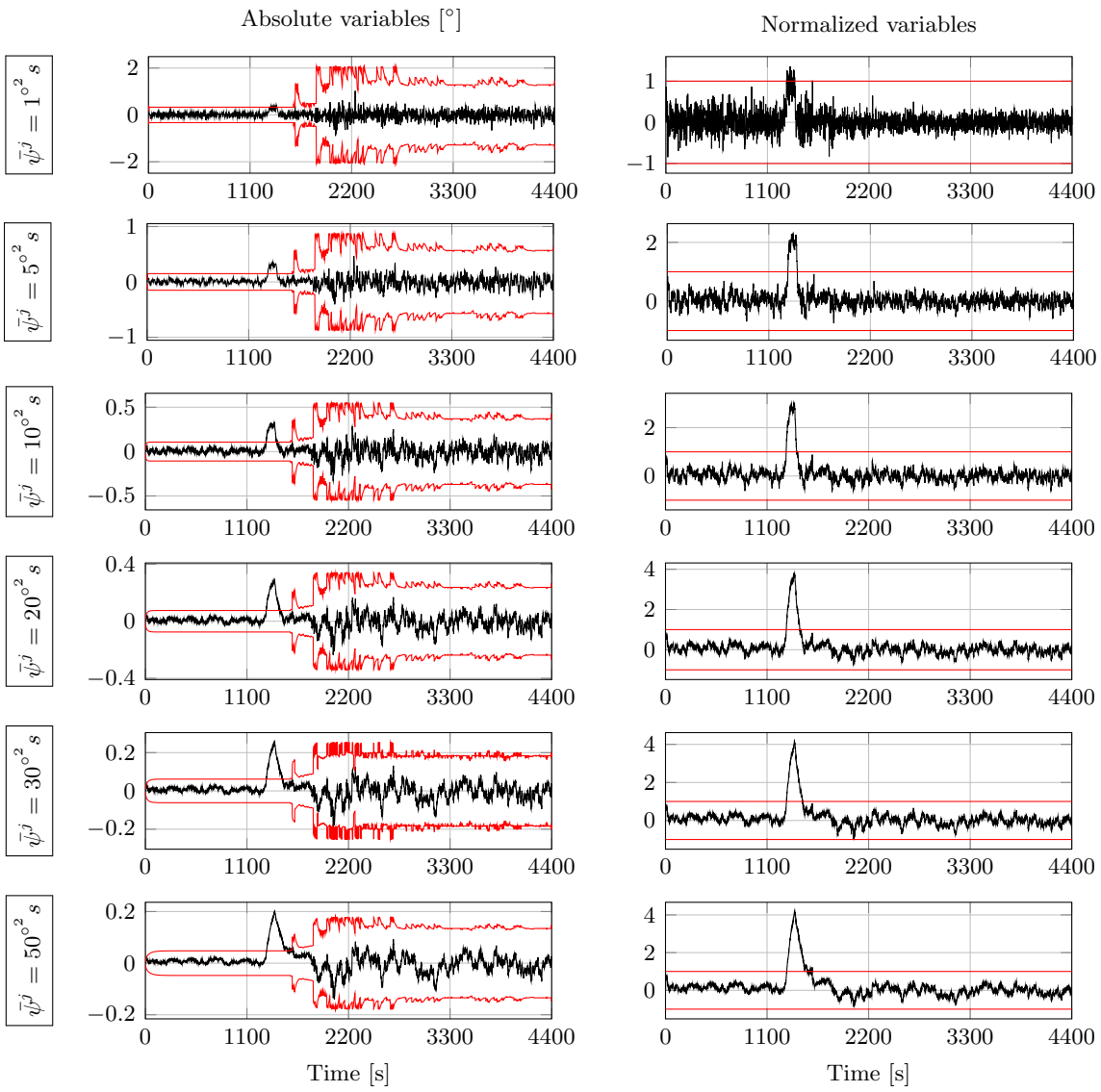

Figure 9.7. FE and FI with different CSE requirements $\bar{\psi}^j$. Turbine ($i = 1$, $j = 1$) of the 0° layout affected by the fault **F1**.

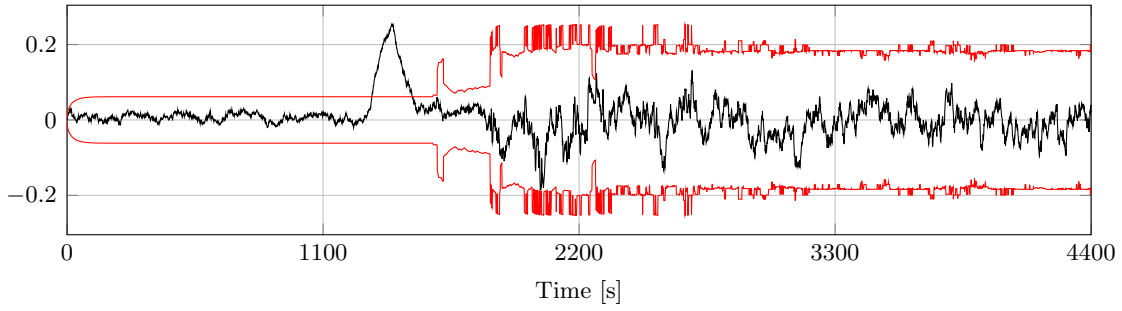

Figure 9.8. Details on the FE and FI results with a CSE requirement of $\bar{\psi}^j = 30^{\circ^2}$s. Turbine ($i = 1$, $j = 1$) of the 0° layout affected by the fault **F1**. Absolute variables in [°].

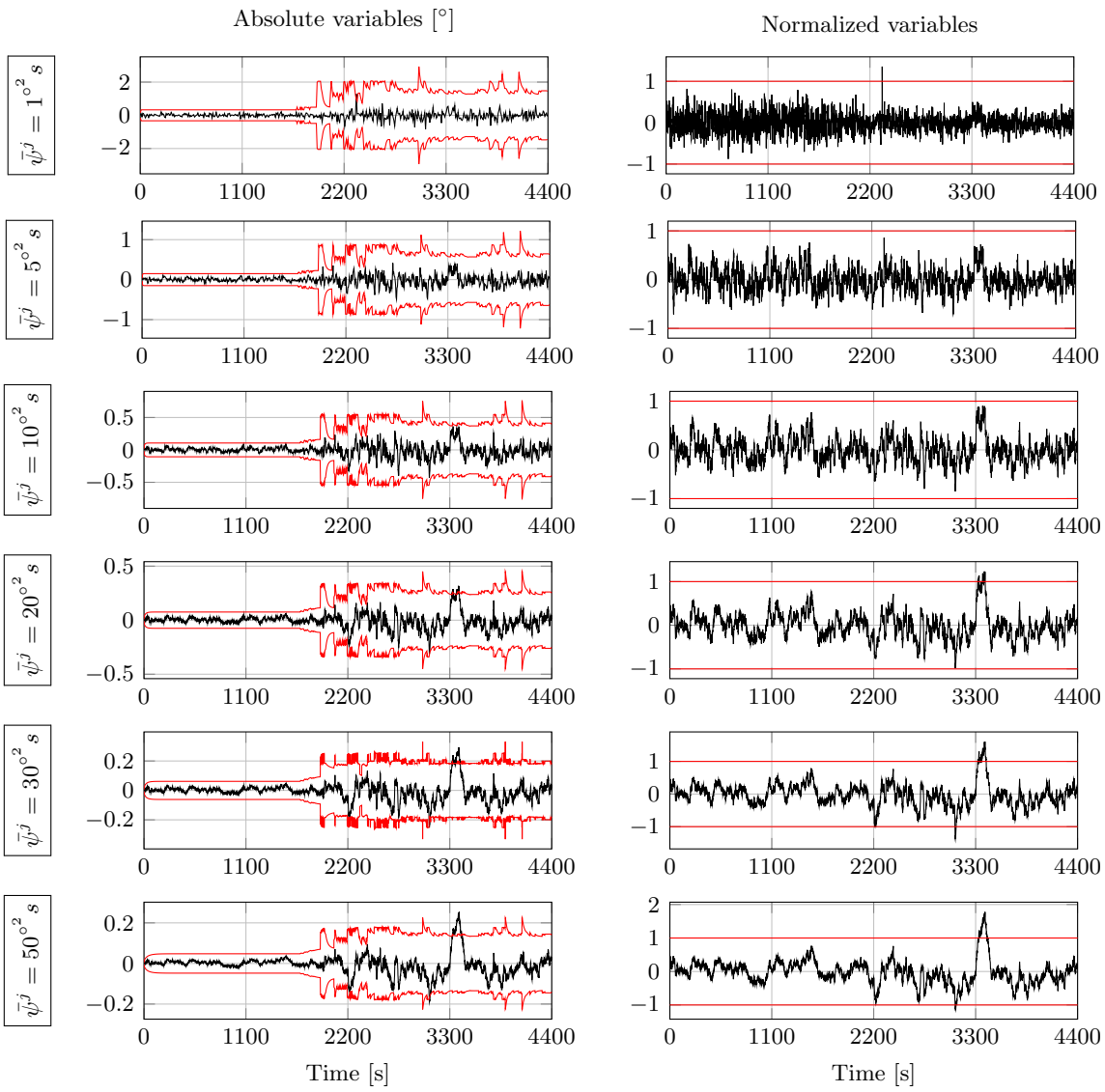

Figure 9.9. FE and FI with different CSE requirements $\bar{\psi}^j$. Turbine $(i = 2, j = 2)$ of the 0° layout affected by the fault **F2**.

Regardless of the value of the CSE requirement, all the figures show that when the power harvested from the wind is much lower than the power required by the WF controller, the achieved minimum isolable faults (MIFs) are smaller. In such cases, the estimated wind speed is low and the pitch reference estimation errors are small because for low wind speeds the pitch reference function is barely constant (see Fig. 9.2). Contrariwise, for high wind speeds the pitch reference function is monotonically increasing and the pitch estimation errors are larger. Let us now analyze the effect of the CSE requirement on the FE and FI performance. We verify that as the CSE requirement becomes more restrictive (i.e., $\bar{\psi}^j$ becomes smaller), the attenuation from the uncertainties and the noises diminishes and the MIFs are larger. On the other hand, the fault tracking behavior is improved and the isolation times (ITs) diminish (as long as the achieved MIFs are smaller than the simulated faults).

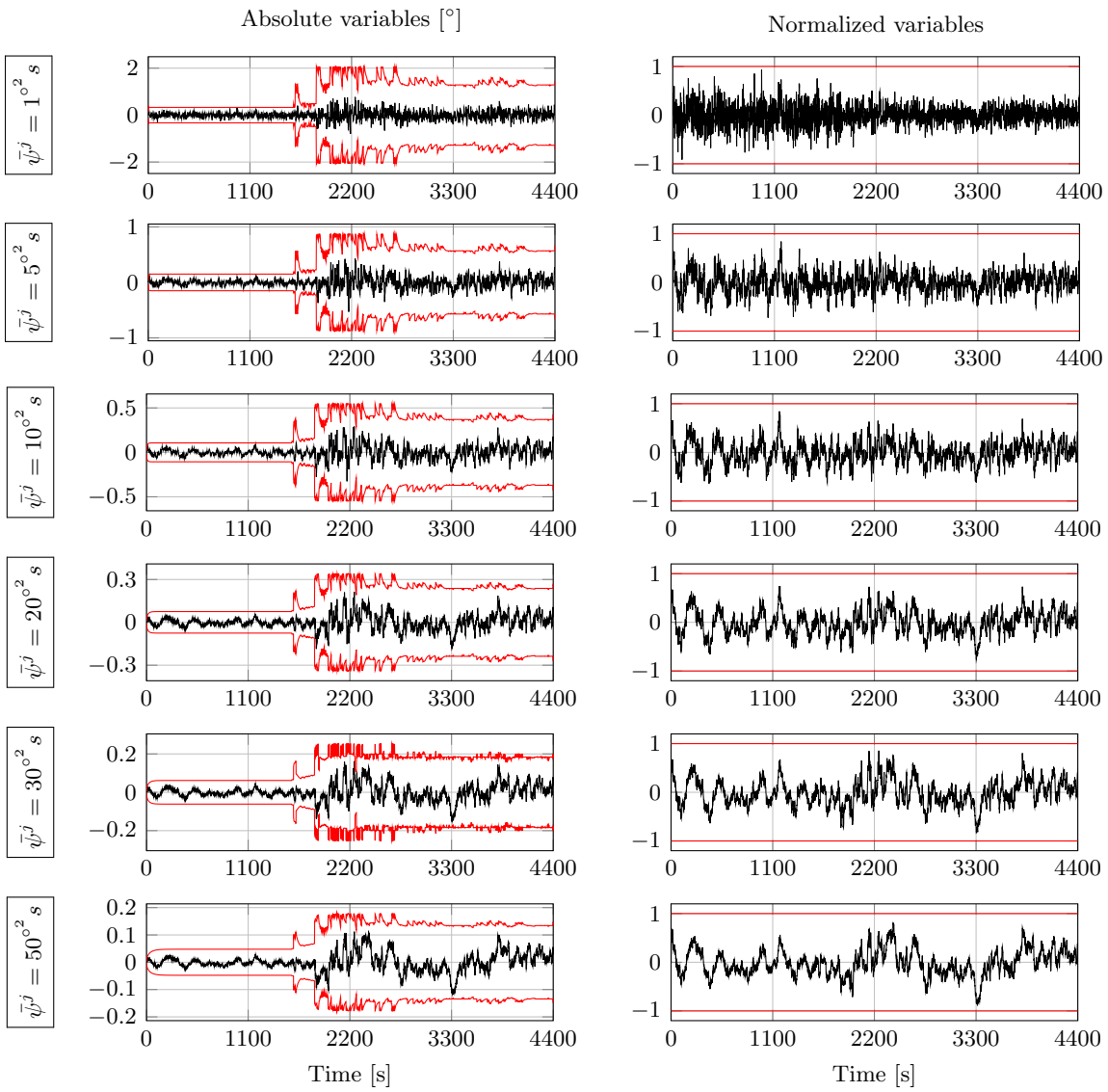

Figure 9.10. FE and FI with different CSE requirements $\bar{\psi}^j$. Turbine $(i = 1, j = 2)$ of the 0° layout in fault-free conditions.

Provided these deductions, it is reasonable that the fault **F1**, which occurs at the low wind speed period, is isolated with all the designed observers. In contrast, the fault **F2**, which occurs at the high wind speed period, is only isolated when using the designs with the less restrictive CSE requirements. Fig. 9.11 compares the isolation of the fault **F1** and of the fault **F2** provided by three designs with a restrictive, an intermediate and a moderate CSE requirement (i.e., $\bar{\psi}^j = 5^{\circ^2}s$, $\bar{\psi}^j = 20^{\circ^2}s$ and $\bar{\psi}^j = 50^{\circ^2}s$). For ease of comparison, the figure includes the normalized variables $\hat{f}[j]/J[j]$ of these three cases. Thus, bigger differences between the value of the variable $\hat{f}[j]/J[j]$ and the unitary threshold imply smaller MIFs. The IT of the fault **F1** is smaller if we use an observer designed with a smaller CSE requirement; in contrast, the difference between the normalized variable $\hat{f}[j]/J[j]$ and the unitary threshold becomes smaller.

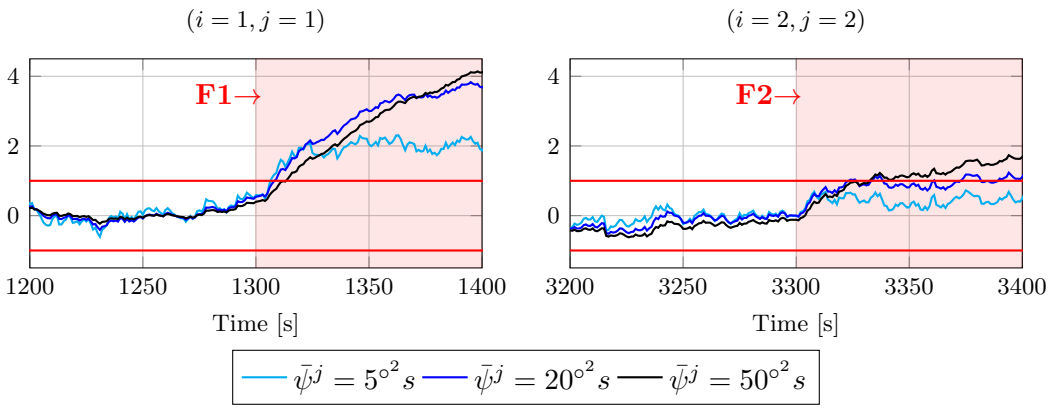

Figure 9.11. Comparison of FE and FI performance with different CSE requirements (0° layout). Normalized variables.

CSE $[^{\circ^2}s]$	MIF at 1300 s [°]		MIF at 3300 s [°]		largest MIF [°]		IT $[s]$	
	$i = 1$	$i = 2$	$i = 1$	$i = 2$	$i = 1$	$i = 2$	**F1**	**F2**
1	0.33	0.33	1.28	1.31	2.07	2.93	10	-
5	0.15	0.15	0.57	0.58	0.88	1.22	7	-
10	0.11	0.11	0.37	0.38	0.55	0.75	8	-
20	0.08	0.08	0.24	0.24	0.34	0.45	9	23
30	0.06	0.06	0.18	0.18	0.25	0.33	10	24
50	0.05	0.05	0.13	0.14	0.18	0.23	14	33

Table 9.2. Comparison of FI performance with different observers (0° layout).

For the fault the fault **F2**, we prove that FI is not achieved if the restrictive CSE requirement is used in the design. The ITs of the other two designs are similar: even if $\bar{\psi}^j = 20^{\circ^2}s$ is smaller than $\bar{\psi}^j = 50^{\circ^2}s$, the achieved MIF at 3300 s for $\bar{\psi}^j = 20^{\circ^2}s$ is very close to 0.30° (see Table 9.2) and FI is compromised. In contrast, the achieved MIF for $\bar{\psi}^j = 50^{\circ^2}s$ at 3300 s is 0.14°. Table 9.2 summarizes these results for all the designs. Let us remark that the maximum values of the MIFs are bigger at the row $i = 2$ than at the row $i = 1$ because the pitch reference estimation errors are higher as the distance to the wind mast increases. At 1300 s and 3300 s these differences are coincidentally minimal. The biggest differences appear at the wind speeds and power references for which the slope of the pitch reference function is more pronounced. Finally, note that the isolation of the fault **F1** is achieved with the design of $\bar{\psi}^j = 1^{\circ^2}s$ even if the MIF at 1300 s is bigger than the fault size (i.e., 0.33° vs. 0.30°). The effect of the noises and uncertainties enhances this isolation; however, the fault estimate oscillates around the threshold of the FI decision and the results are thus misleading in this case.

In the following, we use $\bar{\psi}^j = 30^{\circ^2}s$, and $\bar{\phi}^j = 1 \cdot 10^{-5}$ $(j = 1, \ldots, n_j)$ in the designs. Fig. 9.12 and Fig. 9.13 show the results for all the turbines in the WF when we analyse the 0° layout. To enhance the comprehension of the functioning of the bank of observers and decision mechanisms, let us study each row of turbines in the farm. In the row $i = 1$, between 1300 s and 1400 s, the observer $b = 1$ and the corresponding decision mechanisms are corrupted by the appearance of

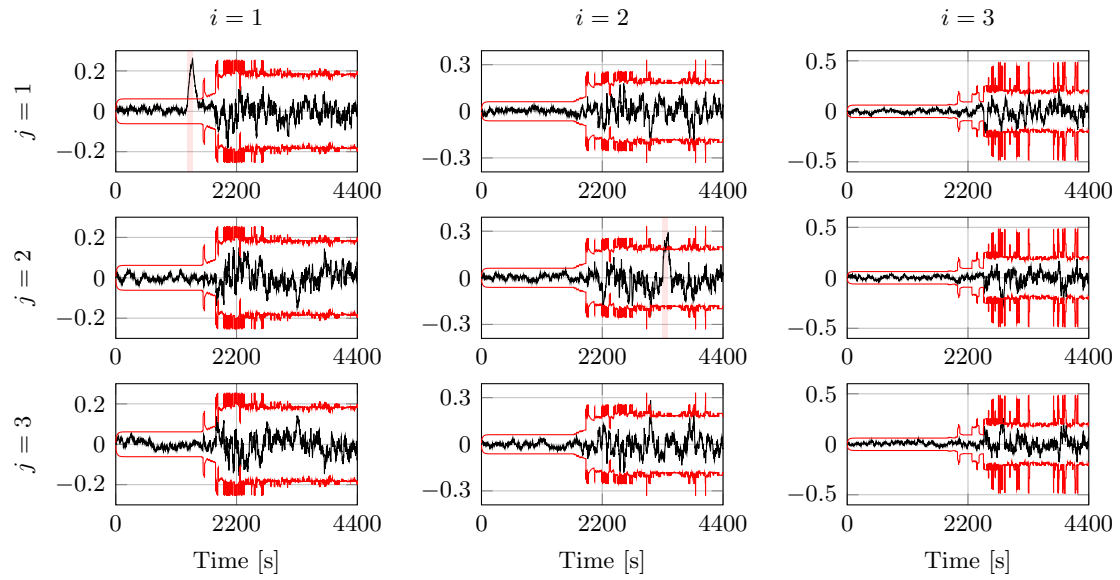

Figure 9.12. FE and FI with $\bar{\psi}^j = 30^{\circ^2}$s (0° layout). Absolute variables in [°].

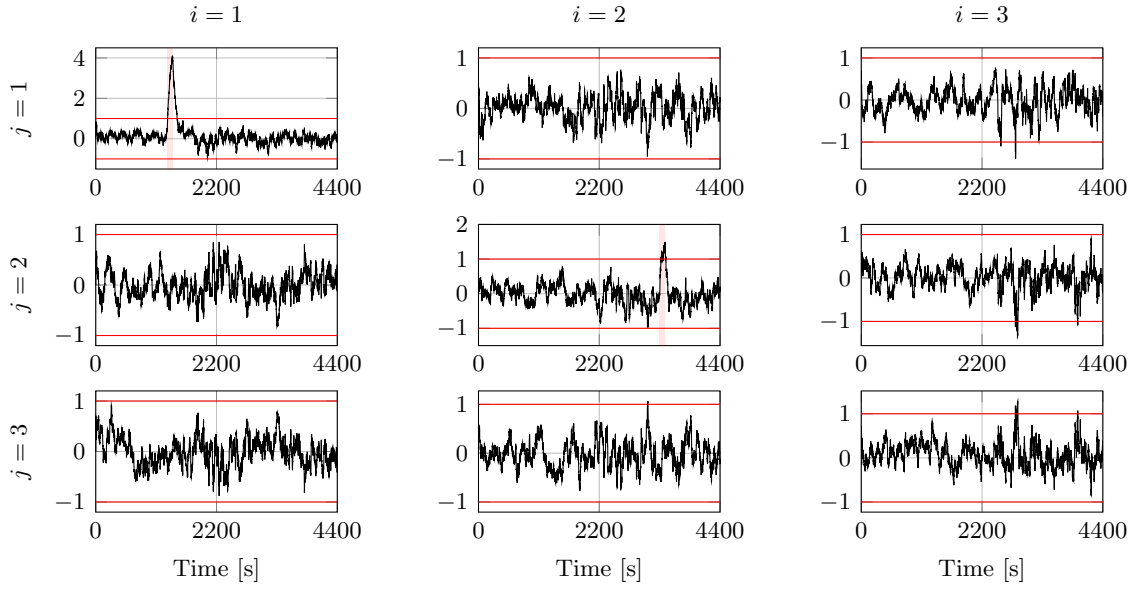

Figure 9.13. FE and FI with $\bar{\psi}^j = 30^{\circ^2}$s (0° layout). Normalized variables.

the fault **F1** in the turbine $(i = 1, j = 1)$ (i.e., $f_k^{1,1} \neq 0$ if $k \in [1300, 1400]$). The estimates of the fault $f^{1,1}$ provided by the observers $b = 2$ and $b = 3$ indicate it. Thus, FE and FI is achieved with the results of $b = 2$ and $b = 3$. Similarly, in the row $i = 2$, between 3300 s and 3400 s, the results are provided by either $b = 1$ or $b = 3$ because $b = 2$ is corrupted by the fault **F2** in the turbine $(i = 2, j = 2)$. Fig. 9.14 includes the results of the non-reliable observer $b = 2$ and the corresponding decision mechanism. They estimate and isolate a non-existent fault in the turbine $(i = 2, j = 3)$. Fortunately, the estimates provided by the observers $b = 1$ and $b = 3$ are reliable and FI is achievable in the WF (Fig. 9.12 and Fig. 9.13).

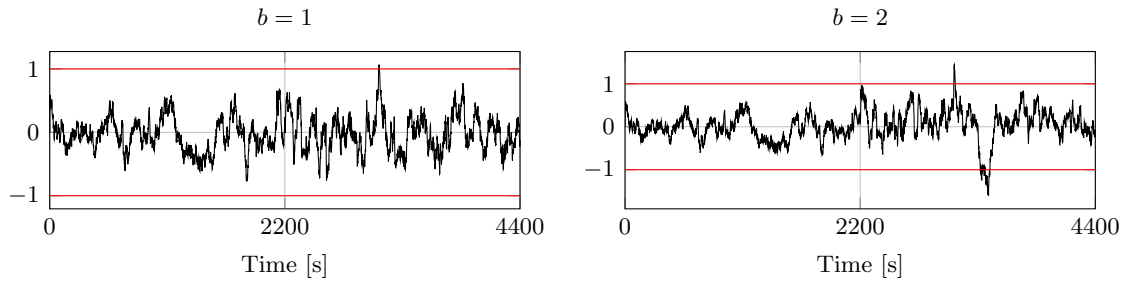

Figure 9.14. Reliability of the observers and decision mechanisms, $\bar{\psi}^j = 30^{\circ^2}$ (0° layout, $i = 2, j = 3$). Normalized variables.

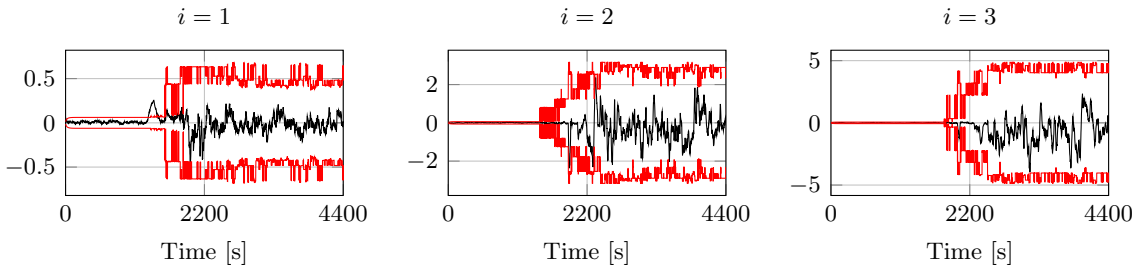

Figure 9.15. FE and FI without fault simultaneity restrictions, $\bar{\psi}^j = 30^{\circ^2}$ (0° layout, $j = 1$). Absolute variables in [°].

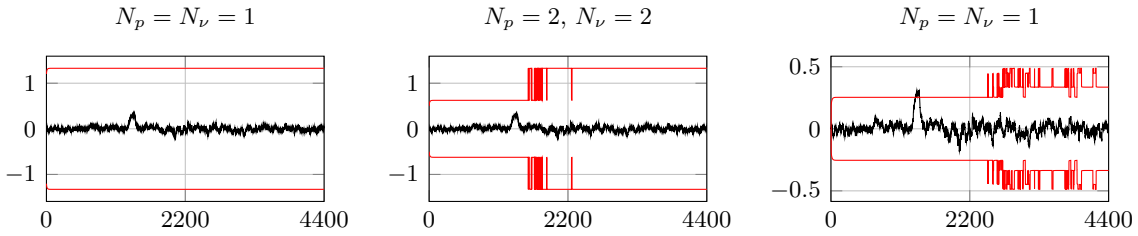

Figure 9.16. FE and FI with different gridding densities, $\bar{\psi}^j = 30^{\circ^2}$s (0° layout, $i = 1$, $j = 1$). Absolute variables in [°].

Let us now design a single observer and a single set of decision mechanisms for each row of turbines of the 0° layout. Fig. 9.15 includes the results for the turbines in the column $j = 1$ when the bank of observers and decision mechanisms is not used. The MIFs at the low wind speed period do not vary significantly. Contrariwise, at the high wind speed period, the MIFs increase drastically and this difference becomes bigger as the distance to the wind mast increases. Thus, we deduce that FE and FI are more difficult when it is not possible to build a bank of observers and decision mechanisms. This is the case where the wind direction is such that there are less than three turbines in a row (e.g., the turbines in the rows $i = 1, 2, 4, 5$ of the 45° layout for which we do not include the results due to space constraints). In such cases, the FE and FI results are similar to the results in Fig. 9.15 . A possible solution to mitigate this effect is to provide the turbines with laser anemometers (LIDAR), which offer a method of remote wind speed measurement ([253]) and thus, the wind estimation errors decrease.

Finally, Fig. 9.16 shows the estimation results when other densities are utilized for gridding the parameter set Θ. We prove that if the number of intervals N_ν and N_p is reduced, the offline computational burden decreases at the cost of some performance conservatism in terms of MIFs. In these cases, fewer changes of subset membership occur and the assumption of infrequent membership switches, which is used to design the FI thresholds, is more realistic. In any case, the chosen number of intervals (i.e., $N_\nu = N_p = 7$) has proved to satisfy an adequate trade-off between computational cost and performance conservatism. Moreover, as show in the figures included in this section, few significant bound changes occur along the simulation of 4400s. Hence, we deduce that there are infrequent membership switches between intervals with significantly different error bounds.

9.8 Conclusion

In this chapter a model-based FE and FI strategy is proposed for WT pitch systems affected by the misalignment of one or more blades. The FE algorithm includes a switched observer that is designed offline to guarantee global stability and local steady-state performance. In the design we use the trade-off between common engineering parameters that describe the fault estimation signals: the cumulative squared error due to faults and the root mean square error due to noises and uncertainties. The FE performance is thus intuitively fixed. The fault estimates are used in statistical-based decision mechanisms for FI. The thresholds of these mechanisms are computed online under the FIR criterion. Under certain restrictions regarding the number of simultaneous faulty turbines in a row, we improve the performance of the FE and FI strategy using a bank of observers and decision mechanisms. The simulations performed on the WF benchmark demonstrate that the proposed strategy is suitable to estimate and isolate pitch misalignments. The algorithm is able to estimate pitch misalignments for all wind directions but its performance is highly ameliorated when more than two turbines are in the same perpendicular row to the wind direction. This proves the effectiveness of following a WF level approach. It should be emphasized that the proposed strategy can be extended for FE and FI in other WT subsystems at a WF level. Future research will include this extension. For its part, the use of the pitch misalignment estimates in individual fault tolerant control highlights as immediate future work.

Chapter 10

Summary and future research

10.1 Summary

This thesis addressed some issues arisen from the application of estimation-based FD strategies to different practical systems such as industrial pipe networks, multistage manufacturing processes, wind turbines and wind farms. We proposed different FE strategies based on augmented observers and we developed various FDI strategies which are based on the evaluation the fault estimates in threshold-based decision mechanisms.

The thesis focused on the performance of the proposed FD strategies. On the one hand, we presented different optimization-based design approaches of the fault estimators and evaluators that allow specifying requirements over different practical FE and FDI performance parameters. In the FE context, we dealt with the cumulative squared error (CSE) due to faults, the fault tracking delay, the variance due to noises and the degree of interfault and UI decoupling. In the FDI framework, we dealt with the minimum isolable fault (MIF), the isolation time (IT) and the false isolation rate (FIR). We also achieved to independently specify the performance of each FE/FDI channel according to its particular diagnostic demands. On the other hand, we presented an enhanced form of augmented observers with an improved performance w.r.t. faults with periodic components. We studied the FE performance trade-offs that arise from the structural complexity of an augmented observer and we presented a probabilistic approach to optimally set these trade-offs. Finally, we extended the proposed approaches to schemes based on banks of fault estimators and evaluators that allow achieving estimation-based FD in systems with numerous faults.

Performance-based fault estimation and evaluation

In the process industry, the demands on diagnostic activities are established in terms of parameters which are barely introduced in theoretical designs. Hence, in this thesis, we presented a variety of designs of fault estimators, designs of fault evaluators and co-designs of fault estimators and evaluators which guarantee an optimal trade-off between this sort of practical FE and FDI parameters.

First, Chapter 3 considered systems affected by faults and stochastic noises. The chapter briefly analyzed the suitability of different estimation approaches (RLS algorithms and SISO PI observers) to establish FD performance-based designs. SISO PI observers having appeared to be more appropriate, the chapter included some preliminarily notes on their design to fix either the CSE towards abrupt faults or the variance due to noises. We subsequently showed how to design the threshold of decision mechanisms that evaluate the fault estimates provided by the observers. In this case, the design deals with the trade-off between the MIF and the FIR.

Second, Chapter 4, considering also systems affected by faults and stochastic uncertainties, extended the previous results and included the performance-based design of a time-varying MIMO PI observer utilizing the Kalman filter theory. By considering the fault variations as uncertainties and their covariance as a multivariate tuning parameter, Chapter 4 presented a design that also fixes either the CSE towards abrupt faults or the variance due to noises. We also showed how to fix the threshold of the decision mechanisms evaluating the fault estimates provided by the observer.

Third, Chapter 5 presented two co-design strategies of time-invariant MIMO PI observers and threshold-based decision mechanisms for systems affected by faults and stochastic noises. The proposed designs take into account the trade-off between the CSE towards abrupt faults, the MIFs and the FIRs. Similarly to Chapter 4, the first co-design approach is based on the Kalman filter theory and it consists on an heuristic optimization problem with Lyapunov equations. The second co-design approach is based on $\mathcal{H}_2$ norms and covariance bounds and it consists on an optimization problem formulated via matrix inequalities. The chapter also included some notes on the suitability of the methods w.r.t. the handling of the appearance of faults in different channels, to which we referred as interfault decoupling capability.

Finally, Chapter 7 considered, along with the presence of stochastic noises and faults, the presence of UIs. It presented a single-step design of time-invariant MIMO PI observers that allows achieving numerical UI decoupling together with other performance requirements over the delays to track incipient faults, the FE covariance due to noises and the degree of interfault decoupling. The design consists on an optimization problem with matrix inequalities utilizing different $\mathcal{H}_\infty$ norms and covariance bounds. Then, we extended these results and we presented a co-design strategy of time-invariant MIMO PI observers and threshold-based decision mechanisms that allows specifying requirements over the FIRS, the MIFs and the ITs.

Fault estimation of complex uncertain fault forms

In certain practical applications, the faults are periodic signals which can be decomposed into sinusoids of known frequencies. In Chapter 6, we thus generalized the formulation of the well-known proportional multiple-integral (PMI) augmented observer by presenting and giving the existence conditions of a novel proportional multiple-integral and multiple-resonant (PMIR) observer for FE in systems with oscillatory faults.

Provided that the form of the faults affecting a practical system is *a priori* uncertain, Chapter 6 also studied the influence of the structural complexity of an augmented observer on the

existing trade-off between its steady-state behavior w.r.t. complex fault forms and its transient behavior w.r.t. simpler fault forms. Along these lines, we also presented a FE design strategy that takes into account the probability of appearance of each of the fault forms considered by an augmented observer.

Fault estimation and evaluation in systems with numerous faults

In practice, the faults affecting a system rarely verify fault isolability conditions. However, standard FE techniques are not applicable to systems with non-isolable faults. Thus, in Chapter 7, we extended the concept of bank of residual generators and evaluators to the FE framework. We presented a bank of observer-based fault estimators and threshold-based fault evaluators that allow achieving FE and FDI in systems with non-isolable faults at the cost of some fault simultaneity restrictions.

In Chapter 8 and Chapter 9, we applied this scheme using banks of fault estimators and evaluators to groups of comparable systems operating under similar conditions. The proposed scheme automatically merges the information provided by the system model inconsistencies and by the inconsistencies between systems and it optimally defines the degree of attention that must be paid to each of these kinds of inconsistencies. It also ameliorates the FE and FDI performance at the cost of some mild restrictions over the simultaneous occurrence of faults.

Fault estimation and evaluation in complex practical applications

This thesis faced the problems related to the application of estimation-based FD strategies to practical engineering cases. First, Chapter 3 considered the problem of leakage diagnosis in real industrial networks of pipelines and tanks. Applying the mass conservation principle, Chapter 3 presented a multiplicative fault estimator based on the RLS identification algorithm and an additive fault estimator based on SISO PI observers. It compared the suitability of these methods w.r.t. leakage FD and it presented an FDI strategy that evaluates the leakage estimates provided by the SISO PI observers.

Second, Chapter 4 presented an observer-based approach for the estimation of variance deviations in multistage manufacturing processes (MMPs). After appropriately modeling the non-stationary behavior of the variances in MMPs, we introduced a time-varying MIMO PI observer for FE and we designed it using common FE performance parameters. Then, the fault estimates were evaluated using statistical confidence intervals for FDI. These intervals were tightened by expressing the fault estimates in terms of infinite weighted sums that approach normal distributions. In comparison with traditional batch-based methods for variance estimation in MMPs, the proposed observer-based approach is more computationally efficient, it has lower data-storage demands and it is more flexible in terms of satisfying different estimation and diagnosis performance requirements.

Third, Chapter 7 presented a solution for FE and FDI in the systems of a wind turbine (WT): the pitch system, the drive train system and the generator and converter system. Provided

that the actuator and sensor faults affecting some WT systems do not verify fault isolability conditions, most estimation-based FD solutions in the bibliography obviate the existence of sensor faults. Chapter 7 presented banks of time-invariant MIMO PI observers and threshold-based decision mechanisms that allow achieving FE and FDI for all the WT actuator and sensor faults. The chapter also included a co-design strategy of these fault estimators and evaluators that allows *a priori* specifying the FI requirements (over false isolation rates and isolation times) indicated in a well-known benchmark for FD in WTs. In the literature, the FI performance is alternatively *a posteriori* studied and the satisfaction of the demanded FI requirements is addressed via iterative procedures.

Finally, Chapter 8 and Chapter 9 addressed the problem of estimation-based FD in wind farms (WFs). Chapter 8 considered the diagnosis of decreased power generation in WFs. For its part, Chapter 9 considered the diagnosis of WT pitch misalignments in WFs. In these chapters, we presented closed-loop FE and FDI approaches that are more actively robust against disturbances than the open-loop methods available in the literature. In the FE step, non-conservative approaches were used to handle the model nonlinearities and the differences in disturbance levels along the operation ranges: Chapter 8 presented a Markovian jump system approach with switched PI observers and Chapter 9 designed switched PI observers considering infrequent mode switchings. The proposed observer designs also allow guaranteeing certain fault sensitivity with optimal disturbance rejection. In the FDI step, we presented adaptive FDI mechanisms that evaluate the fault estimates provided by the observers: Chapter 8 presented a data-driven approach for computing the adaptive thresholds of the mechanisms and Chapter 9 used a model-based statistical procedure making some approximations over the probability distribution function of the fault estimates. Finally, in these chapters, considering some mild fault simultaneity restrictions, the FE and FDI performance is ameliorated by building banks of the previous observers and decision mechanisms for groups of WTs operating under similar wind conditions.

10.2 Future research

The following promising future research directions arise from the contributions in this thesis. We distinguish between the research ideas in the field of estimation-based FD and in the field of active fault tolerant control (FTC).

Fault estimation and evaluation

In the field of estimation-based FD, some likely ideas for future research are listed below.

- Introduction of some practical FE and FDI performance parameters in the design of data-based fault estimators and evaluators, as we did in the design of the model-based fault estimators and evaluators presented in Chapter 3, 4, 5 and 7.

- Formulation of an adaptive version of the Kalman-based time-varying fault estimators presented in Chapter 4 for their adaptation to the actual level of fault variation. Analyzing the possible inclusion of this feature to FE structures that switch among a set of predefined augmented observers.
- Development of the PMIR observers introduced in Chapter 6 for their application in systems with oscillatory faults of unknown frequency.
- Extension of the performance-based fault estimators and evaluators proposed in Chapter 7 to more complex systems, e.g., large-scale system, networked control systems, hybrid systems, etc.
- Application and adaptation of the proposed estimation-based FD strategies to other practical systems. For instance, the extension of the results in Chapter 4 to the estimation and diagnosis of changes in the mean of the variation sources. Also, the application of the PMIR observers in Chapter 6 to FE in power systems of fixed frequency or in wastewater systems.
- Validation of the results in this thesis using experimental verification, which may pose new research challenges. For example, the strategies in Chapter 7, 8 and 9 were tested in realistic numerical simulators in the context of FD in WTs and WFs; future work will include their application to small-scale physical simulators.

Fault tolerant control

In the field of estimation-based FD for FTC, some research challenges are listed below.

- Utilization in active FTC schemes of the estimation-based FD results provided by the fault estimators and evaluators in Chapter 4, 7, 8 and 9. In particular, the application of these results to fault tolerant model predictive control (MPC) seems immediate because MPC structures easily adapt to the differences between faulty and fault-free scenarios.
- Development of co-designs of fault estimators and fault-tolerant controllers for *a priori* guaranteeing FTC performance parameters (in analogy to the co-designs of fault estimators and evaluators presented in Chapter 5 and 7 for *a priori* guaranteeing FDI performance parameters). Comparison of the performance of systems including separately designed or co-designed fault estimators and fault tolerant controllers.
- Development of performance-based co-designs of fault estimators, fault evaluators and fault tolerant controllers. Comparison of the structures with fault estimators and fault tolerant controllers and the structures including also fault evaluators.

Appendix A

Wind energy basics

A.1 Overview of wind power generation status

The combination of the need for climate friendly energy solutions, job creation, price stability, limited fossil fuel resources and security of energy supply are sufficient reasons to shift towards renewable energy [35]. Today, wind energy represents one of the most powerful renewable energy resources and it is one of the world's fastest-growing source of renewable electricity [219]. Both in Europe and worldwide, wind power is being developed rapidly [154,167,320]. In the European Union, the 85% of the new power capacity installed in 2017 came from renewable resources and wind energy represented the 65% of these installations [92], see Fig. A.1

According to the data presented in [12, 58, 60, 91], 204 GW of wind power capacity were installed in the world between 2012 and 2016. 52 GW were installed in Europe, of which 0.3 GW were placed in Spain. As detailed in Table A.1, these installations resulted in a total global capacity of 487 GW by the end of 2016. The European and the Spanish capacity summed 161 GW and 23 GW, respectively. Spain became, then, the fifth world country in terms of wind power capacity, Fig. A.2.

At present, the major wind power capacity is onshore; offshore wind currently accounts for a small amount of the total installed wind power capacity in the world [26]. However, as detailed in [90], offshore wind energy projects are gaining in importance and their growth rates are high, see Fig. A.3.

A.2 Wind turbine operation principle

Wind turbines transform the kinetic energy in the wind into electrical energy. Figure A.4 shows the main components of a horizontal-axis wind turbine. The nacelle, which is set at the higher part of the tower, contains the main elements of the turbine: the rotor, the transmission system and the power generation unit. The blades capture the wind pressure and, through the rotor hub, they make the rotor to turn around his axis converting the wind kinetic energy into

	End 2012	End 2014	End 2016
Spain	22.784	23.025	23.075
EU-28	106.454	129.060	153.730
Europe	109.817	134.253	161.330
World	283.194	369.705	486.790

Table A.1. Installed Wind Power Capacity in GW. (*Source: Prepared by the author on the basis of the data in [12, 13, 58–60, 91]*)

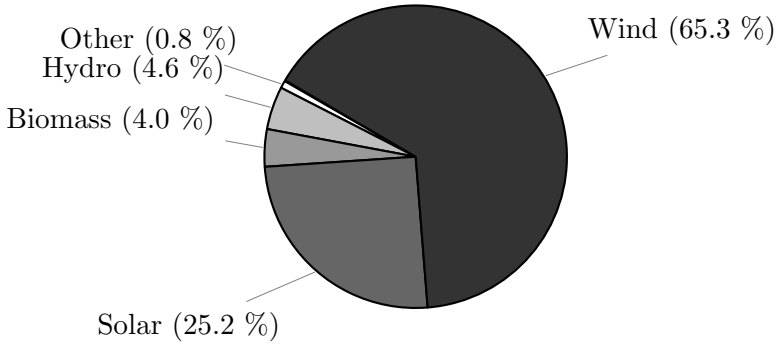

Figure A.1. New renewable power in the European Union in 2017. (*Source: Prepared by the author on the basis of the data in [92]*)

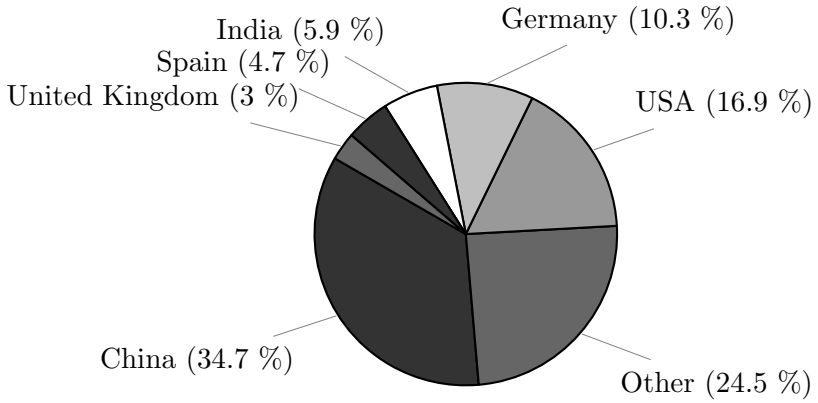

Figure A.2. Top wind cumulative capacity in 2016. (*Source: Prepared by the author on the basis of the data in [60]*)

rotational mechanical energy. A gear box is used to connect the rotor axis to the generator axis, and a converter and a high-voltage transformer are used to connect the generator to the grid. The generator and the converter convert the mechanical energy into electrical energy. Works as [24, 38] show more details on the functioning of this generation system.

Changing the rotor aerodynamics modifies the energy generation. This is achieved by pitching the blades or by fixing a given rotor speed with respect to the wind speed. The converter and its control system set the electromagnetic torque which, indirectly, fixes the rotational speed and, then, the wind energy capture.

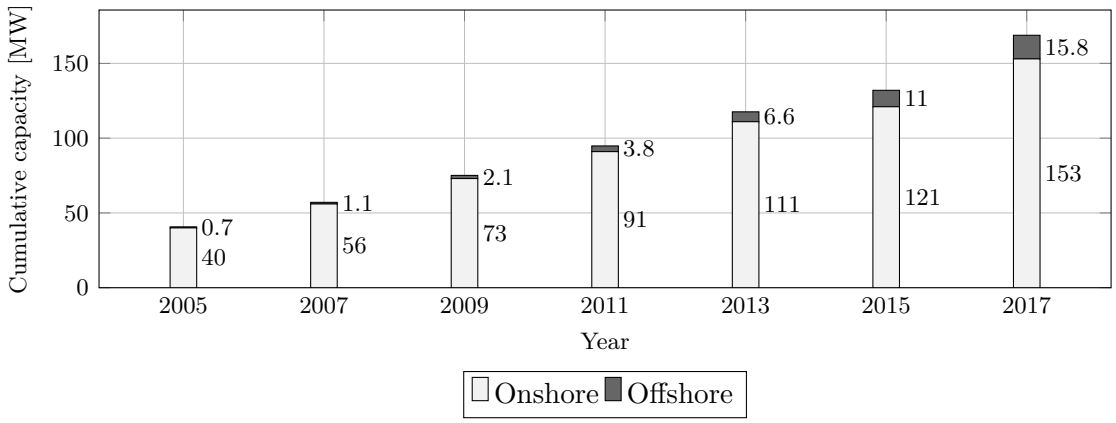

Figure A.3. Cumulative installations of onshore and offshore wind power in the European Union. (*Source: Prepared by the author on the basis of the data in [92]*)

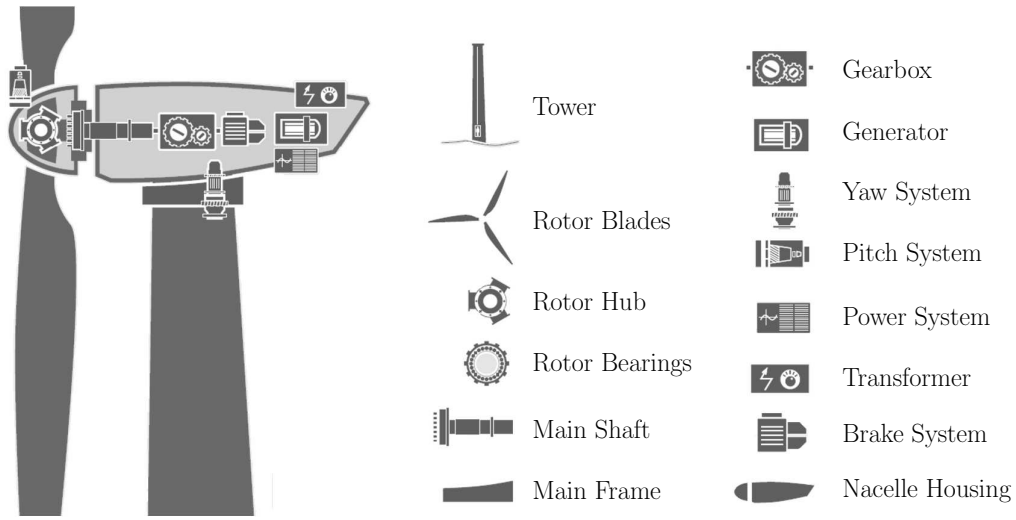

Figure A.4. Wind turbine components. *(Source: Prepared by the authors on the basis of an image in [14])*

Figure A.5 shows an overview of the control system and the relations between the different wind turbine systems (blade and pitch, drive train, generator and converter, and controller). The signals between them are denoted as follows: the torques τ_c, τ_a, τ_g and $\tau_{g,r}$ refer to the captured wind torque moving the turbine blades, the torque acting on the rotor, the electromagnetic torque in the generator and its reference, respectively; the rotational speeds ω_r and ω_g refer to the rotor and to the generator speeds; the pitch reference is denoted as β_r; P_r and P_g refer to the power reference and to the generated power; and, finally, the signals $\tau_{g,m}$, $\omega_{r,m}$, $\omega_{g,m}$ and β_m refer to the measurements of the generator torque, the rotor and the generator rotational speeds, and the pitch angle.

Figure A.6 shows the four control zones in which the controller operates in a different way depending on the mean wind speed for some given time window. This power curve is delimited

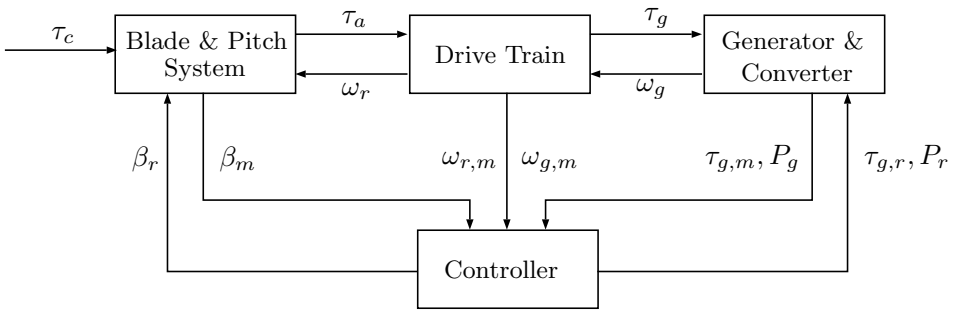

Figure A.5. Control system overview. (*Source: [216]*)

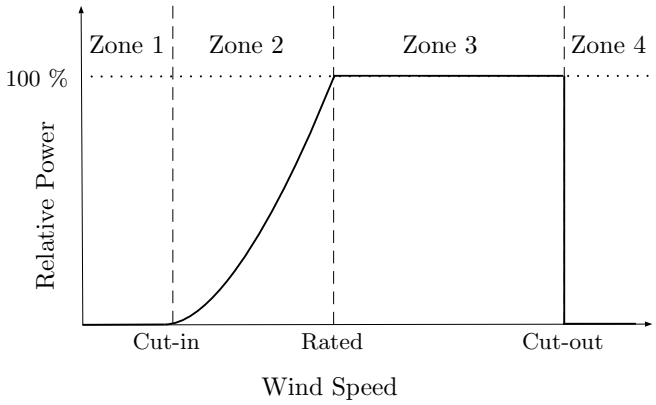

Figure A.6. Control zones of a wind turbine operation. (*Source: [54, 216]*)

by three different wind speeds: the cut-in, the rated and the cut-out wind speed [54].

- In *Zone I*, the aerodynamic torque is not sufficient to overcome the WT inertia and the turbine is halted.
- In *Zone II* or partial load region, the controller maximizes the power production. The pitch angle is held at zero degrees and the generator moment is adjusted to keep the power coefficient of the WT at a maximum value.
- In *Zone III* or full load region, the power production is constant; the pitch angle is controlled to keep the static available power equal to the WT nominal power.
- In *Zone IV*, the turbine is pitched out to stop the rotation due to security reasons.

A.3 Reliability of wind turbines

Wind turbines are subjected to different faults and failures. Unfortunately, the access to wind turbine failures statistics is not always permitted by the manufacturer. Thus, this appendix

refers to the statistics published in some relevant research articles: [65] and [124]. Table A.2 shows the reliability in terms of failure rates and downtimes of the subsystems responsible for the 75% of the breakdowns of wind turbines. One can verify that the pitch and blade subsystem together with the generator, the drive train and the converter cause most of the problems.

The authors in [287] explain that Operation and Maintenance (O&M) costs represent the 12% of the total costs of onshore wind projects and this percentage varies from 18% to 23% in offshore wind farms. These big percentages show that advanced techniques are necessary to ameliorate the reliability of wind turbines and this issue would be thus determinant in the future prospects of wind projects.

Subsystem	Contribution to Total Failure Rate [%]	Contribution to Average Time Lost [%]
Pitch	21,29	23,32
Converter	12,96	18,39
Drive Train	7,16	10,96
Generator	14,33	10,47
Blades	11,28	7,30
Transformateur	1,71	1,84
Tower	2,66	1,75
Brake	1,19	1,42
TOTAL	72,58	75,47

Table A.2. Reliability of wind turbine subsystems. (*Source: Prepared by the author on the basis of the data in [65, 124]*)

Appendix B

Notes on fault detection

On the framework of fault detection based on FE, we can set the following decision:

$$\begin{cases} \text{if } \ \hat{f}(k)^T \, \Lambda \, \hat{f}(k) \geq J_D & \text{Fault} \\ \text{otherwise} & \text{No fault} \end{cases}, \tag{B.1}$$

where Λ and J_D are to be defined and represent, respectively, a weighting matrix and a quadratic scalar threshold for detection.

In analogy to the isolation parameters **i.1**-**i.4**, we define different parameters that characterize the performance of the fault detector:

d.1. the false detection rates,
d.2. the minimum detectable faults,
d.3. the acknowledgement times for detection and
d.4. the detection times.

We define the *false detection rate*, which we denote as ϕ_D, as the probability of rising a detection alarm when no fault exists (i.e., $f = 0$):

$$\phi_D = \mathbb{P}\{\exists k : \hat{f}(k)^T \, \Lambda \, \hat{f}(k) \geq J_D\}. \tag{B.2}$$

Provided $f_{j \neq i} = 0$, $v = 0$ and $d = 0$, we define the *minimum detectable fault* i, which we denote as $\psi_{D,i}$, as the smallest value $\underline{f_i}$ that ensures the detection of the fault (7.26):

$$\psi_{D,i} = \left\{ \begin{array}{l} \min \ \underline{f_i} \\ \text{s.t.} \ \ \exists k \geq \underline{k} : \hat{f}(k)^T \, \Lambda \, \hat{f}(k) \geq J_D \end{array} \right\}. \tag{B.3}$$

Under these conditions (i.e., $f_{j \neq i} = 0$, $v = 0$ and $d = 0$), we define the *acknowledgement time for detection* of the fault i, which we denote as $\vartheta_{D,i}$, as the time elapsed between $\underline{k}$ and the first sample of detection of the fault (7.26):

$$\vartheta_{D,i} = \left\{ \begin{array}{l} \min\limits_{k \geq \underline{k}} \ k - \underline{k} \\ \text{s.t.} \ \ \hat{f}(k)^T \, \Lambda \, \hat{f}(k) \geq J_D \end{array} \right\}. \tag{B.4}$$

We define the *detection time* of the fault i, which we denote as $\tau_{D,i}$, as the time elapsed between the appearance of the fault (7.26) at k_0 and the first sample of detection of this fault:

$$\tau_{D,i} = \underline{k} - k_0 + \vartheta_{D,i}. \tag{B.5}$$

B.1 Mechanisms design with FD requirements

Assume that the model-based observer (7.5) has been designed through the strategies presented in Section 7.3.2 and the FE vector $\hat{f}$ provided by such observer (with prefixed stabilising gains L and K) is used in the decision mechanism (B.1). In the following, we show how to design the weighting matrix Λ and the threshold J_D of the decision mechanism (B.1) for guaranteeing certain requirement over one detection performance index.

Regarding the index **d.1**, if $f = 0$ and perfect UI decoupling is achieved, the FE vector $\hat{f}$ is zero-mean and its covariance is given by Σ, which can be computed through (7.9). Then, if we set $\Lambda = \Sigma^{-1}$, we have that

$$\phi_D \leq n_f / J_D, \tag{B.6}$$

where we have used Chebyshev's multidemensional inequality and the definition (B.2). We can then set J_D as

$$J_D := n_f / \phi_D^*. \tag{B.7}$$

to guarantee the bound $\phi_D \leq \phi_D^*$.

Remark B.1. *Provided perfect UI decoupling, if the noises v are Gaussian and we set $\Lambda = \Sigma^{-1}$, we have that $\hat{f}(k)^T \Lambda \hat{f}(k)$ is a chi-squared random variable of n_f degrees of freedom and the threshold J_D can be seen as the quantile that we set to construct the confidence interval that fixes the false detection rate to ϕ_D^*, i.e.,*

$$J_D := \Phi^{-1}_{\chi^2_{n_f}}(1 - \phi_D^*), \tag{B.8}$$

with $\Phi^{-1}_{\chi^2_{n_f}}(\cdot)$ being the inverse cumulative distribution function of a chi-squared random variable of n_f degrees of freedom.

The minimum detectable fault i depends on the form of the fault signal f_i, see the definition (B.3). Then, we can just ensure certain index **d.2** w.r.t. a specific fault signal form verifying Assumption 7.4 and the conditions (7.26). Consider the occurrence of a non-zero step fault in the i-th fault channel. In this case, the minimum detectable fault i verifies

$$\psi_{D,i} \equiv \sqrt{J_D / \Lambda_{ii}}. \tag{B.9}$$

Note that if Λ is set as $\Lambda = \Sigma^{-1}$, we have that $\psi_{D,i}$ depends on $\Lambda_{ii} = \left[\Sigma^{-1}\right]_{ii}$, which is the inverse of the conditional variance of $\widetilde{f}_i$. Provided (B.9), we can fix the minimum detectable constant fault i to $\psi^*_{D,i}$ by arbitrarily setting Λ_{ii} to some value and

$$J_D := (\psi^*_{D,i})^2 \, \Lambda_{ii}. \tag{B.10}$$

The time indices **d.3** and **d.4** do also depend on the form of the exogenous fault signal f_i, see (7.29) and (7.30). Then, we can just ensure certain time indices w.r.t. a specific fault signal form verifying Assumption 7.4 and the conditions (7.26). In analogy to the performance criteria **i.3** and **i.4**, we consider the occurrence of a ramp fault of slope $\Delta_i \neq 0$ in the i-th fault channel. Similar deductions as the ones detailed for **i.3** and **i.4** apply for **d.3** and **d.4**. First, we have that the acknowledgement time for detection is determined by the observer (i.e., $\vartheta_{D,i} \equiv T_i$) and it cannot be modified by varying J_D nor Σ. Second, we have that the detection time depends on the slope Δ_i of the ramp, which is generally not known. Hence, its expression is omitted here.

B.2 Co-design with FD requirements

The strategies presented in Section B.1 show how to design the decision mechanism (B.1) to ensure one requirement over the index **d.1** or **d.2.** when the gain matrices L and K of the observer (7.5) are prefixed (i.e., the gains are already designed). In order to guarantee two or more requirements over detection indices, it is necessary to perform a co-design of the observer (7.5) and the decision mechanisms (B.1). The following strategies show a proposal of how to perform this co-design for guaranteeing more than one isolation performance requirement.

Strategy B.1. *Assume that we desire to ensure altogether certain false detection rate ϕ_D^*, certain acknowledgement times for detection under ramp faults $\vartheta_{D,i}^*$ ($i = 1, \ldots, n_f$) and we desire to minimize the minimum detectable faults. To ensure these requirements, we first design the observer* (7.5) *through Strategy 7.1 with the value*

$$T_i^* := \vartheta_{D,i}^* \tag{B.11}$$

in (7.23) *for all i. Second, with the obtained gains L and K, we compute Σ through* (7.9)*, we set $\Lambda = \Sigma$ and we set the detection threshold through* (B.7)*with ϕ_D^*.*

Strategy B.2. *Assume that we desire to ensure altogether certain false detection rate ϕ_D^*, certain minimum detectable constant faults $\psi_{D,i}^*$ ($i = 1, \ldots, n_f$) and minimum acknowledgement times for detection under ramp faults (and thus minimum detection times under ramp faults). To ensure these requirements, we first design the observer* (7.5) *through Strategy 7.2 with a modified variance constraint. The constraints* (7.21) *and* (7.25) *are replaced by*

$$[\Xi^{-1}]_{ii} \geq n_f/\phi_D^*/(\psi_{D,i}^*)^2. \tag{B.12}$$

for all i. Second, with the obtained gains L and K, we compute Σ through (7.9)*, we set $\Lambda = \Sigma$ and we set the detection threshold through* (B.7)*with ϕ_D^*.*

Note that the modified constraints (B.12) are nonlinear constraints and iterative procedures must be used to solve Strategy B.2.

Remark B.2. *If the noises v that affect the system are Gaussian, we use* (B.8) *(instead of* (B.7)*) to set J_D in Strategy B.1 and Strategy B.2. Moreover, the constraints* (B.12) *are replaced to*

$$[\Xi^{-1}]_{ii} \geq \Phi_{\chi^2_{n_f}}^{-1}(1 - \phi_D^*)/(\psi_{D,i}^*)^2.$$

Appendix C

Wind speed in the wind farm

C.1 Wind model

Any wind speed v in the wind turbine and wind farm benchmarks [215, 216] consists of four wind speeds: the mean wind speed v_m describing the slow wind variations, a stochastic wind speed component v_s, the wind shear v_{ws} and the tower shadow v_{ts}:

$$v = v_m + v_s + v_{ws} + v_{ts}. \tag{C.1}$$

As explained in [216], these components are generated as follows. Table C.1 shows the wind model parameters.

- The *mean wind speed* is obtained by filtering a measured wind speed dataset with a low-pass filter.
- The *stochastic wind speed* component is modeled as a Kaimal filter [207].
- The *wind shear* is modeled as

  $$v_{ws,i}(t) = \frac{2\,v_m(t)}{3\,R^2}\left(\frac{R^3\,\alpha}{3\,H}\,\chi + \frac{R^4\,\alpha}{4}\,\frac{\alpha-1}{,H^2}\,\chi^2\right) + \frac{2\,v_m(t)}{3\,R^2}\left(\frac{R^5\,\alpha}{30}\,\frac{(\alpha^2-\alpha)\,(\alpha-2)}{H^3}\,\chi^3\right),$$

  where $\chi = \cos(\theta_{ri}(t))$ is the angular position of the three blades,

  $$\begin{aligned}\theta_{r1}(t) &= \theta_r(t),\\ \theta_{r2}(t) &= \theta_r(t) + 2\,\pi/3,\\ \theta_{r3}(t) &= \theta_r(t) + 4\,\pi/3,\end{aligned}$$

  and α and H re two aerodynamic parameters.
- The *tower shadow* is modeled through the following equations:

  $$v_{ts,i}(t) = \frac{m\,\bar{\theta}_{ri}(t)}{3\,r^2}\,(\psi + \upsilon),$$

Parameter		Value
α	Aerodynamic parameter	0.1
H	Aerodynamic parameter	81 m
R	Blades Radius	57.5 m
r_0	Radius of the blade hub	1.5 m

Table C.1. Wind model parameters.

with

$$\begin{aligned}
\psi =& 2\,a^2 \frac{R^2 - r_0^2}{(R^2 - r_0^2)\,\sin(\bar{\theta}_{ri}(t))^2 + k^2}, \\
\upsilon =& 2\,a^2\,k^2 \frac{(r_0^2 - R^2)(r_0^2\,\sin(\bar{\theta}_{ri}(t))^2 + k^2)}{R^2\,\sin(\bar{\theta}_{ri}(t))^2 + k^2}, \\
m =& 1 + \frac{\alpha\,(\alpha - 1)\,r_0^2}{8\,H^2}, \\
\bar{\theta}_{ri}(t) =& \theta_r(t) + \frac{(i-1)\,2\,\pi}{3} - 2\,\pi\,\mathrm{floor}\left(\frac{\theta_r(t) + \frac{(i-1)\,2\,\pi}{3}}{2\,\pi}\right)
\end{aligned}$$

and where floor(x) refers to the largest integer not greater than x, r_0 is the blade hub radius, and k is an aerodynamic parameter.

C.2 Wind speed estimation in the wind farm

From $\hat{v}^0$, it is possible to estimate the mean wind speed acting on the WTs in the i-th row through different propagation models available in the literature, see [159] and the references therein. Provided the wind and wake model of the benchmark in [215], we compute the estimated mean wind speed using the following propagation model:

$$\hat{v}^i(t) = \frac{1}{K_i}\hat{v}^{i-1}(t - t_p^i(t)), \tag{C.2}$$

where K_i is a wake factor and satisfies $K_i = 1$ for $i = 1$ and $K_i = 0.9$ for $i = 2, \ldots, Y-1$. The term $t_p^i(t)$ represents the propagation time between two consecutive rows and we compute it as

$$t_p^i(t) = \frac{l_i}{\hat{v}_f^0(t)/(K_i)^{i-1}},$$

where $\hat{v}_f^0$ results from filtering $\hat{v}^0$ using the low-pass filter $G_f(s) = 1/(s+1)$.

The WF benchmark provides the real effective wind speed signals $\nu^{i,j}$ for numerical validations of the wind propagation schemes. The mean wind speed signals ν^i are not available.

Fig. C.1 shows the wind speed estimation results for the turbines in the rows $i = 1$, $i = 2$ and $i = 3$ of the 0° layout in Fig. 9.1. Recall that the wind speed estimates are common to all the turbines in a row i (see the errors in the second part of Fig. C.1).

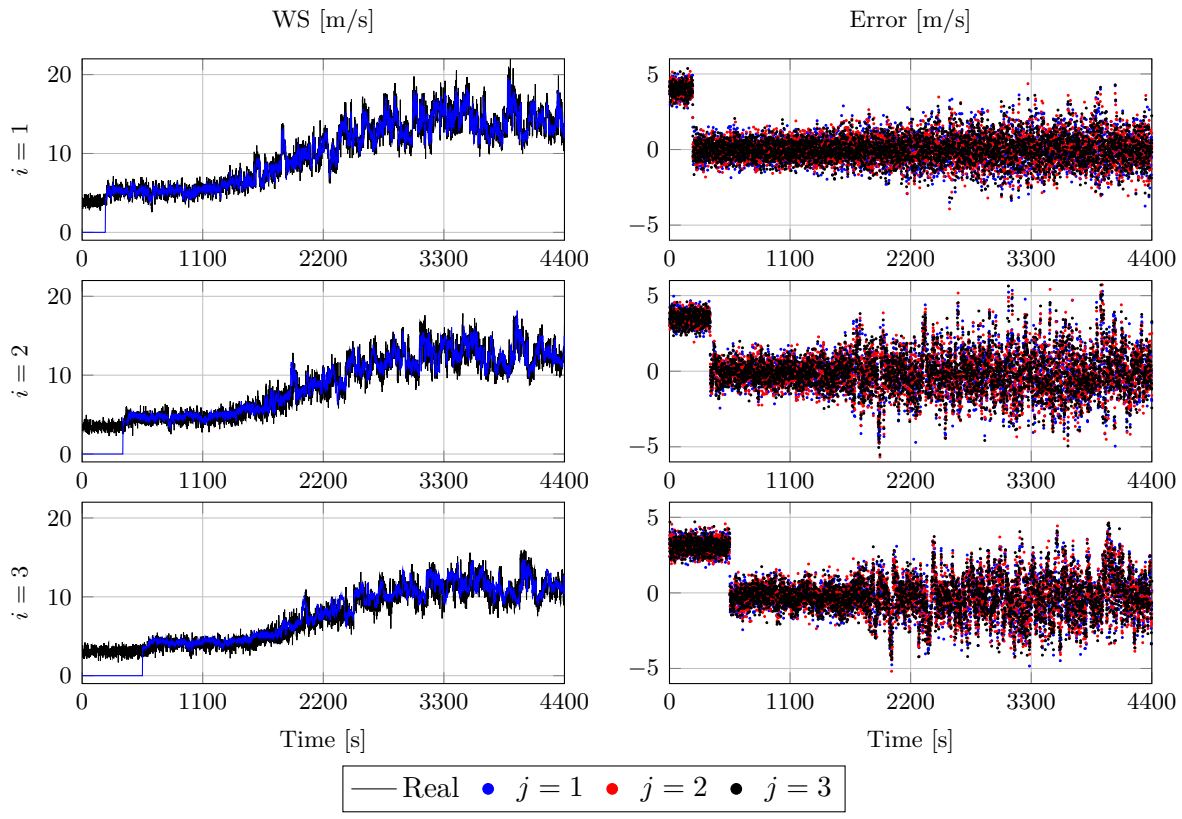

Figure C.1. Wind speed (WS) estimation for the 0° layout.

C.3 Bounding the wind speed estimation errors

Let us bound the wind speed estimation error. Since v^i is not available for numerical validations, we cannot separately compute the turbulence and the propagation error. Hence, we proceed as follows.

- We approximate the turbulence of the turbines to $\widetilde{\nu}_t^{i,j} \approx \nu^{i,j} - 1/3 \sum_{j=1}^{3} \nu^{i,j}$. In the first part of Fig. C.2 we show the results for the turbines in the row $i = 1$ of the 0° layout in Fig. 9.1. For each sample k of the time series, we depict the pair $(\hat{\nu}^i, \widetilde{\nu}_t^{i,j})$. We bound the turbulence as $|\widetilde{\nu}_t^{i,j}| \leq \lambda_t$ with $\lambda_t = 3\,\sigma_t$, which is depicted through a dashed gray line in Fig. C.2.
- We conservatively bound the wind propagation error (i.e.,$|\widetilde{\nu}_p^i| \leq \lambda_p^i$) with the 99-th percentile of the total error $\widetilde{\nu}^{i,j}$, which we compute as $\widetilde{\nu}^{i,j} = \nu^{i,j} - \hat{\nu}^i$. In the second part of the Fig. C.2, we depict the pair $(\hat{\nu}^i, \widetilde{\nu}^{i,j})$ for the turbines in the row $i = 1$. The propagation bound is depicted through a dashed gray line.

Remark C.1. *From* (C.2)*, we deduce that the propagation error is larger for higher wind speeds. Thus, one could consider the bound* $|\widetilde{\nu}_p^i| \leq \lambda_p^i(\widetilde{\nu}_p^i)$*, where* $\lambda_p^i(\hat{\nu}^i)$ *would depend not only on the*

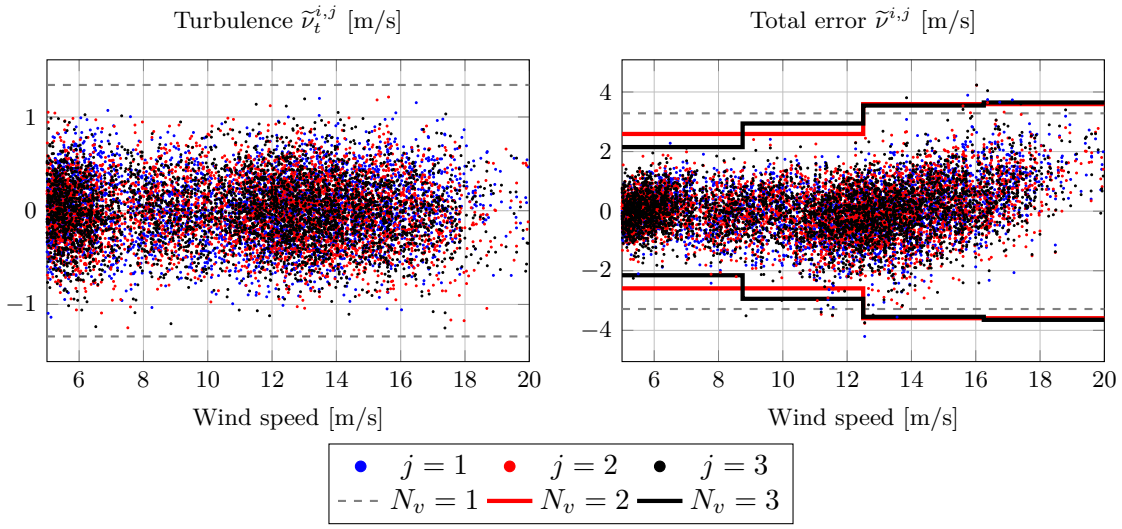

Figure C.2. Wind speed estimation error due to the turbulence and to the propagation model mismatch (0° layout, $i = 1$).

row i but also on the estimated mean wind speed. As shown in Fig. C.2 (including the 99-th percentiles of different intervals), we can neglect the dependence of the bounds on the estimated mean wind speed.

Appendix D

Auxiliary results

D.1 Auxiliary results of Chapter 4

D.1.1 Derivation of the expected value of $m(i)$

Let us first introduce the following lemma.

Lemma D.1. *([256]) Let $A \in \mathbb{R}^{n_a \times n}$, $X \in \mathbb{R}^{n \times n}$ and $B \in \mathbb{R}^{n_b \times n}$ be some matrices. We have that*

$$\operatorname{vec}\left(A\,X\,B^T\right) = B \otimes A \operatorname{vec}(X). \tag{D.1}$$

If matrix X is diagonal, we have that

$$\operatorname{diag}\left(A\,X\,A^T\right) = A^{\circ 2} \operatorname{diag}(X). \tag{D.2}$$

Provided (4.14), we have that

$$\mathbf{E}\{y(i)\,y(i)^T\} = \mathbf{E}\{\Psi(i)\,\zeta(i)\,\zeta(i)^T\,\Psi(i)^T\}. \tag{D.3}$$

Applying (D.1) to (D.3), we get

$$\mathbf{E}\{y(i)\,y(i)^T\} = \operatorname{vec}^{-1}\left(\Psi(i)^{\otimes^2} \operatorname{vec}\left(\mathbf{E}\{\zeta(i)\,\zeta(i)^T\}\right)\right), \tag{D.4}$$

where we have taken into account that $\mathbf{E}\{\Psi(i)\} = \Psi(i)$. Provided (4.12), this relation is simplified as

$$\mathbf{E}\{y(i)\,y(i)^T\} = \Psi(i)\,\Psi(i)^T. \tag{D.5}$$

Taking into account that matrices $D(i)\,D(i)^T$ and $R(i)\,R(i)^T$ are diagonal, we apply (D.2) to (D.5) and we get that the diagonal components of $\mathbf{E}\{y(i)\,y(i)^T\}$ are given by

$$\operatorname{diag}(\mathbf{E}\{y(i)\,y(i)^T\}) = \Gamma^{\circ 2} \operatorname{diag}\left(\mathbf{\Sigma}_u(i)\right) + \mathbf{1}_{n_y}\,\sigma_v^2(i), \tag{D.6}$$

which can be rewritten as

$$\mathbf{E}\{m(i)\} = [\,\Gamma^{\circ 2}\ \ \mathbf{1}_{n_y}\,] \operatorname{diag}\left(\bigoplus\nolimits_j \sigma^2(i)[j]\right). \tag{D.7}$$

D.1.2 Kalman filtering

Let us consider a linear system of the form

$$x(i+1) = A\,x(i) + w(i), \;\; y(i) = C\,x(i) + v(i), \tag{D.8}$$

with $x \in \mathbb{R}^{n_x}$ the state vector, $y \in \mathbb{R}^{n_y}$ the output vector, $A \in \mathbb{R}^{n_x \times n_x}$ the state matrix and $C \in \mathbb{R}^{n_y \times n_x}$ the output matrix. Vector $w(i) \in \mathbb{R}^{n_w}$ contains the process noise and $v(i) \in \mathbb{R}^{n_w}$ contains the measurement noise. We assume that $w(i)$ and $v(i)$ are independent, zero-mean Gaussian noises of time-varying covariances $W(i) = \mathbf{E}\{w(i)\,w(i)^T\}$ and $V(i) = \mathbf{E}\{v(i)\,v(i)^T\}$. A model-based observer for (D.8) is

$$\hat{x}(i) = A\,\hat{x}(i-1) + L(i)\;\left(y(i) - C\,A\,\hat{x}(i-1)\right), \tag{D.9}$$

with $\hat{x}(i)$ the estimated state, see [81]. Then, the dynamics of the estimation error $\widetilde{x}(i) = x(i) - \hat{x}(i)$ is

$$\widetilde{x}(i) = (I_{n_x} - L(i)\,C)\;(A\,\widetilde{x}(i-1) + w(i-1)) - L(i)\,v(i). \tag{D.10}$$

The optimal Kalman gain $L(i)$ for (D.9) is given by

$$\bar{P}(i) = A\,\hat{P}(i-1)\,A^T + Q(i-1), \tag{D.11a}$$

$$L(i) = \bar{P}(i)\,C^T\;\left(C\,\bar{P}(i)\,C^T + V(i)\right)^{-1}, \tag{D.11b}$$

$$\hat{P}(i) = (I_{n_x} - L(i)\,C)\;\bar{P}(i), \tag{D.11c}$$

see [7, 119]. Here, $\bar{P}(i)$ and $\hat{P}(i)$ represent, respectively, the predicted and the estimation error covariance matrix.

D.1.3 Derivation of the statistical properties of the estimator

Let us first remember the Woodbury matrix identity [230]:

$$(D + E\,F\,G)^{-1} = D^{-1} - D^{-1}\,E\,(F^{-1} + G\,D^{-1}\,E)^{-1}\,G\,D^{-1}. \tag{D.12}$$

Now, assuming $\upsilon_j = \upsilon$, for all j, we rewrite (4.33) as

$$P = (I - \nu P\,H^T (H \nu P\,H^T + T)^{-1}\,H)\,\nu\,P \tag{D.13}$$

with $\nu = 1 + \upsilon$. Premultiplying and postmultiplying (D.13) by $(\nu P)^{-1}$, and applying (D.12) to the term $(H\nu P H^T + T)^{-1}$ (with $D = T$, $E = H$, $F = \nu P$ and $G = H^T$) it leads to

$$(\nu^{-1} - \nu^{-2})P^{-1} = \Xi - \Xi(\nu^{-1}P^{-1} + \Xi)^{-1}\Xi \tag{D.14}$$

with $\Xi = H^T T^{-1} H$. Now, applying again (D.12) to the term $(\nu^{-1}P^{-1} + \Xi)^{-1}$ (with $D = \Xi$, $E = I$, $F = \nu^{-1}P^{-1}$ and $G = I$) we obtain that

$$(\nu^{-1} - \nu^{-2})P^{-1} = \left(\nu P + \Xi^{-1}\right)^{-1}. \tag{D.15}$$

Inverting both sides of the equality and substituting $\Xi = H^T T^{-1} H$, we finally have that

$$P = \frac{\nu - 1}{\nu}(H^T T^{-1} H)^{-1}. \tag{D.16}$$

For its part, at steady state, T is given by $T = (\Psi\, \Psi^T)^{\circ 2}$ and

$$\Psi\Psi^T = [\Gamma D\ R][\Gamma D\ R]^T = \Gamma D D^T \Gamma + R R^T. \tag{D.17}$$

From the definition of matrices D and R and using relation (4.3), we have that, at steady state,

$$\Psi\Psi^T = \Gamma\, \mathbf{\Sigma}_u^T\, \Gamma + \mathbf{\Sigma}_v = \mathbf{\Sigma}_y. \tag{D.18}$$

Then, matrix T can be expressed as

$$T = (\Psi\, \Psi^T)^{\circ 2} = \mathbf{\Sigma}_y \circ \mathbf{\Sigma}_y. \tag{D.19}$$

Finally, using (D.19) in (D.16) and substituting $\nu = 1 + \upsilon$, we get (4.34).

D.2 Auxiliary results of Chapter 7

D.2.1 State-space matrices of the wind turbine model

The state-space matrices of the *converter* model are $A^c = -\alpha_{gc}$ and $B^c = \alpha_{gc}$. The matrices C^c, F^c and H^c equal the identity matrix of appropriate dimensions while E^c, G^c and D^c are zero.

The state-space matrices of the *drive train* model are

$$A^c = \begin{bmatrix} a_{11} & a_{12} & a_{13} \\ a_{21} & a_{22} & a_{23} \\ 1 & a_{32} & 0 \end{bmatrix},\ B^c = \begin{bmatrix} 0 \\ b \\ 0 \end{bmatrix},\ G^c = \begin{bmatrix} 0 & 0 & 0 & 0 & 0 \\ 0 & 0 & 0 & 0 & -b \\ 0 & 0 & 0 & 0 & 0 \end{bmatrix},\ D^c = \begin{bmatrix} 1/J_r \\ 0 \\ 0 \end{bmatrix}$$

$$C^c = \begin{bmatrix} 1 & 0 & 0 \\ 1 & 0 & 0 \\ 0 & 1 & 0 \\ 0 & 1 & 0 \end{bmatrix},\ H^c = \begin{bmatrix} 1 & 0 & 0 & 0 & 0 \\ 0 & 1 & 0 & 0 & 0 \\ 0 & 0 & 1 & 0 & 0 \\ 0 & 0 & 0 & 1 & 0 \end{bmatrix}$$

with $a_{11} = \frac{-(B_{dt}+B_r)}{J_r}$, $a_{12} = \frac{B_{dt}}{N_g\, J_r}$, $a_{13} = \frac{-K_{dt}}{J_r}$, $a_{21} = \frac{\eta_{dt,0}\, B_{dt}}{N_g\, J_g}$, $a_{32} = \frac{-1}{N_g}$, $a_{22} = \frac{-(\eta_{dt,0}\, B_{dt} + B_g\, N_g^2)}{N_g^2\, J_g}$, $a_{23} = \frac{\eta_{dt,0}\, K_{dt}}{N_g\, J_g}$ and $b = \frac{-1}{J_g}$. We have that $E^c = 0$ and $F^c = I$.

The state-space matrices of each *pitch* model are

$$A^c = \begin{bmatrix} 0 & 1 \\ 2\,c & 2\,w_{n_0}\,\xi_0 \end{bmatrix},\ B^c = \begin{bmatrix} 0 \\ -2\,c \end{bmatrix},\ E^c = \begin{bmatrix} 0 & 0 & 0 \\ 1 & c & c \end{bmatrix},\ G^c = \begin{bmatrix} 0 & 0 \\ c & c \end{bmatrix},$$

$$C^c = \begin{bmatrix} 1 & 0 \\ 1 & 0 \end{bmatrix},\ F^c = \begin{bmatrix} 0 & 1 & 0 \\ 0 & 0 & 1 \end{bmatrix}$$

with $c = -w_{n_0}^2/2$, $H^c = I$ and $D^c = 0$.

D.2.2 Parameters of the wind turbine model

In the following, we include the values of the parameters of the wind turbine benchmark [216]. Table D.1 includes the parameters of the generator and converter system. Table D.2 includes the parameters of the drive train system. Table D.3 includes the parameters of the blade and pitch system. Table D.4 includes the parameters of the sensors that measure the signal indicated in the table.

Parameter		Value
α_{gc}	Model parameter	50 rad/s
η_g	Efficiency of the generator	0.98

Table D.1. Generator and converter parameters.

Parameter		Value
B_{dt}	Torsion damping coefficient of the drive train	775.49 Nms/rad
B_r	Viscous friction of the low-speed shaft	7.11 Nms/rad
B_g	Viscous friction of the high-speed shaft	45.6 Nms/rad
N_g	Gear ratio	95
K_{dt}	Torsion stiffness of the drive train	$2.7{\cdot}10^9$ Nms/rad
η_{dt}	Efficiency of the drive train	0.97
J_g	Moment of inertia of the high-speed shaft	390 kg/m^2
J_r	Moment of inertia of the low-speed shaft	$55{\cdot}10^6$ kg/m^2

Table D.2. Drive train parameters.

Parameter		Value
ξ_0	Damping factor	0.6
w_{n_0}	Natural frequency	11.11 rad/s

Table D.3. Blade and pitch parameters.

Measurement		Mean	Standard Deviation
v_w	Wind	1.5 m/s	0.71 m/s
ω_r	Rotor speed	0 rad/s	0.16 rad/s
ω_g	Generator speed	0 rad/s	0.22 rad/s
τ_g	Generator torque	0 Nm	9.5 Nm
P_g	Generated Power	0 W	1 31.6 W
β	Pitch Angle	0°	0.45°

Table D.4. Sensors parameters.

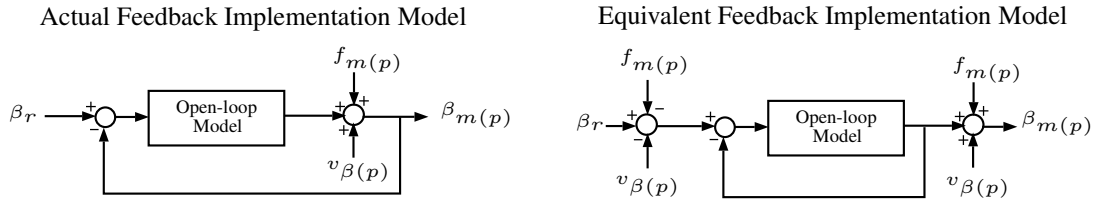

Figure D.1. Pitch system with one faulty and noisy sensor.

D.2.3 Fault observability in the subset S^3 of the pitch system

As stated in Section 7.6.2, condition (7.43) is not verified for the subset S^3. Provided that $n_s = n_y$ and given that input (fault) observability is directly related to system invertibility ([134, 205]), we study the transfer matrix between the faults in f^3 and y.

For ease of clarity, let us consider the analogous case in which the close-loop feedback is the measurement provided by only one sensor, named after $\beta_{m(p)}$, as depicted in Fig. D.1 (instead of the average of the measurements provided by two redundant sensors $\beta_{m_1(p)}$ and $\beta_{m_2(p)}$). In this illustrative appendix, we use a continuous-time formulation.

The transfer matrix of this simplified system satisfies

$$\beta_{m(p)}(s) = \begin{bmatrix} G_0(s) & G_f(s) & G_v(s) \end{bmatrix} \begin{bmatrix} \beta_r(s) \\ f_{m(p)}(s) \\ v_{\beta(p)}(s) \end{bmatrix},$$

with

$$G_0(s) = \frac{\omega_{n_0}^2}{s^2 + 2\,\xi_0\,\omega_{n_0}\,s + \omega_{n_0}^2},$$

$$G_f(s) = G_v(s) = 1 - G_0(s) = \frac{s(s + 2\,\xi_0\,\omega_{n_0})}{s^2 + 2\,\xi_0\,\omega_{n_0}\,s + \omega_{n_0}^2}.$$

The derivative term in $G_f(s)$ ruins the realizability of inverting $G_f(s)$.

Remark D.1. *Any common control loop defined by $H(s)$ has unitary static gain (i.e., $H(0) = 1$). Then, the transfer function $H_f(s) = 1 - H(s)$ between a sensor fault inside a closed loop and the corresponding measurement verifies $H_f(0) = 0$, which ruins the realizability of inverting $H_f(s)$.*

In order to get rid of the derivative term in $G_f(s)$, which causes the instability of the inverse of $G_f(s)$, we consider the derivative of fault $f_{m(p)}(s)$, named after $\dot{f}_{m(p)}(s)$, to be the fault input affecting $\beta_{m(p)}$. Thus, $\beta_{m(p)}(s)$ verifies

$$\beta_{m(p)}(s) = \begin{bmatrix} G_0(s) & G'_f(s) & G_v(s) \end{bmatrix} \begin{bmatrix} \beta_r(s) \\ \dot{f}_{m(p)}(s) \\ v_{\beta(p)}(s) \end{bmatrix},$$

with

$$G'_f(s) = \frac{G_f(s)}{s} = \frac{s + 2\,\xi_0\,\omega_{n_0}}{s^2 + 2\,\xi_0\,\omega_{n_0}\,s + \omega_{n_0}^2}.$$

Note that the inverse of $G'_f(s)$ is realizable.

D.3 Auxiliary results of Chapter 8

D.3.1 Uncertainties and partition of the parameter set

Once the bounds $|\widetilde{\nu}_p^i| \leq \lambda_p^i$ and $|\widetilde{\nu}_t^{i,j}| \leq \lambda_t$ have been computed as detailed Appendix C.2, we determine the bounds of the uncertainties e^i and $\varepsilon^{i,j}$, which are caused by these wind estimation errors. For sake of simplicity, define first the maximum wind propagation error bound as $\rho = \max_i \lambda_p^i$. Define also $\Psi(v^{i,j}) = a(v^{i,j})\bar{x} + \bar{u}(v^{i,j})$ with $\bar{x} = 4.8$ MW. The bounds of e^i and $\varepsilon^{i,j}$ for a certain wind speed $v^{i,j}$ verify

$$\overline{e^i(v^{i,j})} = \max\left\{\left|\Psi(v^{i,j}) - \Psi(v^{i,j} \pm \rho)\right|\right\},$$
$$\overline{\varepsilon^{i,j}(v^{i,j})} = \max\left\{\begin{array}{l} \left|\Psi(v^{i,j} + \rho) - \Psi(v^{i,j} + \rho \pm 3\,\sigma_t)\right| \\ \left|\Psi(v^{i,j} - \rho) - \Psi(v^{i,j} - \rho \pm 3\,\sigma_t)\right| \end{array}\right\}.$$

Fig. D.2 shows the results regarding e^i. Smaller bounds are obtained for $\varepsilon^{i,j}$ (not included here for brevity). Provided these results and given the form of $a(v^{i,j})$ in Fig. 8.2, we divide Ω_v into $N_v = 6$ subsets as shown in Table D.5. The table includes the value of the matrices in (8.18) (B_p^m is deduced from A_p^m) and the bounds of the uncertainties related to the wind speed estimation results in Appendix C.2.

Remark D.2. *At a WT level approach, the bounds $\bar{e}_p$ and $\bar{\varepsilon}_p$ in Table D.5 are independent of the considered wind direction. At a WF level approach, these values are also valid for WF models in which the turbines are grouped by rows. For other WT groupings, $\bar{e}_p$ and $\bar{\varepsilon}_p$ would be modified accordingly (see Remark 8.12).*

Provided the definition of the uncertainties $h^{i,j}$ and given the binary functions $c(\Delta^{i,j})$ and $d(\Delta^{i,j})$, we divide the set Ω_Δ into $N_\Delta = 4$ subsets as detailed in Table D.6. We have here considered that no WT operating mode estimation error appears above the 10% of the nominal power (i.e., 0.48 MW).

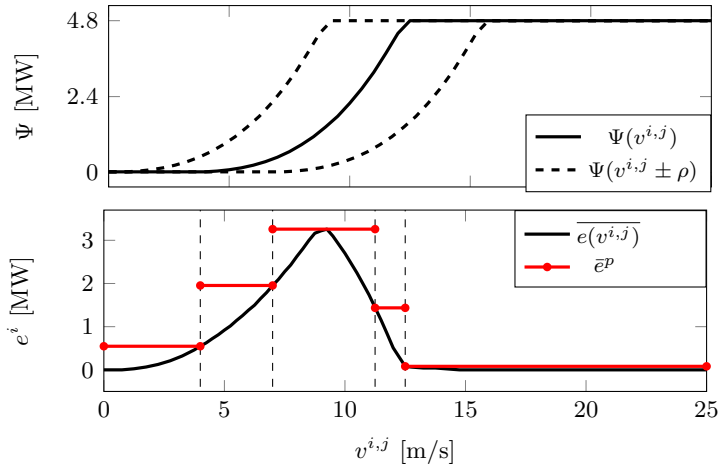

Figure D.2. Bounds $\bar{e}^p$ of the disturbance e^i ($\rho = 4$ m/s).

Table D.5. Partition of the set Ω_v.

p_v	Boundaries	A_p^1	A_p^2	$\bar{e}_p$ [m/s]	$\bar{\varepsilon}_p$ [m/s]
1	$0 \leq v < 4$	0.973 $\oplus$-1	0.973 $\oplus$-1	0.55	0.13
2	$4 \leq v < 7$	0.973 $\oplus$-1	0.934 $\oplus$-1	1.95	0.66
3	$7 \leq v < 11.25$	0.934 $\oplus$-1	0.895 $\oplus$-1	3.25	1.78
4	$11.25 \leq v < 12.5$	0.895 $\oplus$-1	0.891 $\oplus$-1	1.44	1.34
5	$12.5 \leq v < 25$	0.891 $\oplus$-1	0.891 $\oplus$-1	0.82	0.07
6	$25 \leq v < 30$	0.973 $\oplus$-1	0.973 $\oplus$-1	0.55	0.07

Table D.6. Partition of the set Ω_Δ.

p_Δ	Boundaries	C_p	D_p	$\bar{h}_p$ [MW]
1	-4.8 $\leq \Delta <$ -0.48	[1 -1]	0	0
2	-0.48$\leq \Delta <$ 0	[1 -1]	0	0.48
3	0$\leq \Delta <$ 0.48	[0 -1]	1	0.48
4	0.48$\leq \Delta <$ 4.8	[0 -1]	1	0

D.4 Auxiliary results of Chapter 9

D.4.1 Uncertainty and partition of the parameter set

Once the bounds $|\widetilde{\nu}_p^i| \leq \lambda_p^i$ and $|\widetilde{\nu}_t^{i,j}| \leq \lambda_t$ have been computed as detailed Appendix C.2, we determine the bounds of the errors of the pitch reference estimation. In the following, we include the bounds of the errors $\widetilde{u}^i$ (which depend on λ_p^i). A similar procedure is used to determine the bounds of the errors $\widetilde{u}^{i,j}$ (which depend on λ_p^i and λ_t). Fig. D.3 includes the values of the bounds $\lambda_{1,q}^i$ ($|\widetilde{u}^i| \leq \lambda_{1,q}^i$) verifying (9.15) for the wind speed estimation results in Appendix C.2. We include the results which are obtained when using three different numbers of intervals N_ν and

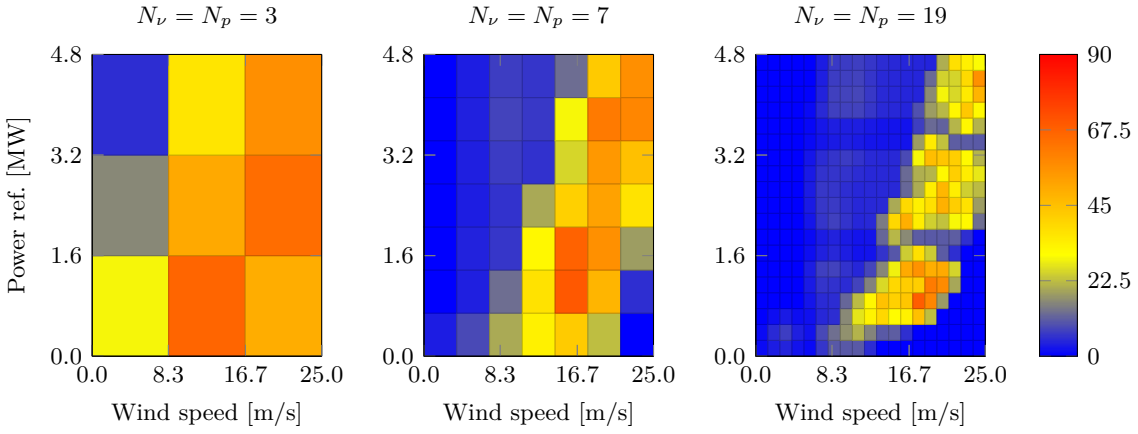

Figure D.3. Bounds of the pitch estimation error due to the propagation model mismatch [°] (0° layout, $i = 1$).

N_p. As the number of gridding intervals increases, the points in the set Θ associated to low pitch estimation errors increase. This enhances better FE and FD performances at the cost of heavier computational times. Thus, we choose the intermediate solution defined by $N_\nu = N_p = 7$.

Bibliography

[1] Ali Abdo, Steven X Ding, Jedsada Saijai, Waseem Damlakhi, and Haiyang Hao. Integration of residual evaluation and threshold computation into switched fault detection system. *IFAC Proceedings Volumes*, 45(20):1238–1243, 2012.

[2] José V Abellán-Nebot, Jian Liu, Fernando Romero Subirón, and Jianjun Shi. State space modeling of variation propagation in multistation machining processes considering machining-induced variations. *Journal of Manufacturing Science and Engineering*, 134(2):021002, 2012.

[3] José V Abellán-Nebot, Ignacio Peñarrocha, Ester Sales-Setién, and Jian Liu. Optimal inspection/actuator placement for robust dimensional compensation in multistage manufacturing processes. In *Computational Methods and Production Engineering*, pages 31–50. Elsevier, 2017.

[4] Muhammad Abid, Wei Chen, Steven X Ding, and Abdul Qayyum Khan. Optimal residual evaluation for nonlinear systems using post-filter and threshold. *International Journal of Control*, 84(3):526–539, 2011.

[5] Saeed Ahmadizadeh, Jafar Zarei, and Hamid Reza Karimi. Robust unknown input observer design for linear uncertain time delay systems with application to fault detection. *Asian Journal of Control*, 16(4):1006–1019, 2014.

[6] P Albertos and A Sala. Fault detection via continuous-time parameter estimation. *IFAC Proceedings Volumes*, 27(5):77–82, 1994.

[7] Pedro Albertos and Sala Antonio. *Multivariable control systems: an engineering approach*. Springer Science & Business Media, 2006.

[8] Halim Alwi and Christopher Edwards. Fault tolerant control using sliding modes with on-line control allocation. *Automatica*, 44(7):1859–1866, 2008.

[9] Johannes H Andersen and Roger S Powell. Implicit state-estimation technique for water network monitoring. *Urban Water*, 2(2):123–130, 2000.

[10] Sabrina Aouaouda, Mohammed Chadli, Peng Shi, and Hamid-Reza Karimi. Discrete-time H_-/H_∞ sensor fault detection observer design for nonlinear systems with parameter uncertainty. *International Journal of Robust and Nonlinear Control*, 25(3):339–361, 2015.

[11] Daniel W Apley and Jianjun Shi. Diagnosis of multiple fixture faults in panel assembly. *Journal of Manufacturing Science and Engineering*, 120(4):793–801, 1998.

[12] European Wind Energy Association. Wind in power. 2012 European statistics. *EWEA*, 2013.

[13] European Wind Energy Association. Wind in power: 2015 European statistics. *EWEA*, page 14, 2016.

[14] Crispin Aubrey. Supply chain: The race to meet demand. *Wind Directions*, pages 27–34, 2007.

[15] Hamed Badihi, Youmin Zhang, and Henry Hong. Active power control design for supporting grid frequency regulation in wind farms. *Annual Reviews in Control*, 40:70–81, 2015.

[16] Hamed Badihi, Youmin Zhang, and Henry Hong. Fault-tolerant cooperative control in an offshore wind farm using model-free and model-based fault detection and diagnosis approaches. *Applied Energy*, 2017.

[17] Bassam Bamieh and Laura Giarre. Identification of linear parameter varying models. *International Journal of Robust and Nonlinear Control*, 12(9):841–853, 2002.

[18] Amitabh Barua and Khashayar Khorasani. Hierarchical fault diagnosis and fuzzy rule-based reasoning for satellites formation flight. *IEEE Transactions on Aerospace and Electronic Systems*, 47(4):2435–2456, 2011.

[19] Richard Vernon Beard. *Failure accomodation in linear systems through self-reorganization.* PhD thesis, Massachusetts Institute of Technology, 1971.

[20] Nadia Bedjaoui and Erik Weyer. Algorithms for leak detection, estimation, isolation and localization in open water channels. *Control Engineering Practice*, 19(6):564–573, 2011.

[21] Mouhacine Benosman. A survey of some recent results on nonlinear fault tolerant control. *Mathematical Problems in Engineering*, 2010, 2010.

[22] Marta Bertelè, Carlo L Bottasso, and Stefano Cacciola. Automatic detection and correction of pitch misalignment in wind turbine rotors. *Wind Energy Science Discussions, in review*, 2018.

[23] Ran Bi, Chengke Zhou, and Donald M Hepburn. Detection and classification of faults in pitch-regulated wind turbine generators using normal behaviour models based on performance curves. *Renewable Energy*, 105:674–688, 2017.

[24] Fernando D Bianchi, Hernan De Battista, and Ricardo J Mantz. *Wind turbine control systems: principles, modelling and gain scheduling design.* Springer Science & Business Media, 2006.

[25] Fernando D Bianchi, Ricardo S Sánchez-Peña, and Marc Guadayol. Gain scheduled control based on high fidelity local wind turbine models. *Renewable Energy*, 37(1):233–240, 2012.

[26] Mehmet Bilgili, Abdulkadir Yasar, and Erdogan Simsek. Offshore wind power development in Europe and its comparison with onshore counterpart. *Renewable and Sustainable Energy Reviews*, 15(2):905–915, 2011.

[27] L Billmann and Rolf Isermann. Leak detection methods for pipelines. *Automatica*, 23(3):381–385, 1987.

[28] Mogens Blanke, Roozbeh Izadi-Zamanabadi, Søren A Bøgh, and Charlotte P Lunau. Fault-tolerant control systems – a holistic view. *Control Engineering Practice*, 5(5):693–702, 1997.

[29] Mogens Blanke, Michel Kinnaert, Jan Lunze, Marcel Staroswiecki, and Jochen Schröder. *Diagnosis and fault-tolerant control*, volume 691. Springer Science & Business Media, 2006.

[30] Joaquim Blesa, Pedro Jiménez, Damiano Rotondo, Fatiha Nejjari, and Vicenç Puig. An interval NLPV parity equations approach for fault detection and isolation of a wind farm. *IEEE Transactions on Industrial Electronics*, 62(6):3794–3805, 2015.

[31] Joaquim Blesa, Vicenç Puig, and Jordi Saludes. Robust identification and fault diagnosis based on uncertain multiple input–multiple output linear parameter varying parity equations and zonotopes. *Journal of Process Control*, 22(10):1890–1912, 2012.

[32] Joaquim Blesa, Damiano Rotondo, Vicenc Puig, and Fatiha Nejjari. FDI and FTC of wind turbines using the interval observer approach and virtual actuators/sensors. *Control Engineering Practice*, 24:138–155, 2014.

[33] Anders B Borcehrsen, Jesper A Larsen, and Jakob Stoustrup. Fault detection and load distribution for the wind farm challenge. *IFAC Proceedings Volumes*, 47(3):4316–4321, 2014.

[34] Jovan D Boskovic, Joseph A Jackson, Raman K Mehra, and Nhan T Nguyen. Multiple-model adaptive fault-tolerant control of a planetary lander. *Journal of Guidance, Control, and Dynamics*, 32(6):1812–1826, 2009.

[35] Ion Bostan, Adrian V Gheorghe, Valeriu Dulgheru, Ion Sobor, Viorel Bostan, and Anatolie Sochirean. *Resilient energy systems: renewables: wind, solar, hydro*, volume 19. Springer Science & Business Media, 2012.

[36] Paul Boulos and Tom Altman. A graph-theoretic approach to explicit nonlinear pipe network optimization. *Applied Mathematical Modelling*, 15(9):459–466, 1991.

[37] James M Buffington, Phillip R Chandler, and Meir Pachter. On-line system identification for aircraft with distributed control effectors. *International Journal of Robust and Nonlinear Control*, 9(14):1033–1049, 1999.

[38] Tony Burton, David Sharpe, Nick Jenkins, and Ervin Bossanyi. *Wind energy handbook*. John Wiley & Sons, 2001.

[39] Eduardo Cabal-Yepez, Armando G Garcia-Ramirez, Rene J Romero-Troncoso, Arturo Garcia-Perez, and Roque A Osornio-Rios. Reconfigurable monitoring system for time-frequency analysis on industrial equipment through STFT and DWT. *IEEE Transactions on Industrial Informatics*, 9(2):760–771, 2013.

[40] A Carpinone, Massimiliano Giorgio, Roberto Langella, and Alfredo Testa. Markov chain modeling for very-short-term wind power forecasting. *Electric Power Systems Research*, 122:152–158, 2015.

[41] Jeang-Lin Chang. Applying discrete-time proportional integral observers for state and disturbance estimations. *IEEE Transactions on Automatic Control*, 51(5):814–818, 2006.

[42] Boli Chen, Gilberto Pin, Wai N Ng, Shu Yuen Hui, and Thomas Parisini. An adaptive observer-based robust estimator of multi-sinusoidal signals. *IEEE Transactions on Automatic Control*, 2017.

[43] Cheng-I Chen and Yeong-Chin Chen. Comparative study of harmonic and interharmonic estimation methods for stationary and time-varying signals. *IEEE Transactions on Industrial Electronics*, 61(1):397–404, 2014.

[44] Jie Chen and Ron J Patton. *Robust model-based fault diagnosis for dynamic systems*, volume 3. Springer Science & Business Media, 2012.

[45] Jie Chen, Ron J Patton, and Hong-Yue Zhang. Design of unknown input observers and robust fault detection filters. *International Journal of Control*, 63(1):85–105, 1996.

[46] Lejun Chen, Ron J Patton, and Philippe Goupil. Robust fault estimation and performance evaluation based upon the ADDSAFE benchmark model. *IFAC Proceedings Volumes*, 45(20):1364–1369, 2012.

[47] Pang-Chia Chen and Jeff S Shamma. Gain-scheduled l^1-optimal control for boiler-turbine dynamics with actuator saturation. *Journal of Process Control*, 14(3):263–277, 2004.

[48] Wei Chen, Steven X Ding, Adel Haghani, Amol Naik, Abdul Qayyum Khan, and Shen Yin. Observer-based FDI schemes for wind turbine benchmark. In *Proceedings of the IFAC World Congress, 2011*, pages 7073–7078, 2011.

[49] Wei Chen, Abdul Khan, Muhammmad Abid, and Steven Ding. Integrated design of observer based fault detection for a class of uncertain nonlinear systems. *International Journal of Applied Mathematics and Computer Science*, 21(3):423–430, 2011.

[50] Wen Chen and Mehrdad Saif. An iterative learning observer for fault detection and accommodation in nonlinear time-delay systems. *International Journal of Robust and Nonlinear Control*, 16(1):1–19, 2006.

[51] Mahmoud Chilali and Pascal Gahinet. Hinf design with pole placement constraints: an LMI approach. *IEEE Transactions on Automatic Control*, 41(3):358–367, 1996.

[52] Charles K Chui, Guanrong Chen, et al. *Kalman filtering with real time applications*. Springer, 1999.

[53] Jérôme Cieslak, Denis Efimov, and David Henry. Transient management of a supervisory fault-tolerant control scheme based on dwell-time conditions. *International Journal of Adaptive Control and Signal Processing*, 29(1):123–142, 2015.

[54] Zafer Civelek, Murat Lüy, Ertuğrul Çam, and Hayati Mamur. A new fuzzy logic proportional controller approach applied to individual pitch angle for wind turbine load mitigation. *Renewable Energy*, 111:708–717, 2017.

[55] Vicente Climente-Alarcon, Jose A Antonino-Daviu, Martin Riera-Guasp, and Miroslav Vlcek. Induction motor diagnosis by advanced notch fir filters and the wigner–ville distribution. *IEEE Transactions on Industrial Electronics*, 61(8):4217–4227, 2014.

[56] Matteo Corno, Sergio M Savaresi, and Gary J Balas. On linear-parameter-varying (LPV) slip-controller design for two-wheeled vehicles. *International Journal of Robust and Nonlinear Control*, 19(12):1313–1336, 2009.

[57] Oswaldo LV Costa, Marcelo D Fragoso, and Ricardo P Marques. *Discrete-time Markov jump linear systems*. Springer Science & Business Media, 2006.

[58] Global Wind Energy Council. Global wind report: Annual market update 2012. *GWEC*, 2012.

[59] Global Wind Energy Council. Global wind report: Annual market update 2015. *GWEC*, 2014.

[60] Global Wind Energy Council. Global wind report: Annual market update 2016. *GWEC*, 2016.

[61] Andrea Cristofaro and Tor Arne Johansen. Fault tolerant control allocation using unknown input observers. *Automatica*, 50(7):1891–1897, 2014.

[62] Jamal Daafouz, Pierre Riedinger, and Claude Iung. Stability analysis and control synthesis for switched systems: a switched Lyapunov function approach. *IEEE Transactions on Automatic Control*, 47(11):1883–1887, 2002.

[63] Xiao-kun Dai, Yang Song, Mira Schüller, and Dieter Schramm. Stability analysis of wind turbines combined with rechargeable batteries based on Markov jump linear systems. In *Advanced Computational Methods in Energy, Power, Electric Vehicles, and Their Integration*, pages 126–136. Springer Science & Business Media, 2017.

[64] N Dalili, Afsaneh Edrisy, and Rupp Carriveau. A review of surface engineering issues critical to wind turbine performance. *Renewable and Sustainable Energy Reviews*, 13(2):428–438, 2009.

[65] Zahra Daneshi-Far, Gérard A Capolino, and Humberto Henao. Review of failures and condition monitoring in wind turbine generators. In *Proceedings of the XIX International Conference on Electrical Machines (ICEM), 2010*, pages 1–6. IEEE, 2010.

[66] Mohamed Darouach, Michel Zasadzinski, and Shi Jie Xu. Full-order observers for linear systems with unknown inputs. *IEEE Transactions on Automatic Control*, 39(3):606–609, 1994.

[67] H d'Assumpcao. Some new signal processors for arrays of sensors. *IEEE Transactions on Information Theory*, 26(4):441–453, 1980.

[68] Iury V de Bessa, Reinaldo M Palhares, Marcos F S V D'Angelo, and João E F Chaves. Data-driven fault detection and isolation scheme for a wind turbine benchmark. *Renewable Energy*, 87:634–645, 2016.

[69] Maurício C de Oliveira, Jacques Bernussou, and José C Geromel. A new discrete-time robust stability condition. *Systems & Control Letters*, 37(4):261–265, 1999.

[70] Steven X Ding. *Model-based fault diagnosis techniques: design schemes, algorithms, and tools*. Springer Science & Business Media, 2008.

[71] Steven X Ding. *Data-driven design of fault diagnosis and fault-tolerant control systems*. Springer Science & Business Media, 2014.

[72] Steven X Ding, Paul M Frank, Eve L Ding, and Torsten Jeinsch. Fault detection system design based on a new trade-off strategy. In *Proceedings of the 39th IEEE Conference on Decision and Control, 2000*, volume 4, pages 4144–4149. IEEE, 2000.

[73] Steven X Ding, Torsten Jeinsch, Paul M Frank, and Eve L Ding. A unified approach to the optimization of fault detection systems. *International Journal of Adaptive Control and Signal Processing*, 14(7):725–745, 2000.

[74] Steven X Ding, Ping N Zhang, Paul M Frank, and Eve L Ding. Threshold calculation using LMI-technique and its integration in the design of fault detection systems. In *Proceedings of the 42nd IEEE Conference on Decision and Control, 2003*, pages 469–474, 2003.

[75] Xianchun Ding, Limin Guo, and Torsten Jeinsch. A characterization of parity space and its application to robust fault detection. *IEEE Transactions on Automatic Control*, 44(2):337–343, 1999.

[76] Yu Ding, Pansoo Kim, Dariusz Ceglarek, and Jionghua Jin. Optimal sensor distribution for variation diagnosis in multistation assembly processes. *IEEE Transactions on Robotics and Automation*, 19(4):543–556, 2003.

[77] Yu Ding, Jianjun Shi, and Dariusz Ceglarek. Diagnosability analysis of multi-station manufacturing processes. *Journal of Dynamic Systems, Measurement, and Control*, 124(1):1–13, 2002.

[78] Yu Ding, Shiyu Zhou, and Yong Chen. A comparison of process variation estimators for in-process dimensional measurements and control. *Journal of Dynamic Systems, Measurement, and Control*, 127:69, 2005.

[79] Jiuxiang Dong, Yue Wu, and Guang-Hong Yang. A new sensor fault isolation method for T–S fuzzy systems. *IEEE Transactions on Cybernetics*, 47(9):2437–2447, 2017.

[80] James Doorhy. Real-time pipeline leak detection and location using volume balancing. *Pipeline & Gas Journal*, 238(2):65–66, 2011.

[81] Richard C Dorf and Robert H Bishop. *Modern control systems*. Pearson, 2011.

[82] Guang-Ren Duan and Ai-Guo Wu. Robust fault detection in linear systems based on PI observers. *International Journal of Systems Science*, 37(12):809–816, 2006.

[83] Eric Duviella, Lisa Serir, and Moamar Sayed-Mouchaweh. An evolving classification approach for fault diagnosis and prognosis of a wind farm. In *Proceedings of the 2nd Conference on Control and Fault-Tolerant Systems (SysTol), 2013*, pages 377–382. IEEE, 2013.

[84] Christopher Edwards, Sarah K Spurgeon, and Ron J Patton. Sliding mode observers for fault detection and isolation. *Automatica*, 36(4):541–553, 2000.

[85] Christopher Edwards and Chee P Tan. Sensor fault tolerant control using sliding mode observers. *Control Engineering Practice*, 14(8):897–908, 2006.

[86] Laurent El Ghaoui, Francois Oustry, and Mustapha AitRami. A cone complementarity linearization algorithm for static output-feedback and related problems. *IEEE Transactions on Automatic Control*, 42(8):1171–1176, 1997.

[87] Omar Ellabban, Haitham Abu-Rub, and Frede Blaabjerg. Renewable energy resources: Current status, future prospects and their enabling technology. *Renewable and Sustainable Energy Reviews*, 39:748–764, 2014.

[88] Jorge O Estima and António J Marques Cardoso. A new algorithm for real-time multiple open-circuit fault diagnosis in voltage-fed pwm motor drives by the reference current errors. *IEEE Transactions on Industrial Electronics*, 60(8):3496–3505, 2013.

[89] John S Eterno, Jerold L Weiss, Douglas P Looze, and Alan Willsky. Design issues for fault tolerant-restructurable aircraft control. In *Proceedings of the 24th IEEE Conference on Decision and Control, 1985*, volume 24, pages 900–905. IEEE, 1985.

[90] Wind Europe. Offshore wind in Europe. Key trends and statistics 2017. *Wind Europe*, 2018.

[91] Wind Europe. Wind in power. 2016 European statistics. *Wind Europe*, 2018.

[92] Wind Europe. Wind in power 2017. Annual combined onshore and offshore wind energy statistics. *Wind Europe*, 2018.

[93] Rosa M Fernandez-Canti, Joaquim Blesa, Sebastian Tornil-Sin, and Vicenç Puig. Fault detection and isolation for a wind turbine benchmark using a mixed bayesian/set-membership approach. *Annual Reviews in Control*, 40:59–69, 2015.

[94] Dieter Filbert. Fault diagnosis in nonlinear electromechanical systems by continuous time parameter estimation. *ISA Transactions*, 24(3):23–27, 1985.

[95] Paul M Frank. Fault diagnosis in dynamic systems using analytical and knowledge-based redundancy: A survey and some new results. *Automatica*, 26(3):459–474, 1990.

[96] Paul M Frank, Steven X Ding, and Teodor Marcu. Model-based fault diagnosis in technical processes. *Transactions of the Institute of Measurement and Control*, 22(1):57–101, 2000.

[97] Paul M Frank and Xianchun Ding. Survey of robust residual generation and evaluation methods in observer-based fault detection systems. *Journal of Process Control*, 7(6):403–424, 1997.

[98] Shasha Fu, Jianbin Qiu, Liheng Chen, and Shaoshuai Mou. Adaptive fuzzy observer design for a class of switched nonlinear systems with actuator and sensor faults. *IEEE Transactions on Fuzzy Systems*, 2018.

[99] Zhiwei Gao. Fault estimation and fault-tolerant control for discrete-time dynamic systems. *IEEE Transactions on Industrial Electronics*, 62(6):3874–3884, 2015.

[100] Zhiwei Gao, Carlo Cecati, and Steven X Ding. A survey of fault diagnosis and fault-tolerant techniques – Part I: Fault diagnosis with model-based and signal-based approaches. *IEEE Transactions on Industrial Electronics*, 62(6):3757–3767, 2015.

[101] Zhiwei Gao, Carlo Cecati, and Steven X Ding. A survey of fault diagnosis and fault-tolerant techniques – Part II: Fault diagnosis with knowledge-based and hybrid/active approaches. *IEEE Transactions on Industrial Electronics*, 62(6):3768–3774, 2015.

[102] Zhiwei Gao and Steven X Ding. Actuator fault robust estimation and fault-tolerant control for a class of nonlinear descriptor systems. *Automatica*, 43(5):912–920, 2007.

[103] Zhiwei Gao and Steven X Ding. Fault estimation and fault-tolerant control for descriptor systems via proportional, multiple-integral and derivative observer design. *IET Control Theory & Applications*, 1(5):1208–1218, 2007.

[104] Zhiwei Gao, Steven X Ding, and Y Ma. Robust fault estimation approach and its application in vehicle lateral dynamic systems. *Optimal Control Applications and Methods*, 28(3):143–156, 2007.

[105] Zhiwei Gao and Daniel WC Ho. Proportional multiple-integral observer design for descriptor systems with measurement output disturbances. *IEE Proceedings-Control Theory and Applications*, 151(3):279–288, 2004.

[106] Zhiwei Gao, Xiaoxu Liu, and Michael ZQ Chen. Unknown input observer-based robust fault estimation for systems corrupted by partially decoupled disturbances. *IEEE Transactions on Industrial Electronics*, 63(4):2537–2547, 2016.

[107] Gerhard Geiger, Thomas Werner, and Drago Matko. Leak detection and locating - a survey. In *Proceedings of the PSIG Annual Meeting, 2003*. Pipeline Simulation Interest Group, 2003.

[108] José C Geromel, Cid C De Souza, and Robert E Skelton. LMI numerical solution for output feedback stabilization. In *Proceedings of the American Control Conference, 1994*, volume 1, pages 40–44. IEEE, 1994.

[109] Janos Gertler. Analytical redundancy methods in fault detection and isolation-survey and synthesis. *IFAC Proceedings Volumes*, 24(6):9–21, 1991.

[110] Janos Gertler. Diagnosing parametric faults: from parameter estimation to parity relations. In *Proceedings of the American Control Conference, 1995*, volume 3, pages 1615–1620. IEEE, 1995.

[111] Janos Gertler. Fault detection and diagnosis in engineering systems. *CRC, Virginia, USA*, 1998.

[112] Janos Gertler. *Fault Detection and Diagnosis*, pages 1–7. Springer London, 2013.

[113] Xiang Gong and Wei Qiao. Imbalance fault detection of direct-drive wind turbines using generator current signals. *IEEE Transactions on Energy Conversion*, 27(2):468–476, 2012.

[114] Xiang Gong and Wei Qiao. Bearing fault diagnosis for direct-drive wind turbines via current-demodulated signals. *IEEE Transactions on Industrial Electronics*, 60(8):3419–3428, 2013.

[115] Elena Gonzalez, Bruce Stephen, David Infield, and Julio J Melero. Using high-frequency scada data for wind turbine performance monitoring: A sensitivity study. *Renewable Energy*, 131:841–853, 2019.

[116] Asier González-González, Alberto Jimenez Cortadi, Diego Galar, and Lorenzo Ciani. Condition monitoring of wind turbine pitch controller: A maintenance approach. *Measurement*, 123:80–93, 2018.

[117] Graham C Goodwin, Stefan F Graebe, and Mario E Salgado. Control system design. *Upper Saddle River*, page 13, 2001.

[118] Philippe Goupil and Andres Marcos. Advanced diagnosis for sustainable flight guidance and control: The European addsafe project. Technical report, SAE technical paper, 2011.

[119] Mohinder S Grewal. Kalman filtering. In *International Encyclopedia of Statistical Science*, pages 705–708. Springer, 2011.

[120] Yuping Guan and Mehrdad Saif. A novel approach to the design of unknown input observers. *IEEE Transactions on Automatic Control*, 36(5):632–635, 1991.

[121] Thierry Marie Guerra, Raymundo Márquez, Alexandre Kruszewski, and Miguel Bernal. H_∞ LMI-based observer design for nonlinear systems via Takagi–Sugeno models with unmeasured premise variables. *IEEE Transactions on Fuzzy Systems*, 26(3):1498–1509, 2018.

[122] Jinchao Guo, Xinhan Huang, and Yu Cui. Design and analysis of robust fault detection filter using LMI tools. *Computers & Mathematics with Applications*, 57(11):1743–1747, 2009.

[123] Vijay Gupta, Richard M Murray, Ling Shi, and Bruno Sinopoli. Networked sensing, estimation and control systems.

[124] Berthold Hahn, Michael Durstewitz, and Kurt Rohrig. Reliability of wind turbines. In *Wind energy*, pages 329–332. Springer, 2007.

[125] Mirza T Hamayun, Christopher Edwards, and Halim Alwi. *Fault tolerant control schemes using integral sliding modes*. Springer Science & Business Media, 2016.

[126] Anca D Hansen, Poul Sørensen, Florin Iov, and Frede Blaabjerg. Centralised power control of wind farm with doubly fed induction generators. *Renewable Energy*, 31(7):935–951, 2006.

[127] Amir Hossein Hassanabadi, Masoud Shafiee, and Vicenc Puig. UIO design for singular delayed LPV systems with application to actuator fault detection and isolation. *International Journal of Systems Science*, 47(1):107–121, 2016.

[128] Carl W Helstrom. *Statistical Theory of Signal Detection: International Series of Monographs in Electronics and Instrumentation*, volume 9. Elsevier, 2013.

[129] Didier Henrion, Johan Löfberg, Michal Kočvara, and Michael Stingl. Solving polynomial static output feedback problems with PENBMI. In *Proceedings of the 44th IEEE Conference on Decision and Control, 2005*, pages 7581–7586. IEEE, 2005.

[130] GM Joselin Herbert, S Iniyan, and Ranko Goic. Performance, reliability and failure analysis of wind farm in a developing country. *Renewable Energy*, 35(12):2739–2751, 2010.

[131] David Mautner Himmelblau. *Fault detection and diagnosis in chemical and petrochemical processes*, volume 8. Elsevier Science Ltd, 1978.

[132] Liu Hong and Jaspreet Singh Dhupia. A time domain approach to diagnose gearbox fault based on measured vibration signals. *Journal of Sound and Vibration*, 333(7):2164–2180, 2014.

[133] Ming Hou and Ron J Patton. An lmi approach to $\mathcal{H}_-/\mathcal{H}_\infty$ fault detection observers. In *Proceedings of the UKACC International Conference, 1996*. IET, 1996.

[134] Ming Hou and Ron J Patton. Input observability and input reconstruction. *Automatica*, 34(6):789–794, 1998.

[135] Sheng-Juan Huang and Guang-Hong Yang. Fault estimation for fuzzy delay systems: A minimum norm least squares solution approach. *IEEE Transactions on Cybernetics*, 47(9):2389–2399, 2017.

[136] Sheng-Juan Huang, Da-Qing Zhang, Liang-Dong Guo, and Li-Bing Wu. Convergent fault estimation for linear systems with faults and disturbances. *IEEE Transactions on Automatic Control*, 63(3):888–893, 2018.

[137] Inseok Hwang, Sungwan Kim, Youdan Kim, and Chze Eng Seah. A survey of fault detection, isolation, and reconfiguration methods. *IEEE Transactions on Control Systems Technology*, 18(3):636–653, 2010.

[138] Rolf Isermann. Supervision, fault-detection and fault-diagnosis methods—an introduction. *Control Engineering Practice*, 5(5):639–652, 1997.

[139] Rolf Isermann. Model-based fault-detection and diagnosis–status and applications. *Annual Reviews in Control*, 29(1):71–85, 2005.

[140] Rolf Isermann. *Fault-diagnosis systems: an introduction from fault detection to fault tolerance*. Springer Science & Business Media, 2006.

[141] Rolf Isermann and Peter Ballé. Trends in the application of model-based fault detection and diagnosis of technical processes. *Control Engineering Practice*, 5(5):709–719, 1997.

[142] Imad M Jaimoukha, Zhenhai Li, and Vasilios Papakos. A matrix factorization solution to the $\mathcal{H}_-/\mathcal{H}_\infty$ fault detection problem. *Automatica*, 42(11):1907–1912, 2006.

[143] Bin Jiang and Fahmida N Chowdhury. Fault estimation and accommodation for linear MIMO discrete-time systems. *IEEE Transactions on Control Systems Technology*, 13(3):493–499, 2005.

[144] Bin Jiang, Marcel Staroswiecki, and Vincent Cocquempot. Fault accommodation for nonlinear dynamic systems. *IEEE Transactions on Automatic Control*, 51(9):1578–1583, 2006.

[145] Tao Jiang, Khashayar Khorasani, and Siamak Tafazoli. Parameter estimation-based fault detection, isolation and recovery for nonlinear satellite models. *IEEE Transactions on control systems technology*, 16(4):799–808, 2008.

[146] Jionghua Jin and Jianjun Shi. State space modeling of sheet metal assembly for dimensional control. *Journal of Manufacturing Science and Engineering*, 121(4):756–762, 1999.

[147] Barry W Johnson, James H Aylor, and Haytham H Hana. Efficient use of time and hardware redundancy for concurrent error detection in a 32-bit vlsi adder. *IEEE Journal of Solid-state Circuits*, 23(1):208–215, 1988.

[148] Gojko M Joksimović, Jakša Riger, Thomas M Wolbank, Nedjeljko Perić, and Mario Vašak. Stator-current spectrum signature of healthy cage rotor induction machines. *IEEE Transactions on Industrial Electronics*, 60(9):4025–4033, 2013.

[149] RB Jørgensen, Ron J Patton, and Jie Chen. Fault detection and isolation using eigenstructure assignment. *IFAC Proceedings Volumes*, 27(5):463–469, 1994.

[150] A Joshuva and V Sugumaran. A data driven approach for condition monitoring of wind turbine blade using vibration signals through best-first tree algorithm and functional trees algorithm: A comparative study. *ISA Transactions*, 67:160–172, 2017.

[151] Thomas Kailath. *Linear systems*, volume 156. Prentice-Hall, 1980.

[152] Rudolph E Kalman. A new approach to linear filtering and prediction problems. *Journal of Fluids Engineering*, 82(1):35–45, 1960.

[153] Elkhatib Kamal and Abdel Aitouche. Robust fault tolerant control of DFIG wind energy systems with unknown inputs. *Renewable Energy*, 56:2–15, 2013.

[154] Yusuf Alper Kaplan. Overview of wind energy in the world and assessment of current wind energy policies in turkey. *Renewable and Sustainable Energy Reviews*, 43:562–568, 2015.

[155] Atef Khedher, Kamel Benothman, Didier Maquin, and Mohamed Benrejeb. State and sensor faults estimation via a proportional integral observer. In *Proceedings of the 6th International Multi-Conference on Systems, Signals and Devices, 2009*, pages 1–6. IEEE, 2009.

[156] Kyung-Soo Kim, Keun-Ho Rew, and Soohyun Kim. Disturbance observer for estimating higher order disturbances in time series expansion. *IEEE Transactions on automatic control*, 55(8):1905–1911, 2010.

[157] Aram Kirakosyan, Mohamed Shawky El Moursi, and Vinod Khadkikar. Fault ride through and grid support topology for the VSC-HVDC connected offshore wind farms. *IEEE Transactions on Power Delivery*, 32(3):1592–1604, 2017.

[158] Genshiro Kitagawa and Will Gersch. *Smoothness priors analysis of time series*, volume 116. Springer Science & Business Media, 2012.

[159] Torben Knudsen, Thomas Bak, and Mohsen Soltani. Prediction models for wind speed at turbine locations in a wind farm. *Wind Energy*, 14(7):877–894, 2011.

[160] Torben Knudsen, Thomas Bak, and Mikael Svenstrup. Survey of wind farm control-power and fatigue optimization. *Wind Energy*, 18(8):1333–1351, 2015.

[161] Michal Kočvara and Michael Stingl. PENNON: A code for convex nonlinear and semidefinite programming. *Optimization Methods and Software*, 18(3):317–333, 2003.

[162] Damien Koenig. Unknown input proportional multiple-integral observer design for linear descriptor systems: application to state and fault estimation. *IEEE Transactions on Automatic Control*, 50(2):212–217, 2005.

[163] Damien Koenig and Said Mammar. Design of proportional-integral observer for unknown input descriptor systems. *IEEE Transactions on Automatic Control*, 47(12):2057–2062, 2002.

[164] Suneel K Kommuri, Michael Defoort, Hamid R Karimi, and Kalyana C Veluvolu. A robust observer-based sensor fault-tolerant control for PMSM in electric vehicles. *IEEE Transactions on Industrial Electronics*, 63(12):7671–7681, 2016.

[165] Józef Korbicz, Jan M Koscielny, Zdzislaw Kowalczuk, and Wojciech Cholewa. *Fault diagnosis: models, artificial intelligence, applications*. Springer Science & Business Media, 2012.

[166] Patrick Kühne, Florian Pöschke, and Horst Schulte. Fault estimation and fault-tolerant control of the FAST NREL 5-MW reference wind turbine using a proportional multi-integral observer. *International Journal of Adaptive Control and Signal Processing*, 2017.

[167] Yogesh Kumar, Jordan Ringenberg, Soma Shekara Depuru, Vijay K Devabhaktuni, Jin Woo Lee, Efstratios Nikolaidis, Brett Andersen, and Abdollah Afjeh. Wind energy: Trends and enabling technologies. *Renewable and Sustainable Energy Reviews*, 53:209–224, 2016.

[168] Andrew Kusiak and Anoop Verma. A data-driven approach for monitoring blade pitch faults in wind turbines. *IEEE Transactions on Sustainable Energy*, 2(1):87–96, 2011.

[169] Josh Kusnick, Douglas E Adams, and Daniel T Griffith. Wind turbine rotor imbalance detection using nacelle and blade measurements. *Wind Energy*, 18(2):267–276, 2015.

[170] Jianglin Lan. *Robust model-based fault estimation and fault-tolerant control: Towards an integration*. PhD thesis, The University of Hull, 2017.

[171] Jianglin Lan and Ron J Patton. A new strategy for integration of fault estimation within fault-tolerant control. *Automatica*, 69:48–59, 2016.

[172] Jianglin Lan and Ron J Patton. Integrated fault estimation and fault-tolerant control for uncertain Lipschitz nonlinear systems. *International Journal of Robust and Nonlinear Control*, 27(5):761–780, 2017.

[173] Jianglin Lan, Ron J Patton, and Xiaoyuan Zhu. Fault-tolerant wind turbine pitch control using adaptive sliding mode estimation. *Renewable Energy*, 2016.

[174] Ioan Doré Landau and Gianluca Zito. *Digital control systems: design, identification and implementation*. Springer Science & Business Media, 2007.

[175] Jing Li, Jionghua Jin, and Jianjun Shi. Causation-based T^2 decomposition for multivariate process monitoring and diagnosis. *Journal of Quality Technology*, 40(1):46–58, 2008.

[176] Shusheng Li and Maiying Zhong. High-precision disturbance compensation for a three-axis gyro-stabilized camera mount. *IEEE/ASME Transactions on Mechatronics*, 20(6):3135–3147, 2015.

[177] Xiao-Jian Li, Jing-Jing Yan, and Guang-Hong Yang. Adaptive fault estimation for TS fuzzy interconnected systems based on persistent excitation condition via reference signals. *IEEE Transactions on Cybernetics*, (99):1–13, 2018.

[178] Xiaohang Li, Hamid Reza Karimi, Yueying Wang, Dunke Lu, and Shenghui Guo. Robust fault estimation and fault-tolerant control for Markovian jump systems with general uncertain transition rates. *Journal of the Franklin Institute*, 355(8):3508–3540, 2018.

[179] Xiaohang Li, Dunke Lu, Guohui Zeng, Jin Liu, and Wei Zhang. Integrated fault estimation and non-fragile fault-tolerant control design for uncertain Takagi–Sugeno fuzzy systems with actuator fault and sensor fault. *IET Control Theory & Applications*, 11(10):1542–1553, 2017.

[180] Xiaohang Li and Fanglai Zhu. Simultaneous time-varying actuator and sensor fault reconstruction based on PI observer for LPV systems. *International Journal of Adaptive Control and Signal Processing*, 29(9):1086–1098, 2015.

[181] Yueyang Li, Hamid Reza Karimi, Maiying Zhong, Steven X Ding, and Shuai Liu. Fault detection for linear discrete time-varying systems with multiplicative noise: The finite-horizon case. *IEEE Transactions on Circuits and Systems I: Regular Papers*, 2018.

[182] Zhenhai Li, Emmanuel Mazars, Ze Zhang, and Imad M Jaimoukha. State–space solution to the H_-/H_∞ fault-detection problem. *International Journal of Robust and Nonlinear Control*, 22(3):282–299, 2012.

[183] Hai Lin and Panos J Antsaklis. Stability and stabilizability of switched linear systems: a survey of recent results. *IEEE Transactions on Automatic control*, 54(2):308–322, 2009.

[184] Zhongwei Lin, Jizhen Liu, Qiuwei Wu, and Yuguang Niu. Mixed H_2/H_∞ pitch control of wind turbine with a Markovian jump model. *International Journal of Control*, 91(1):156–169, 2018.

[185] Zhongwei Lin, Jizhen Liu, Weihai Zhang, and Yuguang Niu. Regional pole placement of wind turbine generator system via a Markovian approach. *IET Control Theory & Applications*, 10(15):1771–1781, 2016.

[186] Robert S Liptser and Albert N Shiryaev. *Statistics of random Processes: I. general Theory*, volume 5. Springer Science & Business Media, 2013.

[187] Jian Liu, Jionghua Jin, and Jianjun Shi. State space modeling for 3-D variation propagation in rigid-body multistage assembly processes. *IEEE Transactions on Automation Science and Engineering*, 7(2):274–290, 2010.

[188] Ming Liu and Peng Shi. Sensor fault estimation and tolerant control for itô stochastic systems with a descriptor sliding mode approach. *Automatica*, 49(5):1242–1250, 2013.

[189] Xiaoxu Liu, Zhiwei Gao, and Michael ZQ Chen. Takagi–Sugeno fuzzy model based fault estimation and signal compensation with application to wind turbines. *IEEE Transactions on Industrial Electronics*, 64(7):5678–5689, 2017.

[190] Xiaoxu Liu, Zhiwei Gao, and Aihua Zhang. Robust fault tolerant control for discrete-time dynamic systems with applications to aero engineering systems. *IEEE Access*, 6:18832–18847, 2018.

[191] Lennart Ljung. *System identification*. Springer, 1998.

[192] Johan Lofberg. YALMIP: A toolbox for modeling and optimization in MATLAB. In *Proceedings of the IEEE International Symposium on Computer Aided Control Systems Design, 2004*, pages 284–289. IEEE, 2004.

[193] Mufeed Mahmoud, Jin Jiang, and Youmin Zhang. *Active fault tolerant control systems: stochastic analysis and synthesis*, volume 287. Springer Science & Business Media, 2003.

[194] Yashwant K. Malaiya and Stephen Y. H. Su. Reliability measure of hardware redundancy fault-tolerant digital systems with intermittent faults. *IEEE Transactions on Computers*, (8):600–604, 1981.

[195] Ramakrishna Mantripragada and Daniel E Whitney. Modeling and controlling variation propagation in mechanical assemblies using state transition models. *IEEE Transactions on Robotics and Automation*, 15(1):124–140, 1999.

[196] Antonino Marvuglia and Antonio Messineo. Monitoring of wind farms' power curves using machine learning techniques. *Applied Energy*, 98:574–583, 2012.

[197] Benoît Marx, Damien Koenig, and Dídier Georges. Robust fault diagnosis for linear descriptor systems using proportional integral observers. In *Proceedings of the 42nd IEEE Conference on Decision and Control, 2003*, volume 1, pages 457–462. IEEE, 2003.

[198] Georgios Mavromatidis, Kristina Orehounig, and Jan Carmeliet. A review of uncertainty characterisation approaches for the optimal design of distributed energy systems. *Renewable and Sustainable Energy Reviews*, 88:258–277, 2018.

[199] Russell C McKenna, P Ostman vd Leye, and Wolf Fichtner. Key challenges and prospects for large wind turbines. *Renewable and Sustainable Energy Reviews*, 53:1212–1221, 2016.

[200] Jelena Milisavljevic, Sesh Commuri, Janet K Allen, and Farrokh Mistree. A concurrent design exploration method for realizing networked manufacturing systems. In *Proceedings of the ASME 2017 International Design Engineering Technical Conferences and Computers and Information in Engineering Conference*.

[201] Saúl Montes de Oca, Vicenç Puig, and Joaquim Blesa. Robust fault detection based on adaptive threshold generation using interval LPV observers. *International Journal of Adaptive Control and Signal Processing*, 26(3):258–283, 2012.

[202] Douglas C Montgomery. *Introduction to statistical quality control*. John Wiley & Sons, 2007.

[203] Ian Morgan, Honghai Liu, Bernardo Tormos, and Antonio Sala. Detection and diagnosis of incipient faults in heavy-duty diesel engines. *IEEE Transactions on Industrial Electronics*, 57(10):3522–3532, 2009.

[204] ApS Mosek. The MOSEK optimization toolbox for MATLAB manual, 2015.

[205] Peter J Moylan. Stable inversion of linear systems. *IEEE Transactions on Automatic Control*, 22(1):74–78, 1977.

[206] Marcin Mrugalski. An unscented kalman filter in designing dynamic GMDH neural networks for robust fault detection. *International Journal of Applied Mathematics and Computer Science*, 23(1):157–169, 2013.

[207] Iulian Munteanu, Antoneta Iuliana Bratcu, Nicolaos-Antonio Cutululis, and Emil Ceanga. *Optimal control of wind energy systems: towards a global approach*. Springer Science & Business Media, 2008.

[208] Pal-Stefan Murvay and Ioan Silea. A survey on gas leak detection and localization techniques. *Journal of Loss Prevention in the Process Industries*, 25(6):966–973, 2012.

[209] Jing Na, Juan Yang, Xing Wu, and Yu Guo. Robust adaptive parameter estimation of sinusoidal signals. *Automatica*, 53:376–384, 2015.

[210] Barry L Nelson. *Stochastic modeling: analysis & simulation*. Courier Corporation, 2010.

[211] Jenny Niebsch and Ronny Ramlau. Simultaneous estimation of mass and aerodynamic rotor imbalances for wind turbines. *Journal of Mathematics in Industry*, 4(1):12, 2014.

[212] Hans H Niemann, Jakob Stoustrup, Bahram Shafai, and Stuart R Beale. LTR design of proportional-integral observers. *International Journal of Robust and Nonlinear Control*, 5(7):671–693, 1995.

[213] Euripedes G Nobrega, Musa O Abdalla, and Karolos M Grigoriadis. Robust fault estimation of uncertain systems using an LMI-based approach. *International Journal of Robust and Nonlinear Control*, 18(18):1657–1680, 2008.

[214] Peter F Odgaard and Jakob Stoustrup. Results of a wind turbine FDI competition. *IFAC Proceedings Volumes*, 45(20):102–107, 2012.

[215] Peter F Odgaard and Jakob Stoustrup. Fault tolerant wind farm control – A benchmark model. In *Proceedings of the IEEE International Conference on Control Applications (CCA), 2013*, pages 412–417. IEEE, 2013.

[216] Peter F Odgaard, Jakob Stoustrup, and Michel Kinnaert. Fault-tolerant control of wind turbines: A benchmark model. *IEEE Transactions on Control Systems Technology*, 21(4):1168–1182, 2013.

[217] Peter F Odgaard, Jakob Stoustrup, Rasmus Nielsen, and Chris Damgaard. Observer based detection of sensor faults in wind turbines. In *Proceedings of the European Wind Energy Conference, 2009*, pages 4421–4430, 2009.

[218] Kasper Zinck Østergaard, Jakob Stoustrup, and Per Brath. Linear parameter varying control of wind turbines covering both partial load and full load conditions. *International Journal of Robust and Nonlinear Control*, 19(1):92–116, 2009.

[219] María del Populo Pablo-Romero Gil-Delgado and Rafael del Pozo-Barajas. Global changes in total and wind electricity (1990–2014). *Energy*, 5(2):290–312, 2017.

[220] Olivier Parent and Adrian Ilinca. Anti-icing and de-icing techniques for wind turbines: Critical review. *Cold Regions Science and Technology*, 65(1):88–96, 2011.

[221] Vahid Pashazadeh, Farzad R Salmasi, and Babak N Araabi. Data driven sensor and actuator fault detection and isolation in wind turbine using classifier fusion. *Renewable Energy*, 116:99–106, 2018.

[222] Ron J Patton. Fault-tolerant control. *Encyclopedia of Systems and Control*, pages 422–428, 2015.

[223] Ron J Patton and Jie Chen. A review of parity space approaches to fault diagnosis. In *Proceedings of the IFAC SAFEPROCESS Conference, 1991*, pages 65–81, 1991.

[224] Ron J Patton and Jie Chen. Robust fault detection using eigenstructure assignment: A tutorial consideration and some new results. In *Proceedings of the 30th IEEE Conference on Decision and Control, 1991*, pages 2242–2247. IEEE, 1991.

[225] Ron J Patton and Jie Chen. On eigenstructure assignment for robust fault diagnosis. *International Journal of Robust and Nonlinear Control*, 10(14):1193–1208, 2000.

[226] Ron J Patton, Jie R Chen, and JHP Miller. A robust disturbance decoupling approach to fault detection in process systems. In *Proceedings of the 30th IEEE Conference on Decision and Control, 1991*, pages 1543–1548. IEEE, 1991.

[227] Ron J Patton, Paul M Frank, and Robert N Clark. *Issues of fault diagnosis for dynamic systems*. Springer Science & Business Media, 2013.

[228] Ron J Patton, Chandrasekhar Kambhampati, Alessandro Casavola, and Giuseppe Framè. Fault-tolerance as a key requirement for the control of modern systems. In *Proceedings of the Fault Detection, Supervision and Safety of Technical Processes 2006*, pages 13–22. Elsevier, 2007.

[229] Ignacio Peñarrocha, Daniel Dolz, and Roberto Sanchis. Performance trade-offs for networked jump observer-based fault diagnosis. *IEEE Transactions on Signal Processing*, 63(10):2692–2703, 2015.

[230] Kaare B Petersen and Michael S Pedersen. The matrix cookbook. *Technical University of Denmark*, 7(15):510, 2008.

[231] Mohammad Pirhooshyaran and Seyed Taghi Akhavan Niaki. A double-max mewma scheme for simultaneous monitoring and fault isolation of multivariate multistage autocorrelated processes based on novel reduced-dimension statistics. *Journal of Process Control*, 29:11–22, 2015.

[232] Marios M Polycarpou and Arun T Vemuri. Learning approach to fault tolerant control: An overview. In *Proceedings of the 1998 IEEE International Symposium on Intelligent Control (ISIC) held jointly with IEEE International Symposium on Computational Intelligence in Robotics and Automation (CIRA)*, pages 157–162. IEEE, 1998.

[233] Z Poulakis, Dimitris Valougeorgis, and Costas Papadimitriou. Leakage detection in water pipe networks using a bayesian probabilistic framework. *Probabilistic Engineering Mechanics*, 18(4):315–327, 2003.

[234] Vicenç Puig, Saúl Montes de Oca, and Joaquim Blesa. Adaptive threshold generation in robust fault detection using interval models: time-domain and frequency-domain approaches. *International Journal of Adaptive Control and Signal Processing*, 27(10):873–901, 2013.

[235] Wei Qiao and Dingguo Lu. A survey on wind turbine condition monitoring and fault diagnosis - Part I: Components and subsystems. *IEEE Transactions on Industrial Electronics*, 62(10):6536–6545, 2015.

[236] Herbert E Rauch. Intelligent fault diagnosis and control reconfiguration. *IEEE Control Systems*, 14(3):6–12, 1994.

[237] H Prashanth Reddy, Shankar Narasimhan, S Murty Bhallamudi, and S Bairagi. Leak detection in gas pipeline networks using an efficient state estimator. Part II. Experimental and field evaluation. *Computers & Chemical Engineering*, 35(4):662–670, 2011.

[238] John Rice. *Mathematical statistics and data analysis*. Nelson Education, 2006.

[239] Jan H Richter. *Reconfigurable control of nonlinear dynamical systems: a fault-hiding approach*, volume 408. Springer, 2011.

[240] Deneb Robles, Vicenç Puig, Carlos Ocampo-Martinez, and Luis E Garza-Castañón. Reliable fault-tolerant model predictive control of drinking water transport networks. *Control Engineering Practice*, 55:197–211, 2016.

[241] Mickael Rodrigues, Hédi Hamdi, Didier Theilliol, Chokri Mechmeche, and Naceur Ben-Hadj Braiek. Actuator fault estimation based adaptive polytopic observer for a class of LPV descriptor systems. *International Journal of Robust and Nonlinear Control*, 25(5):673–688, 2015.

[242] Damiano Rotondo, Andrea Cristofaro, Tor Arne Johansen, Fatiha Nejjari, and Vicenç Puig. Detection of icing and actuators faults in the longitudinal dynamics of small UAVs using an LPV proportional integral unknown input observer. In *Proceedings of the 3rd Conference on Control and Fault-Tolerant Systems (SysTol), 2016*, pages 690–697. IEEE, 2016.

[243] Damiano Rotondo, Fatiha Nejjari, and Vicenç Puig. A virtual actuator and sensor approach for fault tolerant control of LPV systems. *Journal of Process Control*, 24(3):203–222, 2014.

[244] Damiano Rotondo, Fatiha Nejjari, Vicenç Puig, and Joaquim Blesa. Model reference FTC for LPV systems using virtual actuators and set-membership fault estimation. *International Journal of Robust and Nonlinear Control*, 25(5):735–760, 2015.

[245] Evan L Russell, Leo H Chiang, and Richard D Braatz. *Data-driven methods for fault detection and diagnosis in chemical processes*. Springer Science & Business Media, 2012.

[246] Jedsada Saijai, Steven X Ding, Ali Abdo, Bo Shen, and Waseem Damlakhi. Threshold computation for fault detection in linear discrete-time Markov jump systems. *International Journal of Adaptive Control and Signal Processing*, 28(11):1106–1127, 2014.

[247] Karim Salahshoor, Mohsen Mosallaei, and Mohammadreza Bayat. Centralized and decentralized process and sensor fault monitoring using data fusion based on adaptive extended kalman filter algorithm. *Measurement*, 41(10):1059–1076, 2008.

[248] Ester Sales-Setién, Ignacio Peñarrocha, Daniel Dolz, and Roberto Sanchis. Fault detection in the blade and pitch system of a wind turbine with H2 PI observers. *Journal of Physics: Conference Series*, 659(1):012033, 2015.

[249] Ester Sales-Setién, Ignacio Peñarrocha, Daniel Dolz, and Roberto Sanchis. Performance-based design of PI observers for fault diagnosis in LTI systems under gaussian noises. In *Proceedings of the 3rd Conference on Control and Fault-Tolerant Systems (SysTol), 2016*, pages 407–412. IEEE, 2016.

[250] Ester Sales-Setién and Ignacio Peñarrocha-Alós. Banks of estimators and decision mechanisms for pitch actuator and sensor FE in wind turbines. *IFAC-PapersOnLine*, 51(24):1141–1148, 2018.

[251] Hector Sanchez, Teresa Escobet, Vicenc Puig, and Peter Fogh Odgaard. Fault diagnosis of an advanced wind turbine benchmark using interval-based ARRs and observers. *IEEE Transactions on Industrial Electronics*, 62(6):3783–3793, 2015.

[252] Carsten Scherer, Pascal Gahinet, and Mahmoud Chilali. Multiobjective output-feedback control via LMI optimization. *IEEE Transactions on Automatic Control*, 42(7):896–911, 1997.

[253] David Schlipf, Dominik Johannes Schlipf, and Martin Kühn. Nonlinear model predictive control of wind turbines using LIDAR. *Wind Energy*, 16(7):1107–1129, 2013.

[254] Horst Schulte and Eckhard Gauterin. Fault-tolerant control of wind turbines with hydrostatic transmission using takagi–sugeno and sliding mode techniques. *Annual Reviews in Control*, 40:82–92, 2015.

[255] Shayle R Searle, George Casella, and Charles E McCulloch. *Variance components*, volume 391. John Wiley & Sons, 2009.

[256] Shayle R Searle and Andre I Khuri. *Matrix algebra useful for statistics*. John Wiley & Sons, 2017.

[257] Richard Serfozo. *Basics of applied stochastic processes*. Springer Science & Business Media, 2009.

[258] Hui Shao, Zhiwei Gao, Xiaoxu Liu, and Krishna Busawon. Parameter-varying modelling and fault reconstruction for wind turbine systems. *Renewable Energy*, 116:145–152, 2018.

[259] Guoqiao Shen, Xuancai Zhu, Jun Zhang, and Dehong Xu. A new feedback method for PR current control of LCL-filter-based grid-connected inverter. *IEEE Transactions on Industrial Electronics*, 57(6):2033–2041, 2010.

[260] Xiaoling Sheng, Shuting Wan, Lifeng Cheng, and Yonggang Li. Blade aerodynamic asymmetry fault analysis and diagnosis of wind turbines with doubly fed induction generator. *Journal of Mechanical Science and Technology*, 31(10):5011–5020, 2017.

[261] Fengming Shi and Ron Patton. An active fault tolerant control approach to an offshore wind turbine model. *Renewable Energy*, 75:788–798, 2015.

[262] Jianjun Shi and Shiyu Zhou. Quality control and improvement for multistage systems: A survey. *IIE Transactions*, 41(9):744–753, 2009.

[263] Silvio Simani and Paolo Castaldi. Active actuator fault-tolerant control of a wind turbine benchmark model. *International Journal of Robust and Nonlinear Control*, 24(8-9):1283–1303, 2014.

[264] Silvio Simani, Paolo Castaldi, and Saverio Farsoni. Data–driven fault diagnosis of a wind farm benchmark model. *Energies*, 10(7):866, 2017.

[265] Silvio Simani and Cesare Fantuzzi. Fault diagnosis in power plant using neural networks. *Information Sciences*, 127(3-4):125–136, 2000.

[266] Silvio Simani, Cesare Fantuzzi, and Ronald Jon Patton. Model-based fault diagnosis techniques. In *Model-based Fault Diagnosis in Dynamic Systems Using Identification Techniques*, pages 19–60. Springer, 2003.

[267] Silvio Simani, Saverio Farsoni, and Paolo Castaldi. Residual generator fuzzy identification for wind turbine benchmark fault diagnosis. *Machines*, 2(4):275–298, 2014.

[268] Silvio Simani, Saverio Farsoni, and Paolo Castaldi. Data-driven techniques for the fault diagnosis of a wind turbine benchmark. *International Journal of Applied Mathematics and Computer Science*, 28(2):247–268, 2018.

[269] Sigurd Skogestad and Ian Postlethwaite. *Multivariable feedback control: analysis and design*, volume 2. Wiley New York, 2007.

[270] Christoffer Sloth, Thomas Esbensen, and Jakob Stoustrup. Robust and fault-tolerant linear parameter-varying control of wind turbines. *Mechatronics*, 21(4):645–659, 2011.

[271] Torsten Söderström. *Discrete-time stochastic systems: estimation and control*. Springer Science & Business Media, 2012.

[272] Timo Sorsa and Heikki N Koivo. Application of artificial neural networks in process fault diagnosis. *Automatica*, 29(4):843–849, 1993.

[273] Matheus Souza, André R Fioravanti, and Robert N Shorten. On analysis and design of discrete-time constrained switched systems. *International Journal of Control*, 91(2):437–452, 2018.

[274] Rudolph Frederick Stapelberg. *Handbook of reliability, availability, maintainability and safety in engineering design*. Springer Science & Business Media, 2009.

[275] Thomas Steffen. *Control reconfiguration of dynamical systems: linear approaches and structural tests*, volume 320. Springer Science & Business Media, 2005.

[276] Petre Stoica and Arye Nehorai. On the concentrated stochastic likelihood function in array signal processing. *Circuits, Systems and Signal Processing*, 14(5):669–674, 1995.

[277] Anton A Stoorvogel, Hans H Niemann, Ali Saberi, and Peddapullaiah Sannuti. Optimal fault signal estimation. *International Journal of Robust and Nonlinear Control*, 12(8):697–727, 2002.

[278] Liang Sun. Mathematical modeling of the flow in a pipeline with a leak. *Mathematics and Computers in Simulation*, 82(11):2253–2267, 2012.

[279] Shengqi Sun, Liang Dong, Lin Li, and Shusheng Gu. Fault-tolerant control for constrained linear systems based on MPC and FDI. *International Journal of Information and Systems Sciences*, 4(4):512–523, 2008.

[280] Zhendong Sun. *Switched linear systems: Control and design*. Springer Science & Business Media, 2006.

[281] Daoliang Tan, Ron J Patton, and Xi Wang. A relaxed solution to unknown input observers for state and fault estimation. In *Proceedings of the IFAC Symposium on Fault Detection, Supervision and Safety for Technical Processes, 2015*, volume 48, pages 1048–1053, 2015.

[282] Peter Tavner. *Offshore Wind Turbines Reliability, availability and maintenance*. The Institution of Engineering and Technology, 2012.

[283] Poh Sim Teh and H Trinh. Design of unknown input functional observers for nonlinear systems with application to fault diagnosis. *Journal of Process Control*, 23(8):1169–1184, 2013.

[284] Khaoula Tidriri, Nizar Chatti, Sylvain Verron, and Téodor Tiplica. Bridging data-driven and model-based approaches for process fault diagnosis and health monitoring: A review of researches and future challenges. *Annual Reviews in Control*, 42:63–81, 2016.

[285] Adrian Timbus, Marco Liserre, Remus Teodorescu, Pedro Rodriguez, and Frede Blaabjerg. Evaluation of current controllers for distributed power generation systems. *IEEE Transactions on Power Electronics*, 24(3):654–664, 2009.

[286] Lizeth Torres, Cristina Verde, Gildas Besançon, and Omar González. High-gain observers for leak location in subterranean pipelines of liquefied petroleum gas. *International Journal of Robust and Nonlinear Control*, 24(6):1127–1141, 2014.

[287] GJW Van Bussel, AR Henderson, CA Morgan, B Smith, R Barthelmie, K Argyriadis, A Arena, G Niklasson, and E Peltola. State of the art and technology trends for offshore wind energy: operation and maintenance issues. In *Proceedings of the Offshore Wind Energy Special Topic Conference, 2001*, 2001.

[288] D Van Schrick. Investigations of reliability for instrument fault detection state-estimator schemes. *European Journal of Diagnosis and Safety in Automation (Revue Européenne Diagnostic et Sûreté de Fonctionnement)*, 1(1):63–78, 1991.

[289] Venkat Venkatasubramanian, Raghunathan Rengaswamy, Surya N Kavuri, and Kewen Yin. A review of process fault detection and diagnosis: Part III: Process history based methods. *Computers and Chemical Engineering*, 27(3):327–346, 2003.

[290] Venkat Venkatasubramanian, Raghunathan Rengaswamy, Kewen Yin, and Surya N Kavuri. A review of process fault detection and diagnosis: Part I: Quantitative model-based methods. *Computers & Chemical Engineering*, 27(3):293–311, 2003.

[291] Venkat Venkatsubramanian. A review of process fault detection and diagnosis: Part II: Qualitative models and search strategics. *Computers and Chemical Engineering*, 27(3):313–326, 2003.

[292] Cristina Verde. Accommodation of multi-leak location in a pipeline. *Control Engineering Practice*, 13(8):1071–1078, 2005.

[293] Sylvain Verron, Jing Li, and Teodor Tiplica. Fault detection and isolation of faults in a multivariate process with bayesian network. *Journal of Process Control*, 20(8):902–911, 2010.

[294] Yiming Wan, Wei Dong, Hao Wu, and Hao Ye. Integrated fault detection system design for linear discrete time-varying systems with bounded power disturbances. *International Journal of Robust and Nonlinear Control*, 23(16):1781–1802, 2013.

[295] Yiming Wan, Wei Dong, and Hao Ye. Integrated trade-off design of fault detection system for linear discrete time-varying systems. *IET Control Theory & Applications*, 7(3):455–463, 2013.

[296] Jian Liang Wang, Guang-Hong Yang, and Jian Liu. An LMI approach to $\mathcal{H}_-$index and mixed $\mathcal{H}_-/\mathcal{H}_\infty$ fault detection observer design. *Automatica*, 43(9):1656–1665, 2007.

[297] Jing Wang, Wenshuang Ge, Jinglin Zhou, Haiyan Wu, and Qibing Jin. Fault isolation based on residual evaluation and contribution analysis. *Journal of the Franklin Institute*, 354(6):2591–2612, 2017.

[298] Xianghua Wang, Chee Pin Tan, and Donghua Zhou. A novel sliding mode observer for state and fault estimation in systems not satisfying matching and minimum phase conditions. *Automatica*, 79:290–295, 2017.

[299] Zhenhua Wang, Mickael Rodrigues, Didier Theilliol, and Yi Shen. Fault estimation filter design for discrete-time descriptor systems. *IET Control Theory & Applications*, 9(10):1587–1594, 2015.

[300] Michel Weber. A weighted central limit theorem. *Statistics & Probability Letters*, 76(14):1482–1487, 2006.

[301] Marcin Witczak. *Modelling and estimation strategies for fault diagnosis of non-linear systems: from analytical to soft computing approaches*, volume 354. Springer Science & Business Media, 2007.

[302] Marcin Witczak, Mariusz Buciakowski, Vicenç Puig, Damiano Rotondo, and Fatiha Nejjari. An LMI approach to robust fault estimation for a class of nonlinear systems. *International Journal of Robust and Nonlinear Control*, 26(7):1530–1548, 2016.

[303] Marcin Witczak, Damiano Rotondo, Vicenç Puig, Fatiha Nejjari, and Marcin Pazera. Fault estimation of wind turbines using combined adaptive and parameter estimation schemes. *International Journal of Adaptive Control and Signal Processing*, 2017.

[304] Marcin Witczak, Damiano Rotondo, Vicenç Puig, Fatiha Nejjari, and Marcin Pazera. Fault estimation of wind turbines using combined adaptive and parameter estimation schemes. *International Journal of Adaptive Control and Signal Processing*, 32(4):549–567, 2018.

[305] AI-Guo Wu and Guang-Ren Duan. Generalized PI observer design for linear systems. *IMA Journal of Mathematical Control and Information*, 25(2):239–250, 2007.

[306] Ai-Guo Wu, Guang-Ren Duan, and Wanquan Liu. Proportional multiple-integral observer design for continuous-time descriptor linear systems. *Asian Journal of Control*, 14(2):476–488, 2012.

[307] Ai-Guo Wu, Gang Feng, and Guang-Ren Duan. Proportional multiple-integral observer design for discrete-time descriptor linear systems. *International Journal of Systems Science*, 43(8):1492–1503, 2012.

[308] Fen Wu. Switching LPV control design for magnetic bearing systems. In *Proceedings of the IEEE International Conference on Control Applications (CCA'01), 2001*, pages 41–46. IEEE, 2001.

[309] Zedjiga Yacine, Dalil Ichalal, Naïma Ait-Oufroukh, Saïd Mammar, and Saïd Djennoune. Takagi-Sugeno observers: experimental application for vehicle lateral dynamics estimation. *IEEE Transactions on Control Systems Technology*, 23(2):754–761, 2015.

[310] Fuyong Yang, Sun Jin, and Zhimin Li. A comprehensive study of linear variation propagation modeling methods for multistage machining processes. *The International Journal of Advanced Manufacturing Technology*, 90(5-8):2139–2151, 2017.

[311] Fuyong Yang, Sun Jin, and Zhimin Li. A modification of DMVs based state space model of variation propagation for multistage machining processes. *Assembly Automation*, 37(4):381–390, 2017.

[312] Dan Ye, Meng-Meng Chen, and Hai-Jiao Yang. Distributed adaptive event-triggered fault-tolerant consensus of multiagent systems with general linear dynamics. *IEEE Transactions on Cybernetics*, 2018.

[313] Alain Yetendje, Maria M Seron, and José A De Doná. Robust multiactuator fault-tolerant MPC design for constrained systems. *International Journal of Robust and Nonlinear Control*, 23(16):1828–1845, 2013.

[314] Shen Yin, Steven X Ding, Adel Haghani, Haiyang Hao, and Ping Zhang. A comparison study of basic data-driven fault diagnosis and process monitoring methods on the benchmark tennessee eastman process. *Journal of Process Control*, 22(9):1567–1581, 2012.

[315] Shen Yin, Steven X Ding, Xiaochen Xie, and Hao Luo. A review on basic data-driven approaches for industrial process monitoring. *IEEE Transactions on Industrial Electronics*, 61(11):6418–6428, 2014.

[316] Shen Yin, Huijun Gao, Jianbin Qiu, and Okyay Kaynak. Descriptor reduced-order sliding mode observers design for switched systems with sensor and actuator faults. *Automatica*, 76:282–292, 2017.

[317] Shen Yin, Guang Wang, and Hamid Reza Karimi. Data-driven design of robust fault detection system for wind turbines. *Mechatronics*, 24(4):298–306, 2014.

[318] Xiang Yu and Jin Jiang. A survey of fault-tolerant controllers based on safety-related issues. *Annual Reviews in Control*, 39:46–57, 2015.

[319] Shouchao Zhai, Yiming Wan, and Hao Ye. A set-membership approach to integrated trade-off design of robust fault detection system. *International Journal of Adaptive Control and Signal Processing*, 31(2):191–209, 2017.

[320] Dahai Zhang, Jiaqi Wang, Yonggang Lin, Yulin Si, Can Huang, Jing Yang, Bin Huang, and Wei Li. Present situation and future prospect of renewable energy in china. *Renewable and Sustainable Energy Reviews*, 76:865–871, 2017.

[321] Kai Zhang, Haiyang Hao, Zhiwen Chen, Steven X Ding, and Kaixiang Peng. A comparison and evaluation of key performance indicator-based multivariate statistics process monitoring approaches. *Journal of Process Control*, 33:112–126, 2015.

[322] Ke Zhang, Bin Jiang, and Vincent Cocquempot. Robust fault estimation observer design with finite-time convergence specification. *IET Control Theory & Applications*, 11(1):1–9, 2016.

[323] Ke Zhang, Bin Jiang, Vincent Cocquempot, and Huaguang Zhang. A framework of robust fault estimation observer design for continuous-time/discrete-time systems. *Optimal Control Applications and Methods*, 34(4):442–457, 2013.

[324] Ke Zhang, Bin Jiang, and Peng Shi. Observer-based integrated robust fault estimation and accommodation design for discrete-time systems. *International Journal of Control*, 83(6):1167–1181, 2010.

[325] Ke Zhang, Bin Jiang, and Peng Shi. *Observer-based fault estimation and accomodation for dynamic systems*, volume 436. Springer Science & Business Media, 2012.

[326] Ke Zhang, Bin Jiang, Peng Shi, and Vincent Cocquempot. *Observer-based fault estimation techniques*. Springer Science & Business Media, 2018.

[327] Ping Zhang and Steven X Ding. An integrated trade-off design of observer based fault detection systems. *Automatica*, 44(7):1886–1894, 2008.

[328] Xiaodong Zhang, Marios M Polycarpou, and Thomas Parisini. Fault diagnosis of a class of nonlinear uncertain systems with Lipschitz nonlinearities using adaptive estimation. *Automatica*, 46(2):290–299, 2010.

[329] Youmin Zhang and Jin Jiang. Integrated active fault-tolerant control using IMM approach. *IEEE Transactions on Aerospace and Electronic systems*, 37(4):1221–1235, 2001.

[330] Youmin Zhang and Jin Jiang. Bibliographical review on reconfigurable fault-tolerant control systems. *Annual Reviews in Control*, 32(2):229–252, 2008.

[331] Dong Zhao, Dong Shen, and Youqing Wang. Fault diagnosis and compensation for two-dimensional discrete time systems with sensor faults and time-varying delays. *International Journal of Robust and Nonlinear Control*, 27(16):3296–3320, 2017.

[332] Maiying Zhong, Steven X Ding, and Eve L Ding. Optimal fault detection for linear discrete time-varying systems. *Automatica*, 46(8):1395–1400, 2010.

[333] Maiying Zhong, Steven X Ding, James Lam, and Haibo Wang. An LMI approach to design robust fault detection filter for uncertain lti systems. *Automatica*, 39(3):543–550, 2003.

[334] Maiying Zhong, Ligang Zhang, Steven X Ding, and Donghua Zhou. A probabilistic approach to robust fault detection for a class of nonlinear systems. *IEEE Transactions on Industrial Electronics*, 64(5):3930–3939, 2017.

[335] Kemin Zhou, John Comstock Doyle, Keith Glover, et al. *Robust and optimal control*, volume 40. Prentice hall New Jersey, 1996.

[336] Shiyu Zhou, Yong Chen, and Jianjun Shi. Statistical estimation and testing for variation root-cause identification of multistage manufacturing processes. *IEEE Transactions on Automation Science and Engineering*, 1(1):73–83, 2004.

[337] Shiyu Zhou, Yu Ding, Yong Chen, and Jianjun Shi. Diagnosability study of multistage manufacturing processes based on linear mixed-effects models. *Technometrics*, 2012.

[338] Shiyu Zhou, Qiang Huang, and Jianjun Shi. State space modeling of dimensional variation propagation in multistage machining process using differential motion vectors. *IEEE Transactions on Robotics and Automation*, 19(2):296–309, 2003.

[339] Jun-Wei Zhu and Guang-Hong Yang. Fault-tolerant control for linear systems with multiple faults and disturbances based on augmented intermediate estimator. *IET Control Theory & Applications*, 11(2):164–172, 2016.

[340] S Hamideh S Ziyabari and Mahdi A Shoorehdeli. Robust fault diagnosis scheme in a class of nonlinear system based on UIO and fuzzy residual. *International Journal of Control, Automation and Systems*, 15(3):1145–1154, 2017.

[341] Changliang Zou and Fugee Tsung. Directional MEWMA schemes for multistage process monitoring and diagnosis. *Journal of Quality Technology*, 40(4):407–427, 2008.